NASA

QUARTERLY PROGRESS REPORT

No. 84

JANUARY 15, 1967

MASSACHUSETTS INSTITUTE OF TECHNOLOGY
RESEARCH LABORATORY OF ELECTRONICS
CAMBRIDGE, MASSACHUSETTS

The Research Laboratory of Electronics is an interdepartmental laboratory in which faculty members and graduate students from numerous academic departments conduct research.

The research reported in this document was made possible by support extended the Massachusetts Institute of Technology, Research Laboratory of Electronics, by the following agencies.

Joint Services Electronics Programs (U.S. Army, U.S. Navy, U.S. Air Force)
Contract DA 36-039-AMC-03200(E)
U.S. Air Force—Aerospace Medical Division
Contract AF 33(615)-3885
U.S. Air Force—Electronic Systems Division
Contract AF 19(628)-2487
Contract AF 19(628)-6066
U.S. Air Force—Research and Technology Division
Contract F33615-67-C-1148
U.S. Air Force—Office of Scientific Research
Contract F44620-67-C-0030
U.S. Navy—Office of Naval Research
Contract Nonr-1841-(42)
National Aeronautics and Space Administration
Grant NsG-496
Grant NsG-22-009-(163)
Grant NGR-22-009-091
Grant NGR-22-009-114
Grant NGR-22-009-131
Grant NsG-334
Grant NsG-419
Contract NSR-22-009-120
National Institutes of Health
Grant 2 PO1 MH-04737-06
Grant 5 RO1 NB-04332-04
Grant 5 RO1 NB-05462-03
Grant 5 RO1 NB-04897-04
Grant 5 RO1 NB-06251-02
Grant 1 505 FR-07047-01
Grant 5 RO1 NB-04985-04
National Science Foundation
Grant GK-835
Grant GK-57
Grant GK-1165
U.S. Atomic Energy Commission
Contract AT (30-1)-3581
Contract AT (30-1)-3285
Contract AT (30-1)-1842
Bell Telephone Laboratories, Inc. Grant
The Teagle Foundation, Inc. Grant
M.I.T. Cabot Solar Energy Fund
M.I.T. Sloan Fund for Basic Research

Support of projects is acknowledged in footnotes to the appropriate sections

167

1 MASSACHUSETTS INSTITUTE OF TECHNOLOGY, Cambridge 2
2 RESEARCH LABORATORY OF ELECTRONICS 3

QUARTERLY PROGRESS REPORT No. 84

9 January 15, 1967 10 CY

Submitted by: 6 H. J. Zimmermann
G. G. Harvey 9

TABLE OF CONTENTS

Personnel viii

Publications and Reports xvi

Introduction xxii

GENERAL PHYSICS

I. Molecular Beams 1

Square-Wave Phase Modulation in Molecular Beam Resonance Experiments 2

Search for a Shift in the Transverse Electromagnetic Mass of the Electron 9

II. Molecular Collisions 13

III. Microwave Spectroscopy 15

Work Completed 16

Electric Field Effects in the Nuclear Magnetic Resonance of Fluids 16

Expansion of Velocity Surfaces in Spherical Harmonics 17

Ruby Cross Relaxation 26

IV. Atomic Resonance and Scattering 27

V. Electron Magnetic Resonance 31

VI. Radio Astronomy 33

Haystack-Millstone OH Interferometer 34

Millstone-Agassiz OH Interferometer 36

K-band Spectrum Measurements of the Sun 36

Inference of Atmospheric Attenuation near 61.15 GHz from Balloon Flight Results 38

Observations of Microwave Emission from Atmospheric Oxygen: Balloon Flights, Summer 1966 42

Observations of Microwave Emission from Atmospheric Oxygen: Balloon Experiment Results, Summer 1965 42

VII. Solid State Microwave Electronics 49

Work Completed 49

CONTENTS

VIII.	Optical and Infrared Spectroscopy	51
	Work Completed	53
	Temperature Dependence of the Raman Spectrum of $KTaO_3$ and $SrTiO_3$	53
IX.	Ultrasonic Properties of Solids	61
X.	Geophysical Research	63
	High Magnetic Fields	63
	Upper Atomospheric Physics	64
	Possible Relation between Dust and Rainfall	66
XI.	Gravitation Research	69
	Experimental Test of the Freundlich Red-Shift Hypothesis	70
	Measurement of Metastable versus Ground-State Electron Exchange Cross Sections for Helium and Neon	70
XII.	Noise in Electron Devices	75
XIII.	Magnetic Resonance	77
XIV.	X-ray Diffraction Studies	79
XV.	Physical Electronics and Surface Physics	81
	Contact Potential Measurements of the Adsorption of O_2 on (110) Ta	82
	Desorption and Migration Kinetics of Molecules Adsorbed on Nonuniform Surfaces: Steady-State Analysis	89
	Single-Phonon Energy Transfer between Molecular Beams and Solid Surfaces	94
	Theory of Atom-Metal Interactions	94
XVI.	Physical Acoustics	97
	Electric Field Associated with a Sound Wave in a Weakly Ionized Gas	97
	Viscous Effects in a Hydrodynamic Plasma	98
	Interference of Light with Light in a Plasma	103
XVII.	Electrodynamics of Media	113
	Nonlinear Amplification	113
XVIII.	Physical Optics of Invertebrate Eyes	121

CONTENTS

PLASMA DYNAMICS

XIX.	Plasma Physics	123
	Far Infrared Spectrophotometer for Plasma Studies	123
	Experimental Study of Electron Plasma Oscillations	129
XX.	Gaseous Electronics	137
	Electron-Electron Relaxation Rates as Determined from the Observed Time-Dependent Electron Velocity Distribution	137
XXI.	Plasmas and Controlled Nuclear Fusion	141
	Active Plasma Systems	141
	System C: Ion-Cyclotron Wave Generation	142
	Beam-Plasma Discharge: System D	142
	Cross-Field Beam-Plasma Experiment	144
	Sheet Models of the Beam-Plasma Discharge with Plasma Density Gradients along the Beam	145
	Sheet Model of a Plasma Slab	149
	Stability Criteria for Dispersion Relations Containing Branch Points	151
	Finite Larmor Radius Effects in the Interaction of Electrons with High-Frequency Acoustic Waves	155
	Applied Plasma Physics Related to Controlled Nuclear Fusion	157
	Oscillations in the Hollow-Cathode Discharge Arc	159
	Plasma Magnetohydrodynamic Flows, Waves, and Instabilities	164
	Electron Beam Interaction with a Spatially Inhomogeneous Temperate Plasma	164
XXII.	Energy Conversion Research	171
XXIII.	Spontaneous Radiofrequency Emission from Hot-Electron Plasmas	173
XXIV.	Interaction of Laser Radiation with Plasmas and Nonadiabatic Motion of Particles in Magnetic Fields	175
	Nonadiabatic Trapping in Toridal Geometry	162

CONTENTS

COMMUNICATION SCIENCES AND ENGINEERING

XXV.	Statistical Communication Theory	181
	Transfer Functions for a Two-State Modulation System	184
	A New Approach to Echo Removal	194
XXVI.	Processing and Transmission of Information	203
	Low-Rate Upper Bounds on Error Probability for Fading Dispersive Channels	207
	Optical Propagation through a Turbulent Atmosphere	212
XXVII.	Detection and Estimation Theory	225
	Equalization of Dispersive Channels Using Decision Feedback	227
	State-Variable Estimation in the Presence of Pure Delay	243
XXVIII.	Speech Communication	253
	Real-Time Spectral Input System for Computer Analysis of Speech	253
	Children's Perception of a Set of Vowels	254
	Articulatory Activity and Air Flow during the Production of Fricative Consonants	257
XXIX.	Linguistics	261
	Initial Clusters in English	263
	Esquisse à propos d'Une Classe Limitée d'Adjectifs en Français Moderne	275
XXX.	Cognitive Information Processing	287
	Reproduction of Graphical Data by Facsimile	291
	Image Transmission by Two-Dimensional Contour Coding	294
	Fourier-Transform Representation of Pictures	302
	Effect of Multipath Hologram Television Systems	304
	Optical Spatial Filtering for Simultaneous Delay and Doppler Estimates of Radarlike Signals	307
XXXI.	Communications Biophysics	311
	Circuit Model for the Cat's Middle Ear	320
	Multichannel Time-Domain Filtering Employing Time-Division Multiplexing and a Magnetic Delay Drum	327
	Deterministic Nature of Arterial Pressure Receptors	331

CONTENTS

XXXII.	Neurophysiology	333
	On a Calculus for Triadas	335
XXXIII.	Computer Research	347
XXXIV.	Computation Research	349
	Updating of the Computer Indexing Program	350
	A Simple Method for Finding the Roots of an Analytic Function	351
	Roots, a Root-Finding Subroutine Using Muller's Method	352
	Linearizing the Roots of a Polynomial. II	355
	Development of Private Library to Be Searched by TIP	359
XXXV.	Stroboscopic Light Research	363
Author Index		365

PERSONNEL

Administration

Prof. H. J. Zimmermann, Director
Prof. G. G. Harvey, Associate Director
Mr. R. A. Sayers, Assistant Director

Advisory Committee

Prof. R. A. Alberty
Prof. R. L. Bishop
Dean G. S. Brown
Prof. G. G. Harvey
Prof. A. G. Hill
Prof. S. J. Mason
Prof. J. Ross
Prof. I. W. Sizer
Prof. L. D. Smullin
Prof. V. S. Weisskopf
Prof. H. J. Zimmermann
(Chairman)

Research Committee

Dean S. C. Brown
Prof. L. J. Chu
Prof. M. Eden
Prof. M. Halle
Prof. G. G. Harvey
Prof. J. G. King
Prof. S. J. Mason
Prof. D. J. Rose
Prof. W. A. Rosenblith
Mr. R. A. Sayers
Prof. W. M. Siebert
Prof. M. W. P. Strandberg
Prof. P. D. Wall
Prof. J. R. Zacharias
Prof. H. J. Zimmermann
(Chairman)

Professors

Allis, W. P.
Barrett, A. H.
Bitter, F.
Bose, A. G.
Brown, S. C.
Burke, B. F.
Chomsky, N. A.
Chu, L. J.
Eden, M.
Edgerton, H. E.
Elias, P.
Gross, P. L.
Gyftopoulos, E. P.
Halle, M.
Harvey, G. G.
Haus, H. A.
Hill, A. G.
Huffman, D. A.
Ingard, K. U.
Jakobson, R.
Kerrebrock, J. L.
King, J. G.
Lee, Y. W.
Lettvin, J. Y.
Levinthal, C.
Mason, S. J.
Minsky, M. L.
Rose, D. J.
Rosenblith, W. A.
Ross, J.
Schreiber, W. F.
Shannon, C. E.
Shu, C. G. (Visiting)
Siebert, W. M.
Sledd, J. H. (Visiting)
Smullin, L. D.
Stevens, K. N.
Strandberg, M. W. P.
Wall, P. D.
Warren, B. E.
Waugh, J. S.
Wozencraft, J. M. (Absent)
Zacharias, J. R.
Zimmermann, H. J.

Associate Professors

Bekefi, G.
Bers, A.
Brown, G. A.

PERSONNEL

Associate Professors (continued)

Dennis, J. B.
Dupree, T. H.
Fodor, J. A.
Gallager, R. G.
Garland, C. W.
Hennie, F. C., III
Hoffman, M. A.
Jackson, W. D. (Absent)
Katz, J. J.
Kleppner, D.
Klima, E. S.
Kyhl, R. L.
Lee, F. F.
Massey, J. L. (Visiting)
Matthews, G. H.
Mortenson, E. (Visiting)
Oates, G. C.
Peake, W. T.
Pomorska, Krystyna
Rafuse, R. P.
Searle, C. L.
Van Trees, H. L.

Assistant Professors

Anderson, J. (1)
Bernard, G. D.
Billman, K. W.
Black, W. L. (1)
Blum, M.
Bowers, K. W.
Briggs, R. J.
Bromberger, S.
Brown, J. E.
Bruce, J. D.
Carabateas, E. N. (Absent)
Dean, L. W., III
Fiocco, G.
Goutmann, M. M.
Henke, W. L.
Hoversten, E. V. (1)
Huang, T. S.
Ingraham, J. C.
Katona, P. G.
Kennedy, R. S.
Kinsey, J. L.
Kiparsky, R. P. V.
Klatt, D. H. (1)
Kolenkow, R. J.
Lee, H. B.
Lenoir, W. B. (1)
Lidsky, L. M.
Nelsen, D. E.
Oppenheim, A. V.
Penman, S.
Perry, C. H.
Pomeranz, B.
Ross, J. R.
Siambis, J. G. (1)
Snyder, D. L.
Spann, R. N.
Staelin, D. H. (1)
Stickney, R. E.
Troxel, D. E.
Weiss, R.
Weiss, T. F.
Yip, S.

Lecturers

Bever, T. G.
Ferretti, E.
Mark, R. G.
Pitts, W. H.
Rines, R. H.
Teager, H. M.

Instructors

Blesser, B.
Burns, S. K.
Eisenberg, M.
Evans, J. E.
Kukolich, S. G.
McEnally, T. E., Jr.
Parker, R. R.
Schafer, R. W.
Schindall, J. E.
Schneider, H. M.
Speck, C. E.
Tripp, A. P.

Research Associates

Barnett, G. O.
Canfield, J. V.
Chung, K.
Dilly, P. N.
Durlach, N. I.
Garrett, M. F. (2)
Gerschenfeld, Dora J.
Grams, G. W.
Hall, R. D.
Hoffman, R. A.
Ingham, K. R.
Kittelburger, J. S.
Kolers, P. A.
Kornacker, K.
Liss, P. H.
Novotny, D. B.
Papert, S. A.
Sears, R. E. J.
Steinbrecher, D. H.
Zisk, S. H.

(1) Engineering Postdoctoral Fellow

(2) NIH Postdoctoral Trainee

PERSONNEL

Guests

Bailey, C-J. N.
Bullowa, Margaret
Burnham, D. C.
Da Fonseca, J. L. S.
Fomin, S. V.
Heeschen, C.
Kessler, A. R.
Paik, S. F.
Pritchard, D. E.
Walker, D. E.
Winkler, P. F., Jr.

Visiting Scientists

Moreno-Diaz, R.
Nomoto, M. (1)
Suzuki, J.

Research Affiliates

Barlow, J. S.
Brodey, W. M.
Brown, R. M.
Crist, A. H.
Howland, B. (2)
Langbein, D.
McLardy, T.
Ozier, I.

Postdoctoral Fellows

Binford, T. O. (3)
Borbely, A. A.
Fokkens, N.
Franzen, O.
Gruber, J. S. (5)
Hartman, H. (4)
Hellekant, B. C.
Milner, J-C. G.
Natapoff, A. (4)
Schwartz, A. (4)
Smith, N. V.
Songster, G. F. (4)
Taub, A. (4)

R. L. E. Research Staff

Barrett, J. W.
Benhaim, N.
Burgess, R. G.
Cattell, N. R.
Chung, S-H.
Crowther, Patricia P.
Cunningham, A. W. B.
Davis, Heather S.
Fontaine, C. L.
Gambardella, G.
Harwitt, Joan
Ingersoll, J. G.
Isaacs, E. C.
Jensen, E. R.
Kelly, W. F.
Kiang, N. Y. S.
Kierstead, J. D.
Kim, C-W.
Mattison, E. M.
McCaffrey, A.
McCarthy, J. J.
McCulloch, W. S.
Menyuk, Paula
Mulligan, W. J.
Myint, M. T.
O'Brien, F. J.
Pennell, Martha M.
Perkell, J. S.
Pitts, W. H.
Plummer, W. W.
River, Eleanor C.
Rojas-Corona, R. R.
Rosebury, F.
Ryan, L. W.
Shardanand
Shaw, M. L.
Tretiak, O. J.
Viertel, J. J.
Wickelgren, G. L.

Research Assistants

Austin, M. E.
Baggeroer, A. B.
Bartsch, R. R.
Brown, T. S.
Chan, S. W-C.
Chandra, A. N.
Chase, D.
Chen, K. R-S.
Chou, S.
Citron, A.
Davis, J. A.
Dean, Janet P.
DeRijk, R. P. G.
DeWolf, J. B.
Ditz, J. Merle

(1) NIH International Postdoctoral Fellow
(2) Lincoln Laboratory Staff Member
(3) NIH Training Grant
(4) NIH Fellow
(5) NIH Postdoctoral Trainee

Research Assistants (continued)

Eberle, F. W.
Edwards, K. R.
English, R. P.
Ezekiel, S.
Fehrs, D. L.
Fisher, C. H.
Flannery, D. L.
Flynn, R. W.
Frediani, J. K.
Gabrielian, A.
Gadzuk, J. W.
Glaser, J.
Gustafson, K. T.
Ham, D. O.
Herba, F.
Hoff, P. W.
Hougen, M. L.
Huang, T.
Kirk, R.
Kitrosser, D. F.
Klumpp, M. H.
Koons, H. C.
Kurth, R. R.
Kusse, B. R.
Levy, E. K.
Liu, Jane W-S.
Makhoul, J. J.
Mangano, J. A.
Maul, M. K.
McNary, C. A.
Melnick, M.
Milne, D. C.
Moir, R. W.
Moldon, J. C.
Moran, J. M., Jr.
Moses, J.
Murakami, M.
Nahvi, M.
Ng, L. C.
Oates, D. E.
Offenberger, A. A.
Papadopoulos, G. D.
Perozek, D. M.
Poulo, L. R.
Poussart, D. J-M.
Richters, J. S.
Rogers, A. E. E.
Ross, A. H. M.
Sanders, D.
Schumaker, N. E.
Snyder, D. D.
Sugawara, A.
Tomlinson, R. S.
Wagner, C. E.
Weidner, M. Y.
Weiner, B. B.
Wong, Y-M.
Yamamoto, S.
Young, R. A.
Zeiders, G. W., Jr.

Graduate Assistants

Babitch, D.
Brown, T. R.
Davis, W. B.
Ewing, H.
Fertel, Jeanne H.
Forrester, V. G.
Fox, R. L.
Free, J. U., Jr.
Garosi, G. A.
Gschwendtner, A. B.
Langdon, R. M., Jr.
Pleasance, L. D.
Reifenstein, E. C., III
Reznek, S. R.
Silk, J. K.
Smith, T. B.
Vellenga, J. H.
Wilheit, T. T., Jr.
Yung, B. N.

Teaching Assistants

Anderson, G. B.
Bice, P. K.
Bless, S. J.
Ching, H.
Columbant, D. G.
Freeman, J. A. (1)
Guttman, D. S.
Harris, R. V., III
Hartmann, H. P.
Hill, R. A.
Khanna, M.
Kinsley, R. W., Jr.
Kososki, J. F.
Lee, W-H.
Mattison, D. R.
Mazza, C. (2)
Medress, M. F.
Moxon, E. C.
Nedzelnitsky, V.
Nelson, A. C.
Patterson, J. T.
Portner, E. M., Jr.
Schaefer, D. W.
Seitz, C. L.
Singer, J. J.
Tuhy, F. P., Jr.
Wawzonek, J. J.
Williams, J. A.
Woods, J. W.
Yamanaki, B. S.

Graduate Students

Akmajian, A. (3)
Allen, J. L. (5)
Anderson, S. R. (4)
Andrews, M. L.
Arnstein, D. S. (5)
Balcewitz, J. F. (6)

(1) Unites States Air Force
(2) Sci. Teach. Ctr. Grant
(3) National Defense Education Act Fellow
(4) NIH Trainee
(5) Lincoln Laboratory Associate
(6) Jonathan Whitney Fellow

Graduate Students (continued)

Barnwell, T. P., III (4)
Bedell, G. D., IV (6)
Bell, C. M. (31)
Berlinger, J. E. (4)
Bhushnan, A. K. (9)
von Bismarck, G.
Blum, G. D. (4)
Bowers, J. S. (6)
Braida, L. D. (4)
Brame, M. K. (25)
Browne, E. W. (6)
Brueck, S. R. J. (4)
Bucher, E. A. (4)
Callen, J. D. (5)
Carter, R. J. (32)
Chapin, P. G. (1)
Cohen, A. J. (2)
Colburn, S. H. (3)
Collins, L. D. (4)
Cornew, R. W.
Crane, D. E. (5)
Cruise, T. J. (4)
Culicover, P. W. (6)
Decher, R. (7)
Demko, P., Jr. (12)
Dewan, D. P. (4)
Dougherty, R. C. (8)
Ehrenberg, J. E. (9)
Emonds, J. E. (8)
Fidelholtz, J. L. (10)
Gaut, N. E. (7)
George, E. V. (11)
Goldberg, A. J. (12)
Goldfield, R. (6)
Golub, R.
Good, W. E. (13)
Greaves, W. (14)
Greenspan, R. L.
Gross, L. N. (8)
Guinan, J. J., Jr. (4)
Halme, S. (16)
Harris, J. W. (10)
Heggerstad, H. M. (15)
Heller, J. A. (17)
Hofmann, T. R. (8)
Howard, I. J. (6)
Hsiao, H. S.
Hudis, M. (5)
Jackendoff, R. S. (6)
Jameson, P. W.
Kalan, G. R. (18)
Katyl, R. H. (4)
Kayne, R. S. (6)
Kimball, J. P. (8)
Kiparsky, Carol A. (6)
Kolodny, Nancy H. (8)
Krischer, C.
Kronquist, R. L.
Lackner, J. R. (6)
Lawter, J. R. (4)
Leonardi-Cattolica, A. M. (19)
Linford, R. (4)
Lopez, O. (12)
Lubin, M. D.
Manheimer, W. M. (4)
Max, J. (15)
Merrill, E. G. (20)
Mozzi, R. L. (21)
Muehlner, D. J. (4)
Mueller, P. E. (22)
Myers, Amy E. (6)
Naro, A. J. (8)
Nelson, G. P. (10)
Odette, G. (5)
Ohori, D. A. (18)
Parrish, J. H. (4)
Perkins, P. E. (7)
Perlmutter, D. M. (23)
Peterson, D. L.
Pinkston, J. T., III (4)
Pittenger, L. C. (5)
Platts, D. A. (4)
Rabiner, L. R. (4)
Rack, H. J. (24)
Ramshaw, J. D. (4)
Raymond, S. A. (12)
Ritter, J. T. (25)
Robbins, G. M. (9)
Rogoff, G. L.
Rolland, A. E. (26)
Sheena, D. (4)
Sheinson, R. S. (10)
Shupe, D. S. (4)
Simpson, J. I. (4)
Sirbu, M. A. (4)
Snow, M. S. (4)
Stanley, R. J. (8)
Strong, R. M. (27)
Suchard, S. N. (28)
Swain, D. W. (28)
Thiersch, C. L. (4)
Thomae, I. H. (1)
Thongthammachat, S.
Tornberg, N. E. (4)
Tremain, R. E. (4)
Vandamme, F. J. (29)
Vanderbilt, D. H. (4)
Walker, J. L. (26)
Wallace, R. N. (4)
Walpert, G. A. (12)
Wang, C. H. (25)
Watanabe, A. (30)
Weinstein, C. J. (12)
Wiederhold, M. L. (10)
Wilson, T. L. (4)
Wolaver, D. H. (4)
Wolf, J. J.
Woo, Nancy H. (8)
Wright, B. L.
Wright, D. A. (11)
Wright, W. A.

(1) Danforth Foundation Fellow
(2) Shell Oil Co. Fellow
(3) Sperry-Rand Fellow
(4) NSF Fellow
(5) U.S. AEC Fellow
(6) National Defense Education Act Fellow
(7) NASA Fellow
(8) NIH Trainee
(9) Bell Telephone Laboratories Fellow
(10) NIH Fellow
(11) RCA Fellow
(12) NSF Trainee
(13) U.S. Rubber Corporation Fellow
(14) Kennedy Fellow
(15) Lincoln Laboratory Associate
(16) American Scandinavian Foundation
(17) Xerox Fellow
(18) Jonathan Whitney Fellow
(19) Whitney Predoctoral Fellow
(20) Public Health Service Trainee
(21) Raytheon Fellow
(22) American Can Co. Fellow
(23) American Council of Learned Sciences
(24) Vanadium Company Fellow
(25) Woodrow Wilson Fellow
(26) United States Coast Guard
(27) Hertz Foundation Fellow
(28) NASA Trainee
(29) Belgium American Foundation
(30) General Electric Fellow
(31) M.I.T. Fellow
(32) Sci. Teach. Ctr. Grant

PERSONNEL

Undergraduates (Thesis or Special Problems)

Ashton, B.
Bright, K. S.
Cataldo, E. A.
Chappell, R. F.
Cohen, M. H.
Cohen, S. A.
Davidow, J. E.
DeBonte, R. J.
Eckberg, A. E., Jr.
Eckstein, P. F.
Franz, J. M.
Galiger, P. E.
Getting, P. A.
Gill, T. A.
Henckels, L. P. A.
Huie, J. L.
Immerman, E. M.
Juvkam-Wold, H. C.
King, P. A.
Kolb, C. E., Jr.
Kutner, S. R.
Lange, J. H., Jr.
Leary, A. R.
Leighninger, Diana M.
Malpeli, J. G.
Marandino, G. F.
Mase, J. Z.
Mauer, J. L., IV
Neuendorffer, A. C.
Ogan, K. L.
Partridge, L. D.
Pfister, G. F.
Pitegoff, A. D.
Postol, T. A.
Puls, J. H.
Rible, J. W.
Rosenfeld, E.
Rosenkranz, P. W.
Schoman, K. E., Jr.
Sevick, G. E.
Small, J. G.
Smith, R. R.
Solomon, G. S.
Sorensen, K.
Spann, C. W.
Sullivan, K. J.
Toong, H-M. D.
Walker, J. D.
Wandzelak, M.
Warshaw, A. S.
Weatherly, W. P.
Wheeler, G. M.
Wolfe, P. D.
Wringley, J. D., Jr.

Student Employees

Ackerman, W. B.
Bennett, D. W.
Bosel, J. P.
Burgess, L. R.
Chan, M-L.
Drobak, J. N.
Engle, R. H.
Forbes, P. A.
Gibb, B. C.
Granek, H.
Howell, R. P.
Johnson, L. G.
Kinnaman, W. A.
Koehler, R. F.
Laurino, J. A., Jr.
Law, Sara
Masiello, R. D.
Michel, A.
Ray, J. N.
Rich, L. J.
Ruderman, G. S.
Scarlett, D. O.
Solarz, R. W.
Sturges, R. H., Jr.
Waters, J. W.

R. L. E. Administrative Staff

Duffy, D. F.
Hewitt, J. H.
Keyes, R. V., Jr.
Sayers, R. A.
Smith, P. L.
Thomas, Helen L.

Administrative Assistant

Bella, C. J.

Office Clerks

Barron, Gladys G.
Butler, D. F.
Chase, Arbella P.
Engler, R. R.
Gregor, C. A.
Ippolito, Dorothy A.
Mulligan, Maureen F.
O'Toole, J. P.
Peck, J. S.
Ruggere, P. A.
Scalleri, Mary B.
Simon, E.
Toebes, Rita K.

Typists

Dilworth, Doris L.
Foley, Ruth E.
Murphy, Mary R.
Myers, Alberta L.
Smith, Mary L.
Stagliola, Eleanor E.
Young, Nancy E.

PERSONNEL

Technical Typists

Anderson, Linda
Jones, Elizabeth
Kliphan, Evelyn C.
Mullin, Priscilla A.
Schröder, Gertraude L.

Secretaries

Baumann, Irene H. E.
Bedrosian, Isabel
Carbone, Angelina
Cataldo, Donna L.
Cohen, Phyllis J.
Conwicke, Vera
Cook, Elaine J.
Cosgrove, Mary J.
DiPietro, Toni R.
Dunn, Eleanor I.
Fernandez, Teresita M.
Gatton, Tonya K.
Hamilton, Martha C.
Hurvitz, Rose S.
Ingersoll, Nancy L. B.
Johnson, Barbara A.
Kaloyanides, Venetia
Kirk, Marshall A.
Loeb, Charlotte G.
McCarthy, Barbara L.
McEntee, Doris C.
Nunes, Meredith
Owens, Mary E.
Paige, Okella M.
Reid, Gloria C.
Ricker, Barbara J.
Skewes, Anne
Smith, Clare F.
Tomlinson, Ann B.
Tortorici, Camille A.
Van Wezel, Ruth
Wanner, Patricia A.

Engineering Assistants

Berg, A. E.
McKenzie, J. A.
Papa, D. C.
Thompson, J. B.

Technical Assistants

Barger, Z. O.
Byers, F. H.
Grande, Esther D.
Hall, Kyra M.
Iverson, Alice I.
Major, Diane
Newman, Charlotte M.
Rabin, Sylvia G.
Seymour, P. L.
Swenson, Judith E.
Toop, R. W.
Yaffee, M. A.

Technicians

Aucella, Alice G.
Barrows, F. W.
Beaton, Catherine M.
Butler, R. E., Jr.
Cardia, P. F.
Connolly, J. T.
DiPietro, P. J.
Ferrogamo, A. A.
Fitzgerald, E. W., Jr.
Gage, R. B., Jr.
Gay, H. D.
Goodman, L.
Hill, R. F.
Iovine, M. A.
Kaufman, D. E.
Kelly, M. A.
Lewis, R. R.
McLean, J. J.
Neal, R. W.
North, D. K.
Reid, E.
Schwabe, W. J.
Sears, A. R.
Sholder, J. A.
Speredelozzi, A. J.
Sprague, L. E.
Stevens, J. A.
Summers, C. L.
Tortolano, A. J.
Wentworth, A. G., Jr.

Technicians' Shop

Lorden, G. J., Foreman
Fownes, Marilyn R.
MacDonald, K. R.

Laboratory Assistants

Barrows, Helene G.

PERSONNEL

Drafting Room

Navedonsky, C. P. Foreman
DeCesare, Olive J.
Hillier, Anna M.
Porter, Jean M.
Rollins, I. E.

Photographic Shop

Cook, J. F.
Geraigery, R. J.
Karas, P.

Machine Shop

Keefe, J. B. Foreman
Aalrud, R. W.
Bletzer, P. W.
Brennan, J.
Bunick, F. J.
Cabral, M., Jr.
Carter, C. E.
Harvey, A. O.
Liljeholm, F. H.
Muse, W. J.
Reiman, W.
Ryan, J. F.
Sanromá, J. B.

Tube Laboratory

Rosebury, F.
Leach, G. H., Jr.
MacDonald, A. A.
Thibodeau, D. S.

Glass Shop

Ryan, L. W.
DiGiacomo, R. M.
Doucette, W. F.

Stock Clerks

Haggerty, R. H.
Legier, D. O.
Ridge, P. A.
Sharib, G.

Utility and Maintenance

Doiron, E. J. Foreman
Audette, A. G.
Lucas, W. G.
McAteer, T. F., Jr.
Riley, J. F.
Severino, E.
Sincuk, J., Jr.

PUBLICATIONS AND REPORTS

MEETING PAPERS PRESENTED

IAU/URSI Symposium on Radio Astronomy and Galactic Systems, Noorwijk, The Netherlands

August 24-September 1, 1966

A. E. E. Rogers and A. H. Barrett, Anomalous OH Absorption in the Direction of Cassiopeia A

Symposium "Higher Nervous Activity," IV World Congress of Psychiatry, Madrid, Spain

September 5-9, 1966

W. S. McCulloch, Cybernetic Problems of Learning (invited)

XVth General Assembly of the International Scientific Radio Union, Munich, Germany

September 5-15, 1966

A. H. Barrett, Unique Radio Frequencies from Space

Second International Biophysics Congress, Vienna, Austria

September 7-9, 1966

W. A. Rosenblith, The Philosophy of Educating Biophysicists (invited)

Molecular Spectroscopy Symposium, Ohio State University, Columbus, Ohio

September 6-10, 1966

T. F. McNelly and C. H. Perry, The Infrared and Raman Spectra of $KTaO_3$

J. F. Reintjes, Jr. and C. H. Perry, Low-Frequency Vibrations in Ammonium Chloride and Ammonium Bromide

E. F. Young and C. H. Perry, Infrared Transmission Spectra of Single Crystals of Cubic Perovskite Fluorides

Brookhaven Conference on Atomic Beams and Nuclear Moments, University of California, Berkeley

September 12-14, 1966

K. W. Billman, J. G. King, and S. G. Kukolich, Square-Wave Phase Modulation in Beam Resonance Experiments

S. G. Kukolich, Measurement of Hyperfine Structure in the Ammonia Inversion Spectrum with a Two-Cavity Maser

EUCHEM Far Infrared Conference, Culham Laboratory, Culham, Abingdon, England

September 12-16, 1966

C. H. Perry and T. F. McNelly, Ferroelectric "Soft" Mode in $KTaO_3$ (invited)

University of Grenoble Seminars, Grenoble, France

September 18-21, 1966

F. Bitter, Histoire des Champs Magnétiques Intenses, et de Leurs Contributions à la Physique (invited)

National Electronics Conference, Chicago, Illinois

October 3-8, 1966

J. Andersen and H. B. Lee, Realizability Conditions for the Driving-Point Impedances of RLCT Networks in Which the Reactances Exhibit Semiuniform Loss

T. S. Huang, Digital Picture Coding

American EEG Society Annual Meeting, Denver, Colorado

October 6-9, 1966

J. S. Barlow and Thelma Estrin, Spatial and Temporal Aspects of Rhythmic Afterwaves (Afterdischarge) to Flashing in Man

Thirty-first Convention, Audio Engineering Society, New York

October 10-14, 1966

G. C. Maling, Jr. and U. Ingard, Electrothermal Response of Lead-Zirconate-Titanate

Fourth Canadian Symposium on Electronics, Montreal, Quebec

October 13-14, 1966

D. Kleppner and R. F. C. Vessot, Communications System for Spacecraft Relativity Experiments (invited)

Optical Society of America Meeting, San Francisco, California

October 19-21, 1966

C. H. Perry, Solid State Spectroscopy in the Far Infrared (invited)

Conference on Photographic Interaction between Radiation and Matter, Washington, D.C.

October 26-29, 1966

M. U. Palma, The Fate of Holes Photoliberated within the Volume of Silver Halide Crystals

Council of American Science Writers, Gatlinburg, Tennessee

October 30-November 2, 1966

D. Kleppner, Time and the Ultimate Limit to Precision

NEREM-66, Boston, Massachusetts

November 2-4, 1966

S. J. Mason, Reading Machine Studies for Sensory Aids

Seventy-second Meeting Acoustical Society of America, Los Angeles, California

November 2-5, 1966

W. L. Henke, Dynamic Articulatory Model of Speech Production

U. Ingard and M. Schulz, Acoustic Amplification in a Plasma

M. Schulz and U. Ingard, Lateral Acoustic Instability

1966 Thermionic Conversion Specialist Conference, Houston, Texas

November 2-5, 1966

W. Engelmaier and R. E. Stickney, Thermionic and Adsorption Characteristics of Monocrystalline and Polycrystalline Tungsten Filaments Exposed to Oxygen

D. R. Wilkins and E. P. Gyftopoulos, Transport Theory for Low-Energy Plasmas with Applications to Thermionic Converters

Division of Plasma Physics, American Physical Society, Meeting, Boston, Massachusetts

November 2-5, 1966

R. R. Bartsch, Characteristics of the Beam-Plasma Discharge Afterglow

S. R. J. Brueck and A. Bers, Acoustic Instabilities in a Semiconductor in Parallel Applied Electric and Magnetic Fields

J. F. Clarke and L. M. Lidsky, Nonclassical Diffusion Produced by a Resonant Helical Magnetic Field Perturbation

J. A. Davis, A Sheet Model of the Beam-Plasma Interaction

G. Lampis, Afterglow Measurements of a Laser-Produced Helium Plasma

L. M. Lidsky, J. F. Clarke, and D. J. Rose, Experimental and Numerical Investigations of Velocity Diffusion in a Nonadiabatic Injection System

M. A. Lieberman and A. Bers, Ion Oscillations Excited by Electron Beam-Plasma Interactions

M. A. Lieberman and A. Bers, Quasi-linear Theory of Narrow-Bandwidth Convective Instabilities

W. H. Manheimer and T. H. Dupree, Particle Diffusion and the Nonlinear Landau Damping of Waves

R. Parker and A. Bers, Excitation and Propagation of Ion-Cyclotron Waves in a Bounded Plasma

D. J. Rose and J. C. Woo, Physical Model of a Plasma Column Universal Instability

H. M. Schneider, A Charge Sheet Model for Plasma Slab Oscillations

J. C. Woo and D. J. Rose, Generation of a Quiescent High-Density Arc Plasma

B. L. Wright, Relaxation Rates from the Observed Time Dependence of the Electron Velocity Distribution Function

Plasma Physics Seminar, Aerospace Corporation, El Segundo, California

November 4, 1966

M. Schulz, Acoustic Instabilities in a Plasma (invited)

Physics Department Colloquium, Lowell Technical Institute, Lowell, Massachusetts

November 16, 1966

J. G. King, Searching for Nothing, or Null Experiments I Have Known (invited)

Argonne National Laboratory Symposium on Vacuum Technology, Argonne, Illinois

November 17, 1966

F. Rosebury, Vacuum Equipment - Materials of Construction (invited)

MEETING PAPERS PRESENTED (continued)

Eastern EEG Association Meeting, New York

November 28-30, 1966

J. S. Barlow and R. A. Di Perna, A High-Speed Multichannel Analog System for Reconversion of EEG Inked Traces to Their Electrical Forms

JOURNAL PAPERS ACCEPTED FOR PUBLICATION

(Reprints, if available, may be obtained from the Document Room, 26-327, Research Laboratory of Electronics, Massachusetts Institute of Technology, Cambridge, Massachusetts 02139.)

G. D. Blum and R. Weiss, An Experimental Test of the Freundlich Red-Shift Hypothesis (Phys. Rev.)

D. L. Bobroff and H. A. Haus, Impulse Response of Active Coupled Wave Systems (J. Appl. Phys.)

J. D. Bruce, Review of "Matrices and Linear Transformations" by Charles G. Cullen (Proc. IEEE)

N. I. Durlach, On Application of the EC Model to Interaural JND's (J. Acoust. Soc. Am.)

M. Eden, On a Relation between Labelled Graphs and Permutations (J. Combinatorial Theory)

G. Fiocco, On the Production of Ionization by Micrometeorites (J. Geophys. Res.)

M. Halle and S. J. Keyser, Chaucer and the Study of Prosody (College English)

R. P. V. Kiparsky, A Phonological Rule of Greek (Glotta)

G. H. Matthews, Two-Way Languages (Inform. Contr.)

C. H. Perry and T. F. McNelly, Ferroelectric "Soft" Mode in $KTaO_3$ (Phys. Rev.)

R. R. Pfeiffer, Anteroventral Cochlear Nucleus : Waveforms of Extracellularly Recorded Spike Potentials (Science)

A. E. E. Rogers, J. M. Moran, P. P. Crowther, B. F. Burke, M. L. Meeks, J. A. Ball, and G. M. Hyde, The Position and Angular Extent of OH Emission Associated with the H II Regions W3, W24, W49, and NGC 6334 (Astrophys. J.)

C. E. Shannon, R. G. Gallager, and E. R. Berlekamp, Lower Bounds to Error Probability for Coding on Discrete Memoryless Channels (Inform. Contr.)

C. G. Shull, K. W. Billman, and F. A. Wedgwood, Experimental Limit for the Neutron Charge (Phys. Rev.)

M. H. Schulz III, Debye Shielding and Virtual Plasma Oscillations (Am. J. Phys.)

R. E. Stickney, R. F. Keating, S. Yamamoto, and W. J. Hastings, Angular Distribution of Flow from Orifices and Tubes at High Knudsen Numbers (J. Vac. Sci. Tech.)

M. Takata, W. F. Pickard, J. Y. Lettvin, and J. W. Moore, Ionic Conductance Changes in Lobster Axon Membrane when Lanthanum Is Substituted for Calcium (J. Gen. Physiol.)

JOURNAL PAPERS ACCEPTED FOR PUBLICATION (continued)

P. D. Wall, The Laminar Organization of Dorsal Horn and Effects of Descending Impulses (Abstract) (J. Physiol.)

P. D. Wall, The Mechanisms of General Anesthesia (Anesthesiology)

P. D. Wall and W. H. Sweet, Temporary Abolition of Pain in Man (Science)

D. R. Wilkins and E. P. Gyftopoulos, Theory of Thermionic Converter Extinguished-Mode Operation with Applications to Converter Diagnostics (J. Appl. Phys.)

LETTERS TO THE EDITOR ACCEPTED FOR PUBLICATION

D. B. Geselowitz, Green's Theorem and Potentials in a Volume Conductor (IEEE Trans. (BME))

R. Golub and G. L. Guttrich, Level Shifts Due to the Confinement of an Atom by Conducting Walls (Phys. Letters)

G. L. Guttrich and K. W. Billman, A Search for a Shift in the Transverse Electromagnetic Mass of the Electron (Phys. Letters)

U. Ingard and H. Lewenstein, Flexible-Membrane Fabry-Perot Interferometer (Am. J. Phys.)

G. C. Maling, Jr. and U. Ingard, Electric Response of Lead Zirconate Titanate Ceramics to Temperature Fluctuations (Rev. Sci. Instr.)

M. Schulz, Possibility of Ion-Wave Amplification in a Plasma (Phys. Fluids)

TECHNICAL REPORTS PUBLISHED

(These and previously published technical reports, if available, may be obtained from the Document Room, 26-327, Research Laboratory of Electronics, Massachusetts Institute of Technology, Cambridge, Massachusetts 02139.)

453 Herman J. Pauwels, Noise Sources Describing Quantum Effects in the Laser Oscillator

454 J. Charles Ingraham and Sanborn C. Brown, Plasma Diagnostics

455 Robert D. Hall and Roger Greenwood Mark, Acoustically Evoked Potentials in the Rat during Conditioning

SPECIAL PUBLICATIONS

J. Andersen and H. B. Lee, Realizability Conditions for the Driving-Point Impedances of RLCT Networks in Which the Reactances Exhibit Semiuniform Loss (Proc. National Electronics Conference, Vol. 22)

A. B. Baggeroer, Maximum a posteriori Interval Estimation (WESCON/66 Technical Session 7, Paper 7/3)

T. S. Huang, Digital Picture Coding (Proc. National Electronics Conference, Vol. 22)

R. M. Logan, J. C. Keck, and R. E. Stickney, Simple Classical Model for the Scattering of Gas Atoms from a Solid Surface. II. Additional Analyses and Comparisons (Rarefied Gas Dynamics Fifth Symposium, Academic Press, New York, 1967, pp. 49-66)

D. L. Snyder, A Theory of Continuous Nonlinear Recursive Filtering with Application to Communication and Radar Problems (WESCON/66 Technical Session 7, Paper 7/2)

M. W. P. Strandberg, Spectroscopy at Microwave Frequencies (NASA Special Publication, U.S. Government Printing Office, Washington, D.C.)

H. L. Van Trees, Detection and Continuous Estimation : The Fundamental Role of the Optimum Realizable Linear Filter (WESCON/66 Technical Session 7, Paper 7/1)

Introduction

This report, the eighty-fourth in a series of quarterly progress reports issued by the Research Laboratory of Electronics, contains a review of the research activities of the Laboratory for the three-month period ending November 30, 1966. Since this is a report on work in progress, some of the results may not be final.

Following our custom of the past several years, in this issue of January 15, 1967 we preface the report of each research group with a statement of the objectives of the group. These summaries of our aims are presented in an effort to give perspective to the detailed reports of this and ensuing quarters.

GENERAL PHYSICS

I. MOLECULAR BEAMS*

Academic and Research Staff

N 07-cc642

Prof. J. R. Zacharias
Prof. K. W. Billman
Prof. J. G. King
Prof. C. L. Searle
Dr. K. Fokkens ET AL
Dr. S. G. Kukolich
F. J. O'Brien
M. A. Yaffee

Graduate Students

R. Golub
G. L. Guttrich
D. E. Oates
R. S. Stephenson

RESEARCH OBJECTIVES

Our objectives have changed in the last year, partly as a result of the success of the first low-temperature helium beam experiment.

1. RF Spectra, Atomic Clocks, and Null Experiments

It seems unlikely that we shall continue the general study of radio-frequency spectra of atoms and molecules. The development of cesium atomic clocks has proceeded slowly, because of the press of other work, but the techniques already developed, such as high-intensity alkali beam sources and square-wave phase modulation, have been of great use in other experiments. These include the search for permanent electric dipole moment in atoms, for frequency shifts arising from the confinement of atoms between conducting plates, and for small charges carried by atoms.

2. Research with Low-Temperature Atomic Beams

It is now possible to perform many experiments with beams of cold helium and, with some further development, of cold hydrogen. These experiments can be classified as follows.

(i) Studying the scattering of cold He beams by gas, by other beams and from surfaces, both liquid and solid.

(ii) Observing the diffraction of atoms from gratings and apertures.

(iii) Investigating various properties of liquid helium as exhibited by the emitted atoms.

(iv) Using beams of magnetic atoms as microscopic probes of superconductors.

J. R. Zacharias, J. G. King, C. L. Searle

3. Molecular Microscope – Proposed Development

Consider a surface in high vacuum which is emitting neutral molecules. If the molecules moving in the appropriate direction were allowed to pass through a small aperture (pinhole) to strike an array of field-ionization detectors,[1] the resulting ions could be accelerated to a fluorescent screen where a visible image representing the spatial distribution of neutral molecule emission from the surface would be formed.

Improvements in the image would require the development of a suitable atom-light

*This work was supported by the Joint Services Electronics Programs (U.S. Army, U.S. Navy, and U.S. Air Force) under Contract DA 36-039-AMC-03200(E), and in part by the Sloan Fund for Basic Research (M.I.T. Grant 99).

transducer with good resolution and high quantum efficiency and stability. Although the density of field-ionization detectors could be increased, perhaps, by using whiskers or Si fibers instead of needles, a better system might be to adsorb the atoms on a cold surface, where sideways motion is slight, and to read out by simultaneously desorbing and ionizing with a scanning electron beam. The desorbed ions could then strike a fluorescent screen. Methods by which transmitted electrons or generating photons are used directly might also be possible.

Lenses may be used instead of a pinhole to increase the aperture of the system if the molecules have electric or magnetic moments. This is particularly easy when cold beams are used. The effects of the velocity dependence of the focal length can be avoided by chopping the beam and "reading out" the detector at appropriate times. One then also learns about the velocity dependence of the scattering.

Besides observing molecules from desorbing or outgassing surfaces, one could bombard the surface with charged particles and examine the ejected neutrals or expose the surface to beams of neutral molecules and examine the scattered beams. Various properties of the object could be studied by varying both its temperature and that of the incident beam and by using incident molecules with and without electric and magnetic moments. State-selected beams could also be used. It seems likely that one could view a helium surface or a superconductor by emitted or scattered molecules. If the neutral molecule, ion, and light systems can each be made to have a magnification of, say, 100X while preserving adequate resolution, one might be able to observe large molecules; but this is a distant possibility.

Although there are still many unknown problems, and no very elaborate study has yet been undertaken, it seems possible to develop a useful "molecular microscope." Such a device would be a complement to photon, electron, and ion microscopes and might be useful in metallurigical, chemical, and especially biological research.

J. G. King

References

1. W. D. Johnston, Jr. and J. G. King, Rev. Sci. Instr. 37, 475 (1966).

A. SQUARE-WAVE PHASE MODULATION IN MOLECULAR BEAM RESONANCE EXPERIMENTS

The method of square-wave phase modulation was developed by Bates, Badessa, and Searle[1] for use on cesium beam frequency standards. This system offers the advantage over other modulation schemes that very high fidelity modulation, that is, free from distortions and asymmetries, may be easily achieved by modulating the resonant frequency of a tuned rf amplifier. This is especially important in high-precision frequency comparison experiments. This system has the added advantage of providing a convenient method of measuring cavity phase difference, or velocity-dependent shifts arising from $\vec{v} \times \vec{\mathscr{E}}$ in separated oscillating-field resonance experiments.

1. Theory of Sqaure-Wave Phase Modulation

A simplified theory of square-wave phase modulation will be presented elsewhere.[2] In the following discussion there will be no restrictions on frequency or cavity phase deviations, and we shall keep all terms that may have a significant

effect on the shape of the resonance.

The transition probability for a separated oscillating-field resonance apparatus[3] is

$$P = \sin^2\left(\frac{2bl}{v}\right)\cos^2\left[\frac{(\omega_o-\omega)L}{2v}-\frac{\phi}{2}\right],$$

where ω_o is the atomic resonance frequency, L is the cavity separation, v is the velocity of the atoms, l is the RF interaction length, b is the transition rate in the cavities, and ϕ is the cavity phase difference. In an atomic beam apparatus the beam intensity at the detector is proportional to the intergral of P over the velocity distribution.

$$i = i_o + A\int_0^\infty n(v)\sin^2\left(\frac{2bl}{v}\right)\cos\left[\left(\frac{\omega_o-\omega}{v}\right)L-\phi\right]dv.$$

The square-wave modulation steps the phase of the stimulating signal back and forth from approximately +90° to -90°, with a period of approximately four times the average transit time τ_a, the time required for a molecule to travel from the first cavity to the second. The effect of this modulation is to produce an apparent phase difference between the microwave cavities. Immediately after the phase of the stimulating signal is changed, all of the atoms between the cavities will encounter a phase in the second cavity which is different from that in the first cavity. This produces an apparent cavity phase difference, ϕ_1, which persists for the transit time, τ. The cavity phase difference ϕ is composed of two parts, $\phi = \phi_o + \phi_1$, where ϕ_o is a constant (varies at a rate that is slow compared with the modulation) cavity phase difference, and ϕ_1 is the transient, apparent cavity phase difference produced by modulating the phase of the stimulating signal.

$$i(t) = i_o + A\int_0^\infty n(v)\left\{\cos\left[(\omega_o-\omega)\frac{L}{v}-\phi_o\right]\cos\phi_1(t')\right.$$

$$\left.-\sin\left[(\omega_o-\omega)\frac{L}{v}-\phi_o\right]\sin\phi_1(t')\right\}\sin^2\left(\frac{2bl}{v}\right)dv,$$

where $t' = t - \frac{L_1}{v}$, with L_1 the distance from the second cavity to the detector.

The modulation produces steps of $\pm\phi_m$ in the value of ϕ_1, so we may write

$$\cos\phi_1(t) = M(t)\cos\phi_m$$

$$\sin\phi_1(t) = N(t)\sin\phi_m,$$

where M and N may have the values 0, ±1, and the amount of modulation is expressed in ϕ_m. The time dependence of the cavity phase difference ϕ_1, M and N is shown in Fig. I-1. The modulation period is 2T. In an actual resonance experiment the strength

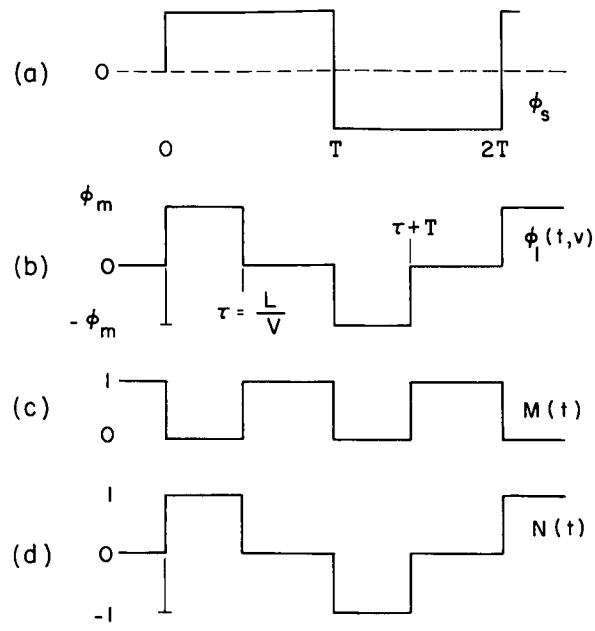

Fig. I-1. Apparent cavity phase difference ϕ_1, M and N as a function of time.

of the rf field is adjusted to give the maximum resonance signal, and this occurs for $2bl/v_a = \tau/2$, where v_a is the average velocity in the beam. Now the expression for the beam intensity is

$$i(t) = i_o + A \cos \phi_m \int_0^\infty n(v) \sin^2\left(\frac{\pi v_a}{2v}\right) \cos\left[(\omega_o-\omega)\frac{L}{v} - \phi_o\right] M\left(t-\frac{L_1}{v}\right) dv$$

$$- A \sin \phi_m \int_0^\infty n(v) \sin^2\left(\frac{\pi v_a}{2v}\right) \sin\left[(\omega_o-\omega)\frac{L}{v} - \phi_o\right] N\left(t-\frac{L_1}{v}\right) dv. \qquad (1)$$

We note that the second term will produce no fundamental component at the modulation frequency $\frac{1}{2T}$, since M has a period, T. The modulation amplitude ϕ_m only comes in through the factor sin ϕ_m, so this will have no effect on the shape of the resonance pattern, and the optimum value is $\phi_m = 90°$.

The effect of a synchronous detector is to perform a Fourier analysis of i(t). Since N(t+T) = -N(t), this is given by

$$\Phi = \frac{\pi}{T}\int_0^T \sin\left(\frac{\pi t}{T} - \phi_1\right) i(t)\, dt,$$

where ϕ_a is the reference phase for the synchronous detector. Since $N\left(t-\frac{L_1}{v}\right)$ is the only nonvanishing factor that is time-dependent, we obtain

$$\Phi(\omega) = A \sin \phi_m \int_0^\infty n(v) \sin\left[(\omega_o - \omega)\frac{L}{v} - \phi_o\right]$$

$$\times \left[\cos\left(\frac{\pi(L_1+L)}{Tv} - \phi_a\right) - \cos\left(\frac{\pi L_1}{Tv} - \phi_a\right)\right] dv. \qquad (2)$$

The optimum modulation frequency, $\frac{1}{2T}$, is approximately $\frac{1}{4\tau_a}$, where L/τ_a is the average velocity in the beam. The optimum value of ϕ_a depends on the length of the region between the second cavity and the detector. The optimum value of ϕ_a for the in-phase synchronous detector is typically 0.2 radian, or less, and is determined experimentally as the phase that gives the maximum amplitude of the resonance signal $\Phi(\omega)$. The quadrature synchronous detector is then operated at a phase of $\phi_a + 90°$ with respect to the modulation.

2. Experimental Results

A cesium beam magnetic resonance apparatus with 125-cm cavity separation was used to test the square-wave phase-modulation system and to obtain values for parameters in the theoretical expression for the resonance function. The cesium hyperfine transition $(4, 0 - 3, 0)$ was observed in this apparatus with a linewidth of 140 Hz. The modulation frequency was $\frac{1}{2T}$ = 53 Hz. The distance from the second cavity to the detector was L_1 = 68 cm, and the optimum value of ϕ_a for the in-phase synchronous detector was −0.21 radian.

The experimental resonance pattern was obtained by sweeping the stimulating signal frequency slowly (~2Hz/sec) through the resonance and recording the output of the synchronous detectors on a strip chart recorder. Theoretical resonance patterns calculated on a computer by putting a velocity distribution n(v) with adjustable parameters into (2),

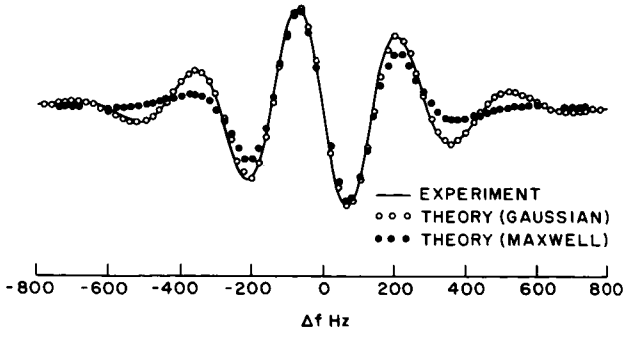

Fig. I-2.
Experimental and theoretical resonance patterns, I(ω), as a function of frequency.

the expression for $\Phi(\omega)$, and adjusting the parameters for a good fit to the experimental pattern. The velocity distributions employed were a modified Maxwellian distribution

$\left(n(v) = n_o v^3 e^{-(v/a)^2}\right)$ and a Gaussian distribution $\left(n(v) = n_o e^{-\beta(v-v_o)^2}\right)$. The experimental and theoretical resonance patterns, $I(\omega)$, are shown in Fig. I-2 $[I(\omega) \equiv \Phi(\omega, \phi_a = -0.21)]$. The Maxwellian distribution contains only one adjustable parameter and when the average velocity is fitted to the data, the resulting Maxwellian velocity distribution is broader than the experimental velocity distribution. This effect is apparent in Fig. I-2. since the width of the envelope of the resonance function is inversely related to the width of the velocity distribution. The Gaussian distribution contains two adjustable parameters and, with the proper values of the parameters v_o and β, provides an accurate fit to the observed resonance pattern. The best fit for the Maxwellian distribution was obtained with $a = 297$ m/sec. The best fit for the Gaussian distribution was obtained with $v_o = 368$ m/sec, $\beta = 6.56 \times 10^{-5}$ (sec/m)^2. We believe that the observed velocity distribution is narrower than the Maxwellian distribution because the narrow gap width of the deflecting magnets removes atoms from the beam if their deflection is much greater or much less than the average deflection.

We have determined the velocity distribution by fitting the resonance pattern, and we shall now use this distribution to determine the behavior of the quadrature signal. The Gaussian distribution was used to calculate the quadrature output signal $Q(\omega)[Q(\omega) \equiv \Phi(\omega, \phi_a = 1.78)]$. The experimental and theoretical values of $Q(\omega)$ are shown in Fig. I-3.

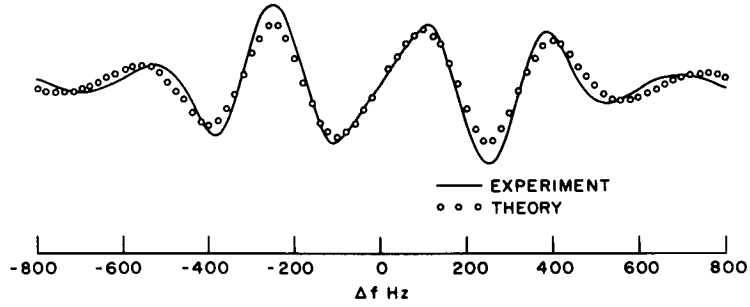

Fig. I-3. Experimental and theoretical values of the quadrature output signal, $Q(\omega)$, as a function of frequency.

In the next experiment the output of the in-phase synchronous detector $I(\omega)$ was used in a servo loop to control the frequency of the stimulating signal. This system maintained the stimulating frequency on the center of the resonance pattern (at $I(\omega) = 0$). Under there conditions, the cavity phase difference, ϕ_o, was varied and the output from the quadrature synchronous detector was measured and calculated as a function of ϕ_o. The results of these measurements and calculations are shown in Fig. I-4. We see that the quadrature signal is linearly related to the cavity phase difference ϕ_o over the range $\phi_o = -60°$ to $+60°$, and that the sensitivity is greater for a wider velocity distribution.

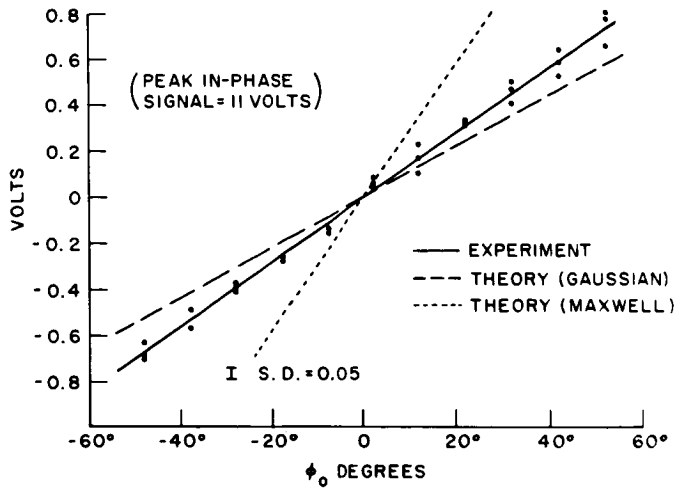

Fig. I-4. Quadrature output signal as a function of cavity phase difference, ϕ_o, with $I(\omega) = 0$.

Therefore, in a two-cavity frequency standard the quadrature signal can be used to control the cavity phase shift.

In experiments in which a large electric field is applied to the region between the cavities, a velocity-dependent frequency shift is produced by the $\vec{v} \times \vec{\mathscr{E}}$ contribution to the magnetic field. In order to show that this system has the same behavior for a velocity-dependent frequency shift such as this $\vec{v} \times \vec{\mathscr{E}}$ term, we note that the transition probability near resonance is approximately

$$P = \frac{1}{2} \cos \left[\left(\omega_o^* - \omega \right) \frac{L}{v} - \phi_o \right]$$

and if

$$\omega_o^* = \omega_o + 2\pi \left(\frac{-\mu_J/h}{8J} \right) \frac{v}{c} \vec{\mathscr{E}}_o \sin \gamma,$$

this is equivalent to using ω_o, ϕ_o^*, where

$$\phi_o^* = \phi_o - 2\pi \left(\frac{-\mu_J/h}{8J} \right) \frac{L}{c} \vec{\mathscr{E}}_o \sin \gamma,$$

so we see that the $\vec{v} \times \vec{\mathscr{E}}$ frequency shift has the same effect on the transition probability as a cavity phase difference of $\left(\phi_o^* - \phi_o \right)$. We note that the $\vec{v} \times \vec{\mathscr{E}}$ shift is only present when a large electric field is applied to the region between the cavities, so we may measure ϕ_o independently by turning off the electric field.

Finally, a more direct experimental check on the velocity spectrum can be made, because, on the center of the resonance, the time derivative of the beam current is

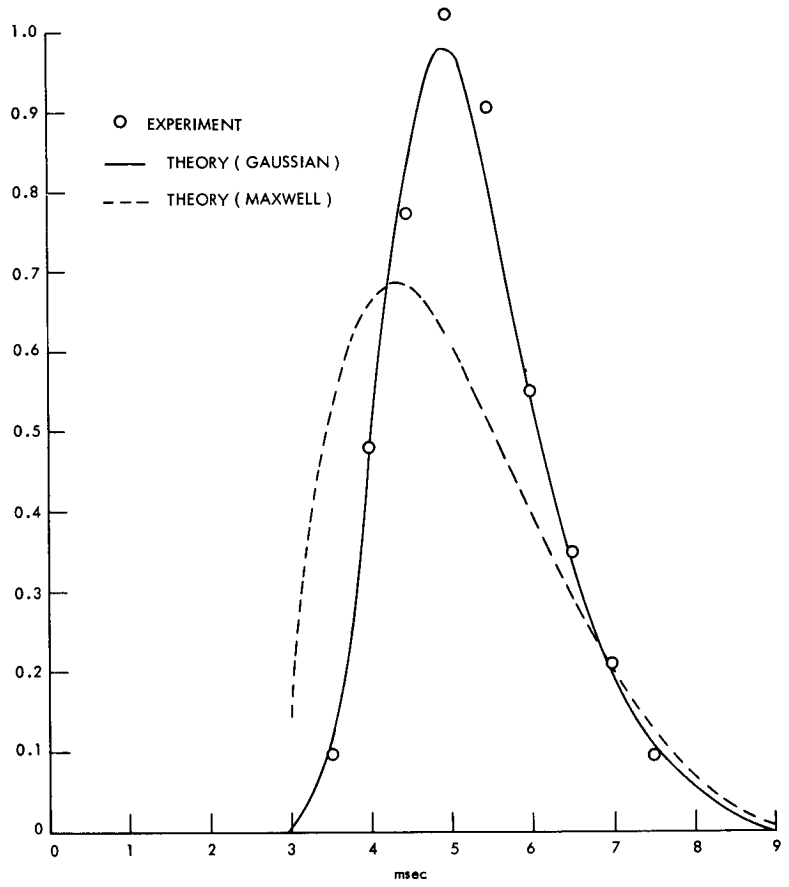

Fig. I-5. Modified distribution of transit times.

related to the velocity distribution in a simple way. For the conditions $\omega_o = \omega$, $\phi = 0$ and $0 < t < T$ we see from Eq. 1 that

$$\frac{di(t)}{dt} = A \cos \phi_m \, n\left(\frac{L+L_1}{t}\right) \sin^2\left(\frac{\pi v_a t}{2(L+L_1)}\right),$$

where n(v) is the velocity distribution, and t is the time measured from the last modulation step. This is just the distribution of transit times from the first cavity to the detector multiplied by the average of a $\sin^2$ factor. The $\sin^2$ term has the effect of making the distribution of transit times appear narrower. The second maximum occurs at times so great that $n\left(\frac{L+L_1}{t}\right)$ is nearly zero. The experimental and theoretical results for this function are shown in Fig. I-5. The experimental data were obtained by averaging over many cycles of the modulation with a multichannel analyzer. The channel number was proportional to time t, and the number of channel counts was proportional to the beam current i(t).

S. G. Kukolich, K. W. Billman

References

1. R. S. Badessa, V. J. Bates and C. L. Searle, IEEE Trans., Vol. IM-13, p. 175, 1964.
2. S. G. Kukolich and K. W. Billman (to appear in J. Appl. Phys.).
3. N. F. Ramsey, Molecular Beams (Oxford University Press, London, 1956), Chap. 5.
4. S. G. Kukolich, Proc. IEEE 52, 211 (1964).

B. SEARCH FOR A SHIFT IN THE TRANSVERSE ELECTROMAGNETIC MASS OF THE ELECTRON

Power has suggested[1] that a shift in the frequency of an atomic clock can be produced by confining the atoms passing through the transition region between conducting plates. The mechanism of this shift can be described as follows: Part of the experimental mass of an electron is due to the presence of a cloud of virtual photons surrounding the "bare" electron. If one should place the electron between conducting walls, virtual photons of a wavelength greater than L, the wall separation, could no longer exist. Hence, the confinement produces a mass shift. A cesium clock utilizes a hyperfine transition involving the reorientation of a single 6s electron outside a closed shell. The frequency of this transition is proportional to the square of the mass of this electron. Hence one might expect $\Delta\nu/\nu = 2\Delta m/m$. Power's calculation gives an estimate of

$$\frac{\Delta\nu}{\nu} \approx 4\alpha\frac{\lambda_c}{L} = \frac{7.1 \times 10^{-11}\ \text{mm}}{L},$$

where α is the fine-structure constant, λ_c is the Compton wavelength of the electron, and L is the separation between the conducting plates.

A search for such a shift was made by using a Cs atomic clock of the usual separated cavity type[2] modified to include movable plates in the "C" region between the RF cavities. Provision for external adjustment of the plate gap (L = 0.4 mm to L = $L_o \approx 25$ mm) necessitated the removal of the usual magnetic shielding of this region which led to some drift uncommon to a high-stability clock; however, as will be explained later, this was easily monitored. A second Cs clock was used as a frequency standard, thereby allowing for simple comparisons to be made to determine any changes in the "experimental clock" frequency as its plates were set to various gaps.

The experimental clock C region between cavities was 126 cm. The linewidth of the resonance at the ($F = 4$, $m_F = 0$) $\longrightarrow$ ($F = 3$, $m_F = 0$) hyperfine transition frequency of 9192 MHz was 140 Hz. The movable, conducting plates, 2.54 cm high and 71 cm long, were made of gold-plated aluminum. Gap adjustment was effected by means of manipulators, one of which was connected to each end of each plate. These allowed for a

simple alignment of the plate axis along the beam axis by observing a sudden decrease in "flop" signal as the gap was narrowed. To obviate direct contact of the beam with the plates, four beam stops were used to limit the beamwidth. Subsequently, the plate gap was never allowed to become smaller than this width, which was 0.4 mm. It should be noted that when the beam was allowed to impinge on the plates, unreproducible frequency shifts were observed which, although interesting, could not be profitably investigated with the present apparatus.

An excellent running check on the sensitivity of the apparatus was obtained by placing a potential difference across the normally grounded plate and observing the Stark shift. This also allowed a simple measurement of the gap size.

Measurements were performed under two different magnetic field configurations in the C region. In Case 1, the magnetic field has a major component vertical, that is, parallel to the conducting plates, of approximately 0.5 Gauss. In Case 2, the major component was perpendicular to the plates and of approximately 0.1-Gauss magnitude. On this basis, it is easy to see that the Case 2 data are expected to be more reliable than those of Case 1, since for the $(4,0) \rightarrow (3,0)$ hyperfine transition $\delta f = 427\ B^2 \frac{\text{Hz}}{\text{Gauss}^2}$, where δf is the second-order magnetic field frequency for the shift B. Thus if the field varies by a small amount ΔB, a shift $\Delta(\delta f) = 854\ B \Delta B \frac{\text{Hz}}{\text{Gauss}^2}$ results. In the Case 1 experiment a 2-milligauss field variation produces a shift of $\Delta\nu = 0.854$ Hz, or $\frac{\Delta\nu}{\nu} \approx 9 \times 10^{-11}$, which was about the largest excursion seen during the experiment. In the Case 2 experiment, however, the same field variation would produce a fivefold smaller shift. One would then expect smaller fluctuations, as was found, and less systematic error with this method of operation.

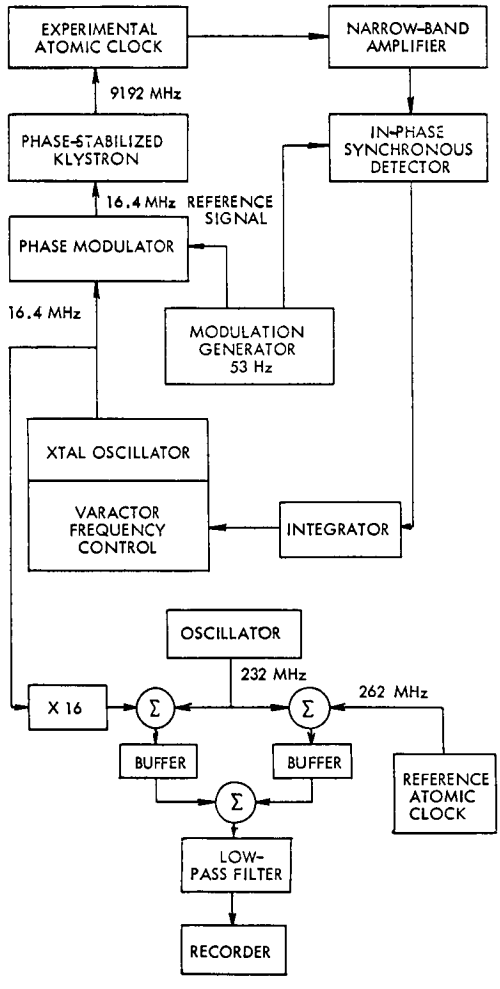

Fig. I-6. Schematic of the electronics.

Data were gathered with the plates alternately wide ($L = L_o = 25$ mm) and narrow. This allowed the effects of drifts to be eliminated to first order. This

correction was generally not necessary for Case 2 data.

Figure I-6 illustrates schematically the electronic apparatus used for the measurement. The reference clock, which utilized a National NC-2001 beam tube, has a measured stability of 3×10^{-12} for a 10^3-sec averaging time. Heterodyning the 262-MHz signals obtained from each clock with a local oscillator allowed a simple display of the beat. Frequency-shift measurements were then made by examination of the beat frequency as the plate gap in the experimental clock was varied.

The experimental results are displayed in Fig. I-7. Each point represents approximately 500 seconds of data with the plates at L_o, and 500 seconds at L. The dashed

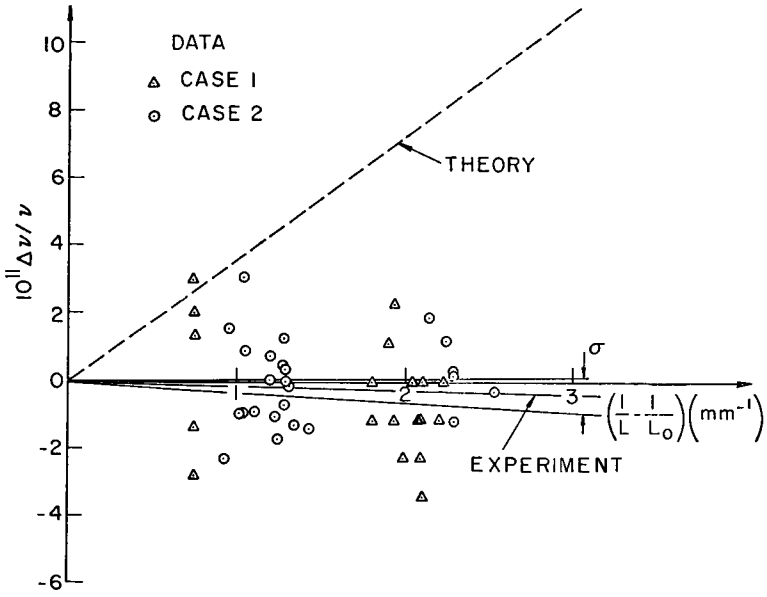

Fig. I-7. Experimental data.

line indicates a frequency shift that would be expected if $\Delta\nu/\nu = (0.56)\,4a\frac{\lambda_c}{L}$, where the numerical factor of 0.56 arises from the fact that the plates only "filled" the C region to this extent. The slope of this line is 4×10^{-11} mm. A least-square fit of the Case 1 data gives a line of slope $\langle a\rangle_1 = (-2.5\pm2.5)\times10^{-12}$, 19 measurements, whereas the slope of the Case 2 data gives $\langle a\rangle_2 = (-0.14\pm1.73)\times10^{-12}$, 25 measurements. Since there is no obvious reason to believe that the field direction affects the predicted hyperfine splitting, these measurements may be combined by using standard weighting with the inverse square of the respective standard deviations, to give $\langle a\rangle_{1+2} = (-0.9\pm1.4)\times10^{-12}$, 44 measurements.

G. L. Guttrich, K. W. Billman

References

1. E. A. Power, Proc. Roy. Soc. (London) A292, 424 (1966).
2. N. F. Ramsey, Molecular Beams (London: Oxford University Press, 1956).

II. MOLECULAR COLLISIONS*

Academic and Research Staff

Prof. J. L. Kinsey
Dr. J. S. Kittelberger

Graduate Students

R. P. English
C. H. Fisher
D. O. Ham
M. H. Klumpp
J. R. Lawter

RESEARCH OBJECTIVES

Our interest is in molecular collisions at thermal energies. These phenomena are studied mainly through crossed molecular beam scattering experiments. Two kinds of collision processes are of interest to this group: (i) collisions which can lead to chemical reactions; (ii) elastic and inelastic nonreactive collisions.

In the chemical studies our aim is to determine some of the finer details of reactive collisions, such as the anisotropy of product velocities and the distribution of available amounts of energy, momentum, and angular momentum among the various accessible modes. The nonreactive studies are mainly concentrated on processes that have some relevance to chemical processes or energy-transfer processes.

This work is supported in part by National Science Foundation Grant GP-5099, which is not administered by the Research Laboratory of Electronics.

J. L. Kinsey

*This work is supported in part by the Joint Services Electronics Programs (U.S. Army, U.S. Navy, and U.S. Air Force) under Contract DA 36-039-AMC-03200(E).

III. MICROWAVE SPECTROSCOPY*

Academic and Research Staff

Prof. M. W. P. Strandberg
Prof. R. L. Kyhl
Dr. T. E. McEnally, Jr.
Dr. M. U. Palma
Dr. Maria B. Palma-Vittorelli
J. G. Ingersoll
J. D. Kierstead
ET AL

Graduate Students

J. U. Free, Jr.
R. M. Langdon, Jr.
L. R. Fox
M. K. Maul
S. R. Reznek
B. N. Yung

RESEARCH OBJECTIVES

This group has a broad general interest in the study of metals and dielectric crystals by means of UHF and microwave frequency experiments with the use of electromagnetic and acoustic radiation. During the past year, the superconducting bolometric detector, developed for use with heat pulses (incoherent phonons), has been used to detect coherent phonons in a crystal rod. These bolometers can be made to be a linear detector of the acoustic power incident on them and, hence, are most suitable for studying the decay of the total coherent acoustic energy in the crystal without having to worry about the phase of the acoustic energy at the quartz surface, as is the case when using coherent detectors. Our studies of superconducting bolometers have indicated how they must be prepared for linear operation, and responsivity and noise measurements have been made by using them as microwave electromagnetic wave detectors. This work will continue.

Work has begun on measurements of acoustic absorption in metals to develop an understanding of the attenuation and boundary-layer thermal resistance at a metal-quartz interface. We have approximated with analytic functions the acoustic velocity surfaces appropriate to NaCl, quartz, and sapphire in the low-frequency limit. The representations will facilitate our understanding of heat-pulse propagation in these crystals, since they make analytic manipulation of the acoustic-wave properties relatively easy. This work will probably be finished in the coming year.

The research on the Fermi surface of gallium has been completed, and work has begun on the copper Fermi surface.

Other work which has been started and will continue is directed toward an analytical understanding of the electromagnetic properties of metals at low temperatures and in magnetic fields. Electron paramagnetic resonance studies of the cross-relaxation process in ruby have been finished and the results have been submitted for publication. A study of NMR signals in static electric fields has been completed. Apparatus designed to detect atomic hydrogen and hydrated electrons in aqueous samples has been completed. Thus far, the results have been negative. It is anticipated that this work will be finished early in the coming year.

Because of the interest of the Radio Astronomy Group in the CH free radical, we have developed very promising instrumentation for detection of CH in an EPR experiment in our laboratory, but these efforts are still inconclusive, and will probably continue for a short time also.

Work with the Department of Chemical Engineering, M.I.T., has been mainly directed at the calibration of a hydrogen atom detector, using the EPR apparatus as an instrument to measure quantitatively atomic hydrogen concentration. Research of a

*This work was supported by the Joint Services Electronics Programs (U.S. Army, U.S. Navy, and U.S. Air Force) under Contract DA 36-039-AMC-03200(E).

different sort, the measurements of chemical reaction-rate constants, is being prepared, also with this group, and will be carried out during the next year.

M. W. P. Strandberg, R. L. Kyhl

A. WORK COMPLETED

1. ELECTRIC FIELD EFFECTS IN THE NUCLEAR MAGNETIC RESONANCE OF FLUIDS

This research has been completed by Terence E. McEnally, Jr., and submitted as a thesis to the Department of Physics, M.I.T., August 1966, in partial fulfillment of the requirements for the degree of Doctor of Philosophy. A summary of the thesis follows.

When a molecule tumbles randomly with an orientational correlation time, τ, much less than the inverse of the linewidth, $\Delta\omega$, predicted for an ensemble of isolated, randomly oriented, nontumbling molecules, the NMR absorption lines become motionally narrowed, and the spectrum exhibits fine structure, because of interactions of the nuclei among themselves. Only the effects of the isotropic (zero-rank) parts of chemical shift and indirect spin-spin interaction tensors is usually observable, as their ranks 1 and 2 parts average to zero isotropically, as do the magnetic dipolar and electric quadrupolar tensors, which are both of rank 2. If the nonspherical molecule tumbles in a potential well of average nonspherical symmetry, then an orientational bias to the motion may ensue, without spoiling its motional narrowing properties. Then the 1^{st} and 2^{nd} rank parts of the nuclear interaction tensors may give an observable effect. Under the assumption of molecules at room temperature having nonzero electric dipole and/or quadrupole moments in a potential described by its first and second derivatives, the calculation of the orientational average of $D^{(\ell)}_{m'm}(\alpha\beta\gamma)$ is carried out by use of the quantum-mechanical density matrix, and the result is found to agree well with the classical result. As $D^{(\ell)}_{m'm}$ describes the transformation of a spherical tensor $T^{(\ell)}$ from the molecular framework to the space-fixed framework, orientational averaging of the tensor can also be effected. Orientation-averaged spin Hamiltonians are developed by using this formalism, and are found to consist, in general, of a sum of terms, in each of which appears a scalar product of the molecule-fixed tensors $T^{(\ell)}$ and the molecule-fixed electric moment tensors, multiplied by the scalar product of space-fixed electric field tensors with space-fixed nuclear operator tensors. The tensors $T^{(\ell)}$ considered are the chemical shift and indirect spin-spin tensors, each with $\ell = 0, 1, 2$, and the magnetic dipolar interaction and intramolecular electric field gradient tensors, each with $\ell = 2$. Diagonalization of the orientation-averaged spin Hamiltonian is described for a general two-spin system in which the Zeeman energy is large and small, respectively, as compared with the electric quadrupole energy. Matrix elements of the nuclear

operators are given for the coupled and uncoupled scheme of two nuclei. The spherical tensor formalism is used throughout.

M. W. P. Strandberg

B. EXPANSION OF VELOCITY SURFACES IN SPHERICAL HARMONICS

The velocity of sound in an elastic medium is given by the roots of a 3×3 secular equation

$$D\left[\Gamma_{ij}(\theta, \phi) - \lambda \delta_{ij}\right] = 0.$$

A method has been developed for expressing the branches of this secular equation in an analytic approximation. The method consists of a least-squares fit of a finite sum of basis functions of the proper symmetry.

$$\lambda_a(\theta, \phi) = \sum_{\ell, m} W_\ell^m(\theta, \phi)\, C_{\ell, m}^a,$$

where $a = 1, 2, 3$ and denotes the branch.

The secular equation has been solved for all points on a grid covering a fundamental symmetry region. The three values of λ at each of these points have been used to determine the value of the C's. The "longitudinal" branch has the greatest λ at all points and is easily separated from the two transverse branches; however, the two "transverse" branches are not easily separable. In certain regions the two curves develop sharp corners and come quite close to one another. Two types of fitting were tried to account for this type of behavior. In the first, we attempted to fit the sharp corners with a small number of terms. In the second, we ignored the sharp corners and assumed that the curves continued smoothly, so that one part of one curve joins onto that of the other. This results in an intersection of the two surfaces which in general does not really exist.

The first approximation is referred to as nonintersecting, and the second as intersecting. Neither method is accurate close to the points of singularity, but the volume over which the error exists should be small.

The velocity of sound as a function of direction in a crystal will have the same symmetry as the crystal. Since our interest is in quartz and sapphire, it was necessary to choose linear combinations that would be invariant under D_{3d}. Table III-1 lists the unnormalized functions that were used. Also listed are the special harmonics proportional to these functions. Table III-2 lists the coefficients for the fourteen basic functions.

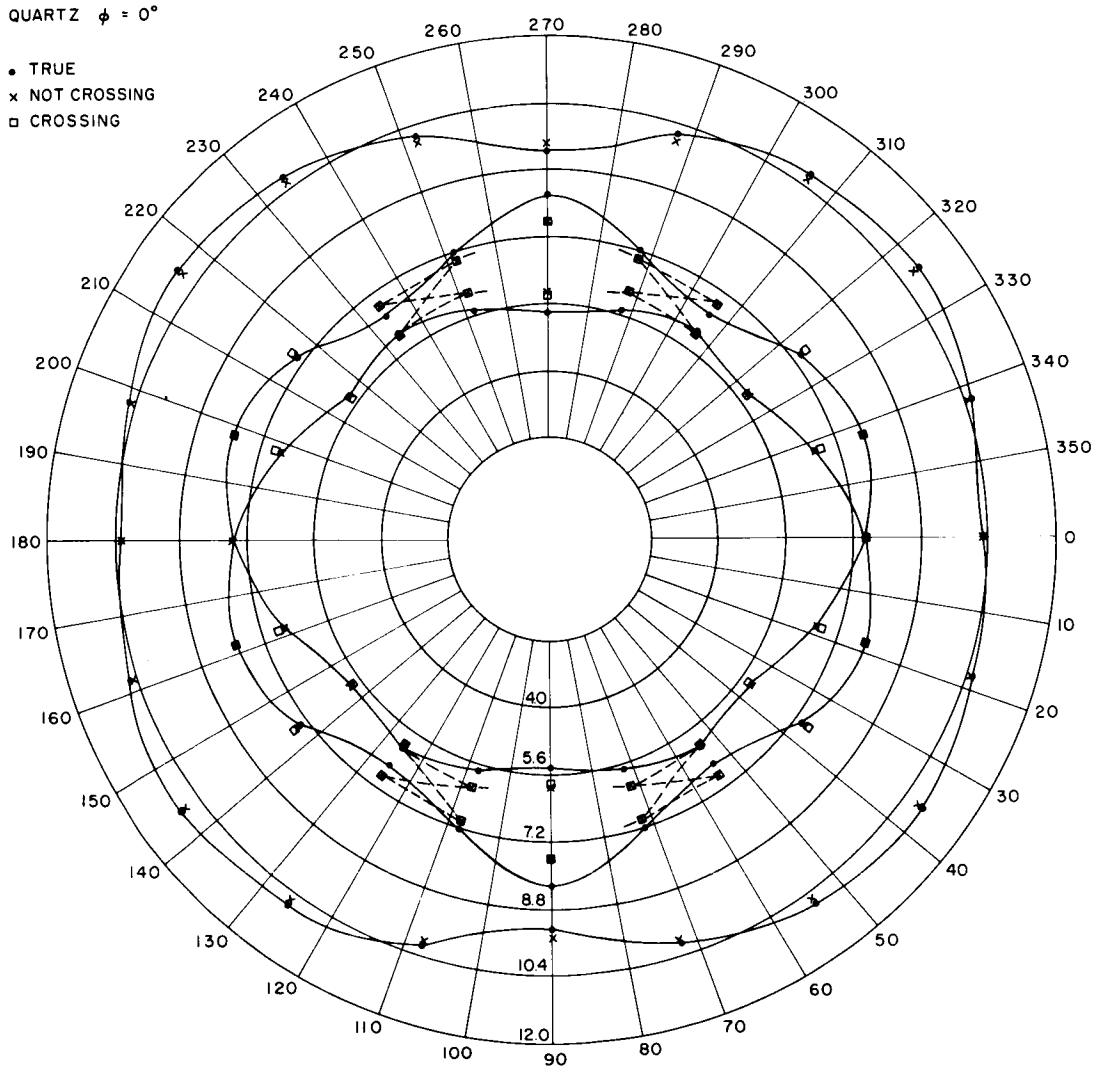

Fig. III-1. True values of λ in crossing and noncrossing approximations for quartz.

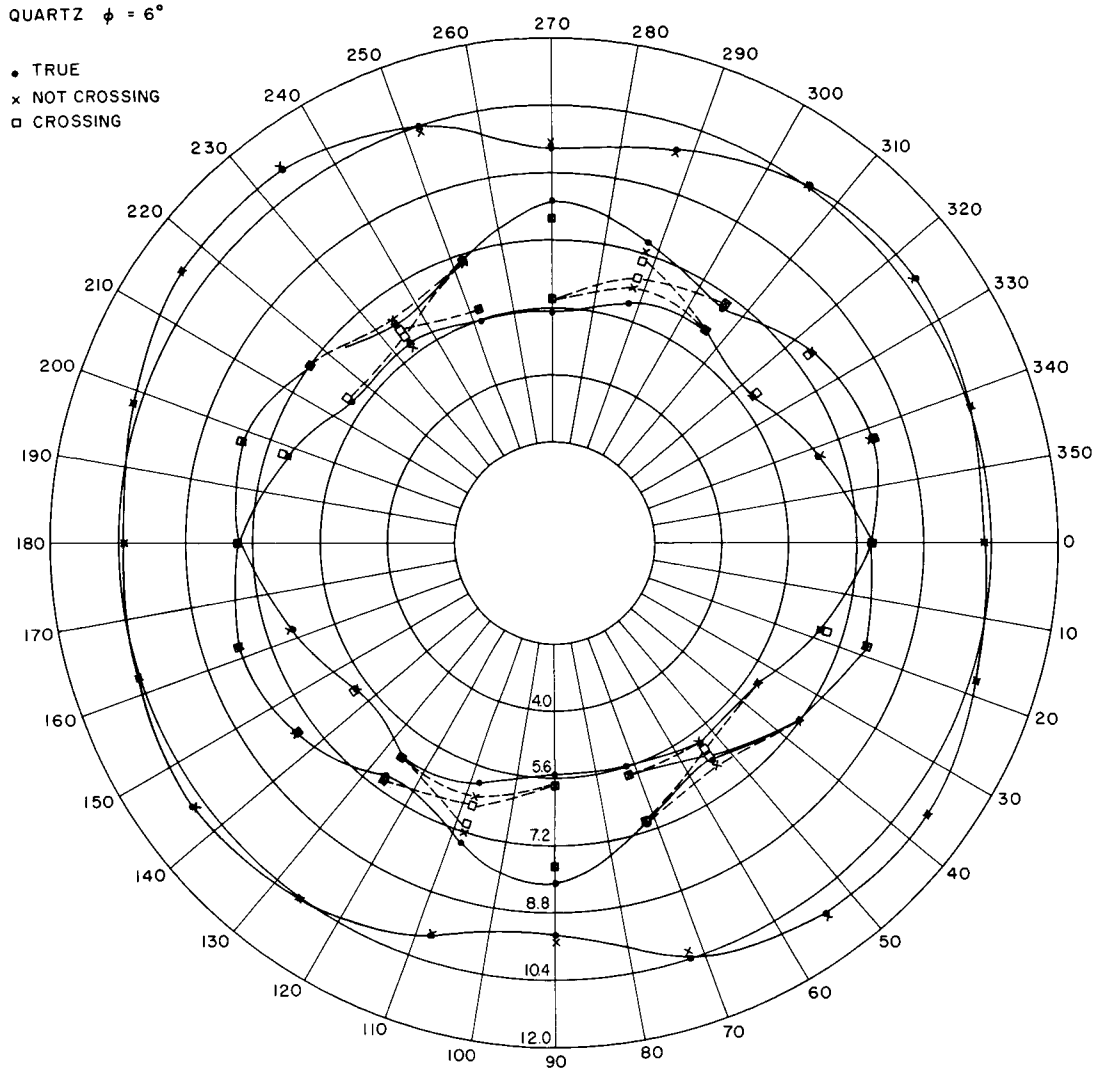

Fig. III-1. Continued.

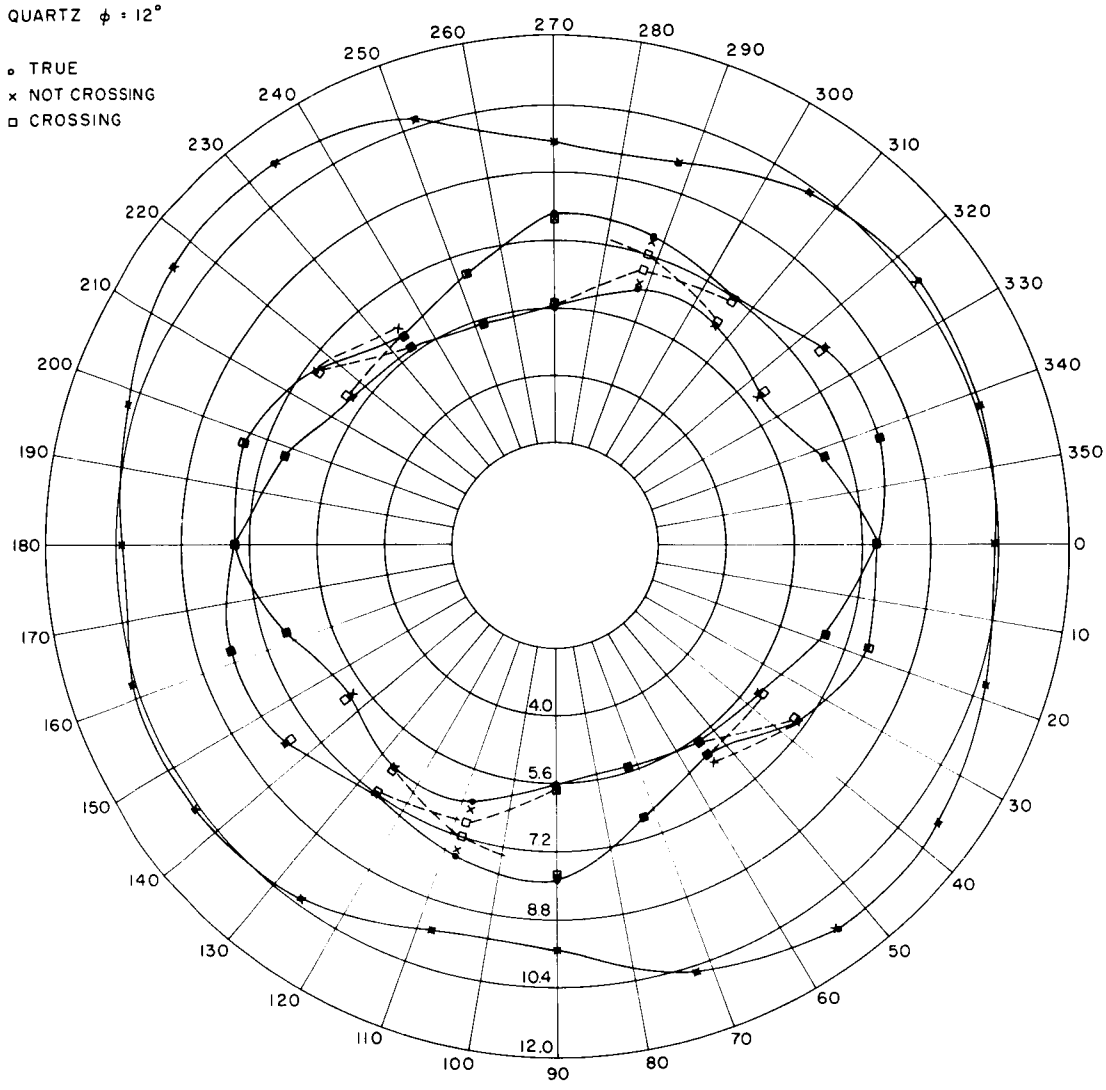

Fig. III-1. Continued.

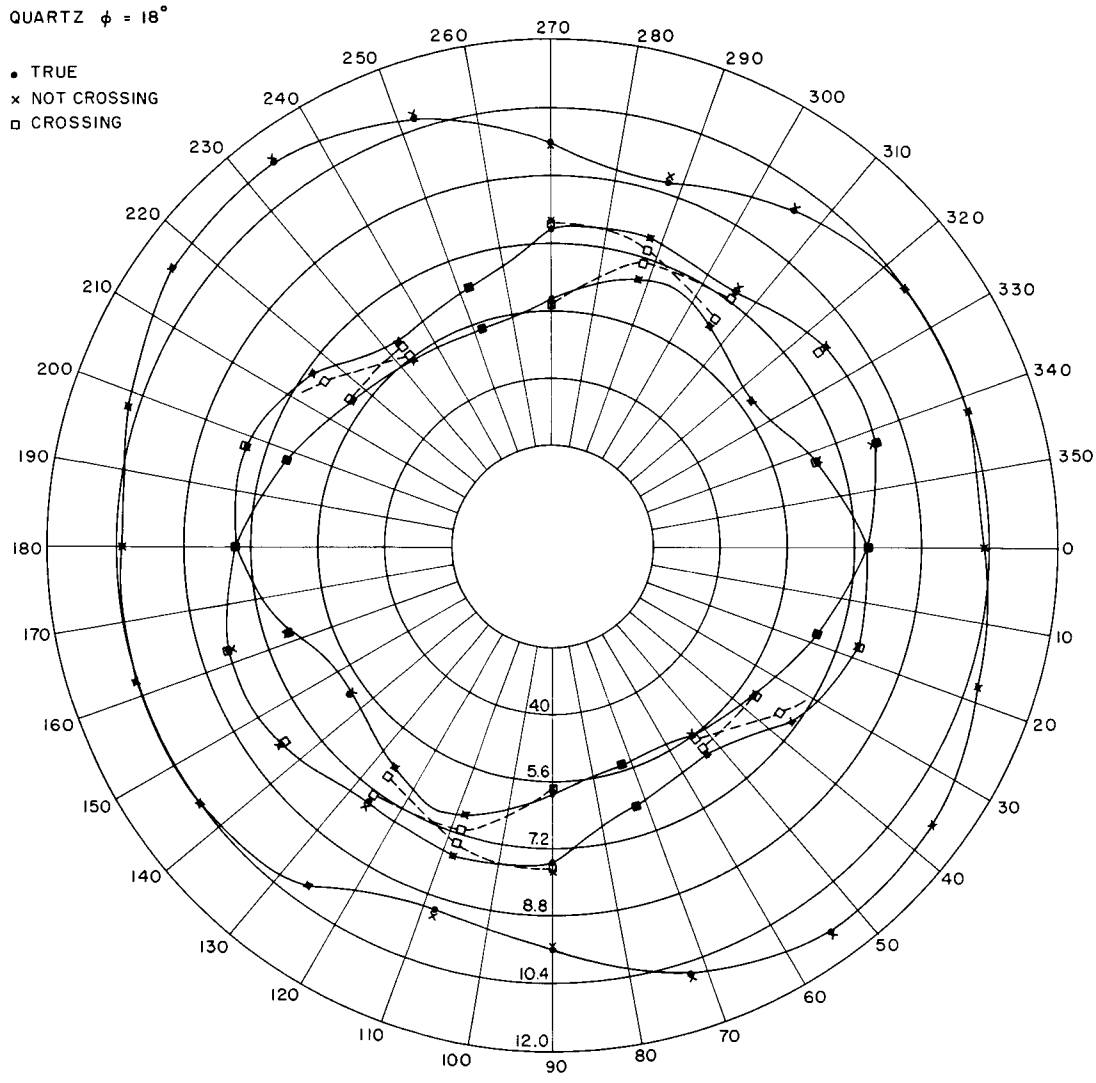

Fig. III-1. Continued.

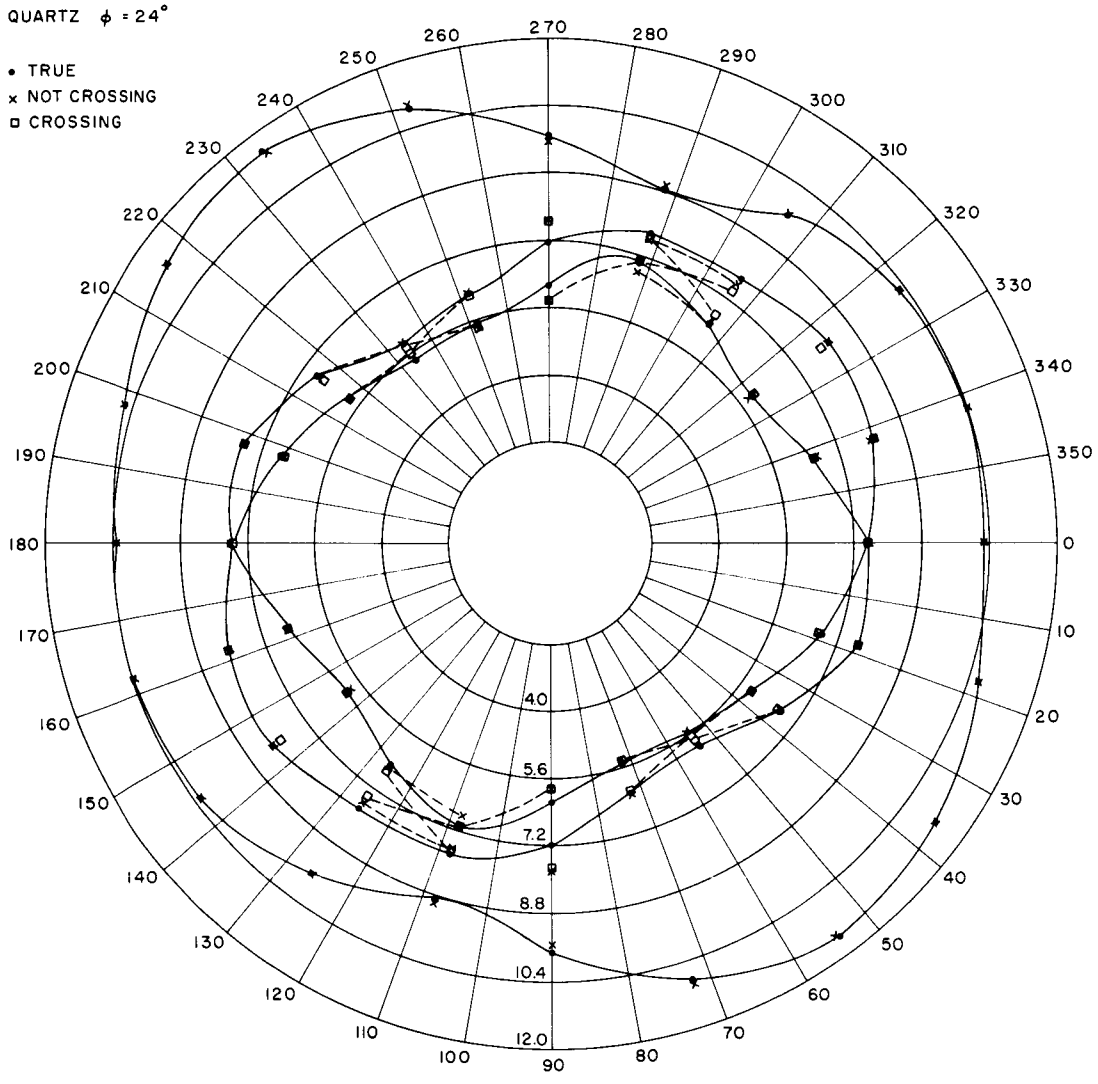

Fig. III-1. Continued.

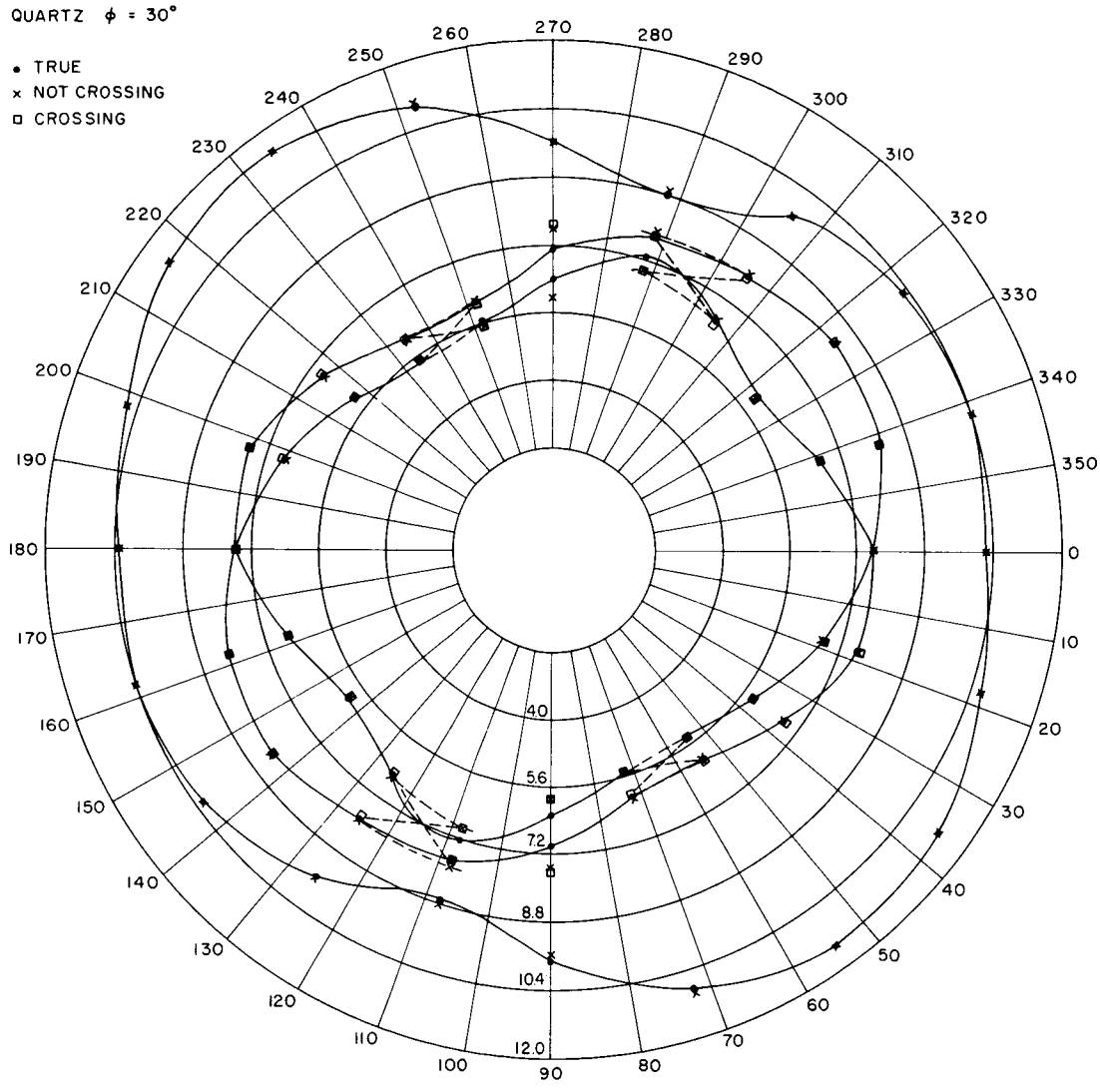

Fig. III-1. Concluded.

Table III-1. Basic functions.

No.	Spherical Harmonic	Function
1	Y_o^o	1
2	Y_2^o	$\frac{1}{2}(3\cos^2\theta - 1)$
3	Y_4^o	$\frac{1}{8}(35\cos^4\theta - 30\cos^2\theta + 3)$
4	$Y_4^3 + Y_4^{-3}$	$(-1)(105)\sin^3\theta\cos\theta\sin(3\phi)$
5	Y_6^o	$\frac{1}{16}[-5 + 105\cos^2\theta - 315\cos^4\theta + 231\cos^6\theta]$
6	$Y_o^3 + Y_o^{-3}$	$\sin^3\theta\left[\frac{945}{2}\cos\theta - \frac{3465}{2}\cos^3\theta\right]\sin(3\phi)$
7	$Y_o^6 - Y_o^{-6}$	$1039\sin^6\theta\sin(6\phi)$
8	Y_8^o	$\frac{1}{128}[35 - 1260\cos^2\theta + 6930\cos^4\theta - 12012\cos^6\theta + 6435\cos^8\theta]$
9	$Y_8^3 + Y_8^{-3}$	$\frac{1}{128}\left[-(6930)\,4!\cos\theta + (12012)\frac{(6!)}{3!}\cos^3\theta - (6435)\frac{8!}{5!}\cos^5\theta\right]\sin^3\theta\sin(3\phi)$
10	$Y_8^6 - Y_8^{-6}$	$\frac{1}{128}\left[-(12012)\,6! + (6435)\frac{8!}{2!}\cos^8\theta\right]\sin^6\theta\sin(6\phi)$
11	Y_{10}^o	$-\frac{63}{256}\left[1 - 55\cos^2\theta + \frac{1430}{3}\cos^4\theta - 1430\cos^6\theta + \frac{12155}{7}\cos^8\theta - \frac{46189}{63}\cos^{10}\theta\right]$
12	$Y_{10}^3 + Y_{10}^{-3}$	$\frac{63}{256}\left[11440\cos\theta - (1430)\frac{6!}{3!}\cos^3\theta + 12155\frac{8!}{5!}\cos^5\theta - \frac{46189}{63}\cos^7\theta\right][\sin^3\theta]\sin(3\phi)$
13	$Y_{10}^6 - Y_{10}^{-6}$	$\frac{63}{256}\left[1430\,(6!) - \frac{12155}{7}\frac{8!}{2!}\cos^2\theta + \frac{46189}{63}\frac{10!}{4!}\cos^4\theta\right]\sin^6\theta\sin(6\phi)$
14	$Y_{10}^9 + Y_{10}^{-9}$	$-\frac{46186}{256}(10!)\cos\theta\sin^9\theta\sin(9\phi)$

Table III-2. Coefficients for basic functions.

A. Quartz

No.	Longitudinal	Noncrossing No. 1	Transverse No. 2	Crossing No. 1	Transverse No. 2
1	1.02694	.72560	.61241	.67827	+.65973
2	.083864	.037667	.023577	.15148	-.090196
3	-.076627	.071489	.045001	-.037285	.15374
4	.093571	-.32044	.26547	.28025	-.30981
5	.0034625	-.066357	.067744	-.0073593	+.0087664
6	.049406	-.16469	.13402	.141368	-.15908
7	$.92088\times10^{-6}$	$.87029\times10^{-6}$	$-.18051\times10^{-5}$	$-.20201\times10^{-5}$	$.10852\times10^{-5}$
8	-.0044750	.0021378	-.0019092	-.020501	.020743
9	.013518	-.045298	.036945	.038948	-.043734
10	$.10264\times10^{-6}$	$-.16674\times10^{-6}$	$.65002\times10^{-7}$	$-.042531\times10^{-6}$	$.30074\times10^{-6}$
11	-.00033281	-.0093415	.0098118	-.0098324	.010285
12	.0015990	-.0053456	.0043559	.0045828	-.0051524
13	$-.33161\times10^{-8}$	$-.829158\times10^{-8}$	$.12186\times10^{-7}$	$-.65656\times10^{-7}$	$.69553\times10^{-7}$
14	$.60771\times10^{-10}$	$-.55847\times10^{-10}$	$.22882\times10^{-10}$	$.11470\times10^{-9}$	$-.14769\times10^{-9}$

B. Sapphire

No.	Longitudinal	Transverse No. 1	Noncrossing No. 2
1	2.30464	1.5426	1.20511
2	.14889	.087645	.065676
3	-.089904	.11134	.036036
4	.010070	-.038211	.032754
5	.0030266	-.14666	.15966
6	.0094793	-.022792	.012749
7	$.42283\times10^{-6}$	$.36553\times10^{-5}$	$-.40537\times10^{-5}$
8	.0098677	-.055929	.044110
9	.0024740	-.006100	.0034896
10	$.47100\times10^{-7}$	$-.22437\times10^{-6}$	$.17464\times10^{-6}$
11	-.0037530	-.012597	.015833
12	.00029974	-.00073529	.00041982
13	$.17323\times10^{-7}$	$-.23263\times10^{-7}$	$.774918\times10^{-8}$
14	$.58666\times10^{-10}$	$-.14354\times10^{-10}$	$-.32633\times10^{-10}$

Figure III-1 shows the true values of λ in the crossing and noncrossing approximations for quartz.

S. R. Reznek

C. RUBY CROSS RELAXATION

The nonexponential behavior of electron cross relaxation in dilute ruby, which was reported in Quarterly Progress Report No. 72 (pages 14-15), has been explained in terms of thermal contact between the Cr^{3+} electron dipole-dipole reservoir and the larger Al^{27} nuclear Zeeman reservoir of the Al_2O_3. Figure III-2 shows the coupling scheme. The basic principle is that the electron dipole-dipole reservoir[1,2] is in better thermal contact with the Al^{27} nuclei than with the rest of the electron-spin system.

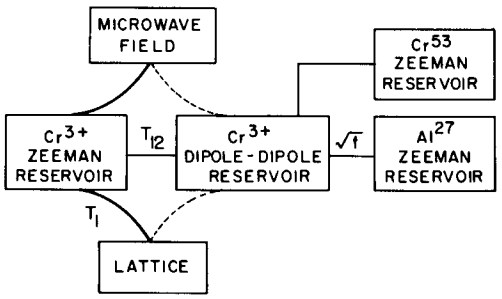

Fig. III-2. Electron and nuclear spin-coupling scheme in dilute ruby.

For two-quantum cross relaxation, which is fast, the bottleneck is the coupling between the dipole-dipole reservoir and the Al^{27} nuclei. The observed square root of time law represents nuclear spin diffusion.

For three-quantum cross relaxation, which is slower, the cross-relaxation process determines the rate, and a good exponential is observed.

R. L. Kyhl

References

1. J. Philippot, Phys. Rev. 133, A471 (1964).
2. J. Jeener, H. Eisendrath, and R. Van Steenwinkel, Phys. Rev. 133, A478 (1964).

IV 3 ATOMIC RESONANCE AND SCATTERING* 6

Academic and Research Staff

Prof. D. Kleppner
Dr. M. T. Myint
Dr. I. Ozier
D. C. Burnham

Graduate Students

D. E. Pritchard ET AL 8
P. F. Winkler

RESEARCH OBJECTIVES AND SUMMARY OF RESEARCH

This group, which was formed in September 1966, is concerned with the properties of atoms and simple molecules as observed by resonance and scattering techniques.

The immediate goal of our resonance experiments is a new determination of the magnetic moment of the proton. In the experiment a hydrogen maser is used, which, for the first time, permits a determination of the proton g-factor in atomic hydrogen. Our scattering efforts are concerned with studying the interactions of atoms with ions, atoms, and electrons, as revealed by electron-spin exchange. This new scattering technique promises to enable a wide class of scattering studies that have not been possible previously.

D. Kleppner

1. Magnetic Moment of the Proton

Our goal is to measure the g-factor of the proton, in terms of the electron g-factor, to a precision substantially higher than has been attained heretofore. The experiment involves the use of a hydrogen maser that allows simultaneous observation of electron and proton transitions in atomic hydrogen. The importance of this experiment lies in the fact that the proton is examined in atomic hydrogen, as contrasted with the molecular environment in which all previous determinations have been made. We hope to achieve a precision of one part in 10^8. We shall also compare the moment of the proton in atomic hydrogen with that of the proton in H_2O and in H_2. This will yield experimental values of the diamagnetic shielding of the proton in water and in molecular hydrogen which should be precise to a few parts in 10^8. These values are of particular interest, since water is a standard reference for NMR and H_2 is the only molecule for which the shielding factor can be predicted with high precision.

Pivotal to all the studies described above is an atomic hydrogen maser, especially designed to work in a magnetic field of 3500 Gauss. The field is provided by a magnet possessing unusual stability and very high homogeneity. The combination of the maser and the magnet produces an electron resonance line that has an excellent signal-to-noise ratio and is considerably narrower than has been possible previously. Resonance lines in the present experiment are typically 150 Hz as contrasted with 20,000 Hz for the same resonance frequency in previous experiments. Previously, it was impossible to study the proton in atomic hydrogen because the coupling of the proton to the electron caused a prohibitive loss in sensitivity to the measurement of the proton moment. For

25

*This work is supported by the Joint Services Electronics Programs (U.S. Army, U.S. Navy, and U.S. Air Force) under Contract DA 36-039-AMC-03200(E), and in part by the Sloan Fund for Basic Research (M.I.T. Grant 95).

END

instance, in order to measure the g-factor ratio to one part in 10^8, it is necessary to obtain a fractional precision in the proton resonance line of nearly two parts in 10^{10}.

As well as the experiments outlined above, there are numerous other g-factor determinations that we are currently considering. Among these are a comparison of the g-factor for the electron in hydrogen with the electron in deuterium to a precision of 1 part in 10^8, and a determination of the temperature dependence of the chemical shift in H_2. We are also considering a determination of the proton moment in nuclear magnetons. By combining this result with the result above for the nuclear moment in Bohr magnetons, a new value of the proton-electron mass ratio can be obtained. This ratio is of particular interest, because of its influence on many of the other fundamental constants.

A preliminary determination of the proton moment has already been obtained.[1] A number of improvements to the maser have been made during the past quarter, including facilities for a stronger beam and a more reliable magnetic-field mapping probe. The next step will be the design of a data acquisition system, which will be undertaken as soon as the maser is again in operation.

D. Kleppner, T. Myint, P. F. Winkler

References

1. T. Myint, D. Kleppner, N. F. Ramsey, and H. G. Robinson, Phys. Rev. Letters 17, 405 (1966).

2. Spin-Exchange Scattering

Spin exchange, the process by which two atoms exchange electrons during a collision, offers a powerful tool for investigating interactions between atoms, ions, and electrons. In particular, it yields detailed information about the singlet and triplet potentials. For atom-atom or ion-atom scattering, extremely small differences in the long-range potentials may be measured by observing oscillations in the spin-exchange cross sections. In electron-atom scattering it is possible to infer all of the important partial wave phase shifts for both singlet and triplet scattering.

Our goal is to observe spin-exchange scattering by means of a crossed-beam scattering apparatus that will allow us to observe differential cross sections for both spin-exchange and non spin-exchange processes. The atom-atom results should be of interest to workers in optical pumping, who can look only at broad terminal averages of total cross sections. The ion-atom results should display a variety of interesting effects. At low energies the oscillations in the spin-exchange cross section can be readily resolved, while at higher ion energy rainbow scattering may be observed. Our observations of electron-atom differential spin-exchange scattering should be of interest to the many workers who have made calculations on this problem, as well as to workers in optical pumping, particularly since the individual phase shifts have not previously been measured. We are especially interested in ion-atom scattering, since we have developed a theory that can be directly compared with our experiments.[1]

A summary of the experiments that we are considering is presented in Table IV-1.

All of our experiments are centered about a scattering apparatus which is under construction and is now approaching completion. The apparatus normally utilizes an alkali beam. The beam passes through a magnetic state selector and into a scattering region where it collides with the target particle (usually provided by a second beam). A portion of the scattered beam passes through collimating slits, a velocity analyzer, and

Table IV-1. SUMMARY OF SPIN-EXCHANGE SCATTERING

Class	Scattered particle	Target particle	Examples	Comments
Ion-Atom	Alkali			Long-range collisions important, perturbation theory yields good results, excellent experimental momentum resolution.
		^2S ion	He^+	Simple system, theory developed by our group.
			Be^+, Mg^+	Theory under development
		^2P ion	Ne^+, Si^+	(Situation complicated by fine structure, qualitative aspects of theory have been developed.)
	^2P atom	^2S ion	$Tl\text{-}He^+$	
	^2P atom	Alkali Ion	$Tl\text{-}Na^+$ $Al\text{-}H^+$	Spin orbit interaction and excitations can be studied, no spin-exchange.
Electron-Alkali	Alkali	Electron	All Alkalis	Possibility of measuring singlet and triplet phase shifts. Differential and differential spin-exchange cross sections can both be measured. Theory developed in detail by various workers. Very low energy results can be compared with optical pumping results. Elastic cross sections can be observed up to 10X excitation energy, with sacrifice in angular resolution.
Atom-Atom				Only system for which theory has been developed in detail is H-H. Possibility of measuring differential cross sections using velocity selected beam. Wide variety of systems can be observed.
	Alkali	Alkali	Na-NA Na-K, etc.	
	Alkali	Hydrogen		
	Alkali	^2P atom	Na-Al Na-Ga etc.	
	^2P	Alkali, Ion		A number of ^2P atoms can be detected by a hot-wire detector, including Al, Ga, Tl. Changes in orbital angular momentum can occur and be detected.
	Alkali	Molecule	Na-O2	
Hydrogen	Hydrogen	-	-	H-electron and H-H spin-exchange of great theoretical interest. However, these experiments will not be possible until a fast, efficient hydrogen detector is developed. We are not currently undertaking this work.

a magnetic spin-state analyzer. The two emerging beams, corresponding to the two electron states, pass into two identical detectors. The ratio of the signals from the detector can be directly related to the fraction of spin-exchange occurring in the scattering process. The sum of the detector readings yields the differential scattering cross section, a quantity also of a considerable interest.

D. C. Burnham, D. Kleppner, I. Ozier, D. E. Pritchard

References

1. D. E. Pritchard, D. C. Burnham, and D. Kleppner, Bull. Am. Phys. Soc. 11, 62 (1966).

V. ELECTRON MAGNETIC RESONANCE*

Academic and Research Staff

Prof. K. W. Bowers

Graduate Students

Nancy H. Kolodny
C. Mazza
A. C. Nelson
R. S. Sheinson
S. N. Suchard
Y.-M. Wong
B. S. Yamanashi

RESEARCH OBJECTIVES

Various problems are being attacked by our group.

1. Excited States. We shall study excited triplet states of simple molecules by the combined technique of flash irradiation and electron spin resonance spectroscopy. We have in our laboratory now a spectrometer capable of scanning 100 gauss, or more, in 25 msec, which with a flash discharge (100 to 10,000 joules into a Xenon-filled tube) of comparable duration provides the most powerful method for the study of excited electronic states extant.

2. Collisional Effects. Gas phase relaxation studies of hydrogen atoms with hydrogen molecules (ortho and para separately and together) and other species are being undertaken to learn more about intermolecular interactions. Other atoms in the gas phase will be similarly studied. We are also looking at collisional cross sections of excited alkali atoms (e.g., $^2P_{1/2}$ and/or $^2P_{3/2}$ states) with their ground states.

3. Charge and Energy Transfer. We are studying, via ESR, charge and energy transfer in semiconductorlike materials in solution and in the solid state, to determine the nature of the donor-acceptor complex.

4. Photoionization. Work is being done on the mechanism of photoionization in large molecules in the vacuum ultraviolet.

5. Radicals in the Gas Phase. Work is going forward in the study of the electronic, vibrational, and rotational structure of alkyl radicals (methyl, ethyl, t-butyl, and so forth) in the gas phase from work with gaseous discharges and flash photolysis.

6. Processes Related to Combustion.

7. Structure of Liquids via electron magnetic relaxation in solution.

8. Electronic Structure of Paramagnetic Species from theoretical and experimental approaches.

9. Relaxation Phenomena at the Orbital Point.

K. W. Bowers

*This work is supported by the Joint Services Electronics Programs (U.S. Army, U.S. Navy, and U.S. Air Force) under Contract DA 36-039-AMC-03200(E).

VI. RADIO ASTRONOMY*

Academic and Research Staff

Prof. A. H. Barrett
Prof. B. F. Burke
Prof. L. B. Lenoir
Prof. D. H. Staelin
Dr. S. H. Zisk
J. W. Barrett
Patricia P. Crowther
E. R. Jensen
P. L. Seymour

Graduate Students

R. J. Allen
M. S. Ewing
N. E. Gaut
M. Melnick
J. M. Moran, Jr.
G. D. Papadopulos
E. C. Reifenstein III
A. E. E. Rogers
K. D. Thompson
T. L. Wilson

RESEARCH OBJECTIVES AND SUMMARY OF RESEARCH

The research objectives of the Radio Astronomy Group may be broadly described as follows.

1. Studies of continuum emission of extraterrestrial radio sources/ The antenna facilities of the Haystack Microwave Research Facility, Lincoln Laboratory, M.I.T., have been used at 2-cm and 3.75-cm wavelengths to study temporal variations in the radio flux from quasi-stellar radio sources,[1] to map the brightness distribution in both the polarized and unpolarized components of the radiation from the strong radio sources,[2] and to determine the absolute flux from the radio sources Cassiopeia A and Taurus A.[3] This work continues and is being extended to other sources. The National Radio Astronomy Observatory interferometer, Green Bank, West Virginia, has been used for determining the brightness distribution of many galatic and extragalatic radio sources at 234 Mc/sec. Studies of Venus and Jupiter at wavelengths near the water-vapor and ammonia resonances have been carried out on the 28-ft radio telescope of Lincoln Laboratory.[4] A radiometer operating at 4-mm wavelength has been installed and tested on the 29-ft radio telescope at the Prospect Park Field Station of Air Force Cambridge Research Laboratories, and planetary observations are planned for the near future.

2. Studies of the radio spectrum of the interstellar medium. The spectral lines of OH have been the subject of extensive observations with the antennas of the Haystack Microwave Research and Millstone Radar Facility, Lincoln Laboratory, M.I.T., and the 140-ft radio telescope of the National Radio Astronomy Observatory, Green Bank, West Virginia. The studies during the past year have led to (a) the detection of circularly polarized OH emission,[5] (b) the detection of the isotopic species $O^{18}H$,[6] and the establishment of an upper limit to the angular size of the OH emitting regions of 15 seconds of arc.[7] Interferometric observations are being extended by using the Millstone and Agassiz (Harvard) radio telescopes as an interferometer to determine the angular size of the emission regions. Searches for other spectral lines are concentrating on the CH radical, with a line expected near 3300 Mc/sec.

3. Study of microwave emission and absorption by the terrestrial atmosphere and

*This work was supported principally by the National Aeronautics and Space Administration (Grant NsG-419 and Contract NSR-22-009-120); and in part by the Joint Services Electronics Programs (U.S. Army, U.S. Navy, and U.S. Air Force under Contract DA 36-039-AMC-03200(E).

surface, with particular emphasis on the meteorological satellite application of microwave sensors. This work has included ground-based observations in conjunction with, and in support of, measurements of planetary microwave emission, and theoretical studies of satellite measurements of atmospheric water vapor and oxygen. An extensive program of balloon observations has been carried out to determine the microwave properties of the upper atmosphere as governed by the resonance lines of molecular oxygen at 5-mm wavelength.[8] These results indicate departures from the Van Vleck-Weisskopf theory of microwave absorption and emission, and further observations are being made to confirm this conclusion. Observations of the water-vapor resonance at 1.35 cm in the terrestrial atmosphere have also been carried out.[9]

A. H. Barrett

References

1. R. J. Allen and A. H. Barrett (to appear in Astron J., November 1966 issue).
2. R. J. Allen and A. H. Barrett, paper presented ath the 123rd Meeting of the American Astronomical Society, Los Angeles, California, December 27-30, 1966.
3. R. J. Allen and A. H. Barrett (to appear in Astron. J., November 1966 issue).
4. D. H. Staelin and R. W. Neal (to appear in Astron. J., November 1966 issue).
5. A. H. Barrett and A. E. E. Rogers, Nature 210, 188 (1966).
6. A. E. E. Rogers and A. H. Barett (to appear in Astron. J., November 1966 issue).
7. A. E. E. Rogers, J. M. Moran, P. P. Crowther, B. F. Burke, M. L. Meeks, J. A. Ball, and G. M. Hyde, Phys. Rev. Letters 17, 450 (1966).
8. A. H. Barrett, J. W. Kuiper, and W. B. Lenoir, J. Geophys. Res. 71, 4723 (1966).
9. D. H. Staelin, J. Geophys. Res. 71, 2875 (1966).

A. HAYSTACK-MILLSTONE OH INTERFEROMETER

Observations of OH emission with an interferometer comprising the Haystack (120-ft) and Millstone (84-ft) antennas have been reported previously.[1] The results can now be extended to include the positions and angular sizes of the emission regions associated with W49, NGC 6334 and Sagittarius, as shown in Table VI-1. The region in Sagittarius was observed to be a point source. W49 is seen to be a double source, whose components remain unresolved. NGC 6334 is at least a double source, but may be more complex. Only one of the components of NCG 6334 was mapped with the interferometer, owing to the poor signal-to-noise ratio and the limited hour angle availability for their source.

Table VI-1. Position and angular sizes of OH emission regions.

Line[a] Velocity km/sec	Polarization	Fringe Amplitude Observed	Effective Source Diameter	Separation from Line with Position Listed	Position-Epoch 1950 α	Position-Epoch 1950 δ
W3 1665 MHz	June 7, 8, 9, 10, 11, 12, 13 July 9, 11				±12 hr	
-45.1	right	1.0 ±0.05	<15"		$02^h23^m16.3\pm1^s$	61°38'57±5"
-43.7	right	1.0 ± 0.1	<20"	<3"		
-41.7	right	1.0 ± 0.2	<25"	<3"		
-45.4	left	1.0 ± 0.1	<20"	<3"		
-46.4	left	1.0 ± 0.1	<20"	<3"		
W3 1667 MHz	June 12, 29 July 8, 9				±12 hr	
-42.3	right	1.0 ± 0.3	<30"	<7"		
-44.8	left	1.0 ± 0.3	<30"		<15" from 1665 Position	
W49 1665 MHz	Position 1 June 29 July 10				±6 hr	
17.0	right	0.9 ± 0.2[b]		<7"		
5.5	left	1.0 ± 0.2	<25"	<15"		
12.0	left	1.0 ± 0.2	<25"	<10"		
16.8	left	0.8 ± 0.3[b]		<7"		
20.9	left	1.0 ± 0.1	<20"		$19^h7^m49.7\pm1^s$	9°1'12±5"
W49 1667 MHz	Position 1 July 8, 9				±6 hr	
2.0	right	1.0 ± 0.3	<30"	<7"		
5.0	right	1.0 ± 0.2	<25"		<7" from 1665 Position 1	
3.0	left	1.0 ± 0.2	<25"	<7"		
5.0	left	1.0 ± 0.21	<20"	<7"		
19.0	left	0.6 ± 0.4[b]		<7"		
W49 1665 MHz	Position 2					
16.0	right	0.8 ± 0.2[b]		<7"		
15.7	left	1.0 ± 0.2	<25"			+8.5[s] R.A.
17.9	left	0.± ± 0.3[b]		<7"		-68" Dec. from Pos. 1
W49 1667 MHz	Position 2					
19.0	left	0.6 ± 4[b]			<10" from 1665 Position 2	
NGC 6334 1665 MHz	July 11, 12				±2 hr	
-12.4	right	1.0 ± 0.2	<25"		$17^h17^m33.5\pm2^s$	-35°45'35±10"
-9.1	left	1.0 ± 0.2	<25"	<7"		
SAG (W24) 1665 MHz	July 10, 11				±3 hr	
74.0	right	1.0 ± 0.2	<25"	<7"	[1] $17^h44^m11\pm2^s$	-28°23'29±10"
67.5	left	1.0 ± 0.1	<20"			

[a]Line velocity based on Radford's (1964) rest frequencies for the $2\pi_{3/2}$, J = 3/2, Λ - doublet of $O^{16}H^1$.

[b]Features that show a systematic fringe amplitude variation.

Most measurements were made with a frequency resolution of 3 kHz; some of the W3 measurements were made with 1 kHz.

None of the components of any OH source is yet resolved, and measurements are now being extended to a longer baseline, in cooperation with the Harvard Agassiz Station (see Sec. VI-B).

B. F. Burke, J. M. Moran, A. E. E. Rogers

References

1. B. F. Burke, J. M. Moran, and A. E. E. Rogers, Quarterly Progress Report No. 83, Research Laboratory of Electronics, M.I.T., October 15, 1966, pp. 7-9.

B. MILLSTONE-AGASSIZ OH INTERFEROMETER

Previous OH interferometer observations, as described in Section VI-A, have clearly demonstrated the need for observations with a larger baseline than the 3800 λ available with the Haystack-Millstone complex. This has led to a joint experiment, involving Research Laboratory of Electronics, Lincoln Laboratory, and Harvard personnel, in which the 84-ft antenna of the Millstone Radar Facility and the 60-ft radio telescope of the George R. Agassiz Radio Astronomy Station of Harvard College Observatory is being used as an interferometer. The telescopes are separated by 74,390 λ (43,925 ft) along a line oriented 22.52° East of North. Phase coherence is maintained by use of a one-way microwave link operating at 7325 Mc/sec on a line-of-sight path between the two stations. The Harvard radiometer has a maser preamplifier and a system temperature of 140°K; the Millstone radiometer has a tunnel-diode amplifier and a system temperature of approximately 700°K. The essential features of the data reduction are the same those as used in the Millstone-Haystack experiment. The OH source W3 has been examined with a bandwidth of 120 kc/sec and a resolution of 3 kc/sec. Preliminary observations have revealed fringes at 1665 Mc/sec.

A. H. Barrett, B. F. Burke, J. M. Moran, A. E. E. Rogers

C. K-BAND SPECTRUM MEASUREMENTS OF THE SUN

The solar brightness spectrum near 1-cm wavelength was measured on several days in the period January-March, 1966. The measurements were made with the Lincoln Laboratory 28-ft millimeter antenna and the Research Laboratory of Electronics 5-channel K-band radiometer.[1] The frequencies observed were 19.0, 21.0, 22.2, 23.5, and 25.5 GHz. This solar band had not been carefully studied before.

The measurements were made by taking drift scans across the center of the sun every 10 minutes for a period of approximately 2 hours each day. The resulting measurements were corrected for atmospheric absorption by extrapolation to zero atmosphere

the observed dependence of solar intensity upon elevation angle.

The results were calibrated by comparison of the solar data with the average lunar brightness temperature observed over a lunation. The comparison was made using the antenna patterns measured at each frequency.[1] The true lunar brightness temperature was estimated from observations by many observers at many wavelengths.[2] The errors involved in this comparison technique are very nearly the same at each frequency and thus the relative errors are small. The relative errors were dominated by the effective receiver noise and system gain fluctuations present during the lunar and solar observations. If it is assumed that the true average lunar brightness temperature is known within 5 per cent, the absolute rms error at each frequency is approximately ±700°K.

The measured average solar brightness temperatures of the center of the sun are listed in Table VI-2, together with the relative rms errors. Only the eight most accurate

Table VI-2. Observed K-band solar spectrum.

Frequency (GHz)	Central Solar Brightness Temperature (°K)	Relative rms Error (°K)
19.0	10,800	±400
21.0	10,800	±400
22.2	11,000	±500
23.5	10,700	±500
25.5	9,800	±300

spectra were averaged. The rest of the data is not included here.

This average spectrum is composed of data obtained on February 10, 18, 23, and 24, and March 3, 10, 11, and 14, 1966. The spectrum did not appear to vary much over this period. These results superseded the data presented earlier,[3] which were based on incomplete calibration data.

D. H. Staelin, N. Gaut, Sara Law, W. T. Sullivan III.

References

1. D. H. Staelin, "Microwave Spectrum of Venus," Sc. D. Thesis, Department of Electrical Engineering, M.I.T., 1965.
2. J. M. Moran, "Radiometric Observations of the Moon near One-Centimeter Wavelength," S.M. Thesis, Department of Electrical Engineering, M.I.T., 1965.
3. W. T. Sullivan III, "Solar Observations at Millimeter Wavelength," NEREM Record (1966), IEEE Cataloge No. F-70.

D. INFERENCE OF ATMOSPHERIC ATTENUATION NEAR 61.15 GHz FROM BALLOON FLIGHT RESULTS

Balloon Flight Experiments such as the 154-P series, which have been previously reported,[1] (see also Sec. VI-F), yield data that can be used to infer the atmospheric attenuation coefficient as a function of height. The ascent and descent portions of the flight are useful in this respect when coupled with accurate measurements of the atmospheric temperature and pressure.

The appropriate measurement geometry is shown in Fig. VI-1. The assumptions made in this inversion method are that the atmosphere may be modeled by infinite planar

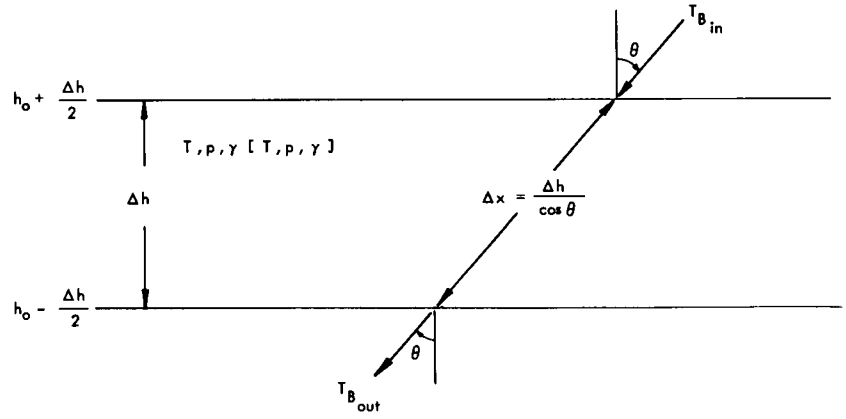

Fig. VI-1. Geometry of the measurements.

layers (valid for $\theta \lesssim 80°$), and within a layer the temperature and pressure may be taken as constant (valid for $\Delta h \lesssim 2.5$ km). The equation of transfer relating the brightness temperatures, $T_{B\,in}$ and $T_{B\,out}$, is

$$T_{B\,out} = T_{B\,in} \exp\left(-\gamma(h_o)\frac{\Delta h}{\cos\theta}\right) + T\left[1-\exp\left(-\gamma(h_o)\frac{\Delta h}{\cos\theta}\right)\right]. \tag{1}$$

This relation can be solved for $\gamma(h_o)$:

$$\gamma(h_o) = \frac{\cos\theta}{\Delta h} \ln\left|\frac{T - T_{B\,in}}{T - T_{B\,out}}\right|, \tag{2}$$

under the assumption that the quantities on the right of (2) are known.

In balloon experiments such as 154-P, the antenna temperature (see Sec. VI-C) is measured, not the brightness temperature. In order to infer the value of $\gamma(h_o)$, the

antenna temperatures at $h_o \pm \frac{\Delta h}{2}$ must be converted to the brightness temperatures along the antenna axis at $h_o \pm \frac{\Delta h}{2}$. The results of flight 154-P indicate a true (measured) antenna temperature that is different from (higher than) the computed values for heights at which the optical depth is not large (that is, at heights above where $T_A = T_B = T$). This would appear to indicate that the true absorption coefficient is higher than the one used in the computations.

Fig. VI-2 shows the mechanics of converting the measured antenna temperatures into brightness temperatures. This conversion is built around the assumption that the

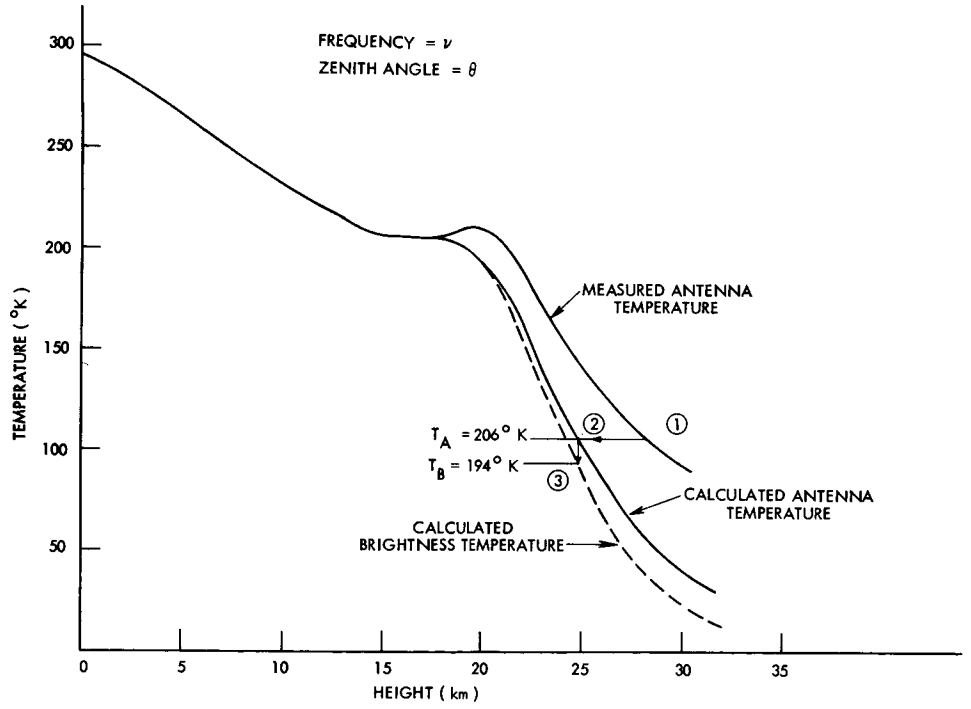

Fig. VI-2. Mechanics of antenna temperature to brightness conversion.

brightness distribution determining a given antenna temperature is the same for the measured antenna temperature and for the computed one. That is, changing the absorption coefficient merely moves the brightness distributions around in height but does not change them. The validity of this assumption can be checked. Thus (in Fig. VI-2) an antenna temperature of 206°K, measured at 28 km is converted to a brightness temperature of 194°K, which is assumed to be appropriate at 28 km.

The effects of noise and uncertainty can be seen by making the following replacement in Eq. 2:

$$T \rightarrow T + \Delta T$$

$$T \rightarrow T_{B\,in} + \Delta T_{B\,in}$$

$$T \rightarrow T_{B\,out} + \Delta T_{B\,out}$$

which yield

$$\gamma(h_o) + \Delta\gamma = \frac{\cos\theta}{\Delta h}\left[\ln\left|\frac{T - T_{B\,in}}{T - T_{B\,out}}\right| + \ln\left|\frac{1 + \dfrac{\Delta T - \Delta T_{B\,in}}{T - T_{B\,in}}}{1 + \dfrac{\Delta T - \Delta T_{B\,out}}{T - T_{B\,out}}}\right|\right] \tag{3}$$

that can be expanded to yield

$$\Delta\gamma_{rms} = \frac{\cos\theta}{\Delta h}\left\{\left|\frac{T_{B\,in} - T_{B\,out}}{(T-T_{B\,in})(T-T_{B\,out})}\right| \Delta T_{rms} + \left[\frac{1}{|T - T_{B\,out}|} + \frac{1}{|T-T_{B\,in}|}\right] \Delta T_{B_{rms}}\right. \tag{4}$$

under

$$\left|\frac{\Delta T - \Delta T_{B\,in}}{T - T_{B\,in}}\right| \ll 1,$$

$$\left|\frac{\Delta T - \Delta T_{B\,out}}{T - T_{B\,out}}\right| \ll 1,$$

and ΔT, $\Delta T_{B\,in}$, and $\Delta T_{B\,out}$ are mutually independent and have rms values of ΔT_{rms}, $\Delta T_{B_{rms}}$, and $\Delta T_{B_{rms}}$, respectively.

The inferred absorption coefficient based on the results of 154-P are shown in Figs. VI-3 and VI-4. Layer thicknesses of 1 km and 2 km were used. The right-hand

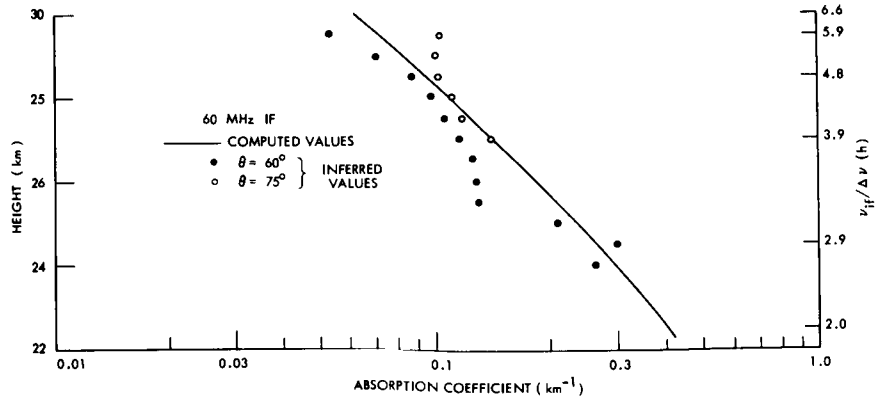

Fig. VI-3. Inferred absorption coefficients, Flight 154-P.

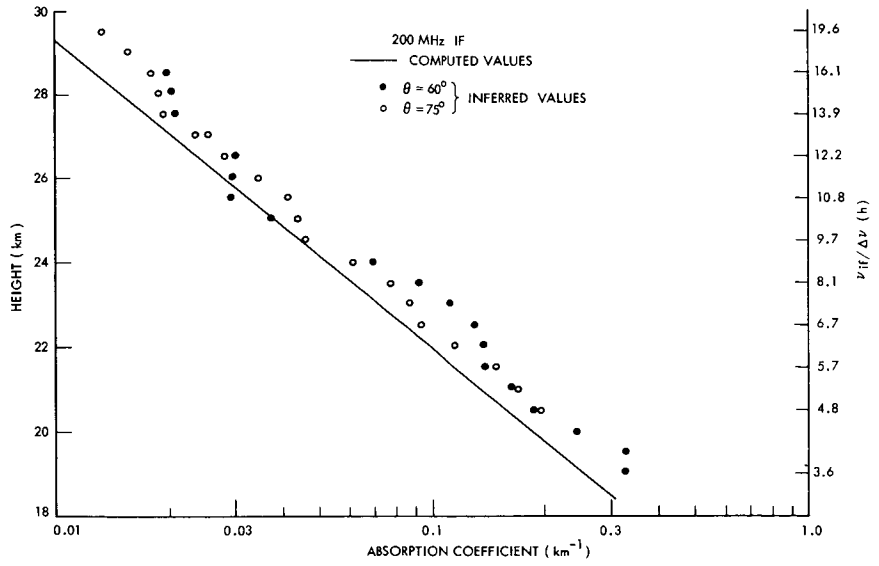

Fig. VI-4. Inferred absorption coefficients, Flight 154-P.

labeling of the vertical axis (essentially frequency in linewidth units) is given to facilitate comparison of inferred values with values computed on the basis of the Van Vleck-Weisskopf line-shape function

$$F(\nu) = \frac{1/\Delta\nu(h)}{\left(\frac{\nu - \nu_{9^+}}{\Delta\nu(h)}\right)^2 + 1}, \tag{5}$$

where $\nu - \nu_{9^+} = \pm\nu_{if}$, and $\Delta\nu$ is the linewidth.

If rms noise fluctuations of $\Delta T_{rms} = 1°K$ and $\Delta T_{B_{rms}} = 2°K$ are assumed, error bars on the inferred points will be approximately ±10-20%.

From Fig. VI-4 it is fairly evident that the absorption coefficient at frequencies well away from the resonance frequency is higher than theory predicts. Two possible changes in the theoretical line shape are being investigated as possible explanations of the higher absorption in the line wings.

The first is a change within the Van Vleck-Weisskopf line-shape theory. On the line-wings Eq. 5 can be expressed as

$$F(\nu) = \frac{\Delta\nu(h)}{(\nu - \nu_{9^+})^2}, \tag{6}$$

which indicates that the wing absorption can be increased by using a larger linewidth;

however, this results in a lower absorption near line center. Whether an absorption coefficient with this correction will adequately agree with the measured values over the entire height range is being investigated.

The second change under investigation is to go to a new line-shape theory. In particular, the impact theory of Gordon[2] should be looked at closely. In this theory it is not assumed that the absorption coefficient of overlapping resonance lines is the sum of the individual absorption coefficients.

Once a better expression for the absorption coefficient is obtained, theoretical computations of the brightness temperature distribution can be made to check the earlier assumption. Any necessary corrections can be made and the method repeated with the correct brightness temperatures.

W. B. Lenoir

References

1. W. B. Lenoir, Quarterly Progress Report No. 82, Research Laboratory of Electronics, M.I.T., July 15, 1966, pp. 36-41.
2. R. G. Gordon, J. Chem. Phys. 45, 1635-1655 (September 1, 1966).

E. OBSERVATIONS OF MICROWAVE EMISSION FROM ATMOSPHERIC OXYGEN: BALLOON FLIGHTS, SUMMER 1966

Two more balloon flight experiments were performed during August, 1966. The characteristics of these flights have been summarized in a previous report.[1] Preliminary analysis indicates that both flights were successful. Further analysis awaits the complete report from the balloon base.

W. B. Lenoir, J. W. Barrett, D. C. Papa

References

1. W. B. Lenoir, Quarterly Progress Report No. 82, Research Laboratory of Electronics, M.I.T., July 15, 1966, pp. 36-41.

F. OBSERVATIONS OF MICROWAVE EMISSION FROM ATMOSPHERIC OXYGEN: BALLOON EXPERIMENT RESULTS, SUMMER 1965

During July 1965, four balloon flight experiments were performed from the NCAR Balloon Base, Palestine, Texas. These flights (150-P, 152-P, 153-P, 154-P) have been described in previous reports.[1,2] Two distinct types of experiments were flown. Flights 150-P and 154-P were experiments to study the shape of the 9^+ resonance line,

Table VI-3. Summary of Flights 150-P and 154-P.

ν_o = 61.151 GHz (9^+ resonance line)

ν_{if} = center frequency of IF passband

B_{if} = bandwidth of IF passband

θ = zenith angle of antenna axis

ΔT_{rms} = output noise fluctuations (measured)

θ (deg)	ν_{if} (MHz)	B_{if} (MHz)	ΔT_{rms} (°K)
60	20	10	1.7
60	60	10	2.0
60	200	15	2.8
75	20	10	2.5
75	60	10	4.5
75	200	15	3.2

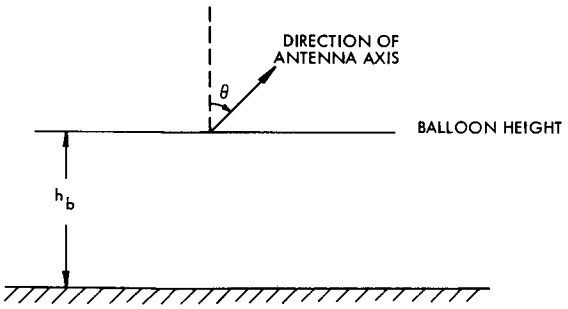

Fig. VI-5. Geometry of Flights 150-P and 154-P.

while flights 152-P and 153-P were experiments to remotely infer the atmospheric temperature profile below the balloon. Data analysis yielding the antenna temperatures of these flights has been completed.

1. Results of Flights 150-P and 154-P

Both of these flights had the same physical characteristics and geometry, as shown in Fig. VI-5 and Table VI-3. The measured quantity is the antenna temperature, T_A, which is the brightness temperature distribution weighted by the antenna gain pattern

$$T_A = \frac{1}{4\pi} \int_{4\pi} T_B(\theta, \phi)\, G(\theta, \phi)\, d\Omega(\theta, \phi), \tag{1}$$

with $G(\theta, \phi)$ being the known antenna gain, and $\Omega(\theta, \phi)$ the solid angle. The brightness

temperature at a zenith angle θ and a frequency ν is given by

$$T_B(\nu, \theta) = \int_{h_0}^{\infty} T(h)\, WF(h, \nu, \theta)\, dh, \tag{2}$$

with

$$WF(h, \nu, \theta) = \frac{\gamma[T(h), p(h), \nu]}{\cos \theta}\, e^{-\tau(h, \nu, \theta)} \tag{3}$$

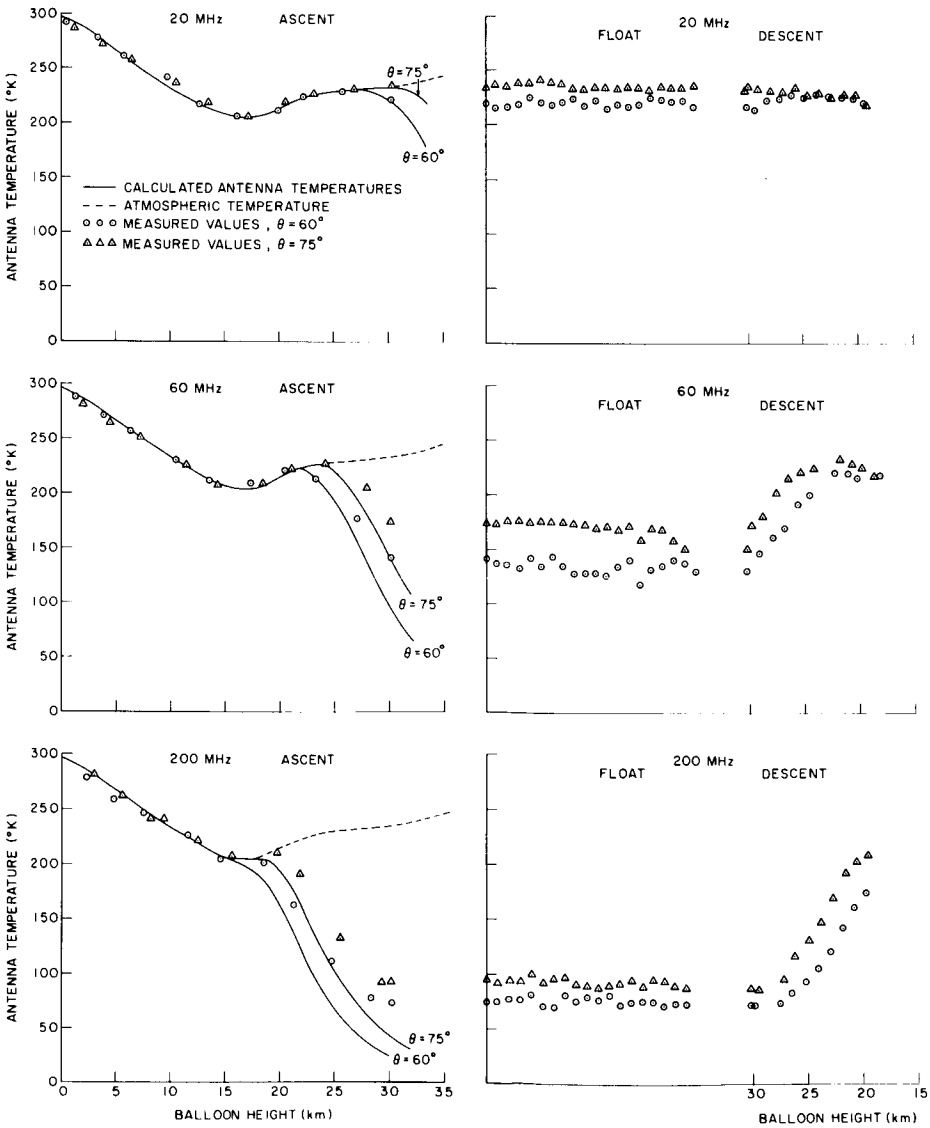

Fig. VI-6. Comparison of experimentally determined antenna temperature with computed values.

Table VI-4. Summary of Flights 152-P and 153-P.

ν_o = 61.151 GHz (9^+ resonance line)

ν_{if} = center frequency of IF passband

B_{if} = bandwidth of IF passband

θ = nadir angle of antenna axis

ΔT_{rms} = output noise fluctuations (measured)

θ (deg)	ν_{if} (MHz)	B_{if} (MHz)	ΔT_{rms} (°K)
60	20	10	1.6
60	60	10	2.8
60	200	15	1.4
0	20	10	2.4
0	60	10	3.5
0	200	15	2.3

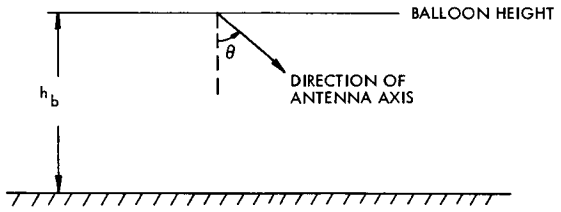

Fig. VI-7. Geometry of Flights 152-P and 153-P.

$$\tau(h, \nu, \theta) = \frac{\int_{A_b}^{h} \gamma[T(\xi), p(\xi), \nu]\, d\xi}{\cos\theta} \qquad (4)$$

T(h) = atmospheric temperature at hight h

p(h) = atmospheric pressure at height h

γ = atmospheric attenuation coefficient.

Preliminary theoretical calculations are based on the use of the Van Vleck-Weisskopf line shape in the expression for the attenuation coefficient. Other parameters are the same as those used by Meeks and Lilley[5] and Barrett, et al.[6]

No useful data for the ascent part of Flight 150-P were taken, because of an equipment problem. Float and descent data are difficult to reduce for this flight, since final calibration temperatures are determined during the ascent part of the flight

Flight 154-P was successful in every respect. The experimentally determined antenna temperatures are compared with the computed values in Fig. VI-6. In the report in Section VI-D the inference of the atmospheric absorption coefficient from these measured antenna temperatures is discussed.

2. Results of Flights 152-P and 153-P

This pair of flights had the characteristics and geometry depicted in Fig. VI-7 and Table VI-4. Equation 1 ist still valid for T_A but T_B is given by

$$T_B(\nu, \theta) = \int_0^{h_0} T(h)\, WF(h, \nu, \theta)\, dh \tag{5}$$

with

$$WF(h, \nu, \theta) = \frac{\gamma[T(h), p(h), \nu]}{\cos \theta} e^{-\tau(h, \nu, \theta)} \tag{3}$$

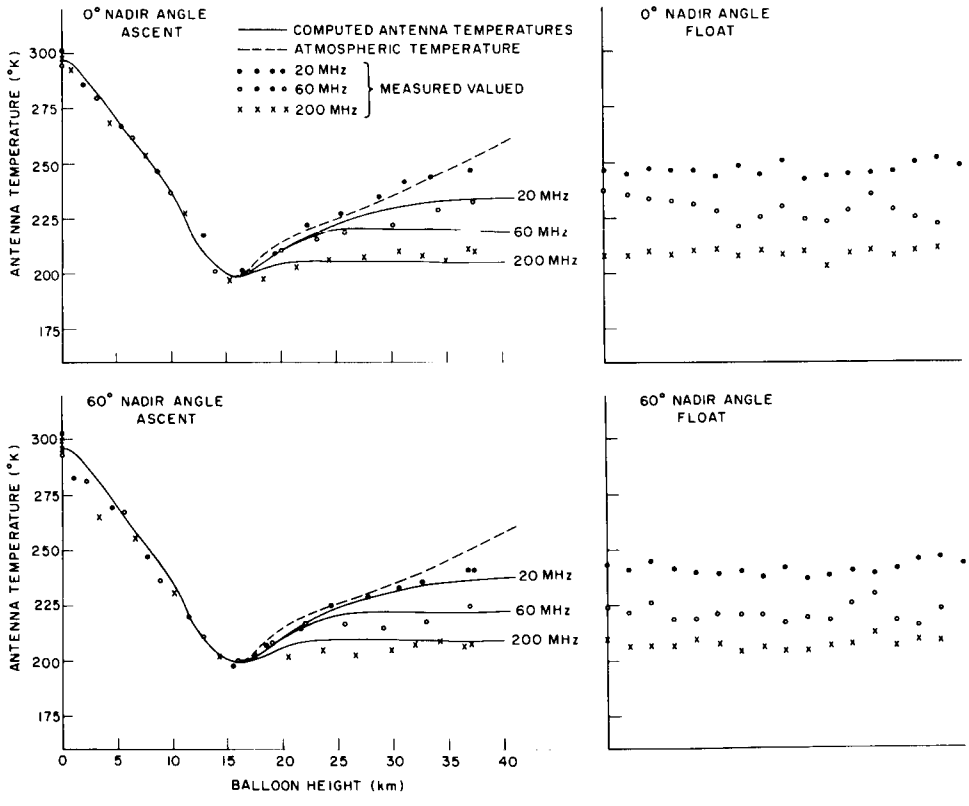

Fig. VI-8. Measured antenna temperatures for ascent and float parts of Flight 152-P.

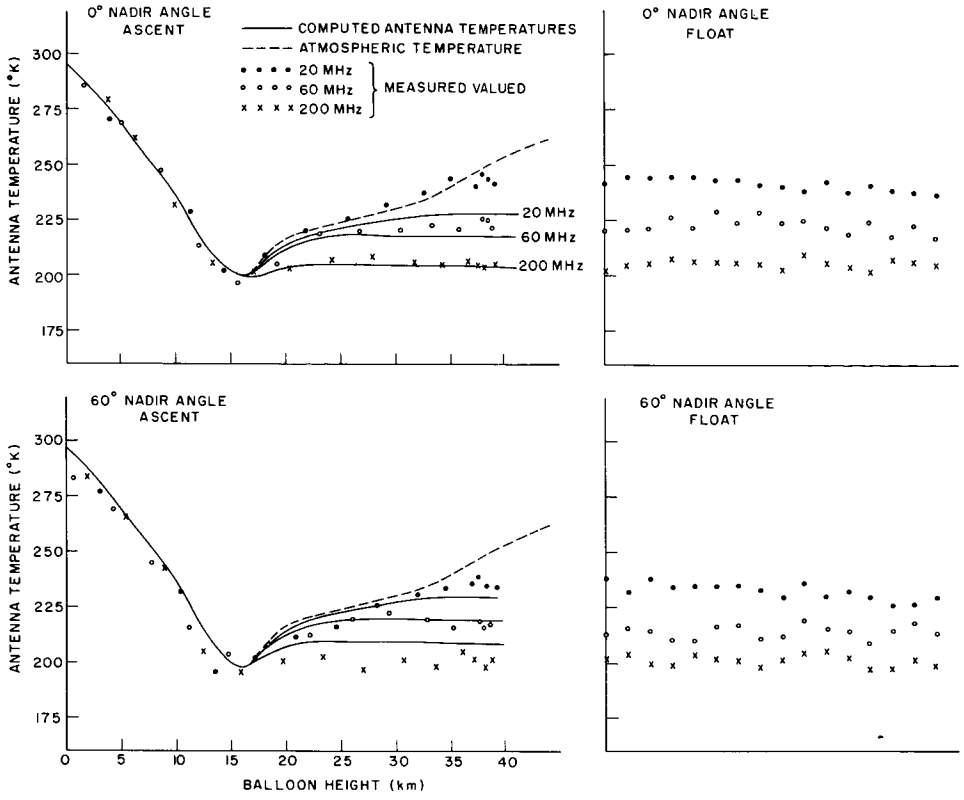

Fig. VI-9. Measured antenna temperatures for ascent and float parts of Flight 153-P.

$$\tau(h, \nu, \theta) = \frac{\int_h^{h_b} \gamma[T(\xi),\ p(\xi), \nu]\, d\xi}{\cos\theta}, \tag{6}$$

and all other parameters are the same as before.

The measured antenna temperatures for the ascent and float part of Flights 152-P and 153-P are presented in Figs. VI-8 and VI-9. Inferences of the atmospheric temperature profile based on these antenna temperature measurements will be made in the future, and the inferred profile will be compared with the profile resulting from measurements made during ascent.

W. B. Lenoir

References

1. W. B. Lenoir, Quarterly Progress Report No. 79, Research Laboratory of Electronics, M.I.T., October 15, 1965, pp. 17-19.

2. W. B. Lenoir, Quarterly Progress Report No. 82, Research Laboratory of Electronics, M.I.T., July 15, 1966, pp. 36-41.

3. J. H. Van Vleck, Phys. Rev. 71, 413 (1947).

4. J. H. Van Vleck and V. F. Weisskopf, Rev. Mod. Phys. 17, 227 (1945).

5. M. L. Meeks and A. E. Lilley, J. Geophys. Res. 68, 1683-1703 (1963).

6. A. H. Barrett, J. W. Kuiper, and W. B. Lenoir, J. Geophys. Res. 71, 4723-4734 (October 15, 1966).

VII. SOLID-STATE MICROWAVE ELECTRONICS*

Academic and Research Staff

Prof. R. P. Rafuse
Dr. D. H. Steinbrecker

Graduate Students

J. Balecewicz
A. M. Davis
A. F. Hillman, Jr.

RESEARCH OBJECTIVES AND STATUS OF RESEARCH

The assembly of a precision S-band test set for varactor diodes is now under way. This test set will permit an evaluation of diode parameters to an accuracy of 1 part in 10^4. The test set consists of a dual-probe slotted line with a precision balancing circuit and a null receiver. By using two probes spaced approximately $\lambda/4$ apart and by adjusting the drive on each probe until the output is balanced, the VSWR may be read directly from the attenuation in the series with one probe. This technique obviates the problems of high dynamic range instrumentation and eliminates gain variations in the receiving apparatus. This test set will be used to characterize devices for use in high-order, high-power multipliers. Again, data reduction will be assisted by the use of a computer.

With the use of MOSFET transistors, a synchronous detector of high dynamic range has been constructed for use in some precision laboratory instrumentation. The dynamic range of this unit approaches 140 db. The output drift is of the order of a few microvolts over a period of several days.

Computer programs have been developed for the analysis of cascaded transmission-line filters and for the design of cascaded transmission-line impedance matching networks. An interesting result of this work was the discovery of an impedance matching network consisting of a one-eighth wavelength transformer and a one-quarter wavelength transformer that can be used to match any impedance to characteristic impedance of a feed line. This permits construction of microwave circuits in which the actual input impedance is unknown, in such a way that the impedance match can always be accomplished in a previously known length of transmission line. This technique hinges on the fact that any impedance can be transformed to a real impedance by a 1/8 wavelength transformer whose characteristic impedance is equal to the magnitude of the load impedance.

R. P. Rafuse

A. WORK COMPLETED

A thesis was completed during the past quarter. It covers the measurement and characterization of avalanche diode oscillators at KU-band and X-band. The major conclusion of this work is that the equivalent circuit of an impatt diode in the avalanche region is similar to that of a tunnel diode over a very wide frequency range. Details may be found in the thesis.[1]

R. P. Rafuse

*This work was supported by the National Aeronautics and Space Administration (Grant NGR-22-009-163).

References

1. A. M. Davis, "Characterization of a Microwave Negative Resitance Diode," S.M. Thesis, Department of Electrical Engineering, M.I.T., December 1966.

VIII. OPTICAL AND INFRARED SPECTROSCOPY*

Academic and Research Staff

Professor C. H. Perry

Graduate Students

Jeanne H. Fertel
D. J. Muehlner
J. F. Parrish
N. Tornberg

RESEARCH OBJECTIVES AND SUMMARY OF RESEARCH

The activities of this group have been concentrated on the study of the optical properties of solids determined by both infrared and Raman spectroscopy. This work is being extended to the study of low-frequency electronic and magnetic transitions in solids at liquid-helium temperatures.

1. Interferometric Spectroscopy[1,2]

The far infrared Michelson interferometer has been operating successfully over the wavelength range 25-1000 μ on a reasonably routine basis. A step-drive sampling interval is being considered and the frequency range has now been extended almost to 650 cm^{-1}. A 2^{12} bit analog-to-digital converter and a new lock-in amplifier are expected to yield more accurate intensity measurements so that full use can be made of the low-temperature bolometer.

References

1. C. H. Perry, R. Geick, and E. F. Young, Appl. Opt. 5, 1171 (1966).
2. C. H. Perry, "Solid-State Spectroscopy in the Far Infrared," Optical Society of America Annual Meeting, San Francisco, California, October 19-21, 1966 (Paper FC3).

2. Lattice Vibrations

a. Infrared Spectra of Solids

The far infrared instrumentation has been described in previous reports and publications.[1,2] Materials investigated have included BN;[3] CdSe;[4] Mg_2Sn;[5] NH_4Cl and NH_4Br;[6] $KTaO_3$;[7] M_2PdX_4, PdL_4X_2, and trans and cis isomers PdL_2X_2 (with $M = NH_4^+$, K^+, Rb^+ or Cs^+; $L = NH_3$; $X = Cl^-$, Br^- or I^-);[8] some ABF_3 fluoride perovskites[9] (with $A = K^+$ or Rb^+; $B = Mg^{2+}$, Ni^{2+}, Co^{2+}, Mn^{2+}, Zn^{2+}, and Mg_x^{2+} Ni_{1-x}^{2+}) and some

*This work was supported in part by the joint services Electronics Programs U.S. Army, U.S. Navy, and U.S. Air Force) under Contract DA 36-039-AMC-03200(E), the U. S. Air Force (ESD Contract AF19(628)-6066), and the Sloan Fund for Basic Research (M.I.T. Grant).

tektites.[10] A temperature-dependent study of the dielectric dispersion of some alkali halides and related ionic crystals continues and will include some mixed crystals of simple alkali halides. Some mixed semiconductors, ferroelectrics, antiferromagnetic materials and other organic solids will be investigated. We also propose to study condensed-phase gases.

b. Raman Spectra of Solids

The temperature-dependent Raman spectrum of NH_4Cl, ND_4Cl, NH_4Br,[11] $(Na_x K_{1-x}) TaO_3$,[12] $KTaO_3$,[13] and $SrTiO_3$ (see Sec. VIII-B) have been studied, and this work continues so that it can be complementary to the far infrared measurements. A Spectra-Physics 125 He/Ne laser is to be incorporated with the present spectrometer, and considerable improvement in signal-to-noise ratio and sample handling is to be expected. A new improved gas-flow Dewar system is being constructed for accurate low-temperature measurements in the region of various phase transitions.

C. H. Perry

References

1. C. H. Perry, Japan. J. Phys., Vol. 4, Suppl. 1, p. 564, 1965.
2. C. H. Perry, R. Geick and E. F. Young, Appl. Opt. 5, 1171 (1966).
3. R. Geick, C. H. Perry, and G. Rupprecht, Phys. Rev. 146, 543 (1966).
4. R. Geick, C. H. Perry, and S. S. Mitra, J. Appl. Phys. 37, 1994 (1966).
5. R. Geick, W. Hakel, and C. H. Perry, Phys. Rev. 148, 824 (1966).
6. J. F. Reintjes, Jr. and C. H. Perry, Symposium on Molecular Structure and Spectroscopy, Ohio State University, Columbus, Ohio, September 1966 (Paper U10); Quarterly Progress Report No. 82, Research Laboratory of Electronics, M. I. T., July 15, 1966, pp. 48-53.
7. C. H. Perry, EUCHEM FAR INFRA-RED Conference, Culham, England, September 12-16, 1966; T. F. McNelly and C. H. Perry, Quarterly Progress Report No. 83, Research Laboratory of Electronics, M.I.T., October 15, 1966, pp. 26-29; (this paper will appear in The Physical Review).
8. C. H. Perry, D. P. Athans, E. F. Young, J. R. Durig, and B. R. Mitchell, Quarterly Progress Report No. 81, Research Laboratory of Electronics, M.I.T., April 15, 1966, pp. 27-32; (this paper will appear in Spectrochimica Acta).
9. E. F. Young, Ph.D. Thesis, Department of Physics, M.I.T., August 1966; E. F. Young and C. H. Perry, Symposium on Molecular Structure and Spectroscopy, Ohio State University, Columbus, Ohio, September 6-10, 1966 (Paper U9); Quarterly Progress Report No. 83, Research Laboratory of Electronics, M. I. T., October 15, 1966, pp. 17-25.
10. C. H. Perry and J. D. Wrigley, Jr., Quarterly Progress Report No. 82, Research Laboratory of Electronics, M.I.T., July 15, 1966, pp. 45-48; (this paper will appear in Applied Optics).
11. J. R. Reintjes, Jr., S.B. Thesis, M.I.T., May 1966; J. F. Reintjes and C. H. Perry, Symposium on Molecular Structure and Spectroscopy, Ohio State University, Columbus, September 6-10, 1966 (Paper U10); Quarterly Progress Report No. 82, Research Laboratory of Electronics, M.I.T., July 15, 1966, pp. 48-53.
12. T. F. McNelly, S.B. Thesis, Department of Physics, M.I.T., May 1966.
13. T. F. McNelly and C. H. Perry, Symposium on Molecular Structure and Spectroscopy, Ohio State University, Columbus, Ohio, September 6-10 (Paper U11).

A. WORK COMPLETED

A thesis, entitled "Normal Vibrations of Cubic Fluoride Perovskites" was submitted by E. F. Young to the Department of Physics, M.I.T., August 1966, in partial fulfillment of the requirements for the degree of Doctor of Philosophy.

C. H. Perry

B. TEMPERATURE DEPENDENCE OF THE RAMAN SPECTRUM OF $KTaO_3$ AND $SrTiO_3$

1. Introduction

The Raman spectrum of single crystals $KTaO_3$ and $SrTiO_3$ have been observed from 30-1200 cm^{-1} frequency shift from the 22,938 cm^{-1} mercury "e" line over the temperature range 4-440°K. The room-temperature Raman spectrum of $SrTiO_3$ has been previously observed by Narayanan and Vedam,[1] and their results are in qualitative agreement with our measurements. Both $SrTiO_3$ and $KTaO_3$ are paraelectric cubic crystals at room temperature and apart from a slight structural change in $SrTiO_3$ at 110°K[2] no observation of the onset of ferroelectricity has been observed above a few degrees Kelvin. These crystals exhibit a Curie-Weiss law behavior,[3] however, and recent theories of ferroelectricity in perovskite crystals[5] have been confirmed experimentally for both of these crystals.[6-8]

The temperature-dependent Raman spectra observed in this work has been interpreted mainly as second-order spectra in both cases. The known cubic symmetry implies three first-order infrared active modes and one infrared and Raman inactive mode, together with the translational modes, none of which are first-order Raman active. Narayanam and Vedam[1] have erroneously interpreted their results as a first-order spectrum for $SrTiO_3$.

2. Experiment

The Raman spectrum was obtained on several different samples by using a Cary 81 spectrophotometer. A gas-flow technique, which has been described previously,[8] was used to obtain sample temperatures at 4-440°K. The spectra at various temperatures for $KTaO_3$ are shown in Fig. VIII-1, and for $SrTiO_3$ in Fig. VIII-2.

3. Discussion

The temperature-dependent spectra for $KTaO_3$ are surprisingly strong and complex. No correlation with the known infrared bands[9] could be seen, however, and the spectra have been interpreted as primarly second order. Table VIII-1

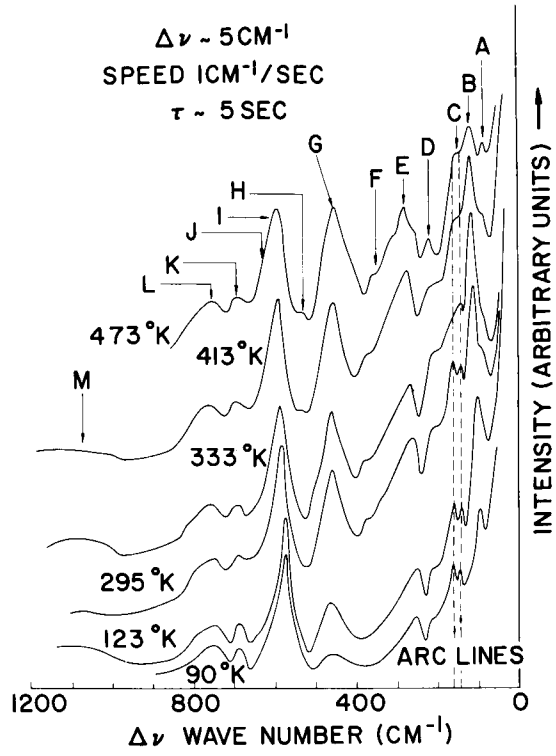

Fig. VIII-1. Spectra for $KTaO_3$ at various temperatures.

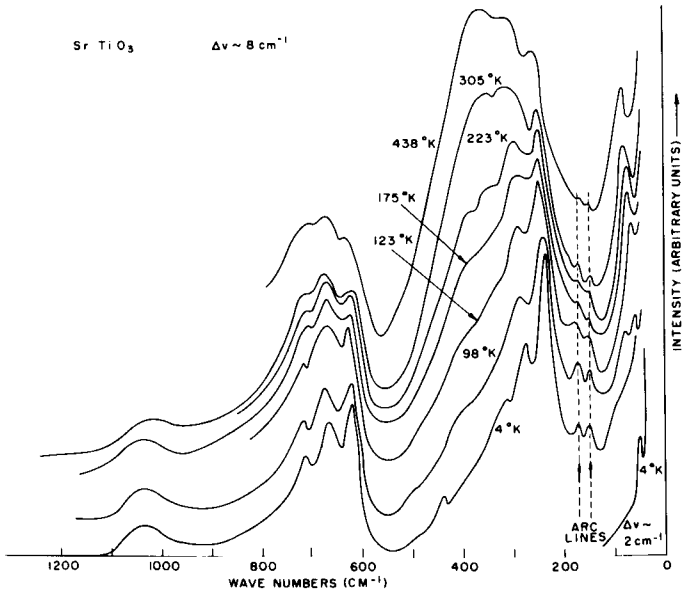

Fig. VIII-2. Spectra for $SrTiO_3$ at various temperatures.

shows the frequency dependence of the various peaks as a function of temperature. Of particular interest are the bands at ~125 cm^{-1} and 460 cm^{-1}. The intensity of the latter band decreases as the temperature is lowered, which indicates the presence of a difference band, whereas the intensity of the former band increases with a decrease in temperature, thereby showing a combination process. This effect is true for a number of other bands, although not to such a marked extent.

From Table VIII-1 it can be seen that most of the frequencies slowly increase with increasing temperature. This behavior is somewhat unusual but may be the influence of the "soft" ferroelectric mode which markedly lowers its frequency as the temperature is lowered toward the "Curie" temperature at 3°K.[8] All of the bands have been interpreted in terms of combinations of phonons at the edge of the Brillouin zone where both energy and momentum considerations can be satisfied and the density of states is high. The assignment of the multi-phonon peaks at 295°K are given in Table VIII-2, together with the averaged energies (in cm^{-1}) at the edge of the Brillouin zone.

Table VIII-1. Temperature dependence of the second-order Raman spectra of $KTaO_3$ (in cm^{-1}).

	90°K	123°K	295°K	333°K	348°K	413°K	473°K
A	–	–	–	100 ± 8sh	100 ± 8sh	100 ± 8	100 ± 8
B	105	110 ± 5	118 ± 5	120 ± 8	122 ± 8	127 ± 10	132 ± 10
C	–	–	–	160 ± 15sh	160 ± 15sh	160 ± 15sh	160 ± 15sh
D	230 ± 10sh	230 ± 10sh	230 ± 10sh	230 ± 10sh	230 ± 10sh	230 ± 10sh	233 ± 10
E	253 ± 5	256 ± 5	265 ± 5	268 ± 5	270 ± 5	277 ± 5	286 ± 5
F	–	–	370 ± 10sh	370 ± 10sh	370 ± 10sh	370 ± 10sh	370 ± 10sh
G	458 ±	458 ± 5	460 ± 5	460 ± 5	461 ± 5	463 ± 5	465 ± 5
H	–	–	–	–	–	530 ± 10sh	530 ± 10
I	580 ± 5	582 ± 5	587 ± 5	592 ± 5	592 ± 8	596 ± 10	598 ± 10
K	685 ± 15	686 ± 15	688 ± 15	693 ± 15	695 ± 15	695 ± 20	695 ± 20
L	750 ± 15	750 ± 15	760 ± 15	760 ± 15	765 ± 20	765 ± 20	770 ± 20
M		1100 ± 50	1100 ± 50	1100 ± 50	1100 ± 50		

sh = shoulder.

Table VIII-2. Assignment to the multi-phonon peaks at 295°K for $KTaO_3$.

	Observed (cm^{-1})	Calculated (cm^{-1})	Assignment
A	100	100	TO_2-LA
B	120	120	TA +LA
C	160	140	O_4-TO_2
		170	LO_2-LA
		170	LO_1-TO_2
D	230	225	TO_1-LA
		225	TO_2+TA
E	270	290	LO_2+TA
		275	TO_2+LA
F	375	360	TO_3-TO_2
G	460	465	TO_3-LA
H	530	530	LO_1+TO_2
I	590	585	TO_3+TA
		585	O_4+LO_2
		595	LO_1+LO_2
J	650	640	O_4+TO_1
		650	LO_1+TO_1
K	690	690	LO_1+ O_4
		705	LO_3+TA
L	760	740	TO_3+TO_2
		755	LO_3+LA
M	1100	1020	LO_3+TO_3
		1210	LO_3+LO_1

H at 473°K only.
J observed in IR only.
K and L observed in IR and Raman.

Average energies (in cm^{-1}) at the edge of the Brillouin zone.
TA 35 TO_1 310 TO_2 190 TO_3 540 O_4 330.
LA 90 LO_1 360 LO_2 255 LO_3 670.

Table VIII-3. Raman bands observed in $SrTiO_3$.

	4°K	78°K	98°K	123°K	175°K	223°K	305°K	438°K
A	45± 5	60±5		65± 5	65± 5	75± 5	80± 5	85± 5
B	63± 8	75±8						
C	85± 8							
D	235± 5		235± 5	240± 5	240± 8	240± 8	250±10	250±15
E	280± 5		285± 8	290±10	295±10	300±15	310±15	320±20
F	315±10		–	325±20	–	350±15	360±15	360±15
G	–		400±20	400±20	375±20	380±20	–	–
H	445± 5							
I	615± 5		620± 5	620± 8	625±10	620±10	620±10	630±10
J	670±10		675±10	675±10	680±10	675±10	675±10	680±10
K	720±10		720±10	720±10	715±10	715±10	720±10	715±10
L	1035±20				1035±20		1030±20	

Cowley[10] has discussed thoroughly the lattice dynamics and phase transitions in $SrTiO_3$, based on both experimental and theoretical studies. The frequency versus wave-vector dispersion curves for some of the normal modes were measured by neutron spectroscopy.[10]

The Raman spectra of $SrTiO_3$ as a function of temperature is shown in Fig. VIII-2 and is drastically different from that of $KTaO_3$.

The spectra consist of three main bands centered around 85, 320, and 640 cm^{-1}. The two broad bands show considerable structure and these smaller peaks are quite temperature-dependent. The highest frequency band appears to consist mainly of summation processes, whilst the central peak, from its marked temperature dependence, appears to consist of both sum and difference multi-phonon processes. The frequency-versus-temperature dependence is shown in Table VIII-3 and the assignments are given in Table VIII-4. In most cases, the interpretation has been made from the neutron dispersion curves given by Cowley.[10] Low-frequency bands observed in the spectra below the phase transition are not fully understood, however. The strongly temperature-dependent line (A) which occurs at 85 cm^{-1} at room temperature and which appears to lower to ~40 cm^{-1} at 4°K could be the first-order ferroelectric "soft" mode (TO_1) at the zone center, although the frequency dependence with temperature is not quite the same as that observed in the infrared and neutron measurements.[6,7] The other bands (B and C), shown at 78°K and 4°K close to the Rayleigh line, are probably due to additional first-order lattice modes appearing with the transition of the crystal to the tetragonal phase, or they may be caused by the crystal splitting up into small domains as proposed by Rimai and de Mars.[2] On the other hand, it is possible to attribute these bands to difference processes but it appears to be unlikely that they would still be present at liquid-helium temperatures.

The temperature dependence of the spectrum between 250 cm^{-1} and 410 cm^{-1} can be explained by assuming that difference multi-phonon processes occur in this region. Possible combinations are the following.

Observed	Assignment	Calculated (cm^{-1})
Broad Band 250-400 cm^{-1}	TO_3-TO_2	330
	LO_2-TO_2	360
	TO_3-LA	365
	LO_2-LA	395
	TO_3-TO_1	405
	TO_3-TA	410

Table VIII-4. Assignment to the multi-phonon peaks at 305°K for $SrTiO_3$.

	Observed (cm^{-1})	Calculated (cm^{-1})	Assignment
D	250	240	TO_1+TA
E	310	285	LA +TA
		290	LA +TO_1
		315	TO_1+TO_2 (in zone)
		320	TA +TO_2
		325	TO_1+TO_2
F	360	365	TO_2+LA
G	380[a]	385	LO_1+TA
		390	LO_1+TO_1
H	445[b]	430	LA +LO_1
		450	TA + O_4
		455	TO_1+ O_4
			LA + O_4^1
I	620	620	O_4+ O_4^1
J	675	670	TO_3+TA
		675	TO_3+TO_1
		680	LO_2+TA
		685	LO_2+TO_1
		695	LO_2+TA
K	720	725	LA +LO_2
L	1030	1025	LO_3+LO_1
		1050	LO_3+ O_4^1

[a] 98°K-223°K.
[b] 4°K.

Table VIII-4a. Average energies (in cm^{-1}) at the edge of the Brillouin zone.

TA – 120	LA – 165
TO_1 – 125	LO_1 – 265
TO_2 – 200	O_4^1 – 290
O_4 – 330	LO_2 – 560
TO_3 – 530	LO_3 – 760

In conclusion, it appears that these multi-phonon Raman spectra are extremely difficult to interpret with any certainty. Cowley's results for $SrTiO_3$ can be assigned, but there is a multiple choice in most cases. The results of the energies of the dispersion curves at the edge of the Brillouin zone for $KTaO_3$ are quite tentative. Consequently, one must await the complete neutron spectrum as a function of wave vector so that worth-while dynamical calculations can be made of the phonon dispersion curves. We would like to thank Professor A. Smakula and Dr. A. Linz of the Materials Center, M.I.T., for the samples.

C. H. Perry, Jeanne H. Fertel, T. F. McNelly

[Mr. T. F. McNelly is now in the Physics Department, Cornell University, Ithaca, New York.]

References

1. P. S. Narayanan and K. Vedam, Physik 163, 158 (1961).
2. L. Rimai and G. A. de Mars, Phys. Rev. 123, 702 (1962).
3. R. O. Bell and G. Rupprecht, Phys. Rev. 129, 90 (1963).
4. G. Rupprecht and R. O. Bell, Phys. Rev. 135, A748 (1964).
5. W. Cochran, Advances in Physics, Vol. 9, p. 387, 1960.
6. A. S. Barker and M. Tinkham, Phys. Rev. 125, 1527 (1962).
7. R. A. Cowley, Phys. Rev. Letters 9, 159 (1962).
8. C. H. Perry and T. McNelly, Quarterly Progress Report No. 82, Research Laboratory of Electronics, M.I.T., October 15, 1966, pp. 26-30.
9. D. B. Hall and C. H. Perry, Quarterly Progress Report No. 78, Research Laboratory of Electronics, M.I.T., pp. 51-61; Phys. Rev. Letters 15, 600 (1965).
10. R. A. Cowley, Phys. Rev. 134, A981 (1964).

IX. ULTRASONIC PROPERTIES OF SOLIDS*

Academic and Research Staff

Prof. C. W. Garland
Dr. D. B. Novotny

Graduate Students

P. E. Mueller
N. E. Schumaker
D. D. Snyder ET AL
B. B. Weiner
R. A. Young

RESEARCH OBJECTIVES

The general goal of our ultrasonic investigations is to obtain information about bulk systems near phase transitions or critical points. In particular, ultrasonic velocities give direct information about equilibrium thermodynamic properties and ultrasonic attenuation provides data about dynamical behavior. The majority of the work is concerned with order-disorder lambda transitions in solids, but other systems (such as a fluid near its critical point) are also being studied. During the past year, a variety of new projects have been started. The design and construction of special equipment is essentially complete for all of these, but detailed experimental results are not yet available. A brief statement of the objectives and progress in each area will be given.

Order-disorder transitions in NH_4Br are of interest, since two different ordered phases are known – a cubic, parallel ordering of NH_4^+ ions and a tetragonal, antiparallel ordering. High-pressure acoustic measurements on NH_4Br have been limited, in the past, by our inability to work below ~240°K. A new high-pressure cell and extensive modifications of the thermostat bath will permit work up to 6 kbar for temperatures constant within ±0.01° and as low as 120°K. In preparation for this work at lower temperatures, changes in transducer size, transducer-sample bonding, and hydraulic pressure fluid have all been made and tested. Most important, several large single crystals of NH_4Br have been grown and (when necessary) oriented and cut for acoustic work. Thus, the preparations are complete and experimental observations have now begun.

Our recent work on NH_4Cl indicates an instability and a first-order transition very close to the expected lambda point. The α-β quartz transition at 847°K is of the lambda type, and there are some indications that this transition may also show a first-order instability. As a precise check on this first-order character, velocity measurements are planned on ultrasonic waves that are not attenuated. Attenuation measurements on other waves are planned as a function of temperature and frequency. These data will provide information about the dynamical relaxation of long-range ordering near this cooperative transition. The principal experimental problems are related to the high temperature of this transition. A furnace and associated control equipment capable of maintaining the temperature constant to better than ±0.1°K has been built and is being tested. A buffer-rod, pulse-echo technique will be used, and a special sample holder is now complete. A large synthetic quartz crystal was obtained from Bell Telephone Laboratories, Inc. and has been oriented and cut into a variety of samples. High-temperature sealing materials are now being tested.

Present interest in the liquid-vapor critical point is very great, and work is in progress on xenon near its critical point at 16.6°C and 58 bar. Recent measurements on helium strongly suggest that the adiabatic sound velocity goes to zero at a critical point,

*This work is supported by the Joint Services Electronics Programs (U.S. Army, U.S. Navy, and U.S. Air Force) under Contract DA 36-039-AMC-03200(E).

in contradiction to the classical theoretical view that it will approach a finite minimum. We plan to measure the velocity for $\Delta T/T_c$ values as small as 3×10^{-6} (an order of magnitude better than the helium work) in order to test this behavior. Accurate acoustic attenuation measurements are also planned over a wide range of frequencies in order to obtain information about the dynamical response of a fluid near its critical point. The difficulties to be overcome are (a) the very high attenuation and therefore the small path lengths required, and (b) the need for excellent temperature and pressure stability. A bath temperature control of ±0.001°C can be achieved, and a quartz thermometer (capable of a resolution of better than 0.001°C) is available for measuring the sample temperature. Pressure stability of $\pm 5 \times 10^{-4}$ bar is expected, and the absolute value of p can be measured with an uncertainty of ±0.01 bar. Major work on a complex, variable-path, high-pressure cell is now complete and testing of this unit has begun. Components for an ultrasonic "sing-around" method are available and this is also being tested.

New ultrasonic attenuation work is just beginning on potassium dihydrogen phosphate (KDP) near its ferroelectric Curie point at ~120°K. Information obtained in the MHz range about the relaxation time of the polarization will be compared with higher frequency data obtained from laser work which is in progress elsewhere.

C. W. Garland

Publications

C. W. Garland, Book review of "Physics of High Pressures and the Condensed Phase," by A. van Itterbeek (ed.), Phys. Today 19, 126 (1966).

C. W. Garland and R. Renard, "Order-Disorder Phenomena I: Instability and Hysteresis in an Ising Model Near its Critical Point," J. Chem. Phys. 44, 1120 (1966).

R. Renard and C. W. Garland, "Order-Disorder Phenomena II: Elastic Constants of a Two-Dimensional Ising Model," J. Chem. Phys. 44, 1125 (1966).

C. W. Garland and R. Renard, "Order-Disorder Phenomena III: Effect of Temperature and Pressure on the Elastic Constants of Ammonium Chloride," J. Chem. Phys. 44, 1130 (1966).

C. W. Garland and C. F. Yarnell, "Temperature and Pressure Dependence of the Elastic Constants of Ammonium Bromide," J. Chem. Phys. 44, 1112 (1966).

C. W. Garland and C. F. Yarnell, "Order-Disorder Phenomena IV: Ultrasonic Attenuation near the Lambda Point in Ammonium Chloride," J. Chem. Phys. 44, 3678 (1966).

C. W. Garland and R. Renard, "Order-Disorder Phenomena V: Pippard Equations and the Phase Diagram for Ammonium Chloride," J. Chem. Phys. 45, 763 (1966).

C. W. Garland and R. Renard, "Ultrasonic Investigation of the Order-Disorder Transition in Ammonium Chloride," Critical Phenomena, Proceedings of a Conference held in Washington, D.C., April 1965, M. S. Green and J. V. Sengers (eds.), NBS Misc. Publ. 273, December 1966, p. 202.

C. W. Garland and N. E. Schumaker, "Effect of Ordering on the Infrared Spectrum of Ammonium Chloride" (in press).

X. GEOPHYSICAL RESEARCH

A. High Magnetic Fields*

Academic and Research Staff

Prof. F. Bitter
Prof. G. Fiocco

Graduate Students

S. J. Bless

RESEARCH OBJECTIVES

The approach to the problem of producing megagauss fields by capacitor discharge has been changed from the conventional one of using a single-turn coil in which the magnetic pressure is directed outward, to the use of a Z-pinch in which the magnetic field surrounds a short straight conductor, and the magnetic pressure is directed inward. The reasons for this change follow.

1. The stored capacitor energy is first converted almost entirely into magnetic energy, and not simultaneously into kinetic energy, because of explosion. A very modest installation, 20 kJ, can produce fields of several megagauss.

2. If the current carrying rod is sufficiently large (a few millimeters in our installation), it is only partly evaporated by a discharge, and the factors influencing performance can be quantitatively studied. In particular, the amount of material melted and evaporated, and the temperatures reached by the current-carrying sheath, called the M-M (metal-megagauss) interface, can be investigated.

3. In certain ranges, the pressure produced by the Z-pinch may be useful for solid-state studies.

The apparatus is to consist of eight 15-μf capacitors operated at 20 kV, connected through spark gaps to the periphery of 2 reinforced metal plates, 3 ft in diameter. They are shorted at the center by replaceable rods of variable length and diameter.

Preliminary experiments with only 4 or 5 of the capacitors used have produced moderately damped discharges with 1/4 period of approximately 1 μsec. A field of 1.5 Mgauss is estimated to have been produced around a Mo rod, 1 cm long and 0.4 cm in diameter.

It is interesting to note that approximately 15 kJ/cc are required to evaporate copper or steel, whereas discharges of this magnitude have passed through rods having a total volume of ~0.25 cc apparent melting and evaporating over only a thin surface layer, ~0.05 cm. Further study is needed to determine how the capacitor energy is dissipated. It is possible that it goes to heating the M-M interface. Further experiments along this line are contemplated during the next few months with the completed apparatus.

An interesting research program in which the methods described above for producing megagauss fields could be used would be to test the theoretical predictions in the paper "High Energy Electromagnetic Conversion Processes in Intense Magnetic Fields" by Thomas Erber, Rev. Mod. Phys. 38, 626 (1966).

F. Bitter, G. Fiocco

*This work is supported in part by the Joint Services Electronics Programs (U.S. Army, U.S. Navy, and U.S. Air Force) under Contract DA 36-039-AMC-03200(E).

X. GEOPHYSICAL RESEARCH

B. Upper Atmospheric Physics*

Academic and Research Staff

Prof. G. Fiocco
Dr. G. W. Grams
Dr. Sharda Nand

Graduate Students

J. B. DeWolf
D. F. Kitrosser
H. C. Koons

RESEARCH OBJECTIVES AND SUMMARY OF RESEARCH

Much of the research in our group is concerned with the properties and use of coherent light in connection with problems of atmospheric physics. The NASA trailer has been instrumented as a mobile laboratory for research in atmospheric optics and contains the optical radar, as well as other instrumentation.

For about a year, we have been analyzing the results of measurements carried out with the optical radar during 1964 and 1965. These measurements provide profiles of the optical backscattering cross section of the atmosphere as a function of altitude and are interpreted to supply information on the dust content of the atmosphere from 10 km to 150 km. The analysis of a large sample of the stratospheric data has been completed and will be published soon. These observations of the stratospheric aerosols were made at Lexington, Massachusetts, during the two-year study and also at College, Alaska, in the summer of 1964.

The data have been compared with various meteorological parameters associated with conditions in the lower stratosphere. A significant negative correlation between fluctuations of dust and ozone has been found in the measurements.

At present, we are concerned with the reduction of data in the 35-150 km range. Although difficulties in the reliable operation of a semiautomatic digitizer have slowed down the data reduction, we hope to complete the reduction early in 1967.

We expect to be able to study the mesospheric dust content, its possible relation to the electron recombination in the D-region, as well as the possible influx of micrometeoric materials and its relation to E-region ionization.

With regard to the first problem, we are interested in the possibility of simultaneously performing dust density measurements by optical radar and electron density measurements by rocket, and are considering collaborative efforts with other groups.

The production of ionization by micrometeorites have been investigated for a simple model based on the acceleration of upper atmospheric molecules by incoming micrometeorites and the successive neutral-neutral ionizing collisions. It is found that a conservative value of 4×10^3 tons/day for the influx rate of cosmic dust on Earth is sufficient to produce ionization in amounts found in the E-region at night; since there is still no satisfactory explanation for the formation of the E-region at night, this is probably a significant result. The results of this will be submitted for publication.

*This work is supported principally by the National Aeronautics and Space Administration (Grants NGR-22-009-131 and NGR-22-009-(114)), and in part by the Joint Services Electronics Programs (U.S. Army, U.S. Navy, and U. S. Air Force) under Contract DA 36-039-AMC-03200(E).

Another aspect of the role of dust in the upper atmosphere with which we are concerned, at present, is its relation with rainfall; we have correlated fluctuations of stratospheric dust amounts with the occurrence and amounts of precipitation, but, thus far, we have been unable to find a relationship. We expect to extend the investigation to include mesospheric dust and thus check the validity of Bowen's hypothesis.

Essential to the interpretation of the optical radar data is the availability of theoretical backscattering cross sections for spheres and ensembles of spheres with specified size distributions. We have extended existing computations to cover a wide range of complex values for the refractive index and have considered a variety of size distributions. The computations are almost complete, although we are facing the task of a meaningful yet compact presentation of the data.

We shall also extend the computations to cover scattering angles different from 180°; these tables will be of use in interpreting photometric and visual observations of scattering from the zodiacal light and from atmospheric stratifications, as well as an aid in estimating the feasibility of forward-scattering optical communication links.

Some estimate will also be carried out of the effects of various aerosol distributions over the response of the Dobson photometric technique for the measurement of atmospheric ozone.

During the summer 1966, the optical radar was taken to Norway to continue the investigation of noctilucent clouds which was initiated in 1964. Several noctilucent displays have been observed and we have collected a very large amount of data that is now being analyzed.

An important advantage of the optical radar technique when applied to noctilucent clouds is that, since our observations are performed at night as well as at twilight, we should be able to describe the development of the cloud when no other techniques of observation are available. From the 1964 data we inferred the possibility of substantial vertical motion for the cloud, and hope with present data to be able to substantiate the earlier findings.

The stratospheric aerosol layer was also observed continuously in Norway during the summer 1966; we intend to draw a comparison with activity in the previous years and establish the presence of a latitudinal gradient in the concentration which was suggested in the earlier work.

An OH airglow meter that utilizes photon counting techniques is being developed and was also operated in Norway during observation of noctilucent clouds. The importance of studying OH is based on (a) its role in the dissociation of H_2O (H_2O is possibly a major constituent of noctilucent clouds), (b) the fact that the excitation of the rotational-vibrational bands of OH probably reflects the ambient temperature of the mesophere, and (c) the relation between OH and Na airglow activity. We are designing a multichannel photometer to scan simultaneously several airglow lines.

Another area of interest in our group is the measurement of atmospheric temperatures by the broadening of laser radiation backscattered by air molecules. We have theoretically analyzed and partially implemented schemes for heterodyne and homodyne detection, as well as more conventional schemes utilizing optical filtering, and we are now assembling a system consisting of a high-power Ar^+ laser of high spectral purity, and a pressure-scanned Fabry-Perot interferometer.

We are now becoming interested in the generation of high power at the wavelength of optical transitions of atmospheric gases; the possibility exists that, because of resonant scattering, cross sections would be greatly enhanced, thereby enabling observation of the presence of even minor constituents in the upper atmosphere and in the laboratory. We are carrying out experiments to explore the practicality of carrying out observations at the following wavelengths: 6560.1 Å(He^+), 3582 Å(N_2^+),

6707.9 (Li), 5973 (O_2), 5889 (Na), 7698.9 and 7665.9 (K), as well as other transitions.

It would appear that it is possible to generate high outputs at these wavelengths by the combination of Raman effects, second-harmonic effects, and thermal tuning of laser light. The possibility of measuring the linewidth of resonant transitions in laboratory plasmas, by tuning the laser to a specific transition, suggests a method for the measurement of the concentration, as well as the temperature, of ionic species.

Further work on the laser scattering-diagnostic technique for plasmas, first developed in this laboratory, is now being carried out. We are making observations of incoherent scattering of pulsed ruby laser light in a reflex discharge and modifying the system to study the possibility of observing scattering from a CW Ar^+ laser light; the use of a relatively low-power, continuous source would be a great advance in the practicality of this diagnostic tool.

G. Fiocco

1. POSSIBLE RELATION BETWEEN DUST AND RAINFALL

Since the nucleating properties of dust provide a mechanism for starting the condensation of water vapor, the vagaries of weather might be somewhat related to fluctuations of the dust content of the atmosphere. Bowen[1,2] has furnished evidence that peaks in average amounts of daily rainfall followed, with approximately one month time lag, the dates of known meteor showers; this suggests that meteor showers influence world rainfall.

These results have been the object of controversy (see, among others, Martyn,[3] Kleine and Brier,[4] and Rosinski and Pierrard[5]). One criticism is that, because of the large variety of sizes expected in the dust influx and of the resultant difference in settling velocities, it would appear difficult to preserve the necessary coherence in the vertical transport process to determine detectable effects.

We have made observations of the dust content of the atmosphere at Lexington, Massachusetts, for almost 2 years, in 1964 and 1965, and data related to the stratospheric dust content are now available. The data were obtained by observing with an optical radar the echoes backscattered by atmospheric constituents and comparing their intensities with the returns that one would obtain from a dust-free atmosphere (see Fiocco and Grams,[6] and Grams and Fiocco[7]).

The optical radar technique is particularly sensitive to particles in the size range ~0.1-1 μ radius, since a transmitted wavelength, $\lambda = 0.094\ \mu$, is utilized. This is the typical spectrum of particle sizes obtained in the stratosphere by balloon and aircraft collections.

The dust content of the stratosphere during the period of study was an order of magnitude larger than usual, because of the injection of volcanic material following the eruption of Mt. Agung, in 1963. It is therefore doubtful whether any of the features of the stratospheric aerosol layer at the time of observation could be attributed to the

influx of extraterrestrial dust.

Since our study has provided us with a record of the stratospheric dust content and its fluctuations, we have correlated the relative dust amounts at heights of 12 km and 16 km with the daily amount of precipitation averaged among 103 stations in New England,[8] in order to establish whether some relationship with rainfall might exist. Although the stratospheric dust smounts are probably not related to meteoric activity, one might expect the incursion of stratospheric dust into the upper troposphere to affect the amount of rainfall, regardless of the source. The time scale for stratospheric-tropospheric exchange is difficult to specify, however, since such processes are, at best, only poorly understood. The times involved in the vertical diffusion from the lower stratosphere to the upper tropopause may be several weeks (Junge et al.[9]). The length of time necessary to introduce stratospheric dust into the troposphere makes it almost naive to assume that a correlation between the two local parameters might be found. Our study of the stratospheric dust layer (Grams and Fiocco,[7]) indicated a degree of persistence of stratospheric dust amounts involving time periods of almost a week. Assuming a wind velocity of 20 m/sec, one may estimate the length scale of a stratospheric dust "cloud" to be of continental dimensions. This lends considerably more justification for comparing the rainfall figure for the New England states with the stratospheric dust

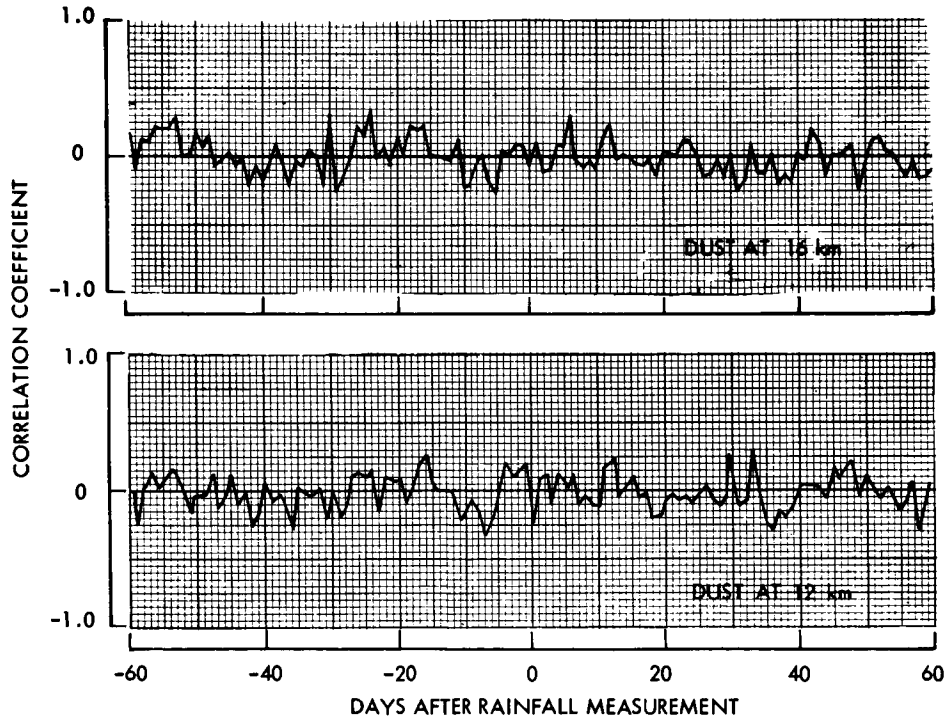

Fig. X-1. Correlation coefficient for rainfall and stratospheric dust measurements as a function of time lag.

measurements carried out at Lexington, Massachusetts.

The curves in Fig. X-1 show the correlation coefficient as a function of the time lag between the measurements of the dust content at different heights and the averaged measurements of rainfall. The correlation coefficients have been computed by using approximately 60 pairs of data. Although small positive peaks are apparent for time lags of 15-25 days, these might be ascribed to the limited size of our statistical sample. No evident trend exists to indicate a correlation between the two physical quantities.

Such correlations are only indirectly a test of Bowen's hypothesis. In order to establish a meteoric effect on rainfall, we should perhaps try to correlate mesospheric amounts of dust with rainfall. In fact, the mesospheric amounts of dust should be related to meteoric influx, and a local measurement of it should exhibit more global features than a local measurement of stratospheric dust. Data related to the mesosphere have also been collected and will be available for such analyses at a future data.

G. Fiocco, G. W. Grams

References

1. E. G. Bowen, "The Influence of Meteoric Dust on Rainfall," Australian J. Phys. 6, 490-497 (1953).
2. E. G. Bowen, "The Relation between Rainfall and Meteor Showers," J. Meteorol. 13, 142-151 (1956).
3. D. F. Martyn, "Comments on a paper by E. G. Bowen entitled 'The Influence of Meteoric Dust on Rainfall'," Australian J. Phys. 7, 358-364 (1954).
4. D. B. Kleine and G. W. Brier, "A Note of Freezing Nuclei Anomalies," Mon. Wea. Rev. 86, 329-333 (1958).
5. J. Rosinski and J. M. Pierrard, "On Bowen's Hypothesis," J. Atmos. Terrestr. Phys. 24, 1017-1030 (1962).
6. G. Fiocco and G. Grams, "Observation of the Aerosol Layer at 20 km by Optical Radar," J. Atmos. Sci. 21, 323-324 (1964).
7. G. Grams and G. Fiocco, "The Stratospheric Aerosol Layer during 1964 and 1965" (submitted to the Journal of Geophysical Research).
8. Hourly Precipitation Data, New England, U.S. Department of Commerce, Weather Bureau, Vols. 14 and 15, 1964 and 1965.
9. C. E. Junge, C. W. Chagnon, and J. E. Manson, "Stratospheric Aerosols," J. Meteorol. 18, 81-108 (1961).

XI. GRAVITATION RESEARCH*

Academic and Research Staff

Prof. R. Weiss

Graduate Students

S. Ezekiel
G. D. Blum

RESEARCH OBJECTIVES

Research in this group is concerned with an experimental investigation of gravitational interaction. Present emphasis is directed toward the experimental consequences of a scalar gravitational interaction, different versions of which have been proposed by Dicke, Jordon, and Nordstrom. In these theories the local value of G, the Newtonian gravitational "constant," can be interpreted as the scalar field variable that becomes a function of the mass distribution surrounding the observer. Two experimental approaches are under consideration.

1. The development of a stable gravimeter to measure annual, and possibly epochal, variations in g, the gravitational field at the surface of the earth. The experiment was described in Quarterly Progress Report No. 77 (page 59). The measurements of g will depend on geophysical factors that must be crosscorrelated to the gravimeter output. Progress in the development of the instrument itself has been disappointing. The main difficulty lies in the geometry of the plate, which is levitated to achieve an unambiguous relation between the Stark transition frequency observed in the molecular beam and the force on the plate. Measurements performed with the originally proposed plate configuration give the ratio

$$\text{Force/Frequency} = K\left(1 + \alpha \frac{d}{d_o}\right),$$

where d is the plate spacing, d_o the fiducial separation. The coefficient $\alpha \sim 10^{-3}$, which is due to the fringing field, is too large by a factor of 100 to allow use of this plate configuration in the experiment. Other plate configurations have been considered, and some of them look promising. Work on the gravimeter has been temporarily suspended.

2. A more direct experiment to search for evidence of a scalar gravitational field is a test for a violation of the strong principle of equivalence. If gravitational and atomic oscillators are placed in an artificial satellite, with the entire system put into free fall toward the sun, the period of one oscillator relative to the other would change by an amount

$$\frac{\Delta\tau}{\tau} \approx \frac{GM_s}{Rc^2},$$

where M_s is the mass of the sun, R the distance between the satellite and the sun, and $\Delta\tau/\tau \sim 10^{-8}$ at 1/10 A.U. Work has begun on the design and construction of an electrostatically suspended torsional gravitational oscillator which is insensitive to tidal forces.

Experiments in gravitation tend to engender advances in instrumentation. An adjunct to the gravimeter program was the development of a long-term stable Earth strain seismometer to try to measure radius changes of the Earth. The basic problem here appears to be the inadequate long-term stability of existing lasers. One of the major efforts of the research in this group is the frequency stabilization of a laser with an optical resonance as observed in an atomic beam used as reference. This has been discussed in Quarterly Progress Report No. 80 (pages 22-23). Since then, several matches between

*This work was supported by the Joint Services Electronics Programs (U.S. Army, U.S. Navy, and U.S. Air Force) under Contract DA 36-039-AMC-03200(E).

existing laser lines and optical resonances that could be observed in atomic or molecular beams have been uncovered. Construction of an atomic-beam magnetic-resonance apparatus has just been completed to exploit a match between an Argon laser line and a magnetic dipole transition in Rubidium.

R. Weiss

A. EXPERIMENTAL TEST OF THE FREUNDLICH RED-SHIFT HYPOTHESIS

A laser interferometer sensitive to 5×10^{-9} of a fringe shift has been employed to test the Freundlich photon-photon scattering hypothesis. This hypothesis was designed to give an alternative explanation to the observed Hubble "red shift" of the galaxies, which is usually attributed to a recessional Doppler shift. Our experiment, which will be published in the Physical Review, showed that 6328°A photons suffered a $\Delta\nu/\nu < 2 \times 10^{-19}$ frequency shift on traversing an X-band radiation field of 3×10^{16} photons/cm^3, 100 cm long. The Freundlich hypothesis would have anticipated $\Delta\nu/\nu \sim 10^{-14}$ for a 3°K cosmic black-body temperature.

G. Blum, R. Weiss

B. MEASUREMENT OF METASTABLE VERSUS GROUND-STATE ELECTRON EXCHANGE CROSS SECTIONS FOR HELIUM AND NEON

In connection with our program on laser frequency stabilization using an atomic beam as a primary frequency reference,[1] measurements of metastable vs ground-state

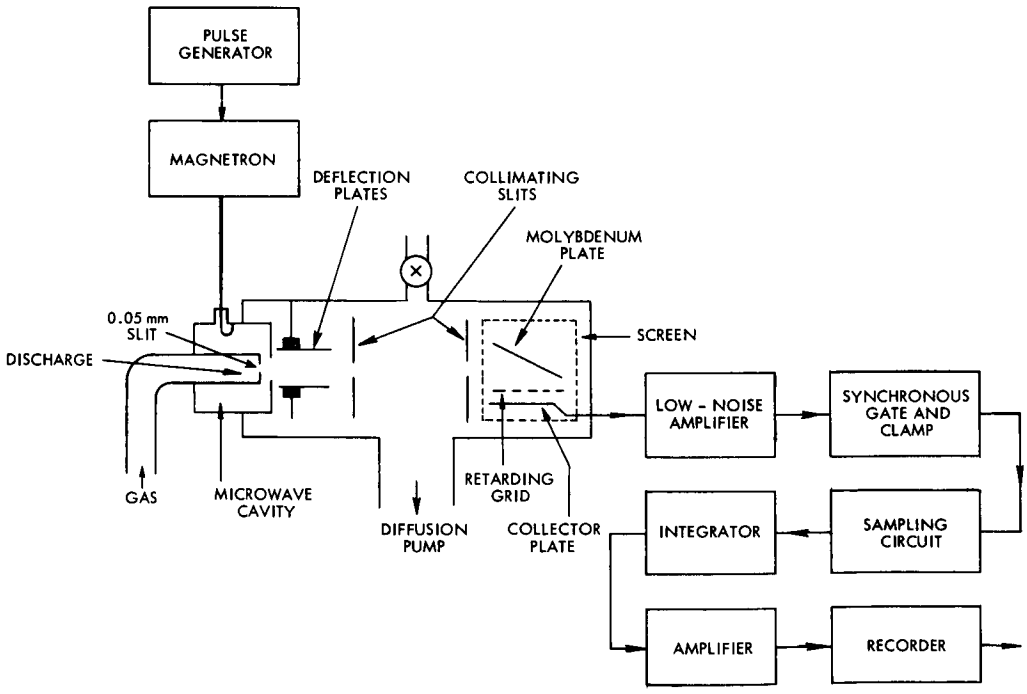

Fig. XI-1. Atomic beam apparatus.

electron exchange cross sections for Helium and Neon have been carried out.

The atomic beam apparatus is shown in Fig. XI-1. Metastables of Helium and Neon are formed in a short discharge tube inside an X-band cavity driven by a QK61 magnetron. Ground-state and metastable atoms effuse through a slit, 0.05-mm wide × 4 mm high × 0.25 mm thick, formed by cementing two soft glass microscope slides onto a soft glass tube with solder glass. Charged particles that come out through the slit are swept out of the beam by deflection plates. Two suitably placed slits farther down the apparatus define the atomic beam. Metastables were detected by electron ejection on a molybdenum surface. The ejected electrons were collected by a stainless-steel plate connected to a low-noise, high-input impedance amplifier. A time-of-flight technique was used to separate metastables from the energetic UV photons coming out of the discharge tube. The discharge was pulsed at a rate of 1000 times per second with a pulse duration of 0.2 msec.

Figure XI-2 shows typical detector data obtained with Helium and Neon metastables.

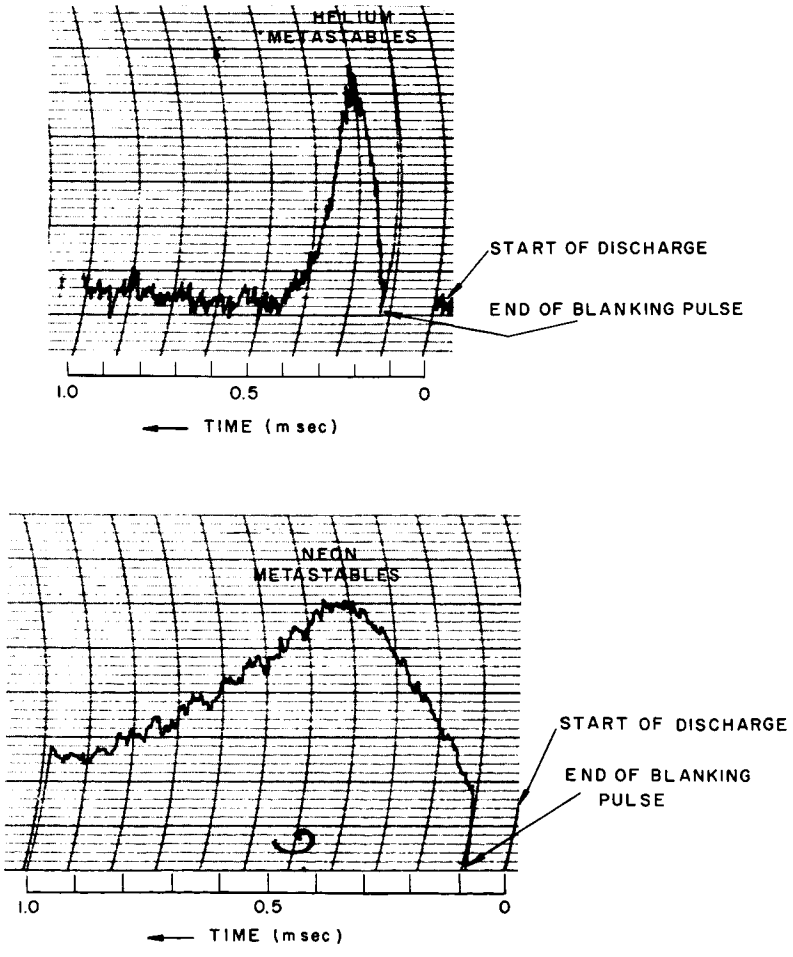

Fig. XI-2. Detector data obtained with the He and Ne metastables.

Metastable vs ground-state electron exchange cross sections were determined by introducing ground-state atoms into the beam chamber and noting the attenuation in the number of metastables with increase in pressure in the chamber. A plot of $\log_e$ (intensity of metastables received at the detector) vs apparatus pressure is shown in Fig. XI-3.

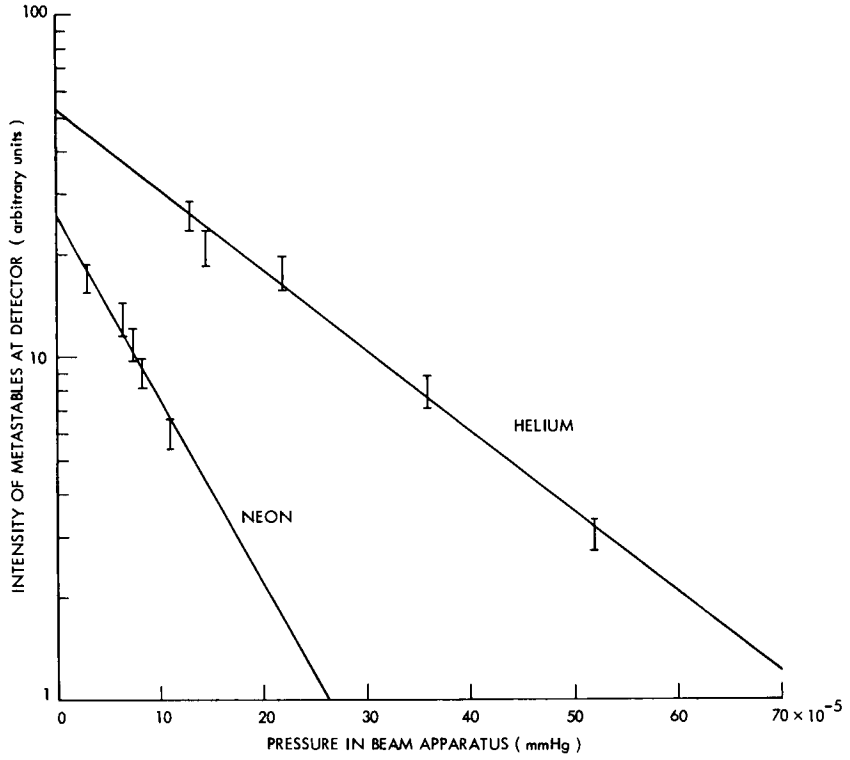

Fig. XI-3. Plot of $\log_e$ (intensity of metastables received at the detector) against apparatus pressure.

The cross sections were found to be 6.8×10^{-15} cm^2 for Helium, and 1.6×10^{-14} cm^2 for Neon. The peak number of metastables leaving the discharge tube was estimated to be 2×10^{12} per second at a discharge pressure of 1.3 mm Hg for Helium, and 6×10^{12} per second at a discharge pressure of 0.8 mm Hg for Neon. The ratio of metastables to ground-state atoms leaving the discharge was 1×10^{-5} for Helium, and 8×10^{-5} for Neon.

In these measurements no effort was made to separate the $2s\ ^3S$ and $2s\ ^1S$ metastable states in Helium, and the $1s_5$ and $1s_3$ metastable states in Neon. An optical absorption was observed, however, in Neon $1s_5$ which could be used in discriminating the Neon $1s_5$ from $1s_3$.

S. Ezekiel

References

1. S. Ezekiel and R. Weiss, "Long-Term Frequency Stabilization of a Laser Employing a Molecular or Atomic Beam as Primary Frequency Reference," Quarterly Progress Report No. 80, Research Laboratory of Electronics, M.I.T., January 15, 1966, pp. 22-23.

XII. NOISE IN ELECTRON DEVICES*

Academic and Research Staff

Prof. H. A. Haus
Prof. R. P. Rafuse

Graduate Students

J. T. Patterson

RESEARCH OBJECTIVES

Our research is concentrated in three areas: noise at optical frequencies, noise in frequency multipliers, and noise in parametric amplifiers.

The past experimental investigation of noise in optical lasers has led to the development of measurement techniques that enable one to discern the amplitude spectrum of incident light with high spectral resolution. These techniques are being developed to study diffusion speeds of small scatterers in liquid suspensions. The same techniques are under study for possible application to detection of microwave acoustic noise vibrations.

H. A. Haus, R. P. Rafuse

*This work is supported by the Joint Services Electronics Programs (U.S. Army, U.S. Navy, and U.S. Air Force) under Contract DA 36-039-AMC-03200(E).

XIII. MAGNETIC RESONANCE*

Academic and Research Staff

Prof. J. S. Waugh
Dr. R. A. Hoffman
Dr. R. E. J. Sears

Graduate Students

J. D. Ellett
W. E. Good
A. Leonardi-Cattolica
D. Mattison
J. D. Ramshaw
D. W. Schaefer
C. H. Wang

RESEARCH OBJECTIVES

1. Nuclear Spin Interactions in Solids

We are investigating a variety of rather elaborate transient NMR experiments whose general aim is to add to the information obtainable about spin interactions in solids. For example, we have shown that by applying RF and DC magnetic fields of appropriate intensities, directions, and time sequences it is possible to measure: (a) a modified fourth moment for dipolar interactions, (b) a modified sixth moment for dipolar interactions, and (c) small chemical shifts in the presence of large dipolar interactions.

2. Nuclear Relaxation and Inelastic Scattering in Gases

We have completed a study of nuclear relaxation in H_2-He mixtures and related it to the anisotropic H_2-He intermolecular potential by means of quantum-scattering calculations. Similar work is now being carried on in HCl-He, ^{13}CO-He, and other systems.

3. Kerr Effect in Nonideal Gases

We are setting up an apparatus for accurate measurement of the Kerr electro-optical effect and equation of state in gases. The nonidealities displayed in these experiments are related to the intermolecular potential, and are expected to give new information about its anisotropic part. The first experiments are being conducted in HCl.

J. S. Waugh

*This work is supported by the Joint Services Electronics Programs (U.S. Army, U.S. Navy and U.S. Air Force) under Contract DA 36-039-AMC-03200(E).

XIV. X-RAY DIFFRACTION STUDIES*

Academic and Research Staff

Prof. B. E. Warren

Graduate Students

R. L. Mozzi

RESEARCH OBJECTIVES

The work of this group is centered on the development and application of x-ray diffraction methods for studying (a) imperfections in crystalline materials, and (b) the structure of amorphous materials.

The present studies of the structures of amorphous materials make use of two improvements over the older methods. By utilizing fluorescence excitation in the detector, it is possible to measure the intensity of the unmodified scattering with the Compton component removed. This makes it possible to obtain significant data out to sin θ/λ values which are twice the previous limit, and this results in radial distribution functions with twice the earlier resolution. By making the interpretation in terms of "pair functions," it is possible to have an exact and rigorous interpretation that is free from the earlier approximations such as considering the different scattering factors as proportional to one another. It is necessary to make corrections for multiple scattering, and a rigorous treatment of this problem has been completed.[1] The present work is concentrated on the structures of simple glasses, such as SiO_2, B_2O_3, GeO_2, Na_2O-B_2O_3, and Na_2O-SiO_2.

B. E. Warren

References

1. B. E. Warren and R. L. Mozzi, Acta Cryst. 21, 459 (1966).

*This work is supported by the Joint Services Electronics Programs (U.S. Army, U.S. Navy, and U.S. Air Force) under Contract DA 36-039-AMC-03200(E).

XV. 3 PHYSICAL ELECTRONICS AND SURFACE PHYSICS* 6

Academic and Research Staff

Prof. 6 R. E. Stickney
Dr. M. L. Shaw

Graduate Students

F. W. Eberle
D. L. Fehrs
J. W. Gadzuk ET AL 8
W. Greaves
H. C. Juvkam-Wold
D. S. Shupe
S. Yamamoto

RESEARCH OBJECTIVES

The general purpose of our research program is to investigate the interaction of electrons, ions, atoms, molecules, and electromagnetic radiation with solid surfaces. At present, we are concentrating on the following problems.

1. Adsorption of Gases and Vapors on Solid Surfaces

The work function of a thermionic cathode may be altered by allowing certain gases or vapors to adsorb upon the surface. Our theoretical and experimental studies are concerned primarily with the adsorption of oxygen and/or cesium on single-crystal refractory metal surfaces. We are attempting to relate the change in work function and desorption energy to the coverage, crystallographic structure, and bare work function of the substrate.

2. Catalysis and Oxidation

Using mass spectrometric techniques, we are investigating the catalytic formation of ammonia on iron and the oxidation of tungsten. Our principal objective is to determine the dependence of these reactions on temperature, pressure, and material properties.

3. Scattering of Gas Atoms and Molecules from Solid Surfaces

Recently, we have developed a simple classical theory for the collisions of atoms and molecules with solid surfaces. The results predict the scattering pattern and energy and momentum transfer. A quantum-mechanical model has also been investigated. In addition to continuing these theoretical approaches, we now are developing an experimental apparatus for measuring the scattering patterns.

4. Photoinduced Surface Processes

Measurements of the photoelectric emission from solids provides us with an additional means of studying surfaces. We plan to determine the photoelectric properties of single-crystal surfaces that are partially covered with adsorbed atoms. Along this same line, we shall look for the existence of photoinduced ion emission from cesiated surfaces.

R. E. Stickney

26 25

*This work was supported by the National Aeronautics and Space Administration (Grant NGR-22-009-091), the M. I. T. Cabot Solar Energy Fund, and the Joint Services Electronics Programs (U. S. Army, U. S. Navy, and U. S. Air Force) under Contract 25 DA 36-039-AMC-03200(E). END

A. CONTACT POTENTIAL MEASUREMENTS OF THE ADSORPTION OF O_2 ON (110) Ta

1. Introduction

During the past two years, we have developed an experimental apparatus for measuring the change in contact potential resulting from the adsorption of various chemical elements on metallic surfaces.[1] We shall report results recently obtained for the adsorption of O_2 on (110) Ta. These results are particularly interesting because they are contrary to the majority of previous experimental results and existing theoretical predictions.

2. Apparatus

Since the apparatus has been described in detail elsewhere,[1] only the major features will be mentioned here. To avoid contamination by background gases the apparatus was mounted within a large Varian ultrahigh vacuum system. With a combination of ion pumping, liquid-nitrogen cryopumping, and titanium sublimation pumping, the background pressure during these runs could be maintained in the mid 10^{-11} Torr range ($\sim 4\text{-}5 \times 10^{-11}$ Torr).

The specimen studied was a tantalum ribbon, $0.0025 \times 0.127 \times 3.0$ cm, mounted upon a rotatable shaft. The ribbon was cut from a larger specimen which, when received, was reported to have a surface oriented in the (110) direction. Unfortunately, the exact orientation of the specimen used in the present study has not yet been determined by x-ray diffraction. The surface was cleaned by direct resistive heating to ~2500°K, with occasional flashes to ~2750° K.

Changes of substrate work function, because of oxygen adsorption, have been measured by the contact-potential method. For this measurement the target was positioned before a simple electron gun. To insure the constant-emitter conditions required by the contact-potential method, the gun filament was continually run at ~2100° K. As well as measuring changes in the surface work function, it was possible to measure the thermionic work function of the bare surface at a thermionic measurement station.

A diffusion leak was used to flood the system to the desired oxygen pressure. The maximum static pressure that could be obtained in the presence of all available pumping was $\sim 10^{-7}$ Torr.

A series of auxiliary runs utilized a General Electric Company monopole partial pressure analyzer. This made it possible to determine the composition of the background gas and, more important, to check the purity of the oxygen admitted by the diffusion leak.

3. Experimental Method and Procedure

The theory, advantages, and limitations of the contact-potential method have been adequately discussed elsewhere[1-3] and will only be briefly mentioned here. Basically we have two electrodes, the electron gun filament and the (110) tantalum target, which form a diode. If we maintain constant conditions at the emitter (electron gun filament), then any changes in the current-voltage characteristic of the diode are due to changes in the properties of the collector (110 Tantalum). In particular, the simple theory of a thermionic diode shows that a voltage shift of the Boltzmann portion of the current-voltage plot will be equal to the change of the collector work function if the reflection coefficient remains constant. The reference point, from which changes are measured, is the current-voltage plot taken when both electrodes are clean.

In this study the experimental method was implemented by the following procedure. After a clean current-voltage plot had been obtained, the diffusion leak was turned on and the system allowed to reach a steady O_2 pressure. Once this steady pressure had been reached, the target was flash-cleaned and current-voltage plots were made as a function of time.

Since these plots could only be taken at 300°K, it was desirable to consider also the effect of target temperature upon the adsorption process. Unfortunately, it was not possible to make the work function-time measurements at elevated temperatures. Instead, we could only study the effect of temperature during the time of adsorption. A few runs were made in which the surface was exposed to the same total oxygen flux, but with the surface maintained at different temperatures (always higher than 300°K) during the time of adsorption. After the adsorption interval, the system was pumped back to the 10^{-11} Torr range and the surface cooled to 300°K. The current-voltage plots were then taken at room temperature.

In addition to oxygen adsorption runs, a few oxygen desorption runs were made. In these a certain oxygen coverage was established, and then the system was pumped back to the 10^{-11} Torr range. The surface was then flashed to some temperature for 15 sec and, upon cooling to 300° K, a current-voltage plot was taken. The 15-sec flashes were continued by stepping the temperature to a higher value each time until the clean surface plot was finally obtained. These runs enabled us to check the reversibility of the data and to estimate the desorption energy of oxygen on (110) Ta.

4. Experimental Results

a. Thermionic Work Function

Measurements of thermionic emission from the target were used to calculate the effective work function.[3] A value of $\phi_o = 4.73 \pm 0.01$ eV was obtained for 5 measurements in the temperature range ~1570°K to ~2360°K.

b. Mass Spectrometer Measurements

When the total pressure was in the mid 10^{-11} Torr range, mass spectrometer analysis of the background gas showed the major components to be H_2O (~18%), He (~16%), CO (~13%), O (~13%), and CO_2 (~10%). Present in smaller amounts were OH, H, Ne, O_2, and H_2. We believe that O, H, and OH are produced in the spectrometer as a result of dissociation and/or desorption induced by electron bombardment.

The oxygen diffusion leak was analyzed at two different steady-state oxygen pressures. At an oxygen pressure of $\sim 10^{-9}$ Torr, none of the background contaminant peaks, such as CO and CO_2, showed any perceptible increase over the initial background values. The temperature of the diffusion leak was increased until a steady-state pressure of $\sim 10^{-7}$ Torr was established. At this pressure the only significant components were O_2, O, and CO. The combination of O and O_2 formed approximately 97% of the total pressure, and CO formed approximately 3%. These results indicate, particularly at lower oxygen pressures, that contamination from such components as CO should not be a major problem.

c. Oxygen Adsorption on (110) Ta

In Fig. XV-1, a portion of the results for oxygen adsorption are shown in the form of work-function change as a function of oxygen exposure. The oxygen exposure is

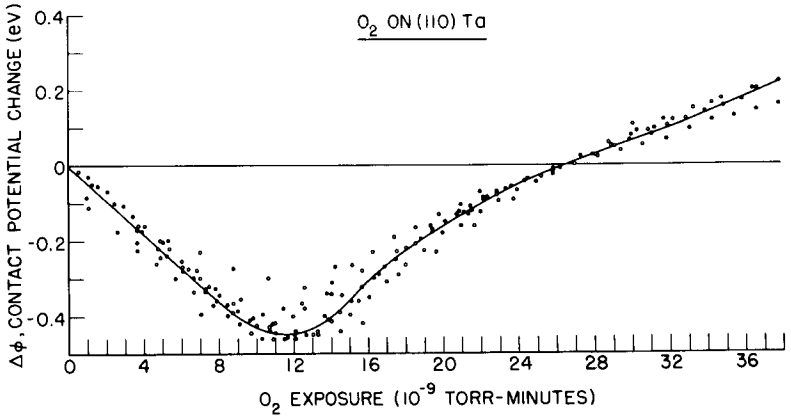

Fig. XV-1. Experimental data for oxygen adsorption on (110) Ta at 300°K; low exposure region.

defined simply as the product of oxygen pressure times the time. In terms of the actual integrated particle flux, an exposure of 1×10^{-9} Torr-minutes, for example, is equal to 4.27×10^{13} oxygen atoms/cm^2.

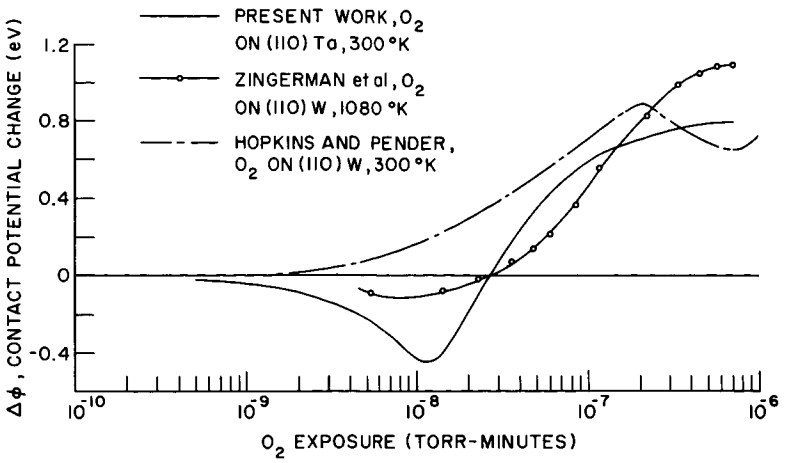

Fig. XV-2. Experimental data for oxygen adsorption on (110) Ta at 300°K compared with data for oxygen on (110) tungsten.

For clarity, only the extreme values of the data and the average curve are shown in Fig. XV-1. The actual plot contains approximately 200 points from 8 separate runs. Also, Fig. XV-2 does not represent the raw data, for there has been some attempt to correlate the raw data and reduce initial scatter that occurred primarily because of inaccuracies of pressure measurement. The correlation has been achieved by multiplying the curve for each run by a factor that would make the curve pass through $\Delta\phi = 0$ at an exposure of $\sim 27 \times 10^{-9}$ Torr-minutes. In the raw data the exposure at which $\Delta\phi$ went to zero ranged from 23 to 30×10^{-9} Torr-minutes, and the average value was $\sim 27 \times 10^{-9}$ Torr-minutes. As we shall see, an interesting comparison can be made between this arbitrary correlation point and other recently published data.

The most interesting feature of the data is that below exposures of 27×10^{-9} Torr-minutes, oxygen adsorption produces a decrease in the work function of the surface. The curve shows a minimum at an exposure of $\sim 12 \times 10^{-9}$ Torr-minutes where the work function has decreased by ~0.45 eV. Though most of the runs in Fig. XV-2 were made at oxygen pressures in the low 10^{-9} Torr range, two runs were made in the middle to high 10^{-8} Torr range, and the points fell within the extremes shown in Fig. XV-2. To insure that the decrease in work function was not due to oxygen adsorption upon the electron-gun filament, this filament was usually flashed to ~2500° K during the course of a run. No effect was ever seen, thereby indicating that the filament remained uncontaminated. Beyond an exposure of $\sim 40 \times 10^{-9}$ Torr-minutes there are data from only 3 runs. These data are fairly consistent, however, and their average is included in Fig. XV-2, which covers the entire exposure range. Beyond $\sim 27 \times 10^{-9}$ Torr-minutes the work function increases, at first rapidly and then more slowly, tending toward a plateau where the work function has increased by ~0.8 eV.

d. Oxygen Desorption from (110) Ta

The results of one desorption run are shown in Fig. XV-3 where the change in work function (always related to the clean surface) is plotted as a function of the temperature of the consecutive 15-sec flashes. Although the quantitative reproducibility of the desorption runs was rather poor in the plateau region of the curve, the qualitative

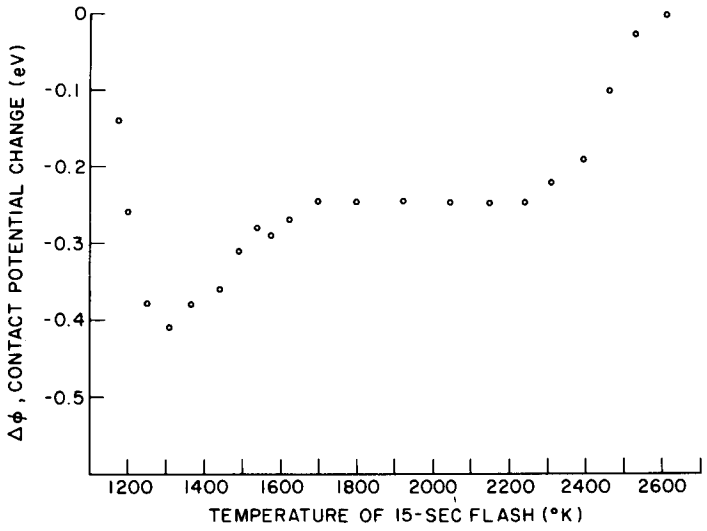

Fig. XV-3. Experimental data for oxygen desorption from (110) Ta.

features were consistently reproduced. In particular, the flashing procedure always reproduced the negative $\Delta\phi$ region of the curve. Also, the negative $\Delta\phi$ always remained up to ~2600°K, where the clean surface was restored. This, then, may indicate a reversibility for the adsorption process. Also, the high-temperature portion has been used to estimate the desorption energy for oxygen on (110) Ta. An assumption of first-order kinetics (i.e., that the oxygen desorbs as atoms[4]) gives a desorption energy of ~6 eV or ~138 kcal/mole.

e. Elevated-Temperature Runs

Wheras the desorption data were obtained in an attempt to determine the effect of temperature on an existing adsorbed film, the data shown in Fig. XV-4 resulted from attempts to investigate the effect of elevated temperature on the adsorption process. Runs were made at ~1000°, 1175°, and 1430°K. At each temperature, the surface was subjected to an oxygen exposure of $\sim 11 \times 10^{-9}$ Torr-minutes. After exposure, and upon cooling to 300°K, the resulting work-function change was measured. In Fig. XV-4 the results show the work-function change as a function of surface temperature during adsorption.

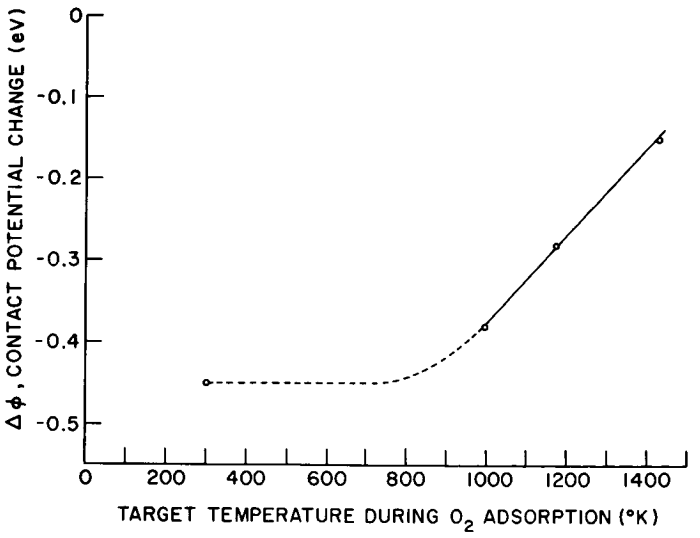

Fig. XV-4. Contact potential change at 300°K as a function of surface temperature during adsorption.

Although the data are insufficient to allow us to draw definite conclusions, two points may be noted. First, for an exposure of 11×10^{-9} Torr-minutes, the work function is observed to decrease for all temperatures in the range 300°-1430°K. Second, the absolute value of the change decreases with increasing temperature. With regard to the first point, it was expected initially that the occurrence of the work-function reduction was due to a metastable state which might disappear at higher temperatures. The results shown in Figs. XV-3 and XV-4 indicate that this expectation may be incorrect. Concerning the second point, there are several possible explanations, and only the simplest will be mentioned here. As may be seen in Fig. XV-1, an exposure of 11×10^{-9} Torr-minutes is near the minimum of the curve at 300°K. If fewer particles remain on the surface at higher temperatures, we would expect from Fig. XV-1 that the absolute value of $\Delta\phi$ would decrease. There are two major possibilities for less oxygen remaining at higher temperatures. First, the sticking probability[5] for oxygen upon tantalum may decrease with temperature; and second, significant desorption and/or migration of oxygen may occur at higher temperatures. Judging from the desorption data of Fig. XV-3, and owing to the lack of any theoretical or experimental data to support the plausibility of the first hypothesis, the desorption and/or migration hypothesis seems to be more reasonable.

f. Comparison with Existing Data

In Fig. XV-2, the data are compared with two recent sets of data for oxygen adsorption upon (110) tungsten. The data of Hopkins and Pender,[6] obtained at 300°K by the Kelvin technique, show a work-function change that is always positive. On the other

hand, the data of Zingerman and co-workers,[7] obtained at 1080°K by the same technique used in our work, are qualitatively similar to our data. Initially, there is a slight decrease in the work function, followed later by an increase. Since Zingerman et al. did not know the intensity of their oxygen beam, it was not possible to assign a quantitative exposure scale. For qualitative comparison only, a scale was assigned by making their data pass through zero at an exposure of 27×10^{-9} Torr-minutes.

Germer and May[8] have recently published data from a low-energy electron-diffraction (LEED) study of oxygen adsorption upon (110) tungsten. Several interesting inferences may be drawn from their data:

1. It appeared that, even at 300°K, oxygen adsorption occurred by reconstruction such that the oxygen occupied substitutional sites in the surface lattice.

2. Average oxygen sticking probabilities at 300°K were inferred for the ranges 0-1/2 monolayer, 1/2-3/4 monolayer, and 3/4-1 monolayer of oxygen. (A monolayer is defined as 1.425×10^{15} atoms/cm^2.) For 0-1/2 monolayer the average value was ~0.6; for 1/2-3/4 monolayer it fell sharply to ~0.003; and for 3/4-1 monolayer it fell to less than 0.003.

3. The half-monolayer structure occurred at an oxygen exposure of $\sim 27 \times 10^{-9}$ Torr-minutes. As shown in Figs. XV-1 and XV-2, our present data for oxygen on (110) Ta indicate that $\Delta\phi$ passes through zero at this value of exposure. At present, it is not clear whether this point is mere coincidence or a matter of physical significance.

g. Comparison of Results with Theoretical Predictions

The data are unusual, in that oxygen adsorption on the (110) Ta initially produces a decrease in the work function. With the use of the concept of electronegativity,[9] oxygen adsorption should lead to a dipole moment that is directly proportional to $X_{Ta} - X_o$, the difference in the electronegativities of tantalum and oxygen. Since X_o is ~3 eV and X_{Ta} is ~1.2-1.6 eV,[10] the formation of a negative dipole leading to an increase in the work function would be expected. The data obviously violate this simple electronegativity model. A similar violation has also been observed in our recent study of nitrogen adsorption upon (110) Ta. Also, studies of oxygen adsorption upon (110), (100), and (111) nickel[11] and nitrogen adsorption upon (100) and (110) tungsten[10] violate this principle.

A possible reason for this violation can be seen most clearly in the work of Farnsworth and Park[12] for oxygen adsorption upon (110), (100), and (111) nickel. On the basis of LEED, contact potential, and photoelectric measurements, they concluded that, with sufficient temperature activation, the work function decreased for lower coverage structures. Up to the formation of a certain high-coverage structure, the photoelectric data closely followed the Fowler plot for metals, thereby indicating that the oxygen-nickel binding was not extremely ionic. Also, once the high-coverage structure was

reached, and data failed to fit the Fowler plot, thereby indicating a change to a more ionic type of binding.

D. L. Fehrs, R. E. Stickney

References

1. D. L. Fehrs and R. E. Stickney, "Report on Twenty-Sixth Annual Conference on Physical Electronics, Massachusetts Institute of Technology, Cambridge, Mass., March 21-23, 1966," p. 287; D. L. Fehrs and R. E. Stickney, Quarterly Progress Report No. 82, Research Laboratory of Electronics, M.I.T., July 15, 1966, p. 77.
2. P. A. Anderson, Phys. Rev. 47, 958 (1935).
3. W. B. Nottingham, Thermionic Emission, Technical Report 321, Research Laboratory of Electronics, M.I.T., December 10, 1956.
4. S. Glasstone, K. J. Laidler, and H. Eyring, The Theory of Rate Processes, (McGraw-Hill Book Company, New York, 1961).
5. G. Ehrlich, Ann. N.Y. Acad. Sci. 101, 722 (1963).
6. B. J. Hopkins and K. R. Pender, Surface Sci. 5, 155 (1966).
7. Ya. P. Zingerman, V. A. Ishchuk, and T. A. Krutilina, Soviet Phys. – Solid State 7, 2078 (1966).
8. L. H. Germer and J. W. May, Surface Sci. 4, 452 (1966).
9. L. Pauling, The Nature of the Chemical Bond (Cornell University Press, Ithaca, N. Y., 3rd rev. ed., 1960).
10. T. A. Delchar and G. Ehrlich, J. Chem. Phys. 42, 2686 (1964).
11. H. E. Farnsworth, "Report on Twenty-Fifth Annual Conference on Physical Electronics, Massachusetts Institute of Technology, Cambridge, Mass., March 24-26, 1965," p. 140.
12. R. L. Park and H. E. Farnsworth, J. Appl. Phys. 35, 2220 (1964).

B. DESORPTION AND MIGRATION KINETICS OF MOLECULES ADSORBED ON NONUNIFORM SURFACES: STEADY-STATE ANALYSIS

1. Introduction

The rate of desorption of atoms and molecules from solid surfaces is a significant factor in a variety of engineering problems. For example, this rate often limits the performance of composite thermionic cathodes, the efficiency of catalytic processes, and the speed of surface oxidation. The practical importance of these applications has served to stimulate many experimental and theoretical investigations of desorption.[1-3]

The majority of the existing analytical treatments of desorption are based on the assumption that the surface properties are uniform over the entire specimen. For polycrystalline specimens, however, it is known that this assumption leads to unsatisfactory results in detailed analyses of similar processes, such as thermionic emission[4-6] and

surface ionization.[6, 7] The results of our recent experimental investigation of oxygen desorption from single-crystal tungsten[8] have led us to attempt to develop a more exact desorption theory for patchy (for example, polycrystalline or nonuniform) surfaces. The first case that we have considered is that of steady-state desorption, and the analysis of a simple model is presented here. After refining this treatment, we plan to consider next the more general problem of flash (that is, transient) desorption.[1]

2. Theoretical Model

To simplify this preliminary analysis we shall adopt a model that is based on a great number of assumptions, many of which may easily be refined or omitted in the final development. Here we shall concentrate on the inclusion of surface patches in the model.

Consider a two-patch model of a cylindrical wire having a circumference 2W, where W is the width of each patch. The distance from the center of patch 1 around the wire is denoted by x. For a given atomic adsorbate, patches 1 and 2 have desorption energies V_1 and V_2, migration energies E_1 and E_2, adatom frequencies of vibration ν_1 and ν_2, adsorbed atom densities n_1 and n_2, and circumferential spacing between adsorption sites a_1 and a_2. (See Fig. XV-5.) The boundary between the two patches is assumed

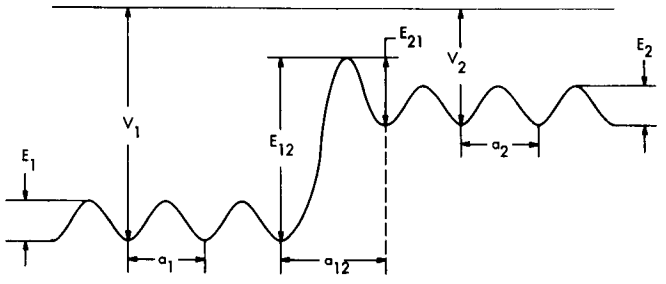

Fig. XV-5. Potential energy diagram for the two-patch model.

to have an energy barrier, with E_{12} and E_{21} being the barrier potentials for an atom migrating from patch 1 to patch 2 and vice versa. The distance between adsorption sites for an atom crossing the boundary is a_{12}. The probability that an atom with sufficient energy to migrate will actually do so is represented by A, where A is assumed to be only a function of surface geometry.

The linear particle flux across the boundary from patch 1 to 2, i_{12}, is given by

$$i_{12} = A_{12} n_1 \left(\frac{W}{2}\right) a_1 \nu_1 e^{-E_{12}/kT}, \tag{1}$$

where $e^{-E_{12}/kT}$ is the probability of an adatom having energy E_{12} or greater, and

$n_1\left(\frac{W}{2}\right) a_1$ is the linear atom density on patch 1 at the boundary. Likewise, the flux form patch 2 to 1 is

$$i_{21} = A_{21} n_2\left(\frac{W}{2}\right) a_2 \nu_2 \, e^{-E_{21}/kT}. \tag{2}$$

The net linear flux then is $i_{12} - i_{21}$.

If now the boundary is considered to lie in patch 1 and E_1 is the migration potential, the expression for the net flux across patch 1 at x is

$$i_1 = A_1 n_1(x)\, a_1 \nu_1 \, e^{-E_1/kT} - A_1 n_1(x+a_1)\, a_1 \nu_1 \, e^{-E_1/kT} \tag{3}$$

$$i_1 = -A_1 a_1^2 \frac{dn_1}{dx} \nu_1 \, e^{-E_1/kT}. \tag{4}$$

The desorbed flux j_i is given by

$$j_1 = n_1(x)\, \nu_1 \, e^{-V_1/kT}, \tag{5}$$

where the probability of an adatom having sufficient energy to escape the surface is given by $e^{-V_1/kT}$, the number of particles per unit area is $n_1(x)$, and the number of attempts made per second is ν_1. From this equation we get

$$n_1(x)\, \nu_1 = j_1 \, e^{V_1/kT} \tag{6}$$

which may be substituted in $(i_{12} - i_{21})$ and i_1:

$$i_{12} - i_{21} = e^{\frac{V_1 - E_{12}}{kT}} (a_1 A_{12} j_1 - a_2 A_{21} j_2) \tag{7}$$

$$i_1 = -A_1 a_1^2 \, e^{\frac{V_1 - E_1}{kT}} \frac{dj_1}{dx}. \tag{8}$$

Here the relation $V_1 - E_{12} = V_2 - E_{21}$ has been used (see Fig. XV-5). The steady-state continuity equation for a control area of width a_1 at point x on patch 1 is

$$i_1(x) + a_1 j_o = i_1(x+a_1) + a_1 j_1, \tag{9}$$

where j_o is the incident flux. This becomes

$$j_o = j_1 + \frac{i_1(x+a) - i_1(x)}{a_1} = j_1 + \frac{di_1}{dx}. \tag{10}$$

Defining λ_1 and λ_2 as

$$\lambda_1^2 = a_1^2 A_1 \, e^{\frac{V_1 - E_1}{kT}} \tag{11}$$

$$\lambda_2^2 = a_2^2 A_2 \, e^{\frac{V_2 - E_2}{kT}} \tag{12}$$

and substituting the derivative of Eq. 4 in Eq. 10 yields

$$j_o = j_1 - \lambda_1^2 \frac{d^2 j_1}{dx^2} \tag{13}$$

$$j_o = j_2 - \lambda_2^2 \frac{d^2 j_2}{dx^2}. \tag{14}$$

Their solutions are

$$j_1 = j_o\left(1 + a_1 \cosh \frac{x - x_1}{\lambda_1}\right), \qquad -\frac{W}{2} \leq x \leq \frac{W}{2} \tag{15}$$

$$j_2 = j_o\left(1 + a_2 \cosh \frac{x - x_2}{\lambda_2}\right), \qquad \frac{W}{2} \leq x \leq \frac{3W}{2}. \tag{16}$$

Since patch 1 is symmetric about x = 0, and patch 2 is symmetric about x = W, the fluxes are

$$j_1 = j_o\left(1 + a_1 \cosh \frac{x}{\lambda_1}\right), \qquad -\frac{W}{2} \leq x \leq \frac{W}{2} \tag{17}$$

$$j_2 = j_o\left(1 + a_2 \cosh \frac{x - W}{\lambda_1}\right), \qquad \frac{W}{2} \leq x \leq \frac{3W}{2} \tag{18}$$

The constants a_1 and a_2 are determined by the boundary conditions

$$i_1\left(\frac{W}{2}\right) = i_{12} - i_{21} = i_2\left(\frac{W}{2}\right). \tag{19}$$

The resulting expressions for the fluxes are

$$\frac{j_1 - j_o}{j_o} = \frac{(A_{21}a_2 - A_{12}a_1) \cosh \frac{x}{\lambda_1}}{\lambda_1 \sinh \frac{W}{2\lambda_1}\left(\frac{A_{21}a_2}{\lambda_2 \tanh \frac{W}{2\lambda_2}} + \frac{A_{12}a_1}{\lambda_1 \tanh \frac{W}{2\lambda_1}} + e^{-\frac{(V_1 - E_{12})}{kT}}\right)} \tag{20}$$

$$\frac{j_2 - j_o}{j_o} = - \frac{(A_{21}a_2 - A_{12}a_1) \cosh \frac{x - W}{\lambda_2}}{\lambda_2 \sinh \frac{W}{2\lambda_2} \left(\frac{A_{21}a_2}{\lambda_2 \tanh \frac{W}{2\lambda_2}} + \frac{A_{12}a_1}{\lambda_1 \tanh \frac{W}{2\lambda_1}} + e^{-\frac{(V_1 - E_{12})}{kT}} \right)} \tag{21}$$

In the limit of small patches with $W \ll \lambda_{1,2}$ the fluxes are given by

$$\frac{j_1 - j_o}{j_1} = \frac{A_{21}a_2 - A_{12}a_1}{A_{21}a_2 + A_{12}a_1 + \frac{W}{2} e^{-\frac{(V_1 - E_{12})}{kT}}} \tag{22}$$

$$\frac{j_2 - j_o}{j_2} = - \frac{A_{21}a_2 - A_{12}a_1}{A_{21}a_2 + A_{12}a_1 + \frac{W}{2} e^{-\frac{(V_1 - E_{12})}{kT}}} \tag{23}$$

Thus we see that different fluxes from different planes are predicted. At present, we are considering the validity of applying the principle of detailed balance in problems of surface migration.

F. W. Eberle, R. E. Stickney

References

1. G. Ehrlich, "Modern Methods in Surface Kinetics: Flash Desorption, Field Emission Microscopy, and Ultrahigh Vacuum Techniques," Advances in Catalysis, Vol. 14, p. 255 (Academic Press, New York, 1963).
2. D. O. Hayward and B. M. W. Trapnell, Chemisorption (Butterworths Ltd., London, 2d edition, 1964).
3. G. C. Bond, Catalysis by Metals (Academic Press, New York, 1962).
4. W. B. Nottingham, "Thermionic Emission," Technical Report 321, Research Laboratory of Electronics, M.I.T., December 10, 1956.
5. C. Herring and M. H. Nichols, "Thermionic Emission," Rev. Mod. Phys. 21, 185 (1949).
6. L. N. Dobretsov, "Electron and Ion Emission," NASA Technical Translation, NASA TT F-73, 1952.
7. E. Ya. Zandberg and N. I. Ionov, "Surface Ionization," Soviet Phys. – Tech. Phys. 67, 255 (1959).
8. W. Engelmaier and R. E. Stickney, "Thermionic and Adsorption Characteristics of a Single-Crystal Tungsten Filament Exposed to Oxygen," Report on Twenty-sixth Annual Conference on Physical Electronics, Massachusetts Institute of Technology, Cambridge, Mass., March 21-23, 1966, p. 260.

C. SINGLE-PHONON ENERGY TRANSFER BETWEEN MOLECULAR BEAMS AND SOLID SURFACES

[This report summarizes a paper that will appear in The Physical Review.]

The quantum-mechanical lattice theory in thermal accommodation coefficient theory is approached from the same point of view as the lattice theory of neutron scattering and Mössbauer effects. Treating the surface atoms from a displacement field theoretic point of view, rather than from the customary single-particle point of view, is more consistent with other solid-state theories. Virtual phonon processes occurring in the field formulation give rise to a nontrivial modification in existing single-phonon accommodation coefficient theories. This modification takes the form of a pseudo Debye-Waller factor.

When the existing theoretical accommodation coefficients are modified by the pseudo Debye-Waller factor, it is found that the resulting accommodation coefficient, obtained herein, displays trends similar to experimental data for helium scattering off of tungsten.

J. W. Gadzuk

D. THEORY OF ATOM-METAL INTERACTIONS

[This report summarizes two papers that will appear in Surface Science.]

1. ALKALI ATOM ADSORPTION

The interaction of a metal with an alkali atom is considered from first principles. It is shown that treating the interaction of the metal with the alkali atom through perturbation theory is a meaningful approach. It is seen that the interaction causes a shift and broadening of the valence level of the alkali atom. Furthermore, it is seen that electron transitions between virtual atomic and metal states are formally equivalent to standard rearrangement processes.

The first-order ns energy-level shift of the alkalis is calculated and the results given in standard form. The shift is found to be $\sim +0.3$ eV. The natural broadening of the originally discrete ns level is calculated in closed form by using time-dependent perturbation theory. The theoretical bandwidth for an alkali atom adsorbed on a metal is found to be $\lesssim 1$ eV.

These results are discussed in relation to previously suggested values for the shifted and broadened level.

It is found that the position of the shifted and broadened level relative to the conduction band of the metal is such that ionic bonds are formed between adsorbate and substrate. The possibility and implications of localized electrons in the interior of the metal near the surface and also around the alkali ion cores are discussed. It is found

that electrons do tend to localize at the surface in the presence of alkali ion cores. The resulting surface dipoles are then discussed in relation to their effects on electron emission properties of the surface. Temperature dependences are included in a semi-quantitative manner, and the origin of thermal depolarization effects is displayed.

J. W. Gadzuk

2. ONE-ELECTRON TRANSITION MATRIX ELEMENTS

The matrix element describing a process in which an electron makes a transition from an atomic s state to a metal conduction band state is considered from the point of view of a rearrangement process. Since the initial and final states are not solutions of the same Hamiltonian, they are not orthogonal. It is shown that by orthogonalizing the initial and final stages, it is possible to obtain a simple, compact matrix element that describes electron transitions between the atom and metal states.

The matrix element is explicitly evaluated for a transition between a hydrogen-like atom and a free electron metal. These closed form results have been previously used to describe alkali-atom adsorption on metals. The present results could also be used to describe resonance ionization of atoms or neutralization of ions by metals.

J. W. Gadzuk

XVI PHYSICAL ACOUSTICS*

Academic and Research Staff

Prof. K. U. Ingard
Prof. L. W. Dean III

Graduate Students

R. H. Katyl
J. L. Macon
W. M. Manheimer ET AL
J. A. Ross
H. M. Schulz III

RESEARCH OBJECTIVES

Our general objective involves the study of the emission, propagation, and absorption of acoustic waves in matter. Specific areas of present research in fluids include generation, propagation, and amplification of sound waves in ionized gases and interaction of acoustic waves with coherent light beams.

K. U. Ingard

A. ELECTRIC FIELD ASSOCIATED WITH A SOUND WAVE IN A WEAKLY IONIZED GAS

Until the present time, it has been believed that an ordinary sound wave in a weakly ionized gas is characterized by equal velocity perturbations in the three fluid components (neutrals, ions, electrons). What actually happens, even for wavelengths much larger that the Debye length, is that the thermal motion of the electrons results in an incomplete screening of the electric fields associated with perturbations in ion density, so that the ions are subjected to competing electrical and collisional forces. The velocity perturbations are, in fact, related by the expressions

$$v_i = v_n\left[1 + \frac{i\omega(T_e/\gamma_n T_n)}{\omega_{in} + m_e\omega_{en}/m_n}\right]^{-1} \equiv v_n[1+ix]^{-1} \tag{1}$$

and

$$v_i = v_e\left[1 + \left(\frac{k}{k_D}\right)^2\right]. \tag{2}$$

Here, (k/k_D) is the ratio of the electronic Debye length to the wavelength, which is assumed to be much less than unity, (T_e/T_n) is the ratio of electron temperature to gas temperature, which is assumed to be much greater than unity, (m_e/m_n) is the ratio of electron mass to neutral mass, γ_n is the specific heat ratio for the gas, and ω_{in} and

*This work was supported principally by the U.S. Navy (Office of Naval Research) under Contract Nonr-1841(42).

ω_{en} are the collision frequencies for ions and electrons, respectively, in the neutral gas. Under usual discharge conditions, the ions and neutrals are seen by (1) to be 45° out of phase for frequencies $\omega/2\pi \sim 10^2$-10^3 Hz. The expressions are somewhat more complicated if one assumes a nonisothermal electron gas or a ratio $T_e/T_n \sim 1$, but the general conclusions remain unchanged.

Equations 1 and 2 imply an electric field perturbation

$$e = \frac{p\sigma}{iq} \frac{x}{1 + ix}, \tag{3}$$

where q is the electronic charge, p is the sound pressure, and σ is the ion-neutral cross section.

The present result affects previously reported acoustic wave amplification in a plasma,[2,3] ion-density measurements in a shock wave,[4] and other effects related to the motion of charged particles in an ordinary sound wave.[5-7]

H. M. Schulz III, U. Ingard

References

1. U. Ingard and K. W. Gentle, Phys. Fluids 8, 1396 (1965).
2. U. Ingard, Phys. Rev. 145, 41 (1966).
3. L. D. Tsendin, Zh. Techn. Fiz. 35, 1972 (1965); [English transl.: Soviet Phys. – Tech. Phys. 10, 1514 (1966)].
4. K. W. Gentle and U. Ingard, Appl. Phys. Letters 5, 105 (1964).
5. J. Berlande, P. D. Goldan, and L. Goldstein, Appl. Phys. Letters 5, 51 (1964).
6. K. J. Nygaard, Phys. Letters 20, 370 (1966).
7. K. J. Nygaard and G. Meltz, "Acoustic Transients in a Weakly Ionized Gas" (submitted for publication).

B. VISCOUS EFFECTS IN A HYDRODYNAMIC PLASMA

We shall consider some dissipative effects in a hydrodynamic plasma. The plasma is treated as if it were a classical viscous fluid, and the hydrodynamic equations describing such a fluid are used. This approach is valid only for phenomena involving characteristic frequencies much less than the collision frequency (which, in turn, is generally less than the plasma frequency), since only then is the dependent assumption of a local Maxwellian distribution justified. In the following analysis we shall show that longitudinal and transverse waves propagate independently (with different dispersion relations) in such a plasma. The discarding of the assumption of isentropic flow will lead to additional roots of the dispersion equation; all of the roots will lead, however to heavily damped waves.

The equations describing a hydrodynamic plasma are

$$\frac{\partial \rho}{\partial t} + \text{Div}\,(\rho \underline{v}) = 0 \tag{1}$$

$$\frac{\partial}{\partial t}(\rho \underline{v}) + \text{Div}\,(\rho \underline{v}\underline{v}) = -\text{Grad}\,P + \frac{4}{3}\mu\,\text{Grad Div}\,\underline{v} - \mu\,\text{Curl Curl}\,\underline{v} - \frac{e}{m}\rho\left[\underline{E} + \frac{\underline{v}}{c} \times \underline{B}\right] \tag{2}$$

$$\text{Div}\,\underline{E} = -4\pi\,\frac{e}{m}\,(\rho - \rho_o) \tag{3}$$

$$\text{Curl}\,\underline{E} = -\frac{1}{c}\,\frac{\partial \underline{B}}{\partial t} \tag{4}$$

$$\text{Div}\,\underline{B} = 0 \tag{5}$$

$$\text{Curl}\,\underline{B} = \frac{1}{c}\,\frac{\partial \underline{E}}{\partial t} - \frac{4\pi}{c}\,\frac{e}{m}\,(\rho \underline{v}), \tag{6}$$

where

ρ = the mass density

$\underline{v}$ = the velocity

P = the pressure

μ = the coefficient of viscosity

$-e/m$ = the electronic charge-to-mass ratio

$\underline{E}$ = the electric field

$\underline{B}$ = the magnetic field

ρ_o = the equilibrium (average) mass density

and we are assuming that the plasma is an "electron fluid" superimposed on an immobile background of positive charge. To complete the formulation of the basic equations of the system, we must also introduce an equation of state and an equation expressing the conservation of energy. For the former, we shall merely use the ideal gas law

$$P = \frac{\rho KT}{m}, \tag{7}$$

so that the latter is given[1] by

$$\frac{\partial}{\partial t}\left[\frac{3}{2}\,\frac{\rho KT}{m} + \frac{1}{2}\,\rho v^2 + \frac{E^2}{8\pi} + \frac{B^2}{8\pi}\right] + \text{Div}\left[\left[\frac{3}{2}\,\frac{\rho KT}{m} + \frac{1}{2}\,\rho v^2\right]\underline{v} + \underline{S}\right.$$

$$\left. + P\underline{v} - \kappa\,\text{Grad}\,T + \frac{5}{3}\,\mu \underline{v}\,\text{Div}\,\underline{v} - \mu\,\text{Div}\,(\underline{v}\underline{v}) - \frac{1}{2}\,\mu\,\text{Grad}\,(v^2)\right] = \frac{e}{m}\,\rho \underline{E} \cdot \underline{v}, \tag{8}$$

where $\underline{S}$ is the Poynting vector, and κ is the coefficient of thermal conductivity.

If we assume that there are no external sources of electromagnetic fields, then longitudinal and transverse waves can propagate through the system independently of one another (to first order), and with different dispersion relations. To show this, we

linearize the basic equations, which then become

$$\frac{\partial \rho^{(1)}}{\partial t} + \rho_o \operatorname{Div} \underline{v}^{(1)} = 0 \tag{9}$$

$$\rho_o \frac{\partial \underline{v}^{(1)}}{\partial t} = -\operatorname{Grad} P^{(1)} + \frac{4}{3}\mu \operatorname{Grad} \operatorname{Div} \underline{v}^{(1)} - \mu \operatorname{Curl} \operatorname{Curl} \underline{v}^{(1)} - \frac{e}{m} \rho_o \underline{E}^{(1)} \tag{10}$$

$$\operatorname{Div} \underline{E}^{(1)} = -4\pi \frac{e}{m} \rho^{(1)} \tag{11}$$

$$\operatorname{Curl} \underline{E}^{(1)} = -\frac{1}{c} \frac{\partial \underline{B}^{(1)}}{\partial t} \tag{12}$$

$$\operatorname{Div} \underline{B}^{(1)} = 0 \tag{13}$$

$$\operatorname{Curl} \underline{B}^{(1)} = \frac{1}{c} \frac{\partial \underline{E}^{(1)}}{\partial t} - \frac{4\pi}{c} \frac{e}{m} \rho_o \underline{v}^{(1)} \tag{14}$$

$$\frac{T^{(1)}}{T_o} = \frac{P^{(1)}}{P_o} - \frac{\rho^{(1)}}{\rho_o} \tag{15}$$

$$\frac{3}{2} \frac{\partial P^{(1)}}{\partial t} + \frac{5}{2} P_o \operatorname{Div} \underline{v}^{(1)} - \kappa \nabla^2 T^{(1)} = 0. \tag{16}$$

Considering longitudinal waves first, we take the divergence of Eq. 10, and with the aid of Eqs. 9 and 11, obtain

$$\left[\frac{\partial^2}{\partial t^2} - \frac{4}{3} \frac{\mu}{\rho_o} \nabla^2 \frac{\partial}{\partial t} + \omega_p^2\right] \rho^{(1)} = \nabla^2 P^{(1)}, \tag{17}$$

where $\omega_p = (4\pi\rho_o e^2/m^2)^{1/2}$ is the plasma frequency. Similarly, Eqs. 9, 15, and 16 reduce to

$$\left[\frac{5}{3} c_T^2 \frac{\partial}{\partial t} - \frac{2}{3} \kappa \frac{T_o}{\rho_o} \nabla^2\right] \rho^{(1)} = \left[\frac{\partial}{\partial t} - \frac{2}{3} \kappa \frac{T_o}{\rho_o} \frac{1}{c_T^2} \nabla^2\right] P^{(1)} \tag{18}$$

where $c_T = (KT/m)^{1/2}$ is the thermal velocity of the electrons. Assuming a time dependence of the form $\exp(-i\omega t)$, where $\omega \neq 0$, we solve Eqs. 17 and 18, and obtain

$$L\rho^{(1)} = 0, \tag{19}$$

where the linear operator L is given by

$$L = \kappa\nabla^2\nabla^2 - i\frac{4}{3}\frac{\mu\kappa}{\rho_o c_T^2}\omega\nabla^2\nabla^2 - \kappa\frac{\omega_p^2}{c_T^2}\nabla^2 + i\frac{5}{2}\frac{c_T^2\rho_o}{T_o}\omega\nabla^2$$

$$+\left[\frac{\kappa}{c_T^2}+\frac{2\mu}{T_o}\right]\omega^2\nabla^2 - i\frac{3}{2}\frac{\rho_o}{T_o}\omega\left(\omega_p^2-\omega^2\right). \tag{20}$$

Notice that L is independent of c, the speed of light, but does depend on c_T, μ, and κ; furthermore, all spatial dependence contained in L appears in the form of Laplacian operators.

Since Div $\underline{v}^{(1)}$ is related to $\rho^{(1)}$ by Eq. 9, we conclude that Eq. 19 also implies

$$L \text{ Div } \underline{v}^{(1)} = 0 \tag{21}$$

The dispersion relation for longitudinal waves is thus obtained by replacing ∇^2 by $-k^2$ in Eq. 20, and setting the resulting expression equal to zero; the result is

$$\kappa k^4 - i\frac{4}{3}\frac{\mu\kappa}{\rho_o c_T^2}\omega k^4 + \kappa\frac{\omega_p^2}{c_T^2}k^2 - i\frac{5}{2}\frac{c_T^2\rho_o}{T_o}\omega k^2 - \left[\frac{\kappa}{c_T^2}+\frac{2\mu}{T_o}\right]\omega^2 k^2$$

$$- i\frac{3}{2}\frac{\rho_o}{T_o}\omega\left(\omega_p^2-\omega^2\right) = 0 \tag{22}$$

For isentropic flow $\mu = \kappa = 0$, and we have

$$k^2 = -\frac{\left(\omega_p^2-\omega^2\right)}{\frac{5}{3}c_T^2}. \tag{23}$$

Since $\omega \ll \omega_p$, this implies that all waves are heavily damped, decaying in a distance of the order of c_T/ω_p. For nonisentropic flow (and $\omega \ll 1/\tau$, where τ is the "collision time"), Eq. 22 has two solutions, both of which are heavily damped:

$$k^2 = -\frac{\omega_p^2}{c_T^2} \tag{24}$$

$$k^2 = i\frac{3}{2}\frac{\rho_o}{T_o}\frac{c_T^2}{\kappa}\omega. \tag{25}$$

The removal of the isentropic condition thus creates an additional root of the dispersion relation (consideration of additional mobile species in the system would presumably

create even more), although neither one reduces to the isentropic result, Eq. 23, in the zero-frequency limit.

To derive the dispersion relation for transverse waves, we take the curl of Eq. 14, and with the aid of Eq. 12, obtain

$$\left[\nabla^2 - \frac{1}{c^2}\frac{\partial^2}{\partial t^2}\right]\underline{B}^{(1)} = \frac{4\pi}{c}\frac{e}{m}\rho_o \text{ Curl } \underline{v}^{(1)}. \tag{26}$$

Combining this result with that obtained by taking the curl of Eq. 10,

$$\left[\rho_o \frac{\partial}{\partial t} - \mu\nabla^2\right] \text{Curl } \underline{v}^{(1)} = \frac{e}{m}\frac{\rho_o}{c}\frac{\partial \underline{B}^{(1)}}{\partial t}, \tag{27}$$

we find that Curl $\underline{v}^{(1)}$ must satisfy the condition

$$\left[\frac{\partial}{\partial t}\nabla^2 - \frac{1}{c^2}\frac{\partial^3}{\partial t^3} - \frac{\mu}{\rho_o}\nabla^2\nabla^2 + \frac{\mu}{\rho_o}\nabla^2\frac{1}{c^2}\frac{\partial^2}{\partial t^2} - \frac{\omega_p^2}{c^2}\frac{\partial}{\partial t}\right] \text{Curl } \underline{v}^{(1)} = 0. \tag{28}$$

If an exp $(-i\omega t)$ dependence is assumed, the result is

$$M \text{ Curl } \underline{v}^{(1)} = 0, \tag{29}$$

where

$$M = -i\omega\nabla^2 - i\frac{\omega^3}{c^2} - \frac{\mu}{\rho_o}\nabla^2\nabla^2 - \frac{\mu}{\rho_o}\frac{\omega^2}{c^2}\nabla^2 + i\omega\frac{\omega_p^2}{c^2}. \tag{30}$$

Notice that M is independent of c_T and κ, but does depend on c and μ; furthermore, as was the case with the operator L, all spatial dependence appears in the form of Laplacian operators.

The dispersion relation for transverse waves is obtained by replacing ∇^2 by $-k^2$ in Eq. 30, and setting the resulting expression equal to zero:

$$-\frac{\mu}{\rho_o}k^4 + \frac{\mu}{\rho_o}\frac{\omega^2}{c^2}k^2 + i\omega k^2 + i\frac{\omega}{c^2}\left(\omega_p^2 - \omega^2\right) = 0. \tag{31}$$

For isentropic flow, $\mu = 0$, and we have

$$k^2 = -\frac{\left(\omega_p^2 - \omega^2\right)}{c^2}, \tag{32}$$

so that all waves are heavily damped, decaying in a distance of the order of c/ω_p. For nonisentropic flow, Eq. 31 has two solutions, both of which are heavily damped:

$$k^2 = i\frac{\omega}{2}\frac{\rho_o}{\mu}\left[1 \pm \left(1 - i\frac{4\mu}{\rho_o}\frac{\omega_p^2}{\omega c^2}\right)^{1/2}\right]. \tag{33}$$

If $\mu\omega_p^2 \ll \rho_o\omega c^2$, the two roots become

$$k^2 = i\omega\frac{\rho_o}{\mu} \tag{34}$$

$$k^2 = -\frac{\omega_p^2}{c^2}. \tag{35}$$

Notice that Eq. 35 is the same as the isentropic solution, Eq. 32

To find the most general solution for all first-order quantities, we must realize that it is possible for both longitudinal and transverse phenomena to be present in a plasma at the same time. Thus we separate the first-order velocity $\underline{v}^{(1)}$ into irrotational and solenoidal parts:

$$\underline{v}^{(1)} = -\text{ Grad }\phi + \text{Curl }\underline{A}. \tag{36}$$

Then

$$\text{Div }\underline{v}^{(1)} = -\nabla^2\phi \tag{37}$$

$$\text{Curl }\underline{v}^{(1)} = -\nabla^2\underline{A}, \tag{38}$$

in which we assume Div $\underline{A} = 0$. Equations 21 and 22 thus become

$$L\nabla^2\phi = 0 \tag{39}$$

$$M\nabla^2\underline{A} = 0, \tag{40}$$

and these equations plus the appropriate boundary conditions uniquely determine ϕ and $\underline{A}$. The quantities $\rho^{(1)}$, $P^{(1)}$, $T^{(1)}$, $\underline{E}^{(1)}$ and $\underline{B}^{(1)}$ can then be found by using one or more of Eqs. 9-16 in conjunction with Eq. 36.

J. A. Ross

References

1. U. Ingard, Class Notes for "Introduction to the Physics of Fluids and Plasmas," Massachusetts Institute of Technology, 1964, p. 19.

C. INTERFERENCE OF LIGHT WITH LIGHT IN A PLASMA

We shall consider the perturbation effects of externally produced electromagnetic waves on a homogeneous, collisionless, nonrelativistic plasma; such waves can be

generated, for example, by klystrons or lasers, the choice depending on the frequencies desired. These waves tend to interfere with each other, primarily by the interaction of their magnetic fields with the induced oscillations of the charged particles. This $\underline{v} \times \underline{B}$ interaction thus leads to second-order waves having frequencies and wave vectors equal to the sum and difference of those of the primary waves. There is also a resonance if the difference in frequency of the primary waves is equal to the plasma frequency.

The (classical) analysis presented here is original, and the author thought, at first, that it was still totally unpublished. He has since discovered a paper by Montgomery,[1] in which a number of the results presented in this report are given for the special case of linearly polarized, parallel, perturbing waves. The results presented here reduce to those of Montgomery in the special case considered by him, but are presented here for the general case of arbitrary polarization of the waves, with arbitrary angles between their wave vectors. The results are thus given in a more general form than those of Montgomery, and have a more general validity in view of the fact that in practice two interacting beams will never be strictly parallel.

For mathematical simplicity, we shall assume that the plasma is "cold," that is, that its temperature is very low; to state this another way, we shall assume that the thermal velocities of all the species in the plasma system are much less than the phase velocity of any wave considered.[2] In this case the equations for the conservation of particles and momentum in a plasma may be written[2]

$$\frac{\partial n_a}{\partial t} + \text{Div}\,(n_a \underline{v}_a) = 0 \qquad \text{(Conservation of Particles)} \tag{1}$$

$$\frac{\partial}{\partial t}(m_a n_a \underline{v}_a) + \text{Div}\,(m_a n_a \underline{v}_a \underline{v}_a) = q_a n_a \left[\underline{E} + \frac{\underline{v}_a}{c} \times \underline{B}\right] \qquad \text{(Conservation of Momentum)} \tag{2}$$

where $\underline{E}$ and $\underline{B}$ are the electric and magnetic fields; q_a and m_a are the charge and mass, respectively, of a particle of the a^{th} species, and

$$n_a(\underline{x}, t) = \int d\underline{v}\, f_a(\underline{x}, \underline{v}, t) \qquad \text{(particle density)} \tag{3}$$

$$n_a \underline{v}_a(\underline{x}, t) = \int d\underline{v}\, \underline{v}\, f_a(\underline{x}, \underline{v}, t) \tag{4}$$

$$n_a \underline{v}_a(\underline{x}, t)\, \underline{v}_a(\underline{x}, t) = \int d\underline{v}\, \underline{v}\, \underline{v}\, f_a(\underline{x}, \underline{v}, t), \tag{5}$$

where f_a is the distribution function for the a^{th} species. Maxwell's equations are

$$\text{Div}\,\underline{E} = 4\pi \sum_a q_a n_a \tag{6}$$

$$\text{Curl } \underline{E} = -\frac{1}{c}\frac{\partial B}{\partial t} \tag{7}$$

$$\text{Div } \underline{B} = 0 \tag{8}$$

$$\text{Curl } \underline{B} = +\frac{1}{c}\frac{\partial E}{\partial t} + \frac{4\pi}{c}\sum_a q_a n_a \underline{v}_a. \tag{9}$$

Taking the curl of Eq. 7, and using Eq. 9, we obtain the following equation for $\underline{E}(\underline{x}, t)$:

$$\left[\nabla^2 - \frac{1}{c^2}\frac{\partial^2}{\partial t^2} - \text{Grad Div}\right] E = \frac{4\pi}{c^2}\frac{\partial}{\partial t}\sum_a q_a n_a \underline{v}_a. \tag{10}$$

We next expand the relevant variables in perturbation series about their equilibrium values, and remembering that we are dealing with a homogeneous plasma with no zero-order electromagnetic fields, take

$$n_a^{(0)} = N_a \tag{11}$$

$$\underline{v}_a^{(0)} = 0. \tag{12}$$

Hence the first-order expansions of Eqs. 1 and 2 become

$$\frac{\partial n_a^{(1)}}{\partial t} + N_a \text{ Div } \underline{v}_a^{(1)} = 0 \tag{13}$$

$$\frac{\partial v_a^{(1)}}{\partial t} = \frac{q_a}{m_a}\underline{E}^{(1)}. \tag{14}$$

Solving Eq. 10 to first order with the aid of Eq. 14, we obtain

$$\left[\nabla^2 - \frac{1}{c^2}\frac{\partial^2}{\partial t^2} - \text{Grad Div}\right]\underline{E}^{(1)} = \frac{\omega_p^2}{c^2}\underline{E}^{(1)}, \tag{15}$$

where

$$\omega_p^2 = \sum_a \omega_{pa}^2 = \sum_a \frac{4\pi N_a q_a^2}{m_a}.$$

Assuming a wave dependence of the form $\exp[i(kz-\omega t)]$ for $\underline{E}^{(1)}$, we conclude that either $\omega = \omega_p$ or else $\underline{E}_z^{(1)} = 0$. We consider first the last case; the waves are purely transverse (as opposed to the natural oscillations, which are purely longitudinal), and, from Eq. 15, the dispersion relation is

$$k^2c^2 = \omega^2 - \omega_p^2. \tag{16}$$

Thus only waves having frequencies greater than the natural oscillation frequency ω_p can propagate through the plasma.

Such waves, being purely transverse, do not induce a separation of charge. They do, however, cause a transverse oscillatory motion of the particles, and this motion couples with the magnetic field of the wave to produce a second-order longitudinal wave. To see this mathematically, consider the first-order wave

$$\underline{E}^{(1)} = E_A \cos(kz-\omega t)\,\hat{x}, \tag{17}$$

where the symbol $\hat{x}$ is used to designate the unit vector in the x-direction. Then Eqs. 7, 13, and 14 yield

$$\underline{B}^{(1)} = \frac{kc}{\omega} E_A \cos(kz-\omega t)\,\hat{y} \tag{18}$$

$$\underline{v}_a^{(1)} = -\frac{q_a}{m_a}\frac{1}{\omega} E_A \sin(kz-\omega t)\,\hat{x} \tag{19}$$

$$n_a^{(1)} = 0. \tag{20}$$

The second-order electric field $\underline{E}^{(2)}$ is found from Eq. 10 to satisfy

$$\left[\nabla^2 - \frac{1}{c^2}\frac{\partial^2}{\partial t^2} - \text{Grad Div}\right] E^{(2)} = \frac{4\pi}{c^2}\sum_a q_a N_a \frac{\partial \underline{v}_a^{(2)}}{\partial t}. \tag{21}$$

Now the second-order velocity $\underline{v}_a^{(2)}$ is related to $\underline{E}^{(2)}$ and the first-order quantities by the second-order expansion of Eq. 2:

$$\frac{\partial \underline{v}_a^{(2)}}{\partial t} + \text{Div}\left(\underline{v}_a^{(1)}\underline{v}_a^{(1)}\right) = \frac{q_a}{m_a}\left[\underline{E}^{(2)} + \frac{\underline{v}_a^{(1)}}{c}\times \underline{B}^{(1)}\right]. \tag{22}$$

Thus Eq. 21 may be written

$$\left[\nabla^2 - \frac{1}{c^2}\frac{\partial^2}{\partial t^2} - \text{Grad Div} - \frac{\omega_p^2}{c^2}\right]\underline{E}^{(2)} = \sum_a \frac{\omega_{pa}^2}{c^2}\left[\frac{\underline{v}_a^{(1)}}{c}\times \underline{B}^{(1)} - \frac{m_a}{q_a}\text{Div}\left(\underline{v}_a^{(1)}\underline{v}_a^{(1)}\right)\right]. \tag{23}$$

This equation is valid for any situation in which $n_a^{(1)} = 0$. For our particular example, Div $\left(\underline{v}_a^{(1)}\underline{v}_a^{(1)}\right)$ vanishes, and $\underline{E}^{(2)}$ is given by

$$\underline{E}^{(2)} = -\sum_a \frac{q_a}{m_a}\frac{\omega_{pa}^2}{2}\frac{1}{\left(4\omega^2-\omega_p^2\right)}\frac{k}{\omega^2}E_A^2 \sin\left[2(kz-\omega t)\right]\hat{z}; \tag{24}$$

it is thus a longitudinal wave having a frequency and wave vector that are twice those of the perturbing transverse wave. Associated with this electric field $\underline{E}^{(2)}$ is a longitudinal particle oscillation; thus although a transverse wave produces no charge separation of first order, it does induce one to second order.

A more interesting situation is that involving the interaction between the plasma and two perturbing sources, that is, the interference of light with light in a plasma. In this case we expect that, in addition to the waves generated by the two sources separately, their interaction will produce second-order waves having frequencies and wave vectors equal to the sum and difference of those of the first-order waves. We expect, furthermore, that some kind of resonance will occur when the difference in frequency of the two first-order waves is equal to the plasma frequency ω_p. That this is indeed the case will be borne out of our analysis.

Once again, the first-order dispersion relation, Eq. 15, requires that the perturbing waves be transverse. This in turn implies, with Eqs. 13 and 14, that $n_a^{(1)} = 0$; hence Eq. 23 is again valid. Designating the two first-order waves by the subscripts 1 and 2 we take the direction of propagation of $\underline{E}_1$ to be the z-direction, and that of $\underline{E}_2$ to be a direction in the xz-plane making an angle β with the z-axis; that is

$$\underline{k}_1 = k_1 \hat{z} \tag{25}$$

$$\underline{k}_2 = k_2 \sin\beta \hat{x} + k_2 \cos\beta \hat{z}. \tag{26}$$

Allowing for arbitrary polarization of the two waves, we thus take

$$\underline{E}_1 = E_{1A} \cos(\underline{k}_1 \cdot \underline{x} - \omega_1 t - \delta_1)\, \hat{x} + E_{1B} \cos(\underline{k}_1 \cdot \underline{x} - \omega_1 t - \phi_1)\, \hat{y} \tag{27}$$

$$\underline{E}_2 = -E_{2A} \cos\beta \cos(\underline{k}_2 \cdot \underline{x} - \omega_2 t - \delta_2)\, \hat{x} + E_{2B} \cos(\underline{k}_2 \cdot \underline{x} - \omega_2 t - \phi_2)\, \hat{y}$$
$$+ E_{2A} \sin\beta \cos(\underline{k}_2 \cdot \underline{x} - \omega_2 t - \delta_2)\, \hat{z}, \tag{28}$$

where δ_1, ϕ_1, δ_2 and ϕ_2 are arbitrary phase angles. Then from Eqs. 7, 13, and 14, we have

$$B_1 = -\frac{k_1 c}{\omega_1} E_{1B} \cos(\underline{k}_1 \cdot \underline{x} - \omega_1 t - \phi_1)\, \hat{x} + \frac{k_1 c}{\omega_1} E_{1A} \cos(\underline{k}_1 \cdot \underline{x} - \omega_1 t - \delta_1)\, \hat{y} \tag{29}$$

$$\underline{B}_2 = -\frac{k_2 c}{\omega_2} E_{2B} \cos\beta \cos(\underline{k}_2 \cdot \underline{x} - \omega_2 t - \phi_2)\, \hat{x} - \frac{k_2 c}{\omega_2} E_{2A} \cos(\underline{k}_2 \cdot \underline{x} - \omega_2 t - \delta_2)\, \hat{y}$$
$$+ \frac{k_2 c}{\omega_2} E_{2B} \sin\beta \cos(\underline{k}_2 \cdot \underline{x} - \omega_2 t - \phi_2)\, \hat{z} \tag{30}$$

$$\underline{v}_a^{(1)} = -\frac{q_a}{m_a}\left[\frac{E_{1A}}{\omega_1}\sin(\underline{k}_1\cdot\underline{x}-\omega_1 t-\delta_1) - \frac{E_{2A}}{\omega}\cos\beta\,\sin(\underline{k}_2\cdot\underline{x}-\omega_2 t-\delta_2)\right]\hat{x}$$

$$-\frac{q_a}{m_a}\left[\frac{E_{1B}}{\omega_1}\sin(\underline{k}_1\cdot\underline{x}-\omega_1 t-\phi_1) + \frac{E_{2B}}{\omega_2}\sin(\underline{k}_2\cdot\underline{x}-\omega_2 t-\phi_2)\right]\hat{y}$$

$$-\frac{q_a}{m_a}\frac{E_{2A}}{\omega_2}\sin\beta\,\sin(\underline{k}_2\cdot\underline{x}-\omega_2 t-\delta_2)\,\hat{z} \tag{31}$$

$$n_a^{(1)} = 0. \tag{32}$$

To find $\underline{E}^{(2)}$ we must first evaluate the right-hand side of Eq. 23. After a considerable amount of tedious algebra, we obtain

$$\frac{\underline{v}_a^{(1)}}{c}\times\underline{B}^{(1)} - \frac{m_a}{q_a}\,\mathrm{Div}\left(\underline{v}_a^{(1)}\underline{v}_a^{(1)}\right) = -\frac{q_a}{m_a}\,\frac{1}{2}\,\mathrm{Grad}\left|\int dt\,\underline{E}^{(1)}\right|^2 \tag{33}$$

where

$$\underline{E}^{(1)} = \underline{E}_1 + \underline{E}_2 \tag{34}$$

$$\underline{B}^{(1)} = \underline{B}_1 + \underline{B}_2 \tag{35}$$

Thus there will be no interference effects between the two waves, regardless of their frequencies or wave vectors, unless $\underline{E}_1\cdot\underline{E}_2 \neq 0$.

The right-hand side of Eq. 33 appears to be nonlinear; it is actually a linear expression, however, and may be written as a sum of purely sinusoidal terms with the aid of the trigonometric identity

$$2\sin a\cos b = \sin(a+b) + \sin(a-b). \tag{36}$$

Using this identity, we may solve Eq. 23 for the second-order electric field $\underline{E}^{(2)}$, and, after a considerable amount of algebra, obtain

$$\underline{E}^{(2)} = -\sum_a \frac{q_a}{m_a}\,\frac{\omega_{pa}^2}{2}\left[\frac{1}{\left(4\omega_1^2-\omega_p^2\right)}\left[E_{1A}^2\sin\left[2(\underline{k}_1\cdot\underline{x}-\omega_1 t-\delta_1)\right]+E_{1B}^2\sin\left[2(\underline{k}_1\cdot\underline{x}-\omega_1 t-\phi_1)\right]\right]\frac{\underline{k}_1}{\omega_1^2}\right.$$

$$+\frac{1}{\left(4\omega_2^2-\omega_p^2\right)}\left[E_{2A}^2\sin\left[2(\underline{k}_2\cdot\underline{x}-\omega_2 t-\delta_2)\right]+E_{2B}^2\sin\left[2(\underline{k}_2\cdot\underline{x}-\omega_2 t-\phi_2)\right]\right]\frac{k_2}{\omega_2^2}$$

$$\left.+\frac{1}{\left(\omega_+^2-\omega_p^2\right)}\left[-E_{1A}E_{2A}\cos\beta\,\sin(\underline{k}_+\cdot\underline{x}-\omega_+ t-\delta_+)+E_{1B}E_{2B}\sin(\underline{k}_+\cdot\underline{x}-\omega_+ t-\phi_+)\right]\frac{\underline{k}_+}{\omega_1\omega_2}\right.$$

$$- \frac{1}{\left(\omega_-^2 - \omega_p^2\right)}\left[-E_{1A}E_{2A}\cos\beta \sin(\underline{k}_- \cdot \underline{x} - \omega_- t - \delta_-) + E_{1B}E_{2B}\sin(\underline{k}_- \cdot \underline{x} - \omega_- t - \phi_-)\right]\frac{\underline{k}_-}{\omega_1\omega_2}\Bigg], \tag{37}$$

where $\underline{k}_\pm = \underline{k}_1 \pm \underline{k}_2$, $\omega_\pm = \omega_1 \pm \omega_2$, $\delta_\pm = \delta_1 \pm \delta_2$, and $\phi_\pm = \phi_1 \pm \phi_2$.

Thus $\underline{E}^{(2)}$ is the sum of two kinds of longitudinal waves: those of the form observed in Eq. 24 representing "self-interactions" of the first-order waves; and "sum and difference" waves representing interference of the two first-order waves with each other. Notice that the interference terms contain the factor $\underline{k}_\pm/\omega_1\omega_2$, rather then $\underline{k}_\pm/\omega_\pm$; this is necessary to insure that $\underline{E}^{(2)}$ reduces to the proper result for the special case $\underline{k}_1 = \underline{k}_2$, $\omega_1 = \omega_2$. Notice also that, although $\omega_1 > \omega_p$ and $\omega_2 > \omega_p$, ω_- can have any value. Thus, by this means, it is possible to generate a longitudinal wave of arbitrary frequency and wave number. As expected, there is a resonance at $|\omega_-| = \omega_p$. The occurrence of this resonance is independent of the angle β, however, so that the produced resonant wave can have any wave number. The wave number is, in fact, given by

$$|\underline{k}_1 - \underline{k}_2| = \left(k_1^2 + k_2^2 - 2k_1k_2\cos\beta\right)^{1/2}, \tag{38}$$

where (Eq. 16)

$$k_i^2c^2 = \omega_i^2 - \omega_p^2.$$

For $\omega_i \gg \omega_p$ and $\beta = 0$, we have $|\underline{k}_1 - \underline{k}_2| \approx |\omega_1 - \omega_2|/c \approx \omega_p/c$, a rather small wave number; for $\beta = \pi/2$, however, we obtain $|\underline{k}_1 - \underline{k}_2| = \left(\omega_1^2 + \omega_2^2 - 2\omega_p^2\right)^{1/2}/c$, a relatively large wave number if $\omega_i \gg \omega_p$. Last, but not least, we wish to point out that only those particles with very large values of q_a/m_a (the electrons) participate significantly in the oscillations described.

Thus far we have been dealing only with transverse waves. We now wish to consider the effects of the addition of longitudinal waves to our analysis. By Eq. 16, such a wave must oscillate at the plasma frequency ω_p, although its wave number k is arbitrary. We shall consider now the situation involving interference between a longitudinal and a transverse wave in a plasma. In contrast to the case involving two transverse waves, we shall find that the second-order "sum and difference" waves produced by the interaction are both longitudinal and transverse, and are generated regardless of the angle between the two first-order waves. As expected, there is a resonance when the frequency difference between the two waves is ω_p (that is, the frequency of the transverse wave is $2\omega_p$), but there are also additional resonances that depend on the wave vectors of the primary waves.

Our starting point is the second-order expansion of Eq. 10:

$$\left[\nabla^2 - \frac{1}{c^2}\frac{\partial^2}{\partial t^2} - \text{Grad Div}\right]\underline{E}^{(2)} = \frac{4\pi}{c^2}\sum_a \frac{\partial}{\partial t} q_a (n_a \underline{v}_a)^{(2)}. \tag{39}$$

With the aid of the second-order expansion of Eq. 2,

$$\frac{\partial}{\partial t}(n_a \underline{v}_a)^{(2)} + N_a \,\text{Div}\,(\underline{v}_a \underline{v}_a)^{(2)} = \frac{q_a}{m_a}\left[(n_a \underline{E})^{(2)} + N_a \frac{\underline{v}_a^{(1)}}{c} \times \underline{B}^{(1)}\right], \tag{40}$$

we obtain

$$\left[\nabla^2 - \text{Grad Div} - \frac{1}{c^2}\frac{\partial^2}{\partial t^2} - \frac{\omega_p^2}{c^2}\right]\underline{E}^{(2)} = \sum_a \frac{\omega_{pa}^2}{c^2}\left[\frac{\underline{v}_a^{(1)}}{c} \times \underline{B}^{(1)} - \frac{m_a}{q_a}\,\text{Div}\left(\underline{v}_a^{(1)}\underline{v}_a^{(1)}\right) + \frac{n_a^{(1)}}{N_a}\underline{E}^{(1)}\right]. \tag{41}$$

This is the most general form of the equation governing the generation of second-order fields in a plasma.

Allowing full generality for the polarization and phase difference between the two waves, we take

$$\underline{E}_1 = E_{1A} \cos(\underline{k}_1 \cdot \underline{x} - \omega_1 t - \delta)\,\hat{x} + E_{1B} \cos(\underline{k}_1 \cdot \underline{x} - \omega_1 t - \phi)\,\hat{y} \tag{42}$$

$$\underline{E}_2 = E_2 \sin\beta \cos(\underline{k}_2 \cdot \underline{x} - \omega_p t)\,\hat{x} + E_2 \cos\beta \cos(\underline{k}_2 \cdot \underline{x} - \omega_p t)\,\hat{z}, \tag{43}$$

where δ and ϕ are arbitrary phase angles, and $\underline{k}_1$ and $\underline{k}_2$ are given by

$$\underline{k}_1 = k_1 \hat{z} \tag{44}$$

$$\underline{k}_2 = k_2 \sin\beta\,\hat{x} + k_2 \cos\beta\,\hat{z}. \tag{45}$$

Then, from Eqs. 7, 13, and 14, we have

$$\underline{B}_1 = -\frac{k_1 c}{\omega_1} E_{1B} \cos(\underline{k}_1 \cdot \underline{x} - \omega_1 t - \phi)\,\hat{x} + \frac{k_1 c}{\omega_1} E_{1A} \cos(\underline{k}_1 \cdot \underline{x} - \omega_1 t - \delta)\,\hat{y} \tag{46}$$

$$\underline{B}_2 = 0 \tag{47}$$

$$\begin{aligned}\underline{v}_a^{(1)} = &-\frac{q_a}{m_a}\left[\frac{E_{1A}}{\omega_1}\sin(\underline{k}_1 \cdot \underline{x} - \omega_1 t - \delta) + \frac{E_2}{\omega_2}\sin\beta \sin(\underline{k}_2 \cdot \underline{x} - \omega_p t)\right]\hat{x} \\ &- \frac{q_a}{m_a}\frac{E_{1B}}{\omega_1}\sin(\underline{k}_1 \cdot \underline{x} - \omega_1 t - \phi)\,\hat{y} \\ &- \frac{q_a}{m_a}\frac{E_2}{\omega_2}\cos\beta \sin(\underline{k}_2 \cdot \underline{x} - \omega_p t)\,\hat{z}\end{aligned} \tag{48}$$

$$n_a^{(1)} = -\frac{q_a}{m_a}\frac{k_2}{\omega_2^2} N_a E_2 \sin(\underline{k}_2\cdot\underline{x} - \omega_p t). \tag{49}$$

With these expressions for the first-order quantities (and the relation $\omega_2 = \omega_p$), we find, after a considerable amount of algebra, that Eq. 41 can be written

$$\left[\text{Curl Curl} + \frac{1}{c^2}\frac{\partial^2}{\partial t^2} + \frac{\omega_p^2}{c^2}\right]\underline{E}^{(2)} = \sum \frac{\omega_{pa}^2}{c^2}\frac{q_a}{m_a}\left[\frac{1}{2}\text{Grad}\left|\int \underline{E}^{(1)}\,dt\right|^2 + \left[\int \underline{E}^{(1)}\,dt\right]\left[\int \text{Div}\,\underline{E}^{(1)}\,dt\right] + \underline{E}^{(1)}\int dt\left[\int \text{Div}\,\underline{E}^{(1)}\,dt\right]\right]. \tag{50}$$

This is a general expression governing the interference of waves with waves in a plasma, and shows that although there is no interference between perpendicular transverse waves, there is always interference between transverse and longitudinal waves, regardless of the angle between them.

To find the second-order electric field $E^{(2)}$, we again use Eq. 36; the result is

$$\begin{aligned}
\underline{E}^{(2)} = -\sum_a \frac{q_a}{m_a}\frac{\omega_{pa}^2}{2}\Bigg[&\frac{1}{\left(4\omega_1^2-\omega_p^2\right)}\Big[E_{1A}^2\sin[2(\underline{k}_1\cdot\underline{x}-\omega_1 t-\delta)] \\
&+ E_{1B}^2\sin[2(\underline{k}_1\cdot\underline{x}-\omega_1 t-\phi)]\Big]\frac{\underline{k}_1}{\omega_1^2} + \frac{E_2^2}{\omega_p^2}\sin[2(\underline{k}_2\cdot\underline{x}-\omega_p t)]\frac{\underline{k}_2}{\omega_p^2} \\
&+ \frac{1}{\left(\omega_+^2-\omega_p^2\right)}E_{1A}E_2\sin(\underline{k}_+\cdot\underline{x}-\omega_+ t-\delta)\frac{\underline{k}_+}{\omega_1\omega_p} \\
&- \frac{1}{\left(\omega_-^2-\omega_p^2\right)}E_{1A}E_2\sin(\underline{k}_-\cdot\underline{x}-\omega_- t-\delta)\frac{\underline{k}_-}{\omega_1\omega_p} \\
&+ \frac{k_2\sin\beta}{k_+^2}\frac{1}{\left(\omega_+^2-\omega_p^2\right)}\frac{k_2}{\omega_p}\left(\frac{1}{\omega_p}+\frac{1}{\omega_1}\right)E_{1A}E_2\sin(\underline{k}_+\cdot\underline{x}-\omega_+ t-\delta)\,\underline{k}_+ \\
&- \frac{k_2\sin\beta}{k_-^2}\frac{1}{\left(\omega_-^2-\omega_p^2\right)}\frac{k_2}{\omega_p}\left(\frac{1}{\omega_p}-\frac{1}{\omega_1}\right)E_{1A}E_2\sin(\underline{k}_-\cdot\underline{x}-\omega_- t-\delta)\,\underline{k}_- \\
&+ \frac{1}{k_+^2}\frac{1}{\left(k_+^2c^2+\omega_+^2-\omega_p^2\right)}\frac{k_2}{\omega_p}\left(\frac{1}{\omega_p}+\frac{1}{\omega_1}\right)\left[E_{1A}E_2\sin(\underline{k}_+\cdot\underline{x}-\omega_+ t-\delta)\,\underline{k}_+\times(\hat{x}\times\underline{k}_+)\right. \\
&\left.+ E_{1B}E_2\sin(\underline{k}_+\cdot\underline{x}-\omega_+ t-\phi)\,\underline{k}_+\times(\hat{y}\times\underline{k}_+)\right] \\
&- \frac{1}{k_-^2}\frac{1}{\left(k_-^2c^2+\omega_-^2-\omega_p^2\right)}\frac{k_2}{\omega_p}\left(\frac{1}{\omega_p}-\frac{1}{\omega_1}\right)\left[E_{1A}E_2\sin(\underline{k}_-\cdot\underline{x}-\omega_+ t-\delta)\,\underline{k}_-\times(\hat{x}\times\underline{k}_-)\right. \\
&\left.+ E_{1B}E_2\sin(\underline{k}_-\cdot\underline{x}-\omega_- t-\phi)\,\underline{k}_-\times(\hat{y}\times\underline{k}_-)\right]\Bigg].
\end{aligned} \tag{51}$$

As expected, we have both longitudinal and transverse interference waves. We also have a resonance when the frequency of the transverse waves equals $2\omega_p$, but there are additional resonances at other frequencies, which depend to a considerable extent on the wave vectors of the two primary waves.

In this report we have dealt only with plane waves. Our analysis can easily be extended to cases involving cylindrical and/or spherical waves, but, at the present time, there is no way to generate such waves. An analysis of such a situation is thus rather meaningless, and hence has been omitted here.

J. A. Ross

References

1. D. C. Montgomery, Physica 31, 693 (1965).
2. D. C. Montgomery and D. A. Tidman, Plasma Kinetic Theory (McGraw-Hill Book Company, Inc., New York, 1964), pp. 118, 122.

XVII. ELECTRODYNAMICS OF MEDIA*

Academic and Research Staff

Prof. L. J. Chu
Prof. H. A. Haus
Prof. G. C. Shu

Graduate Students

J. Glaser T. K. Gustafson ET AL P. W. Hoff

RESEARCH OBJECTIVES

During the several years past, work has been in progress on the formulation of the fundamental equations of electrodynamics, with particular attention devoted to obtaining correct expressions for the macroscopic force density distributions for various media of interest. The results of this work, including some results of last year's research will be published as a research monograph by The M. I. T. Press, Cambridge, Massachusetts.[1]

In a self-consistent formulation of electrodynamics, an important question is concerned with the correct identification of momentum density of other than kinetic origin. The feasibility study of a deflection experiment of a polarizable body in a magnetic field to distinguish between a widely accepted expression for the momentum density and the one that we have concluded to be the correct one is now under way.

The study of electrodynamics of moving media led unavoidably into a general treatment for nonlinear media. Such media are of present interest in the optical frequency range and some of their properties are of great engineering importance. In this connection a study is under way of the utilization of nonlinear amplification to obtain from an (optical) amplifier output pulses of duration that is short compared with the inverse (linear) bandwidth of the amplifier.

L. J. Chu, H. A. Haus

References

1. Paul Penfield, Jr. and Hermann A. Haus, Electrodynamics of Moving Media (The M. I. T. Press, Cambridge, Mass., in press); also Special Technical Report Number 14, Research Laboratory of Electronics, M. I. T., Cambridge, Mass.

A. NONLINEAR AMPLIFICATION

1. Introduction

An investigation of the possibility of obtaining and amplifying laser pulses of duration shorter than the inverse bandwidth of the active medium has been initiated. Of particular interest is the CO_2 transition at 10.6 μ. The transitions can be pumped efficiently; however, in the linear region pulse lengths not shorter than ~80 nsec can be obtained, because

*This work was supported by the Joint Services Electronics Programs (U.S. Army, U.S. Navy, and U.S. Air Force) under Contract DA 36-039-AMC-03200(E).

of the inherent bandwidth limitation of any linear amplifier.

In the nonlinear region, the rate at which inversion of a two-level system can be achieved is determined by the field intensity of the applied pulse, and not by the inverse linewidth. Moreover, if the pulse length is shorter than the transverse relaxation time, or becomes so, inertial terms associated with the polarization of such a two-level system become important.

For a linear bandwidth of 50 MHz, and gains and saturation levels typical of a CO_2 system, our results indicate that a peak power intensity $\approx$1.5 kW for a Gaussian pulse of 20 nsec in width should be sufficient to show some sharpening in 6 m. These power densities are obtainable with a Q-switched pulse. The realizability of the pulse lengths is more questionable.

Even though the model of a homogeneously broadened two-level system is an oversimplification of CO_2 laser operation, it is believed that guidelines for future work on CO_2 systems can be gleaned from these results.

2. Equations of Motion

The equations describing the amplifying medium and the amplifying wave are the density matrix equations for a two-level system and a forward traveling-wave equation for the field. The derivations can be found in several publications.[1-5] The resultant equations are

$$(\dot{\rho}_{22}-\dot{\rho}_{11}) = -\frac{(\rho_{22}-\rho_{11}) - \left(\rho^e_{22}-\rho^e_{11}\right)}{T_1} + \frac{2}{n\hbar\omega_o}\left(E_o J_p^* + E_o^* J_p\right) \tag{1}$$

$$\dot{J}_p = i\omega_o J_p - \frac{J_p}{T_2} - \frac{\omega_o n |p_{12}|^2}{\hbar}(\rho_{22}-\rho_{11})E_o \tag{2}$$

$$\frac{\partial E}{\partial t} + c\frac{\partial E_o}{\partial t} + \frac{\sigma}{2\epsilon}E_o = -\frac{J_p}{2\epsilon} \tag{3}$$

Here E_o is the field amplitude; J_p, the polarization current; ω_o, the optical frequency, which is assumed to coincide with the atomic frequency; n, the density of particles, which is assumed to be constant; T_1, the lifetime of the excited state; T_2, the polarization relaxation time; $\rho_{22} - \rho_{11}$, the difference between the probability of the upper state being occupied and the probability of the lower state being occupied; and $\rho^e_{22} - \rho^e_{11}$, the equilibrium value of $\rho_{22} - \rho_{11}$. The polarization matrix element connecting the two states is given by p_{12}.

It is convenient to normalize the time with respect to T_2,[1] and the field quantities with respect to the energy content associated with the equilibrium population difference,

so that

$$F_o = \frac{\sqrt{2\epsilon_o}\, E_o}{\sqrt{n\hbar\omega_o\left(\rho_{22}^e - \rho_{11}^e\right)}} \tag{4}$$

$$K_o = \frac{T_2 J_p}{\sqrt{2\epsilon_o n\hbar\omega_o\left(\rho_{22}^e - \rho_{11}^e\right)}} \tag{5}$$

$$Z = \frac{z}{cT_2}; \qquad T = \frac{t}{T_2} \tag{6}$$

$$N = \frac{\rho_{22} - \rho_{11}}{\rho_{22}^e - \rho_{11}^e} \tag{7}$$

The equations then become

$$\frac{dN}{dT} = -\frac{N-1}{\tau_1} + 4F_oK_o; \qquad \tau_1 = \frac{T_1}{T_2} \to \infty \tag{8}$$

$$\frac{dK_o}{dT} = -K_o - ANF_o \tag{9}$$

$$\frac{\partial F_o}{\partial T} + \frac{\partial F_o}{\partial Z} + \frac{F_o}{\tau_o} = -K_o; \tag{10}$$

with

$$\frac{1}{\tau_o} = \frac{\sigma T_2}{2\epsilon_o}$$

$$A = \frac{|p_{12}|^2\, n\left(\rho_{22}^e - \rho_{11}^e\right)\hbar\omega_o T_2^2}{2\hbar^2\epsilon}$$

3. Integration of the Equations and Results

The set of three equations (8), (9), and (10) can be integrated numerically along the characteristics, two of which are along z = constant, and the other of which is given by V = Z − T = constant. The system is then essentially an infinite set of coupled ordinary differential equations. The Runge-Kutta fourth-order scheme was used. Spatial smoothing was added to the time-smoothed scheme, thereby creating a highly stable predictor-corrector algorithm.

The pulse-sharpening process can be described as follows. The leading edge of the

pulse, if intense enough, will cause a depopulation of the upper state, which, if the maximum pulse amplitude is chosen correctly, becomes fully depleted only when the entire pulse has passed. This causes a preferred increase in the amplitude of the leading edge of the pulse. As the maximum amplitude tends to increase, however, the population becomes fully depleted before the entire pulse has passed. The polarization is zero for the fully depleted system; however, inertial effects cause "overshoot" and hence it changes sign. This causes the medium to become an absorber and thus the two-level system tends to re-invert at the expense of the field. Eventually the lagging edge of the field or polarization changes sign once more. This creates another region of population depletion (Eq. 8) trailing the preceding alternating regions of inversion and depletion. The consequence is a pulse which, upon traversing the medium, sharpens, increases in maximum intensity, and develops ringing (Fig. XVII-1).

Several things influence the behavior described above. If the relaxation time T_2 is so small that relaxation overshadows the gain, the polarization and population tend to relax very rapidly and the effect upon the field is diminished. The ringing is highly damped. In the limit when inertial effects are negligibly small, no ringing occurs; and no sharpening occurs except when the front of the pulse is extremely steep (slope of the

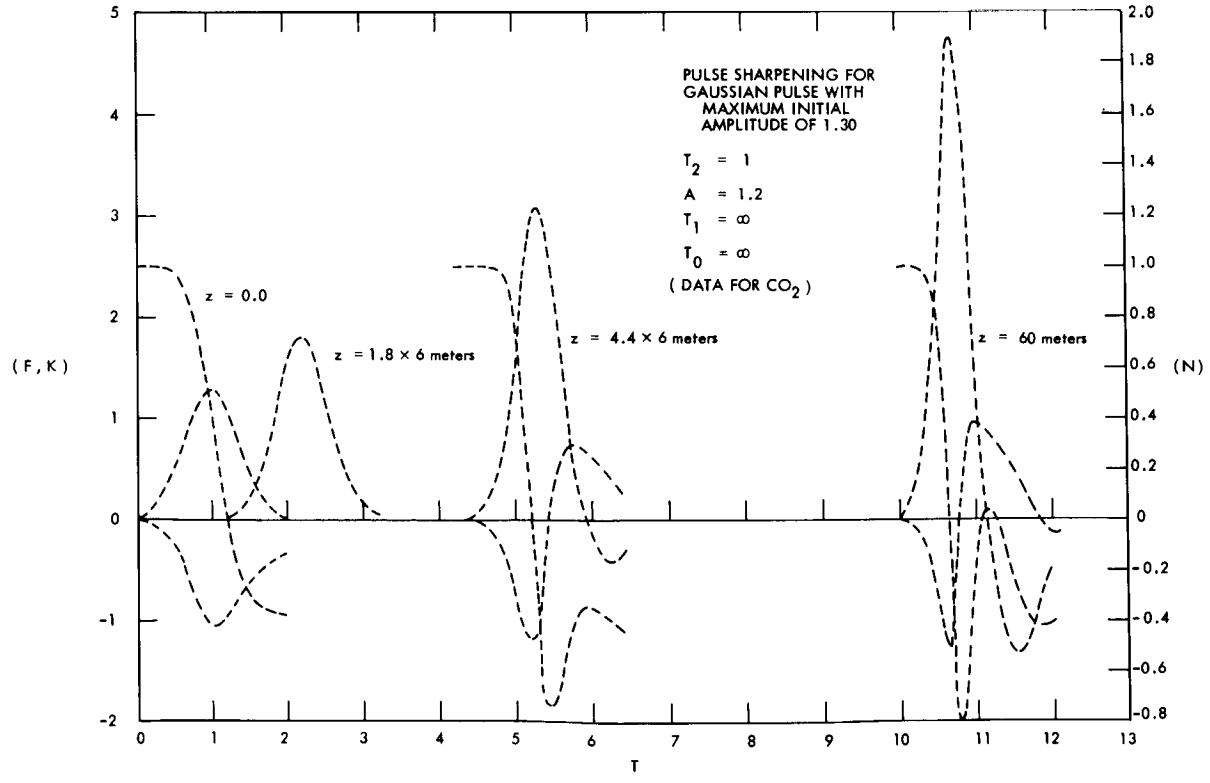

Fig. XVII-1. Pulse sharpening and developing ringing.

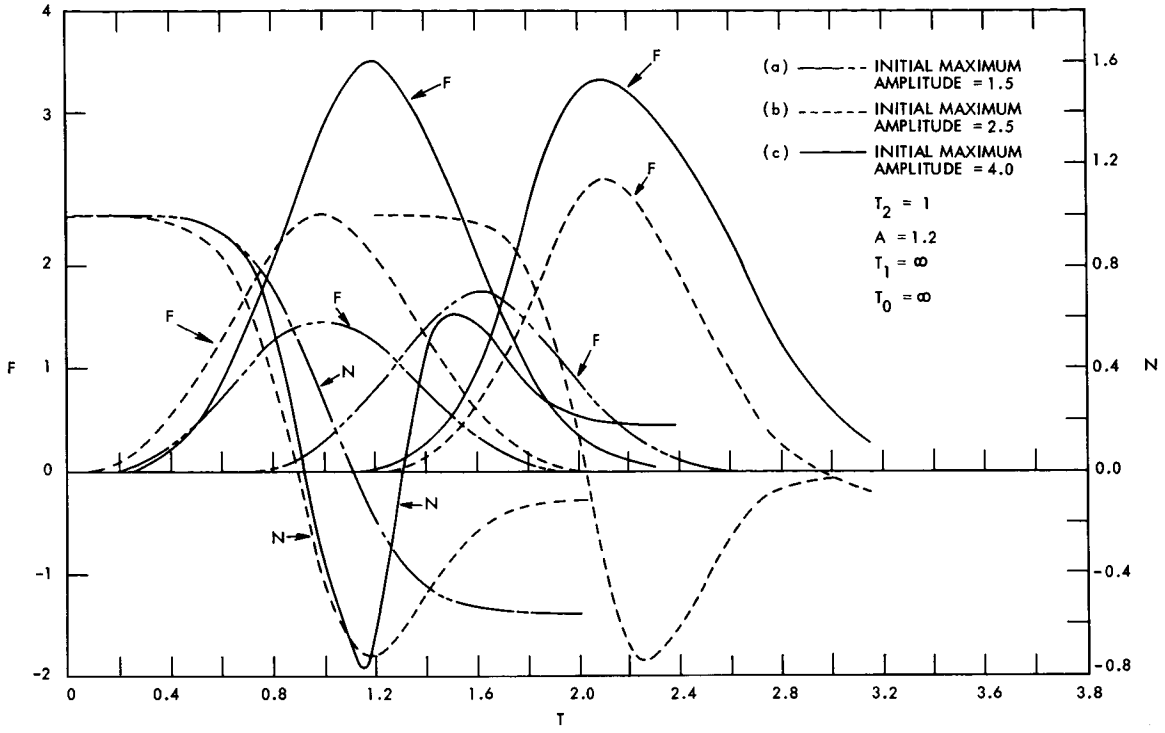

Fig. XVII-2. Initial changes of a Q-switched pulse penetrating an inverted medium.

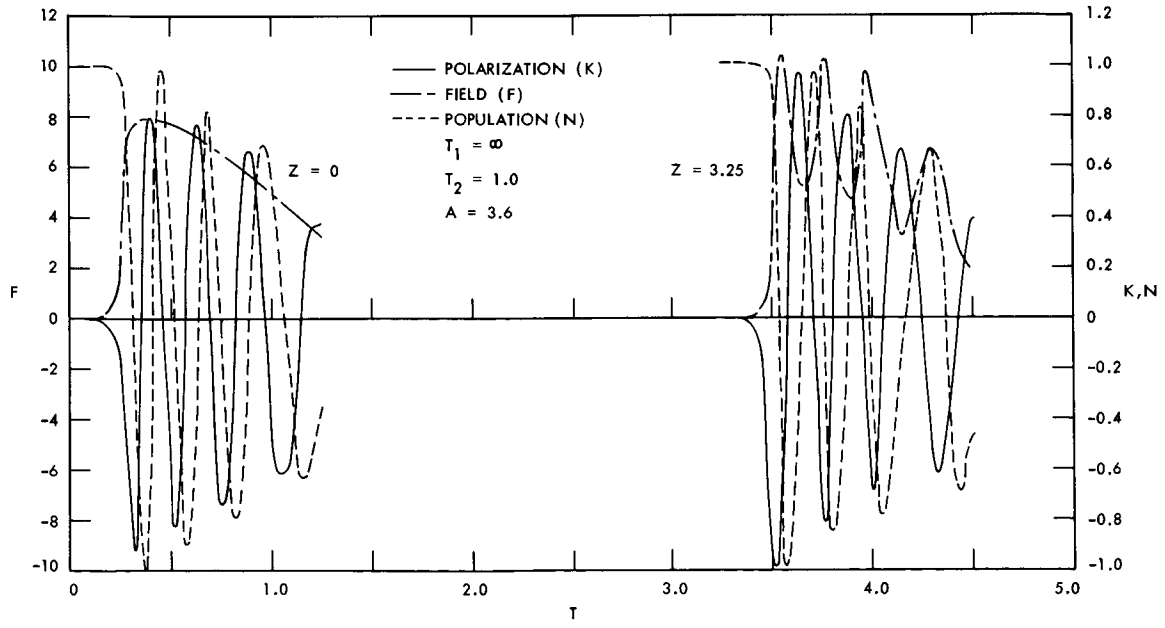

Fig. XVII-3. Development of a pulse with a short initial rise time.

order of $1/T_2$) and the amplitude very large. This case has been discussed by Basov and co-workers.[4] They also consider the effect of a saturable absorber on the sharpening of the characteristics when inertial effects are small. It then becomes a process of sharpening by preferred absorption, rather than by preferred amplification.

If the field amplitude is large, the population can become fully depleted before the peak value of the field has arrived. This causes a pronounced ringing to set in, and can cause the maximum amplitude to initially decrease as the pulse penetrates the medium. This effect is illustrated in Fig. XVII-2 (curve c), in which case the peak energy density associated with the field is much greater than that stored in the medium. The greatest gain in the pulse occurs well ahead of the maximum, which is itself contributing to re-inversion. Hence the maximum is decreasing and the pulse is broadening.

One means of achieving a very narrow pulse would be to chop the initial Q-switched pulse in such a way that its rise time would be very short. Then a much larger amplitude pulse could be used because, for maximum sharpening, the population should be fully depleted in a time comparable to the rise time and the energy required to accomplish this should almost be a constant. Figure XVII-3 shows the development of such a very short pulse. A strong ringing develops because of the large trailing pulse energy. This is essentially the step response obtained by Tang.[2]

The sharpening process can be enhanced by using saturable dyes in conjunction with the amplifying medium. This influence is now being studied with the same program.

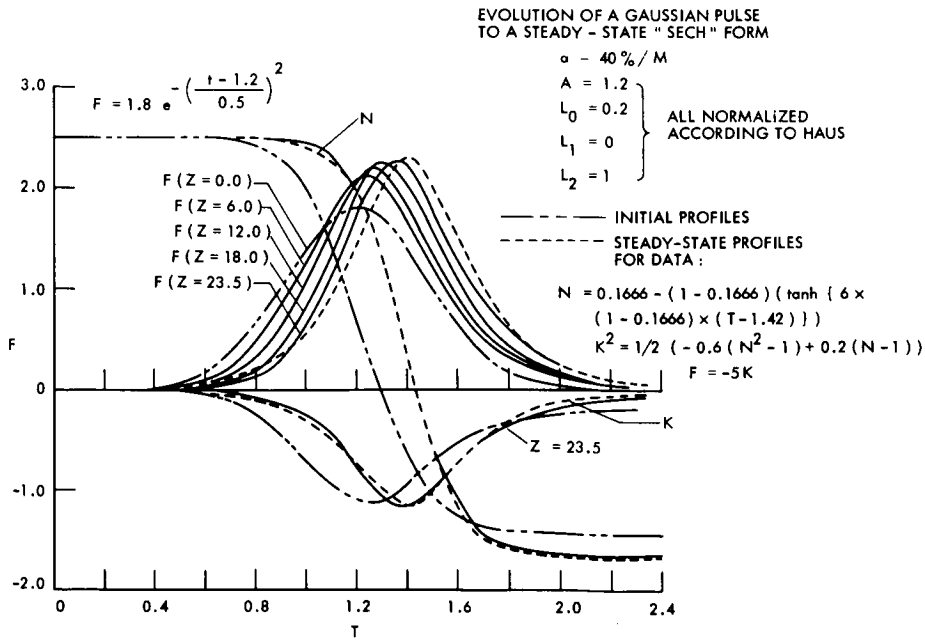

Fig. XVII-4. Evolution of a Gaussian pulse to a steady-state sech profile.

Field loss limits the amount of sharpening and gain which can be obtained from the inverted medium. If the pulse energy is less than a critical value, the pulse at first gains energy and then propagates in a steady-state manner. Similarly, if the pulse energy is greater than the critical value, the energy difference is lost to the medium. A steady-state solution for propagation at the speed of light is given[4,5] by

$$N = \frac{L_o L_2}{A} - \left(1 - \frac{L_o L_2}{A}\right)\left[\tanh \frac{A}{L_o}\left\{1 - \frac{L_o L_2}{A}\ (T+T_o)\right\}\right]$$

$$K_o^2 = \frac{A}{4}\left(1 - \frac{L_o L_2}{A}\right)^2 \operatorname{sech}^2\left[\frac{A}{L_o}\left(1 - \frac{L_o L_2}{A}\right)(T+T_o)\right]$$

$$F_o = -\frac{K_o}{L_o}$$

$$L_o = \frac{1}{\tau_o}; \qquad L_2 = 1.0.$$

We have shown that an initial waveform of a Gaussian shape does tend to the sech $\{A/L_o(1-L_oL_2/A)(T+T_o\}$ profile (Fig. XVII-4). Thus, for a small L_o ($L_o \ll A/L_2$), the limiting pulsewidth is

$$\frac{1}{c}\left(\frac{L_o}{A}\right).$$

For CO_2, the pertinent data are

$$\lambda = \frac{2\pi c}{\omega_o} = 10.6\ \rho.$$

$$T_2 \approx 20 \times 10^{-9}\ \text{sec}.$$

These data give

$$n\left(\rho_{22}^e - \rho_{11}^e\right) = 3.73 \times 10^{12}/\text{cm}^3$$

and

$$\hbar\omega_o\left(\rho_{22}^e - \rho_{11}^e\right) n = 0.69 \times 10^{-7}\ \text{J/cm}^3.$$

For a 20-nsec pulse, a maximum amplitude of $F_o \approx 1.3$ is necessary for sharpening. This gives a peak-power intensity of ~1.5 KW/cm^2.

T. K. Gustafson, H. A. Haus

References

1. H. A. Haus and W. Wagner, "High-Rate Optical Amplification" (unpublished).

2. C. L. Tang and B. D. Silverman, in Physics of Quantum Electronics, Edited by P. Kelley, B. Lax, and P. Tannenwald (McGraw-Hill Book Company, New York, 1966), p. 280.

3. J. P. Wittke, P. J. Warter, J. Appl. Phys. 35, 1668 (1964).

4. N. G. Basov and others, Soviet Phys. – JETP 23, 16-22 (July 1966).

5. F. T. Arecchi and R. Bonifacio, IEEE, J. Quantum Electronics, Vol. 4, pp. 169-178, July 1965.

XVIII. PHYSICAL OPTICS OF INVERTEBRATE EYES*

Academic and Research Staff

Prof. G. D. Bernard

Graduate Students

J. L. Allen
F. Beltran

RESEARCH OBJECTIVES

The dioptrics of the compound eyes of invertebrates may contain a number of structures with dimensions of the order of a wavelength of light. Examples are corneal nipples on the front corneal surface, layers within the cornea and crystalline cone, rhabdomeres, and pigment granules.

We are interested in understanding the effect of such structures on light scattered from and transmitted through the eye, and in understanding what they are doing for the animal.

This work involves: (i) determination of the geometry and electrical properties; (ii) measurements of optical scattering and transmission properties with actual eyes used; (iii) microwave measurements of scaled models; and, (iv) theoretical models.

G. D. Bernard

*This work is supported by the Joint Services Electronics Programs (U. S. Army, U. S. Navy and U. S. Air Force) under Contract DA 36-039-AMC-03200(E).

END

PLASMA DYNAMICS

XIX. PLASMA PHYSICS

Academic and Research Staff

Prof. S. C. Brown
Prof. W. P. Allis
Prof. G. Bekefi
Prof. J. C. Ingraham
Dr. G. Lampis ET AL
J. J. McCarthy
E. M. Mattison
W. J. Mulligan

Graduate Students

M. L. Andrews
A. J. Cohen
D. L. Flannery
V. G. Forrester, Jr.
E. V. George
P. W. Jameson
R. L. Kronquist
D. T. Llewellyn-Jones
J. E. McClintock
G. L. Rogoff
J. K. Silk
D. W. Swain
J. H. Vellanga

RESEARCH OBJECTIVES

As in the past few years much of our effort continues to be the study of plasma-wave interactions. Most recently, particular emphasis has been placed on the properties of longitudinal electron and ion waves and the effect of plasma inhomogeneities on these oscillations. Many of these studies are made in the regime where the waves are weakly or highly unstable; in the latter situation the plasma may become turbulent and we are looking into methods of studying such turbulent media.

We are continuing our program of developing new plama diagnostic methods of measuring electron and ion densities, temperatures, and distribution of particle velocities. These techniques are based largely on the interaction of transverse electromagnetic waves with the ionized medium. The plasma is either illuminated by radiation of appropriate wavelength and then analyzed, or the noise spontaneously emitted by the plasma is studied. The investigations are made at wavelengths ranging from the visible through the infrared and microwave to the long radio waves. Laser and incoherent sources are used in these studies.

The plasmas used in the aforementioned experiments are made in a variety of ways. In addition to the conventional method of breaking down the gas by DC and RF fields, we ionize the medium by means of a high-powered Q-spoiled laser or by injecting electron beams into a neutral un-ionized gas.

S. C. Brown

A. FAR INFRARED SPECTROPHOTOMETER FOR PLASMA STUDIES

1. Introduction

A double-beam optical-null spectrophotometer is being developed for measuring the absorption of far infrared radiation ($0.1 < \lambda < 1$ mm) by a plasma in order to determine experimentally the plasma mechanisms responsible for the emission of incoherent far infrared radiation. The spectrophotometer operates essentially as follows (see Fig. XIX-1). Two beams of radiation from a far infrared source, S, follow separate optical paths, one beam passing through the plasma, P, the other through a calibrated

*This work was supported by the United States Atomic Energy Commission under Contract AT(30-1)-1842.

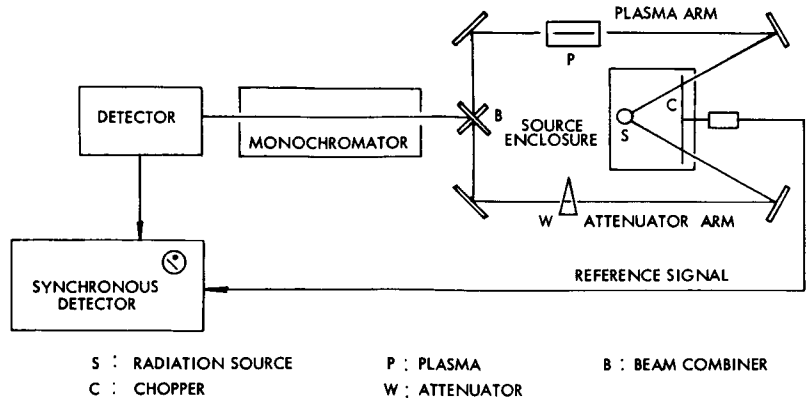

Fig. XIX-1. Schematic illustration of the spectrophotometer.

variable attenuator, W (shown as a movable wedge). The beams are combined at B (by two plane mirrors, one above the other) and are directed to a detector through a grating monochromator, which is set for a particular wavelength. A chopper wheel, C, located near the source permits only one of the beams to pass at a time, effectively switching radiation from S between the two paths at a fixed frequency. A phase-sensitive detector (lock-in amplifier) registers only that part of the detected signal which has this frequency. Thus, the output signal from the synchonous detector corresponds to a difference in the amount of source radiation reaching the detector along the two paths. The attenuator is adjusted to null the detector output, first with the plasma off and then with it on, the difference in attenuator setting in the two cases giving the plasma attenuation.

The relation between attenuator setting and plasma attenuation actually includes the effects of extraneous emission, reflection, and transmission of the various components of the optical system and of its environment, as well as the minimum detectable power of the detection system. If the assumptions are made, however, that all radiation reaching the detector from the chopper plane does so along the intended optical path (that is, stray chopped radiation is negligible), the state of the plasma does not affect the chopped power in either arm, all transmittances in the system (except for the plasma and attenuator) remaining unchanged during the measurement, and the chopped power reaching the detector in either arm is large compared with the minimum detectable power, then the plasma transmittance is given simply by

$$T_p = \frac{T_{wb}}{T_{wa}}. \tag{1}$$

Here T_{wa} is the attenuator transmittance that nulls the detector output with the plasma off, and T_{wb} is the attenuator transmittance that nulls the detector output with the plasma on. Note that the transmittance of the atmosphere and optical components in the

arms need not be equal to make the measurement. They need only remain constant.

The only radiant power, J, that must be considered in determining T_p is that introduced into either beam at the chopper plane, since the synchronous detector responds only to the radiation that is modulated by the chopper. When a chopper blade intersects the beam, J includes radiation from the chopper blade itself, as well as radiation from elsewhere (optical components, plasma, and surroundings) that is reflected into the beam by the blade. When the beam is not obstructed by the chopper, J includes source radiation already attenuated by the mirrors and atmosphere in the source enclosure, radiation from parts of the source enclosure that are now exposed, and radiation from elsewhere that enters the source enclosure and is reflected back out into the beam. For Eq. 1 to hold, care must be taken to insure that, in each beam, the difference between these two power levels with the plasma on is equal to their difference with the plasma off.

2. Optical Arrangement

The optical arrangement has many important features, most of which are concerned with maximizing the radiant flux through the system. This is essential, because of the limited amount of far infrared radiation emitted by the source, S, which is a high-pressure Hg arc lamp. Although, for clarity, much of the following discussion refers to the plasma beam, it is equally applicable to the attenuator beam.

(i) Front-surfaced mirrors are used throughout to avoid the transmission losses and dispersion associated with lenses in the far infrared. The reflectivity of aluminized mirrors is excellent in this spectral region.

(ii) The entire system is designed so that the grating monochromator is the only component that limits the radiant flux through the system. The source is imaged at the monochromator slit. Thus, the grating is the aperture stop of the system and the slit is the field stop. (Note that the monochromator is not overfilled. If it were overfilled, the chopped radiation that misses the grating might reach the detector by an unintended optical path.)

(iii) The radiation beam through the plasma has the smallest possible diameter that is consistent with feature (ii), according to which the monochromator limits the flux through the system. Unfortunately, space does not permit a detailed discussion of this important feature. It turns out that for a plasma length, L, in an ideal optical system, the minimum beam diameter, w, that is consistent with feature (ii) is $w = \sqrt{KL}$, where K is a constant determined by the monochromator dimensions ($K = 0.374$ cm). This beam diameter is obtained by locating a slit conjugate at one end of the plasma (either end) and a grating conjugate at the other end, with both conjugates being of equal diameter, w. Although the boundaries of this beam are parallel with the optical axis, rays within the beam are at angles θ with respect to the axis up to θ_{max}, given by

$\tan \theta_{max} = w/L$. Note that if the plasma tube diameter is smaller than w, the tube itself limits the maximum possible flux through the system. This is an important factor when only weak radiation sources are available, as is the case in the present experiment. (This discussion applies for $w \ll L$.)

(iv) To reduce stray chopped radiation, conjugates of both the monochromator slit and grating are located between the source and chopper and apertures of the conjugate dimensions are placed at these locations. These apertures allow only radiation that reaches the real slit and grating by the intended optical path to be chopped. (An ideal optical system is assumed.) Since the beam diameter must have a relative minimum at one member of such a pair of conjugates, one conjugate is small compared with the chopper blade and is located very near the chopper plane to obtain a sharply chopped signal. The other conjugate is large enough to allow for reductions in aperture size without introducing significant diffraction effects.

(v) A beam combiner is located at a grating conjugate just before the monochromator entrance slit. The beam combiner consists of two plane mirrors, one located above the other, each directing one of the two beams into the monochromator. The size of this grating conjugate is large enough to be split conveniently by the two mirrors (with negligible diffraction effects), and it is located relatively close to the monochromator, permitting reasonable flexibility in arranging the remaining mirrors for the two separate beams. (Since there is a focusing mirror between the monochromator and beam combiner, the beam combiner can be located closer to the monochromator if it is located at a grating conjugate rather than at a slit conjugate.) The grating conjugate in the source enclosure is made larger than its corresponding slit conjugate (which is small and near the chopper plane) so that one-half of its aperture may be obstructed, thereby allowing chopped radiation to reach only the half of the beam combiner that directs the radiation into the monochromator. Radiation from one beam that reaches the half of the beam combiner intended for the other beam will be reflected out of the optical path, and may reach the detector by an unintended path (for example, without passing through the monochromator).

(vi) Since high-quality image formation is not of primary importance in the system, spherical mirrors are used for focusing purposes. At all such mirrors the incident and reflected beams are as close to being on-axis as possible.

(vii) The system contains only mirrors that are conveniently available from suppliers' stock, in order to facilitate initial construction, component replacement, and system alterations in the future. It was possible to design the system from a mirror selection with focal lengths 7.5, 10, 15, 20, 30 cm and diameters of 5, 7.5, 10 cm.

(viii) The optical path lengths in the system are limited as much as possible to reduce atmospheric absorption and diffraction losses and to facilitate construction. The system is designed to accommodate an enclosure if purging becomes necessary.

(It may be possible to avoid this necessity by operating at appropriately selected wavelengths.)

(ix) The system can be operated as a single-beam instrument if in one beam the obstacle over one-half of the grating conjugate in the source enclosure is removed and the beam-combiner mirrors are made parallel to direct that beam into the monochromator. In this case the entire radiant flux is utilized on one arm, rather than being divided between two arms. The other beam should be blocked at the source enclosure, to prevent it from contributing stray chopped radiation to the detector.

(x) The source enclosure openings face away from the monochromator and detector to reduce stray chopped radiation, and the radiation beams intersect the chopper plane and source enclosure face at an angle, so that radiation from components in the system, particularly from the plasma, will not be reflected back into the beam.

Figure XIX-2 illustrates the optical arrangement of the system from the source

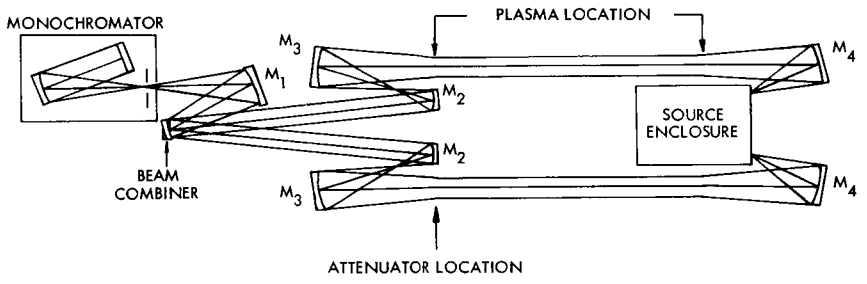

Fig. XIX-2. Optical layout of the spectrophotometer (showing only focusing mirrors).

enclosure to the monochromator. To avoid unnecessary confusion, the plane mirrors that are required are omitted from the illustration. Plane mirrors are used to bend the beam, to insure that the incident and reflected beams at each spherical mirror are as close to being on-axis as possible, and to compress a long beam section into a small space (by "folding" the beam) where this is necessary. The portion of the system between the source and monochromator is illustrated again in Fig. XIX-3 for the plasma arm, where, for simplicity, the mirrors are represented as lenses. The part of the system between the source and beam combiner is duplicated in both beams, with the attenuator being located at σ_p in its arm. In each beam radiation traverses only one-half of each grating conjugate so that at the beam combiner and at the grating itself the two beams are adjacent, one above the other. At the slit and its conjugates following the beam combiner the two beams overlap. Consequently, in double-beam operation each beam contributes one-half of the radiant flux through the monochromator.

The slit and grating conjugates at the plasma ends are arranged as shown so that the

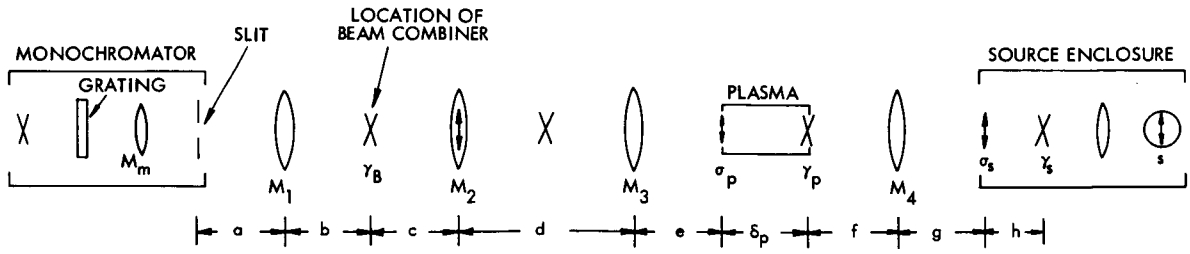

↕ : CONJUGATE OF SLIT
X : CONJUGATE OF GRATING
σ = DIAMETER OF SLIT CONJUGATE
γ = DIAMETER OF GRATING CONJUGATE
f = MIRROR FOCAL LENGTH

f_m = 27 cm	a = 26 cm
f_1 = 20	b = 23
f_2 = 10	c = 65
f_3 = 15	d = 30
f_4 = 15	e = 30
γ_B = 5	f = 30
σ_p = 5	g = 18
γ_p = 5	h = 10
σ_s = 0.75	δ_p = 67
γ_s = 2.5	

Fig. XIX-3. Locations of the slit and grating conjugates in the system.

required conjugates in the source enclosure can be obtained with a single concave mirror between the source enclosure and plasma. This is convenient because the experimental space in this region is limited.

Three concave mirrors (M_1, M_2, M_3) are used between the plasma and the monochromator to produce the required slit and grating conjugates at the plasma ends and at the beam combiner. The mirror, M_4, was selected to give convenient dimensions between the plasma and the source enclosure apertures, as well as convenient sizes for these apertures. The focal lengths of these mirrors are listed in Fig. XIX-3, along with some calculated system dimensions. These dimensions actually only approximate the final dimensions of the optical layout, since no attempt was made to account accurately for such things as aberrations or deviations of the actual focal lengths from the expected values. To adjust for these effects, slight alterations were made experimentally in the dimensions and aperture sizes.

Several different kinds of attenuators are being considered for use in the system. At present, a simple wedge of low-absorption material is being tried.

The monochromator is a Perkin-Elmer prism monochromator (Model 99) that has been modified for use as a single-pass grating instrument. The f number of this Littrow-type instrument is approximately 3.8. The slit height is 12 mm, and the maximum slit width has been increased to appoximately 8 mm.

When required, radiation filters (wire-mesh reflection filters) will be located

between the monochromator and detector in order to act on both beams simultaneously. The detector is a Mullard Indium Antimonide photoconducting detector.

The plasma will be a DC discharge (5 cm in diameter, 50 cm long). "Bubble windows"[1] will be on the ends of the plasma tube.

The basic optical system has been completed and tested in a preliminary manner, with very encouraging results.

G. L. Rogoff

References

1. G. L. Rogoff, Quarterly Progress Report No. 82, Research Laboratory of Electronics, M. I. T., July 15, 1966, pp. 114-121.

B. EXPERIMENTAL STUDY OF ELECTRON PLASMA OSCILLATIONS

Observations of microwave scattering from density fluctuations in a beam-plasma have been previously reported,[1,2] and it has been established[2] that the density fluctuations are associated with standing waves along the axis of the plasma column. The experimental study of these waves has continued, and we present in this report the experimentally determined disperison relation for the waves and a measurement of their temporal growth rate.

The experimental geometry is the same as described previously,[2] and is illustrated in Fig. XIX-4. Briefly, the plasma is produced by firing an electron beam into un-ionized

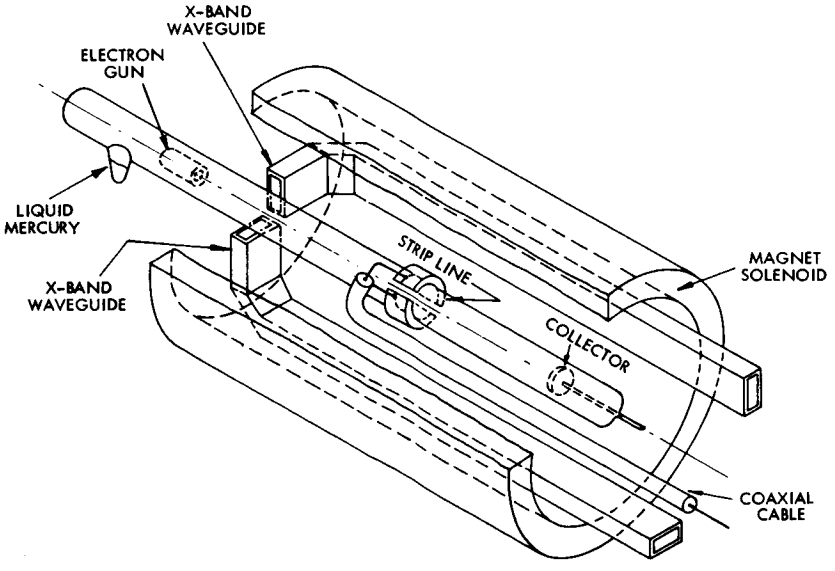

Fig. XIX-4. Experimental geometry.

mercury vapor at a pressure of 2×10^{-4} mm Hg. The axis of the plasma tube is aligned along a uniform magnetic field. Two open-ended pieces of X-band waveguide, which serve as microwave horns in the scattering experiments, and a strip-line antenna, which couples capacitively to the plasma and picks up the oscillations directly, are mounted on a platform that can be moved along the axis of the plasma tube.

The spectra of oscillations at three different axial positions of the strip line are shown in Fig. XIX-5. At each position, peaks occur at the same frequencies, but the

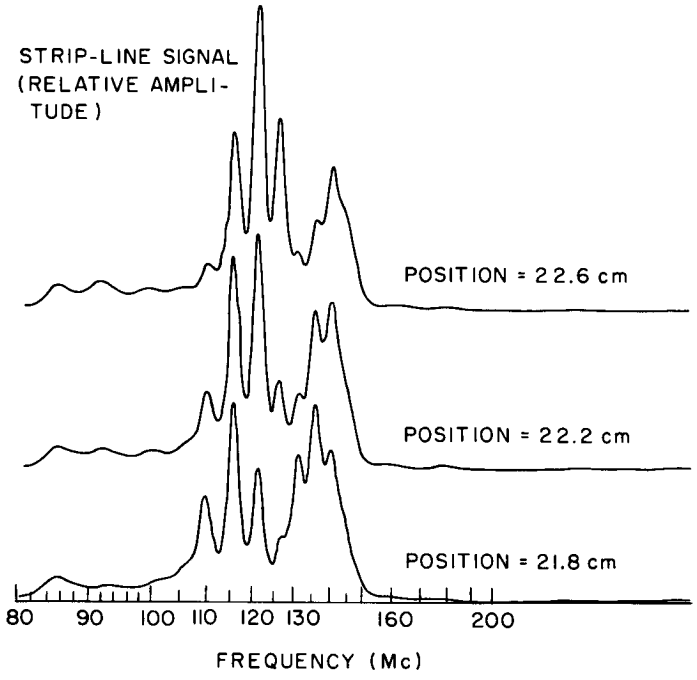

Fig. XIX-5. Amplitude of strip-line signal vs frequency.

relative amplitudes of the peaks are different in each of the spectra. A series of such spectra was taken for axial positions 2 mm apart along the length of the plasma tube which was accessible to the strip line. It was thus possible to follow each frequency peak or mode along the axis and plot its amplitude against distance, as shown in Fig. XIX-6. The minima and maxima, representing nodes and anti-nodes, indicate that each mode can be identified with a standing wave, in which the wavelength is given by twice the distance between two adjacent anti-nodes.

The collector for the electron beam is a helically shaped cathode, which was previously used to run a discharge in the plasma tube. Because of nickel sputtered onto the walls of the tube from this collector cathode, data taken near the collector are not meaningful. Nevertheless, it can be seen from Fig. XIX-6 that for all of the modes shown, the first maximum is spaced almost exactly a half-wavelength from

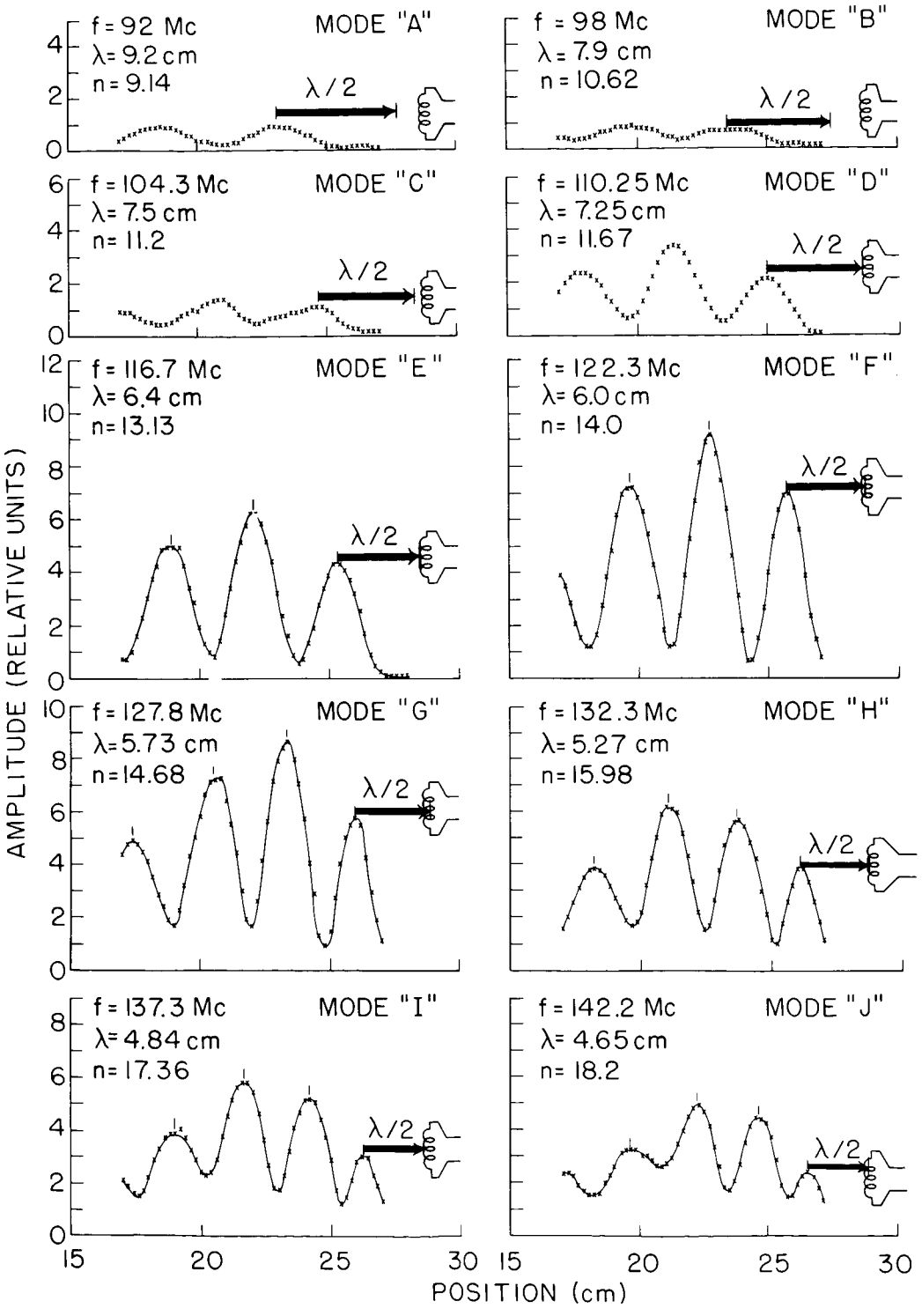

Fig. XIX-6. Amplitude of strip-line signal at fixed frequency vs distance.

the collector. This indicates that the boundary condition at the collector is that it should be an anti-node. This seems reasonable if we assume that the amplitude of the strip-line signal represents the amplitude of the electron density modulation resulting from the wave. The electron density in a plasma wave is roughly analogous to the pressure in an ordinary sound wave in a gas, and for a sound wave the pressure modulation has an anti-node at a rigid end wall. The measurements described above were made with the collector floating, so no current could be drawn, and the analogy of a rigid end wall for a pressure wave seems reasonable. We plan to repeat these measurements with the voltage of the collector variable, to see if the boundary condition of an anti-node at the collector can be changed.

The dispersion relation for the waves can be determined from the set of plots in Fig. XIX-6, since the frequency and wavelength for each mode have been measured. Before plotting the dispersion relation, however, it is interesting to identify with each mode a mode number n, where n is the number of half-wavelengths, $\lambda/2$, along the plasma column of length L = 42 cm. (It is assumed that the electron gun is also at an anti-node.) Therefore, we calculate for each of the modes in Fig. XIX-6 a mode number, $n = 2L/\lambda$, which will be close to, but not exactly equal, an integer, since there is some experimental error in the measurement of λ. From inspection of the n's calculated from Fig. XIX-6, we can identify these modes as corresponding to n = 9, 10, ..., 18. When we plot the dispersion relation, we eliminate the small experimental error in the measurement of λ, by using the λ corresponding to the integral mode numbers instead of the measured λ.

A series of peaks lower in frequency and amplitude than those shown in Fig. XIX-5 were also observed, but their wavelengths were too long to be measured. Nevertheless their mode numbers are known, since the mode numbers of the higher modes have been determined as described above. The dispersion relation is plotted in Fig. XIX-7, where the modes whose wavelengths were measured directly are denoted by x's and the modes whose wavelengths were not measured are denoted by circles.

The straight line in Fig. XIX-7 represents a wave whose phase velocity would be equal to the beam velocity, and it is interesting to note from Figs. XIX-7 and XIX-6 that the waves whose phase velocities are nearest to the beam velocity are most strongly excited. (These are the modes labeled F and G in Fig. XIX-6.) The experimentally determined dispersion relation qualitatively resembles that for plasma waves propagating along the axis of a plasma cylinder with a finite radius,[3] but no comparisons have been made with theory, since measurements have not yet been made of the plasma and electron beam densities.

Additional measurements have also been made of the microwave scattering from these waves. Previously,[2] scattering measurements and direct observations of the waves by means of the strip line were made but not with identical experimental

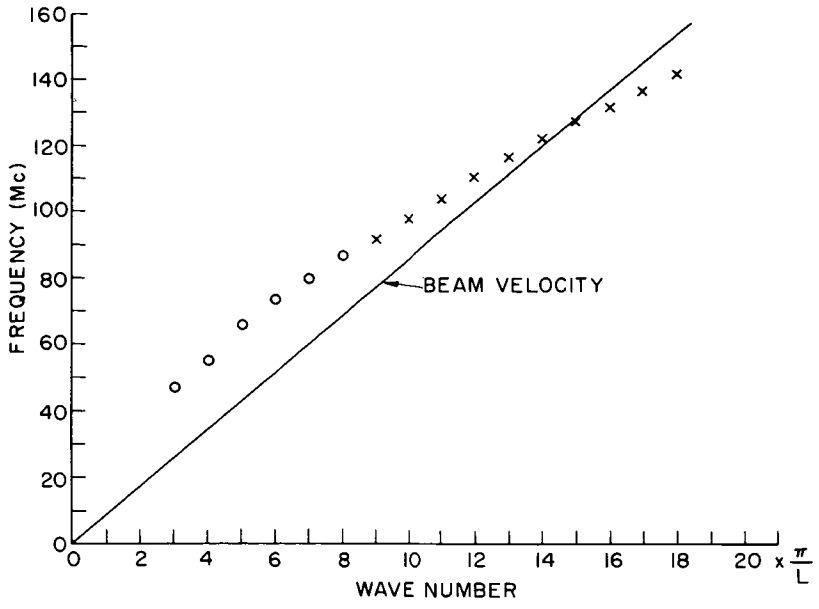

Fig. XIX-7. Frequency vs wave number, $k_n = \frac{n\pi}{L}$.

parameters, so a direct comparison could not be made between the scattering and the strip-line data. The new data are shown in Fig. XIX-8, where we plot on the same graph the direct signal from the antenna against frequency and data points representing

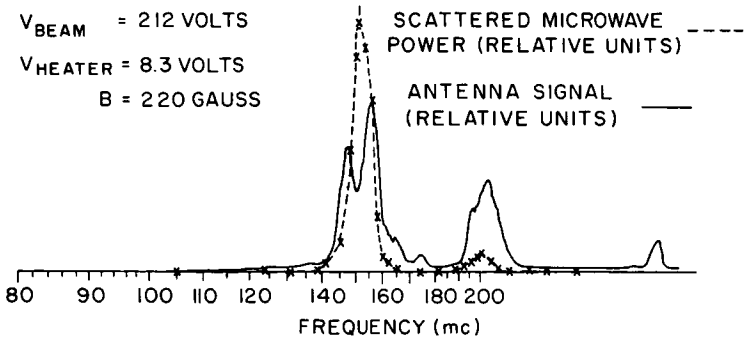

Fig. XIX-8. Antenna signal vs frequency and scattered power vs frequency shift.

the amplitude of the scattered microwave power against frequency shift between incident and scattered frequencies. These data were taken with the microwave horns at the same axial position as the antenna and with identical experimental parameters. The amplitudes and shapes of the peaks for the scattering and direct-signal data differ considerably, but the frequencies of the peaks coincide quite well. The double peak seen in the

signal picked up by the antenna is not resolved in the scattering data, probably because of the wide bandwidth of the IF strip in the X-band radiometer (10 Mc) as compared with the bandwidth of the radio receiver (2 Mc) which detected the signal from the antenna.

Measurements of the temporal behavior of these waves have also been made. The strip line was connected directly to an oscilloscope and the voltage on the electron gun was pulsed. Figure XIX-9 shows the voltage pulse and the envelope of the signal picked

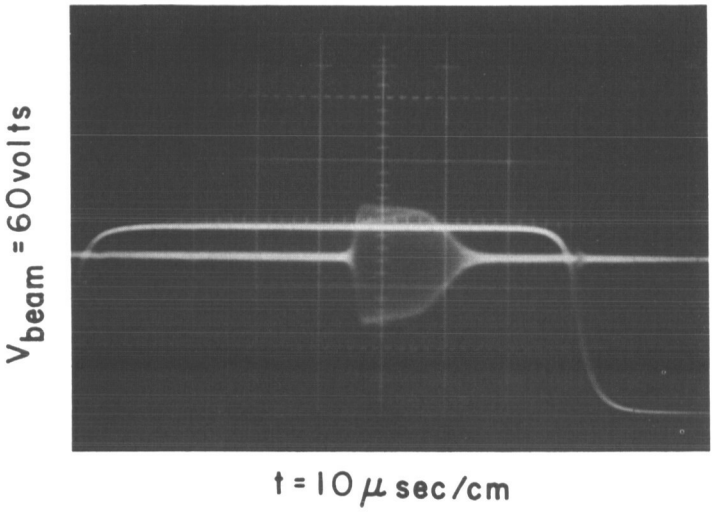

Fig. XIX-9. Voltage applied to electron gun and strip-line voltage vs time.

up by the strip line. The oscillations appear approximately 40 μsec after the voltage has been applied to the gun. This time delay may be ascribed to two effects, the time required for the beam to ionize enough neutral atoms so that the plasma frequency reaches the value required for instability, and the time required for the wave to grow from noise to an amplitude that can be detected. It can also be seen that the amplitude of the wave saturates after approximately 2 μsec, and then remains approximately constant for approximately 10 μsec, after which it decays with a longer time constant than that which characterized its growth. It should be noted that the decay begins well before the voltage on the electron gun is turned off. When the pulsewidth was increased, it was found that an instability again appeared several microseconds after the decay of the first instability. This also saturated and decayed and was followed by subsequent bursts of oscillations. Figure XIX-10 shows the growth of the instability shown in Fig. XIX-9, but with an expanded time scale so that both the frequency and the growth rate can be determined. The frequency is 20.7 Mc, which seems to correspond to one of the lower standing-wave modes of the dispersion relation in Fig. XIX-7. The higher modes may correspond to the bursts occurring at later times, but this is not yet clear. The wave

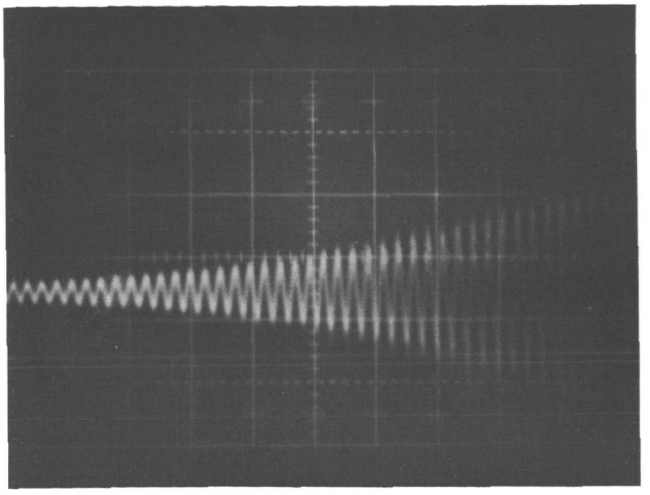

t = 0.2 μsec/cm

Fig. XIX-10. Strip-line voltage vs time.

amplitude is plotted against time in Fig. XIX-11 on a semi-log scale, and the straight line indicates that the growth is exponential until saturation occurs. The frequency of the wave is $\omega = \omega_r + i\omega_i$, with $\omega_r = 2\pi \times 20.7 \times 10^6$ and $\omega_i = 1.33 \times 10^6$, giving $\omega_i/\omega_r \approx 0.01$. Thus $\omega_i/\omega_r \ll 1$, satisfying a basic assumption of quasi-linear theory which

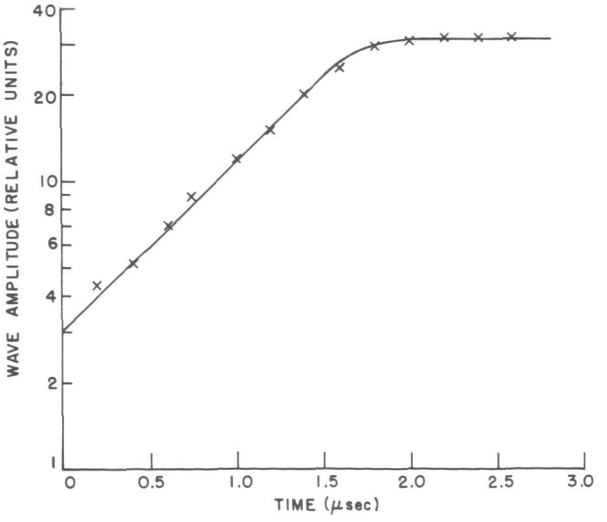

Fig. XIX-11. Wave amplitude vs time.

describes the saturation of a slowly growing plasma wave by action of the wave back on the electron velocity distribution function. It is hoped that the observed saturation can be explained in terms of this theory.

R. L. Kronquist

References

1. R. L. Kronquist, "Microwave Scattering from an Electron-Beam Produced Plasma," Quarterly Progress Report No. 82, Research Laboratory of Electronics, M. I. T., July 15, 1966, pp. 109-114.

2. R. L. Kronquist, "Microwave Scattering from Standing Plasma Waves," Quarterly Progress Report No. 83, Research Laboratory of Electronics, M. I. T., October 15, 1966, pp. 53-58.

3. A. W. Trivelpiece and R. W. Gould, J. Appl. Phys. 30, 1784 (1959).

XX. GASEOUS ELECTRONICS*

Academic and Research Staff

Prof. S. C. Brown
Prof. W. P. Allis
Prof. G. Bekefi
Prof. J. C. Ingraham
E. M. Mattison
J. J. McCarthy
W. J. Mulligan

Graduate Students

W. B. Davis
G. A. Garosi
L. D. Pleasance
T. T. Wilheit, Jr.
B. L. Wright

RESEARCH OBJECTIVES

A great deal of effort continues to be spent on the fundamental interaction of the particles of plasma physics. In this group we have concentrated on measuring diffusion coefficients, collision probabilities, particularly in partially ionized and fully ionized gases, and on the mechanism of production of radiation. Within the last few years we have studied the production of microwave radiation, and we are pushing this toward shorter and shorter wavelengths in the direction of the very long infrared. Our objective in this area is to study as many of the mechanisms involved in electron-atom and electron-molecule collisions as are susceptible to our microwave, infrared, and probe techniques.

S. C. Brown

A. ELECTRON-ELECTRON RELAXATION RATES AS DETERMINED FROM THE OBSERVED TIME-DEPENDENT ELECTRON VELOCITY DISTRIBUTION

Experimental observations of the time-dependent electron velocity distribution function, $f(v, t)$, during the early afterglow of an argon discharge have been previously reported.[1] Solution of an appropriate theoretical model showed good agreement with both the observed steady-state distribution during the DC voltage pulse and the instantaneous energy loss rate at the beginning of the afterglow.[2] Under the conditions of the experiment (argon pressure ~1 Torr and electron density $\sim 10^{10}$ cm^{-1}), electron-electron and electron-atom collisions are found to represent competing mechanisms with comparable characteristic rates. In interpreting the observed time dependence of $f(v, t)$, it is desirable to examine quantities which to some extent separate these two effects. Thus, since mean electron energy is conserved by electron-electron interactions, the rate of energy loss previously analyzed is largely determined by electron-atom collisions. Electron-electron effects, however, play an indirect role in the cooling by replenishing $f(v)$ at higher velocities where (in argon) the energy loss rate is greater.

To obtain a more direct measure of the rate of electron-electron interaction, we

*This work was supported by the Joint Services Electronics Programs (U.S. Army, U.S. Navy, and U.S. Air Force) under Contract DA 36-039-AMC-03200(E).

note that the ultimate effect of this interaction is the attainment after a few microseconds of a nearly Maxwellian velocity distribution with a temperature (~10,000°K) well above that of the neutral gas. Parameters which in some sense measure the departure of f(v) from a Maxwellian should consequently provide information on the electron-electron relaxation rate. In defining such parameters f(v) is to be compared with a Maxwellian that has the same average electron energy, and only the over-all shape of f(v) is important. We thus define a dimensionless velocity variable, $z = v/w$, in terms of the characteristic velocity, w, defined by

$$\frac{3}{2}w^2(t) = 4\pi \int_0^\infty v^4 f(v,t)\, dv.$$

Here f(v, t) is normalized so that $4\pi \int_0^\infty v^2 f\, dv = 1$. The distribution function for scaled velocities, g(z, t), is now given by

$$g(z,t) = w^3 f(wz,t)$$

which satifies both $4\pi \int_0^\infty z^2 g\, dz = 1$ and $4\pi \int_0^\infty z^4 g\, dz = \frac{3}{2}$. This function is to be compared with the correspondingly scaled Maxwellian,

$$\hat{g}(z) = \pi^{-3/2} e^{-z^2}.$$

Perhaps the most classic measure of the departure of a velocity distribution from a Maxwellian is Boltzmann's parameter H. It represents a generalization of the concept of entropy to systems not in thermal equilibrium. For the scaled distribution function, H is given by

$$H(t) = 4\pi \int_0^\infty z^2 g \ln g\, dz$$

which is to be compared with the Maxwellian (minimum) value, $\hat{H} = -\frac{3}{2}(\ln \pi + 1)$. Other less physically justifiable parameters may also be used. For example, the quasi-moments given by

$$Q_n(t) = 4\pi \int_0^\infty z^{2+n} g\, dz$$

can (for $n \neq 0, 2$) differ from the corresponding Maxwellian values

$$\hat{Q}_n = \Gamma\left(\frac{3+n}{2}\right) \Big/ \Gamma\left(\frac{3}{2}\right).$$

Finally, a crude gauge of the departure from Maxwellian may be determined from the mean absolute difference,

$$A_o(t) = 4\pi \int_0^\infty z^2 |g-\hat{g}|\, dz.$$

Thus $H - \hat{H}$, $Q_n - \hat{Q}_n$, and A_o are all quantities that should approach zero as f(v, t) relaxes to equilibrium. Semi-logarithmic plots of the time dependence of these quantities are shown in Fig. XX-1. The open squares represent experimental values based

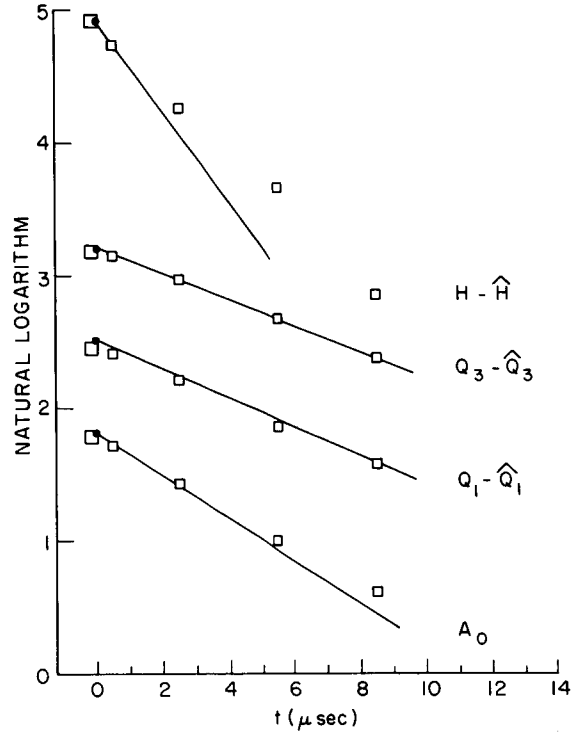

Fig. XX-1. Afterglow time dependence of quantities that measure the departure of f(v) from a Maxwellian.

on the same data ($p = 0.72$ Torr, $n = 1.1 \times 10^{10}$ cm^{-3}) discussed in the previous reports.[1,2] In Fig. XX-1, the vertical positions of some of the plotted quantities have been shifted for purposes of display.

In comparing the observed decay rates with a theoretical model, at this stage, we are still dependent upon solution of a steady-state problem which provides $\dot{f} = \frac{\partial}{\partial t} f(v, t)$ only at the beginning of the afterglow (t=0). Nonetheless, if f and $\dot{f}$ are known, the time dependence of the scaled distribution is given by

$$\dot{g} = w^3 \left[3 \frac{\dot{w}}{w} f + \frac{\dot{w}}{w} v f' + \dot{f}_a \right] + w^3 \dot{f}_e,$$

where f' is the partial derivative of f(v, t) with respect to v. In this expression we have separated $\dot{f}$ into $\dot{f}_a$, attributable to collisions with atoms, and $\dot{f}_e$, attributable to electron-electron interactions only. In the absence of electron-atom impacts or for a collision frequency independent of velocity, the term in brackets vanishes.

When $\dot{H}$, $\dot{Q}_n$ and $\dot{A}_o$ are evaluated from $\dot{g}$ at t = 0, positive theoretical slopes are obtained. Initially, electron-atom effects are dominant, and the distribution is driven farther away from a Maxwellian. Experimentally this has never been seen to occur. Indeed, simplified analysis of the electron-atom collision-dominated case shows that the initial trend at t = 0 is quickly reversed in a time of approximately 1 μsec after which Maxwellization can occur. Thus it seems inadvisable to compare the instantaneous theoretical rates at t = 0 with the observed relaxation of these parameters. On the other hand, if, after some interval, collisions with atoms cease to dominate, $\dot{g}$ will depend, for the most part on $\dot{f}_e(v, t)$. The relaxation rates resulting from electron-electron effects are not expected to vary much with time. It is therefore not too surprising that slopes obtained simply by using $\dot{g} = w^3\dot{f}_e(t=0)$ (shown as solid lines in Fig. XX-1) agree fairly well with the experiment.

We find, then, that the time dependence of parameters that measure the departure of f(v, t) from a Maxwellian can be correctly given by our simple collisional model, provided electron-electron interactions dominate. Reconciling this fact with the theoretical result that electron-atom collisions are initially important will require a full time-dependent solution of the model equation.

B. L. Wright

References

1. B. L. Wright, "Microwave Measurements of a Time-dependent Electron Velocity Distribution Function," Quarterly Progress Report No. 80, Research Laboratory of Electronics, M.I.T., January 15, 1966, pp. 99-103.

2. B. L. Wright, "Comparison of Measured Time-dependent Electron Velocity Distributions with a Theoretical Model," Quarterly Progress Report No. 83, Research Laboratory of Electronics, M.I.T., October 15, 1966, pp. 59-64.

XXI. PLASMAS AND CONTROLLED NUCLEAR FUSION

A. Active Plasma Systems*

Academic and Research Staff

Prof. L. D. Smullin Prof. G. D. Bernard Prof. R. J. Briggs
Prof. A. Bers Prof. J. G. Siambis

Graduate Students

R. R. Bartsch
S. R. J. Brueck
S-L. Chou
J. A Davis
F. N. Herba
B. R. Kusse
O. Lopez
J. A. Mangano
R. R. Parker
D. M. Perozek
H. M. Schneider
R. E. Tremain, Jr.
R. N. Wallace

RESEARCH OBJECTIVES

1. Beam-Plasma Discharge

Our principal research effort will go into the study of means of transferring the greatest amount of power from a beam to its resultant plasma. Experimentally, this will involve the redesign of System D in such a way as to permit easier variation of gun parameters, and beam powers up to 1 MW, or so, will be used. Also, the redesign will provide greater pumping speed and will allow the use of highly conducting end plates just outside the mirrors to provide "magnetic line-tieing."

Other studies will continue the work on excitation of ion motion by modulating the beam at an appropriate frequency between the ion-cyclotron and the hybrid frequency.

2. Beam-Plasma Interactions: Experiments and Theory

During the past year, we have observed beam-plasma interactions that lead to self-excited ion oscillations in the vicinity of the ion plasma frequency ω_{pi}. Our effort now is to establish an appropriate theoretical model that will explain these observations and ellucidate the role of hot electrons.

A velocity analysis of the emerging beam in System A has been obtained. Theoretical work on the nonlinear aspects of beam-plasma interactions is being carried out in order to obtain a quantitative picture of the energy loss by the beam.

Experiments have been initiated to study the nature of beam-plasma interactions when the injected beam has a considerable fraction of its energy across the applied magnetic field. Low-frequency oscillations and a diocotron-type breakup of the beam have been observed.

3. Active Plasma Effects in Solids

We plan to continue our theoretical studies of plasma instabilities in solids that may be of interest for high-frequency generation and amplification. An analysis of acoustic-wave growth in the presence of electron drift along an applied magnetic field has been completed. The analysis of quantum effects that become important at high frequencies continues. Other modes under study are the drifted-helicon wave with its self-magnetic field, and nonlocal effects on the helicon surface-wave mode.

L. D. Smullin, A. Bers, R. J. Briggs, R. R. Parker

*This work was supported by the National Science Foundation (Grants GK-57 and GK-1165).

1. SYSTEM C: ION-CYCLOTRON WAVE GENERATION

The study of ion-cyclotron wave excitation and propagation in System C has been completed and the results will be submitted to the Department of Electrical Engineering, M. I. T., as an Sc. D. thesis.

One of the results of this study is the solution of the eigenvalue problem previously posed.[1] In addition to the exact solution, we have obtained good approximate solutions in two mutually exclusive regions of plasma parameters, one of which corresponds to the "zero-electron mass" approximation.

R. R. Parker

References

1. R. R. Parker, Quarterly Progress Report No. 82, Research Laboratory of Electronics, M. I. T., July 15, 1966, pp. 127-131.

2. BEAM-PLASMA DISCHARGE: SYSTEM D

Oscillations Stimulated by a DC Beam

A DC beam has been injected into the afterglow of the beam-plasma discharge to study the interaction of a low-energy (<1 kV) beam with a plasma that has a significant fraction of its electron density in the form of hot electrons. We see oscillations in the 250-1000 Mc range, which cease at the times corresponding to the electron plasma frequency (as determined by the previously measured density decay), dropping below the particular frequency that is being observed. Low-frequency oscillations in the range 1-50 Mc are observed 50-150 msec after the main discharge. We are now attempting to correlate these observations with the work of Lieberman.[1]

Characteristics of the Unstable Afterglow

The DC beam described above triggers an instability when the gas pressure is below the level of normal operation. One characteristic of this instability is a sharp drop in the diamagnetism. Since we can interpret rapid (<5-10 msec) changes in the diamagnetism, we can use this instability to determine the plasma diamagnetism at times in the afterglow that are greater than the flux diffusion time through the discharge-tube wall. The range of observed diamagnetism is shown in Fig. XXI-1, wherein we have assumed that all of the hot electrons are lost in the instability, that is, the diamagnetism of the plasma drops to zero.

Previously reported observations[2] of oscillations following the occurrence of an instability have been extended. The oscillations are observed as low as 1 kMc – lower than the electron cyclotron frequency (~3 kMc). Raising the magnetic field ~50 per cent

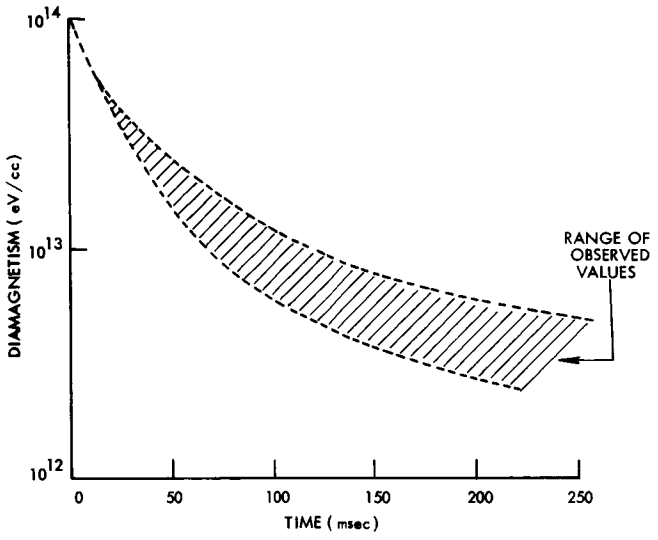

Fig. XXI-1. Plasma diamagnetism determined from triggered instability.

does not eliminate the oscillations near 1 kMc.

The particle flux to the walls and ends of the system following an instability has been observed. The net current out of the ends of the system is negative, and the net current to the walls is positive. If this is interpreted as meaning that electrons are lost axially and ions radially, the currents approximately account for the total number of particles in the system at the time of the instability.

Pressure Measurements

The Veeco-Gauge gauge factor has been determined with a McLeod gauge to be two for hydrogen, in agreement with data furnished by Veeco.[3] The pressure transient for the Marshall valve is shown in Fig. XXI-2. The upper curve is the pressure ~2 inches in front of the collector, and the lower curve is the pressure at the gun end of the system. The peak pressure was adjusted to be the same as the peak pressure used for previously reported measurements of the discharge characteristics.

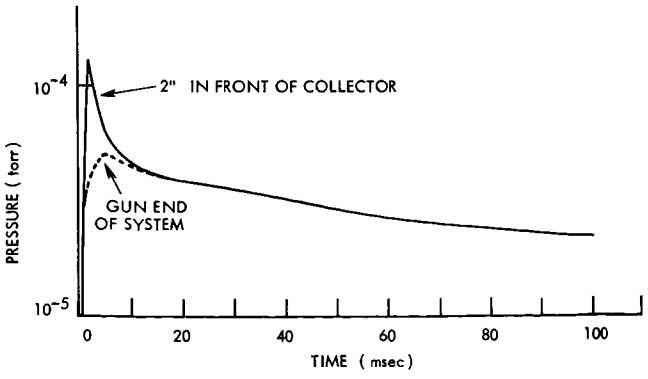

Fig. XXI-2. Marshall valve pressure transient.

X-ray spectrum measurements are now being made to determine the temperature of the hot electrons. A

beryllium window and a thin sodium iodide scintillation crystal are being installed to facilitate measurement of the spectrum down to 10 keV.

The author wishes to acknowledge the use of the facilities of the National Magnet Laboratory for the experiments described above.

R. R. Bartsch

References

1. M. A. Lieberman, Ph.D. Thesis, Department of Electrical Engineering, M.I.T., June 1966.
2. R. R. Bartsch, Quarterly Progress Report No. 83, Research Laboratory of Electronics, M.I.T., October 15, 1966, pp. 65-72.
3. P. Becker, Veeco Instruments, Inc. (Private communication, 1966).

3. CROSS-FIELD BEAM-PLASMA EXPERIMENT

Preliminary experiments have been carried out on the cross-field beam-plasma apparatus described in a previous report.[1] In these initial observations three types of beams have been used: (i) an axially flowing hollow beam obtained by having B_r and B_L, as previously described,[1] pointing in the same direction and equal in magnitude; (ii) an axially flowing hollow beam rotating about its axis obtained by having B_L and B_r oppositely directed and equal in magnitude; and (iii) an axially flowing scalloped beam obtained by setting $B_L = 0$.

With any of these beams it is possible to operate the discharge in two regimes. The first regime is characterized by ionization of the gas only in the region of the beam. The second regime is encountered by increasing the pressure of the background gas and the perveance of the beam. In the last regime a beam-plasma discharge takes place, and gas in the entire drift region can be ionized.

The initial measurements have shown low-frequency, narrow-bandwidth oscillations to be present in the low pressure-low perveance regime. These oscillations range in frequency from 10 to 200 kHz, and in some cases are essentially pure sine waves. Oscillations also have been observed in the beam-plasma-discharge regime. These oscillations are of wider bandwidth and higher in frequency (~100 mHz) than the low-frequency oscillations.

Experiments are now being carried out to verify a thin-beam electrostatic model of the system operating in the low pressure-low perveance regime.

B. R. Kusse, A. Bers

References

1. B. Kusse and A. Bers, "Cross-Field Beam-Plasma Interactions," Quarterly Progress Report No. 82, Research Laboratory of Electronics, M.I.T., July 15, 1966, pp. 154-157.

4. SHEET MODELS OF THE BEAM-PLASMA DISCHARGE WITH PLASMA DENSITY GRADIENTS ALONG THE BEAM

Previously, we found we had to include a very large collision frequency ($\nu = 0.2\omega_p$) to justify our assumption that the plasma remained linear at the point of initial beam overtaking.[1] In this case the plasma had a uniform density, and we velocity-modulated the beam at the plasma frequency. We find that the introduction of a longitudinal plasma density gradient produces a much less intense interaction, even in the absence of collisions or temperature. If we velocity-modulate the beam at the local plasma frequency near the gun, this frequency will be different from the local plasma frequency at the point of initial overtaking. That is, the bunches formed at overtaking will strike the plasma off-resonance, and the fields there will be much less.

Linear Theory: Continuum Model

We shall now derive the linearized equations for a beam-plasma interaction with the plasma density increasing linearly from the gun. We shall then compare computer experiments with these linearized results.

The model is one-dimensional, with a cold, collisionless plasma whose density is given by

$$\omega_p^2(z) = \omega^2 + a\,z. \tag{1}$$

We assume that all variables oscillate at ω, the local plasma frequency at $z = 0$.

$$i\,m\,\omega\,v_p = e\,E$$

$$i\,m\,\omega\,v_b + m\,v_{ob}\frac{\partial v_b}{\partial z} = e\,E \tag{3}$$

$$\frac{\partial E}{\partial z} = \frac{\rho_p + \rho_b}{\epsilon_o} \tag{4}$$

$$\frac{\partial}{\partial z}\left[\rho_{op}(z)\,v_p\right] = -i\,\omega\,\rho_p \tag{5}$$

$$\frac{\partial}{\partial z}\left[\rho_{ob}\,v_b + \rho_b\,v_o\right] = -i\,\omega\,\rho_b, \tag{6}$$

where v_p, ρ_p, v_b, ρ_b are the first-order velocities and charge densities, and ρ_{ob} is assumed constant. By manipulation of Eqs. 1-6, we obtain

$$v_o\,a\,z\frac{\partial^2 v_b}{\partial z^2} + \left[a\,v_o + i\,2\omega\,a\,z\right]\frac{\partial v_b}{\partial z} + \left[i\,\omega\,a - \frac{\omega^2}{v_o}\left(a\,z + \omega_{pb}^2\right)\right]v_b = 0. \tag{7}$$

The solutions to Eq. 6, for $z < 0$, are

$$v_{bI} \sim \exp\left(\frac{-i\omega z}{v_o}\right) J_o\left[\frac{2\omega\omega_{pb}}{v_o}\left(\frac{-z}{a}\right)^{1/2}\right] \tag{8}$$

$$v_{bII} \sim \exp\left(\frac{-i\omega z}{v_o}\right) Y_o\left[\frac{2\omega\omega_{pb}}{v_o}\left(\frac{-z}{a}\right)^{1/2}\right], \tag{9}$$

and for $z > 0$,

$$v_{bI} \sim \exp\left(\frac{-i\omega z}{v_o}\right) I_o\left[\frac{2\omega\omega_{pb}}{v_o}\left(\frac{z}{a}\right)^{1/2}\right] \tag{10}$$

$$v_{bII} \sim \exp\left(\frac{-i\omega z}{v_o}\right) K_o\left[\frac{2\omega\omega_{pb}}{v_o}\left(\frac{z}{a}\right)^{1/2}\right]. \tag{11}$$

The expressions for the other variables can be obtained from Eqs. 1-6. In particular,

$$E_I = v_{bI}\frac{m}{e}\frac{\omega\omega_{pb}}{v_o\sqrt{az}} \exp\left(\frac{-i\omega z}{v_o}\right) I_1\left[\frac{2\omega\omega_{pb}}{v_o}\left(\frac{z}{a}\right)^{1/2}\right]; \quad z > 0 \tag{12}$$

The physical meanings of the v_{bII} solutions are still unclear. Attempts to excite them in computer experiments have failed, thus far. We note that if "a" were negative (a linearly decreasing density) the solutions for $z > 0$ and $z < 0$ would be reversed.

Nonlinear Theory: Computer Sheet Model

For "a" positive, the I_o solution is easily excited in a computer experiment. This calculation was done as reported previously,[1] except a Runge-Kutta integration technique was used throughout, in place of the Milne method. Energy conservation is now better than 0.5 per cent. Snapshots of normalized beam-sheet velocity and acceleration (-eE/m) versus distance are shown in Figs. XXI-3 and XXI-4. The solid lines in each figure indicate the predictions of the linear theory. Times are normalized to ω_{po}, distances to $0.4 v_o/\omega_{po}$. The density is $\rho_o(z) = 0.15\,\rho_o + 0.001\,z$.

The plasma first-order charge density is approximately 11 per cent of $\rho_o(z)$ at the point of maximum field. With a suitable correction for finite beam diameter, it should be even less. This matter is under study at present.

J. A. Davis

References

1. J. A. Davis, Quarterly Progress Report No. 81, Research Laboratory of Electronics, M.I.T., April 15, 1966, p. 146.

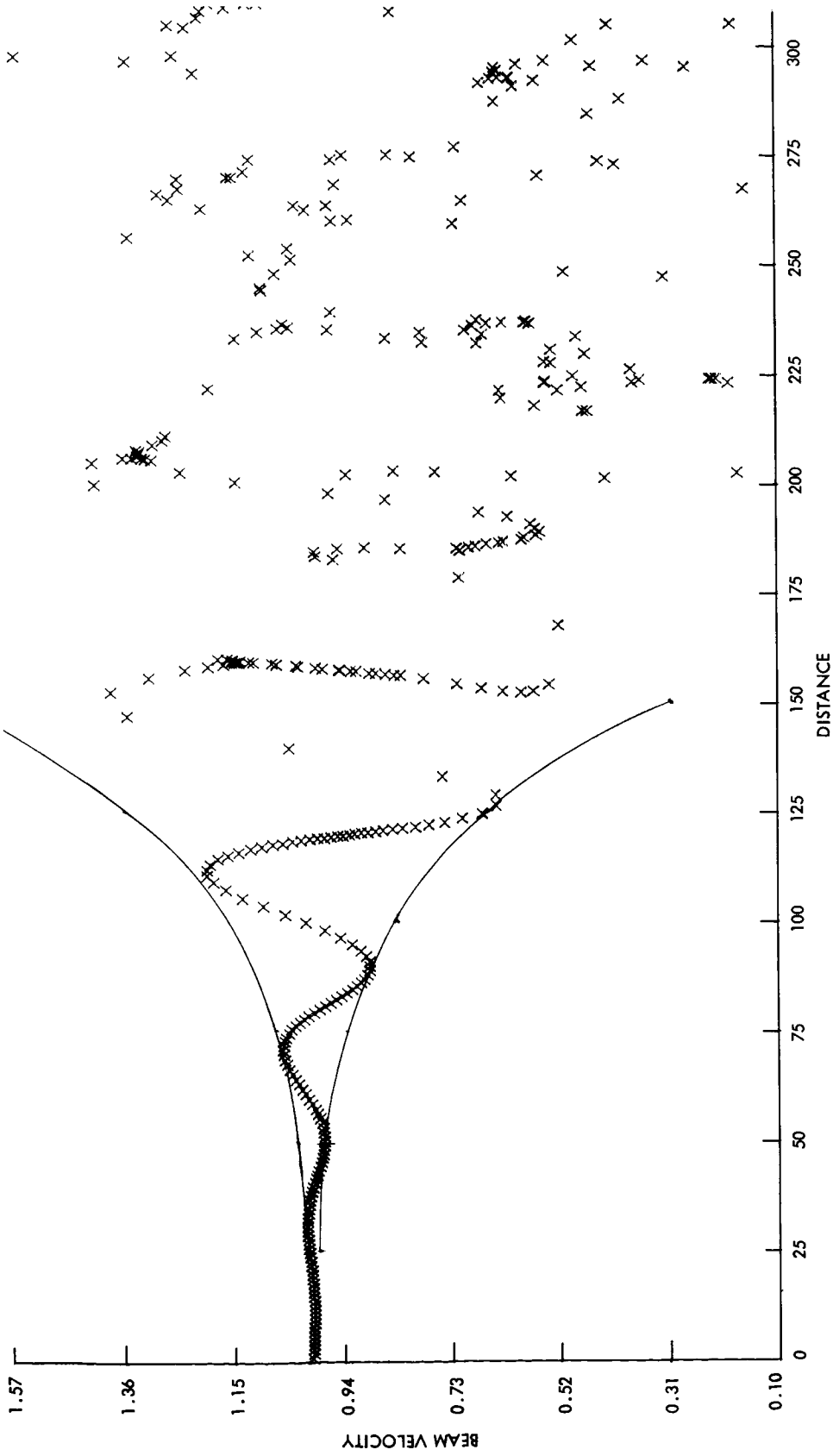

Fig. XXI-3. Instantaneous beam-sheet velocity at $t = 300\ \omega_{po}^{-1}$, where $\omega_{po}^2 = e\rho_o/m\epsilon_o$, $\rho_o(z) = 0.15\ \rho_o + 0.001\ z$. Beam velocity is 0.1 per cent modulated at $\omega = \sqrt{0.15}\ \omega_{po}$.

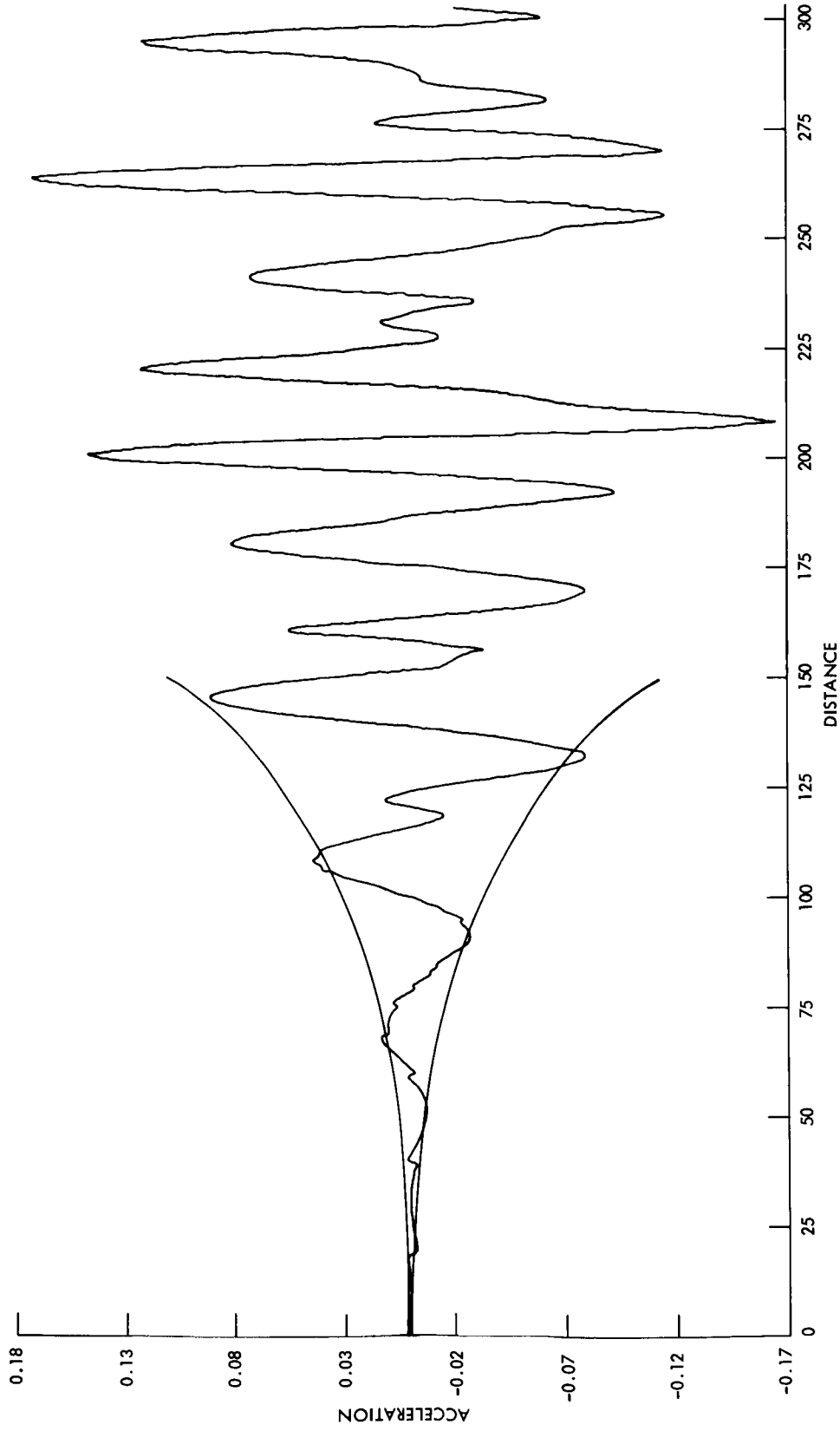

Fig. XXI-4. Instantaneous acceleration of a test particle at z. Times normalized to ω_{po}^{-1}, distances to $0.4\ v_o\ \omega_{po}^{-1}$.

5. SHEET MODEL OF A PLASMA SLAB

We have continued the study of nonlinear plasma slab oscillations with a charge-sheet model.[1,2] The oscillations were initiated by a uniform displacement δ of an electron cloud that is cold in equilibrium and has thickness d. Several new aspects of the investigation are reported here.

Dependence of the Scrambling Rate on Initial Perturbation

From electron-sheet trajectories given previously,[2] it can be seen that for small initial displacements the scrambling which originally occurs near the surface propagates in toward the center of the slab at a constant rate. It has been noted that the rate of scrambling propagation is a function of the initial displacement. For the data points shown in Fig. XXI-5, the rate of scrambling propagation is directly proportional to the initial displacement. The rate R_s is described by

$$R_s = 1.33 f_p \delta, \tag{1}$$

where f_p is the plasma frequency in cycles per second, and δ is the initial displacement. The numerical factor was determined from Fig. XXI-5. Since the scrambling propagates

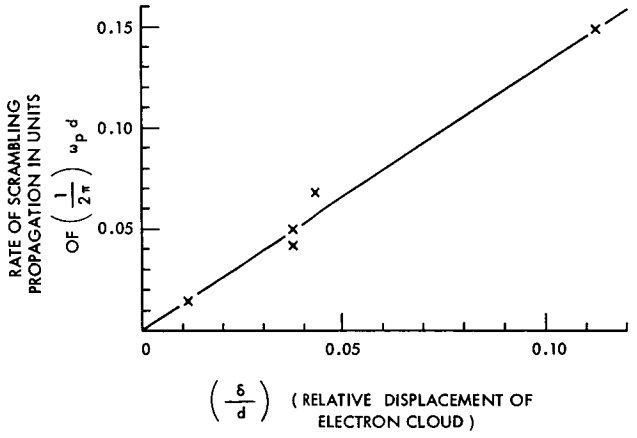

Fig. XXI-5. Rate of scrambling propagation as a function of initial displacement.

in from both sides of the slab, the time, Δt, at which the ordered plasma oscillations in the entire slab have been destroyed is given by

$$\frac{\Delta t}{T_p} = 0.38\left(\frac{d}{\delta}\right),$$

where T_p is one plasma period, $T_p = 1/f_p$.

Maximum Energy in the Random Motion

The initial energy given to the slab by a uniform displacement perturbation is entirely in the form of potential energy. If U_o denotes the initial energy per unit area of the slab, we have

$$U_o = \frac{1}{2} m(\omega_p \delta)^2 N\left[1 - \frac{1}{3}\left(\frac{\delta}{d}\right)\right], \tag{2}$$

where N is the total number of particles per unit area, and m is the mass of an electron. The second term inside the brackets is due to the nonuniform electric field near the boundary. Note that for small displacements, $U_o \approx \frac{1}{2} m(\omega_p \delta)^2 N$.

As the scrambling propagates into the slab, the number of particles N_s that have scrambled (those that are no longer oscillating coherently at the plasma frequency) steadily increases. These particles initially had a total energy given by

$$U_s \cong \frac{1}{2} m(\omega_p \delta)^2 N_s. \tag{3}$$

If the scrambled particles are assumed to have a Maxwellian velocity distribution f(V) given by

$$f(V) = \frac{N_s}{\sqrt{2\pi}} \left(\frac{d}{\lambda_D}\right) \frac{1}{\omega_p d} \exp\left[-\frac{1}{2} V^2 \left(\frac{d}{\lambda_D}\right)^2\right], \tag{4}$$

where $V = \frac{v}{\omega_p d}$ and $\lambda_D^2 = \frac{kT}{m\omega_p^2}$, the total kinetic energy of these particles would be

$$U_{Th} = \int_{-\infty}^{+\infty} \frac{1}{2} m\, v^2 f(v)\, dv \tag{5}$$

or

$$U_{Th} = \frac{1}{2} m\, N_s (\omega_p \lambda_D)^2. \tag{6}$$

We can obtain an upper bound to the temperature or Debye length, λ_D, of the scrambled particles by assuming that all of the initial energy given to the scrambled particles appears as random kinetic energy. Using Eq. 3 and 6, we find

$$\lambda_D \approx \delta. \tag{7}$$

Numerical Example

The bar-graph velocity distribution for scrambled particles is shown in Fig. XXI-6 for a slab modeled by 129 electron sheets. The distribution was averaged in time over one plasma period when $t/T_p \approx 16$. The initial displacement was $(\delta/d) = 0.0117$, so that

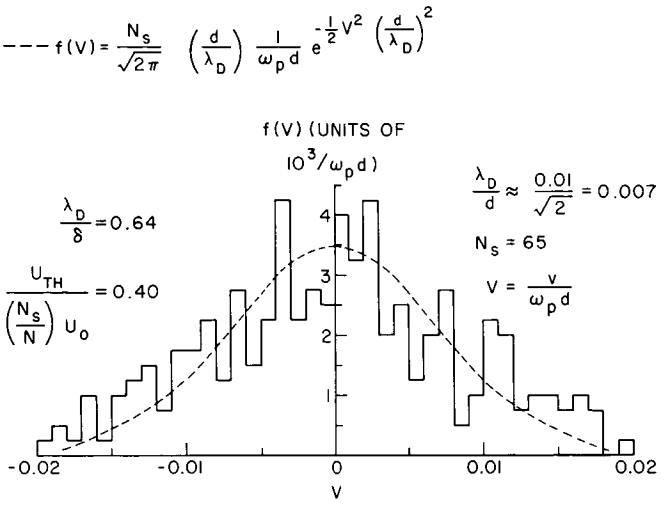

Fig. XXI-6. Time average velocity distribution of scrambled particles for $t/T_p \approx 16$, and $\frac{\delta}{d} = 0.0117$.

at this time (in agreement with Fig. XXI-5) approximately half of the particles have scrambled, or $N_s = 65$. A Maxwellian was fitted to the bar-graph and the Debye length was determined to be

$$\frac{\lambda_D}{d} = 0.007. \tag{8}$$

Thus $\frac{\lambda_D}{\delta} = 0.64$, and we find that approximately 40 per cent of the initial energy given to the scrambled particles appears as energy in the random motion.

H. M. Schneider

References

1. H. M. Schneider and A Bers, "Dynamics of the Plasma Boundary," Quarterly Progress Report No. 78, Research Laboratory of Electronics, M. I. T., July 15, 1965, pp. 114-119.
2. H. M. Schneider, "Dynamics of the Plasma Boundary," Quarterly Progress Report No. 80, Research Laboratory of Electronics, M. I. T., January 15, 1966, pp. 128-129.

6. STABILITY CRITERIA FOR DISPERSION RELATIONS CONTAINING BRANCH POINTS

The stability criteria of Bers and Briggs were developed for plasma dispersion relations, $\Delta(\omega, k)$, which are single-sheeted in the k-plane.[1] The application of the criteria to dispersion relations which have branch cuts has been studied,[2] and some additional thoughts concerning this last type of dispersion relation are presented here.

Many dispersion relations have no branch points with the k-plane and can be analyzed

perfectly well by the original formulation of the stability criteria. It should be pointed out that the expression for the roots, $\omega(k)$, obtained from the dispersion relation $\Delta = 0$, has branch points in the k-plane, and a number of sheets corresponding to the number of roots of ω for a given k. This does not mean that the dispersion relation has branch points. The original formulation of the stability criteria only breaks down when the dispersion relation itself is associated with more than one sheet in the k-plane.

One example of a dispersion relation with a branch line in the k-plane is the following one for longitudinal plasma waves in a single-species plasma:

$$\Delta(\omega, k) = 1 - \frac{\omega_p^2}{k^2} \int_{-\delta}^{+\delta} \frac{\frac{\partial f_o(u)}{\partial u}}{u - \frac{\omega}{k}}\, du. \qquad (1)$$

$\lim \delta \to \infty$

This function has branch points in the k-plane at $\left(\frac{\mathrm{Re}\ \omega}{\delta}, \frac{\mathrm{Im}\ \omega}{\delta}\right)$ $\left(\frac{-\mathrm{Re}\ \omega}{\delta}, \frac{-\mathrm{Im}\ \omega}{\delta}\right)$. See Fig. XXI-7. This can be demonstrated by taking as f_o a resonance function $f_o = \frac{1}{u^2 + a^2}$. Then $\Delta(\omega, k)$ becomes

$$\Delta(\omega, k) = \frac{1}{\frac{\omega^2}{k^2} + a^2} \left[\log \left(\frac{\delta - \frac{\omega}{k}}{\delta + \frac{\omega}{k}} \right) - \frac{2\omega}{ak} \tan^{-1} \frac{\ell}{a} \right].$$

It can be seen that this function has branch points as described above.

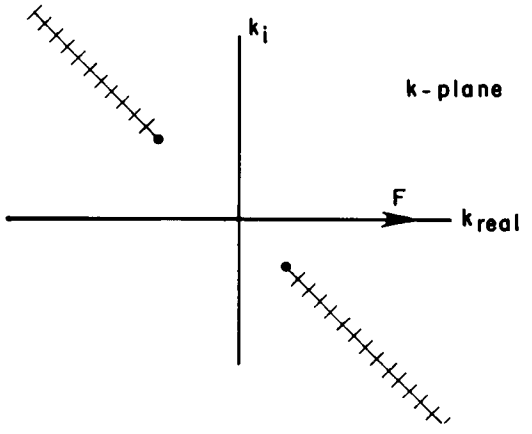

Fig. XXI-7. Branch cut in k-plane for $\Delta(\omega, k)$ describing logitudinal plasma waves, under the assumption of real ω positive and imaginary ω negative.

The Fourier contour of the stability criteria is taken along the real k-axis. In applying the stability criteria for single-sheeted dispersion relations, one investigates the roots $k = k(\omega)$ as ω is swept from the lower half ω-plane to the real ω-axis. Absolute instabilities occur when k-roots pinch the deformed Fourier contour during these sweeps.

It will be shown that this same condition applies to dispersion relations with branch points in the k-plane, Care must be taken however, to make sure that the Fourier contour is really pinched.

The dispersion relation $\Delta(\omega, k)$ in Eq. 1 can be approximated by $\Delta_1(\omega, k)$ and $\Delta_2(\omega, k)$, where

$$\Delta_1(\omega, k) = 1 - \frac{\omega_p^2}{k^2} \int_{-\infty}^{\infty} \frac{\frac{\partial f_o}{\partial u}}{u - \frac{\omega}{k}} du; \qquad \text{Im}\,\frac{\omega}{k} < 0$$

$$\Delta_2(\omega, k) = 1 - \frac{\omega_p^2}{k^2} \int_{-\infty}^{\infty} \frac{\frac{\partial f_o}{\partial u}}{u - \frac{\omega}{k}} du; \qquad \text{Im}\,\frac{\omega}{k} > 0.$$

This approximation is good, except near the origin of the k-plane, around the branch points, and becomes better as $\delta \to \infty$. The regions of validity are shown in Fig. XXI-8, with the Fourier contour on only one sheet.

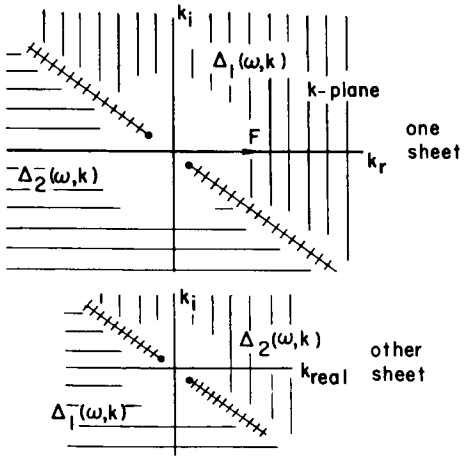

Fig. XXI-8. Δ_1 and Δ_2 approximations to $\Delta(\omega, k)$.

Now consider the roots $k = k(\omega)\big|_{\Delta_1}$ obtained from Δ_1 for sweeps of ω. If they behave as shown in Fig. XXI-9, they most definitely pinch the deformed Fourier contour and predict an absolute instability. If, however, they collide as shown in Fig. XXI-10, more care must be taken to determine whether or not the deformed Fourier contour is really pinched.

In order to see these poles collide, analytic continuation must be performed and the branch lines deformed. In doing this it can be seen the Fourier contour is pushed up and the collision does not pinch the contour. Consequently, no absolute instability is predicted.

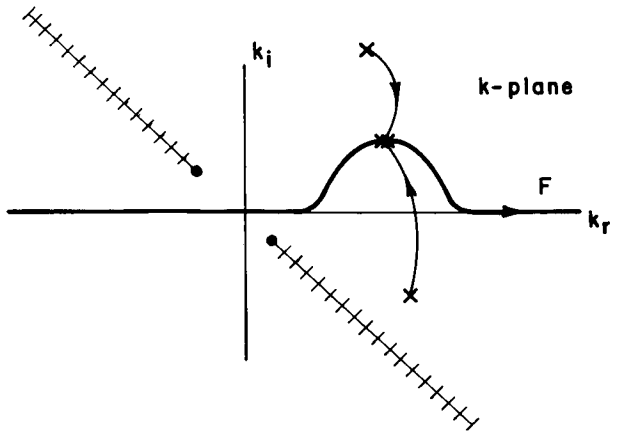

Fig. XXI-9. Absolute instability roots of $\Delta_1(\omega, k)$.

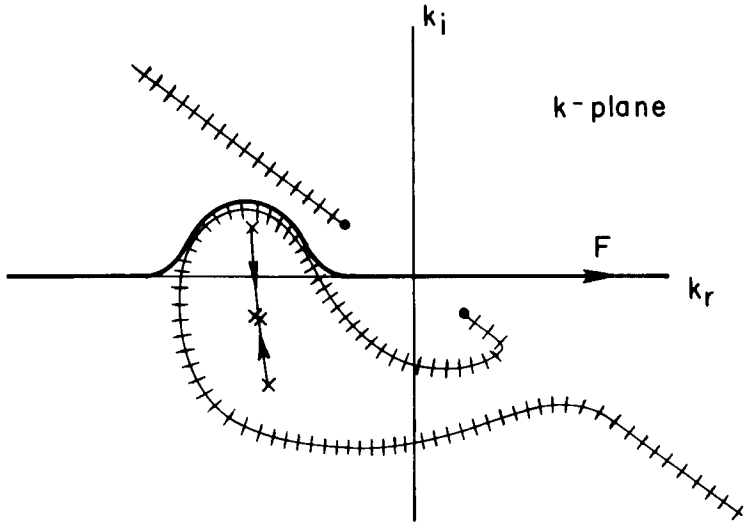

Fig. XXI-10. Roots of $\Delta_1(\omega, k)$ that do not pertain to an absolute instability.

By extending these arguments, it can be seen that a collision of k-roots obtained from $\Delta_1(\omega, k)$ leads to an absolute instability if one root crosses the positive real k-axis, but does not lead to an absolute instability if the collision occurs as a result of a crossing of the negative real k-axis. Similarly, a collision of k-roots obtained from $\Delta_2(\omega, k)$ leads to an absolute instability only if one root crosses the negative real k-axis.

B. R. Kusse

References

1. R. J. Briggs, Electron-Stream Interaction with Plasmas (The M. I. T. Press, Cambridge, Mass., 1964).

2. B. R. Kusse, "Plasma Dispersion Relations and the Stability Criteria," S. M. Thesis, Department of Electrical Engineering, M. I. T., 1964.

7. FINITE LARMOR RADIUS EFFECTS IN THE INTERACTION OF ELECTRONS WITH HIGH-FREQUENCY ACOUSTIC WAVES

We have previously reported[1] on an analysis of the classical dispersion relation for electrons interacting with acoustic waves in a solid.

A physical picture of the interaction and, in particular, the effects of a finite Larmor radius, which come into the electron dielectric constant through the Bessel functions, can be obtained by considering the particle motion along the wave. The energy exchanged between any given particle and the electric field of the wave is given by $\overline{E} \cdot \overline{v}$. As we are considering a longitudinal acoustic wave, $\overline{E}$ is along $\overline{q}$, the wave vector. Thus it is sufficient to consider the zero-order trajectory of a particle along a coordinate axis in the $\overline{q}$ direction as a function of time given by

$$x_q = x_o + (w_{||} \cos\theta)t - \frac{w_\perp \sin\theta}{\omega_c} \cos(\omega_c t + \phi),$$

where x_o and ϕ are the arbitrary initial position and phase, $w_{||}$ is the velocity along the external magnetic field, $\overline{B}_o$, $w_\perp$ is the velocity across the magnetic field, ω_c is the electron-cyclotron frequency, and θ is the angle between the wave vector and B_o. If we consider a longitudinal wave of the form

$$\overline{E} = E_o \frac{\overline{q}}{|q|} \cos(qx - \omega t),$$

then the force on the electron is

$$\overline{F} = -eE_o \frac{\overline{q}}{|q|} \cos\left(qx_o + (q_{||}w_{||} - \omega)t - \frac{q_\perp w_\perp}{\omega_c} \cos(\omega_c t + \phi)\right),$$

where $q_{||} = q\cos\theta$, and $q_\perp = q\sin\theta$. The results of computations on this equation for a particular value of initial position and phase are shown in Fig. XXI-11. Figure XXI-11a is just the electron velocity along $\overline{q}$ attributable to the Larmor orbit; Fig. XXI-11b and 11c are the force on a particle for parameters such that the resonance at $\omega - q_{||}w_{||} + \omega_c = 0$ is satisfied. The first is for a value of $p = \frac{q_\perp w_\perp}{\omega_c}$ (which is 2π times the ratio of the electron Larmor radius to the wavelength) near the first maximum of J_1, and the second for a value of p near the first zero. Figure XXI-11d and 11e are similar, except that here the resonance is $\omega - q_{||}w_{||} + 3\omega_c = 0$ and the p values refer to the first maximum and zero of J_3. It is easily seen that the value of $\overline{E} \cdot \overline{v}$ averaged over a cyclotron period is much larger for p values near the maximum of the Bessel functions, and decreases rapidly for values of p near a zero of the Bessel functions.

No conclusions can be drawn about the direction of energy flow between the particles

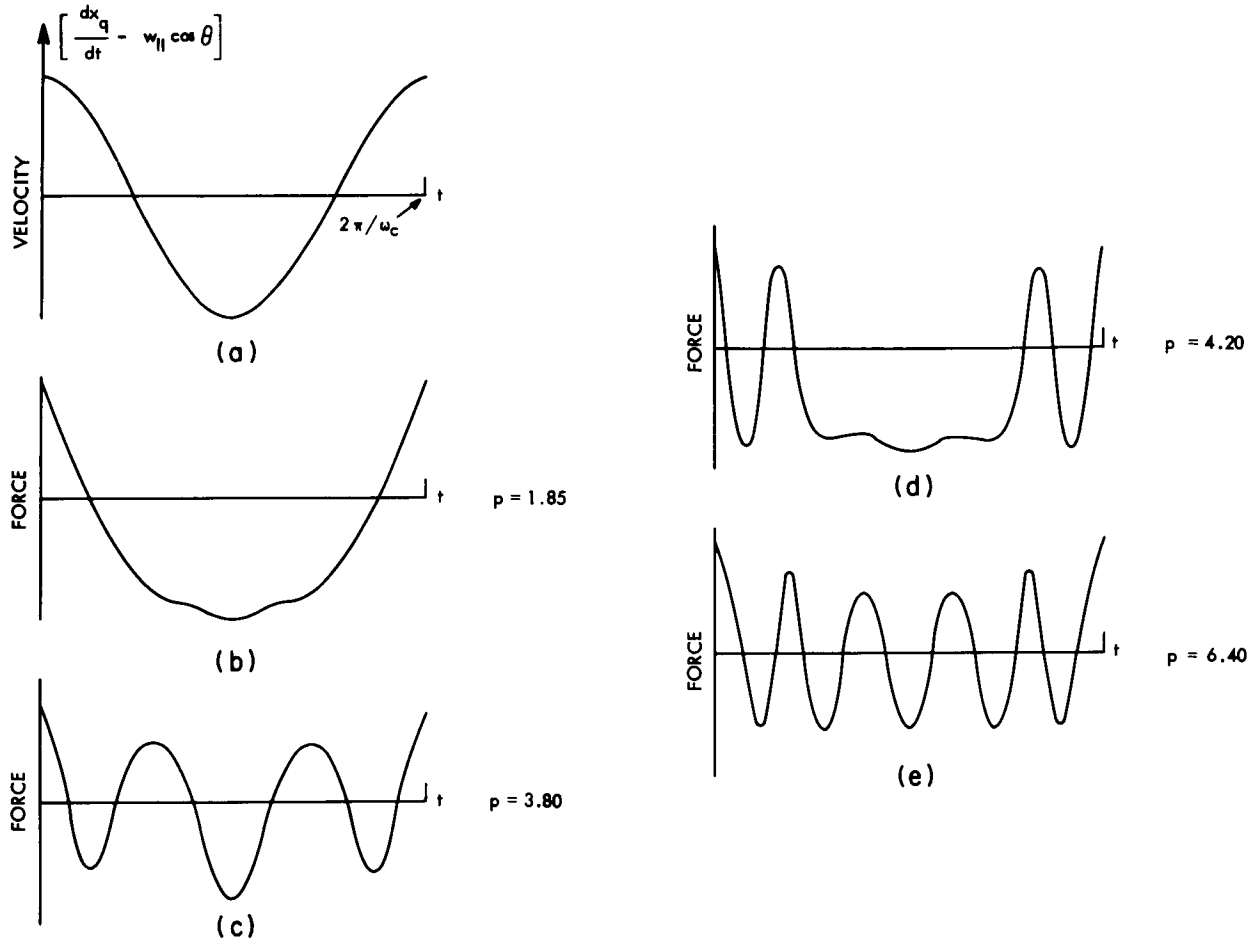

Fig. XXI-11. (a) Unperturbed velocity of a particle along the wave, owing to its Larmor orbit. (b) Force on the particle caused by the wave for parameters such that $\omega - q_{||}w_{||} + \omega_c = 0$ and p is near the first maximum of J_1. (c) Same as (b), except that p is near first zero of J_1. (d) and (e) Same as (b) and (c), except that the parameters are such that $\omega - q_{||}w_{||} + 3\omega_c = 0$.

and the wave on the basis of this picture. The reason for this is that if the total energy exchange averaged over the randomly distributed initial position and phase is considered, it is easily seen that $\langle \overline{F} \cdot \overline{v} \rangle_{x_o, \phi} = 0$. The direction of energy flow depends, of course, on the derivatives of the distribution function in the manner previously discussed.[1]

S. R. J. Brueck

References

1. S. R. J. Brueck and A. Bers, Quarterly Progress Report No. 83, Research Laboratory of Electronics, M. I. T., October 15, 1966, pp. 72-76.

XXI. PLASMAS AND CONTROLLED NUCLEAR FUSION*

B. Applied Plasma Physics Related to Controlled Nuclear Fusion

Academic and Research Staff

Prof. D. J. Rose
Prof. T. H. Dupree
Prof. L. M. Lidsky
Prof. E. P. Gyftopoulos
Prof. H. Cheng
Prof. S. Yip
Dr. K. Chung

Graduate Students

K. R-S. Chen
D. G. Colombant
R. W. Flynn
R. A. Hill
M. Hudis
W. M. Manheimer
G. R. Odette
L. C. Pittenger
A. Sugawara
C. E. Wagner
A. Watanabe

RESEARCH OBJECTIVES

1. Material and Engineering Experiments Related to Controlled Fusion

We have continued studies of material damage by 14-MeV neutrons, which will be a serious problem in any controlled nuclear fusion reactor. Irradiation of small metal samples continues, with the use of the weak (10^{10} neutrons/sec) Texas Instrument Company accelerator that is available. A radiation damage-detection technique that enables observation of the small expected damage has been used. The measured damage will be compared with theoretical estimates.

We hope to continue experiments on the neutron and gamma-ray spectra from mock-up fusion blanket assemblies.

D. J. Rose, G. R. Odette

2. Feasibility Studies of Controlled Fusion

Calculations of hypothetical controlled fusion system parameters will be carried out to determine the improvement expected by modifying the moderator to contain pure liquid metal, and by modifying other material specifications.

D. J. Rose, L. M. Lidsky

3. Intense Neutron Sources

Preliminary calculations indicate that it may be possible to build a 14-MeV neutron source with 10^{15} n/cm^2 sec intensity at the target position by using the Mach cone of a freely expanding jet as a windowless gas target. A detailed investigation of such neutron sources has been started with the primary objective of solving the hydrodynamic equations for duct flow with intense heating. This will be followed by an analysis of the system to find the optimal pressure ratios, expansion factors, diffusor design, and so forth.

L. M. Lidsky, D. G. Colombant

*This work was supported by the National Science Foundation (Grant GK-1165).

4. Experimental Plasma Turbulence

Work continues on the long "quiescent" plasma column developed during the last two years. To be studied now are (a) ion temperature, including comparison with various theoretical estimates; (b) determination of onset conditions for various unstable modes prevalent in such columns; (c) determination of the conditions for most nearly quiescent operation; (d) propagation of weak (linear) perturbing waves in the quiescent plasma; (e) measurement of the correlation function of the fluctuations in the plasma under various operating conditions; (f) a comparison of conditions in the plasma during "quiescent" operation with predictions of quasi-linear theory.

We have listed more research work than can be accomplished in one year; there are many projects waiting for this popular and useful device.

K. Chung, L. M. Lidsky, D. J. Rose

5. Confinement of Hot-Electron Plasmas

We have generated beam-plasma discharge plasmas in mirror, cusp, and stuffed-cusp magnetic fields and are engaged in measurements of their similarities and differences. The mirror-contained plasma is distinguished from the cusp-contained plasma, for example, by a much higher temperature for the energetic group (35 kev vs ~10 kev) and a higher level of density fluctuation. We plan to identify the types of instabilities present in these several systems, giving special attention to distinguishing the instabilities driven by the high- and low-energy electron groups.

L. M. Lidsky, C. E. Wagner

6. Particle Diffusion in Weakly Turbulent Plasma

We have studied the motion of particles in weakly turbulent plasma. Particular emphasis has been given to the conditions under which the distribution function satisfies a diffusion equation. Explicit expressions for the diffusion coefficient have been derived. The growth (or damping) rates of the turbulent wave spectrum can be calculated from the rate of energy and momentum transfer between particles and waves.

W. M. Manheimer, T. H. Dupree

7. Particle Motion in Large Amplitude Waves

We are attempting to calculate the time evolution of the distribution function for a single nonlinear wave. It is hoped that the solution of this problem can then be applied to strong narrow-band turbulence. In this regime particle trapping, or strong reflections from potential maxima, is an important feature of the motion. This feature is not included in present weak-turbulence theory.

T. S. Brown, T. H. Dupree

8. Computer Experiments on Turbulent Plasma

A computer program has been written to compute the particle distribution function for a given arbitrary spectral density of the electric field. The influence of the spectrum on particle motion can be studied in detail and compared with various theories. The distribution function and the electric field are not required to satisfy Maxwell's equation. Dropping this "self-consistency" constraint leads to a much more accurate computer simulation of the Vlasov equation, and also

gives the experimenter complete freedom to specify the spectrum.

R. W. Flynn, T. H. Dupree

1. OSCILLATIONS IN THE HOLLOW-CATHODE DISCHARGE ARC

We report here the observation of plasma oscillations in the highly ionized Argon plasma produced by the hollow-cathode discharge arc (HCD).[1] Oscillations were detected by Langmuir probes at various values of plasma parameters. As expected, we observed a close relation between the oscillations and the plasma stability.

In our HCD,[1] we can vary the confining magnetic field in the drift-tube region, the magnetic field over the source region, the neutral pressure in the drift-tube region, the gas-feed rate through the hollow cathode, the gas-feed rate through the hollow anode, the current flow to the anode plate and the column length of the drift tube. Although varying each parameter may affect others, we can vary them rather freely in some restricted regions. In this observation we set the column length at its maximum, and the cathode feed rate at 1 atm-cc/sec, unless it is otherwise noted. We used 1/8" I.D., 0.015" thick, tantalum tube for the cathode, and the inner radius of each baffle was 1 5/8". The probes were located in the drift tube near the baffle and also near the axial mid-point. The radial positions of the probes were changed, and the probes were either floated or biased to the ion saturation voltages. Typically, the plasma density was around 10^{13}/cc and the radius of the arc column was 1/2".

At fixed gas-feed rate and drift-tube magnetic field, we found significant changes in the frequencies and magnitudes of the oscillations as we varied the source magnetic field. In Fig. XXI-12 we show a series of oscilloscope pictures of power spectra and time-resolved responses of the oscillations. The probes were located 1/4" from the axis and floating. At lower source magnetic fields (a, b or e), there are distinctive signals at 75 kc and its multiples. In fact, we observed similar oscillations at other drift field values. The interesting point is that the fundamental frequency is almost at the ion-cyclotron frequency, which is 75 kc for this particular case. Harmonics are very strong for these oscillations. We also noticed that this oscillation disappears abruptly as we increase the source magnetic field over a certain value. If we compare Fig. XXI-12d and 12e, we see that the disappearance of this oscillation is very sudden, and the plasma column itself undergoes sudden changes in its density and brightness. Note the doubling of the neutral pressure despite the very small change in the source magnetic field. Also, the current to the anode plate changes a lot, although we do not change the gas-feed rate or the external load resistance. Notice in Fig. XXI-12b that when we increased the neutral pressure by an additional anode gas feed, we found that the harmonics were very much subdued, and the oscillation could be relatively reduced somewhat, as compared with the density changes of the plasma.

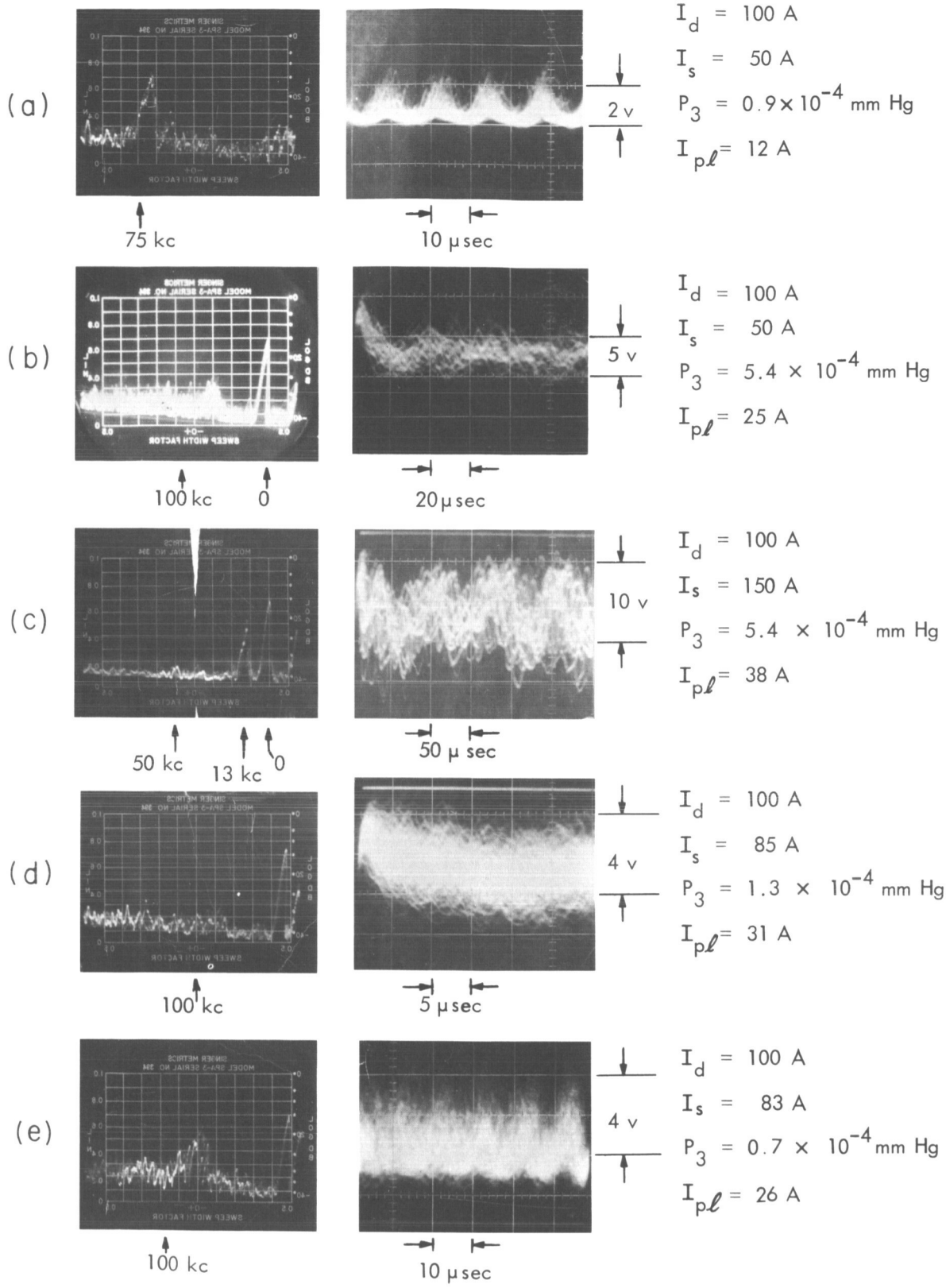

Fig. XXI-12. Power spectra and time-resolved responses of the oscillations.

As we increased the source magnet far beyond the critical value, we found a new kind of oscillation at lower frequencies (Fig. XXI-12c). Contrary to the other kind of oscillations, these new oscillations are very strong at the edge of the plasma, and we could detect a sizable signal far from the axis. In the series of pictures in Fig. XXI-13,

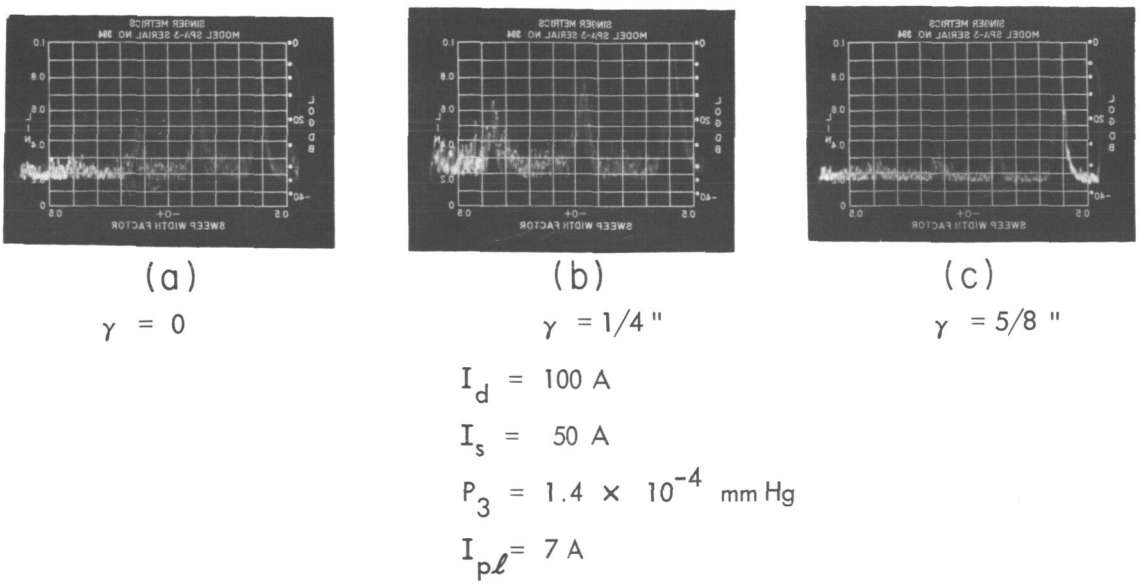

(a) $\gamma = 0$

(b) $\gamma = 1/4$"

(c) $\gamma = 5/8$"

$I_d = 100$ A

$I_s = 50$ A

$P_3 = 1.4 \times 10^{-4}$ mm Hg

$I_{p\ell} = 7$ A

(d) $\gamma = 1$"

(e) $\gamma = 3/8$"

(f) $\gamma = 1/8$"

$I_d = 85$ A

$I_s = 117$ A

$P_3 = 4.3 \times 10^{-4}$ mm Hg

Fig. XXI-13. Radial profile of the oscillations.

we display the signals from different radial positions. We note smaller signals near the center (Fig XXI-13e vs 13f) in the case of lower frequency oscillations. Previously reported "quiet" plasma,[2] which was produced by the same HCD machine, could be

obtained by controlling the magnetic fields to somewhere near the critical values at which the sudden change of plasma density and the onset of plasma oscillation occurred. In order to obtain the "quiet" plasma, we must reduce the low-frequency type of oscillation by lowering the source magnetic field to its critical

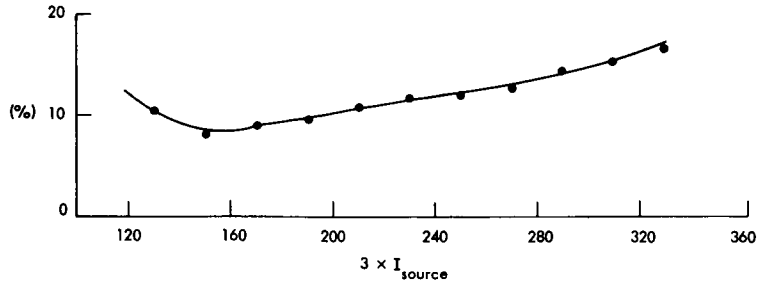

Fig. XXI-14. Percentage of fluctuations with respect to the plasma density.
Cathode Feed ≈ 1 atm-cc/sec
I_d = 125 A $\Longrightarrow$ $B_d \approx 2.5$ kGauss
Anode Feed = 0.1 atm cc/sec
$\gamma = \frac{1}{2}$ in. (near the edge of the plasma).

value and introducing a small amount of the anode gas feed. In Fig. XXI-14 we see the percentage density fluctuation with respect to the source magnetic field. The minimum value of the fluctuation percentage in this particular set of parameters is rather high (8%). If we had measured at the center of the plasma column, we would have recorded a much lower value. This is due to higher plasma densities and lower fluctuation level at the center. Incidentally, the fluctuation illustrated by Fig. XXI-14 was measured by the probes biased at ion-saturation voltages.

The probes biased to ion-saturation voltages registered similar responses with the probes floated. Thus we speculate that the oscillations are electrostatic. Using several probes located at different positions axially and azimuthally, we studied the propagation of the oscillation. We found that the higher frequency oscillations associated with the ion-cyclotron frequency propagate from the anode to the cathode with the phase velocity very close to the ion acoustic wave phase velocity. On the contrary, the lower frequency oscillation, which appeared at higher source magnetic fields, was detected as moving from the source region to the anode. We speculate that this oscillation may be due to the relative motion of layers of the plasma in the baffle region and thus has a hydrodynamic origin. An independent study of the effects of the baffles is under way.

To summarize, we observed two types of plasma oscillations in the Argon plasma produced by the HCD and established the close relation between the plasma oscillations and the plasma stability, which is very helpful in obtaining the "quiet" plasma.

K. Chung

References

1. J. C. Woo, L. M. Lidsky, and D. J. Rose, Quarterly Progress Report No. 76, Research Laboratory of Electronics, M.I.T., January 15, 1965, pp. 130-133.

2. J. C. Woo and D. J. Rose, Quarterly Progress Report No. 82, Research Laboratory of Electronics, M.I.T., July 15, 1966, pp. 163-169.

XXI. PLASMAS AND CONTROLLED NUCLEAR FUSION

C. Plasma Magnetohydrodynamic Flows, Waves, and Instabilities

Academic and Research Staff

Prof. W. P. Allis Prof. H. A. Haus

Graduate Students

C. A. McNary K. R. Edwards

RESEARCH OBJECTIVES

1. In an MHD plasma, small disturbances of density and temperature are accompanied by small changes in constituent properties, such as conductivity and Hall parameter. An analytic description of all waves that can be supported by a moderate magnetic Reynolds number MHD plasma for all directions of propagation is under study, including the effects of parameter variations on magnetoacoustic and Alfvén wave propagation. A delineation of the MHD environments for which absolute and convective instabilities, if any, can occur is to be found. A study of oscillator and/or amplifier device application feasibility will be undertaken.

H. A. Haus

2. It is well known that glow discharges often exhibit bright spots, and the bright "meniscus" which develops in a hot-cathode discharge has been studied experimentally by Emeleus. Its origin is due to the interaction of the beam of fast electrons from the cathode with the inhomogeneous plasma in this neighborhood. The phenomena of plasma wave amplification and Landau damping are involved. An exact mathematical theory for this and similar phenomena is being developed.

W. P. Allis

1. ELECTRON BEAM INTERACTION WITH A SPATIALLY INHOMOGENEOUS TEMPERATE PLASMA

This theoretical analysis of an electron beam-plasma interaction is an attempt to model some of the experimentally observed phenomena that are typical of such a system. Various experimental investigators have observed the randomization of the beam energy and direction, and the abrupt commencement of plasma oscillations at a point a small distance from where the beam enters the plasma.

In the theoretical model now under study, the beam and plasma are considered as separate entities, coupled electrostatically by Poisson's equation. The plasma is assumed to be collisionless and temperate, and the beam is sufficiently diffuse that it does not significantly perturb the plasma as a result of collisions. The geometry of the beam-plasma system consists of a z-directed electron beam having the same

*This work was supported principally by the National Science Foundation (Grant GK-1165).

cross-section dimensions as the plasma. The beam is assumed to be spatially homogeneous and to have a directed velocity, v_o, which is a constant. The plasma has a one-dimensional density distribution, $G_k(z)$, and is spacially homogeneous in the other two directions. Under these initial assumptions, the plasma and the beam may be modeled by the collisionless Vlasov equation. This equation is written separately for each species: plasma ions, plasma electrons, and beam electrons. The distribution functions involved are split into zero- and first-order parts, and zero-order parts are assumed to be independent of time and separable in the remaining space and velocity variables. The first-order portions are assumed to be periodic in time; and, because of the comparatively large mass and inertia of the plasma ions, first-order perturbations of the ions are neglected. Substitution of these distribution functions in the Vlasov equation and linearization yields first-order equations for the plasma and beam electrons of the form

$$\frac{\partial \delta f}{\partial t} + \vec{v} \cdot \vec{\nabla} \delta f - \frac{e}{m} \vec{E} \cdot \vec{\nabla}_v \delta f - \frac{e}{m} \delta \vec{E}\, G(z) \cdot \vec{\nabla}_v f = 0. \tag{1}$$

In Eq. 1, $\vec{E}$ and $\delta\vec{E}$ are the zero- and first-order electric fields respectively, $f(\vec{v})G(z)$ is the separable zero-order distribution function, and δf is the first-order distribution function. If we assume that the electric fields are z-directed and functions of z only, Eq. 1 may be simplified to

$$\frac{\partial \delta f}{\partial t} + v_z \frac{\partial \delta f}{\partial z} - \frac{e}{m} E(z) \frac{\partial \delta f}{\partial v_z} = \frac{e}{m} \delta E(z)\, G_e(z) \frac{\partial f(\vec{v})}{\partial v_z} = 0. \tag{1a}$$

With the following definitions, Eq. 1a may be put into the form

$$\left[\frac{\partial}{\partial v_z} + H\right] \delta f = \frac{\Gamma}{a} \frac{\partial f}{\partial v_z}, \tag{2}$$

where the time dependence is assumed to be of the form $\exp(-j\omega t)$; $eE/m \equiv a$; $\frac{e\delta E(z)\, G(z)}{m} \equiv \Gamma(z)$; H is the operator $\frac{1}{a}(j\omega - v_x D)$; and $D \equiv \frac{\partial}{\partial z}$. Note that only when $a \neq a(z)$, but is a constant, can this formalism be carried out; otherwise commutativity difficulties arise. An additional operator U is so difined that $[\partial/\partial v_z + H]U = 0$, with $U(v_z=0) = 1$ and $UU^{-1} = U^{-1}U = 1$. Straightforward integration then yields

$$U = U(v_z=0) \exp\left[-\frac{1}{a}\left(j\omega v_z - \frac{v_z^2}{2} D\right)\right] = \exp \frac{-1}{a}\left(j\omega v_z - \frac{v_z^2}{2} D\right). \tag{3}$$

Then the particular solution for δf may be written in the form

$$\delta f = U \int_0^{v_z} dv_z'\, U^{-1} Q + U \delta f(v_z=0), \tag{4}$$

where

$$Q \equiv \frac{\Gamma(z)}{a} \frac{\partial f}{\partial v_z'} \quad \text{and} \quad U^{-1} \equiv \exp \frac{1}{a}\left(j\omega v_z - \frac{v_z^2}{2} D\right).$$

The formal solution indicated in Eq. 4 may be verified by direct substitution.[1] Although Eq. 4 is only the particular solution of Eq. 1a, it should be noted that the homogeneous solution if of no interest in this analysis. Carrying out the operations indicated in Eq. 4 for a distribution function of the form

$$f_k(\vec{v}) = (\pi v_k)^{-3/2} \exp - \frac{1}{v_k^2}\left[u^2 + (v_z - v_{o,k})^2\right], \tag{5}$$

where $u^2 = v_x^2 + v_y^2$, v_k is the thermal velocity, and $v_{o,k}$ is the directed velocity of the k^{th} specie, yields the following result for δf:

$$\delta f_k(\vec{v}, v_o) = f_k(\vec{v}, v_o)\left\{1 - \frac{D}{2Aa} + \frac{[j\omega + BD/2A]}{2Aa(v_z + B/2A)}\left[1 + \sum_{n=1}^{\infty} \frac{(-1)^n (2n)!}{n!\left[2\sqrt{A}\,(v_z + B/2A)\right]^{2n}}\right]\right\} \frac{\Gamma}{a}. \tag{6}$$

The infinite series of Eq. 6 results from an asympototic expansion of an error function that arises from the finite limits of integration of the exponential of Eq. 5. Also, $A = 1/v_k^2 + D/2a$, and $B = -\left[j\omega/a + 2v_{o,k}/v_k^2\right]$. Equation 6 is an infinite-order differential equation, and is formally the solution for δf_k.

Integration of Eq. 6 over velocity space yields a formal result for the first-order particle number density, δn_k, or the first-order charge density $\delta\rho_k = -e\delta n_k$:

$$\delta\rho_k = -\sum_{n=1}^{\infty} \left[\frac{C_n\left(a + \frac{v_k^2}{2} D\right)^{2n-1}}{\left[\frac{v_k^2}{2}(v_o D - j\omega)^2\right]^n} + \frac{(-1)^n (2n)!}{n!}\left(\frac{2a}{v_k^2}\right)^n \frac{\left(a + \frac{v_k^2}{2} D\right)^{n-1}}{(v_o D - j\omega)^{2n}}\right.$$
$$\left.\cdot\left\{1 + \sum_{m=1}^{\infty} F_{m,n} \frac{\left(a + \frac{v_k^2}{2} D\right)^{2m}}{\left[\frac{v_k^2}{2}(v_o D - j\omega)^2\right]^m}\right\}\right] e\Gamma_k(z), \tag{7}$$

where $C_n = 1 \cdot 3 \cdot 5 \cdot \ldots \cdot (2n-1)$, and

$$F_{m,n} = \frac{[1 \cdot 3 \cdot \ldots \cdot (2m-1)][(2n+1)(2n+2) \cdot \ldots \cdot (2n+2m)]}{(2m)!}.$$

In the case of current interest, two species k are considered, plasma electrons and

beam electrons. By identifying the plasma electrons with the subscript k = e and the beam electrons with k = b; substitution of Eq. 7 in Poisson's equation, with $v_{o,e} = 0$ for the plasma electrons, yields

$$D\delta E = \frac{\Sigma\delta\rho_k}{\epsilon_o} = -\omega_p^2 \sum_{n=1}^{\infty} \left[\frac{C_n \left(a + \frac{v_e^2}{2} D\right)^{2n-1}}{\left(\omega^2 \frac{v_e^2}{2}\right)^n} (-1)^n + \frac{(2n)!}{n!} \left(\frac{2a}{v_e^2}\right)^n \frac{\left(a + \frac{v_e^2}{2} D\right)^{n-1}}{\omega^{2n}} \right.$$

$$\left. \left\{ 1 + \sum_{m=1}^{\infty} F_{m,n} \frac{\left(a + \frac{v_e^2}{2} D\right)^{2m}}{\left(\frac{v_e^2}{2} \omega^2\right)^m} (-1)^m \right\} \right] g_e(z)\, \delta E(z)$$

$$-\omega_b^2 \sum_{n=1}^{\infty} \left[\frac{C_n \left(a + \frac{v_b^2}{2} D\right)^{2n-1}}{\left[\frac{v_b^2}{2} (v_o D - j\omega)^2\right]^n} + \frac{(-1)^n (2n)!}{n!} \left(\frac{2a}{v_b^2}\right)^n \frac{\left(a + \frac{v_b^2}{2} D\right)^{n-1}}{(v_o D - j\omega)^{2n}} \right.$$

$$\left. \left\{ 1 + \sum_{m=1}^{\infty} F_{m,n} \frac{\left(a + \frac{v_b^2}{2} D\right)^m}{\left[\frac{v_b^2}{2} (v_o D - j\omega)^2\right]^m} \right\} \right] \delta E(z). \qquad (8)$$

In Eq. 8, $G_e(z) = N_e g_e(z)$, and $G_b(z) = N_b$. Also, $\omega_p^2 = N_e e^2/m_e\epsilon_o$, and $\omega_b^2 = N_b e^2/m_e\epsilon_o$. Equation 8 is the formal differential equation for $\delta E(z)$.

Possible solutions of Eq. 8 have been considered for the case in which a = 0, the zero-order velocity distribution function of the beam is a delta function, $\delta(v_z - v_o)$, and only first-order terms in the plasma temperature, $T_e = \frac{3}{2} v_e^2$, are retained. Then Eq. 8 may be simplidied to

$$D\delta E(z) = -\omega_p^2 \left\{ \left[\frac{T_e D^3}{\omega^4} - \frac{D}{\omega^2} \right] g_e(z)\, \delta E(z) + \frac{N_b}{N_e} \frac{D}{(v_o D - j\omega)^2} \delta E \right\}. \qquad (8a)$$

For a cold plasma T_e is small and the first term in square bracketts may be neglected. Then, one integration of (8a) yields

$$\left[1 - \frac{\omega_p^2}{\omega^2} g_e(z)\right] D^2\delta E - \frac{2j\omega}{v_o}\left[1 - \frac{\omega_p^2}{\omega^2} g_e(z) + \frac{v_o}{j\omega}\frac{\omega_p^2}{\omega^2} g_e'(z)\right] D\delta E$$

$$+\left[\frac{\left(\omega_b^2 - \omega^2\right)}{v_o^2} - \frac{\omega_p^2}{\omega^2}\left(g_e''(z) - \frac{2j\omega}{v_o} g_e'(z) - \frac{\omega^2}{v_o^2} g_e(z)\right)\right] \delta E = K_1, \tag{8b}$$

where K_1 is the integration constant.

For a linear plasma density variation, the coefficient of the second derivative term is of the form

$$1 - a^2(z) = 1 - a_1^2 z,$$

in which it is assumed that

$$a^2(z) = \frac{\omega_p^2}{\omega^2} g_e(z)$$

$$a^2(z) = a_1^2 z$$

$$a^2(z=0) = 0$$

$$a^2(z=1) = a_1^2.$$

Then Eq. 8 may be put in the form of the general Bessel differential equation

$$x^2 D^2\delta E + x[2+2\epsilon x]\, D_x\delta E + \left[\frac{\omega_b^2/v_o^2}{a_1^2} x + 2\epsilon x + \epsilon^2 x^2\right] \delta E = K_1, \tag{9}$$

where $x \equiv \frac{1}{a_1^2} - z$, and $\epsilon = \frac{j\omega}{v_o}$. The homogeneous solution of Eq. 9 is

$$\delta E(x) = x^{-1/2} \exp\left[\frac{-j\omega|x}{v_o}\right]\left\{C_1 J_1\left[\frac{2\omega_b}{a_1 v_o} x^{1/2}\right] + C_2 Y_1\left[\frac{2\omega_b}{a_1 v_o} x^{1/2}\right]\right\},$$

or in terms of z,

$$\delta E\left(\frac{1}{a_1^2} - z\right) = \frac{a_1}{\left(1-a_1^2 z\right)^{1/2}} \exp \frac{j\omega}{v_o}\left[z-1/a_1^2\right] \cdot \left\{ C_1 J_1 \left[\frac{2\omega_b}{a_1^2 v_o}\left(1-a_1^2 z\right)^{1/2}\right] + C_2 Y_1 \left[\frac{2\omega_b}{a_1^2 v_o}\left(1-a_1^2 z\right)^{1/2}\right]\right\}. \quad (10)$$

Note that Eq. 10 is singular for $a^2(z) = 1$, the point where the local plasma frequency $\omega_p(z)$ equals the excitation frequency, ω. Figure XXI-15 illustrates the typical wave growth indicated for a plasma density distribution of the form $a_1^2 z$.

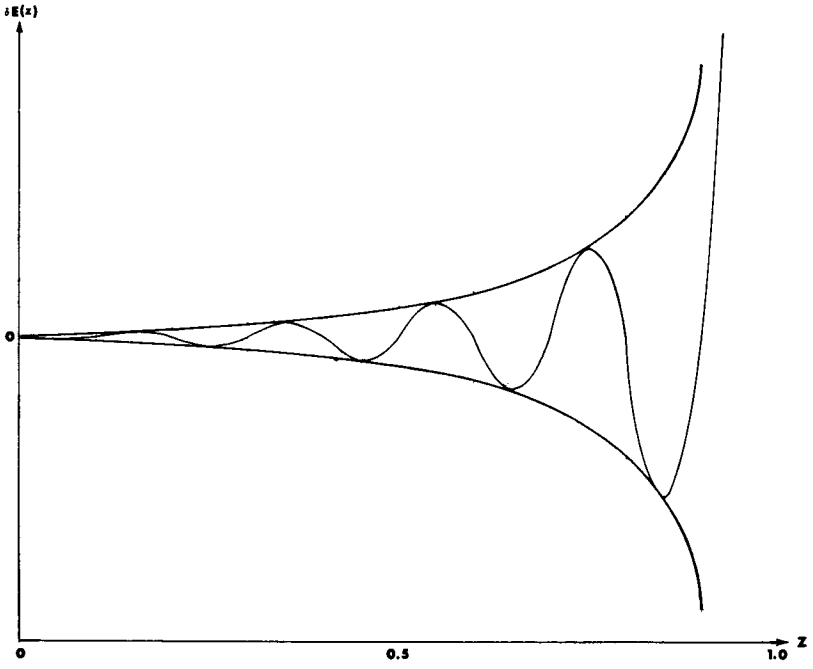

Fig. XXI-15. Typical growth of the first-order electric field; $\omega_b \ll \omega_p$, $a_1^2 = 1$.

The author wishes to acknowledge frequent and invaluable discussions with Professor W. P. Allis which have aided in the development of this analysis to its present state.

C. A. McNary

References

1. J. C. de Almeida Azevedo, "The Oscillations of an Inhomogeneous Plasma," Ph. D. Thesis, Department of Physics, Massachusetts Institute of Technology, June 1966, pp. 98-101.

XXII. ENERGY CONVERSION RESEARCH*

Academic and Research Staff

Prof. G. A. Brown
Prof. J. L. Kerrebrock
Prof. C. C. Oates

Graduate Students

R. Decher
M. L. Hougen
E. K. Levy
G. W. Zeiders, Jr.

RESEARCH OBJECTIVES AND SUMMARY OF RESEARCH

A. LIQUID-METAL MHD POWER GENERATION

1. Experimental Progress

The analytical solutions obtained from the "rod" flow model (see "Research on New Concepts in Energy Conversion," Quarterly Technical Progress Report Nr. 12, p. 2) suggest that the Mach number of the vapor entering the mixing section is slightly greater than unity and that the thickness of the wall of the liquid nozzle can significantly affect the values of liquid and vapor flow at which transition from subsonic to supersonic inlet vapor Mach number occurs. During the last quarter, liquid nozzles with various wall thicknesses (0.010"-0.080") were tested, and we found that the inlet Mach number is indeed greater than unity. Values of the Mach number ranged from approximately 1.01 for a wall thickness t = 0.080" to approximately 1.07 for t = 0.010". Also, we found that the value of the average liquid velocity at which the transition from supersonic to subsonic vapor flow occurs depends upon the nozzle wall thickness. Because of this "lip" effect, we decided to conduct all remaining experiments with the "sharp" nozzle (0.461" O.D.; 0.441" I.D.).

During the next quarter, detailed impact pressure profiles of the various single-phase and two-phase flow regions will be obtained in an attempt to determine the causes of the observed pressure discontinuities and to determine when they can and cannot occur.

2. Analytical Progress

A digital computer program has been written for a constant-area tube containing a rodlike liquid stream and an annular vapor stream, the vapor being an equilibrium two-phase mixture. This program becomes important for the case in which the steam reaches the liquid-vapor saturation line and subsequently becomes wet. This program was found to give good agreement with experimentally obtained axial static pressure distributions.

G. A. Brown, E. K. Levy

B. ALKALI-METAL MHD GENERATORS

The principal objective of this research program is to assess the feasibility of alkali-metal MHD generators for space power generation. The emphasis for the coming year

*This work was supported by the U.S. Air Force (Research and Technology Division) under Contract AF33(615)-3489 with the Air Force Aero Propulsion Laboratory, Wright-Patterson Air Force Base, Ohio.

will be on study of the behavior of a large nonequilibrium generator, which was first operated this year, and on analysis of data obtained in a supersonic stream of potassium vapor.

J. L. Kerrebrock

XXIII. SPONTANEOUS RADIOFREQUENCY EMISSION FROM HOT-ELECTRON PLASMAS*

Academic and Research Staff

Prof. A. Bers

Graduate Students

C. E. Speck

RESEARCH OBJECTIVES AND SUMMARY OF RESEARCH

The production of a hot plasma usually results in an anisotropic velocity distribution function for the constituent particles. Such distribution functions are known to be unstable (velocity-space instabilities), and are often identified experimentally by the radio-frequency emissions that they produce. The pulsed electron-cyclotron discharge, which we have studied in the past, produces a hot-electron plasma. In the "afterglow" (in between the applied microwave pulses) we have observed strong emission near the electron-cyclotron frequency and its harmonics.

During the past year, we have carried out a theoretical stability analysis of plasmas with anisotropic velocity distributions. This includes a classification and description of such instabilities in terms of negative energy modes that we have proposed. Also, during the past year we have observed three types of enhanced RF emissions from a pulsed electron-cyclotron discharge, one that is accompanied by a loss of diamagnetic signal, one that is accompanied by an oscillatory variation in cold-plasma density, and one that is not accompanied by any appreciable plasma loss.

We plan to emphasize our experimental study of the proper identification and classification of the observed instabilities that occur in between the applied microwave pulses that form and maintain the plasma. Further supporting theoretical work on stability theory will be carried out as needed for interpreting experimental data.

A. Bers

*This work is supported by the United States Atomic Energy Commission under Contract AT(30-1)-3581.

XXIV. INTERACTION OF LASER RADIATION WITH PLASMAS AND NONADIABATIC MOTION OF PARTICLES IN MAGNETIC FIELDS*

Academic and Research Staff

Prof. D. J. Rose
Prof. T. H. Dupree
Prof. L. M. Lidsky
Prof. S. Yip

Graduate Students

T. S. Brown
J. D. Callen
H. Ching
D. E. Crane
M. D. Lubin
R. W. Moir
M. Murakami
A. A. Offenberger
M. A. Samis

RESEARCH OBJECTIVES

1. Mechanisms of the Hollow Cathode Arc

The present experiment to determine the gaseous electronic mechanisms that are important in sustaining the hollow cathode arc will, in all probability, be completed. The relative importance of thermionic emission, secondary electron emission by ions, photons, metastable atoms, and so forth will be evaluated quantitatively and compared with theoretical calculations.

M. D. Lubin, D. J. Rose

2. Interaction of Coherent Radiation and Plasmas

With the 70-80 watt cw nitrogen-carbon dioxide laser completed and the (approximately) 10^{-13} watt-Hz bandwidth detector completed, we shall complete experiments on coherent scattering of 10.6-μ radiation from a steady-state plasma with electron density $\approx 10^{14}$ cm^{-3}, electron temperature $\approx$3-10 eV, 50-95% ionized.

A doctoral program will be started to measure electron temperatures parallel to and perpendicular to the magnetic field, by using laser scattering to give more direct information on thermalization rates in the plasma.

A. A. Offenberger, L. M. Lidsky, D. J. Rose

3. Laser-Plasma Science and Technology

This heading includes gaseous electronics, plasma physics and technological aspects of devices that are likely to be of interest as gas lasers. This work continues, with changes of detailed topics. A small program to maximize the power-handling capability of an insulating tube-type argon laser will be completed, with a study of the utility of high-alumina tubes (G. E. Co. Lucalox) in such applications. A simple optical device is being constructed which will detect incipient thermal failure of such laser column tubes. A hollow cathode arc with side gas feed and plasma coming from both ends will be built to see whether the hollow cathode arc type of argon plasma can be made to "lase."

Finally, a pulsed variation of the nitrogen-carbon dioxide laser will be completed. Preliminary estimates show that it should be possible to pulse the plasma and increase the 10.6-μ output very substantially in the afterglow.

D. E. Crane, L. M. Lidsky, D. J. Rose

---

*This work was supported by the United States Atomic Energy Commission (Contract AT(30-1)-3285).

4. Nonadiabatic Scattering

The first stage in our study of nonadiabatic scattering has been completed. We have measured the lifetime of electrons resonantly trapped in a magnetic-mirror field and developed a theoretical explanation of our experimental results. The theory, which predicts the point at which first-order perturbation theoretical estimates of velocity-space diffusion will become inadequate and furnishes a higher order estimate of the diffusion coefficient, has applicability to a wide range of problems. We are now investigating the following problems.

(i) Scattering in long coherence length, nonresonant perturbations.

(ii) Small-angle (in velocity space) scattering in very weak resonant perturbations. The toroidal device developed for this study provides over 100 transits of the perturbation region and very high sensitivity to changes in the direction of the velocity vector.

(iii) The possibility of using the techniques developed in our study of the corkscrew system to study wave-particle scattering with a view toward furnishing an experimental test of some predictions of plasma kinetic theory.

L. M. Lidsky, D. J. Rose, R. W. Moir, M. Murakami

A. NONADIABATIC TRAPPING IN TOROIDAL GEOMETRY

One goal of the toroidal injection experiment has been achieved: The nonadiabatic injection of a cw electron beam into a toroidal magnetic field to produce a circulating electron stream.

The experiment (described more fully in previous reports[1]) is a 6-meter circumference torus, with 11-cm minor diameter and 70 Gauss main field. An electron beam of a few microamperes at 1500 eV was injected through an injector snout with 80% of the energy perpendicular to $\vec{B}$. A magnetic field periodically perturbed in space (corkscrew) acted on the beam, converting perpendicular energy to parallel energy. The beam's

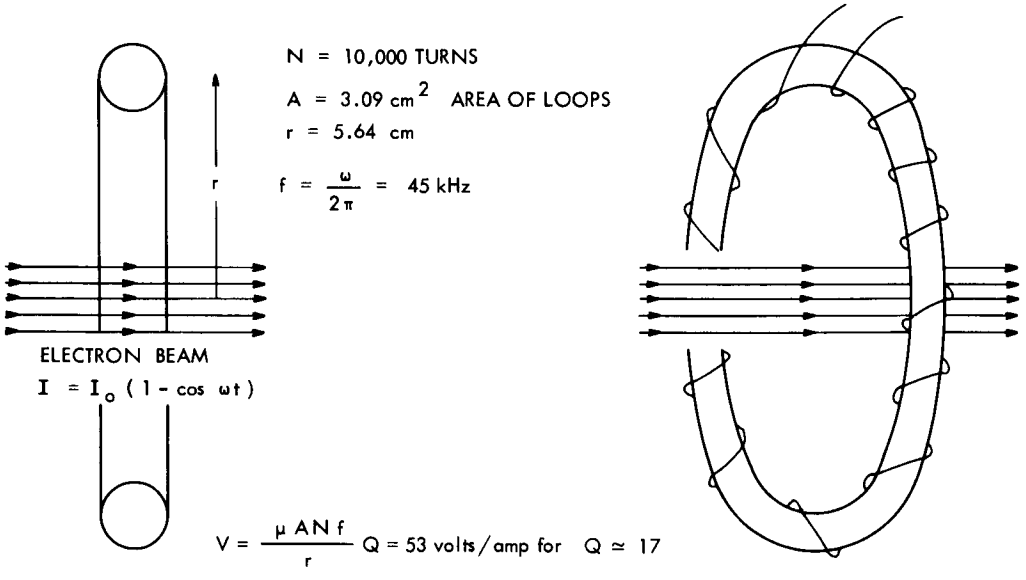

Fig. XXIV-1. Rogowsky coil.

guiding center remained on the axis, and 95% of the energy was parallel to B. This beam then circulated around the torus until it hit the injector snout or the walls. The beam lifetime was measured with an ion collector[1] and a new diagnostic, and Rogowsky coil, which is shown in Fig. XXIV-1. The electron beam was modulated at 45 kHz, the self-resonant frequency of the coil; this procedure enabled detection of less than 60 namps of current. The Rogowsky coil was chosen because of its insensitivity to the low-energy secondary electrons that plague charge collector techniques.

The Rogowsky coil measurements agreed within 5% with the ion collector measurements, both of which indicated 4-5 transits of the beam around the torus.[2] This number is in fair agreement with the 6.4 transits obtained by means of a computer calculation.[3]

We found that the resonant perturbation, even at the field strength ($B_\perp/B = 4.3\%$) used for injection, preferentially scattered the beam energy into perpendicular motion, thereby resulting in very rapid loss. This preferential scattering was also seen by Clarke in his experiments on nonadiabatic scattering in mirror systems.[4]

In order to increase the number of transits, we decided to inject the beam into the torus by means of a pulsed E field. After the E field is switched off, the remaining fields are fairly uniform, yielding adiabatic motion and many transits. Figure XXIV-2

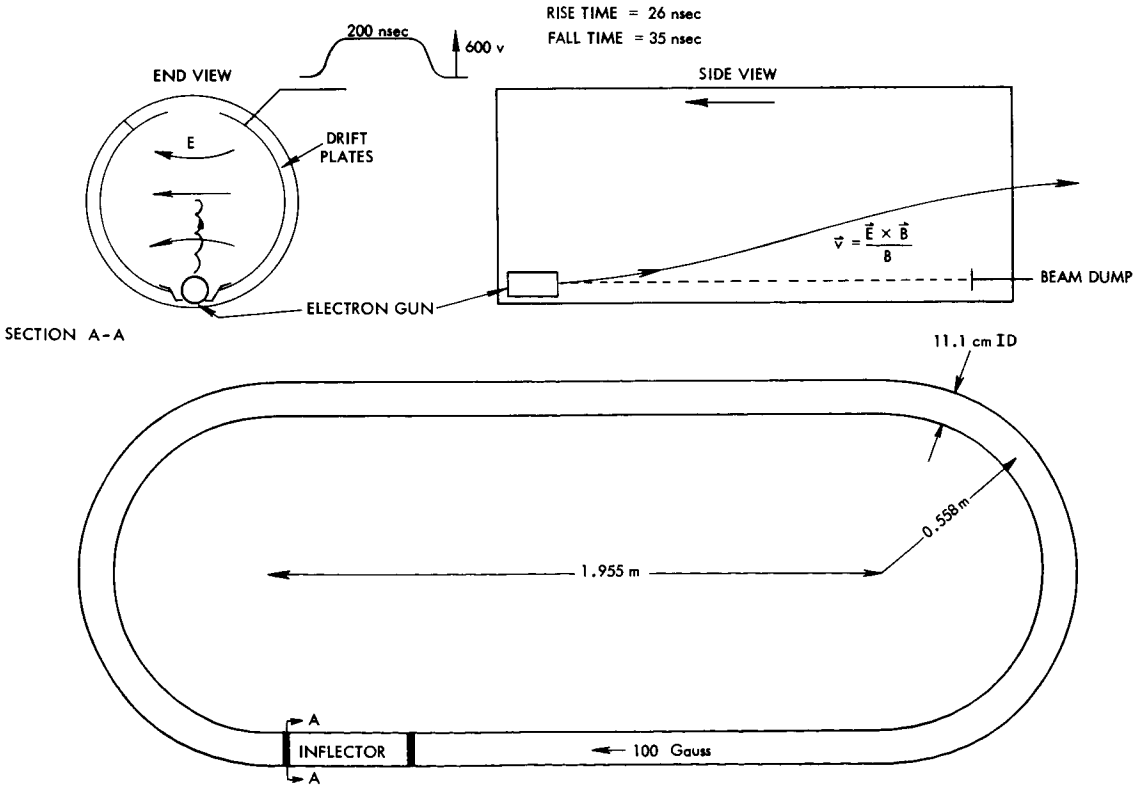

Fig. XXIV-2. Electron injection system.

shows the injection system.

The curved "drift" plates produce a horizontal $\vec{E}$ field which causes the beam to drift vertically at the E/B speed. In order to minimize the transverse energy contained in the cycloidal motion of the drifting electrons, the plates were made quite long (20 inches), which gave 4 or more complete cycloids for drifting to the torus axis.

With the injection field off, the electron beam from the continuously operating gun follows the magnetic field lines near the bottom of the torus to the collector electrode. Beam inflection is produced by a flat-topped 600-V pulse with ~30 nsec rise and fall times and variable width. The nominal injection time is ~200 nsec (slightly less than one transit time of the beam in its motion around the torus), but is variable over a wide range around this value. Injection for larger than a single transit time results in spillage of the beam that is already trapped. The injection pulse is repeated every 16 msec, and the beam decay (~30 μsec for complete loss) is observed during the interpulse periods.

The beam, which is actually a long column of electrons, then circulates around the axis until it diffuses to the walls.

The diagnostic was a cylindrical tube, 3 1/4" in diameter, through which the beam

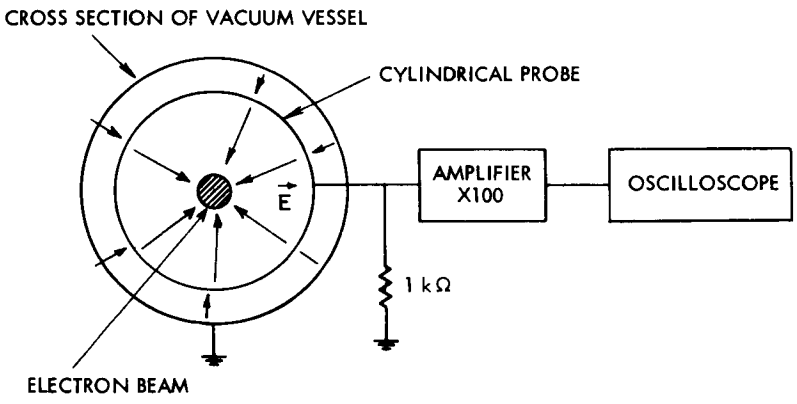

Fig. XXIV-3. Pickup probe.

passed. The E-field from the beam electrons induces a voltage on the cylinder (Fig. XXIV-3).

Figure XXIV-4a (lower trace) shows the voltage on the drift plates, and the upper trace shows the probe signal. Each oscillation indicates one transit. The oscillation period scales as $1/\sqrt{E_{\|}}$ (period = $\ell/v_{\|}$) where E is the parallel energy of the beam. The amplitude dies away as the beam is lost to the walls. The lower frequency oscillation period is caused by rotational transform of the magnetic field (ℓ = 2 Stellarator coils), and is thought to be due to the transform rotating the beam around an axis displaced from the axis of the torus, which thus brings the beam closer and then farther

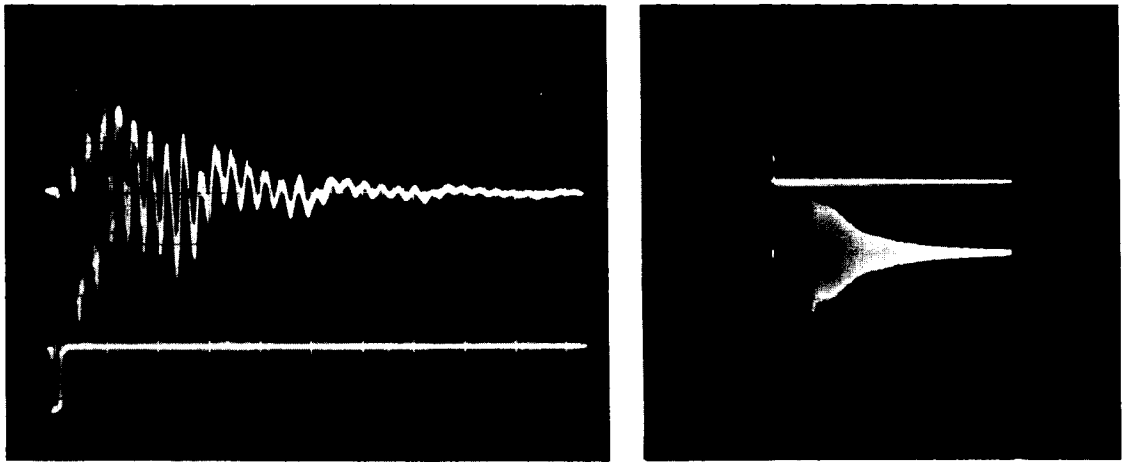

(a) (b)

Fig. XXIV-4. Pickup probe data.
(a) Horizontal: 1 μsec/cm; 0.3 μsec/transit
Upper: 0.2 volt/cm
Lower: 500 volts/cm
(b) Horizontal: 5 μsec/cm; 0.3 μsec/transit
Lower: 5 mV/cm.

from the pickup probe. The transform angle a is found to be proportional to the square of the current in the Stellarator coil. $a \approx 360°/N = 50°$ for N = 7, where N is the number of oscillations during one period of the low-frequency oscillation (see Fig. XXIV-4a). Figure XXIV-4b shows a beam contained in a longer time; 37 transits for an e-folding, and 128 transits still observable.

While our results are preliminary, the rather long lifetime of the circulating beam meets our requirements for perturbation studies, and also provides a tool for investigating the closure of drift surfaces in closed B-field systems.

R. W. Moir, L. M. Lidsky

References

1. Quarterly Progress Report No. 77, pp. 164-167; Quarterly Progress Report No. 78, pp. 126-127; Quarterly Progress Report No. 79, pp. 131-132; Quarterly Progress Report No. 81, pp. 141-147.
2. We previously reported (Quarterly Progress Report No. 81, p. 145) 15 transits, but this enhanced value was due to secondary electrons.
3. Ibid; loc. cit.
4. Ibid; p. 147.

COMMUNICATION SCIENCES
AND
ENGINEERING

XXV. STATISTICAL COMMUNICATION THEORY*

Academic and Research Staff

Prof. Y. W. Lee
Prof. A. G. Bose
Prof. J. D. Bruce
Prof. A. V. Oppenheim
Prof. D. E. Nelsen
G. Gambardella

Graduate Students

T. Huang
V. Nedzelnitsky
L. R. Poulo
A. E. Rolland
R. W. Schafer
J. E. Schindall
F. P. Tuhy
J. L. Walker
J. J. Wawzonek
C. J. Weinstein
D. H. Wolaver

RESEARCH OBJECTIVES

1. Investigation of Switching Systems

There is an increasing need for systems that handle analog signals but operate in a switching mode. Such switching systems offer efficiency, size, and weight advantages over conventional analog systems. The analysis of these systems, however, is complicated by the fact that they often take the form of closed-loop nonlinear systems. Analysis and synthesis procedures are necessary in order to optimally design these systems and to determine their ultimate performance capabilities.

The principal efforts during the past three years have been devoted to static analysis. An exact static analysis has been achieved by A. G. Bose[1] and has provided useful design guidelines. The noise analysis has been carried out for the special case of a tunnel-diode switching circuit by D. E. Nelsen.[2]

Work is now under way to determine the dynamic performance of these systems. During the coming year it is hoped that a better understanding of the transient response and spectrum properties will be obtained. We also plan to extend the noise studies to other switching devices and circuits. An eventual goal in this project is to obtain noise models for switching devices in much the same way as we have done for noise models of devices operating in the linear mode.

2. Modulation Noise in Tape Recording

Modulation noise in tape recording is a wide-band noise whose intensity increases with increasing recorded signal on the tape. The phenomenon has been well documented, but adequate explanations and models are not available. We hope that a proper model will aid in the development of lower noise tapes.

Extensive experiments have been made to isolate noises of other origins (electrical and mechanical) from the modulation noise. The spectral properties of modulation noise have been measured under varying conditions of recording and playback. A theoretical model has been derived which relates the modulation noise to particle interaction on the tape.

---

*This work was supported by the Joint Services Electronics Programs (U.S. Army, U.S. Navy, and U.S. Air Force) under Contract DA 36-039-AMC-03200(E), the National Aeronautics and Space Administration (Grant NsG-496), and the National Science Foundation (Grant GK-835).

Further experiments are necessary to correlate the predictions indicated by the model with physical observations on tape noise. Recommendations for reduction of the noise will be made after verification of the noise model.

3. Recording and Reproduction of Sound

The design of loudspeakers and of recording techniques has remained a controversial and poorly understood area for decades. Standards committees have not been able to agree upon an acceptable design criterion or measurement technique for evaluation of the commom loudspeaker. This subject is complicated by the fact that objective criteria are desired for transducers whose ultimate use involves subjective evalution.

A design criterion has been developed which makes use of Green's function to produce recordings of sound as they would be heard if reproduced in a room through an ideal transducer. A computer-aided design program has yielded the design of a practical transducer whose performance is subjectively indistinguishable from that of the ideal transducer.[3]

Efforts will now be directed toward problems in the recording of sound. The effects of the normal mode structure of the recording environment will be investigated and the constraints that this structure imposes upon the techniques and procedures of recording will be determined.

4. Optimum Quantization

Exact expressions for the quantization error as a function of the quantizer parameters, the error-weighting function, and the amplitude probability density of the quantizer-input signal have been derived by J. D. Bruce.[4] An algorithm based on these expressions, which permits the determination of the specific values of quantizer parameters that minimize the quantization error (with respect to some particular error-weighting function) has been developed. The error expressions and the algorithm have been extended to the case in which the quantizer-input signal is a message signal contaminated by a noise signal.

During the past year studies have been concentrated in two particular areas.

a. Subjective evaluation of speech quantizer levels is small and there are requirements of high intelligibility and naturalness.

b. Theoretical investigation of optimum quantizers for quantizer-input signals that are message signals contaminated by noise.

Results have been obtained in each of these areas and are being reported.[5,6] In particular, it is now possible to characterize a quantizer by certain of its properties so as to be able to say whether or not it is desirable for use in a speech-transmission system. Also, these same properties classify the type of distortion that the quantizer will introduce. With respect to the second area, results have been obtained for the case in which the message signal is discrete. These results are identical to those obtained from the ideal observer point of view in classical decision theory.

Studies in both of these areas will continue during the coming year.

5. Localization of Acoustical Phenomena

For some time, there has been evidence to indicate that the pinna (external ear) plays a primary role in the localization of acoustical phenomena. It is proposed that this role be studied in the forthcoming year with a view toward modeling the external ear and simulating its role in localization.

6. Superposition in a Class of Nonlinear Systems

In 1964, a new characterization of nonlinear systems was developed, and its application to problems in nonlinear filtering was suggested by A. V. Oppenheim.[7] This approach to nonlinear filtering represented a generalization of the linear filtering problem and appeared to be particularly suited to the nonlinear separation of signals that have been nonadditively combinded.

Specific cases of interest, at present, are in the application of this technique to the separation of convolved signals and the separation of multiplied signals. The need for such techniques arises, for example, in the processing of signals after transmission over multipath and fading channels, the removal of echoes from recorded speech and music, and the analysis and bandwidth reduction of speech. It also appears, at present, that the ability to apply these techniques to speech and music suggest some fundamentally new means for modifying their characteristics and for preprocessing before recording or transmission to enhance their quality.

Primary empahsis during the past year has been directed toward the separation of convolved signals. The filter was simultated on a digital computer and initial studies were carried out with both artificially generated waveforms and speech. A preliminary investigation of the effect of additive noise on the processing was initiated.

Work will continue on a study of the separation of convolved signals. In particular, speech with artificially generated echoes will be processed to recover the original speech. Uncorrupted speech will also be processed in an attempt to separate the glottal waveform and the impulse response of the vocal tract.

Attention will also be directed toward the extraction of the low-frequency envelope from music and the processing of waveforms that have been subject to low-frequency fading.

7. Wiener Theory of Nonlinear Systems

The study of this theory was initiated at the Research Laboratory of Electronics in 1949. Many doctoral theses and technical reports have been written on the subject by members of this group. The latest doctoral thesis on the Wiener nonlinear theory was written by R. B. Parente.[8] It contains the first solution of the dynamic stability problem of a magnetic suspension device associated with inertial guidance systems. Present work is directed toward other applications, and the relationship between differential equation representation and functional representation of nonlinear systems.

Y. W. Lee

References

1. A. G. Bose, "A Two-State Modulation System," WESCON, Section 7.1, San Francisco, August 20-23, 1963.

2. D. E. Nelsen, "Statistics of Switching-Time Jitter for a Tunnel Diode Threshold-Crossing Detector," Sc.D. Thesis, Department of Electrical Engineering, M.I.T., June 1966.

3. A. G. Bose, "Relative Effects of Normal Mode Structure of Loudspeakers and Rooms on the Reproduction of Sound," a paper presented at the Sixty-eighth Meeting of the Acoustical Society of America, October 1964.

4. J. D. Bruce, "Optimum Quantization," Technical Report 429, Research Laboratory of Electronics, Massachusetts Institute of Technology, Cambridge, Massachusetts, March 1, 1965.

5. R. W. Koralek, "Speech Quantization Studies," S.B. Thesis, Department of Electrical Engineering, M.I.T., May 1966.

6. J. D. Bruce, "Fixed Representation-Value Quantization of a Discrete Message Signal Plus Noise," to be published.

7. A. V. Oppenheim, "Superposition in a Class of Nonlinear Systems," 1964 IEEE International Convention Record, Part 1, pp. 171-177.

8. R. B. Parente, "Functional Aanlysis of Systems Characterized by Nonlinear Differential Equations," Technical Report 444, Research Laboratory of Electronics, Massachusetts Institute of Technology, July 15, 1966.

A. TRANSFER FUNCTIONS FOR A TWO-STATE MODULATION SYSTEM

1. Introduction

Bose[1,2] has described the simple two-state modulation system diagrammed in Fig. XXV-1 and has demonstrated that the average of the output switching waveform is approximately equal to the negative of the input voltage for fixed values of input signal. The system has application as an efficient switching amplifier, or can operate as a voltage regulator by having the input fixed at a reference voltage and powering the output switching element from the voltage that is to be regulated.

In this report, transfer functions for the modulator are derived for fixed- and ramp-input waveforms. Other aspects of modulator operation are being explored; this work will not be reported here.

2. Transfer Function, Static Input

First, consider the modulator of Fig. XXV-1 with zero delay, and denote the fixed input x_o. It is expedient to visualize the averaging of the two-state output waveform y(t) as taking place in two stages. This is diagrammed (with representative waveforms) in Fig. XXV-2. The two-state waveform y(t) is first passed through a lowpass RC network, with the same time constant as the RC network appearing within the modulator feedback loop. The intermediate signal, $y_i(t)$, which results – identical to the modulator feedback signal f(t) – is then passed through an ideal lowpass filter to yield output $\bar{y}$. Of course, y(t) could just as well be passed directly through the ideal lowpass filter to yield the same $\bar{y}$ as does the two-stage filtering process; however, the modulator error is graphically evident by examination of the intermediate waveform $y_i(t)$.

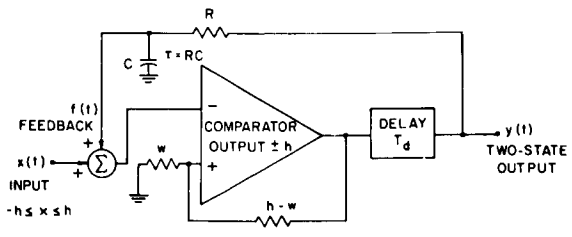

Fig. XXV-1. Two-state modulation system.

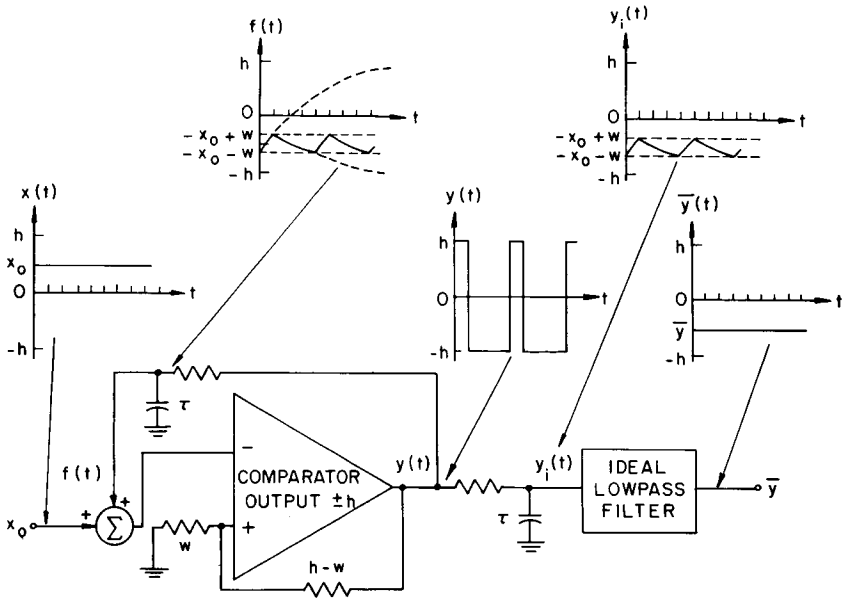

Fig. XXV-2. Modulator waveforms with two-stage output filter (zero-delay).

Since $y_i(t)$ is identical to f(t), the operation of the modulator loop contrains it to vary between $-x_o - w$ and $-x_o + w$ in an exponential manner. This is shown in Fig. XXV-2. The desired output, $-x_o$, is the midpoint value of $y_i(t)$. The ideal lowpass filter yields output $\bar{y}$ as the average value of $y_i(t)$. Because of the unequal curvature associated with the charge and discharge portions of the waveform $y_i(t)$, the average is equal to the midpoint only for $x_o = 0$. In fact, it is apparent that the discrepancy between average and midpoint (the modulator error) increases as $|x_o|$ and as w (the half-width of the exponential window) increase and acts to produce a modulator gain or transfer function slightly greater than unity.

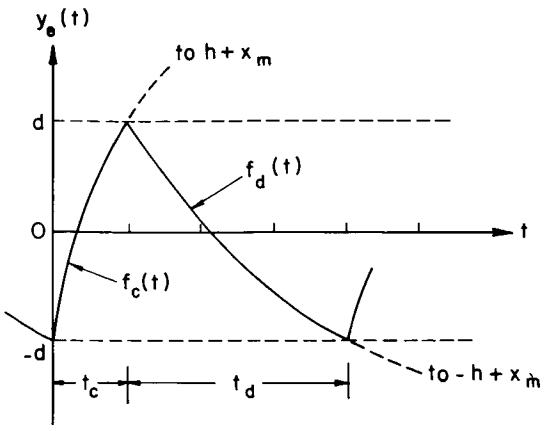

Fig. XXV-3. Exponential-error waveform.

Consider an exponential waveform charging and discharging toward h and -h between limits $-x_m + d$ and $-x_m - d$, where $-x_m$ is the midpoint of the exponential window, and d is the half-width of the window. The object is to derive an expression for the average value of this waveform in terms of its midpoint value and its half-width. To avoid masking

the output error, consider subtracting the midpoint value $-x_m$ from the exponential waveform. The resulting waveform $y_e(t)$ has midpoint zero and varies exponentially between d and -d as sketched in Fig. XXV-3.

The average of $y_e(t)$ is precisely $\overline{y} - (-x_m)$. During the charge portion of the cycle,

$$f_c(t) = (h+x_m) + (-h-x_m-d)\, e^{-t/\tau}. \tag{1}$$

So

$$f_c(t_c) = d = h + x_m + (-h-x_m-d)\, e^{-t_c/\tau}, \tag{2}$$

and

$$t_c = \tau \ln \frac{h + x_m + d}{h + x_m - d}. \tag{3}$$

From (1) and (3),

$$\int_0^{t_c} f_c(t)\, dt = \tau \left[(h+x_m) \ln \left(\frac{h + x_m + d}{h + x_m - d} \right) - 2d \right]. \tag{4}$$

Similarly, for the discharge portion of the cycle,

$$\int_{t_c}^{t_c+t_d} f_d(t)\, dt = -\tau \left[(h-x_m) \ln \left(\frac{h - x_m + d}{h - x_m - d} \right) - 2d \right]. \tag{5}$$

The average over a cycle is given by

$$\frac{1}{t_c + t_c} \int_0^{t_c+t_d} y_e(t)\, dt = \frac{(h+x_m) \ln \dfrac{h + x_m + d}{h + x_m - d} - (h-x_m) \ln \dfrac{h - x_m + d}{h - x_m - d}}{\ln \dfrac{h + x_m + d}{h + x_m - d} + \ln \dfrac{h - x_m + d}{h - x_m - d}}. \tag{6}$$

Expanding, since $\ln \left[\frac{a+\epsilon}{a-\epsilon} \right] = 2 \left[\frac{\epsilon}{a} + \frac{1}{3} \left(\frac{\epsilon}{a} \right)^3 + \frac{1}{5} \left(\frac{\epsilon}{a} \right)^5 + \ldots \right]$ for $\left| \frac{\epsilon}{a} \right| < 1$, we have

$$\frac{1}{t_c + t_d} \int_0^{t_c+t_d} y_e(t)\, dt = \frac{(h+x_m)\, 2 \left[\dfrac{d}{h+x_m} + \dfrac{1}{3} \left(\dfrac{d}{h+x_m} \right)^3 + \ldots \right] - (h-x_m)\, 2 \left[\dfrac{d}{h-x_m} + \left(\dfrac{d}{h-x_m} \right)^3 + \ldots \right]}{2 \left[\dfrac{d}{h+x_m} + \dfrac{1}{3} \left(\dfrac{d}{h+x_m} \right)^3 + \ldots \right] + 2 \left[\dfrac{d}{h-x_m} + \dfrac{1}{3} \left(\dfrac{d}{h-x_m} \right)^3 + \ldots \right]}. \tag{7}$$

Combining terms, to second order we obtain

$$\overline{y} = -x_m \left[1 + \frac{2}{3} \frac{\left(\frac{d}{h}\right)^2}{1 - \left(\frac{x_m}{h}\right)^2} \right] \tag{9}$$

which is the desired transfer function. The result of (9) is under the assumption that $\frac{d}{h \pm x_m} \ll 1$, in that terms of the order of $\left[\frac{d}{h \pm x_m}\right]^4$ have been neglected. The "excess-gain" error term is of order $\left(\frac{d}{h}\right)^2$ and contains a nonlinearity of the form $\left[1 - \left(\frac{x_m}{h}\right)^2\right]$.

For the case of static input and zero delay, the exponential window waveform $y_i(t)$ has midpoint $-x_o$ and half-width w. For this case, then, (9) leads to

$$\overline{y} = -x_o \left[1 + \frac{2}{3} \frac{\left(\frac{w}{h}\right)^2}{1 - \left(\frac{x_o}{h}\right)^2} \right]. \tag{10}$$

Now the effect of nonzero delay in the modulator loop will be considered. Because of the delay, the output does not change until T_d seconds after the feedback waveform has reached $-x_o + w$ or $-x_o - w$. During this time, the feedback waveform and the intermediate waveform $y_i(t)$ overshoot. The effect of delay on $y_i(t)$ is to enlarge the

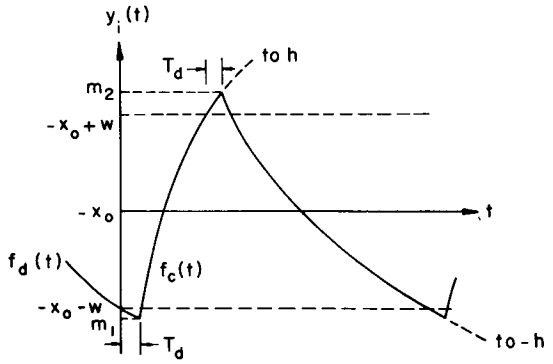

Fig. XXV-4. Intermediate waveform, static input.

exponential window and to displace its midpoint from $-x_o$. This is diagrammed in Fig. XXV-4. Notice that the delay-induced overshoot is more pronounced on the steeper of the two exponential segments, tending to displace the midpoint of the waveform toward the more distant asymptote and thus decrease the magnitude of the modulator gain. From Fig. XXV-4,

$$f_d(t) = -h + (h - x_o - w)\, e^{-t/\tau}, \tag{11}$$

so

$$m_1 = -h + (h - x_o - w)\, e^{-T_d/\tau}. \tag{12}$$

Similarly,

$$m_2 = h + (-h - x_o + w)\, e^{-T_d/\tau}. \tag{13}$$

The midpoint of the exponential window, $-x_m$, is given by

$$-x_m = \frac{m_1 + m_2}{2} = -x_o\, e^{-T_d/\tau}. \tag{14}$$

The half-width of the exponential window, d, is given by

$$d = \frac{m_2 - m_1}{2} = h\left(1 - e^{-T_d/\tau}\right) + w\, e^{-T_d/\tau}. \tag{15}$$

Substituting the delay-altered values of midpoint and half-width from (14) and (15) in Eq. 9 gives

$$\overline{y} = -x_o e^{-T_d/\tau}\left\{1 + \frac{2}{3}\,\frac{\left[\left(1 - e^{-T_d/\tau}\right) + \frac{w}{h}\, e^{-T_d/\tau}\right]^2}{1 - \left[\frac{x_o e^{-T_d/\tau}}{h}\right]^2}\right\}. \tag{16}$$

The modulator gain is reduced by a factor of $e^{-T_d/\tau}$ from the zero-delay case, while the nonlinearity and parameter dependence of the result, introduced by the second term in brackets, are increased. Under the assumption that $\frac{T_d}{\tau} \ll 1$, (16) can be written

$$\overline{y} = -x_o\left(1 - \frac{T_d}{\tau}\right)\left[1 + \frac{\left(\frac{T_d}{\tau} + \frac{w}{h}\right)^2}{1 - \left(\frac{x_o}{h}\right)^2}\right]. \tag{17}$$

And, for use of the modulator as a symmetric regulator, (17) predicts

$$\frac{dy}{dh} = 2\,\frac{x_o}{h}\,\frac{\left(\frac{T_d}{\tau} + \frac{w}{h}\right)\left(\frac{x_o^2}{h^2}\,\frac{T_d}{\tau} + \frac{w}{h}\right)}{\left(1 - \frac{x_o^2}{h^2}\right)^2}. \tag{18}$$

3. Dynamic Transfer Function, Ramp Input

An explicit expression for the modulator transfer function with arbitrary dynamic input waveforms cannot be obtained. The problem arises because the modulator switches at time t_s in such a manner that the exponential feedback waveform added to the input signal equals w or -w. This produces an implicit transcendental equation for t_s which admits an explicit solution for t_s only when the input signal is a constant.

A useful approach is to select a particular input waveform appropriate for characterizing the modulator behavior, and seek an approximate solution for this excitation. For a linear system the sinusoidal response provides an effective characterization. In nonlinear systems such as the two-state modulator, however, the sinusoidal response is difficult to express (it is a function of the amplitude and DC level of the input, as well as its frequency) and provides no general information about the system (since superposition does not apply).

The main effect of a dynamic input on modulator operation is that the modulator must track or "keep up" with the time rate of change of the input waveform. This time rate of change, or slope, is characterized by a ramp waveform. With this motivation, characterizing the dynamic response of the modulator by its ramp response leads to an unexpected bonus: although the equations describing the transfer function are transcendental, they can be manipulated to yield an accurate and explicit solution for the particular case of a ramp input. It should be noted that many waveforms can be adequately modeled as a series of ramp segments, each segment being one modulator switching period long.

Derivation of the modulator transfer function with a ramp input is facilitated by characterizing the ramp as altering the effective width and midpoint of the exponential window function $y_i(t)$. Because the modulator operation is asynchronous, one cannot specify or predict "charging" or "discharging" operation of the modulator at any particular instant of time. The desired transfer function will first be obtained by assuming input mean x_o to take place at the center of a modulator charge cycle to give $t_c(x_o) = t_{co}$; then assuming the same mean, x_o, to have occurred at the center of a modulator discharge cycle to give $t_d(x_o) = t_{do}$; and taking the output to be

$$\overline{y} \equiv h \frac{t_{co} - t_{do}}{t_{co} + t_{do}}. \tag{19}$$

This is plausible in view of the asynchronous operation of the modulator. It will then be shown that (19) remains unchanged when the output is defined more rigorously as the average of y(t) over a complete cycle, and x_o is taken as the input mean over the complete cycle.

Consider an input ramp x(t), with mean x_o and slope x' during the feedback charge

cycle. The resulting exponential window waveform is plotted in Fig. XXV-5. The switching limits plotted are the loci of $y_i(t) = -x(t) + w$ and $y_i(t) = -x(t) - w$; the

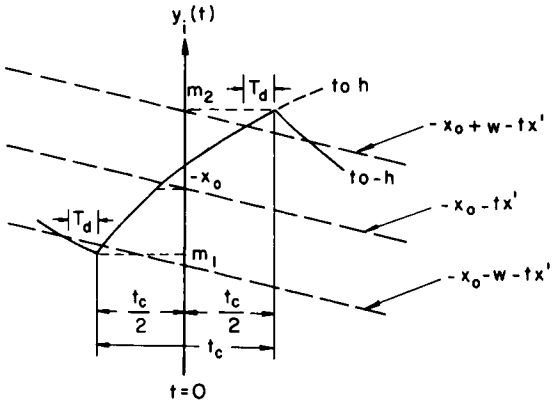

Fig. XXV-5. Intermediate waveform, ramp input.

overshoot occurs because of the delay T_d. From Fig. XXV-5,

$$m_1 = -h + \left[h - x_o - w + x'\left(\frac{t_{co}}{2} + T_d\right)\right] e^{-T_d/\tau} \tag{20}$$

$$m_2 = h + \left[-h - x_o + w - x'\left(\frac{t_{co}}{2} + T_d\right)\right] e^{-T_d/\tau}. \tag{21}$$

Therefore

$$d = \frac{m_2 - m_1}{2} = h\left(1 - e^{-T_d/\tau}\right) + w\, e^{-T_d/\tau} - \frac{x'}{2} e^{-T_d/\tau} t_{co} \tag{22}$$

$$-x_m = \frac{m_1 + m_2}{2} = -(x_o - x'T_d)\, e^{-T_d/\tau}. \tag{23}$$

Similar values of d and x_m are obtained by regarding x_o as the mean of the input ramp during a discharge cycle.

The problem is that d is expressed as a function of t_{co}, hence (22) and (23) cannot be plugged directly into (9) to obtain an explicit expression for $\overline{y}$.

Recall that (9) arose from the expression

$$t_{co} = \tau \ln \frac{h + x_m + d}{h + x_m - d}. \tag{24}$$

Or, to second order, since $\ln\left[\frac{a+\epsilon}{a-\epsilon}\right] = 2\left[\frac{\epsilon}{a} + \frac{1}{3}\left(\frac{\epsilon}{a}\right)^3 + \ldots\right]$,

$$t_{co} = \frac{2\tau d}{h + x_m}. \tag{25}$$

If the implicit expressions for d and x_m are substituted in Eq. 25, we have

$$t_{co} = \frac{2\tau\left[h\left(1-e^{-T_d/\tau}\right)+we^{-T_d/\tau}\right]}{h+\left[x_o-T_dx'\right]e^{-T_d/\tau}} - \frac{\left[\tau x'e^{-T_d/\tau}\right]t_{co}}{h+\left[x_o-T_dx'\right]e^{-T_d/\tau}}. \tag{26}$$

Iterative substitution for t_{co} yields a ratio series

$$t_{co} = \frac{2\tau\left[h\left(1-e^{-T_d/\tau}\right)+we^{-T_d/\tau}\right]}{h+\left[x_o-T_dx'\right]e^{-T_d/\tau}}\left[\frac{1}{1+\dfrac{\tau x'e^{-T_d/\tau}}{h+\left[x_o-T_dx'\right]e^{-T_d/\tau}}}\right] \tag{27}$$

or

$$t_{co} = \frac{2\tau\left[h\left(1-e^{-T_d/\tau}\right)+we^{-T_d/\tau}\right]}{h+\left[x_o+(\tau-T_d)x'\right]e^{-T_d/\tau}}. \tag{28}$$

Comparison of Eq. 28 and Eq. 25 enables identification of equivalent midpoint and half-widths, denoted x_e and d_e, in explicit form:

$$x_e = \left[x_o+(\tau-T_d)x'\right]e^{-T_d/\tau} \tag{29}$$

$$d_e = \left[h\left(1-e^{-T_d/\tau}\right)+we^{-T_d/\tau}\right]. \tag{30}$$

Now equations (29) and (30) may be substituted in Eq. (9) to give the desired transfer function.

$$\boxed{\bar{y} = -\left[x_o+(\tau-T_d)x'\right]e^{-T_d/\tau}\left\{1+\frac{\left[\left(1-e^{-T_d/\tau}\right)+\frac{w}{h}e^{-T_d/\tau}\right]^2}{1-\left[\frac{\left[x_o+(\tau-T_d)x'\right]e^{-T_d/\tau}}{h}\right]^2}\right\}} \tag{31}$$

It will be demonstrated next that (31) remains valid if a complete modulator cycle is considered, with output $\bar{y} = h\dfrac{t_c-t_d}{t_c+t_d}$ and input mean x_o over the complete cycle. The input mean during t_c, from Fig. XXV-6, is

$$x_{oc} = x_o - \frac{t_d}{2} x'. \tag{32}$$

And, during t_d the input mean is

$$x_{od} = x_o + \frac{t_c}{2} x'. \tag{33}$$

Rewriting (28) in terms of the charge and discharge means yields

$$t_c = \frac{2\tau d_e}{h + [x_o + (\tau - T_d)x'] e^{-T_d/\tau} - \frac{t_d}{2} x' e^{-T_d/\tau}} \tag{34}$$

$$t_d = \frac{2\tau d_e}{h - [x_o + (\tau - T_d)x'] e^{-T_d/\tau} - \frac{t_c}{2} x' e^{-T_d/\tau}}. \tag{35}$$

Recalling that t_{co} was defined as the charge period with input mean x_o, and t_{do}

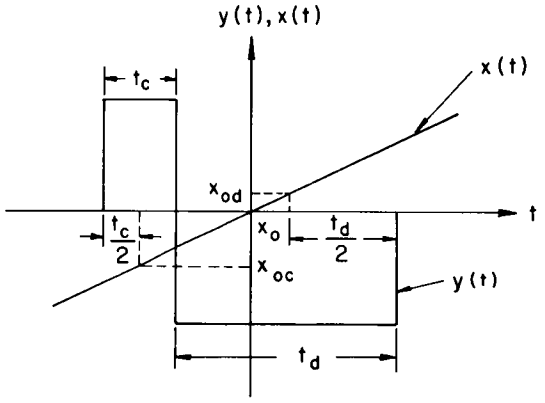

Fig. XXV-6. Complete modulator cycle, ramp input.

as the discharge period with input mean x_o, we can rewrite (34) and (35) as

$$t_c = t_{co} \frac{1}{1 - t_{co} \frac{x' e^{-T_d/\tau}}{4\tau d_e} t_d} \tag{36}$$

$$t_d = t_{do} \frac{1}{1 - t_{do} \frac{x' e^{-T_d/\tau}}{4\tau d_e} t_c}. \tag{37}$$

By identifying $\frac{x' e^{-T_d/\tau}}{4\tau d_e} = A$, iterative substitution gives

$$t_c = t_{co} \cfrac{1}{1 - At_{co}t_{do} \cfrac{1}{1 - At_{co}t_{do} \cfrac{1}{1 - At_{co}t_{do} \cfrac{1}{\ddots}}}} \tag{38}$$

$$t_d = t_{do} \cfrac{1}{1 - At_{co}t_{do} \cfrac{1}{1 - At_{co}t_{do} \cfrac{1}{\ddots}}} \tag{39}$$

It is sufficient to note that

$$t_c = Bt_{co} \tag{40}$$

$$t_d = Bt_{do}. \tag{41}$$

Whence

$$\overline{y} = h\frac{t_c - t_d}{t_c + t_d} = h\frac{Bt_{co} - Bt_{do}}{Bt_{co} + Bt_{do}} = h\frac{t_{co} - t_{do}}{t_{co} + t_{do}}. \tag{42}$$

This is the desired proof that the output average over a full cycle in terms of the input mean x_o during this cycle is the same as that obtained by superposition of the charge-cycle and discharge-cycle results, each taken separately to have input mean x_o.

It should be pointed out that most of the transfer functions obtained here can also be obtained by direct brute-force algebraic expansion and approximation methods on the transfer function obtained by Bose. Indeed, it was not until direct algebra and computer evaluation had predicted the form of the result that the procedure described in this report was developed. The exponential window technique presented here is, however, simpler to apply, more intuitive, and yields results of a higher order of accuracy than could be obtained by using direct methods and a finite quantity of paper.

A computer program has been written to check the accuracy of the transfer function given by Eq. 31. For a given set of parameter values, the result predicted by (31) is compared with the exact output found by numerical analysis methods. Results of the program will be outlined in greater detail at a later date; however, it will be mentioned here that over a wide range of parameters the error in (31) is typically less than 0.2 per cent of the modulator hysteresis height. Even for the rather poor operating values of $h = 1$, $\frac{w}{h} = 0.05$, $T_d/\tau = 0.05$, $\frac{\tau x'}{h} = 0.2$ and $x_o = 0.95$, the output

predicted by (31) is only 0.006 higher than the exact result, $\overline{y} = 0.716$.

The exponential window approach can be applied to evaluate a broader class of systems than the two-state modulator. For example, the response of a bang-bang servomechanism can be effectively characterized by utilizing this technique.

J. E. Schindall

References

1. A. G. Bose, Quarterly Progress Report No. 66, Research Laboratory of Electronics, M.I.T., July 15, 1962, pp. 187-189.
2. A. G. Bose, Quarterly Progress Report No. 67, Research Laboratory of Electronics, M.I.T., October 15, 1962, pp. 115-119.

B. A NEW APPROACH TO ECHO REMOVAL

In many situations one is faced with the problem of processing signals that have been combined by convolution. Such signals occur in high-fidelity recording, sonar, multipath communication channels, and seismology. In general, the problem is one of extraction of one signal from the convolution of two or more. For example, if a signal s(t) is passed through an environment that introduces echoes, the result is a signal x(t) of the form

$$x(t) = s(t) + \alpha s(t-t_o). \tag{1}$$

This signal can be thought of as the convolution of s(t) with an impulse train as in Eq. 2a and Eq. 2b.

$$x(t) = s(t) \otimes u_\alpha(t) \tag{2a}$$

$$u_\alpha(t) = u_o(t) + \alpha u_o(t-t_o). \tag{2b}$$

If the signal s(t) is to be recovered, the impulse train must be removed. Alternatively, if only information regarding the presence and the timing of the echo is required, it might be desirable to remove the signal s(t) and recover only the impulses.

The system shown in Fig. XXV-7 has been proposed for the purpose of separating convolved signals.[1] It has been shown[2,3] that such a system is a member of a larger class of nonlinear systems called homomorphic systems which obey a generalized principle of superposition. In Fig. XXV-7a, the system L is a linear system obeying superposition in the conventional sense, and the system $A_\otimes$ is specified by Fig. XXV-7b, where X(f) is the Fourier transform of x(t), and

$$\hat{X}(f) = \log X(f).$$

The system $A_\otimes^{-1}$ is simply the inverse of $A_\otimes$. From the definition of $A_\otimes$, it can be

shown that if

$$x(t) = x_1(t) \otimes x_2(t),$$

then

$$\hat{x}(t) = \hat{x}_1(t) + \hat{x}_2(t). \tag{3}$$

In this report, some results pertaining to the removal of echoes, by using the system of Fig. XXV-7a, will be given and an example will be discussed.

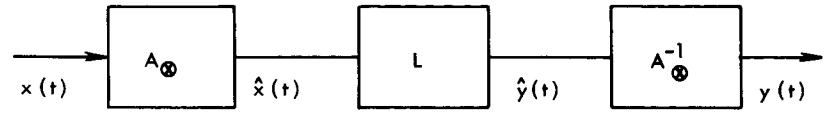

(a)

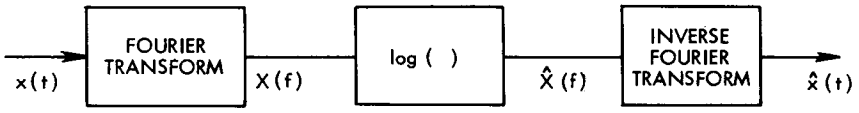

(b)

Fig. XXV-7. (a) Canonic form for convolution filter.
(b) Realization of the system $A_{\otimes}$.

In order to understand how to choose the linear system L in any filtering application, it is necessary to characterize the signals that will be present at the output of system $A_{\otimes}$. Some results will be given without proof for some typical signals that arise in the removal of echoes from speech signals. Following the presentation of these results, is a discussion of their application.

1. Echoes

Equation 2 shows the form of a signal with a single echo of amplitude a and delay t_o. From Eq. 3, it is seen that

$$\hat{x}(t) = \hat{s}(t) + \hat{u}_a(t). \tag{4}$$

The signal $\hat{u}_a(t)$ can be shown to be

$$\hat{u}_a(t) = \sum_{n=1}^{\infty} (-1)^{n+1} \frac{a^n}{n} u_o(t-nt_o) \qquad \text{if } a < 1. \tag{5}$$

2. Aperiodic Waveforms

General results are not known about the response of system $A_{\otimes}$ to an arbitrary waveform. For an aperiodic function p(t), which is zero for $t < 0$ and has a Fourier transform that is a rational function of $j2\pi f$, however, something can be said about the response p(t) for $t > 0$.

It is found, that for $t > 0$, the output of system $A_{\otimes}$ is of the form

$$\hat{p}(t) = \frac{-1}{j2\pi t} \int_{-\infty}^{\infty} \frac{P'(f)}{P(f)} e^{j2\pi ft}\, df, \tag{6}$$

where P(f) is the Fourier transform of the input p(t). From Eq. 6, it can be shown that if the transform of the input has all its poles and zeros in the left half-plane, then

$$|\hat{p}(t)| \leq A \frac{e^{-bt}}{t} \qquad t > 0, \tag{7}$$

where A and b are positive constants, and -b is greater than the real parts of all the poles and zeros of the transform of p(t). This means simply that although p(t) goes to zero exponentially, $\hat{p}(t)$ will go to zero even faster.

3. Periodic Signals

Consider a signal x(t) of the form

$$x(t) = \sum_{m=0}^{M-1} p(t-mT). \tag{8}$$

Equation 8 could be rewritten

$$x(t) = p(t) \otimes u(t) \tag{9a}$$

$$u(t) = \sum_{m=0}^{M-1} u_o(t-mT). \tag{9b}$$

Such a signal could represent a segment of a speech waveform during an interval corresponding to a voiced sound. In this case, p(t) would be an exponentially decaying aperiodic function, and T would correspond to the pitch period. The response of system $A_{\otimes}$ to the input of Eq. 8 is

$$\hat{x}(t) = \hat{p}(t) + \hat{u}(t), \tag{10}$$

where $\hat{u}(t)$ can be shown to be

$$\hat{u}(t) = \sum_{n=1}^{\infty} \frac{1}{n} u_o(t-nT) - \sum_{n=1}^{\infty} \frac{1}{n} u_o(t-nMT). \tag{11}$$

The output of system $A_{\otimes}$ thus consists of the sum of a signal $\hat{p}(t)$, which is going to zero as in Eq. 7, and two impulse trains for which the areas approach zero as $\frac{1}{n}$ and whose spacings are T and MT.

4. Exponential Weighting of Inputs

Suppose the input given by Eq. 8 is multiplied by an exponential to give

$$x_1(t) = e^{-at} x(t).$$

This expression can be rewritten

$$x_1(t) = \sum_{m=0}^{M-1} p_1(t-mT)\, e^{-amT},$$

where

$$p_1(t) = e^{-at} p(t).$$

The output of system $A_{\otimes}$ then becomes

$$\hat{x}_1(t) = \hat{p}_1(t) + \sum_{n=1}^{\infty} \frac{e^{-anT}}{n} u_o(t-nT) - \sum_{n=1}^{\infty} \frac{e^{-anMT}}{n} u_o(t-nMT). \tag{12}$$

In a similar way, it can be shown that the effect of exponentially weighting an input containing echoes (Eq. 1) is to produce the output

$$\hat{x}_1(t) = \hat{s}_1(t) + \sum_{n=1}^{\infty} (-1)^{n+1} \frac{\alpha^n e^{-ant_o}}{n} u_o(t-nt_o) \tag{13}$$

where $\hat{s}_1(t)$ is the response to $s_1(t) = e^{-at} s(t)$.

It can be seen from the results just presented that the effect of system $A_{\otimes}$ is to tend to produce outputs that occupy different regions of time. In general, aperiodic pulse-type waveforms produce outputs that approach zero after a very short time, while impulse trains of finite duration produce impulse trains of infinite duration that go to

zero at least as fast as $\frac{1}{n}$. This suggests that in some situations, the outputs will occupy different intervals of time so that a "frequency-invariant"[1] linear filter should be used for system L in Fig. XXV-7a. For example, if x(t) is a speech signal with an echo

$$x(t) = s(t) \otimes u_a(t) \tag{14a}$$

$$s(t) = p(t) \otimes u(t), \tag{14b}$$

x(t) is the convolution of three signals and the response of the system $A_{\otimes}$ will be the sum of the corresponding responses to these three inputs

$$\hat{x}(t) = \hat{p}(t) + \hat{u}_a(t) + \hat{u}(t). \tag{15}$$

If $T \ll t_o$, the three components of the response essentially occupy different time intervals, as can be seen from Eqs. 7, 5 and 11. For example, if the echo is to be removed, a "frequency-invariant comb filter," as shown in Fig. XXV-8, could be used. In using

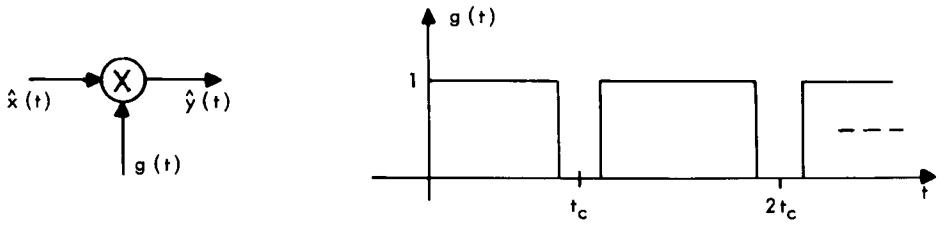

Fig. XXV-8. Ideal frequency-invariant filter for echo removal.

such a system it is clear that the echo timing need not to be known exactly but must only fall in the region around t_c.

It should be pointed out that for speech signals the character of the waveform changes as time increases, so that it is neither possible nor desirable to perform a Fourier transformation of a speech signal of long duration, even if the complete waveform is available (e.g., a recording). For this reason, the Fourier transformation indicated in Fig. XXV-7b should be replaced by a "short-time" Fourier transform defined as

$$X(f,t) = \int_{-\infty}^{\infty} w(t-\tau)\, x(\tau)\, e^{-j2\pi f\tau}\, d\tau. \tag{16}$$

In Eq. 16, $w(\tau)$ is a "window" function of finite duration. Such an operation on the signal $x(\tau)$ can be interpreted as a Fourier transformation of $x(\tau)$ when viewed through a

window that slides along as t increases.

It should be clear that the logarithmic operation in Fig. XXV-7a takes advantage of the fact that if two signals are convolved, their transforms are multiplied. For a short-time transform of Eq. 1, it can be shown that

$$X(f,t) = S(f,t) + \alpha S(f,t-t_o)\, e^{-j2\pi f t_o}.$$

If S(f,t) does not change too rapidly as t changes, we can see that in some sense

$$X(f,t) \approx S(f,t)\left[1+\alpha\, e^{-j2\pi f t_o}\right]. \tag{17}$$

Therefore taking the logarithm of X(f,t) produces approximately the same behavior as before. Intuitively, the requirement that the approximation of Eq. 17 hold is equivalent to requiring that the window be wide compared with the echo time t_o.

Whether a short-time transform is required or not, it is necessary to give some attention to the computational aspects of realizing the system of Fig. XXV-7. A system of this type has been programmed for the PDP-1 computer and has been used to obtain results that are consistent with the previous discussion. The Fourier analysis is done by using the Cooley-Tukey algorithm[4] for evaluating the equations

$$X(k) = \sum_{t=0}^{N-1} x(t)\, e^{-j\frac{2\pi}{N}kt} \qquad k = 0, 1, \ldots, N-1 \tag{18a}$$

$$x(t) = \frac{1}{N}\sum_{k=0}^{N-1} X(k)\, e^{j\frac{2\pi}{N}kt} \qquad t = 0, 1, \ldots, N-1. \tag{18b}$$

The results for the response of system $A_{\otimes}$ given in the previous equations assume that time and frequency are continuous variables. All of these results have their counterparts in the case for which time and frequency are discrete as in Eqs. 18a and 18b. There are two major differences. First, unit impulses are replaced by unit samples. Second, because of the sampled nature of the time function and the frequency function, Eqs. 18a and 18b are actually periodic with period N. This means, for example, that in the infinite sum in Eq. 5 all values of nt_o must be taken mod N. Therefore a unit sample of height $\frac{\alpha^n}{n}(-1)^{n+1}$, which is supposed to occur at $t = nt_o$ with $2N > nt_o > N$, will actually occur at $(nt_o - N)$. This aliasing effect is minimized computationally by exponential weighting of the input, since it is clear from Eq. 13 that the corresponding weighted sample has height $(-1)^{n+1}\frac{\alpha^n}{n}e^{-ant_o}$.

As an example of the type of processing that is proposed, consider Fig. XXV-9. Figure XXV-9a shows a section of the vowel "ah" which has an echo at t_o = 300 samples

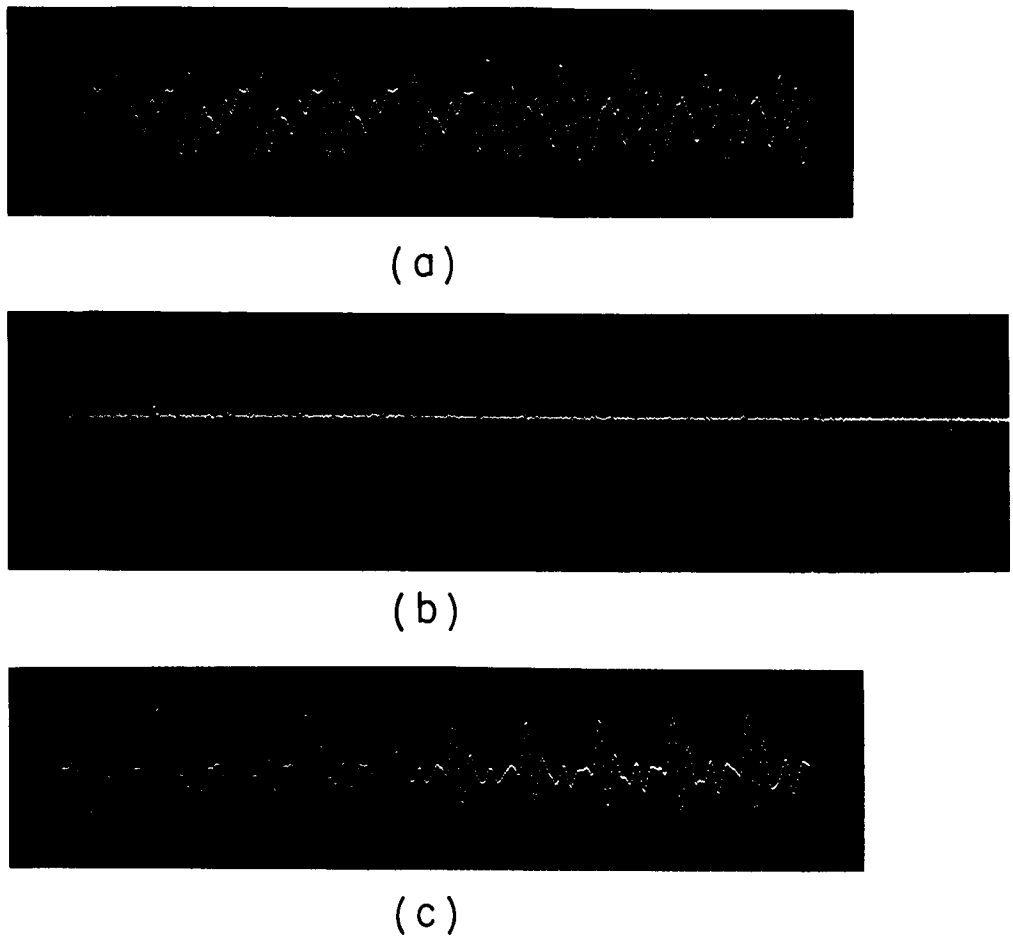

Fig. XXV-9. (a) Segment of the vowel "ah" with an echo at 300 samples.
(b) Output of the system $A_{\otimes}$ for the exponentially weighted input of (a).
(c) Output of system after the removal of echo.

(sampling rate of 10 kHz). Figure XXV-9b shows the corresponding output of system $A_{\otimes}$ for the exponentially weighted input. The peaks at t = 300 and 600 are due to the echo, and the peaks at multiples of 46 (the pitch period) are due to the middle term in Eq. 12. The points that are due to p(t) are seen to be essentially limited to the region between 0 and 46. The peaks predicted by the last term in Eq. 12 do not appear because MT is greater than N and e^{-aMT} is very small. The waveform of Fig. XXV-9c shows the

output of the system of Fig. XXV-7a when the linear system L is a frequency-invariant filter with g(t), as shown in Fig. XXV-8.

Many theoretical and computational problems remain to be resolved. The ideas and results reported here do seem to hold promise of application in a wide variety of waveform-processing situations.

R. W. Schafer

References

1. A. V. Oppenheim, "Nonlinear Filtering of Convolved Signals," Quarterly Progress Report No, 80, Research Laboratory of Electronics, M.I.T., January 15, 1966, pp. 168-175.

2. A. V. Oppenheim, "Superposition in a Class of Nonlinear Systems," Technical Report 432, Research Laboratory of Electronics, Massachusetts Institute of Technology, Cambridge, Massachusetts, March 31, 1965.

3. A. V. Oppenheim, "Optimum Homomorphic Filters," Quarterly Progress Report No. 77, Research Laboratory of Electronics, M.I.T., April 15, 1965, pp. 248-260.

4. J. W. Cooley and J. W. Tukey, "An Algorithm for the Machine Calculation of Complex Fourier Series," Mathematics of Computation, Vol. 19, pp. 297-301, April 1965.

XXVI. PROCESSING AND TRANSMISSION OF INFORMATION

Academic and Research Staff

Prof. P. Elias	Prof. E. V. Hoversten	Prof. E. Mortenson
Prof. R. M. Gallager	Prof. D. A. Huffman	Prof. C. E. Shannon
Prof. M. M. Goutmann	Prof. R. S. Kennedy	Prof. R. N. Spann
Prof. F. C. Hennie III	Prof. J. L. Massey	Prof. J. T. Wagner

Graduate Students

D. S. Arnstein	M. Khanna	J. T. Pinkston III
E. A. Bucher	Jane W-S. Liu	E. M. Portner, Jr.
D. Chase	J. Max	J. S. Richters
R. L. Greenspan	J. C. Moldon	A. H. M. Ross
H. M. Heggestad	R. Pilc	S. Thongthammachat
J. A. Heller		D. A. Wright

RESEARCH OBJECTIVES AND SUMMARY OF RESEARCH

1. Communications

The work of this group is focused on the dual problems of ascertaining the best performance that can be attained with a communication system, and developing efficient techniques for actually achieving performances substantially this good.

a. Convolutional Codes and Decoding

A technique has been investigated for combining block coding with convolutional coding.[1] Using a combination of sequential decoding and algebraic decoding, we have demonstrated that reliable communication can be achieved at all rates below channel capacity. While this technique is more complicated than sequential decoding alone, it operates at higher rates and has less buffer storage requirements than sequential decoding.

Preliminary results have been achieved on the relative probability performance of nonsystematic versus systematic convolutional codes.[2] Surprisingly, the results indicate that for nonsystematic codes, the exponential decay of error probability with code constraint length is much faster than for systematic codes.

A theoretical investigation has been undertaken on the capabilities of tree codes for error-correction purposes, fixed convolutional codes being treated as an important special case. Minimum distances of an appropriate type have been defined for both feedback decoding and nonfeedback or definite decoding of tree codes. Some new upper and lower bounds on minimum distance have been obtained and effort in this direction continues. The error-propagation effect resulting from feedback decoding is also being investigated. A new decoding technique, called semidefinite decoding, which has some of the features of feedback decoding but avoids the error-propagation effect, is being simulated for a wide variety of convolutional codes on the binary symmetric channel to determine whether it offers an over-all advantage over feedback decoding.

J. L. Massey, R. G. Gallager

*This work was supported in part by the National Aeronautics and Space Administration (Grants NsG-334 and NsG-496), and in part by the Joint Services Electronics Programs (U.S. Army, U.S. Navy, and U.S. Air Force) under Contract DA 36-039-03200(E), the National Science Foundation (Grant GP-835), and the Sloan Fund for Basic Research (M.I.T. Grant).

References

1. D. Falconer, "A Hybrid Sequential and Algebriac Decoding Scheme," Ph.D. Thesis, Department of Electrical Engineering, M.I.T., September 1966.
2. E. A. Bucher, "Error Probability for Systematic Convolutional Codes," Thesis research, in preparation.

b. Optical Communication

The extension of communication theory to optical channels has been focused on the effects of atmospheric turbulence. A model that is appropriate for the analysis of communication systems has been developed with the techniques of geometric optics. Since our approach provides some insights into more general problems of atmospheric propagation, it is being developed beyond the level required for communication theory to its natural conclusion. The character of these conclusions is discussed in this report (see Sec. XXVI-B).

A 4-km one-way propagation path operating at 6328 Å has been established with the with the cooperation of the Harvard College Observatory.[1] The facility has been used to investigate the statistical properties of intensity, and is now being modified for round-trip transmission. An interferometric system has also been developed to study turbulence-induced phase fluctuations.[2] A theoretical and experimental study concerning depolarization caused by turbulence has led to the conclusion that depolarization is negligible.[3] The experimental aspects of the study were carried on at Bell Telephone Laboratories, Inc., Crawford Hill.

Recently initiated investigations include studies of the communication reliability of free space and atmospheric channels in the absence of quantum effects, the reliability of quantum channels, the potential of forward-scatter communication systems, and the estimation of incoherently illuminated objects viewed through a turbulent atmosphere.

R. S. Kennedy, E. V. Hoversten

References

1. J. E. Roberson, "A Study of Atmospheric Effects on Intensity Spatial and Temporal Properties at 6328 Å," S.M. Thesis, Department of Electrical Engineering, M.I.T., October 1966.
2. R. Yusek, "Interferometric Measurement of Optical Phase Noise over Atmospheric Paths," S.M. Thesis, Department of Electrical Engineering, M.I.T., October 1966.
3. A. A. M. Saleh, "Laser Wave Polarization by Atmospheric Transmission," S.M. Thesis, Department of Electrical Engineering, M.I.T., November 1966.

c. Specific Channels and Coding

One of the major types of channels which is being investigated is a class of fading dispersive channels such as HF and Tropo. Particular emphasis is being placed upon the situation in which the information rate is comparable to, or exceeds, the available bandwidth; the complementary situation has been considered elsewhere.[1]

The performance that can be achieved with one particular signaling scheme when

both the coherence bandwidth and the frequency dispersion of the channel are small has been investigated analytically and experimentally.[2] The results suggest that a very large energy-to-noise ratio is required for satisfactory communication when the rate is comparable to the bandwidth. A comprehensive analytical study of the attainable reliability is now in progress. Partial results are presented in this report (see Sec. XXVI-A).

A number of coding theorems have been developed for statistically related parallel channels in the absence of cross talk.[3] Such models can be applied, for example, to frequency-multiplexed channels and also yield insight into the behavior of channels with memory.

A theoretical investigation of the use of coding on unsynchronized, noisy channels is in progress.[4] The lack of synchronization does not change the random coding exponent, but appears to radically change the exponent to error probability at low rates or for channels with little noise.

R. S. Kennedy, R. G. Gallager

References

1. R. S. Kennedy, Fading Dispersive Communication Channels (John Wiley and Sons, Inc., in press).
2. J. Moldon, "High Rate Reliability over Fading Dispersive Communication Channels," S. M. Thesis, M. I. T., Department of Electrical Engineering, June 1966.
3. J. Max, "Parallel Channels without Cross Talk," Thesis research, in preparation.
4. D. Chase, "Communication over Noisy Channels with No a priori Synchronization Information," Thesis research, in preparation.

d. Coding and the Processing of Information

The problem of performing reliable computation with unreliable computing elements has been reviewed by Winograd and Cowan.[1] Earlier work in this field has led to results that enable improvement in the reliability of computation only by increasing the number of unreliable elements used per unit computation, or increasing the complexity of each such element without reducing its reliability. Results analogous to the noisy-channel coding theorem of information theory, which would permit increasing the reliability of computation while performing more of it at once, with a fixed redundancy of equipment per unit computation, have not been available. Michael C. Taylor[2] has shown that application of low-density parity-check codes[3] to the problem of reliable storage of information in a noisy register leads to a result of coding theorem character: Doubling both the number of nosiy components and the amount of stored information reduces the probability of error or, alternatively, increases the mean time until an error occurs.

Two other topics relating coding to information processing are now under investigation. The first is the efficient addressing of stored data. The second is the trade-off between informational efficiency in encoding the output of an analog source and the ability to answer a variety of questions from the encoded output, or to tolerate a range of possible source characteristics. The second question is of interest for telemetry and other analog-digital conversion applications.

P. Elias, R. Gallager

References

1. S. Winograd and J. C. Cowan, Reliable Computation in the Presence of Noise (The M. I. T. Press, Cambridge, Mass., 1963).
2. M. C. Taylor, "Randomly Perturbed Computer Systems," Ph.D. Thesis, Department of Electrical Engineering, M. I. T., September 1966.
3. R. G. Gallager, Low Density Parity Check Codes (The M. I. T. Press, Cambridge, Mass., 1963).

e. Networks of Nosiy Channels

Earlier results concerning particular two-terminal networks of channels perturbed by additive Gaussian noise[1] have been extended to a large class of such networks, including, among others, series-parallel and bridge networks. The best signal-to-noise ratio attainable at the output by taking linear combinations of signals arriving at a node has been determined for this class, and has been bounded for all two-terminal networks. This work has been presented orally[2] and submitted for publication. Further work on numerical evaluation of cases of feedback networks not included in the solved class is under way.

P. Elias

References

1. P. Elias, "Channel Capacity without Coding," Quarterly Progress Report, Research Laboratory of Electronics, M. I. T., October 15, 1956, pp. 90-93.
2. P. Elias, "Networks of Gaussian Channels with Application to Feedback Systems," presented at the International Congress of Mathematicians, Moscow, August 1966.

f. Source Coding with a Distortion Measure

The interrelations between source and channel coding have been investigated for discrete memoryless sources and channels.[1] The results indicate that for combined source and channel coding with block length n, the theoretical minimum distortion is approached with increasing n, the dependence of the rate of approach with n being between $1/n$ and $\sqrt{\ln n/n}$.

In another investigation, a distortion measure for a discrete source was considered with a distortion of 1 for error, and 0 for no error. This led to a complete solution for the minimum probability of error achievable for a discrete memoryless source when transmitting over a channel with capacity less than the source entropy.[2]

Further investigations are being made on techniques for source coding and on the effect of quantizers in source coding.

R. G. Gallager, R. S. Kennedy

References

1. R. Pilc, "Coding Theorems for Discrete Source-Channel Pairs," Ph.D Thesis, Department of Electrical Engineering, M.I.T., November 1966.

2. J. T. Pinkston, "An Application of Rate Distortion Theory to a Converse to the Coding Theorem" (submitted for publication to IEEE Transactions on Information Theory).

A. LOW-RATE UPPER BOUNDS ON ERROR PROBABILITY FOR FADING DISPERSIVE CHANNELS

1. Introduction

A scatter communication channel such as an orbital dipole belt can frequently be considered as a collection of K equal-strength diversity paths, each with independent additive Gaussian noise.[1] We consider using such a channel to transmit amplitude information, x, on some basic unit energy signal. Under these conditions, it is possible to define a statistic, y, at the channel output that is sufficient for the estimation of x, where

$$p_K(y|x) = \frac{y^{2K-1} \, e^{-\frac{y^2/2}{\frac{x^2}{K}+N_o}}}{2^{K-1}\,\Gamma(K)\left(\frac{x^2}{K}+N_o\right)^K} \tag{1}$$

and the noise power density is $N_o/2$ watts/cps. This abstraction results in a continuous input-continuous output channel with input x and output y governed by the probability function $p_K(y|x)$.

By transmitting time and frequency translates of the basic signal, and providing sufficient guard space in both time and frequency, we can obtain N independent channel uses. We consider transmission of one of $M = e^{NR}$ equally probable input signals and represent the m^{th} input signal as an N-tuple $\{x_{1m}, x_{2m}, \ldots, x_{Nm}\}$, where x_{nm} is the amplitude of the n^{th} channel use. Such a communication scheme allows us to explicity take into account a bandwidth constraint for communication over a fading dispersive channel, by relating N and K to W, the total input bandwidth, and T, the total time duration of the input signals.

2. Error Probability

Under the conditions just outlined above, we may apply the random coding upper bound to error probability, as discussed by Gallager.[2] For simplicity, we shall

consider here only the low-rate, expurgated portion of the bound, which involves a much simpler problem than the maximization required at higher rates. This restriction will still allow us to obtain the straight-line bound.

After a suitable normalization, the expurgated bound has the essential form

$$Pe \leq \exp -N[E_{xK}(\rho, \underline{p}, r)-\rho R] \tag{2}$$

$$E_{xK}(\rho, \underline{p}, r) = -\rho \ln \left[\int_0^\infty \int_0^\infty p(x)\, p(x_1)\, e^{r[f(x)+f(x_1)]}\, H(x, x_1)^{K/\rho}\, dx dx_1 \right] \tag{3}$$

$$H(x, x_1) = \frac{(1+x^2)^{1/2}\left(1+x_1^2\right)^{1/2}}{1+\frac{1}{2}\left(x^2+x_1^2\right)}. \tag{4}$$

In these equations, $p(x)$ is the probability density on the input for any one channel use, $r \geq 0$, and $\rho \geq 1$. Also, $\int_0^\infty f(x)\, p(x)\, dx = 0$, where $f(x) = x^2 - \frac{A}{K}$, representing an input energy constraint (i.e., $A = \frac{1}{N}\frac{PT}{N_o}$, where $PT = \frac{1}{M}\sum_{m=1}^{M}\sum_{n=1}^{N} x_{nm}^2$ is the average input signal energy). For the expurgated bound, maximization of the exponent for a given K, ρ, A can be simplified by assuming $K = 1$ and replacing ρ by $\frac{\rho}{K} = \rho'$ and A by $\frac{A}{K} = A'$, and then maximizing, for if we let

$$E_{xK}(\rho, A) = \max_{p(x), r} E_{xK}(\rho, \underline{p}, r) \tag{5}$$

for a given A and ρ, then

$$E_{xK}(\rho, A) = K E_{x1}(\rho', A'). \tag{6}$$

This reduces the maximization to a two-parameter one, although now the range of ρ' is $\rho' > 0$ when $\rho \geq 1$, to provide for all values of K.

3. Optimization over p(x)

It is possible to derive sufficient conditions on $p(x)$ and r to maximize $E_{x1}(\rho, \underline{p}, r)$, subject to the energy constraint. For $0 < \rho < \infty$ the derivation depends on the fact that $H(x, x_1)^{1/\rho}$ is non-negative definite for the particular $H(x, x_1)$ considered here. The resulting sufficient condition is

$$\int_0^\infty p(x_1)\, e^{r[f(x)+f(x_1)]}\, H(x,x_1)^{1/\rho}\, dx_1 \geq \int_0^\infty \int_0^\infty p(x)\, p(x_1)\, e^{r[f(x)+f(x_1)]}\, H(x, x_1)^{1/\rho}\, dx dx_1 \tag{7}$$

for all x, with equality when $p(x) > 0$.

At zero rate, when $\rho = \infty$, the situation changes somewhat, for the problem now

becomes

$$\max_{p(x)} -\int_0^\infty \int_0^\infty p(x)\, p(x_1) \ln H(x, x_1)\, dx dx_1$$

with the same energy constraint as before, but now $\ln H(x, x_1)$ is not non-negative definite. All that the proof actually requires, however, is that $\ln H(x, x_1)$ be non-negative definite with respect to all functions that can be represented as the difference of two finite energy probability distributions, and it is possible to show that such is indeed the case. For $\rho = \infty$, the resulting sufficient condition for the maximization is

$$\int_0^\infty p(x_1) \ln H(x, x_1)\, dx_1 \geq \int_0^\infty \int_0^\infty p(x)\, p(x_1) \ln H(x, x_1)\, dx dx_1 + \lambda(x^2 - A) \qquad (8)$$

for all x, again with equality when $p(x) > 0$. Note that the conditions above have only been proved sufficient and not necessary. Hence it is conceivable that some other probability density exists which results in an exponent equal to the one obtained by a p(x) satisfying the conditions. There cannot, of course, be a p(x) that gives a larger exponent.

For a range of A and ρ, it is possible to show that a p(x) consisting of two impulses, one of which is at the origin, will satisfy the applicable sufficient condition. In particular, for $\rho = \infty$ and all A, such a probability density will satisfy conditions (8). For any ρ, $0 < \rho < \infty$, there is an $A_2 < \infty$ such that, for $A \leq A_2$, a two-impulse p(x) satisfies condition (7) and thus is optimum. Also, as $A \to 0$, this type of p(x) is optimum for all ρ, and the resulting exponent is the same as the infinite-bandwidth, orthogonal signal exponent obtained by Kennedy[3] (actually, this is true for the whole random coding bound, and not just the expurgated portion). When a two-impulse solution is optimum, it signifies that it is sometimes advantageous to conserve energy by not using an individual channel, so that when a channel is used, it is with an "optimum" value of energy-to-noise ratio per diversity path.

4. Zero-Rate Upper Bound

As we have mentioned, the case of zero rate is especially simple because the optimum probability density always consists of two impulses, regardless of the other system parameters. Also, holding $R = 0$ implies $\rho = \infty$ independent of other parameters, while if R exceeds zero, a change in system parameters will usually require a corresponding change in the value of ρ.

To illustrate the character of the results we consider a specific waveform set which, although often useful, is not always an efficient one. Let the basic signals have bandwidth W_s, and last for a time T_s, $T_s W_s = 1$. A guard space between signals of $B + 1/L$ cps in frequency and $L + 1/B$ sec in time should serve to make the signals

independent and orthogonal at the channel output, where B is the channel Doppler spread, and L is the multipath spread. Then if we consider a total signaling interval of T sec and a bandwidth of W cps, we can roughly express N and K in terms of the preceding parameters.[1] For example, with the choice of $BT_s > 1$, $LW_s < 1$,

$$K \cong BT_s \tag{9}$$

and

$$N \cong \frac{TWS}{(1+S+K)\left(1+S+\frac{S}{K}\right)}, \tag{10}$$

where S = BL is the channel-spread factor.

We want to choose K (and thereby N) to maximize the exponent $NE_{xK}(\infty, A)$. Since

$$\text{exponent} = \frac{PT}{N_o}\left\{\frac{E_{x1}\left(\infty, \frac{A}{K}\right)}{\frac{A}{K}}\right\}, \tag{11}$$

we see from Fig. XXVI-1 that to maximize the exponent, we must minimize $\frac{A}{K} = \frac{PT}{N_o}\frac{1}{NK}$, which requires making K as large as possible. From (9) we that this can be

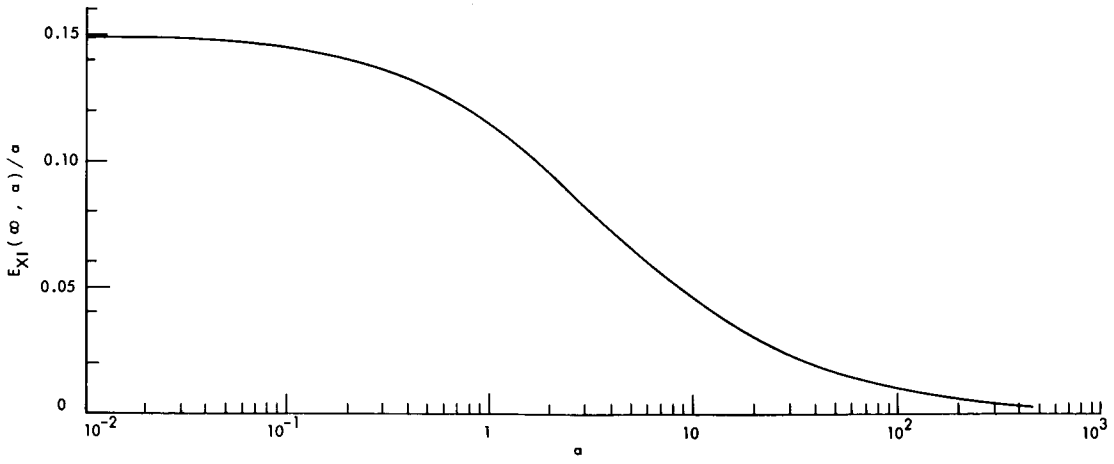

Fig. XXVI-1. $\frac{E_{x1}(\infty, \alpha)}{\alpha}$ vs α.

done by using very long basic signals, with a resulting value

$$\frac{A}{K} \cong \frac{1+\frac{1}{S}}{W}\left(\frac{P}{N_o}\right). \tag{12}$$

As we have noted, $W \to \infty$ means $A/K \to 0$ and $\frac{E_{x1}(\infty, A/K)}{A/K} \simeq .15$, which results in the infinite-bandwidth exponent found by Kennedy. Note that, for finite bandwidths, the exponent obtained here is still a function of W, even at zero rate. This contrasts with the case of the additive Gaussian noise channel, for which the zero-rate exponent is independent of bandwidth.

5. Rates Greater than Zero

For positive rates, the situation becomes more complex, and the best p(x) is still unknown. It has not been possible to show that the exponent is always maximized by a discrete p(x) (the proof for two impulses involves solving for the probabilities and positions, and this quickly becomes laborious for more than two), but it seems reasonable to believe that such is the case. If, for example, we let p(x) consist of a grid of impulses spaced along the x-axis, and numerically optimize on the impulse probabilities, we find that most probabilities are zero, and the nonzero ones are widely separated. As the grid spacing is reduced, the nonzero impulses change positions and probabilities slightly, and the others remain zero. If the distribution that is arrived at in this manner involved more and more impulses with smaller and smaller probabilities as the grid spacing was

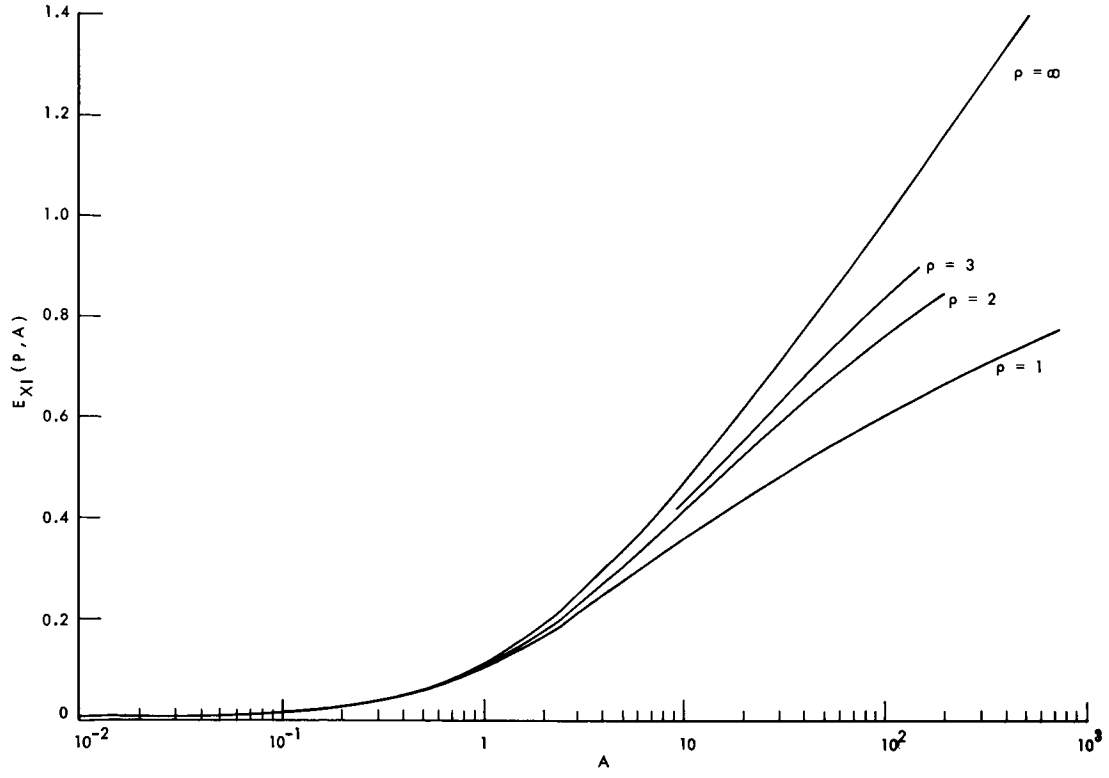

Fig. XXVI-2. $E_{x1}(\rho, A)$ vs A for several values of ρ.

reduced, we would say that it was beginning to approximate a continuous distribution. Instead, the only effect of reduced grid spacing is an apparent relocation of the impulses to better postiions, and the distribution still looks impulsive.

As A is increased from zero for a given value of ρ, the optimum probability distribution starts as two impulses, then appears to become three, then four, etc. This has been true for all values of ρ for which distributions have been computed.

Whether or not discrete solutions are always exactly optimum, the type of computation described above indicates that they are approximately optimum, and consequently allows computation of approximate results, such as those illustrated in Fig. XXVI-2.

If we consider one-channel use when $\rho = \infty$, with fixed energy but variable diversity, or, equivalently, fix N and A but allow K to vary, increasing K results in a monotonically increasing exponent, and $K \rightarrow \infty$ gives the infinite-bandwidth result. When $\rho < \infty$, it appears that we cannot get the infinte-bandwidth result merely by increasing K with N and A fixed, for there is a value of K beyond which the exponent starts decreasing again. Of course, allowing N to become large, for example, by increasing the bandwidth, will always lead to the infinite-bandwidth exponent.

J. S. Richters

References

1. R. S. Kennedy and I. L. Lebow, "Signal Design for Dispersive Channels," IEEE Spectrum, Vol. 1, No. 3, p. 231, March 1964.
2. R. G. Gallager, "A Simple Derivation of the Coding Theorem and Some Applications," IEEE Trans. Vol. IT-11, No. 1, pp. 3-18, January 1965.
3. R. S. Kennedy, Performance Limits for Fading Dispersive Channels (to be published by John Wiley and Sons, Inc., New York).

B. OPTICAL PROPAGATION THROUGH A TURBULENT ATMOSPHERE

It is known that atmospheric turbulence severely affects the performance of optical communication systems that involve propagation through the earth's atmosphere. Neither the fundamental limitations that this turbulence imposes upon the attainable communication reliability nor the signal and receiver structures that are most effective in combating it are known, however. To answer these questions it is necessary to determine the statistical properties of the received signal, or field, that exists over the receiving aperture.

The most casual examination convinces one that a rigorous, diffraction-theory treatment of the problem is unappealing, if not impossible. A further examination suggests that the most generally accepted technique of approximation is that due to Rytov,[1] as presented by Tatarski.[2] For point sources, plane waves, and "uncollimated

beams" this approach yields results that are in good agreement with experiment.[3] Recently, this technique has been applied to the near field of collimated beams by Tatarski,[4] but the complexity of the results limits their utility in a communication analysis. Moreover, the behavior of the far field is still unknown.

Another technique of approximation is provided by geometric optics.[5] Its utility in the study of atmospheric optical propagation has been in doubt because it has yielded results that fail to agree with experiment and because heuristic arguments have been advanced to suggest that diffraction effects are of basic importance in such studies.[6-8] Geometric optics does lead, however, to a relatively simple, and unified, model for the effects of turbulence in both the near and far fields. Such simplicity is almost as important to any subsequent communication analysis as is extreme precision. Moreover, the arguments suggesting that diffraction effects are important only consider the behavior of small isolated elements of the atmosphere and ignore the averaging, or masking, of diffraction effects that results from the superposition of numerous such elements. Therefore, a study of atmospheric optical propagation predicated upon geometric optics was initiated. The preliminary results suggest that the lack of agreement between theory and experiment has resulted from a failure to distinguish between rays and their mean values and between points on rays and points in space. This has led us to pursue the geometrical optics approach beyond the level required for communication analysis.

1. Atmospheric Model

The random space-time variations of the atmospheric refractive index cause the statistical fluctuations observed in optical propagation. These variations can be reasonably treated as locally isotropic and, for simplicity, one also often supposes that they are homogeneous. This latter supposition is not crucial, and can be removed at the cost of complicating the results. We shall limit our discussion here to the behavior of the field at a single instant of time. Temporal problems will be treated subsequently.

The only knowledge that we require of the refractive-index variations is that they be quite small, the variation at points separated by distances of the order of meters be independent, and the mean and correlation function, or the structure function, of the variations be given. The most realistic choice for a structure function is probably that obtained from the Obukhov-Kolmogorov theory of turbulence.[9] Since this choice leads to rather complicated expressions, however, we shall often consider other simpler functions to illustrate the results. Reiger[10] has developed an approximation to the turbulence spectrum in the inertial subrange which is useful in many calculations because of its form. With the Reiger spectrum the calculations are reduced to those required for a Gaussian-shaped correlation function.

2. Geometric Optics

It suffices to consider the sinusoidal steady state. The complex fields are then of the form

$$E(\vec{r}) = \vec{e}(\vec{r}) \exp\left[j\frac{2\pi}{\lambda}\mathcal{L}(\vec{r})\right] \tag{1a}$$

$$H(\vec{r}) = \vec{h}(\vec{r}) \exp\left[j\frac{2\pi}{\lambda}\mathcal{L}(\vec{r})\right]. \tag{1b}$$

By the approximation of geometric optics, $\mathcal{L}(\vec{r})$, satisfies the Eikonal equation

$$|\nabla\mathcal{L}(\vec{r})|^2 = n^2(\vec{r}), \tag{2}$$

where $n(\vec{r})$ is the refractive index as a function of position, $\vec{r}$. In this expression we have employed the notion of a frozen atmosphere and have suppressed the time variation of the refractive index. The quantity $\mathcal{L}(\vec{r})$ is the optical path length, while $\frac{2\pi}{\lambda}\mathcal{L}(\vec{r})$ is the phase function.

For our purposes, the utility of geometric optics lies in the ray picture that it provides. These rays are defined to be the set of trajectories perpendicular to the constant phase surfaces ($\mathcal{L}(r)$ = constant). Each ray can be specified by the variation of its position vector, $\vec{r}_\tau$, with the parameter τ. The parameter τ specifies position along the ray and is roughly proportional to arc length ℓ as $d\ell = nd\tau$. It is also convenient to introduce the ray direction, $\vec{u}_\tau$, which is the derivative of $\vec{r}_\tau$ with respect to τ. These vectors are related to each other and to the optical phase length by the expressions

$$\vec{u}_\tau = \frac{d\vec{r}_\tau}{d\tau} = \nabla\mathcal{L}(\vec{r}_\tau) \tag{3a}$$

and

$$\frac{d\vec{u}_\tau}{d\tau} = \frac{\nabla n^2(\vec{r}_\tau)}{2}. \tag{3b}$$

Integration of these equations yields

$$\vec{u}_\tau = \vec{u}_o + \frac{1}{2}\int_0^\tau \left[\nabla n^2(\vec{r}_\sigma)\right] d\sigma \tag{4a}$$

and

$$\vec{r}_\tau = \vec{r}_o + \vec{u}_o\tau + \frac{1}{2}\int_0^\tau (\tau-\sigma)\left[\nabla n^2(\vec{r}_\sigma)\right] d\sigma, \tag{4b}$$

where the quantities $\vec{u}_o$ and $\vec{r}_o$, the initial ray direction and position at the source of radiation, serve to specify the ray in question.

The field quantities $\mathscr{L}(\vec{r})$, $\vec{e}(\vec{r})$, and $\vec{h}(\vec{r})$ also can be evaluated by integrals along the rays. In particular, the variation of the phase along any given ray is governed by the differential equation

$$\frac{d\,\mathscr{L}(\vec{r}_\tau)}{d\tau} = n^2(\vec{r}_\tau) \tag{5a}$$

which yields

$$\mathscr{L}(\vec{r}_\tau) = \mathscr{L}_o + \int_0^\tau n^2(\vec{r}_\sigma)\, d\sigma, \tag{5b}$$

where $\mathscr{L}_o$ is the initial phase. For simplicity, $\mathscr{L}(\vec{r}_\tau)$ will often be written as $\mathscr{L}(\tau)$. Also,

$$\frac{|\vec{e}(\vec{r}_\tau)|^2}{|\vec{e}_o|^2} = \exp\left[-\int_0^\tau \left[\nabla^2 \mathscr{L}(\vec{r}_\sigma)\right] \frac{d_\sigma}{n(\vec{r}_\sigma)}\right] \tag{6a}$$

and

$$\frac{|\vec{h}(\vec{r}_\tau)|^2}{|\vec{h}_o|^2} = \frac{|\vec{e}(\vec{r}_\tau)|^2}{|\vec{e}_o|^2}, \tag{6b}$$

where $\vec{e}_o$ and $\vec{h}_o$, are the initial vlaues. In Eq. 6 we have approximated $\left[\frac{n(\vec{r}_\tau)}{n(\vec{r}_o)}\right]^2$ by unity.

To avoid the necessity of evaluating the Laplacian of $\mathscr{L}(\vec{r}_\tau)$, it is sometimes desirable to employ the approximation

$$\nabla^2 \mathscr{L}(\vec{r}_\sigma) \approx \frac{\partial \ln n(\vec{r}_\sigma)}{\partial \sigma} + \int_0^\sigma \nabla^2 n^2(\vec{r}_\rho)\, d\rho. \tag{7}$$

Upon introducing this into Eq. 6a, evaluating two integrals, and again approximating $\frac{n(\vec{r}_\tau)}{n(\vec{r}_o)}$ by unity we obtain

$$\frac{|\vec{e}(\vec{r}_\tau)|^2}{|\vec{e}_o|^2} = \frac{|\vec{h}(\vec{r}_\tau)|^2}{|\vec{h}_o|^2} \approx \exp\left[-\int_0^\tau (\tau-\sigma)\left[\nabla^2 n^2(\vec{r}_\sigma)\right] d\sigma\right]. \tag{8}$$

To complete the specification of the fields, it is necessary to specify their directions.

By the approximations of geometric optics, the $\vec{e}$ and $\vec{h}$ vectors are perpendicular to each other and to the ray direction vector. Thus it suffices to determine the angle, θ, between the direction of $\vec{e}_o$ and of $\vec{e}(\vec{r}_\tau)$, i.e., the depolarization angle. Although a precise evaluation of this angle is difficult, it can be shown that it is essentially equal to the change in the ray direction vector.[11] That is, there is no depolarization as such but only the rotation of $\vec{e}(\vec{r}_\tau)$ that is associated with the changing direction of $\vec{u}(\tau)$. In particular, subject to the suppostion that θ is not too large, it is easy to show that

$$\theta_\tau \approx \frac{|\vec{e}_o \cdot \vec{u}_\tau|}{|\vec{e}_o|^2}. \tag{9}$$

Equations 4 through 9, in conjunction with the Central Limit theorem, lead to a complete statistical description of the field at any point, τ, on a ray. Specifically, for any given value of τ that is sufficiently large $\vec{r}_\tau$, $\vec{u}_\tau$, $\mathscr{L}(\vec{r}_\tau)$ and $\ln\left[|\vec{e}(\vec{r}_\tau)|^2\right]$ will be Gaussian random (vector) variables. More generally, it is reasonable to suppose that the values of these quantities at different points on the same ray, or on different rays, are jointly Gaussian. Finally, the remaining quantities $\vec{h}(\vec{r}_\tau)$ and θ_τ are determined by Eqs. 6b and 9.

3. Moments

Since all of the field quantities are determined by a set of Gaussian random variables, it suffices to know their means and covariances. To evaluate these quantities, we invoke an approximation that is best explained by an example, By virtue of Eq. 4b, the expected value of $\vec{r}_\tau$ at the parameter point τ is

$$E[\vec{r}_\tau] = \vec{r}_o + \tau\vec{u}_o + \frac{1}{2}\int_0^\tau (\tau-\sigma)\, E_{\vec{r}}\left[\nabla E_{n|\vec{r}}\left[n^2(\vec{r}_\sigma)\right]\right] d\sigma, \tag{10}$$

where $E_{n|\vec{r}}$ denotes the conditional expected value of $n^2(\vec{r}_\sigma)$ at the parameter point σ on the ray, given that the position at that point is $\vec{r}_\sigma$.

We next claim that the conditional average is approximately equal to the unconditional average evaluated at the (random) point $\vec{r}_\sigma$. This is so because $\vec{r}_\sigma$ is controlled by the large-scale behavior of the atmosphere, while $n(\vec{r})$ is a local quantity: hence, knowledge of $\vec{r}_\sigma$ yields little information about $n(\vec{r}_\sigma)$. Thus we obtain

$$E[\vec{r}_\tau] \approx \vec{r}_o + \tau\vec{u}_o + \frac{1}{2}\int_0^\tau (\tau-\sigma)\, E_{\vec{r}_\sigma}\left[\nabla E_n\left[n^2(\vec{r}_\sigma)\right]\right] d\sigma, \tag{11}$$

where E_n is the unconditional average of n^2 evaluated at the random position $\vec{r}_\sigma$, and

$E_{\vec{r}_\sigma}$ denotes the average of the indicated quantity with respect to the ray position vector, $\vec{r}_\sigma$. The approximation that leads from Eq. 10 to Eq. 11 can be used to evaluate all of the required averages.

For example, the approximation, in conjunction with the supposition that the refractive index is homogeneous in space, leads one to conclude that

$$E[\vec{r}_\tau] = \vec{r}_o + \tau\vec{u}_o \tag{12a}$$

$$E[\vec{u}_\tau] = \vec{u}_o \tag{12b}$$

$$E[\mathscr{L}(\vec{r}_\tau)] = \mathscr{L}_o + \tau \tag{12c}$$

and

$$E\left[\ln \frac{|\vec{e}(\vec{r}_\tau)|^2}{|\vec{e}(o)|^2}\right] = 0. \tag{12d}$$

Here, we have supposed that the unconditional average of $n^2(\vec{r})$ is unity.

The covariance of the quantities above can be obtained by straightforward, but laborious, calculation. Since the results are cumbersome, we shall only discuss the covariance of the position vector along a single ray. This quantity is chosen because it involves more difficulties than do the other covariances.

The covariance of the i^{th} component of the position vector at the parameter value τ and the j^{th} component at parameter value τ' is easily shown to be

$$C_{y_i y_j}(\tau, \tau') = E[y_i(\tau)y_j(\tau')]$$

$$\approx -\frac{1}{2}\int_0^\tau \int_0^{\tau'} (\tau-\sigma)(\tau'-\sigma')\, E_{\vec{r}_\sigma, \vec{r}_{\sigma'}}\left[\frac{\partial^2}{\partial q_i \partial q_j'} D_n(\vec{r}_\sigma, \vec{r}_{\sigma'})\right] d\sigma d\sigma', \tag{13a}$$

where $\vec{y}(\tau)$ is the zero mean position vector defined as

$$\vec{y}(\tau) = \vec{r}_\tau - E(\vec{r}_\tau)$$

$$\vec{y}(\tau) = \sum_{k=1}^{3} y_k \vec{i}_k, \tag{13b}$$

q_i and q_j are the variables associated with the i^{th} and j^{th} rectangluar coordinates, respectively, and the refractive index structure function is defined by the relation

$$D_n(\vec{r}_\sigma, \vec{r}_{\sigma'}) = E_n\left\{[n(\vec{r}_\sigma) - n(\vec{r}_{\sigma'})]^2\right\}. \tag{13c}$$

In the derivation of Eq. 13a the assumptions that the refractive index is homogeneous and that the variations are small have been exploited to approximate

$$\frac{\partial^2}{\partial q_i \partial q_j'} E\left[n^2(\vec{r}_\sigma) n^2(\vec{r}_{\sigma'})\right]$$

by

$$-2 \frac{\partial^2}{\partial q_i \partial q_j'} D_n(\vec{r}_\sigma, \vec{r}_{\sigma'}).$$

Note that the covariance of the ray position enters into both sides of Eq. 13a. Thus it provides an equation which the covariance must satisfy, rather than an expression from which it can be directly evaluated. A direct solution of this equation appears to be quite difficult although it may be possible in some special situations.

An alternative, and commonly employed, approach is to replace the position vectors in the integrand by their average values so as to avoid the expectation operation with respect to the position vectors. That is, one ignores the ray motion and evaluates the integrals along the average, or unperturbed, ray to obtain a first-order estimate of the covariance. If desired, the resulting expression for the ray covariance can be used to obtain a second-order estimate: more generally, one can iterate the scheme indefinitely. We have not yet established, however, that the higher order estimates converge to the true covariance function.

Once the ray position vector covariance has been determined, the other covariances can be obtained by straightforward calculations. With the exception of the covariance for the ray direction vector, which is required later, the covariances of the other quantities will be omitted in the interest of brevity. The covariance of the i^{th} and j^{th} components of the ray direction vector, $\vec{u}_\tau$, is

$$\begin{aligned} C_{\mu_i \mu_j}(\tau, \tau') &= E[\mu_i(\tau)\mu_j(\tau')] \\ &= -\frac{1}{2} \int_0^\tau \int_0^{\tau'} E_{\vec{r}_\sigma, \vec{r}_{\sigma'}} \frac{\partial^2}{\partial q_i \partial q_j'} D_n(\vec{r}_\sigma, \vec{r}_{\sigma'}) \, d\sigma d\sigma', \end{aligned} \tag{14a}$$

where $\vec{\mu}(\tau)$ is the zero-mean ray direction vector defined as

$$\begin{aligned} \vec{\mu}(\tau) &= \vec{u}_\tau - E[\vec{u}_\tau] \\ \vec{\mu}(\tau) &= \sum_{k=1}^{3} \mu_k \vec{i}_k. \end{aligned} \tag{14b}$$

Certain conclusions can be drawn from Eqs. 13a and 14a without explicity solving them. One conclusion, which is needed later, is that the components of $\vec{y}(\tau)$ are uncorrelated and also that the components of $\vec{\mu}(\tau)$ are uncorrelated. Also, we can conclude that the two components of $\vec{y}(\tau)$ perpendicular to the direction of propagation have the same variance. A similar statement is also true for $\vec{\mu}(\tau)$.

Rather than pursue the moment calculations further, we now consider the distinction between the quantities defined on rays and those measured in space. This distinction will then be illustrated by considering the phase covariance function.

4. Ray-to-Space Transformations

The results stated above do not directly specify the field at any fixed point in space; rather, they specify the field values at points on rays and also the statistical behavior of the ray spatial position. Thus, to determine the behavior of the field at a point in space, one must, in principle, determine the probability that any particular ray passes through the point in question and then determine the conditional statistics of the field on that ray. This ray-to-space transformation appears to have been overlooked in previous applications of geometric optics.

In the ray-to-space transformation, the question of how many rays may go through a given point in space arises. This is essentially the question of whether interference effects are important or can be neglected. It seems clear that interference effects must be accounted for in some situations, e.g., converging beams. The large coherent bandwidths observed in optical propagation through the atmosphere suggest, however, that interference is not a first-order effect for unfocused beams over path lengths of several kilometers.[12,13] In the sequel interference will be neglected, and at most a single ray will be assumed to go through any given point.

Although the ray-to-space transformation has not yet been completed for all of the field quantities, the preliminary results suggest that it will remedy many of the defects normally attributed to geometrical optics, and permit the solution of some previously unsolved problems. To illustrate the possiblities, we shall now examine the phase covariance in more detail.

5. Phase Covariance

In this section the source distribution is assumed to be a uniform plane wave propagating in the z-direction. Thus all rays have the same initial direction vector and phase value. As usual, homogeneity and local isotropy of the refractive-index variations are assumed.

A calculation of the phase covariance for two points lying on a line parallel to the direction vectors at the source provides an illustration of the importance of accounting for ray motion. The solution presented here is only a first-order solution because most

integrations will be carried out along unperturbed ray paths. The ray parameter τ is thus assumed to be the same for any two points in a plane perpendicular to the source direction vectors. Furthermore, as we have mentioned, it is assumed that only one ray goes through each point in space.

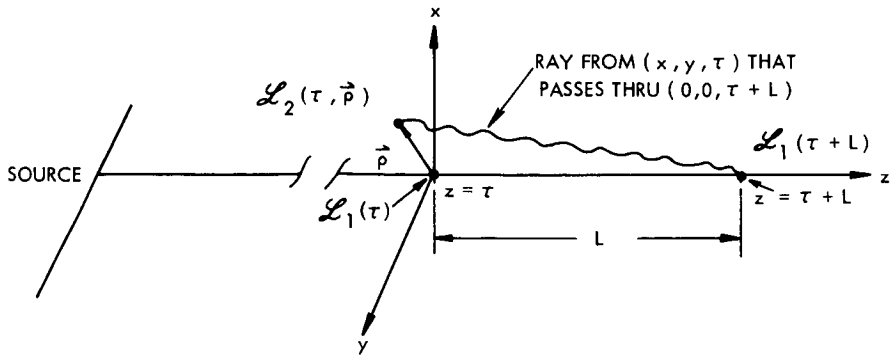

Fig. XXVI-3. Coordinate frame for calculation of phase covariance.

The situation of interest is shown in Fig. XXVI-3 where the coordinate system is indicated. The quantity to be calculated is $E[(\mathscr{L}_1(\tau) - \overline{\mathscr{L}_1(\tau)})(\mathscr{L}_1(\tau+L) - \overline{\mathscr{L}_1(\tau+L)})]$, the joint central moment of the phase at the intersection of the z-axis and the planes $z = \tau$ and $z = \tau + L$. Note that, because of the ray motion, the ray that passes through the last point may not pass through the former point. Instead it passes through another point in the plane $z = \tau$ whose position is indicated by the vector $\vec{\rho} = x\vec{i}_x + y\vec{i}_y$. The phase at this second point in the plane $z = \tau$ is denoted by $\mathscr{L}_2(\tau;\vec{\rho})$.

To simplify the notation, let

$$S_1 = \mathscr{L}_1(\tau) - \overline{\mathscr{L}_1(\tau)} \tag{15a}$$

$$S_2 = \mathscr{L}_2(\tau+L) - \overline{\mathscr{L}_1(\tau+L)} \tag{15b}$$

$$S_3(\vec{\rho}) = \mathscr{L}_2(\tau;\vec{\rho}) - \mathscr{L}_2(\tau;\vec{\rho}) \tag{15c}$$

The quantity to be calculated now is $E[S_1S_2]$. It is convenient to first compute the conditional average, given that the ray passing through $(0, 0, \tau+L)$ has the position vector $\vec{\rho}$ in the plane $z = \tau$, and then to average over $\vec{\rho}$. Thus

$$\begin{aligned} E[S_1S_2|\vec{\rho}] &= E[S_1(S_3(\vec{\rho}) + \Phi(\vec{\rho}))] \\ &= E[S_1S_3(\vec{\rho})] + E[S_1\Phi(\vec{\rho})], \end{aligned} \tag{16}$$

where $\Phi(\vec{\rho})$ is the zero-mean increment in the phase as the ray propagates from (x, y, τ) to $(0, 0, \tau + L)$. If L is large relative to the correlation distance of the refractive-index variations, then the second expectation on the right can reasonably be assumed to be approximately zero. The conditional expectation then becomes

$$E(S_1 S_2 | \vec{\rho}) = C_s(\rho; \tau), \tag{17}$$

where $C_s(\rho; \tau)$ is the spatial phase covariance function in a plane perpendicular to the direction of propagation.

To remove the conditioning in Eq. 17, it is necessary to average the conditional expectation over $\vec{\rho}$. To do this exactly, the probability must be used that the ray from (x, y, τ) goes through $(0, 0, \tau+L)$ and that all other rays do not. A much simpler approximate method is to think of replacing the ray through $(0, 0, \tau+L)$ with a pseudoray directed from the point $(0, 0, \tau+L)$ back toward the plane $z = \tau$. This pseudoray is assumed to have a direction vector which is the negative of the direction vector of the ray that goes through $(0, 0, \tau+L)$.

It is now possible to use this pseudoray to calculate the probability that the actual ray emanated from various parts of the $z = \tau$ plane and thus to carry out the desired averaging. Since the direction vector of the actual ray is also random, one must average over its value. This average involves the density of the direction vector components at a point in space which, in turn, requires a ray-to-space transformation. In the following discussion this ray-to-space transformation will be neglected, and it will be assumed that the form of the density is not changed and, furthermore, that the variance associated with the direction vector components for a ray parameter value of $\tau + L$ can be used. We believe that these assumptions do not significantly alter the results.

As we have noted, the ray position vector components are independent Gaussian random variables. The ray direction vector components are also independent and Gaussian. Thus, the conditional density of the x component of the pseudoray position is

$$p_{x|u_x}(X) = \frac{1}{\sqrt{2\pi}\,\sigma_x} \exp\left[-\frac{1}{2}\,\frac{(X - u_x L)^2}{\sigma_x^2}\right], \tag{18}$$

where u_x is the x component of the pseudoray direction vector. As u_x has a zero mean, its density is

$$p_{u_x}(U) = \frac{1}{\sqrt{2\pi}\,\sigma_{u_x}} \exp\left[-\frac{1}{2}\,\frac{U^2}{\sigma_{u_x}^2}\right]. \tag{19}$$

Similar equations can be written for the y component of the pseudoray position and direction vectors. It is thus possible, by using the independence, to obtain the

unconditional joint density for the two lateral ray position coordinates, x and y. Finally, the density of $\rho = |\vec{\rho}| = \sqrt{x^2 + y^2}$ is given by

$$p_\rho(P) = \frac{P}{\left(L^2\sigma_{u_x}^2 + \sigma_x^2\right)} \exp\left[-\frac{1}{2}\frac{P^2}{L^2\sigma_{u_x}^2 + \sigma_x^2}\right], \tag{20}$$

where the facts that $\sigma_x^2 = \sigma_y^2$ and $\sigma_{u_x}^2 = \sigma_{u_y}^2$ have been used.

Before this density can be used to complete the determination of $E[S_1S_2]$ it is necessary to determine the lateral spatial covariance function of the phase. The first-order solution (integration along the unperturbed rays) is

$$C_s(\rho;\tau) \approx 4\int_0^\tau \int_0^\tau C_n(|\vec{r}_\sigma - \vec{r}_{\sigma'}|)\, d\sigma d\sigma', \tag{21}$$

where $C_n(|\vec{r}_\sigma - \vec{r}_{\sigma'}|)$ is the refractive index covariance function, and the integration is along two parallel paths separated by a distance, ρ. The refractive index can be written

$$n = 1 + \delta, \tag{22}$$

where δ is very small, and the approximation exists because terms in δ^3 and δ^4 have been dropped.

Under the assumption of a Gaussian covariance function for the refractive-index variations,

$$C_n(\rho) = \overline{\delta^2} \exp\left[-\frac{\rho^2}{a^2}\right], \tag{23}$$

the equation above reduces to

$$C_s(\rho;\tau) = 4\sqrt{\pi}\ \overline{\delta^2}\ a\ \tau \exp\left(-\frac{\rho^2}{a^2}\right). \tag{24}$$

With the Gaussian covariance function of Eq. 23, and a first-order solution neglecting terms in δ^3 and δ^4, the variance of a lateral component of the ray direction vector and a lateral component of the ray position vector can be written

$$\sigma_{u_x}^2(\tau) = 2\sqrt{\pi}\,\frac{\overline{\delta^2}}{a}\,\tau \tag{25}$$

$$\sigma_x^2(\tau) = \frac{2}{3}\sqrt{\pi}\,\frac{\overline{\delta^2}}{a}\,\tau^3. \tag{26}$$

It is now possible to calculate the desired expectation. Using the density of Eq. 20

to remove the conditioning in Eq. 17, where the value of $C_s(\rho;\tau)$ is given by Eq. 21, one obtains

$$E[S_1S_2] = \frac{4\sqrt{\pi}\,\overline{\delta^2}\,a\,\tau}{1+\frac{2\left[L^2\sigma_{u_x}^2(\tau+L)+\sigma_x^2(L)\right]}{a^2}}, \tag{27}$$

and by using the results of Eqs. 25 and 26 this reduces to

$$E[S_1S_2] = \frac{4\sqrt{\pi}\,\overline{\delta^2}\,a\,\tau}{1+\frac{2\,\overline{\delta^2}\,\sqrt{\pi}}{a^3}\left(2L^2\tau+\frac{8}{3}L^3\right)}. \tag{28}$$

In order to provide a result for comparison, we shall now consider the phase convariance, using unperturbed rays with no ray-to-space transformation. The equation of interest,

$$E[S_1S_2] = 4\int_0^{\tau+L}\int_0^{\tau} C_n(|\vec{r}_\sigma-\vec{r}_{\sigma'}|)\,d\sigma d\sigma', \tag{29}$$

is readily obtained by modifying Eq. 21. The integration in Eq. 29 is along the z-axis in Fig. XXVI-3. For the assumption of the Gaussian covariance function of Eq. 23 the result is

$$E[S_1S_2] \approx 2\overline{\delta^2}\left[(2\tau+L)\sqrt{\pi}\,a - L\,\mathrm{Erf}\left(\frac{\sqrt{2L}}{a}\right)\right], \tag{30}$$

where Erf(·) is the error function, and it is assumed that $\tau \gg a$. Note that this phase covariance does not decrease as L increases but rather assumes a value equal to the phase variance at the point closest to the source.

The Gaussian covariance function of Eq. 23 is not a good model of the covariance of the refractive-index variations, but it does facilitate comparison of the results that are obtained with and without the ray-to-space transformation. As L becomes large relative to a, Eq. 30 reduces to the numerator of Eq. 28, and the difference in functional form is evident. Moreover, the extension to more realistic convariances, although cumbersome, is straightforward.

R. S. Kennedy, E. V. Hoversten

References

1. S. M. Rytov, "Diffraction of Light by Ultrasonic Waves," Izv. Akad. Nauk SSSR, Ser. Fiz., No. 2, 223 (1937).

2. V. I. Tatarski, Wave Propagation in a Turbulent Medium (translated by R. A. Silverman)(McGraw-Hill Book Company, New York, 1961), Chap. 7.

3. Ibid., Chap. 12.

4. A. I. Kon and V. I. Tatarski, "Fluctuation of the Parameter of a Spatially Bounded Light Beam in a Turbulent Atmosphere," Izvest. Vyss. Uch. Zav., Ser. Radiophysika 8, 870 (1965).

5. M. Born and E. Wolf, Principles of Optics (Pergamon Press, New York, 1959), Chap. III.

6. V. I. Tatarski, op. cit., p. 120 and Chap. 12.

7. L. A. Chernov, Wave Propagation in a Random Medium (translated by R. A. Silverman)(McGraw-Hill Book Company, New York, 1960), Chap. II.

8. G. E. Meyers, D. L. Fried, and M. P. Keister, Jr., "Experimental Measurements of the Character of Intensity Fluctuations of a Laser Beam Propagating in the Atmosphere," Technical Memorandum No. 252, IS-TM-651146, Electro-Optical Laboratory, Space and Information Systems Division, North American Aviation, Inc., September 1965.

9. J. L. Lumley and H. A. Panofsky, The Structure of Atmospheric Turbulence (Interscience Publishers, New York, 1964).

10. S. H. Reiger, "Starlight Scintillation and Atmospheric Turbulence," Astron. J. 68, 395 (1963).

11. A. A. M. Saleh, "Laser Wave Depolarization by Atmospheric Transmission," S.M. Thesis, Department of Electrical Engineering, M.I.T., Febuary 1967.

12. A. H. Mikesell, A. A. Hoag, and J. S. Hall, "The Scintillation of Starlight," J. Opt. Soc. Am. 41, 689 (1951).

13. E. G. Chatterton, "Optical Communications Employing Semiconductor Lasers," Technical Report 392, Lincoln Laboratory, M.I.T., June 1965.

XXVII. DETECTION AND ESTIMATION THEORY*

Academic and Research Staff

Prof. H. L. Van Trees
Prof. D. L. Snyder

Graduate Students

M. E. Austin
A. B. Baggeroer
L. D. Collins
T. J. Cruise
R. R. Kurth
A. P. Tripp, Jr.

RESEARCH OBJECTIVES AND SUMMARY OF RESEARCH

The work of this group may be divided into four major areas.

1. Sonar

The central problem of interest is the development of effective processing techniques for the output of an array with a large number of sensors. Some specific topics of interest in this connection are the following.

(i) A state-variable formulation for the waveform estimation problem when the signal is a sample function from a possibly nonstationary random process that has passed through a dispersive medium before arriving at the array. Some preliminary results have been obtained.[1]

(ii) The effects of array velocity on the system performance when operating in a reverberation-limited environment.[2]

(iii) Iterative techniques to measure the interfering noise field and modify the processor to reduce its effect.

(iv) A hardware-efficient analog transversal equalizer has been designed, and the basic components built and tested. With some additional work, a completed transversal filter will enable us to apply actual channel measurements to its time-variable tap gains, thus making possible laboratory simulations of dispersive channels. Such simulations are expected to provide a convenient means of evaluating channel parameter estimation techniques, and to prove useful in the development of better models of the sonar channel.

2. Communications

a. Digital Systems

Decision-feedback systems offer an effective method for improving digital communications over dispersive channels. A new structure has been derived whose performance should be appreciably better than previous systems. Theoretical work on this decision-feedback scheme will continue; it will be viewed as an integral part of an adaptive receiver whose acquisition and tracking behavior are of interest in equalization of dispersive channels. The analog transversal filter that is being constructed as a channel-measuring and channel-simulation device (see (iv) above) will also prove useful in evaluating the performance of algorithms that have been developed for adjusting the parameters of these adaptive receivers.

*This work was supported by the Joint Services Electronics Programs (U.S. Army, U.S. Navy, and U.S. Air Force) under Contract DA 36-039-AMC-03200(E).

The optimum receiver for the detection of Gaussian signals in Gaussian noise is well known. Except for limiting cases it is difficult to evaluate the error behavior. Work continues on developing performance measures for evaluating the performance, emphasizing techniques that are computationally tractable and, at the same time, give a good measure of the system performance. Both tight upper bounds and computational algorithms have been developed for the probability of error which emphasize the fundamental role of optimum linear systems in detection problems. Future work includes the application of these techniques to the analysis and design of radar, sonar, and communication systems.

The availability of a noiseless feedback channel from receiver-to-transmitter enables a significant increase in performance. By utilizing the continuous feedback signal at the modulator, the behavior system performance at the end of the transmission interval is greatly improved. The feedback link could be used to obtain the same performance over a shorter transmission interval. The actual structure of the system is very flexible and simple.

Noise in the feedback channel degrades the achievable system performance with the simple feedback system. Improvement over the no-feedback system is obtained, but it is not as dramatic as when noiseless feedback is available.

b. Analog Systems

(i) Investigations of the performance of analog modulation systems operating in additive noise channels are essentially completed.[3]

(ii) When a noiseless feedback link is available from receiver-to-transmitter simple modulation schemes can be developed which achieve the rate-distortion bound. Realizible feedback systems perform very close to the rate-distortion bound.

The effects of additive noise in the feedback link depend on the relative noise levels in the two channels. For relatively small feedback channel noise, the system performance is close to the rate-distortion bound. For large feedback noise the availability of a feedback link does not significantly improve the system performance.

(iii) A new approach has been developed for estimating continuous waveforms in real time. The approach is formulated with continuous Markov processes and use is made of state-variable concepts. The approach has been applied successfully to the problem of estimating continuous stochastic messages transmitted by various linear and nonlinear modulation techniques over continuous random channels; particular emphasis has been given to phase and frequency modulation. An advantage of this approach over alternative schemes is that it leads automatically to physically realizable demodulators that can be readily implemented.[4]

3. Seismic

A substantial portion of our effort in this area is devoted to acquiring an adequate understanding of geophysics in order to formulate meaningful problems. An area of concentration is exploration seismology in land and ocean environments. Some specific problems of interest include array design and effective quantization techniques.

4. Random Process Theory and Application

a. State-Variable and Continuous Markov Process Techniques

(i) In the theory of signal detection and estimation, it is frequently of interest to determine the solutions to a Fredholm integral equation. A state-variable approach to the problem of determining the eigenfunctions and eigenvalues associated with the problem has been formulated.

The random process(es) is represented as the output of a linear dynamic system that is described by a state equation. The Fredholm integral equation is reduced to a vector differential equation that is directly related to the state equation of the dynamic system. From this equation, a determinant is found which must vanish in order that an eigenvalue exist. Once the eigenvalue is found, the eigenfunction follows from the transition matrix of the vector differential equation.

The technique is general enough to handle a large class of problems. Constant-parameter (possibly nonstationary) dynamic systems for both scalar and vector processes can be handled in a straightforward and analytic manner. Time-varying systems can also be treated by computational techniques.[5]

(ii) The problem of formulating a state-variable model for random channels encountered in practice is being investigated. A particular class of channels of interest are those exhibiting frequency-selective fading.

(iii) The system identification problem is being studied. Applications include measurement of noise fields, random process statistics, and linear system functions.

b. Detection Techniques

Various extensions of the conventional detection problem to include nonparametric techniques, sequential tests, and adaptive systems are being studied.

H. L. Van Trees

References

1. A. Baggeroer, "MAP State-Variable Estimation in a Dispersive Environment," Internal Memorandum, December 10, 1966 (unpublished).
2. A. P. Tripp, Jr., "Effects of Array Velocity on Sonar Array Performance," S. M. Thesis, Department of Electrical Engineering, M. I. T., 1966.
3. T. L. Rachel, "Optimum F. M. System Performance – An Investigation Employing Digital Simulation Techniques," S. M. Thesis, Department of Electrical Engineering, M. I. T., 1966.
4. D. L. Snyder, "The State-Variable Approach to Continuous Estimation," Ph.D. Thesis, Department of Electrical Engineering, M. I. T., 1966.
5. A. B. Baggeroer, "A State-Variable Technique for the Solution of Fredholm Integral Equation" (submitted to IEEE Transactions on Information Theory).

A. EQUALIZATION OF DISPERSIVE CHANNELS USING DECISION FEEDBACK

1. Introduction

Several authors have recently considered decision feedback as a means of improving digital communication over dispersive channels. Lucky[1] applied decision feedback to the equalization of telephone lines, effectively enabling him to achieve dispersion measurements via the message sequence, rather than having to send additional signals to "sound" the channel before information transmission. Aein and Hancock[2] have analyzed the performance of a nonlinear decision-feedback receiver, applicable to channels in which the dispersion is restricted to less than two baud durations. Drouilhet and

Neissen[3] have studied and are constructing a decision-feedback equalizer, differing from that of Lucky in that they use a matched-filter ahead of their equalization filter, and use decision feedback to "subtract out" the effects of the message in order to improve their continuous, "sounding-signal" channel measurement.

The equalizer structure considered by Lucky is the conventional tapped delay line (TDL), which has long been used in correcting telephone lines, while Drouilhet and Niessen are using the MF-TDL structure, arrived at through different approaches and criteria by several persons (for example, Tufts,[4] George,[5] and Austin[6]). Both efforts are examples of how decision feedback has been used to facilitate channel measurement and the adjustment of parameters of what we shall refer to henceforth as "conventional" equalizers. We shall show in this report that decision feedback can be used to additional advantage in channel equalization, if one adopts the new equalizer structure developed in the sequel, hereafter referred to as the "decision-feedback" equalizer to distinguish it from the conventional equalizers mentioned above.

We want to consider the problem of determining the structure of a receiver for digital communication over a linear dispersive channel whose equivalent impulse response, h(t), is known. The receiver input is

$$r(t) = \sum_{k=-\infty}^{\infty} \xi_k h(t-kT_b) + n(t), \tag{1}$$

where T_b is the baud duration, and ξ_k contains the information transmitted on the k^{th} baud. Our problem is to decide between the hypothesis H_o that $\xi_o = +1$ and hypothesis H_1 that $\xi_o = -1$. We make the following assumptions.

(i) The ξ_k are independent.

(ii) H_o and H_1 are equally likely.

(iii) n(t) is white Gaussian noise, $R_n(\tau) = \frac{N_o}{2}\delta(\tau)$.

At this point we would like to derive the optimal receiver structure, assuming only that $\xi_k = +1$ or -1 on each baud. This, however, proves analytically intractable, and therefore we shall adopt an approach leading to a suboptimal receiver structure, which nonetheless exhibits definite advantages over existing conventional equalizer structures. This requires us to make additional assumptions.

(iv) The ξ_k are $N(0,\sigma)$ for $k > 0$.

(v) The ξ_k are known for $k < 0$.

We note that assumption (iv) renders our model inaccurate for binary AM or PSK systems in which $\xi_k = +1$ or -1 for all k, while assumption (v) is only valid for decision-feedback equalizers in the absence of decision errors.

Using these assumptions, we shall be led to the desired suboptimal receiver structure

(Fig. XXVII-4); then we shall optimize its parameters for the binary communication problem of interest (Eqs. 5 and 6). Finally, we shall work a simple example demonstrating that our new decision-feedback equalizer is capable of rendering far better performance than the conventional MF-TDL receiver.

2. Structure of the Decision-Feedback Equalizer

We want to determine the optimum receiver structure for the problem and assumptions that have been introduced, but first we introduce some notation and definitions that will prove useful in the derivation that is to follow.

Definitions: 1. $\underline{\xi}^- = \{\xi_k \,|\, k<0\}$

2. $\underline{\xi}^+ = \{\xi_k \,|\, k>0\}$

3. $a_k = \frac{1}{N_o}\int r(t)\, h(t-kT_b)\, dt = \frac{1}{N_o}\int r(t+kT_b)\, h(t)\, dt$

4. $b_k = \frac{1}{N_o}\int h(t)\, h(t-kT_b)\, dt.$

Under our assumptions, $\underline{\xi}^-$ is known correctly via decision feedback, and with this taken into account, the optimum receiver calculates the likelihood ratio

$$\Lambda = \frac{p\left[r(t)\,|\,\underline{\xi}^-, H_o\right]}{p\left[r(t)\,|\,\underline{\xi}^-, H_1\right]} = \frac{\int p\left[r(t)\,|\,\underline{\xi}^-, H_o, \underline{\xi}^+\right] p(\underline{\xi}^+)\, d\underline{\xi}^+}{\int p\left[r(t)\,|\,\underline{\xi}^-, H_1, \underline{\xi}^+\right] p(\underline{\xi}^+)\, d\underline{\xi}^+}.$$

We shall first consider the numerator. Under assumption (v) we have

$$p\left[r(t)\,|\,\underline{\xi}^-, H_o, \underline{\xi}^+\right] =$$

$$K_1 \exp\left[-\frac{1}{N_o}\int \left\{r(t) - \sum_{k<0} \xi_k h(t-T_b) - \xi_o h(t) - \sum_{\ell>0} \xi_\ell h(t-\ell T_b)\right\}^2 dt\right]\Bigg|_{\xi_o=1}$$

and since

$$K_1 \exp\left[-\frac{1}{N_o}\int \left\{r(t) - \sum_{k<0} \xi_k h(t-kT_b)\right\}^2 dt\right]$$

is independent of $\underline{\xi}^+$ and ξ_o, it will factor out of the integral and cancel with the same term arising in the denominator of Λ. Thus the terms of importance remaining in the integrand of the numerator are

$$\exp\left[\frac{2}{N_o}\int\left\{r(t)-\sum_{k<0}\xi_k h(t-kT_b)\right\}\left\{\xi_o h(t)+\sum_{\ell>0}\xi_\ell h(t-\ell T_b)\right\}dt\right.$$

$$\left.-\frac{1}{N_o}\int\left\{\xi_o h(t)+\sum_{\ell>0}\xi_\ell h(t-\ell T_b)\right\}^2 dt\right]\Bigg|_{\xi_o=1}.$$

By applying definitions 3 and 4, this may be written

$$\exp\left[2\xi_o a_o+2\sum_{\ell>0}\xi_\ell a_\ell-2\sum_{k<0}\sum_{\ell>0}\xi_k\xi_\ell b_{|k-\ell|}-2\xi_o\sum_{k<0}\xi_k b_k\right.$$

$$\left.-\xi_o^2 b_o-2\xi_o\sum_{\ell>0}\xi_\ell b_\ell-\sum_{j>0}\sum_{\ell>0}\xi_j\xi_\ell b_{|j-\ell|}\right]\Bigg|_{\xi_o=1}.$$

Now under assumption (iv) we may write

$$p(\underline{\xi}^+)=K_2\exp\left[-\frac{1}{2\sigma^2}\sum_{\ell>0}\xi_\ell^2\right]=K_2\exp\left[-\sum_{j>0}\sum_{\ell>0}\xi_j Q_{j\ell}\xi_\ell\right],$$

where we have defined $Q_{j\ell}=\frac{1}{2\sigma^2}\delta_{j\ell}$. Thus, by factoring out of the integral those terms that are independent of $\underline{\xi}^+$, the numerator of Λ becomes proportional to

$$\exp\left[2\xi_o a_o-2\xi_o\sum_{k<0}b_k\xi_k-\xi_o^2 b_o\right]\int\exp\left[-\sum_{j>0}\sum_{\ell>0}\xi_j(b_{|j-\ell|}+Q_{j\ell})\xi_\ell\right.$$

$$\left.+2\sum_{\ell>0}\xi_\ell\left(a_\ell-\sum_{k<0}b_{|k-\ell|}\xi_k-\xi_o b_\ell\right)\right]d\underline{\xi}^+\Bigg|_{\xi_o=1}.$$

By completing the square in the exponent of the integrand, it is straightforward to show that this numerator of Λ is

$$\exp\left[2\xi_o a_o - 2\xi_o \sum_{k<0} b_k \xi_k - \xi_o^2 b_o + \sum_{j>0} \sum_{\ell>0} \left(a_j - \sum_{k<0} b_{|j-k|}\xi_k - \xi_o b_j\right) P_{j\ell} \left(a_\ell - \sum_{m<0} b_{|\ell-m|}\xi_m - \xi_o b_\ell\right)\right]_{\xi_o=1},$$

where the $P_{j\ell}$ are elements of the matrix $\underline{P}$ defined by $\underline{P} = (\underline{B}+\underline{Q})^{-1}$ (for $j, \ell > 0$), and $Q_{j\ell}$ are as defined above. This same expression evaluated at $\xi_o = -1$ gives the denominator of Λ. It thus follows that the optimum receiver computes

$$\Lambda = \exp\left[4a_o - 4\sum_{k<0} b_k\xi_k - 4\sum_{\ell>0} b_\ell \left\{\sum_{j>0}\left(a_j - \sum_{k<0} b_{|k-j|}\xi_k\right) P_{j\ell}\right\}\right],$$

and decides H_o if $\Lambda \geq 1$, and decides H_1 if $\Lambda < 1$. Equivalently, if one defines

$$g_j \triangleq -\sum_{\ell>0} P_{j\ell} b_\ell \tag{2}$$

$$f_k \triangleq b_k + \sum_{j>0} g_j b_{|j-k|}, \tag{3}$$

then the optimum decision rule may be written

$$\boxed{a_o + \sum_{j>0} g_j a_j - \sum_{k<0} f_k \xi_k \underset{H_1}{\overset{H_o}{\lessgtr}} 0} \tag{4}$$

The receiver structure may now be found from this decision rule. From definition 3, it is seen that the sufficient statistics a_j may be generated by using a TDL having taps spaced at the baud duration T_b, as shown in Fig. XXVII-1. Moreover, since the weightings on the a_j may be placed before the integration and multiplication operations, and the multipliers and integrators are common to all taps of Fig. XXVII-1, then clearly we can generate

$$\sum_{j\geq 0} g_j a_j$$

as shown in Fig. XXVII-2, in which we define $g_o = 1$.

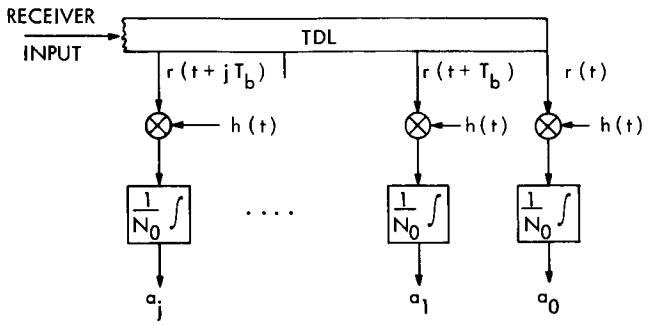

Fig. XXVII-1. Generation of sufficient statistics.

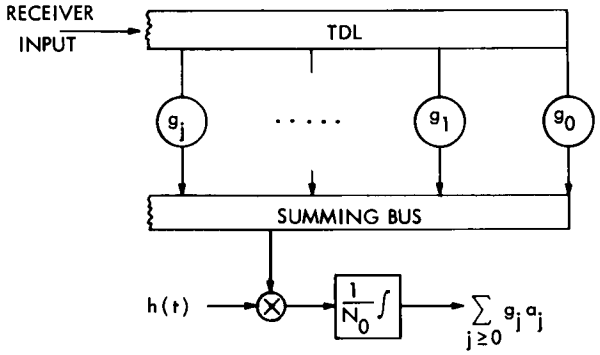

Fig. XXVII-2. Generating the first term of the decision rule.

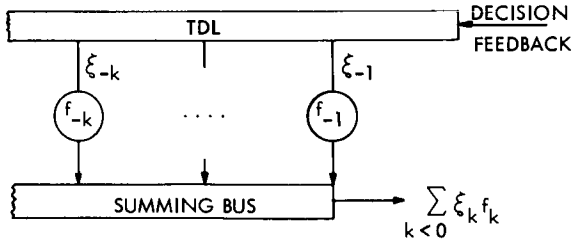

Fig. XXVII-3. Generating the second term of the decision rule.

Similarly, the decision-feedback term may be generated as indicated in Fig. XXVII-3. Noting that the integration need last only over the interval where h(t) is significantly non-zero in Fig. XXVII-2, then we would sample the output at some time, say T, to obtain the desired weighted sum of the a_j. The multiplication-integration procedure is clearly equivalent to a matched filter. Since the MF and TDL are both linear, we may put the MF ahead of the TDL. Also, sampling the TDL output means that one may instead sample the MF output at the baud rate. Thus we have arrived at the final structure of the decision-feedback equalizer shown in Fig. XXVII-4.

We note that this decision-feedback equalizer structure is similar to the conventional MF-TDL equalizer, except that the TDL now only accounts for future bauds, while the feedback TDL accounts for past bauds upon which decisions have been made. Further differences will become apparent in the discussion.

3. Minimum-Output-Sample-Variance Decision-Feedback Equalizer

We now want to adopt the equalizer structure derived above (Fig. XXVII-4) and determine the forward and feedback TDL tap gains that minimize the sum of the signal sidelobes and noise power at the receiver output in the absence of decision errors. We first introduce some additional notation and definitions that will prove useful in the following discussion.

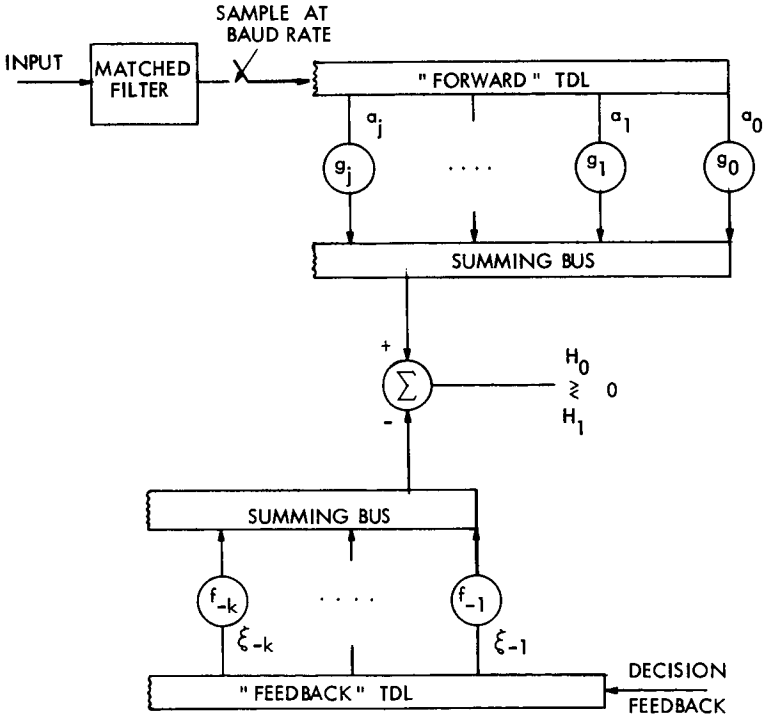

Fig. XXVII-4. Structure of the decision-feedback equalizer.

Definitions:

5. q_ℓ = signal component of the forward-TDL output at the ℓ^{th} sample time, when a single $\xi_o = +1$ baud is transmitted
6. $\phi_k = \int h(t)\, h(t+kT_b)\, dt$ = sampled channel autocorrelation function at $\tau = kT_b$.
7. $\underline{Y}$ = matrix with elements $Y_{jk} = \phi_{j-k}$ for $j, k \geq 0$
8. $\underline{X}$ = matrix with elements $X_{jk} = \sum_{\ell \leq 0} \phi_{j+\ell}\phi_{k+\ell}$ for $j, k \geq 0$
9. $\underline{\phi}$ = column vector with elements ϕ_i for $i \geq 0$
10. $\underline{g}$ = column vector with elements g_i for $i \geq 0$
11. $\underline{f}$ = column vector with elements f_{-i} for $i \geq 1$.

A typical response of the decision-feedback equalizer to a single transmitted baud of $\xi_o = +1$ is shown in Fig. XXVII-5a. It is always an asymmetrical waveform, having

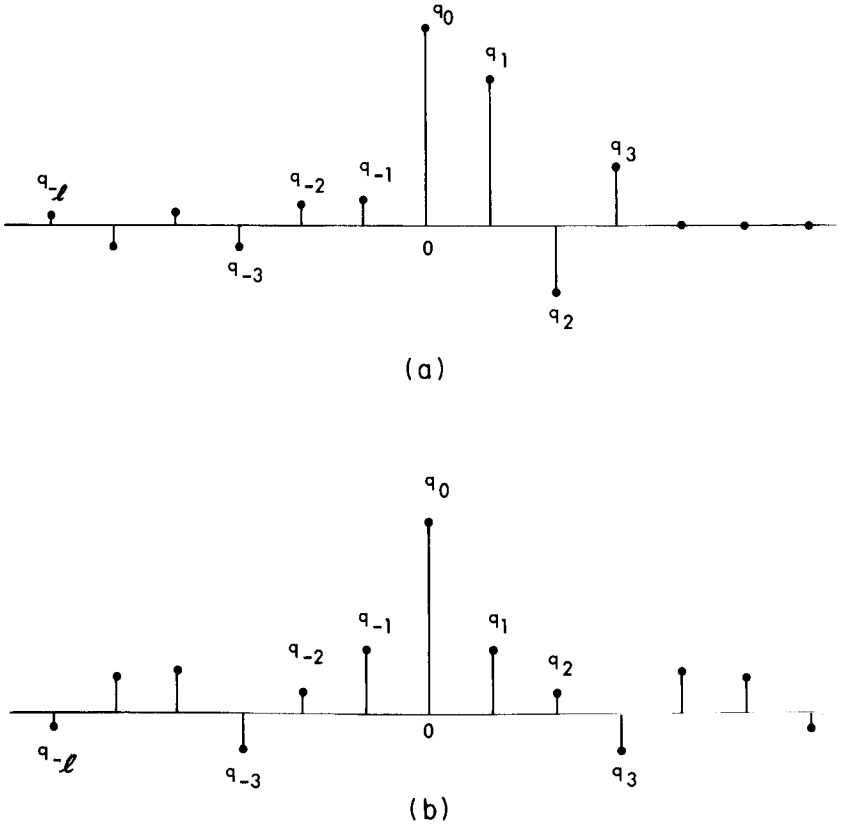

Fig. XXVII-5. Typical responses to a single transmitted $\xi_o = +1$ baud in the absence of noise: (a) decision-feedback equalizer; and (b) conventional MF-TDL equalizer.

N more samples occurring before the main sample (which is denoted sample number 0) than after it, where the MF output has 2N + 1 nonzero samples. This is in contrast with the typical output from the conventional MF-TDL equalizer, which is seen in Fig. XXVII-5b to always exhibit symmetry about the main sample.

Before we can proceed to determine the optimum choices of $\underline{g}$ and $\underline{f}$ under our minimum-output-sample-variance criterion, we must first understand the effect of the decision feedback on the output distortion. Consider the signal component out of the forward TDL at the first sample time:

$$\sum_{j\geq 0} g_j [a_{j+1}]_{\text{signal}} = \sum_{j\geq 0} g_j \left[\frac{1}{N_o} \int \left\{ \sum_k \xi_k h(t-kT_b) \right\} \{h(t-(j+1)T_b)\}\, dt \right].$$

The contribution to this component, which is due to the bauds for which decisions have already been made (that is, on all the ξ_k up to and including ξ_o), is then

$$\sum_{j\geq 0} \sum_{k\leq 0} g_j b_{|j+1-k|} \xi_k.$$

Next, consider the output of the feedback TDL at this same first sample time. With the use of Eq. 3 for the f_k, this becomes

$$\sum_{k<0} f_k \xi_{k+1} = \sum_{k<0} \left(b_k + \sum_{j>0} g_j b_{|j-k|} \right) \xi_{k+1},$$

and if we let $k^* = k + 1$,

$$= \sum_{k^*\leq 0} \left(b_{k^*-1} + \sum_{j>0} g_j b_{|j+1-k^*|} \right) \xi_{k^*}$$

$$= \sum_{j\geq 0} \sum_{k^*\leq 0} g_j b_{|j+1-k^*|} \xi_{k^*}.$$

Here, we have used $b_{k^*-1} = b_{1-k^*}$ and our earlier definition, $g_o \triangleq 1$. Thus we see that in the absence of decision errors the feedback-TDL output is exactly the same as the contribution to the forward-TDL output at the first sample time, attributable to past bauds, and hence there is no net contribution to the distortion from those bauds upon which decisions have already been made. We now see the three important advantages that the decision-feedback equalizer enjoys over the conventional equalizer.

(i) The conventional equalizer cannot completely eliminate interference due to past bauds, due to noise-enhancement considerations, as well as the practical constraint of a finite TDL length. The decision-feedback equalizer, in the absence of decision errors, completely eliminates the intersymbol interference due to past bauds.

(ii) For the decision-feedback equalizer, the forward-TDL gain-vector $\underline{g}$ may be optimized without consideration of the q_ℓ for $\ell > 0$, since these are eliminated by the decision-feedback, while the conventional equalizer must be designed to simultaneously suppress all of the q_ℓ for $\ell \neq 0$. This additional freedom enables the decision-feedback equalizer to achieve much better suppression of the intersymbol interference due to future bauds.

(iii) Since the intersymbol interference due to past bauds is suppressed through the noiseless feedback-TDL rather than through using additional taps on the forward-TDL as in the conventional equalizer, then clearly the output noise power is significantly reduced.

Each of these advantages contributes to a much better performance for the decision-feedback equalizer compared with that of its conventional counterpart, as we shall show in the example. In view of the conclusions, stated above, it is clear that the output sample variance is given by

$$\sum_{\ell<0} q_\ell^2 + \text{Output noise variance.}$$

Under the constraint that the main sample be unity, we may include q_o in the summation to find that

$$\sum_{\ell\leq 0} q_\ell^2 = \sum_{j\geq 0}\sum_{k\geq 0} g_j X_{jk} g_k = \underline{g}^T \underline{X} \underline{g},$$

while the output noise variance can be shown[7] to be

$$\frac{N_o}{2}\sum_{j\geq 0}\sum_{k\geq 0} g_j Y_{jk} g_k = \frac{N_o}{2}\underline{g}^T \underline{Y}\underline{g}.$$

Thus under the constraint that $q_o = \underline{g}^T\underline{\phi} = 1$, we want to minimize the quantity

$$J = \underline{g}^T\left[\underline{X} + \frac{N_o}{2}\underline{Y}\right]\underline{g} + \lambda(1-\underline{g}^T\underline{\phi})$$

over the choice of the forward-TDL gain vector $\underline{g}$. The unique solution is given by

$$\underline{g} = \frac{\left[\underline{X} + \frac{N_o}{2}\underline{Y}\right]^{-1} \underline{\phi}}{\underline{\phi}^T \left[\underline{X} + \frac{N_o}{2}\underline{Y}\right]^{-1} \underline{\phi}} \tag{5}$$

This result appears formally the same as that for the optimum tap-gain vector in the conventional MF-TDL equalizer.[7] The difference is that for the conventional equalizer the summation of definition 8 is taken over all ℓ, while the vector of definition 9 has elements for all i. Thus $\underline{X}$ matrix for the conventional equalizer becomes symmetrical and Toeplitz, while the $\underline{\phi}$ vector becomes symmetrical, and these properties do not hold for the decision-feedback equalizer.

The proper choice of the $\underline{f}$ vector now follows directly from Eq. 3, except that we have dropped the $1/N_o$ factor common to all terms of Eq. 4 (that is, the a_j contained this factor, while it is not included in the MF output in the present discussion) and thus replace the b_k there by ϕ_k:

$$f_k = \sum_{j \geq 0} g_j \phi_{|j-k|}.$$

If we define a matrix $\underset{\sim}{Y}$ with elements $\underset{\sim}{Y}_{jk} = \phi_{j-k}$ for $j \geq 0$ and $k < 0$ (note that it is the range of k which distinguishes this matrix $\underset{\sim}{Y}$ from the matrix $\underline{Y}$ of definition 7), then the feedback-TDL tap-gain vector may be conveniently written as

$$\underline{f} = \underset{\sim}{Y}\underline{g} \tag{6}$$

Thus, once the sampled channel autocorrelation function and additive noise level have been specified, one can use Eqs. 5 and 6 to determine the parameters of the minimum-variance decision-feedback equalizer. This is illustrated by the example that follows.

4. Conventional Equalizer versus Decision-Feedback Equalizer: An Example

We shall now work out an example, applying the derived decision-feedback structure to the equalization of the channel whose sampled autocorrelation function is shown in Fig. XXVII-6a. This particular example was chosen, not because it necessarily provides a realistic model of channels of practical importance, but because it illustrates the important advantages that the decision-feedback equalizer has over the conventional MF-TDL equalizer. More complex examples could have been chosen, for they pose no additional difficulties.

We thus want to find the conventional equalizer and decision-feedback equalizer

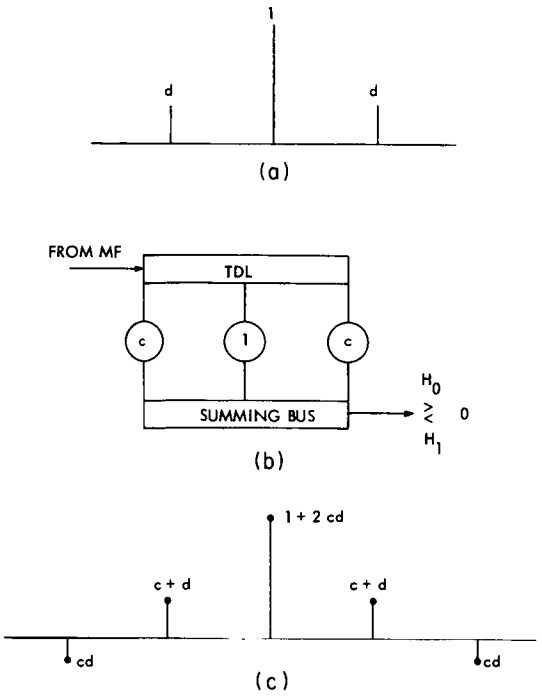

Fig. XXVII-6.

(a) Sampled-channel autocorrelation function. (b) 3-tap conventional equalizer. (c) Output for a single $\xi_0 = +1$ transmitted baud.

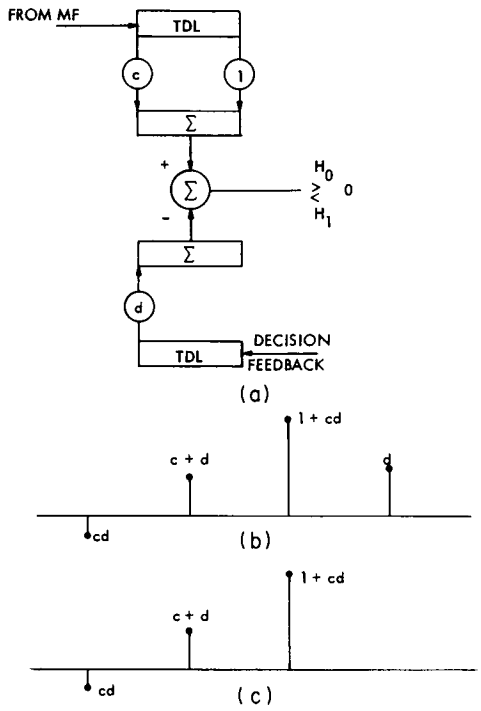

Fig. XXVII-7.

(a) Decision-feedback equalizer. (b) Forward-TDL output. (c) Effective output with decision feedback.

structures as a function of the noise level, $N_0/2$, and the sidelobe level, d, of Fig. XXVII-6a.

Using the 3-tap conventional equalizer shown in Fig. XXVII-6b, one can solve Eq. 5 (with appropriate $\underline{X}$ and $\underline{\phi}$, and normalizing the result so that $g_0 = 1$) to find that

$$c = \frac{2d^3 - d}{1 - d^2 + \frac{N_0}{2}(1-2d^2)} \tag{7}$$

minimizes the output-sample variance, which results in the response to a single transmitted $\xi_0 = +1$ baud shown in Fig. XXVII-6c. The noise present at the output has variance given by

$$\sigma^2 = \frac{N_0}{2}(1+4dc+2c^2). \tag{8}$$

Given σ^2 and an arbitrary set of sidelobes, we can determine the probability of error very efficiently, using an "error tree" algorithm developed by the author.[7] This

algorithm was applied to the present problem for d = .4, d = .48, and d = .50, with the resulting performance curves for the conventional MF-TDL equalizer shown in Figs. XXVII-8, XXVII-9, and XXVII-10. These curves are discussed further below, when we compare them with the corresponding curves of the decision-feedback equalizer.

For the channel of Fig. XXVII-6a, the decision-feedback equalizer is as shown in Fig. XXVII-7a, where we consider it to be the counterpart of Fig. XXVII-6b, since the delay and tap-gain requirements are the same with both equalizers. We should note at this point that although the forward TDL of the decision-feedback equalizer appears to be half of the conventional-equalizer TDL, this is not the case, in general. In general, if the sampled-channel autocorrelation has M sidelobes, then the feedback TDL requires M taps, with the remaining in the forward TDL. Thus, for example, if one had a conventional equalizer of 55 taps to equalize a channel having 10 autocorrelation sidelobes, then the hardware-equivalent decision-feedback equalizer would have 45 forward-TDL gains and 10 feedback-TDL gains.

Solving Eq. 5 and normalizing so that $g_o = 1$, one finds that

$$c = \frac{d^3 - d}{1 + \frac{N_o}{2}(1-d^2)} \tag{9}$$

minimizes the output-sample variance, and results in the response to a single $\xi_o = +1$ transmitted baud shown in Fig. XXVII-7b. The effective output after decision feedback is shown in Fig. XXVII-7c, where the samples occurring after the main sample have been eliminated. The noise present at the output has variance

$$\sigma^2 = \frac{N_o}{2}(1+2dc+c^2). \tag{10}$$

As discussed further below, the output noise is smaller than that appearing at the output of the conventional equalizer after appropriate normalizations have been made. Note that the parameter c of Eqs. 9 and 10 is numerically different from that of Eqs. 7 and 8.

The performance of the decision-feedback equalizer was determined through digital computer simulations, with the results shown in Figs. XXVII-8, XXVII-9 and XXVII-10. The signal-to-noise ratio in these figures is given by

$$\text{SNR} = 10 \log_{10}\left(\frac{2}{N_o}\right),$$

since we have assumed unit signal energy on each baud. Also, to place the performance curves of the conventional and decision-feedback equalizers in better perspective, Figs. XXVII-8, XXVII-9, and XXVII-10 show the performance curves of an unequalized receiver (matched filter only) and of the ideal receiver (that obtained when transmitting

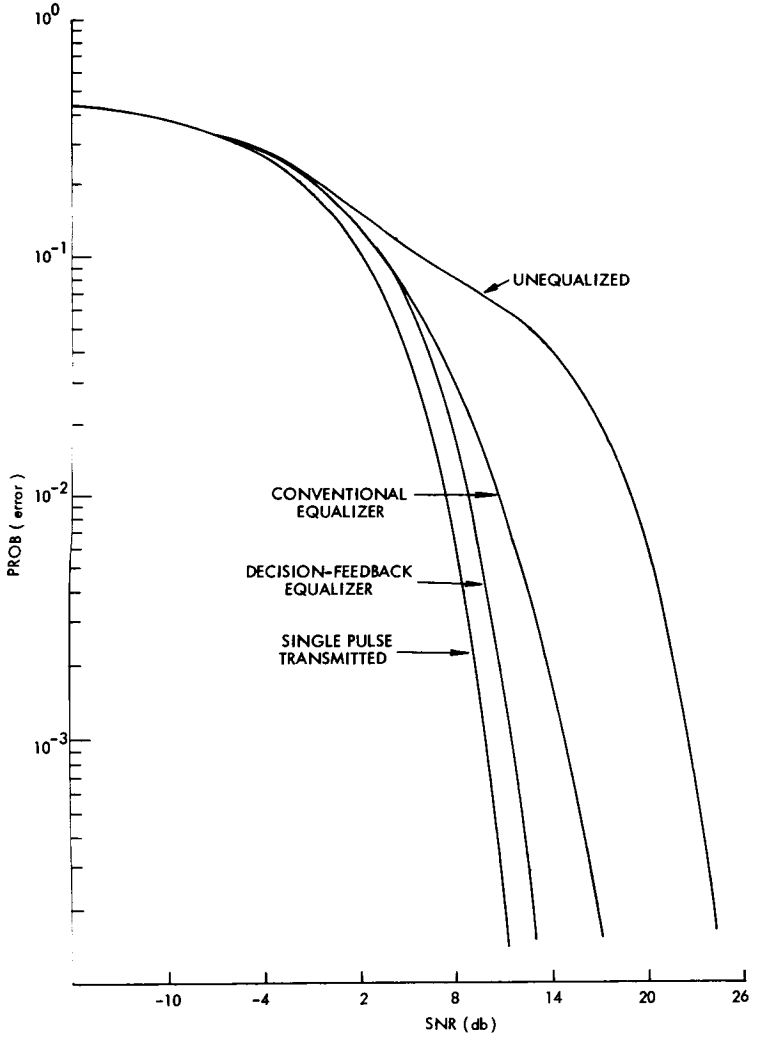

Fig. XXVII-8. Performance for the channel indicated in Fig. XXVII-6a, with d = .40.

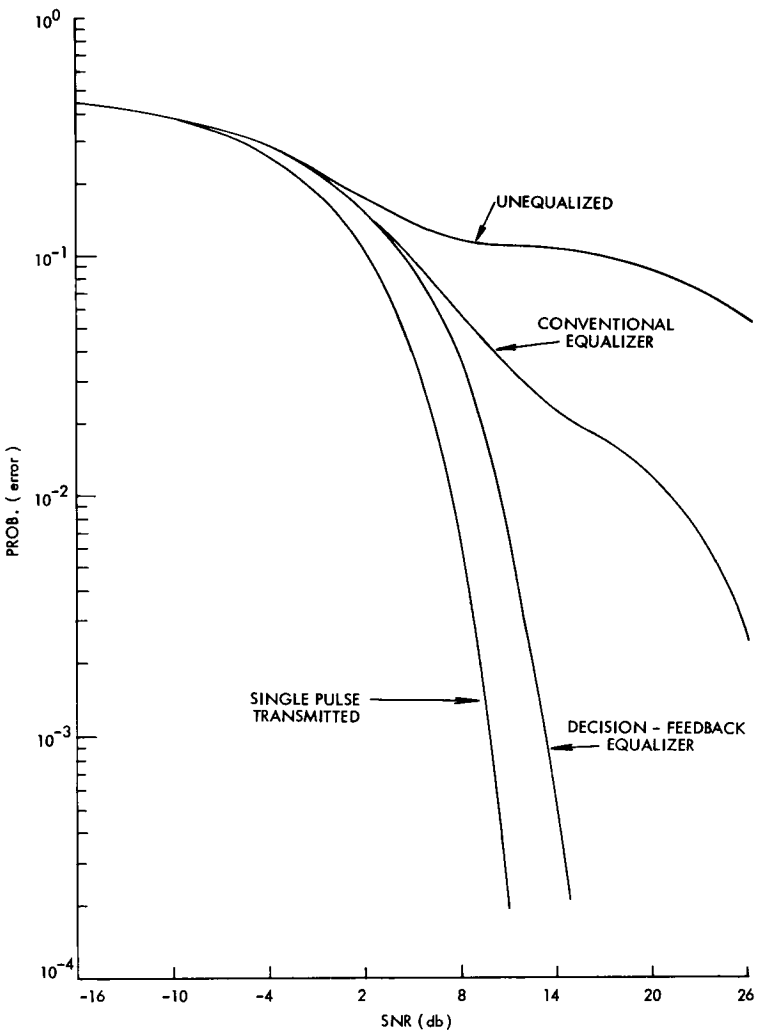

Fig. XXVII-9. Performance for the channel indicated in Fig. XXVII-6a, with d = .48.

only a single pulse, where intersymbol interference is no longer a problem).

When the sidelobe energy is approximately one-third that of the main sample (the d = .40 case), the decision-feedback equalizer is only approximately 2 db away from the ideal at high SNR, while it is approximately 4 db better than the conventional equalizer.

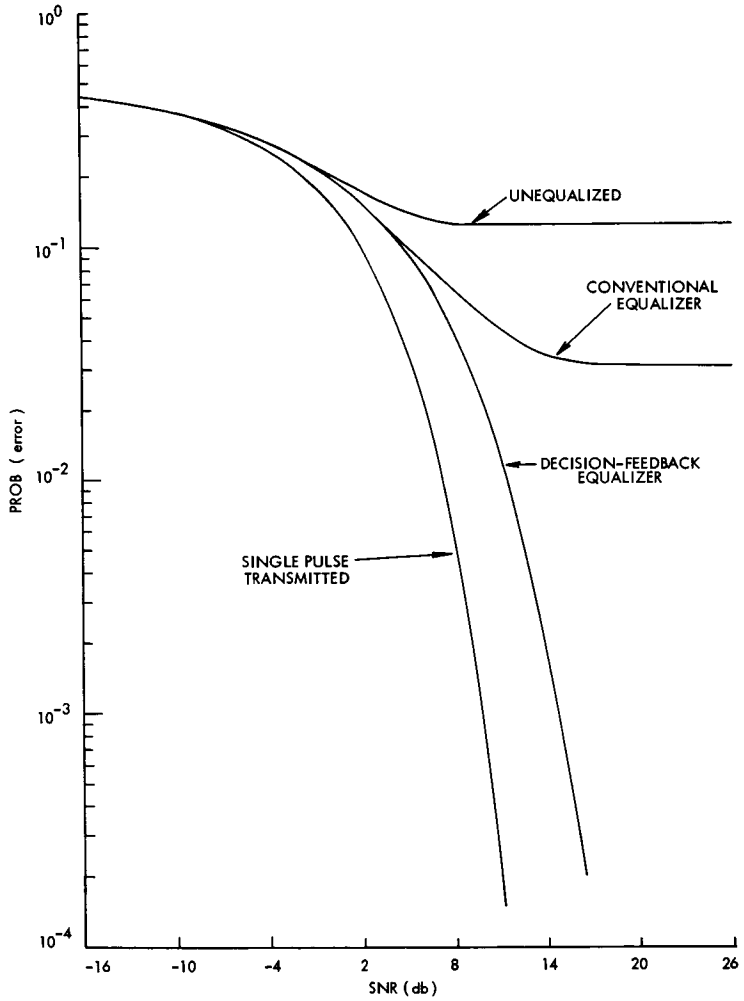

Fig. XXVII-10. Performance for the channel indicated in Fig. XXVII-6a, with d = .50.

As the sidelobe energy is increased (Figs. XXVII-9 and XXVII-10), the decision-feedback equalizer becomes 3-5 db off the ideal, and approximately 12 db better than the conventional equalizer at d = .48. For d = .50, the conventional equalizer is seen in Fig. XXVII-10 to approach a limiting performance with increasing SNR, while the decision-feedback equalizer continues to improve rapidly beyond ~5 db. The behavior of the conventional equalizer here is due to the fact that d = .50 renders an input distortion

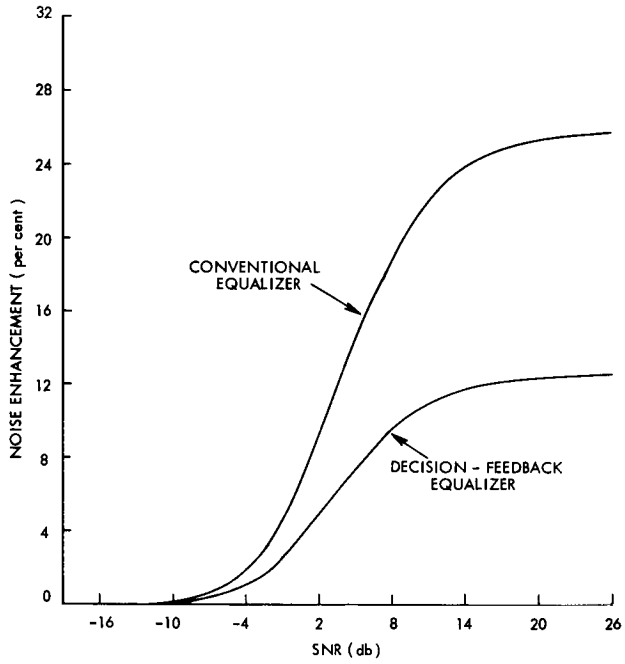

Fig. XXVII-11. Noise enhancement for the channel indicated in Fig. XXVII-6a, with d = .40.

of unity (with a sum of the side-lobe magnitudes used as measure; thus the "eye" was closed even in the absence of noise, for those familiar with "eye diagrams"), and a (2M+1)-tap TDL conventional equalizer exhibits a limiting performance of 2^{-2M-3} with increasing SNR.

If one normalizes the main output samples to unity, and correspondingly normalizes the output noise variances, the noise enhancement is considerably more with the conventional equalizer than with the decision-feedback equalizer in this example, as shown in Fig. XXVII-11 for d = .40. This illustrates advantage (iii), which we listed for the decision-feedback equalizer.

Note that at low SNR the performance of the two equalizers coincides in Figs. XXVII-8, XXVII-9, and XXVII-10. This is not perhaps what one might have expected from heuristic arguments, which point out that when an error is made by the decision-feedback equalizer the feedback-TDL contribution enhances rather than eliminates the q_1 sample (see Fig. XXVII-7b and 7-c), thereby resulting in this example in an additional equivalent interfering sample whose magnitude exceeds that of the main sample by $|cd|$. This gives a large probability of error on the next decision ($\approx 1/3$ for intermediate SNR, calculated under the assumption of uncorrelated distortion), and thus it appears quite possible that "one bad decision will lead to another," and cause the performance at low SNR to become eventually worse than that of the conventional equalizer.

Such behavior was not observed in this example, however, and the decision-feedback equalizer appears at least as good as the conventional equalizer at all SNR.

For more complex channels that we have studied, in which the energy in the side lobes is much greater than in the simple case considered here, the anticipated thresholding effect has been noted,[7] but only at high conventional equalizer error rates, and the decision-feedback equalizer still exhibits far better performance at all SNR of practical importance.

M. E. Austin

References

1. R. W. Lucky, "Techniques for Adaptive Equalization of Digital Communication Systems," Bell System Tech. J., Vol. XLV, No. 2, pp. 255-286, February 1966.
2. J. M. Aein and J. C. Hancock, "Reducing the Effects of Intersymbol Interference with Correlation Receivers," IEEE Trans., Vol. IT-9, No. 3, pp. 167-175, July 1963.
3. P. Drouilhet and C. W. Niessen, Private discussions, Lincoln Laboratory, M. I. T., February 1966.
4. C. W. Tufts, "Matched Filters and Intersymbol Interference," Technical Report 345, Cruft Laboratory, Harvard University, Cambridge, Massachusetts, July 20, 1961.
5. D. A. George, "Matched Filters for Interfering Signals," IEEE Trans., Vol. IT-11, No. 1, pp. 153-154 (Correspondence), January 1965.
6. M. E. Austin, "Adaptive Signal Processing – Part III," unpublished memoranda, February 1966-October 1966.
7. M. E. Austin, "Adaptive Signal Processing – Part IV," unpublished memoranda, October 1966-January 1967.

B. STATE-VARIABLE ESTIMATION IN THE PRESENCE OF PURE DELAY

1. Introduction

We shall present a state-variable approach for the processing of sonar or seismic array data. In the processing of data from these arrays, one often encounters delayed versions of the same signal, or signals that are correlated by means of a delay, in the same waveform.

Because of the inherent nonrationality of the delay factors, the classical Weiner approach, even for stationary processes, requires finding the impulse response of a filter with an infinite number of poles. When one wishes to use existing state-variable techniques, one requires an infinite dimensional state representation in order to develop the estimation equations. Here, we shall develop a finite set of estimation equations that specify the estimate maximizing the a posteriori probability density of the process.

2. Signal Model

Let us now discuss the equations which describe the system of interest (see

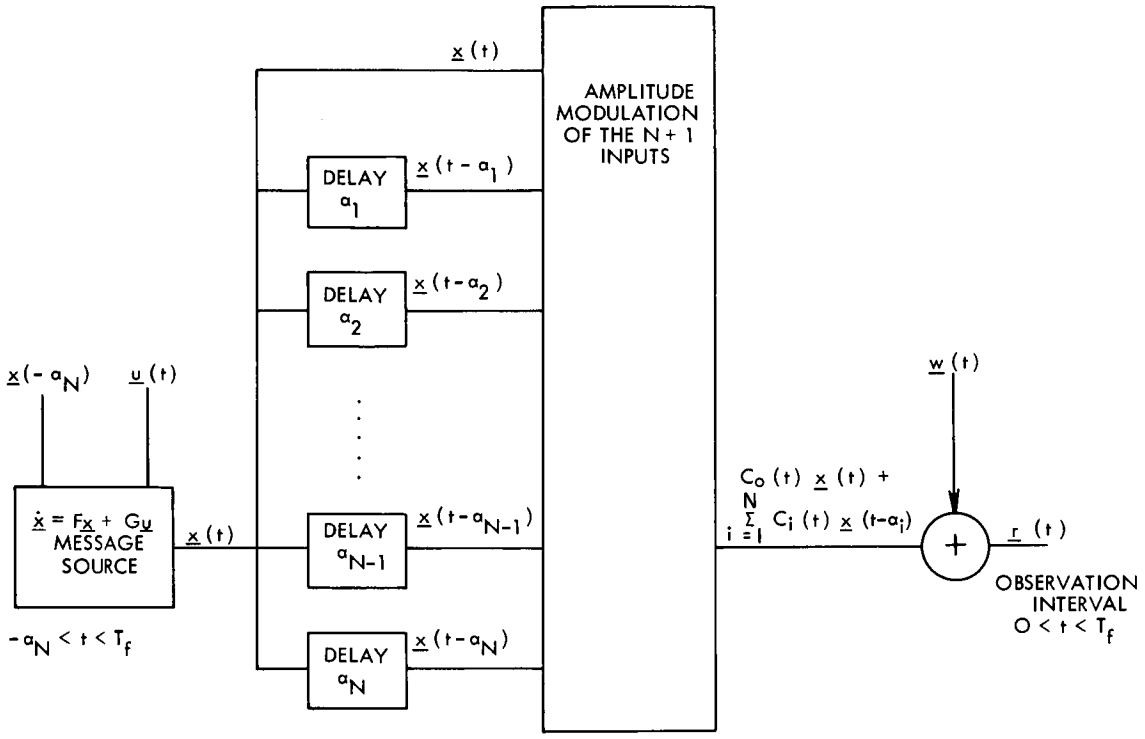

Fig. XXVII-12. System model.

Fig. XXVII-12). We assume that the dynamics of the message process are determined by a linear state equation

$$\frac{d\underline{x}(t)}{dt} = F(t)\,\underline{x}(t) + G(t)\,\underline{v}(t) \tag{1}$$

over the time interval $-a_N < t < T_f$, where F(t), G(t) are matrices determining the dynamics of the state equation, and v(t) is a white Gaussian source noise with

$$E[\underline{v}(t)\underline{v}^T(\tau)] = Q\delta(t-\tau). \tag{2}$$

In order to completely specify this random process, we need to make some assumptions about the conditions of the initial state. We assume that the initial state is a Gaussian random vector with

$$E[\underline{x}(-a_N)] = \overline{\underline{x}}(-a_N) \tag{3}$$

$$E\left[(x(-a_N)-\overline{\underline{x}}(-a_N))(\underline{x}(-a_N)-\overline{\underline{x}}(-a_N))^T\right] = P(-a_N). \tag{4}$$

We shall now discuss the observation process. We assume that we observe N different delayed versions of an amplitude modulation of the state vector in the presence of a white Gaussian observation noise. Our observation is, therefore,

$$\underline{r}(t) = C_o(t)\,\underline{x}(t) + \sum_{i=1}^{N} C_i(t)\,\underline{x}(t-\alpha_i) + \underline{w}(t), \tag{5}$$

where

$$0 < t < T_f$$

$$0 < \alpha_1 < \alpha_2 < \ldots < \alpha_{N-1} < \alpha_N \tag{6}$$

$$E[\underline{w}(t)\underline{w}^T(\tau)] = R\delta(t-\tau). \tag{7}$$

Notice that our observation equation is defined over a different time interval from the state equation. For convenience, let us define

$$\underline{y}_i(t) = \underline{x}(t-\alpha_i). \tag{8}$$

Aside from the delay terms that enter, our assumptions do not differ from the usual ones made in state-variable estimation procedures.

3. Derivation of the MAP Estimation Equations

It can be shown that the problem of maximizing the a posteriori density is equivalent to minimizing the following quadratic functional:

$$J(\underline{v}(t), \underline{x}(-\alpha_N)) = \|\underline{x}(-\alpha_N) - \overline{\underline{x}}(-\alpha_N)\|_{P^{-1}(-\alpha_N)}$$

$$\int_0^{T_f} \left\| \underline{r}(t) - C_o(t)\,\underline{x}(t) - \sum_{i=1}^{N} C_i(t)\,y_i(t) \right\|_{R^{-1}} dt$$

$$+ \int_{-\alpha_N}^{T_f} \|\underline{v}(t)\|_{Q^{-1}}\, dt \tag{9}$$

Subject to the constraint of the state equation (1) and the delay operations specified by Eq. 6 $\left(\|x\|_A = x^T A x\right)$.

Let us first consider the state-equation constraint. We can introduce this by using a Lagrangian multiplier. This is done by adding to the quadratic functional the term

$$L_o = \int_{-\alpha_N}^{T_f} \underline{p}^T(t) \left(\frac{d\underline{x}(t)}{dt} - F(t)\, \underline{x}(t) - G(t)\, \underline{v}(t) \right) dt. \tag{10}$$

It will be useful to integrate the first term of the integrand by parts. Doing this, we have

$$L_o = \underline{p}^T(T_f)\, \underline{x}(T_f) - \underline{p}^T(-\alpha_N)\, \underline{x}(-\alpha_N)$$

$$\int_{-\alpha_N}^{T_f} \left\{ \frac{d\underline{p}^T(t)}{dt}\, \underline{x}(t) + \underline{p}^T(t)\, F(t)\, \underline{x}(t) + \underline{p}^T(t)\, G(t)\, \underline{v}(t) \right\} dt. \tag{11}$$

When we incorporate the constraints imposed by the delays, we encounter much more difficulty. In order to impose the constraints, we must find a differential equation that the delay operation satisfies. As we would expect from the infinite-state requirement imposed by the delay operation, we cannot find a finite-dimensional ordinary differential equation. It is easy to show, however that the delay operation satisfies the partial differential equation

$$\frac{\partial \underline{\phi}_i(t,\tau)}{\partial t} + \frac{\partial \underline{\phi}_i(t,\tau)}{\partial \tau} = 0, \tag{12}$$

where

$$\underline{\phi}_i(t,0) = \underline{x}(t).$$

We show this by noting that the general solution to Eq. 12 is

$$\underline{\phi}_i(t,\tau) = \underline{f}_i(t-\tau). \tag{13}$$

Imposing the boundary condition at $\tau = 0$ yields

$$\underline{\phi}_i(t,0) = \underline{f}_i(t) = x(t). \tag{14}$$

We see that we now have

$$\underline{\phi}_i(t,\alpha_i) = \underline{f}_i(t-\alpha_i) = \underline{x}(t-\alpha_i) = \underline{y}_i(t). \tag{15}$$

As a result, we are able to impose the constraint of each delay term by using a Lagrangian multiplier that is a function of two variables, that is, we want to add to the quadratic functional terms of the form

$$L_i = \int_0^{T_f} \int_0^{\alpha_i} \underline{\mu}_i^T(t,\tau) \left(\frac{\partial \underline{\phi}_i(t,\tau)}{\partial t} + \frac{\partial \underline{\phi}_i(t,\tau)}{\partial t} \right) dt d\tau, \tag{16}$$

in which we have

$$\underline{\phi}_i(t,\tau) = \underline{x}(t-\tau). \tag{17}$$

We again want to perform some integrations by parts. This yields

$$L_i = \int_0^{T_f} \left(\underline{\mu}_i^T(t,a_i)\underline{\phi}_i(t,a_i) - \underline{\mu}_i^T(t,0)\underline{\phi}_i(t,0) \right) dt$$

$$+ \int_0^{a_i} \left(\underline{\mu}_i^T(T_f,\tau)\underline{\phi}_i(T_f,\tau) - \underline{\mu}_i^T(0,\tau)\underline{\phi}_i(0,\tau) \right) d\tau$$

$$- \int_0^{T_f} \int_0^{a_i} \left(\frac{\partial \underline{\mu}_i^T(t,\tau)}{\partial t} + \frac{\partial \underline{\mu}_i^T(t,\tau)}{\partial \tau} \right) \underline{\phi}_i(t,\tau)\, dt d\tau. \tag{18}$$

When we add the Lagrangian multiplier constraints L_o, L_1, ... L_N imposed by the state equation and the delay terms to the quadratic functional described by Eq. 9, we have

$$J(\underline{v}(t), \underline{x}(-a_N)) = \| \underline{x}(-a_N) - \overline{\underline{x}}(-a_N) \|_{P^{-1}(-a_N)}$$

$$\int_0^{T_f} \left\| \underline{r}(t) - C_o(t)\, \underline{x}(t) - \sum_{i=1}^{N} C_i(t)\, \underline{y}_i(t) \right\|_{R^{-1}} dt$$

$$+ \int_{-a_N}^{T_f} \| \underline{v}(t) \|_{Q^{-1}} dt + \underline{p}^T(T_f)\, \underline{x}(T_f) - \underline{p}^T(T_o)\, \underline{x}(T_o)$$

$$- \int_{-a_N}^{T_f} \left\{ \frac{d\underline{p}^T(t)}{dt}\, \underline{x}(t) + \underline{p}^T(t)\, F(t)\, \underline{x}(t) + \underline{p}^T(t)\, G(t)\, \underline{v}(t) \right\} dt$$

$$+ \sum_{i=1}^{N} \left[\int_0^{T_f} \left(\mu_i^T(t,a_i)\underline{y}_i(t) - \underline{\mu}_i^T(t,0)\underline{x}(t) \right) dt \right.$$

$$+ \int_0^{a_i} \left(\underline{\mu}_i^T(T_f,\tau)\underline{x}(T_f-\tau) - \underline{\mu}_i^T(0,\tau)\underline{x}(-\tau) \right) d\tau$$

$$\left. - \int_0^{T_f} \int_0^{a_i} \left(\frac{\partial \mu_i^T(t,\tau)}{\partial t} + \frac{\partial \mu_i^T(t,\tau)}{\partial \tau} \right) \phi_i(t,\tau)\, dt d\tau \right]. \tag{19}$$

We now are in a position to minimize the quadratic functional by applying variational techniques. We proceed by perturbing v(t) and $x(-a_N)$ from their optimal estimates, that is,

$$\underline{x}(-a_N) = \hat{\underline{x}}(-a_N) + \epsilon\delta\hat{\underline{x}}(-a_N) \tag{20}$$

$$\underline{v}(t) = \hat{\underline{v}}(t) + \epsilon\delta\hat{\underline{v}}(t). \tag{21}$$

The response of the state equation to the perturbed input is

$$\underline{x}(t) = \hat{\underline{x}}(t) + \epsilon\delta\hat{\underline{x}}(t), \tag{22}$$

where $\delta\underline{x}(t)$ satisfies the differential equation

$$\frac{d\delta\hat{\underline{x}}(t)}{dt} = F(t)\ \delta\hat{\underline{x}}(t) + G(t)\ \delta\underline{v}(t). \tag{23}$$

The variation by the quadratic functional which results from these perturbations is given by

$$\begin{aligned}
J(\underline{v}(t),\underline{x}(-a_N)) = J(\hat{\underline{v}}(t),\hat{\underline{x}}(-a_N)) + \epsilon\Bigg\{&\left[x(-a_N)-x(-a_N)\right]^T P^{-1}(-a_N)\ \delta x(-a_N) \\
&+ \int_0^{T_f} -\left[\underline{r}(t) - C_o(t)\ \hat{\underline{x}}(t) - \sum_{i=1}^{N} C_i(t)\ \hat{\underline{y}}_i(t)\right]^T R^{-1}\left[C_o(t)\ \delta x(t)\right. \\
&\left. + \sum_{j=1}^{N} C_j(t)\ \delta\hat{\underline{y}}_j(t)\right] \\
&+ \int_{-a_N}^{T_f} \hat{\underline{v}}(t)^T Q^{-1}\delta\hat{\underline{v}}(t)\ dt + \underline{p}^T(T_f)\ \delta\hat{\underline{x}}(T_f) - \underline{p}^T(T_o)\ \delta\hat{\underline{x}}(-a_N) \\
&- \int_{-a_N}^{T_f} \left\{\frac{d\underline{p}^T(t)}{dt}\ \delta\hat{\underline{x}}(t) + \underline{p}^T(t)\ F(t)\ \delta\hat{\underline{x}}(t) + \underline{p}^T(t)\ G(t)\ \delta\hat{\underline{v}}(t)\right\} dt \\
&+ \sum_{i=1}^{N}\left[\int_0^{T_f}\left(\underline{\mu}_i^T(t,a_i)\delta\underline{y}_i(t) - \underline{\mu}_i^T(t,0)\delta\hat{\underline{x}}(t)\right) dt\right] \\
&+ \sum_{i=1}^{N}\left[\int_0^{a_i}\left(\mu_i^T(T_f,\tau)\delta\underline{x}(T_f-\tau) - \underline{\mu}_i^T(0,\tau)\delta\hat{\underline{x}}(-\tau)\right) d\tau\right] \\
&+ \sum_{i=1}^{N}\left[\int_0^{T_f}\int_0^{a_i} \frac{\partial\underline{\mu}_i^T(t,\tau)}{\partial t} + \frac{\partial\underline{\mu}_i^T(t,\tau)}{\partial\tau}\ \delta\hat{\underline{\phi}}_i(t,\tau)\ dtd\tau\right]\Bigg\} + 0(\epsilon^2).
\end{aligned} \tag{24}$$

We now want to combine the various variations into common factors. We have

$$J(\underline{v}(t),\underline{x}(-a_N)) = J(\hat{\underline{v}}(t),\hat{\underline{x}}(-a_N)) + \epsilon \left\{ \left(\left[\hat{\underline{x}}(-a_N) - \underline{\bar{x}}(-a_N) \right]^T P^{-1}(-a_N) - p^T(-a_N) \right) \delta x(-a_N) \right.$$

$$+ \int_0^{T_f} \left(- \left[\underline{r}(t) - C_o(t)\, \hat{\underline{x}}(t) - \sum_{j=1}^{N} C_i(t)\, \hat{\underline{y}}_i(t) \right]^T R^{-1} C_o(t) \right.$$

$$- \left(\frac{d\underline{p}^T(t)}{dt} - \underline{p}^T(t)\, F(t) - \sum_{i=1}^{N} \mu_i^T(t,0) \right) \delta\hat{\underline{x}}(t) \Bigg) \, dt$$

$$+ \int_{-a_N}^{T_f} \left((\hat{\underline{v}}(t)^T Q^{-1} - \underline{p}^T(t) G(t)) \delta\hat{\underline{v}}(t) \right) dt$$

$$+ \sum_{i=1}^{N} \left[\int_0^{T_f} \left(- \left(r(t) - C_o(t)\, \hat{\underline{x}}(t) - \sum_{j=1}^{N} C_j(t)\, \hat{\underline{y}}_j(t) \right)^T R^{-1} C_i(t) \right. \right.$$

$$\left. \left. + \mu_i^T(t, a_i) \right) \delta\hat{\underline{y}}_i(t) \right] dt$$

$$+ \int_{-a_1}^{0} \left(- \frac{d\underline{p}^T(t)}{dt} - \underline{p}^T(t)\, F(t) - \sum_{j=1}^{N} \underline{\mu}_j^T(0,-t) \right) \delta\hat{\underline{x}}(t)\, dt$$

$$+ \sum_{i=1}^{N-1} \left[\int_{-a_{i+1}}^{-a_i} \left(- \frac{d\underline{p}^T(t)}{dt} - \underline{p}^T(t)\, F(t) - \sum_{j=i+1}^{N} \underline{\mu}_j^T(0,-t) \right) \delta\hat{\underline{x}}(t)\, dt \right]$$

$$+ \sum_{j=1}^{N} \left[\int_0^{a_j} \underline{\mu}_j^T(T_f, \tau)\, \delta\hat{\underline{x}}(T_f - \tau)\, d\tau \right] + \sum_{j=1}^{N} \left[\int_0^{T_f} \int_0^{a_j} \left(\frac{\partial \underline{\mu}_j^T(t,\tau)}{\partial t} \right. \right.$$

$$\left. \left. + \frac{\partial \underline{\mu}_j^T(t,\tau)}{\partial \tau} \right) \delta\phi_j(t,\tau)\, dt d\tau \right]. \qquad (25)$$

We shall now make a series of arguments to cause the ϵ variation of the functional to vanish. We shall require that the Lagrangian multiplier functions satisfy some equations so that the coefficients of some of the variations vanish.

First we require the delay constraints to have the functional form

$$\underline{\mu}_i(t,\tau) = \underline{\mu}_{o_i}(t-\tau) \qquad (26)$$

so that the last term in the equation vanishes identically ($\underline{\mu}_i$ is the adjoint function for the delay equation). Furthermore, we require that

$$\underline{\mu}_{o_i}(t-\tau) = 0 \tag{27}$$

$$a_i < \tau < T_f \tag{28}$$

and, for $0 < t < T_f$,

$$\underline{\mu}_{o_i}(t-a_i) = C_i^T(t)\, R^{-1} \left(\underline{r}(t) - C_o(t)\, \hat{\underline{x}}(t) - \sum_{j=1}^{N} C_j(t)\, \underline{y}_j(t) \right) . \tag{29}$$

This completes our restrictions of the Lagrangian multipliers for the delay constraints. Notice that the restrictions may be made independently of all the other constraints, including the state-equation constraint.

Now we shall impose some restrictions on the Lagrangian multiplier for the state-equation constraint. First we impose the restriction, $0 < t < T_f$,

$$\frac{d\underline{p}(t)}{dt} = F^T(t)\, \underline{p}(t) - C_o^T(t)\, R^{-1} \left(r(t) - C_o(t)\, \hat{\underline{x}}(t) - \sum_{j=1}^{N} C_j(t)\, \hat{\underline{y}}_j(t) \right) - \sum_{j=1}^{N} \underline{\mu}_{o_j}(t). \tag{30}$$

Finally, we impose restrictions for the time before the observation interval. Within this region, for $-a_1 < t < 0$, we require

$$\frac{d\underline{p}(t)}{dt} = -F^T(t)\, \underline{p}(t) - \sum_{j=1}^{N} \underline{\mu}_{o_j}(t), \tag{31}$$

and, for $-a_{i+1} < t < a_i$, $\quad i = 1, 2, \ldots, N-1$,

$$\frac{dp(t)}{dt} = -F^T(t)\, \underline{p}(t) - \sum_{j=i+1}^{N} \underline{\mu}_{o_j}(t). \tag{32}$$

As a result, we have defined $\underline{p}(t)$ over the entire interval of the process. Therefore we have

$$\begin{aligned} J(v(t), \underline{x}(-a_N)) = {} & J(\hat{\underline{v}}(t), \hat{\underline{x}}(-a_N)) \\ & + \epsilon \left\{ \left[(\hat{\underline{x}}(-a_N)) - \overline{\underline{x}}(-a_N)^T P^{-1}(-a_N) - \underline{p}^T(-a_N) \right] \delta \hat{\underline{x}}(-a_N) \right. \\ & \left. + \int_{-a_N}^{T_f} (\hat{\underline{v}}(t)^T Q^{-1} - \underline{p}^T(t) G(t))\, \delta \hat{\underline{v}}(t) + 0(\epsilon^2) \right\}. \end{aligned} \tag{33}$$

Because of the optimality of $\hat{\underline{v}}(t)$ and $\hat{\underline{x}}(-a_N)$, we have

$$\underline{p}(-a_N) = P^{-1}(-a_N)((\hat{\underline{x}}(-a_N))-\overline{\underline{x}}(-a_N)) \tag{34}$$

$$Q^{-1}\hat{v}(t) = G^T(t)\,\underline{p}(t). \tag{35}$$

Equation 34 imposes an initial boundary condition, and Eq. 35 relates the terms $\underline{v}(t)$ and $\underline{p}(t)$. By using Eq. 35, our state equation becomes

$$\frac{d\hat{\underline{x}}(t)}{dt} = F(t)\,\hat{\underline{x}}(t) + G(t)\,QG^T(t)\,\underline{p}(t). \tag{36}$$

We shall now summarize our equations determining the MAP interval estimate of the process $\underline{x}(t)$. For convenience, we shall define

$$a_o = 0$$

$$\hat{\underline{y}}_o(t) = \hat{\underline{x}}(t).$$

For $-a_N < t < T_f$, we have

$$\frac{d\hat{\underline{x}}(t)}{dt} = F(t)\,\hat{\underline{x}}(t) + G(t)\,QG^T(t)\,p(t).$$

By using the definitions stated above, we may write Eqs. 33 and 35 in the same manner. for $-a_{i+1} < t < -a_i$ these equations become

$$\frac{d\underline{p}(t)}{dt} = -F^T(t)\,\underline{p}(t) - \sum_{j=i+1}^{N} \mu_{o_j}(t),$$

where i may assume the values

$$i = 0, 1, \ldots N-1.$$

For $0 < t < T_f$, we have

$$\frac{d\underline{p}(t)}{dt} = -F^T(t)\,\underline{p}(t) - C_o(t)\,R^{-1}\left(\underline{r}(t) - \sum_{j=0}^{N} C_j(t)\,\underline{y}_j(t)\right) - \sum_{j=1}^{N} \underline{\mu}_{o_j}(t).$$

The functions $\underline{\mu}_i$ are defined to be, for $0 < \tau < a_i$,

$$\underline{\mu}_{oi}(T_f-\tau) = 0,$$

and for $0 < t < T_f$,

$$\underline{\mu}_{oi}(t-a_i) = C_i^T(t)\,R^{-1}\left(\underline{r}(t) - \sum_{j=0}^{N} C_j(t)\,\hat{\underline{y}}(t)\right).$$

The result of our derivation is a set of differential-difference equations with a two-point boundary-value condition. In the absence of any delay terms, the equations are identical to those for the interval estimator with no-memory modulation, that is, amplitude modulation. At the present time, the equation may be solved only for the case of an equally spaced delay, $\alpha_i = i\Delta\alpha$. We are now working on more general methods of solution, the performance of the estimator in a delay environment, and realizable filters for such an environment.

A. B. Baggeroer

References

1. A. C. Bryson and M. Frazier, "Smoothing for Linear and Nonlinear Dynamic Systems," Proc. Optimum Systems Conference, Wright-Patterson Air Force Base, Ohio, September, 1962.
2. R. E. Kalman and R. S. Bucy, "New Results in Linear Filtering and Prediction Theory," ASME Paper 60-JAC, May 31, 1960.
3. M. Athans and P. Falb, Optimal Control (McGraw-Hill Book Company, Inc., New York, 1966).
4. A. Baggeroer, "Maximum A Posteriori Interval Estimation," WESCON/66 Technical Papers, Session 7, Paper 7/3.

XXVIII. SPEECH COMMUNICATION*

Academic and Research Staff

Prof. K. N. Stevens	Prof. A. V. Oppenheim	C.-W. Kim
Prof. M. Halle	Dr. Margaret Bullowa	N. Benhaim
Prof. W. L. Henke	Dr. Paula Menyuk	J. S. Perkell
Prof. D. H. Klatt	Dr. J. Suzuki†	Eleanor C. River
	K. Fintoft‡	

Graduate Students

J. K. Frediani	L. R. Rabiner	M. Y. Weidner
A. J. Goldberg	R. S. Tomlinson	J. J. Wolf

RESEARCH OBJECTIVES

The objective of the research in speech communication is to gain an understanding of the processes whereby (a) discrete linguistic entities are encoded into speech by human talkers, and (b) speech signals are decoded into meaningful linguistic units by human listeners. Our general approach is to formulate theories or hypotheses regarding certain aspects of the speech processes, obtain experimental data to verify these hypotheses, and simulate models of the processes and compare the performances of the models and of human talkers or listeners. Research in progress or recently completed includes: observations of the acoustic and articulatory aspects of speech production in English and in other languages through spectrographic analysis; study of cineradiographic data and measurement of air-flow events; study of the perception of speech sounds by children and examination of the acoustic properties of the utterances of children; computer simulation of articulatory movements in speech; investigation of the mechanism of larynx operation through computer modeling and acoustic analysis; examination of new procedures for analysis of speech signals using deconvolution techniques; experimental studies of the perception of vowel sounds; speech synthesis by rule with a computer-simulated terminal analog synthesizer; a re-examination of the system of features used to describe the phonetic segments of language; and the development and improvement of interface equipment for spectral analysis of speech with a computer and for synthesis of speech from computer-generated control signals.

K. N. Stevens, M. Halle

A. REAL-TIME SPECTRAL INPUT SYSTEM FOR COMPUTER ANALYSIS OF SPEECH

On-line operation of a real-time spectral input system for computer analysis of speech was achieved during the period covered by this report. The system, mentioned in a previous report,[1] was used with a bank of 36 bandpass filters and a PDP-1 computer to analyze recorded utterances played back in real time. A block diagram of the complete analyzing configuration is shown in Fig. XXVIII-1.

*This work was supported principally by the U.S. Air Force (Electronic Systems Division) under Contract AF19(628)-5661, and in part by the National Institutes of Health (Grant 5-RO1-NB-04332-04).

†On leave from Radio Research Laboratories, Tokyo, Japan.

‡On leave from Norges Laererhogskole, Trondheim, Norway.

Operation of the system is, at present, completely under program control. When in data-taking mode, the program continually pulses the real-time analyzer, thereby causing it to read and convert the output of each channel. Channel stepping is performed

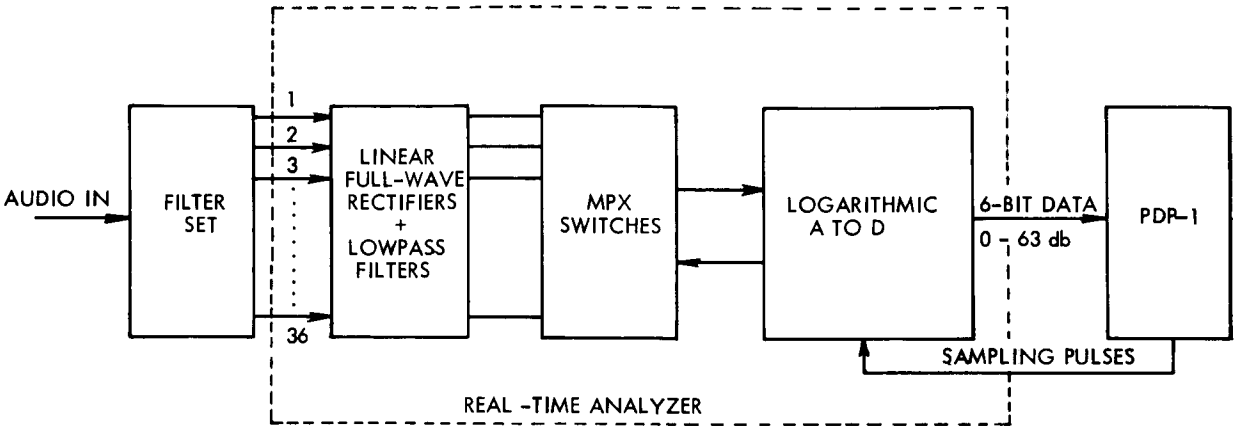

Fig. XXVIII-1. Diagram of the real-time analyzer as used with analyzing filter bank and PDP-1 computer.

at the end of each conversion by the internal logic of the analyzer. Digitized channel information is sent back to the computer and stored in the core. When the sum of the outputs of three selected channels rises above a set threshold, the program recognizes the onset of speech. Termination of speech is similarly recognized. The beginning and end thresholds and the sampling rate are program parameters. At present, 4000 words of data may be stored, representing approximately 3.4 seconds of speech at a 10-msec sampling rate. The program can display any given 36-channel spectrum sample and also each spectrum sample in sequence throughout the utterance. A display of selected channels outputs as a function of time is also available.

N. Benhaim, Eleanor C. River

References

1. N. Benhaim, "Real-Time Spectral Input System," Quarterly Progress Report No. 80, Research Laboratory of Electronics, M.I.T., January 15, 1966, p. 197.

B. CHILDREN'S PERCEPTION OF A SET OF VOWELS

In experiments comparing identification and discrimination functions for vowels in isolation and in consonantal context, it has recently been found that vowels in context tend to be perceived in a categorial fashion. Discrimination functions are characterized by peaks at the phoneme boundaries, whereas isolated vowels form a perceptual continuum. It is felt that these results support the theory that experience with the

generation of speech movements and with simultaneous observation of the acoustic consequences of these movements plays an important role in shaping the process whereby speech is perceived.[1]

In the case of a child the acoustic consequences of his speech movements differ quite radically from the consequences produced by the adults in his environment. The question asked in this experiment was: Are the phoneme boundaries for a set of vowels in consonantal context the same for the child as for the adult. Six children and 5 adults constituted the population of this study. The children, three boys and three girls, ranged in age from 5 to 11 years.

Each subject listened through earphones to 90 stimuli consisting of random presentation of 9 different synthetically produced CVC syllables. Two of the 9 syllables (steps 2 and 8) formed a typical version of b/i/l and b/I/l spoken by an American male. Five additional stimuli were produced by computing a set of interpolated formant contours that were equally spaced between b/i/l and b/I/l (steps 3-7). Two more were produced by extrapolating one step before b/i/l and one step after b/I/l (steps 1 and 9). These step sizes were equal to those between the interpolated stimuli. This produced 9 different syllables. (For a more detailed discussion of the stimuli see Stevens.[1])

Three black and white drawings pasted to a black surface were placed before each subject and identified by the experimenter as b/i/l (a truck), b/I/l (a bird's bill) and b/ɛ/l (a church bell). The subjects were asked to point to the picture that the speaker was naming. The percentage of judgments for each subject as /i/, /I/ or /ɛ/ for each of the 9 steps was then computed and a mean for adults and children was obtained. Table XXVIII-1 gives the numerical results.

Table XXVIII-1. Per cent of judgments /i/, /I/, /ɛ/ as a function of step.

Step	ADULTS % i	CHILDREN % i	ADULTS % I	CHILDREN % I	ADULTS % ɛ	CHILDREN % ɛ
1	100	100	0	0	0	0
2	100	97	0	3	0	0
3	79	90	20	9*	1	0
4	62	73	36	27	2	0
5	15	24	81	75	3	0
6	0	5	97	95	3	0
7	0	1	95	98	5	1
8	0	0	86	85	14	15
9	0	0	42	32	58	68

*p > .05.

There were no significant differences between adults' and children's judgments on each step except for step 3 as computed by chi-square comparison. The tendency is for the adults to begin to perceive /I/ "sooner" in the continuum than the children, and for the children to do so with /ɛ/, although not significantly so. Figure XXVIII-2 shows that phoneme boundaries for the vowels in this experiment are the same, in terms of steps, for the children and for adults.

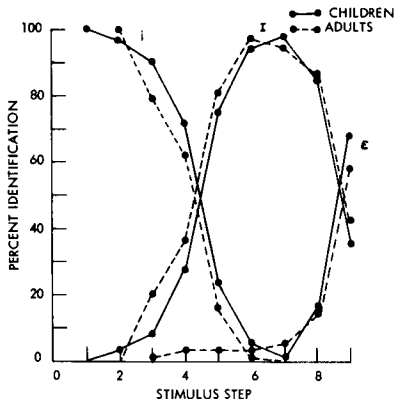

Fig. XXVIII-2. Phoneme boundaries for vowels in the experiment.

The answer to the question that was raised, therefore, is yes for the set of vowels in this experiment. This leaves us, however, with the task of trying to explain how the child can identify vowels in much the same way as adults when he produces these vowels so that they are, in terms of formant frequency, a poor match with those of the adults. We might also ask how the adult identifies the vowels produced by children.

There are several possibilities concerning the perceptual cues that may be in operation. Although the child's vowels do not match the adult's, his set of vowels are clearly differentiated from each other in formant frequencies. Furthermore, the direction that differences take for F_1 and F_2 between vowels is the same for adults and children. Also, there is no overlap between the vowels produced by children and adults. That is, for example, the /I/ produced by the child is not like the /i/ produced by the adult in terms of formant frequencies. Therefore, a system of distinctive differences exists between the vowels produced by children, as well as between the vowels of children and adults. (The data will be reported in detail elsewhere.[2]) Two further speculations would be that acoustic characteristics other than formant frequencies provide cues for identification and that articulatory gestures used by children to produce the vowels might be analogous to those used by adults. The first speculation is now being examined from data obtained in a previous experiment.[3] We have, at this time, no data on the articulatory gestures of children. We have the task of identifying those parameters by which the

child matches what he produces to what the adult produces and those by which the adult matches what he produces to what the child produces so that there is mutual understanding, which does, in fact, exist.

We have found that the child identifies certain vowels in consonantal context categorially, as does the adult, and that the boundaries of these vowels are strikingly similar for both children and adults. We would like to explore this question with other speech sounds; primarily, with those sounds that create difficulty developmentally, such as w, r, l, y.

Paula Menyuk

References

1. K. N. Stevens, "On the Relations between Speech Movements and Speech Perception, a paper presented at the 18th International Congress of Psychology, Moscow, August 1966.
2. Paula Menyuk, "Children's Production and Perception of a Set of Vowels" (in preparation).
3. Paula Menyuk, "Cues Used in the Perception and Production of Speech by Children," Quarterly Progress Report No. 77, Research Laboratory of Electronics, M.I.T., April 15, 1965, pp. 310-313.

C. ARTICULATORY ACTIVITY AND AIR FLOW DURING THE PRODUCTION OF FRICATIVE CONSONANTS

One of the principal objectives of research in speech is to understand the mechanism underlying the control of the speech-generating system. Several kinds of experimental observations can be made in order to investigate the nature of this process. Among these, air-flow and pressure measurements can provide useful information concerning the activities of the various articulatory structures. The purpose of this report is to describe one result of a larger study that has been reported on elsewhere.[1] Measurements of air flow during speech production have led to certain conclusions about the manner in which voiceless fricatives are produced in intervocalic position.

A face mask incorporating a linear flow resistance and a pressure transducer was used to measure the volume velocity of the air stream expelled from the lungs during speech production.[1-3] Figure XXVIII-3 is an example of the graphic record for the utterance "Say the word /hə'fɑf/ again." A double peak in the air flow occurs for each /f/ phone as indicated by the arrows. This type of double peak is characteristic of the voiceless fricatives /f, θ, s, š/ in the context of this frame sentence for all 5 speakers studied.

The double peak is probably a consequence of the relative timing of laryngeal and articulatory gestures. In Fig. XXVIII-4 a tracing of average air flow is compared with

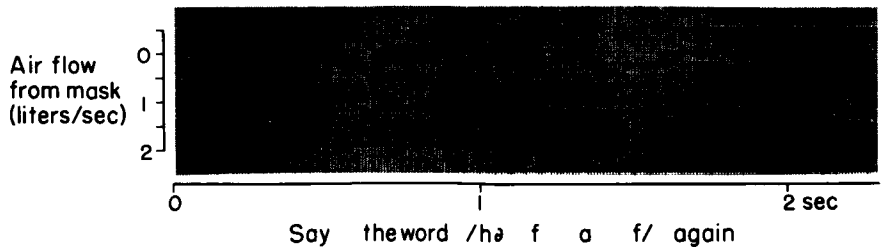

Fig. XXVIII-3. Example of the air-flow record (inverted) from the graphic recorder for the utterance "Say the word /hə'fɑf/ again." (Speaker: KNS.)

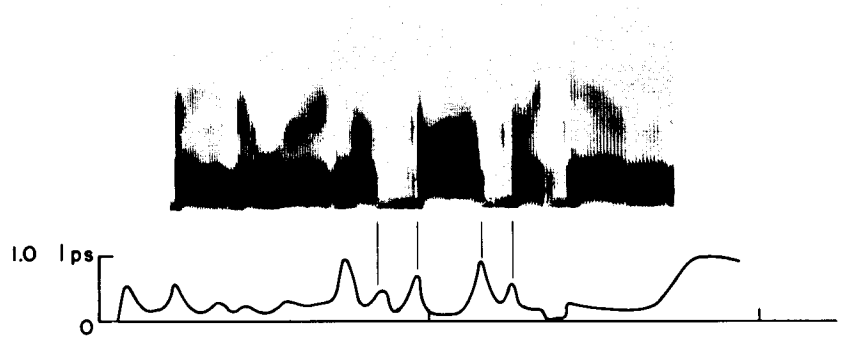

Fig. XXVIII-4. Spectrogram and tracing of average air flow utterance "Say the word /hə'fɑf/ again." The lines indicate the times of cessation and initiation of voicing in the syllable /fɑf/.

a spectrogram of the utterance to indicate the times of voicing onset and cessation. The lines that mark these times occur approximately at air-flow peaks.

An interpretation of these results in articulatory terms is suggested in Fig. XXVIII-5. During the unstressed vowel/ə/, the glottis begins to open while the vocal cords continue to vibrate. At the first peak in air flow (indicated by the first dashed line) the lower teeth begin to make contact with the upper lip, and the constriction that is formed causes a rise in mouth pressure. As a result, vocal-cord vibration ceases rather abruptly. The supraglottal articulator continues to constrict until vocal-tract resistance reaches a maximum value. The articulator then begins to move away in anticipation of the next phone, thereby lowering vocal-tract resistance. Air flow through the glottis thus increases, the vocal cords approximate as a consequence of the reduced pressure, and vocal-cord vibration begins (at the point indicated by the second dashed line). Finally, the vocal cords assume a mode of vibration which is characteristic of the vowel, with higher glottal resistance. A similar pattern of the air flow occurs in the

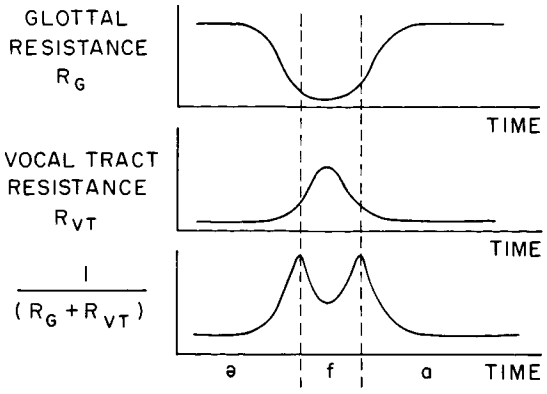

Fig. XXVIII-5. Interpretation of the articulatory events causing a double peak in the air-flow trace for a voiceless fricative in intervocalic position. Total resistance to flow is assumed to be the sum of glottal resistance and vocal-tract resistance. Dashed lines indicate times of cessation and initiation of voicing.

final /f/ of the utterance illustrated in Fig. XXVIII-4.

The voiced fricatives, /vð z ž/ display similar air-flow traces, except that air flow is reduced relative to that of the voiceless fricatives, and the double peak is less pronounced. Voicing occurs throughout these sounds, but the flow becomes higher than for a vowel in spite of the turbulence-producing supraglottal constriction. Thus the laryngeal mode of vibration for voiced fricatives must differ from that occurring during vowels; the vocal cords probably remain separated during a vibratory cycle, with the result that there is an appreciable DC component to the flow.

In the course of the study,[1] data were gathered on other consonants of English. Some consonant clusters were recorded and found to have air-flow traces exhibiting coarticulation effects. Word stress was found to have some effect on air flow. The data suggest certain limits on the speed of reaction and coordination of larynx and vocal-tract structures during speech production.

The experimental data reported here were obtained at the Harvard School of Public Health, in collaboration with Dr. Jere Mead of its Department of Physiology.

D. H. Klatt

References

1. D. H. Klatt, K. N. Stevens, and J. Mead, "Studies of Articulatory Activity and Air Flow during Speech," Proc. Conference on Sound Production in Man, New York Academy of Sciences, 1966 (in press).

2. J. F. Lubker and K. L. Moll, "Simultaneous Oral-Nasal Air Flow Measurements and Cinefluorographic Observations during Speech Production," The Cleft Palate Journal, Vol. 2, pp. 257-273, July 1965.

3. N. Isshiki and R. Ringel, "Air Flow during the Production of Selected Consonants," J. Speech Hearing Res. 7, 233 (1964).

XXIX. LINGUISTICS*

Academic and Research Staff

Prof. R. Jakobson
Prof. M. Halle
Prof. S. Bromberger
Prof. J. A. Fodor
Prof. J. J. Katz
Prof. R. P. V. Kiparsky
Prof. E. S. Klima
Prof. G. H. Matthews
Prof. Krystyna Pomorska
Prof. J. R. Ross
Prof. J. H. Sledd
Dr. J. V. Canfield
Dr. Elinor K. Charney
Dr. J. B. Fraser
Dr. M. F. Garrett
Dr. J. S. Gruber
Dr. A. Schwartz
Dr. N. V. Smith
Dr. D. E. Walker
Dr. Anna Wierzbicka
Dr. Kay R. M. Williamson
C-J. N. Bailey
N. R. Cattell
B. E. Gaines
J-C. Milner
J. J. Viertel

Graduate Students

A. Akmajian
S. R. Anderson
J. S. Bowers
M. K. Brame
E. W. Browne III
R. J. Carter
S. W-C. Chan
P. G. Chapin
P. W. Culicover
Janet P. Dean
R. P. G. De Rijk
R. C. Dougherty
J. E. Emonds
J. L. Fidelholtz
R. Goldfield
L. N. Gross
J. W. Harris
T. R. Hofmann
I. J. Howard
R. S. Jackendoff
R. S. Kayne
J. P. Kimball
Carol A. S. Kiparsky
R. Kirk
J. R. Lackner
Amy E. Myers
A. J. Naro
D. M. Perlmutter
J. T. Ritter
M. S. Snow
R. J. Stanley
R. J. Thiersch
F. J. Vandamme
Nancy Woo

RESEARCH OBJECTIVES

There have been two main traditions in the study of language in modern times. The first is the tradition of "universal" or "philosophical grammar," which flourished in the seventeenth and eighteenth centuries in intimate connection with philosophy and speculative psychology. The second is the tradition of modern linguistics, a nineteenth and twentieth century phenomenon that was also closely interwoven with the philosophy, psychology, and anthropology of its day. Philosophical grammar was concerned with general, universal principles of language structure; it attempted to ground these principles in a theory of mental processes, and to illustrate them with detailed study of particular languages. By modern standards, the work lacked care and attention to detail, and the conclusions that were reached, though often highly insightful, were deficient in empirical support and sharpness of formulation. In comparison, modern nineteenth and twentieth century linguistics has achieved a much higher standard of rigor, and has accumulated linguistic data of an incomparably greater scope and variety. It has been limited, however, by a much narrower interpretation of the purposes and goals of linguistic science. It has eschewed theory construction in favor of elaboration of methods of analysis, and it has not been concerned with linguistic universals – often, in fact, it has denied that there are, in any significant sense, genuine and deep universal principles that constrain the form and use of human language.

*This work was supported principally by the U.S. Air Force (Electronics Systems Division) under Contract AF 19(628)-2487; and in part by the Joint Services Electronics Programs (U.S. Army, U.S. Navy, and U.S. Air Force) under Contract DA 36-039-AMC-03200(E), the National Science Foundation (Grant GK-835), the National Institutes of Health (Grant 2 PO1 MH-04737-06), and the National Aeronautics and Space Administration (Grant NsG-496).

The work in linguistics at the Massachusetts Institute of Technology represents, in a sense, a synthesis of these two major traditions. In terms of its general goals and even many of its specific hypotheses, this work has a very classical flavor. But in the range and reliability of evidence and precision of formulation, this work accepts and attempts to surpass the standards of modern structuralism.

For classical linguistics, a central property of human language is what we can call its "creative" aspect, that is, its unboundedness and freedom from stimulus control. Under ordinary circumstances, what a person says is not determined by the stimuli that impinge on him or by identifiable physiological states, to any significant degree. The unboundedness of normal language is evident from the fact that almost every linguistic utterance produced and understood is quite new, not similar in any physically defined sense to those that have been produced in the past experience of the language user, and not conforming to familiar or memorized patterns, in any meaningful sense of the notion "pattern." Nor are these utterances "generalizations" from past experience, in any sense of "generalization" known to psychology or philosophy. Nor can language use be described in terms of "habits" or "repertoires of responses." In recognizing these facts, philosophical grammar was entirely correct and to the point.

To account for this creative aspect of normal language use, we must attribute to the language user knowledge of a certain organized system of rules that establish a sound-meaning relation for an infinite class of sentences. This knowledge is, of course, quite unconscious, but it is nonetheless perfectly real. Thus it is quite likely that no one reading this report has ever seen, heard, or produced the sentence

(1) What disturbed John was being disregarded by everyone.

Yet every reader will understand that the sentence may be roughly paraphrased by either (2) or (3):

(2) Everyone was disregarding the thing that disturbed John.

(3) The fact that everyone was disregarding him disturbed John.

Thus sentence (1) is ambiguous, its possible interpretations being (2) or (3). If the word "our" is inserted in (1), giving (4), the sentence is unambiguous.

(4) What disturbed John was our being disregarded by everyone.

The interpretation of (4) can only be along the lines of (3), with "him" replaced by "us." Or, to choose an example from a totally different sphere of language, speakers of English would know that the plural of the word dap is daps, whereas that of linch is linches (with es rather than s), in spite of the fact that most of the speakers would neither know the meanings of these words nor have heard them before.

A speaker of English has knowledge of these facts and numerous others without having been exposed to these sentences or to any explicit "teaching." He has mastered a system of rules that determine both the phonetic form of sentences (1)-(4) and their various semantic interpretations. The first task of the linguist who is investigating the structure of English is to try to determine this system of rules, the system that is called the "generative grammar of English." This generative grammar has in some manner been internalized by every speaker of English; it determines the pairing of sound and meaning for an indefinitely large range of possible sentences. It is this internalized generative grammar that makes possible the normal, "creative" use of language.

The discovery of the generative grammar of English, and other languages, is, however, only the first task that faces the linguist. To the extent that such grammars have been developed and validated, the linguist can then turn to the question of how they are put to use, by the speaker or hearer, in normal conversation, in literature, in internal monologue, and so on. Furthermore, he can turn to the basic problem of classical linguistics: What are the universal principles that limit the form of such generative grammars? Clearly, there must be universal principles with a very narrow and limiting character. If this were not true, it would be impossible for the child, presented with

scattered samples of a language for an extremely short period, to determine for himself the generative grammar of this language. But this is a task that normal humans accomplish with great facility. This indicates that they must approach the task forearmed with highly specific advance knowledge (obviously, unconscious) of the possible form that a generative grammar must assume. To put it loosely, although the child cannot "know" in advance whether the language to which he is exposed is English, Chinese, and so on, he must "know" that it is a "human language" of a highly special sort, which can only vary in very restricted ways. The problem of "universal grammar," now, as in the seventeenth century, is to determine the principles that limit the variety of human language and make possible the acquisition of language. To the extent that such principles can be formulated and validated, we gain insight of an unparalleled kind into the innately determined character of human mental processes.

We feel that recent work, much of it carried out at M. I. T., makes it possible to formulate a fairly precise theory of universal grammar in this sense, a theory which is, furthermore, reasonably well supported by substantial empirical evidence from a variety of languages. The major goal of our research, then, is to sharpen and deepen the theory of generative grammar, and to use it as a basis for the study of cognitive processes.

Since many of the problems of language lie in the area in which several disciplines overlap, an adequate and exhaustive treatment of language demands close cooperation of linguistics with other sciences. The inquiry into the structural principles of human language suggests a comparison of these principles with those of other sign systems, which, in turn, leads naturally to the elaboration of a general theory of signs, semiotics. Here linguistics touches upon problems that have been studied by philosophy. Other problems of interest to logicians – and also to mathematicians – are touched upon in the studies devoted to the formal features of a general theory of language. The study of language in its poetic function brings linguistics into contact with the theory and history of literature. The social function of language cannot be properly illuminated without the help of anthropologists and sociologists. The problems that are common to linguistics and the theory of communication, the psychology of language, the acoustics and physiology of speech, and the study of language disturbances are too well known to need further comment here. The exploration of these interdisciplinary problems, a major objective of this group, will be of benefit not only to linguistics; it is certain to provide workers in the other fields with stimulating insight and new methods of attack, as well as to suggest to them new problems for investigation and fruitful reformulations of questions that have been asked for a long time.

M. Halle, N. A. Chomsky

A. INITIAL CLUSTERS IN ENGLISH

In examining the range of possible consonant clusters at the beginning of a word in English, we find not merely a lot of redundancy (as is well known), but a particular kind of redundancy, a type that allows us to re-analyze these clusters as single segments. This leads us to suspect that the structure of words may be much simpler than has yet been suggested. Chomsky and Halle[1] have shown how and why the complex vowel nuclei of syllables must be derived from simple vocalic segments and in this report we extend this same concept, finding that many complex consonant clusters can be derived also from single segments.

1. Preliminary

In English, all words begin with the following sequence: (C = a consonant, V = a vowel;

parentheses enclose optional elements and brackets alternate possibilities. The positions are numbered for ease of reference.)

(1)
$$\underset{1}{(s)}\ \underset{2}{(C)}\ \underset{3}{\left(\left\{\begin{matrix}l\\r\\w\\y\end{matrix}\right\}\right)}\ V \ldots$$

Not all possibilities of the formula above are realized, however – there are principled restrictions on what may occur with what. For example, l never occurs with a preceding dental stop – any word that began *dl... would simply not be an English word.

Various methods have been proposed to schematize the possibilities of occurrence and non-occurrence, ranging from (earliest) a simple list of possible initial clusters to (later) what we may call "phoneme order charts" as exemplified by Harris[2] to (recently) morpheme structure rules which effectively forbid certain sequences of elements. Another method of expressing these restrictions is proposed below.

It is well to notice first that the y following a consonant is itself always followed by [u] as in beauty, cute and is unlike the other position 3 possibilities in that it does occur after voiced non-obstruents as in view, mute, lieu, new. (In some dialects this y has dropped after dentals.) For these reasons, then, we may consider it to be part of the [u] which necessarily follows it, treating the combination as a single vowel in the underlying representation. This treatment may be found in Chomsky and Halle,[1] and will not be duplicated here.

2. Position 3 Elements

We may now revise the original statement (1) of possibilities of word-beginnings to (such statements we shall call 'canonical forms'):

(2)
$$\underset{1}{(s)}\ \underset{2}{(C)}\ \underset{3}{\left(\left\{\begin{matrix}l\\r\\w\end{matrix}\right\}\right)}\ V \ldots$$

If we ignore the s in position 1 for the moment, we see that in position 3 there are 4 possibilities; either nothing at all (which I shall call $\emptyset$), r, l, or w. A choice between 4 possibilities involves 2 bits of information. The maximally simple description would be obtained if we could use but 2 distinctive features to specify which possibility is found in a particular word.

Arranging the possibilities as in

(3)
$$\begin{array}{c|c} r & l \\ \hline w & \emptyset \end{array},$$

we see that in the horizontal dimension, r and w oppose l in flatness.[3] And in the vertical dimension, there is a distinction in both consonantality and vocalicity between r and l on the one hand and w on the other. Let us use the feature vocalicity for the vertical dimension. We then have (vertical bars enclose a conjunction of features, vocl = vocalicity, and flat = flatness):

(4) $$r = \left|\begin{matrix}+\text{vocl}\\+\text{flat}\end{matrix}\right|, \qquad l = \left|\begin{matrix}+\text{vocl}\\-\text{flat}\end{matrix}\right|, \qquad w = \left|\begin{matrix}-\text{vocl}\\+\text{flat}\end{matrix}\right|$$

and the last combination, $\left|\begin{matrix}-\text{vocl}\\-\text{flat}\end{matrix}\right|$, is realized as $\emptyset$.

If we can specify that a consonant occupies position 2 by marking $|+\text{cons}|$, then the feature vocl, along with flat, is not used in specifying anything about that segment. It is proposed, then, that rather than use a separate segment (position 3) to hold the 2 features needed to specify how that segment is to be actualized, we now place these features in the second segment and thus simplify the canonical form of words in English. A segmentalization rule will be introduced to spell the features flat and vocl out of a consonantal segment into a position immediately following it. The canonical form for English is thus

(5) $$\underset{1}{(s)}\ \underset{2}{(C)}\ V \ldots$$

This segmentalization rule is placed, of course, after the stress assignment rule and simplifies it by allowing a definition of a strong cluster as "2 or more $|+\text{cons}|$ segments" instead of "any cluster that is not a weak cluster, where a weak cluster is $C(\left\{\begin{matrix}l\\r\\w\end{matrix}\right\})$".[4] The problem in stress assignment where ll must be a strong cluster (e.g., costello) in spite of its natural inclusion in the formulation of a weak cluster is now nonexistent, as each l well have to be a separate segment. We are assuming that the segmentalization rules also account for those medial and final clusters that are the same as permitted initial ones. As will be seen in section 5, there is a principled restriction forbidding initial clusters composed of any combination of r, l, or w. In particular, there can be no ll initial. Hence, if ll occurs medially, it must be 2 segments: one associated with the preceding vowel, and the other an initial, associated with the following vowel.

3. Remarks

There are several points that should be remarked upon here. First, notice that only by using an arrangement such as (3) can we specify both how position 3 is realized (as r, l, or w) and whether or not there is a position 3 type segment by using only 2 features. Any other system must use 2 features to contrast the 3 possibilities r, l, and w and one additional feature to specify the existence of nonexistence of the

position 3 segment. That is, to specify whether a segment after a consonant and before a vowel is a position 3 item or simply a vowel or a consonant, we would need one additional feature. For example, we must specify a segment to be |+cons| in addition to being $\left|\begin{matrix}+\text{flat}\\+\text{vocl}\end{matrix}\right|$ in order that r is output rather than u or o, whereas with the present system the features $\left|\begin{matrix}+\text{flat}\\+\text{vocl}\end{matrix}\right|$ are located in the position 2 segment and the extra feature needed in the earlier system is inserted by the segmentalization rule. Of course, using 3 features to specify what 2 can specify entails some redundancy that will have to be expressed by rule.[6]

Another point is that a maximally efficient set of distinctive features can be hoped for only if each feature divides roughly into halves the classes defined by other features. Heretofore, this has been conspicuously lacking between the features cons and vocl, the classes defined by one being almost duplicated by the other. With this change, however, where we previously had one consonant, $\left|\begin{matrix}+\text{cons}\\-\text{vocl}\end{matrix}\right|$, we now have, in general, 4 consonantal |+cons| segments,

(6)

	k	kr	kl	kw
cons	+	+	+	+
vocl	−	+	+	−
flat	−	+	−	+

and the class defined by |+cons| is roughly divided in half by vocl. Both of these simplifications are facets of the same inner simplification.

It should also be remarked that using the feature vocl in the way we do in some sense imputes a different definition to it. Of course, we so use it only on a very deep level, where features are little more than abstract markers. If we want to put the requirement of phonetic realism on the underlying forms, we shall either have to find another feature to play the role of vocl in this analysis or alternatively re-define vocl so that tr can be both vocalic and consonantal. I believe that the second alternative would be more productive, as we would then not need an "erasure" rule to mark position 2 segments |-vocl| (after the vocl has been segmentalized, of course). This is not unreasonable, as we cannot have an erasure rule to mark position 2 segments |-flat| because a position 2 consonant is always rounded when followed by an r. Flatness also involves itself in the difference between the t and the ch series, which accounts in part for s becoming sh when followed by r and for the similarity in acoustic impression between trip and chip, etc. On the other hand, we shall need an erasure rule to mark position 2 segments |-strid|, as stridency is missing in the nasal in smile or snide.

4. Leading s

Returning now to the optional s at the beginning of a word, we may notice that it contrasts only with its absence. This is just 1 bit of information or 1 distinctive feature — all else is redundant. We need only 1 unused feature of its following consonant to use in

specifying its presence. There are several possibilities, but let us assume that stridency (strid) is available on this deep level, i.e., that f and s do not contrast with anything by virtue of their values of stridency. (We shall soon return to s and θ.) Then we may say that if a consonant is strident, an s is created before it by the s-segmentalization rule. To develop s alone as an initial, the full form of s is entered in the dictionary. The s-segmentalization rule will add an s before it and geminate simplification will reduce the resultant ss to s.

The s-segmentalization rule is formalized as[7]

(7) $$\left|\begin{matrix}+\text{strid}\\ \left\{\begin{matrix}-\text{voic}\\ +\text{nasl}\end{matrix}\right\}\end{matrix}\right| \Longrightarrow \left|\begin{matrix}+\text{cons}\\ -\text{vocl}\\ +\text{strid}\\ -\text{voic}\\ +\text{cont}\end{matrix}\right| + 1$$

and is followed by the stridency-erasure rule

(8) $$\left|\begin{matrix}-\text{cont}\\ +\text{nasl}\end{matrix}\right| \longrightarrow |-\text{strid}| / (|+\text{strid}|) \_\_\_\_$$

D. Perlmutter has pointed out that, by such an arrangement, the effect of a morpheme structure rule is obtained at no extra cost. If a strident b ($\underline{b}_s$) occurs in the dictionary, rule (7) does not apply and rule (8) erases the stridency. In contrast, if p_s (a strident p) occurs, rule (7) applies to form sp_s, and rule (8) applies only to the p_s by virtue of the disjunctive ordering (roughly, if a parenthesized term in a rule environment can be matched by some part of the material to which the rule is to be applied, then the rule cannot be applied without so matching).

Consider the case in which positions 1, 2, 3 are all filled. While we previously needed only |+cons| in first segment to specify it as s, we now need 1 feature, strid on both s and non-s-beginning words. This means that in the case of the leading s, our present system will require more feature mentions in the dictionary, although the use of markedness can make the 2 systems equivalent again. I am inclined to believe that we now have the proper result. A word with a leading s carries no more and no less information than one without s. If the number of binary distinctions needed to identify a word is any function of the information content (or "surprise value") of that word, the s-less and s-ful words must be specified with the same number of features.

5. Details

To meet the facts of English, we must disallow the following combinations.

(9)

position 2	position 3
labial	w
dental	l
voiced continuant	any (i.e., r, l, or w)

By effecting this restriction before the segmentalization rule applies, we can handle this with segment-structure rules that are equivalent to the morpheme structure rules that were necessary for handling these restrictions before. The only difference between the 2 systems is that now we need not assign values for the features vocl and flat in position 2, as we had to before. The following rules will suffice, but are not the only ones that will do so. The chosen ones are interesting in that they approximate the acoustic impressions experienced by a native when hearing forbidden clusters:

(10) $$\begin{vmatrix} +\text{cons} \\ +\text{grav} \\ +\text{diff} \\ \underline{+\text{flat}} \end{vmatrix} \longrightarrow |-\text{vocl}|$$

(11) $$\begin{vmatrix} +\text{cons} \\ +\text{vocl} \\ -\text{flat} \\ \underline{-\text{cont}} \end{vmatrix} \longrightarrow |+\text{grav}|$$

and one that does not have this property

(12) $$\begin{vmatrix} +\text{cons} \\ +\text{cont} \\ \underline{+\text{voic}} \end{vmatrix} \longrightarrow \begin{vmatrix} -\text{flat} \\ -\text{vocl} \end{vmatrix}$$

Actually, something fundamental is happening here that is hard to capture without introducing the concept of markedness, which is beyond the scope of this introductory sketch. After labials, a w (a labial) is forbidden; after dentals, an l (a dental) is forbidden; and after voiced continuents, any position 3 item (all voiced continuents) is forbidden. Although this can be expressed with markedness, what really should be said is that w (l) is not segmentalized out of a labial (dental) because such segmentalization would be pure redundancy. All of the essential characteristics of the w (l) are already expressed by the presence of the labial (dental). Such considerations are valid for the languages with which I am familiar, but these are at best a small sample. Let us pose this as a supposition, and if it holds water for a large number of languages, we can build it into the theory of segmentalization. Note that the testing of this supposition rests on deeper analyses of languages than are now generally available, and although languages like Spanish do have pw..., the w does not result from segmentalization but derives from an underlying vowel.[8]

But recalling how we used the s-segmentalization rule with its associated erasure rule to effect a restriction, we may ask if it is possible to play such a trick here, thereby saving the cost of these segment-structure rules. It is easy to do for rule (12) but more difficult for rules (10) and (11). The "3"-segmentalization rule will be the following.

(13) $\begin{vmatrix} +\text{cons} \\ -\text{nasl} \\ \gamma\,\text{fric} \\ -\gamma\,\text{voic} \\ \alpha\,\text{vocl} \\ \beta\,\text{flat} \end{vmatrix} \Longrightarrow 1 + \begin{vmatrix} \alpha\,\text{cons} \\ \alpha\,\text{vocl} \\ \beta\,\text{flat} \\ \vdots \end{vmatrix}$

The $|-\text{nasl}|$ forbids position 3 creation with a nasal and the γ specifications do the same for voiced fricatives. All will have to be marked $\begin{vmatrix} -\text{flat} \\ -\text{vocl} \end{vmatrix}$, which is motivation for a vocl erasure rule if this tack is taken. To disallow w after labials, we shall need as additional features (14a), and to disallow l after dentals, we shall need (14b) added to the left side of rule (13).

(14) (a) $\begin{vmatrix} +\text{diff} \\ +\text{grav} \\ +\text{vocl} \end{vmatrix}$ (b) $\begin{vmatrix} +\text{diff} \\ -\text{grav} \\ -\text{flat} \end{vmatrix}$

Addition (14a) will disallow w and y from being segmentalized out of labials, and the y will be erased anyhow to give the plain labial. Addition (14b) will disallow l and y from a dental. The derivation for the plain consonants has been supposed to originate in the underlying forms as $\begin{vmatrix} -\text{vocl} \\ -\text{flat} \end{vmatrix}$, which was spelled out as y, after which the y was erased. We see, however, that for the labials and dentals it is easier to block the w and l by also blocking[9] the y, hence the simple labials and dentals are not marked for flat and vocl, respectively. This is a verification of our original arrangement (3) of the position 3 elements. There is no clear method to combine (14a) and (14b) with (13). We can obviate the need for this by using a rule of the following form before the "3"-segmentalization rule to cause it not to apply to any segments to which this rule is applicable.

(15) $\begin{vmatrix} +\text{diff} \\ \alpha\,\text{vocl} \\ -\alpha\,\text{flat} \\ \alpha\,\text{grav} \end{vmatrix} \longrightarrow [-\text{next rule}]$

Let us consider how l, r, w are handled when they do not follow a consonant. The underlying form of l is $\begin{vmatrix} +\text{cons} \\ +\text{vocl} \\ -\text{flat} \\ \zeta \end{vmatrix}$, where ζ is the set of features necessary to make l distinct from such consonants as kl, t, n, δ. The segmentalization rule applies giving $\begin{vmatrix} +\text{cons} \\ +\text{vocl} \\ -\text{flat} \\ \zeta \end{vmatrix} \begin{vmatrix} +\text{vocl} \\ -\text{flat} \\ \xi \end{vmatrix}$ where ξ is the redundant set of features inserted in position 3 by the segmentalization rule. If the sets ξ and $\begin{vmatrix} +\text{cons} \\ \zeta \end{vmatrix}$ are the same, then the segmentalization rule will change a single l into ll and the geminate-simplification rule (which is externally motivated) will then change the ll into l. An identical process is undergone by r, except that all $|-\text{flat}|$ specifications are replaced by $|+\text{flat}|$. If for both r and l

(16) $$\zeta = \begin{vmatrix} -\text{grav} \\ +\text{diff} \\ -\text{nasl} \\ +\text{cont} \\ -\text{fric} \end{vmatrix},$$

then the complete form of the "3"-segmentalization rule is

(17) $$\begin{vmatrix} +\text{segment} \\ +\text{cons} \\ \alpha\,\text{vocl} \\ \beta\,\text{flat} \\ -\text{nasl} \end{vmatrix} \Longrightarrow 1 + \begin{vmatrix} \alpha\,\text{vocl} \\ \beta\,\text{flat} \\ \alpha\,\text{cons} \\ -\alpha\,\text{grav} \\ +\text{diff} \\ -\text{nasl} \\ +\text{cont} \\ -\text{fric} \end{vmatrix}$$

Notice that in the more traditional analysis employing morpheme structure rules there was a large number of consonants, $\begin{vmatrix} +\text{cons} \\ -\text{vocl} \end{vmatrix}$, but only 2 liquids, $\begin{vmatrix} +\text{cons} \\ +\text{vocl} \end{vmatrix}$, and as a result the 2 liquids r and l could be specified by only 3 features apiece, while most other consonants required more. In this analysis, the number of liquids is comparable to the number of consonants (kl, kr, etc. are now liquids on the more abstract levels) and the 2 "simple liquids," r and l, must be specified to an extent that is comparable to the specification of a simple stop.

The simple glide w, $\begin{vmatrix} -\text{cons} \\ -\text{vocl} \\ +\text{flat} \end{vmatrix}$, is unaffected by the "3"-segmentalization rule because this rule affects only $|+\text{cons}|$ segments. It may seem surprising, at first, that the treatment required of simple w by this solution is not parallel to the treatment of simple r and l, but this nonparallelness is also found in the data. A (position 3) w after a consonant is never followed by U' ([u] or [ʊ], usually spelled oo). If a w is in position 2 (i.e., not following a consonant), such a vowel following is possible, e.g., woo, woozy, wood, would, wool, woof. To explain these data within the framework of morpheme structure rules is considerably more difficult than rule (18) placed before "3"-segmentalization.

(18) $$\begin{vmatrix} +\text{cons} \\ -\text{vocl} \end{vmatrix} \longrightarrow |-\text{flat}| \;/\; \underline{\quad} \; \text{U'}$$

This rule will also enable us to explain why there is no w in two [tu] in contrast to the w in twin, twelve, twain, between, etc. (courtesy of D. Perlmutter). Further, notice that we have gained without cost the effect of a morpheme structure rule which forbids all initial combinations of r, l, and w.

The treatment of s will solve 2 problems that are lurking in the background of the segment-structure rules mentioned above. First, s being a dental, it ought not to occur with l yet it does (and is the only exception to the rule). Hence we shall enter sl in the

dictionary as a strident l. The l is duplicated by the "3"-segmentalization rule, and the leading s is inserted by the s-segmentalization rule. With geminate simplification, this becomes sl.

The second problem was that although w does not occur in environments, C_U', swU' does, i.e., there is swoon, swoop. Thus we write it as a strident w, which as we have found, will not be affected by the "3"-segmentalization rule or by rule (18). In this case, it is necessary to consider the s to be in the 1st position and the main consonant to be w rather than an expected 2nd position s consonant with a w in the 3rd position (i.e., that it is a strident w, $\begin{vmatrix} -\text{cons} \\ -\text{vocl} \\ +\text{flat} \\ +\text{strid} \\ \vdots \end{vmatrix}$, not a rounded s, $\begin{vmatrix} +\text{cons} \\ -\text{vocl} \\ +\text{flat} \\ +\text{strid} \\ \vdots \end{vmatrix}$).

Usual formulations of English phonology employ stridency to distinguish s from θ. This option is left open to us as long as an sθ cluster is forbidden as it clearly is (sthenic and sthanakvasi undoubtedly being foreign). We see that leading s occurs with consonants p, t, k in spot, stop, and scot; with nasals in smart, snot; and with f as in sphere. We have strident stops, nasals, and f, and it would seem unlikely if we did not also have a strident θ parallel to the f. But indeed we do, and we call it s. It is doubled by the s-segmentalization rule and then re-singled by the geminate-simplification rule. Thus the simple strident consonants may be charted:

(19)

sp	st	sk
sm	sn	
sf	s	

In English, there is no initial sr except in Srinigar, which is clearly foreign, and there are no palatals with l, w, or r, except that shr.. is common (shwa, shluh, schlimazel, schlemiel are foreign). These facts have prompted many to suggest that sr obligatorily becomes shr. Of course, the more traditional phonology cannot accept this unless Srinigar is represented with a word boundary, s#ringer, or is an exception to the rule that converts s to sh before r. The present system captures the distinction nicely, shrink beginning with an s that is $\begin{vmatrix} -\text{vocl} \\ +\text{flat} \end{vmatrix}$, and Srinigar beginning with an s followed by an r, i.e., a true cluster, which is forbidden initially in English.

6. Problem

Referring back to (14) and (15), we saw that to block w and l after labials and dentials, respectively, the position 3 y, which would have been deleted anyhow, was also blocked. But now notice that the rule needed to remove this y will be useful only with velars (i.e., there is no ky,[10] gy). It is very tempting at this point to map these velars + y into the ch series (č ǰ š), thereby explaining their presence in English and why they are never accompanied by a position 3 element, and also removing the need of the

y-deletion rule. Unfortunately, if we do this, there is no source for plain k. If we could make up an ad hoc feature, |+3|, which would specify whether or not a position 3 is to be created, k and ch could contrast on their being |-3| and |+3|. respectively. It may well be that this is cheaper (it depends on the relative weighting of feature mentions in the dictionary and feature mentions in phonological rules); we shall not argue it here. It is significant, however, that an analogous situation is found in Mandarin Chinese phonology, that for the sake of 2 types of syllable finals, a feature must be introduced which serves only to specify whether or not the final has a position 4 element (y, w, n, or ng). We may ask if this is a general property of segmentalization systems, but for the present we shall have to be content with hypothesizing that such an extra feature is sometimes necessary to capture the full generality of the phonemic system.[10]

7. Comments

A few comments are in order concerning the interpretation of these processes of segmentalization. First, it is observed that the posited underlying segments are nigh on impossible to pronounce; for example, a strident nasal or liquid or a rounded "liquidic" (i.e., |+vocl|) t, etc. It such underlying forms existed, there would need to be spelling-out rules to de-focus the various components of such a segment into time-wise distinct segments so that all would be pronounceable. It seems that in some languages (e.g., English), there is a strong tendency to move some of the features on a segment in one direction and others in another, until what was originally one segment may appear to be several distinct segments in the phonetic output. In other languages (e.g., Kabardian[11]), most of the features on a segment are realized in the output more or less concurrently. (It is doubtful that in any language, for any segment, any 2 features begin and end simultaneously.) But even in nonsegmentalizing languages, many of the features on a consonant are spread out onto surrounding segments in the phonetic output. For example, in East Indian languages, the retroflection of the retroflex series of consonants appears recognizably only on the vowels before and after the consonants. It is clear that the only reason that these languages are not analyzed as having pseudo clusters like the English initial clusters is that the phonetic realization of the segmentalized features appears on both sides of the basic segment, and thus there is no way to decide on which side to place them. Contrariwise, treating the pseudo clusters found at the beginning of an English word as genuine clusters, e.g., chm in Lechmere, is a hang-over from the theory of classificatory phonemics.

The major difference between the use of segmentalization techniques and morpheme structure restrictions is that with the latter the simpler case is the one in which there is greater freedom of occurrence between elements of a cluster, whereas with the former strong restrictions not only are expected but required.

This segmentalization technique applies only to clusters in which the combinatorial

possibilities are severely restricted. Note that in the analysis above, the features needed to naturally specify positions 1 and 3 were unused in the specification of the 2nd segment. Requiring such a condition seems to place a natural limitation on the possibilities of this segmentalization technique. It is clear that without creating a lot of ad hoc features, the initial consonant cluster and its following vowel could not be spelled out of a single segment, since at least the features grave, diffuse, and vocalic would necessarily have one value for the initial cluster and one value for the vowel, which values would not in general be identical.

Even more natural than having the features on one segment unused in the other segment (as above) is the situation in which a feature that is necessary on one of the segments predicts the occurrence of itself or similar feature(s) on another segment within the cluster. An example of this can be found in Mandarin Chinese, which I shall not discuss now.

This solution for initial clusters is as simple as any that has been previously entertained. It is simpler, in fact, in terms of the number of features used in the rules. Thus if this type of solution is to be rejected, the present phonological theory will have to be modified in some non ad hoc manner, in order to exclude it automatically.

Last, consider a mutated form of English, where r, l, and w in position 3 are replaced by k, t, and p. This language would be more complex, yet the list and the phoneme-order methods of description would not show it. Another mutation, where r, l, and w in position 3 are supplemented by k, t, and p, would be simpler in terms of morpheme structure rules (since less restrictions would have to be stated). In both of these cases, it is only when we find that the clusters thus formed cannot be reduced to single segments that we understand the reason why these mutations result in a more complex language.

A forthcoming paper by J. E. Emonds, to whom I am indebted for some points brought out in this report, will give a more general description of consonant clusters in English, although the author disagrees with me on some points and does not go as far in some directions as I have in the present report.

T. R. Hofmann

Footnotes and References

1. N. A. Chomsky and M. Halle, The Sound Pattern of English (to be published by Harper and Row).

2. Z. S. Harris, Methods of Structural Linguistics (University of Chicago Press, Chicago, Ill., 1951), p. 153.

3. This is realized as lip-rouding, or tongue retroflection, or both. Actually, we could simply use rounding for this contrast, since the prevocalic r, as well as w, is always rounded. Post vocalic r, with which we are not concerned here, is a beast of an other nature, and is never rounded.

4. M. Halle (in class lectures) has treated kw as a single segment (thereby allowing a weak cluster "formula," $C(\{^{l}_{r}\})$), but was unwilling to treat tw and dw similarly. Our direction here requires us to go on and accept not only tw but also kr, kl, tr, pl, and pr as single segments. Recently G. Bedell[5] has proposed such an analysis for the 'final' part of the syllable in Mandarin Chinese. The only thing new here, as with Bedell's analysis, is the use to which this technique is put, that of creating canonical positions. But even this is not novel, we may view the canonical position of the vowel off-glides in English as being created and filled by the influence of the preceding vowel.

5. G. D. Bedell IV, "Syllable Finals in Chinese Phonology, Quarterly Progress Report No. 81, Research Laboratory of Electronics, M. I. T., April 15, 1966, pp. 186-190.

6. Although one part of this redundancy is perhaps universal, the impossibility of $\begin{vmatrix}-\text{cons}\\-\text{flat}\\-\text{vocl}\end{vmatrix}$ in position 3 will have to be mentioned, which will have the effect of, and will cost the same as, the rule in our new system which deletes such a segment.

7. We shall assume that f is |-strid| at this level of abstraction, and that it is stridentized later.

8. J. A. Foley, Jr., "Spanish Morphology," Ph. D. Thesis, Department of Modern Languages and Linguistics, M. I. T., June 1965 (unpublished).

9. Here, to block means "to cause not to appear," rather than the more usual "to mark as deviant."

10. Notice the similarity in saying that k is |-3| and that k is an exception to the "3"-segmentalization rule.

11. A. Kuipers, Phoneme and Morpheme in Kabardian (Mouton and Company, The Hague, 1960).

B. ESQUISSE À PROPOS D'UNE CLASSE LIMITÉE D'ADJECTIFS EN FRANÇAIS MODERNE

Il existe en Français moderne une variation souvent observèe, qui transforme le sens de l'adjectif, suivant qu'il suit ou précède le nom auquel il se rapporte:

(1) un simple soldat / un soldat simple
une simple robe / une robe simple

(2) un ancien roi / un roi ancien
une ancienne armoire (=un meuble qui a été une armoire, et sert à présent à d'autres usages) / une armoire ancienne

(3) une épopée vraie / une vraie épopée

(4) une vague idée (=quelque chose qui mérite à peine le nom d'idée) / une idée vague (=une idée imprécise)

(5) une apparente folie / une folie apparente

D'ordinaire, on ramène ce phénomène à celui, plus général, de la place de l'adjectif épithète en Français, et de sa variation.[1] Ainsi les oppositions mentionnées sont rapprochées de l'opposition entre homme grand et grand homme, qui change le sens, ou entre verts pâturages et pâturages verts, courageux soldat et soldat courageux etc., qui change la nuance. C'est même dans ce dernier type de variation qu'est trouvée la clef de l'ensemble: avant le nom, verts, dira-t-on, n'est pas un adjectif descriptif, mais désigne un attribut permanent du nom; au contraire, après le nom, verts est descriptif et désigne un attribut accidentel. Ainsi, dira-t-on, il existe une opposition générale gouvernant la place et le sens de l'adjectif, entre par exemple le propre (après le nom) et le figuré (avant le nom), comme on peut le voir, semble-t-il, dans les couples (1) à (5) ou dans le couple homme grand / grand homme.

Notre hypothèse est au contraire que la série des variations (1) à (5)[2] est à séparer des autres phénomènes apparemment analogues (y compris l'alternance présentée par grand), et que les adjectifs qu'elle affecte forment une classe limitée, reconnaissable à certains caractères.

Par exemple, ils n'admettent pas les degrés de comparaison: on ne dit pas

(6) *une moins simple simple robe, une robe moins simple
*une plus simple robe, une robe plus simple

(7) *un moins ancien professeur, un professeur moins ancien
*un plus ancien professeur, un professeur plus ancien

du moins au sens de une simple robe, un ancien professeur.

Il est illégitime de les coordonner avec des adjectifs ordinaires, ce qui, suivant les règles de la coordination, suffit à prouver la différence des statuts. On ne dit pas *une

simple et petite porte, *un vieil et ancien professeur.

Mais de façon plus radicale encore, il n'est que de rechercher leur origine profonde pour manifester une singularité essentielle de ces adjectifs: on ne peut les employer en attributs après la copule. Une robe est simple ne peut avoir que le sens de une robe simple, un professeur est ancien, le sens de un professeur ancien. Cela suffit à interdire de dériver ces adjectifs de relatives prédicatives: (8) ne peut venir de (9).

(8) je porte une simple robe

(9) je porte une robe [une robe est simple]

En même temps qu'il les distingue, ce caractère dèfinit le véritable problème syntaxique que posent ces adjectifs: s'il est impossible de les dériver des relatives, quelle est leur origine profonde?

On peut remarquer ici que l'impossibilité de prédiquer est l'aspect le plus important d'un phénomène plus général, l'impossibilité de séparer les éléments du syntagme, par exemple en supprimant l'élément nominal dans une anaphore. Ainsi (10) est possible, (11) ne l'est pas.

(10) Quel crayon voulez-vous? __Le petit.

(11) *Quelle robe voulez-vous? __La simple.

De même (10a) C'est le petit que je veux.

(11a) *C'est la simple que je veux.

Tout se passe donc comme si le groupe formé par l'adjectif et le nom était inséparable, et provenait en bloc de tours prédicatifs tels que

(12) Louis est un ancien professeur[3]

(13) Ceci est une simple robe.

S'il en est bien ainsi, ce seront ces groupes unitaires que l'analyse devra expliquer à partir de la prédication qui les constitue, et d'abord il convient d'en examiner la signification exacte.

En effet, l'on peut admettre sans difficulté que l'énoncé Ceci est une belle robe exprime que l'objet appartient à l'ensemble des robes, au sous-ensemble des belles robes, une belle robe étant une robe caractérisée par sa beauté. En revanche, par l'énoncé Ceci est une simple robe, on exprime que l'objet appartient à l'ensemble des robes, mais il n'y a pas de sous-ensemble des simples robes; une simple robe en effet n'est pas une robe caractérisée par sa simplicité, mais une robe tout simplement. Ce qui se trouve ainsi défini, ce n'est pas l'appartenance à un sous-ensemble, mais une modalité de l'appartenance à l'ensemble.[4]

Or il est remarquable que tout naturellement, pour paraphraser l'énoncé à

interpréter, nous soyons parvenu plus haut à un tour adverbial: une simple robe est une robe tout simplement. Il ne s'agit pas là d'un hasard; il apparait en effet que l'on peut relier les adjectifs que nous traitons à des adverbes synonymes:

(14) a. Jean était anciennement un professeur
b. Ceci est une robe tout simplement
c. Ceci est apparemment une folie
d. Jean est faussement un prêtre
e. Jean est vraiment un héros

(15) a. Jean est un ancien professeur
b. Ceci est une simple robe
c. Ceci est une apparente folie
d. Jean est un faux prêtre
e. Jean est un vrai héros

Bien que les phrases (14) soient inégalement acceptables, il est clair que toutes peuvent recevoir une interprétation, dont relèvera tout aussi bien la phrase (15) correspondante. La relation prédicative donc parait modifiée (modalisée) de manière identique par l'adjectif et l'adverbe.

Sans les analyser pour eux-mêmes, nous pouvons cependant reconnaitre à ces adverbes certaines particularités qui les opposent aux adverbes de manière avec lesquels on les confond aisément.

1. Il est impossible de les coordonner avec ces derniers. On peut par exemple dire:

(16) Il conduit rapidement et bien

mais non pas

(17) *Il conduit vraiment (apparemment) et bien

2. De façon plus révélatrice encore, il est impossible d'employer ces adverbes pour répondre a une interrogation Comment?, De quelle manière?.

(18) De quelle manière conduit-il?

a. __Prudemment
b. __Rapidement
c. __*Apparemment
d. __*Anciennement
e. __*Vraiment

En revanche, (18) c, d, e répondent à la question Conduit-il?.

3. Pas plus que leurs correspondants adjectifs, ils n'admettent les degrés de comparaison:

(19) *Jean est plus (moins) vraiment (apparemment) malade que Louis

4. Du point de vue de leur origine profonde, le sens même interdit que ces adverbes proviennent d'un tour Préposition + Nom. En effet, dans les phrases que nous considérons, simplement ne peut signifier 'avec simplicité', ni anciennement 'avec ancienneté', ni vraiment 'avec vérité', ni apparemment 'avec apparence', La seule paraphrase possible serait ici composée de l'adjectif qualifiant un nom tel que manière, façon etc., soit de manière simple, ancienne, vraie, apparente, fausse, réelle etc.[5]

Seule correcte pour le sens, cette paraphrase fournit aussi la base de l'analyse syntaxique. Il suffit de reconnaitre qu'en vérité, le nom n'est doué ici d'aucune autonomie sémantique: tel la copule dans l'énoncé prédicatif, il n'est là que pour effectuer la complétude et l'autonomie syntaxique du syntagme, qui réduit au seul adjectif ne pourrait en Français obtenir de statut plein.[6] C'est en fait le représentant superficiel de ce qui doit être dans la structure profonds un "dummy element", un élément non spécifiable, sinon par sa catégorie et sa fonction.

Nous parvenons dès lors a la représentation suivante:

$$\left[\text{MOD}\left[\text{NP}\ \text{Adjectif}\quad \underset{[+\text{Oblique}]}{\text{D}}\right]\right]$$

où D représente un N non spécifié,

MOD désigne la catégorie Modalité, que nous introduisons dans la grammaire afin de nommer la structure sous-jacente aux adverbes dont nous avons reconnu la spécificité.

La figuration [+Oblique] tient compte du fait que, vraisemblablement, de et à ne sont pas en Français des prépositions ordinaires et jouent plutôt comme des traits conférés à un élément nominal par sa place dans le P. M., c'est-à-dire assignés à certaines fonctions (donc analogues a des cas).[7]

Devant la synonymie des phrases (14) et (15), nous avançons l'hypothèse que l'adjectif dans les phrases (15) est un adjectif modal, dérivé du syntagme de modalité, sous-jacent à l'adverbe dans les phrases (14). En rigueur, l'adverbe en -ment étant lui-même dérivé du syntagme de modalité, le processus dérivant l'adjectif ne passera pas par l'adverbe lui-même, mais deplacera directement l'adjectif (issu d'une relative réduite) hors de la structure de modalité, et l'adjoindra par une transformation que nous ne tenterons pas ici de mieux définir au NP Attribut de la phrase prédicative. Ainsi, adjectif épithète ordinaire dans le syntagme [$_{\text{NP}}$Adjectif D], celui-ci devient adjectif modal (issu d'un tour adverbial) dans le syntagme attributif dérivé.[7b]

Nous n'avons pas à décider ici de la place hiérarchique de la Modalité; l'hypothèse la moins coûteuse, sinon la plus vraisemblable, est de la placer au même niveau que VP. Nous admettrons donc que pour dériver Jean est un ancien professeur, nous devrons

partir de la description suivante:

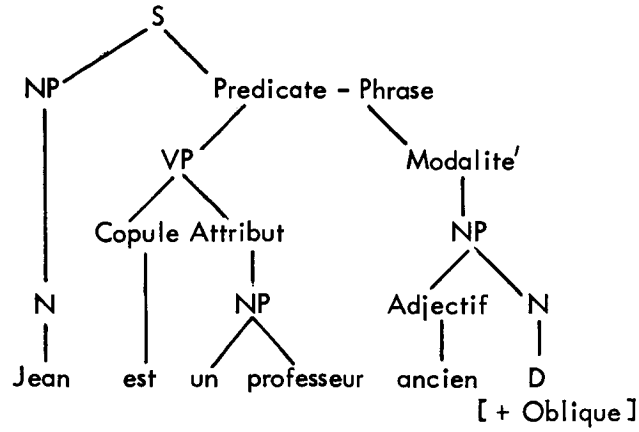

Diagram XXIX-1.

La dérivation procédera comme suit:

1. Adjonction de l'Adjectif dominé par la catégorie Modalité, au NP dominé par la catégorie Attribut.
2. Plutôt qu'une délétion particulière, le "dummy element" D suivra une règle générale conférant à tous les "dummy" non explicitement remplacés une interprétation phonétique zéro. Dès lors on pourra conserver le noeud Modalité dans le PM généralisé, et l'on parlera de phrases modales, caractérisées par sa présence. D'où

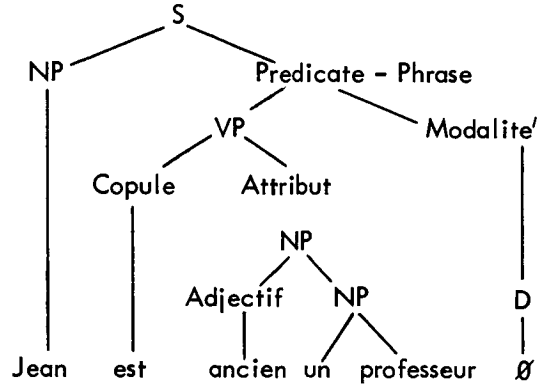

Diagram XXIX-2.

La transformation se décrit ainsi: (# dénote l'Adjonction)

$$+ X\ [_{PredP}\ [_{VP}\ \text{Copule NP}]\ Y\ [_{MOD}\ [_{NP}\ \text{Adj D}]]\ Z + \xrightarrow{\text{OPT}}$$

1 2 3 4 5 6 7 8 9

1 2 3 6 # 4 5 0 7 8 9

Remarques: 1. Si la transformation sur la Modalité n'est pas appliquée en ce sens prend place la transformation adverbiale: [simple D] devient simplement. Entre l'une et l'autre transformations, il y a choix optionnel, mais il est obligatoire de transformer. On peut alors parler d'un couple obligatoire de transformations optionnelles sur la Modalité.

2. La transformation adjective est cyclique (d'où la présence des + marquant les "phrase boundaries"). Témoin les phrases

(19) Jean est un simple ancien professeur

(20) Jean est un parfait simple soldat

3. La place de l'adjectif modal est fixe: il précéde tous les éléments du NP auquel il est adjoint, non pas évidemment l'article, toujours en tête (une règle spéciale y pourvoira), mais tout adjectif non-modal, ou tout adjectif modal issu d'une dérivation antérieure. Ainsi s'expliquent les apparentes infractions aux règles d'ordre rythmiques (pourtant si contraignantes), suivant lesquelles un adjectif polysyllabe suit un nom monosyllabe (cf. pour cette règle Grévisse, Le bon Usage, § 398). On dira donc Un ancien roi, un parfait sot, un véritable don. Si le nom est déjà précédé d'un adjectif, on dira par exemple: Une simple petite porte, Un faux grand homme et non *Une petite simple porte, *Un grand faux homme. Il faut reconnaitre du reste que la rencontre de deux adjectifs devant le nom est d'ordinaire évitée grâce au tour adverbial; plutôt que Un vrai bel appartement, on dira Un appartement vraiment beau etc.

Ainsi se trouve développée l'origine des tours prédicatifs du type Ceci est une simple robe, et de même que l'adjectif épithète ordinaire, ce sera de ces tours que l'adjectif modal sera dérivé dans ses emplois non-prédicatifs

(21) a. Je porte une simple robe
b. une simple robe suffira

(22) a. Je vois un ancien professeur
b. Un ancien professeur arrive

Comme pour l'adjectif ordinaire, il faut partir d'une relative, celle-ci ne qualifiant pas un nom spécifié cependant, mais ici encore un N non spécifié, analogue à quelqu'un, quelque chose. En effet nous avons vu, c'était notre point de départ, que les groupes simple robe, ancien professeur étaient inséparables, ils devront donc provenir ensemble de la relative et dans la principale ne subsiste plus qu'un zéro phonétique, représentant un "dummy"sous-jacent.

On obtient alors la description suivante:

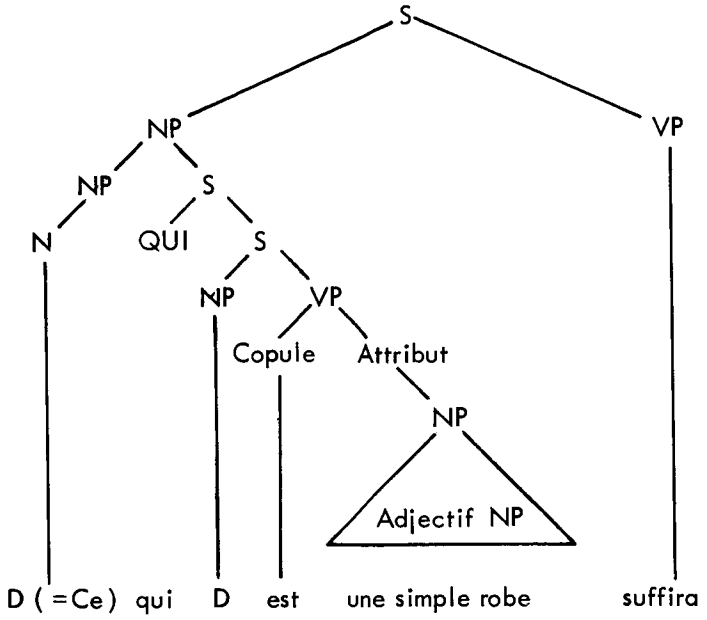

Diagram XXIX-3.

Il est aisé de voir que la transformation appropriée sera ici la réduction des relatives, dont la description structurale sera obtenue à partir de celle valable pour l'Anglais, soit

$$X\,[_{NP}\ NP\,[_{S}\ QUI\ Copule\ Y]]\ Z \xrightarrow{OPT}$$

1	2	3	4	5
1	2	0	4	5

Cependant, pour des raisons en partie indépendantes de notre présent objet, la présence de D doit être spécifiée dans la description structurale, et entraine certaines modifications. Il convient en effet de préciser que la réduction n'est pas possible si l'antécédent du relatif est cet élément non-spécifié D, et l'attribut un adjectif: Tout ce qui est bon ne se réduit pas à *Tout bon.
En revanche, si l'attribut est un nom pourvu ou non d'un adjectif modal ou non, la réduction est possible: Tout ce qui est une belle robe se réduit à Toute belle robe, Toute ce qui est une simple robe a Toute simple robe, Tout ce qui est une robe à Toute robe.

Une version particulière de la réduction des relatives apparait ainsi nécessaire:

$$X\ [_{NP}\ D\ [_{S}\ QUI\ Copule\ [_{ATT}\ [_{NP}\ Y\ NP]]]]\ Z \xrightarrow{OPT}$$

1	2	3	4	5	6
1	2	0	4	5	6

Dans cette formulation, la spécification de l'ancienne variable 4 est liée à la spécification de l'élément 2. Il est clair que ce n'est pas là une règle ad hoc, formulée pour rendre compte seulement des tours modaux non-prédicatifs, mais une règle concernant l'ensemble des réductions de relatives attachées à un élément non-spécifié nominal: en fait une règle mineure (minor rule). Il est vrai aussi cependant que cette formulation précisée permet seule d'obtenir la dérivation que nous souhitons. Grâce à elle, nous pouvons dériver de D [D est une simple robe] suffira, Une simple robe suffira.

D recevra une interprétation phonétique zéro, mais l'on peut admettre comme énoncé dérivé D l'ancien professeur, D une simple robe.[8] Une simple robe, l'ancien professeur se trouvent ainsi engendrés comme des caractérisations apposées d'un élément non-spécifié, et de ce fait même générique, ce qui correspond bien au sentiment intuitif que ces énoncés comportent une référence vague à un ensemble plus vaste; on entendra par exemple (En fait de vêtements) une simple robe-...; on peut observer du reste que le tour est bien plus fréquent avec un article indéfini.

Au terme de cette double dérivation qui nous a procuré d'abord les phrases modales prédicatives, puis par une réduction particulière, les non-prédicatives, il apparait que les alternances dont nous étions parti sont illusoires: ce n'est pas le même adjectif qui, changeant de place, change de sens, mais il y a deux adjectifs de forme identique et d'origine différente, dont l'un, l'adjectif modal, a une place fixe, devant le nom, et en exclut l'adjectif non-modal homonyme.

Cependant cette homonymie n'est pas un fait de hasard, puisque l'adjectif modal est bien issu de l'adjectif non-modal, par l'intermédiaire de l'adverbe de modalité, soit le processus

Adjectif non-modal — Adverbe de modalité — Adjectif modal

$$Simple^{(1)} > Simplement > Simple^{(2)}$$

Du même coup s'expliquent et la parenté et la différence des sens entre les deux adjectifs homonymes: parenté du fait d'une commune origine lexicale, différence dans les processus de dérivation.

On peut affirmer sans grave erreur que les alternances ainsi réduites formaient l'élément principal des variations de place affectant le sens de l'adjectif; si l'on

démontre d'autre part que parmi les alternances non-réduites, les plus apparentes sont également illusoires, pour d'autres raisons, on aura écarté l'ensemble des variations de place entrainant d'importantes polarisations sémantiques.[9] Or bien évidemment une grammaire transformationnelle pouvait difficilement traiter ces phénomènes, tels qu'ils apparaissaient à première vue; deux solutions se présentaient ici (elles ont été effectivement proposées par G. Lakoff et J. R. Ross): ou bien attribuer le déplacement à une règle mineure (minor rule), mais alors une transformation se trouvait affecter le sens,[10] ou bien conserver deux entrées lexicales, ce qui ne rendait pas compte de la parenté des sens. C'est donc simplifier et généraliser la grammaire du Français que d'y admettre la nouvelle transformation et la nouvelle classe dérivée des adjectifs modaux.

Il faut prendre garde que par là ne se trouve nullement résolu le problème général de la place de l'épithète. Bien au contraire, alors que les grammaires traditionnelles apercevaient dans les variations sémantiques polarisées le phénomène le plus caractéristique et la clef générale du système adjectif, notre hypothèse entend les mettre à part et ne préjuger en rien de ce que doit être l'analyse des adjectifs ordinaires. Tout au plus, dissipant une apparence dont celle-ci prenait jusqu'à présent son départ, peut elle prétendre en former une étape préliminaire.[11]

J. C. Milner

Notes

1. De ce fait, des phénomènes différents se trouvent mélangés dans les listes données par les grammaires et les descriptions (cf. e.g., Brunot, La Pensée et la Langue, pp. 638-643, Damourette et Pichon, Des Mots à la Pensée, II, par. 512-516, Grevisse, Le bon Usage, par. 398). Les relevés les plus complets de ces variations apparaissent chez les grammairiens du XVIIIe siècle, qui les considéraient comme essentielles à la précision et l'exactitude du style (Des références sont données par Damourette et Pichon, ibid.; y ajouter pour une expression caractéristique du point de vue général Rivarol, Prospectus d'un nouveau dictionnaire de la langue française.).

2. Si les exemples (1) à (5) relèvent tous de la classe que nous entendons décrire, ils n'en épuisent pas l'extension. D'autres adjectifs apparaitront occasionnellement dans la suite, mais nous ne tenterons pas ici de dresser une liste complète.

   De plus, dans l'examen du comportement particulier des adjectifs concernés, la brièveté nous impose de faire valoir un ou deux cas (en général, simple et ancien) pour l'ensemble. Nous ne prétendons pas que certains ne présentent pas parfois certaines idiosyncrasies, mais nous les négligerons ici.

3. Notons encore un trait particulier des adjectifs considérés: de même que l'on peut avoir, sans article, Jean est soldat, Jean est professeur (noms de fonction), on aura Jean est simple soldat, simple professeur. En revanche, un adjectif ordinaire entraine automatiquement l'article: les énoncés *Jean est pauvre soldat, Jean est vieux professeur sont exclus.

4. La même analyse pourrait être faite de Jean est un ancien professeur, Ceci est une apparente folie, mais la relation n'est pas simple, un ancien professeur n'étant plus professeur, une apparente folie n'étant pas une folie. Cependant ici encore l'adjectif ne modifie pas le nom en le caractérisant, mais la relation elle-même en la modalisant.

On peut ainsi comprendre que tout adjectif probatif (excellent, parfait, mauvais, vrai, faux, réel etc.) peut entrer dans le système des adjectifs considérés, puisqu'ils sont prédisposés à exprimer que les conditions déterminant l'appartenance à une classe (définie en intension, non en extension, soit un concept fregéen) sont ou non remplies.

5. On pourrait objecter que tous les adverbes de manière en -ment admettent également cette interprétation. Mais il est clair que, pour le sens, il est indifférent de dériver par exemple rapidement de avec rapidité ou de de manière rapide. Le trait discriminant n'est pas que l'analyse proposée soit possible, mais qu'elle soit dans certains cas précis la seule possible.

6. De même que dans bien des langues, en certains cas, la copule peut être représentée par un zéro phonétique, de même le "dummy" auquel se rapporte l'adjectif dans les tours sous-jacents à l'adverbe. Comparer e.g., certains adverbes de manière en latin: crebro, cito, falso.

Le fait que le français, s'opposant au latin de la même manière dans les deux cas, soit obligé d'employer un mot de statut grammatical plein et de sémantisme vide pour soutenir l'adjectif, qu'il s'agisse de la prédication ou du tour adverbial, pourrait manifester une corrélation typologique importante.

7. L'hypothèse a été avancée et solidement fondée par E. Benveniste, notre présentation n'en est qu'une interprétation plus formelle.

Le trait [+Oblique] recevra l'interprétation phonétique de ou à suivant les contextes syntaxiques (ici de). On peut même penser que par, introduisant l'agent, est la réécriture de ce même trait dans le contexte de la transformation passive.

7b. Cette adjonction n'est pas sans rapport avec la règle reportant la négation du verbe subordonné au verbe recteur dans une phrase telle que:

I didn't believe that he would leave until tomorrow

Cela malgré des différences évidentes: dans cette règle, il s'agit d'un trait [+Neg], non d'un constituant; de plus le déplacement de l'élément se fait du syntagme dominé au syntagme dominant, non pas entre syntagmes de même niveau hiérarchique.

8. Il est possible que ce soit là l'explication de la place de tout dans les énoncés tels que Toute la maison, tout le corps, si l'on admet qu'ils soient à dériver de Tout ce qui est la maison, tout ce qui est le corps, c'est-à-dire Tout [D qui est] la maison, Tout [D qui est] le corps.

9. Ainsi par exemple la célèbre alternance homme grand / grand homme. En effet
1. cette alternance ne vaut que pour le mot homme; partout ailleurs, grand a une place fixe, avant le nom,

2. malgré l'apparence grand conserve le même sens dans tous ses emplois: la différence entre les énoncés un grand tapis / un grand pianiste réside seulement dans la classe sémantique des éléments nominaux. Néanmoins certains traits lexicaux du nom peuvent affecter l'adjectif; ainsi grand sera ou non adjectif de mesure suivant que le nom sera ou non marqué du trait lexical [+Mesure]. On posera donc une règle d'assimilation, comparable à une règle phonologique:

$$\text{Grand} \longrightarrow [\alpha\ \text{Mesure}] \,/\, \underline{\quad}_{N}\ [\alpha\ \text{Mesure}]$$

3. s'il y a une apparente variation du sens de grand entre homme grand et grand homme, elle ne peut être due qu'à une dualité du nom, et en effet le mot homme a deux séries d'emplois: dans l'une, il est syntaxiquement analogue aux noms de fonction; on peut alors le prédiquer sans article (Je suis homme, comme Je suis pianiste, fonctionnaire, professeur etc.) et il faut l'affecter du trait [-Mesure]. Dans ce cas, grand est à sa place régulière et n'est pas adjectif de mesure.

Dans l'autre emploi, homme est un terme "biologique", comparable aux noms d'animaux, et il est affecté du trait [+Mesure] (cf. un homme de 1,80 m), le conférant du même coup à grand. C'est l'homonymie avec le premier tour, phénomène purement idiosyncratique, qui exclut alors grand de la place précédant le nom.

A titre de contre-épreuve, on observera que femme, n'ayant que le sens "biologique", ne présente pas la même alternance; non seulement Une femme grande aurait le même sens que Une grande femme, mais le premier énoncé serait bien inférieur au second, et à peine acceptable (Noter l'opposition nominale grande femme [+Mesure] / grande dame [-Mesure]).

10. Ajoutons que les variations de sens joueraient alors de manière déconcertante; si l'on admet en effet, comme il est vraisemblable, que la place régulière de l'adjectif est devant le nom et la place dérivée, après le nom, comment expliquer que le sens "propre" apparaisse à la place dérivée, et le sens figuré (qu'on imaginerait plutôt issu de la transformation) à la place régulière?

11. Si toutes les variations sémantiques se trouvent réduites, seules subsistent des variations de nuance (cf. e.g., verts pâturages / pâturages verts, courageux soldats / soldats courageux). Il est possible, dans ces conditions, que le déplacement de l'adjectif épithète ordinaire relève à nouveau d'une règle mineure (minor rule), et que les variations de nuance soient attribuées à des phénomènes de discours (essentiellement d'intonation); peut-être faut-il aussi tenir compte de la différence entre relatives restrictives et non-restrictives.

Note ajoutée à la relecture: Nous avons pris connaissance trop tard pour en faire état ici de l'article d'E. Bach "Nouns and Noun Phrases in English" (non publié), où pp. 12 et 13, des remarques et des hypothèses analogues aux nôtres se trouvaient déjà énoncées.

Nous ne discuterons pas les suggestions de Bach et remarquerons seulement la différence qui s'établit nécessairement entre la grammaire de l'Anglais et celle du Français; dans les deux langues, la spécificité des adjectifs modaux est claire et s'atteste par le même trait: l'absence de prédication (cf. pour l'Anglais, former, alleged, real, mere cités par Bach.); mais le problème qui se pose alors en Anglais est seulement de rendre compte de la dérivation syntaxique de cette classe. En Français, à une hypothèse de cet ordre, s'en ajoute encore une autre touchant la place de ces adjectifs; nous avons avancé ainsi deux hypothèses distinctes et, il faut le remarquer, indépendantes:

1] les adjectifs modaux proviennent de tours adverbiaux

2] ils ont une place fixe

Il n'y a aucune relation d'implication entre ces deux hypothéses: la première seule pourrait prétendre être étendue à l'Anglais et ainsi s'opposed à celle de Bach; la seconde est propre au Français et, en tout état de cause, n'est nullement affectée par le sort de la première.

XXX3 COGNITIVE INFORMATION PROCESSING*6

Academic and Research Staff

Prof. W. L. Black
Prof. M. Eden
Prof. T. S. Huang
Prof. F. F. Lee
Prof. S. J. Mason ET AL 8
Prof. W. F. Schreiber
Prof. D. E. Troxel
Dr. K. R. Ingham
Dr. P. A. Kolers
Dr. P. H. Liss
Dr. O. J. Tretiak
C. L. Fontaine
E. R. Jensen
G. L. Wickelgren

Graduate Students

E. I. Ancona
G. B. Anderson
T. P. Barnwell III
A. K. Bhushan
B. A. Blesser
A. L. Citron
R. W. Cornew
D. P. Dewan
A. Gabrielian
R. V. Harris III
H. P. Hartmann
G. R. Kalan
R. W. Kinsley, Jr.
J. I. Makhoul
W. H. Lee
L. C. Ng
D. L. Peterson
H. J. Rack
G. M. Robbins
A. H. M. Ross
C. L. Seitz
D. Sheena
R. M. Strong
G. A. Walpert
J. A. Williams

RESEARCH OBJECTIVES AND SUMMARY OF RESEARCH

The primary research interest of this group is in the real-time acquisition and processing of visual information for display to the visual and nonvisual senses, and in the psychology of human utilization of such information, for both communication and control. The motivation is an interest in human capabilities for information processing and in human information requirements. Applications include sensory-aids systems for the blind and the blind-deaf, picture-transmission systems, and special information-display systems for enhancement of human performance under conditions of stress.

Major projects now in progress include studies on reading machines, picture processing, pattern recognition, and automatic processing of visual data of significance in studies of biology and medicine.

1. Reading Machine Studies

Research during the past few years in the Cognitive Information Processing Group of the Research Laboratory of Electronics has led to the construction and operation of an experimental reading system for the blind. In its present configuration the system consists of a document-handling carriage, a flying-spot opaque scanner, a digital scanner control unit, and a general-purpose medium-sized computer (PDP-1). Focusing, black-and-white threshold setting and document loading are manually controlled by a sighted operator. The scanner control unit operating under control of the computer program reports coordinate letter contour and other statistical information of the view in the scanner field. This information is used for the generation of signatures that are searched in a signature table for the identification of the letters. The signature table is built up through training sessions. Identified letters are spelled out, one at a time, through the use of digitized speech samples. The present output rate of the spelled

*This work was supported in part by the Joint Services Electronics Programs (U. S. Army, U. S. Navy, and U. S. Air Force) under Contract DA 36-039-AMC-03200(E), and in part by the National Science Foundation (Grant GK-835), the National Institutes of Health (Grant 2 PO1 MH-04737-06), and the National Aeronautics and Space Administration (Grant NsG-496).

speech is 60-80 words per minute. Experience has indicated an identification error rate of approximately 0.3% with a type font which the machine has been trained on.

One long-term objective is to provide a real-time connected speech output for the reading machine. The steps required are the translation of English words in conventional spelling into phonetic spellings, the addition of intonation to utterances and the generation of synthetic speech. Other intermediate forms of outputs are also contemplated.

Another objective for future research is to develop a field version of a reading system and evaluate its characteristics under conditions of actual use by blind subjects. This will involve consideration of the problems encountered by a blind operator in the adjustments of focus and threshold, the alignment of the document, and in specifying which portion of the text is to be read next. Naturally, considerable research will be required both on the hardware and software of the present reading system before a field version is to be designed and constructed.

a. Character Recognition

The character recognition algorithm used in the reading machine system described above is being tested on several other type fonts, including news print. Variation of this and new algorithms will be investigated with a view toward further simplification and applicability to multiple type fonts. Consideration will also be given to the problems of broken and touching letters.

b. Opaque Scanners

The character recognition work thus far has been carried out with a scanner that has a small field of view and is fairly slow. Work will proceed on other types of scanners which will allow less sophisticated document handling and a faster throughput of characters.

c. Tactile Displays

Two tactile displays are under development, both of which are two-dimensional arrays of Braille-like tactile "dot" elements, in which each dot is either present or absent, according to external control. The first display, made up of solenoid-controlled poke probes, has a size of 6×8 and is designed to present a Braille-like cell to each of 8 fingers. The second display is of the "moving-belt" variety, with size 64×128, and a frame rate of three or more per minute. These displays will be used as tactile outputs for the reading-machine system and also for general studies of tactile pattern perception, both dynamic and static.

d. Spelled-Speech Storage, Display, and Compression

Spelled-speech offers a slower, but simpler, auditory display than artifical speech. Under construction are magnetic and optical storage and read-out of the spoken-letter sounds, and the compression of spelled speech by sampling in sections, temporal truncation, and temporal-overlap superposition has been examined.

e. Phonetic Translation of English Text

The transliteration of spelled English words into phonetic spellings depends on the use of morphographemic rules, morphophonemic rules, as well as syntax and semantics. Although the dependence on semantics is relatively weak in an engineering sense, the dependence on syntax is heavy, in that intonation (a suprasegmental feature of speech

such as English) cannot be determined without a certain amount of syntactic analysis. The problem of the selection of important morphographemic, morphophonemic, and syntactic rules, and the make-up of an accompanying morpheme lexicon are crucial to the generation of connected speech from text string input.

f. Artificial-Speech Generation

Rapid human adaptation to a sentence of synthesized speech under repeated exposure makes it very difficult for the experimenter himself to judge the quality and performance of his synthesizer and the procedure used. A facility that allows the experimenter to input phonetic strings to the synthesizer and to manipulate the procedure parameters easily should allow better artificial speech to be synthesized. The development of the equipment and the accompanying computer program is part of the reading-machine research effort.

g. Real-Time Data-Processing Facilities

Work continues on the development of real-time remote input-output subsystems that make it possible for two small general-purpose digital computers to be utilized simultaneously and cooperatively in the reading-machine system, one computer being mainly occupied with scanner control, character recognition, phonetic translation, and the other with the generation of speech from phonetic symbolic input.

F. F. Lee, D. E. Troxel, S. J. Mason

2. Picture-Processing Studies

Picture-processing research is concerned principally with processing and encoding picture signals for efficient transmission, subject to a quality constraint in the received picture. Subsidiary matters concern picture processing for quality improvement or for feature recognition.

a. Picture Quality

Our long-range goal is to develop objective measures correlating with subjective rating of picture quality. As a preliminary goal, we need to establish subjective rating on a more satisfactory basis. At present, it is not possible to compare such evaluations made on different systems, using different subjects, different observers, at different times. To facilitate such comparison, we plan to produce a new set of standard subjects. For each subject we shall produce a set of standard photographs in which the quality and data rate are varied, and in which, for each data rate, the system parameters have been varied, for optimum quality. The system will be PCM, with additive random noise of uniform probability distribution. These sets of pictures should permit accurate evaluation of quality and coding efficiency of new systems by a matching process.

b. Picture Coding

During the past year, we have made good progress on picture compression by two-dimensional contour coding. A technique has been developed for artifact-free reconstruction of pictures from the two-dimensional gradient or Laplacian. In the coming year, emphasis will be placed on more efficient coding and interpolation techniques for transmitting the contour data. Some effort may also be put into coding of textural information.

c. Optical Image Processing

Our principal interest is in using optics as a tool for picture processing. In particular, we are interested in developing links between digital computers and coherent optics so that the two can be used to complement each other. Applications under consideration include matched-filter detection, and holographic television systems.

W. F. Schreiber, T. S. Huang

3. Pattern-Recognition Studies

"Pattern Recognition" is a common theme underlying the projects described above, whether the task is accomplished by human cognition, by computer data processing or, most commonly, by a combination of the two.

Complementary to the task-oriented projects, the following research studies in the general area of pattern recognition are being carried out.

a. Psychophysics of Depth Perception

This project is designed to provide information on a subject's ability to make accurate distance and orientation judgments with respect to real and illusory three-dimensional objects. The variation of such judgments will be studied without feedback, as well as with a continuous auditory or visual error signal.

b. Effects of Spatial Transformation of Text upon Reading and Writing Performance

It has been shown that systematic transformations or printed text (such as inversions or rotations of letters and of words) produce regular changes in the learning rate, as well as in the asymptotic reading rate. These studies are being extended to a wider class of transformations and also to reading and writing performance, with cursive script used as the text.

c. Automatic Extraction of Information from Printed Sheet Music

With the aid of the scanner and ancillary equipment developed for the projects described above, it is possible to program a computer to determine note value, duration, phrasing, and certain other music indicators from ordinary printed sheet music. This study is being continued to see what additional parameters can be extracted by automatic recognition.

d. Cognitive Processes – Language Comprehension

Research will be directed toward clarifying the nature of the quick perception and comprehension of written information by studying how normal and speed readers interpret words and sentences presented tachistiscopically. The ability to detect various syntactic and semantic differences between a known sentence and a briefly presented one will be especially studied.

e. Visual Perception and Eye-Movement Relations

We shall explore the ability of the system controlling eye movements to learn to follow points or scan lines whose positions are modified in determinate ways by

movement of the eyes. Of especial interest will be the effect of eye-movement adaptation on the perception of motion and form.

M. Eden, P. A. Kolers, P. H. Liss

4. Biological Image Processing

Biological image processing deals with the acquisition and analysis of visual patterns that are important to medicine and biology. The picture-processing facilities described above are being used to explore the feasibility of using fully automatic techniques or machine aids to human classification of such objects as white cells, chromosome counting, particle counting in micro-autoradiographs, and three-dimensional visualization of micro-anatomic structures.

a. Chromosome Project

As an exploratory venture into Biological Image Processing, we have started assembling a procedure for karyotyping human chromosomes. In particular, we are addressing ourselves to the problems presented by touching and overlapping chromosomes. We hope to achieve our aim of distinguishing overlapping chromosomes by obtaining photographs in which the density in the overlap regions is different from that in the nonoverlapping regions, then to outline the chromosomes through appropriate programming.

b. Blood Cell Inventorying

The objective is to see if the distinctions between the various blood cells are sufficiently well understood to allow us to devise an automatic inventorying procedure. Standard blood smears stained with Wright's solution are photo-micrographed, and then scanned through three color filters on a flying-spot scanner. The digital data are then entered into the computer, where various algorithms will be employed to attempt separation. Ultimately, we hope to construct a computer-controlled microscope scanner.

c. Branching Structures

Algorithms have been devised for generating two-dimensional venation patterns such as are typified by tree leaves. The parameters of the algorithm serve as data for a possible classification of leaf type according to species. The work will be extended to measure the analogous parameters of actual leaves by picture-processing techniques.

M. Eden, W. L. Black, O. J. Tretiak

A. REPRODUCTION OF GRAPHICAL DATA BY FACSIMILE*

There is a broad category of documentary and graphical data which is commonly transmitted by facsimile and in which only two brightnesses, black and white, exist in the input. Although substantial savings in channel capacity could be made by restricting the transmitted information to these two levels, it is found in practice that a continuous

*This work was done by the author while he was at the Indian Institute of Technology, Kanpur, U. P., India, under the Kanpin Indo-American Program, a project financed by USAID.

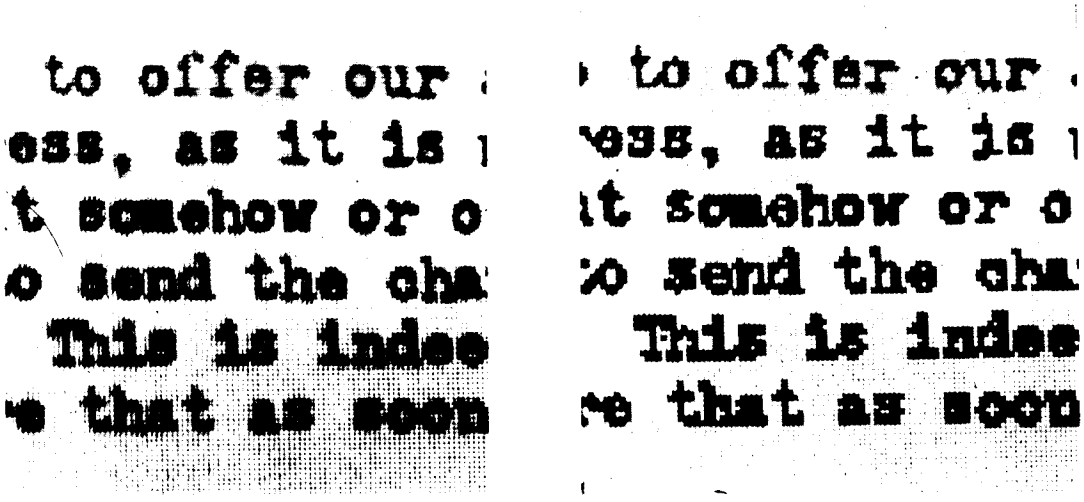

(a) (b)

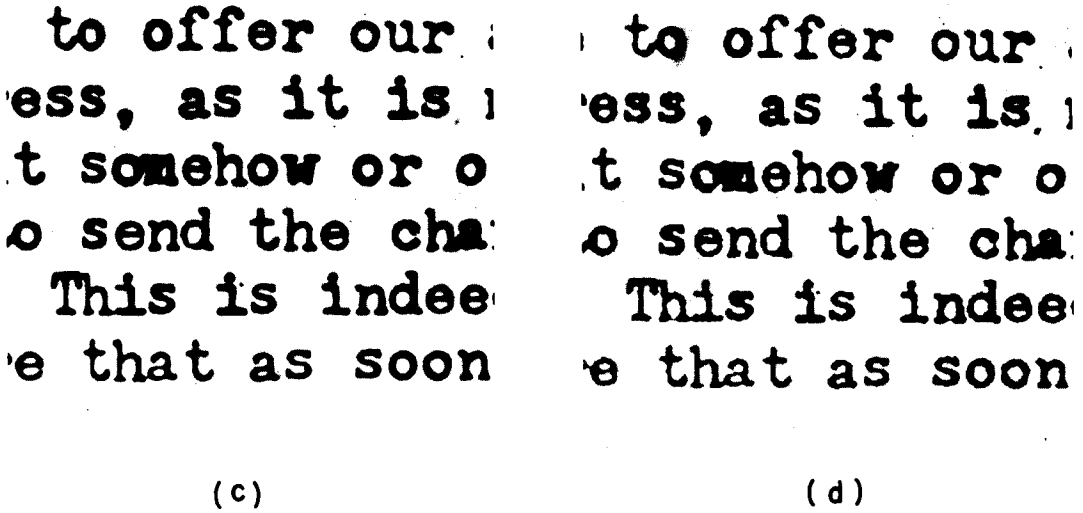

(c) (d)

Fig. XXX-1. (a) 70 samples/inch, continuous tone scale.
(b) 70 samples/inch, binary tone scale.
(c) 200 samples/inch, continuous tone scale.
(d) 200 samples/inch, binary tone scale.

These pictures should be viewed at approximately twice normal viewing distance. The resolution refers to the original copy.

(analog) tone scale gives superior results. It is the purpose here to report some experiments along these lines and to present some preliminary conclusions.

Eight examples of original documents, including typing, book, newspaper, and magazine print, and several non-Roman scripts, were converted into transparencies, with careful attention paid to photographic quality, including sharpness, graininess, and the preservation of the original tone scale. These transparencies were then scanned at approximately 70, 100, 140, and 200 samples per inch (of the original) in each direction. The sampled data were displayed on a cathode-ray tube and photographed with the original continuous tone scale, and also quantized into various numbers of steps. Attention was given to comparison of the analog and two-level reproductions. The scanning aperture was small (sharply focussed) in all cases, but the reproduction aperture was made just large enough to reduce the visibility of the dot structure to a low level.

The results show that at the lower sampling densities analog transmission does give superior quality, but the difference between analog and binary reproduction becomes less as the sampling density increases. The two reproductions seem nearly comparable at 200 samples/inch or less, the difference depending on the copy. On the basis of these tests, we have reached the following preliminary conclusion:

> Very high-quality transmission of graphical data is possible, by using discrete sampling in both directions with only two transmitted levels of brightness.

There is a subsidiary matter of importance in binary transmission, however. When only two brightness levels are used, the decision level of the quantizer is of great importance. Factors such as different reflectivity of background, color and darkness of ink, quality of print, focus, and so forth, make it highly desirable to use some local averaging to adjust the decision level to an optimum value. Preliminary qualitative work shows this approach to have merit. We hope to do further studies at a later date.

Some examples are shown in Fig. XXX-1 above.

W. F. Schreiber

B. IMAGE TRANSMISSION BY TWO-DIMENSIONAL CONTOUR CODING

This research is an extension of the work done by J. W. Pan,[1] as suggested by Professor W. F. Schreiber.[2] A block diagram of the proposed system is shown in Fig. XXX-2.

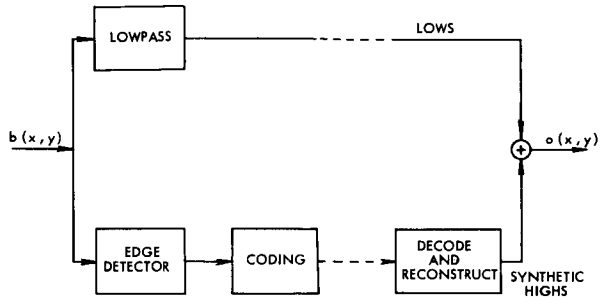

Fig. XXX-2. Block diagram of the proposed system.

In this system an image is treated as a two-dimensional signal of the spatial coordinates x and y. The large changes in brightness in a picture occur at the edges of objects and are accentuated by the visual system. The edge points can be isolated by the gradient or Laplacian operator. The fact that these edge points lie along connected contours in two dimensions is used to code the location and characteristics of each point efficiently. Two-dimensional reconstruction filters are derived to synthesize the high-frequency picture from the decoded-edge information. A two-dimensional lowpass or out-of-focus picture is also formed which can be transmitted with a relatively small number of bits. After a possible accentuation to make the picture appear "sharper," the "synthetic highs" signal is added to the lowpass picture to yield the final output. A reduction in the total number of bits required to describe a picture by a factor of 4 to 23 is possible as compared with 6-bit PCM.

The pictures used in this investigation were flying-spot-scanned, quantized to 256 levels, which permits an 8-bit representation, and recorded on digital magnetic tape by the picture-processing equipment constructed in our laboratory. The IBM 7094 II and other facilities of the Computation Center, M. I. T., were used to process these pictures, and the equipment in our laboratory was used to display and photograph the output from the simulation. Limitations of core storage and processing speed led to the choice of pictures that were sampled with a 256 × 256 array.

The lowpass filter, $\ell(x, y)$, used in this study was a circularly symmetric Gaussian function with $\sigma = 4$ samples. This spreads over approximately 10 per cent of the picture height. The original and the lowpass pictures are shown in Fig. XXX-3. In an earlier report[3] it was shown that the gradient operator could be used as an edge

(a)

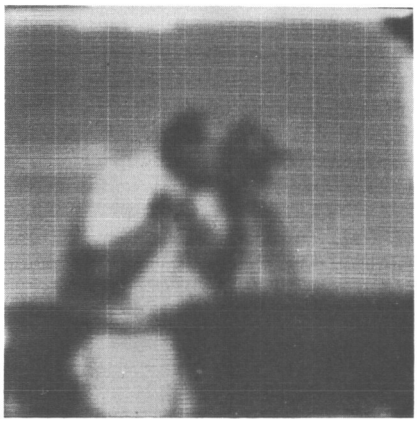

(b)

Fig. XXX-3. (a) Original picture.
(b) Lowpass picture.

detector and that it is possible to reconstruct the high-frequency part of the picture by operating on the gradient signal with a two-dimensional linear filter. It is also possible to use the Laplacian operator and to derive a reconstruction filter for this signal.[4]

The principal edges in a picture lie along contours in two dimensions which are continuous. A large "contour start threshold" is set to isolate the important edges in the picture. After finding a point for which the magnitude of the gradient exceeds the contour start threshold, the neighboring points are examined and the contour extended in the direction of the maximum magnitude. This process continues until no neighbor point exceeds the "edge-point threshold" when an "end-of-contour" signal is sent. The starting point is examined again to see if the contour extends in the opposite direction to that first taken.

In transmitting the location of the contour points a great deal of advantage can be taken of their connectivity. The beginning point of a contour requires 16 bits to specify its location, although some sort of two-dimensional run-length coding could reduce this. The first sample on the contour can be in any direction, so that 3 bits are necessary to specify this. Because contours tend to be long, straight or curved lines, it is expected that the next point will lie in the same direction as the last, or perhaps 45° to either side. A variable-length code can be generated to describe these vector direction changes (vdc) efficiently. At any point that is on a contour, the gradient is quantized into 4 possible magnitudes and 8 directions. Since we expect the gradient to be in the same direction along a contour with occasional changes, the gradient direction change (gdc) can be coded in the same way as the vdc. In fact, changes in these two quantities are probably highly correlated. Since we search for the maximum value of the magnitude along a contour, we can also expect that to change slowly. An efficient code for the gradient magnitude change (gmc) can be derived from the conditional probabilities

Table XXX-1. Contour coding data for the figures.

Figure	XXX-5	XXX-6	XXX-7	XXX-8
Number of edge points	3994	8900	13980	2301
Number of contours	125	263	485	55
Number of bits for				
vdc	9850	20300	38400	5900
gdc	8420	17400	30600	4260
gmc	4840	11200	18900	2880
start point	2625	5513	10185	1155
lows	3000	3000	3000	3000
Total number of bits	28735	57413	101085	17195
Reduction factor	13.7	6.85	3.9	22.9

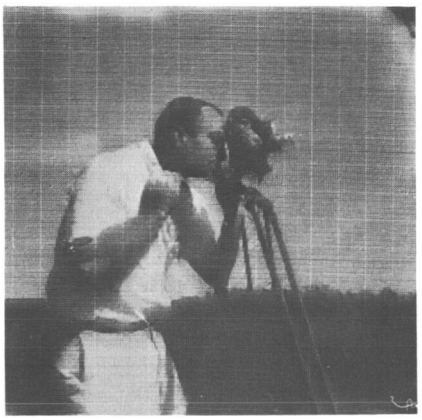

Fig. XXX-4. Output picture reconstructed after tracing and quantizing.

Contour Start Threshold = 38
Edge-Point Threshold = 12

Fig. XXX-5. Two-dimensional bandlimiting.

Reduction Factor = 16

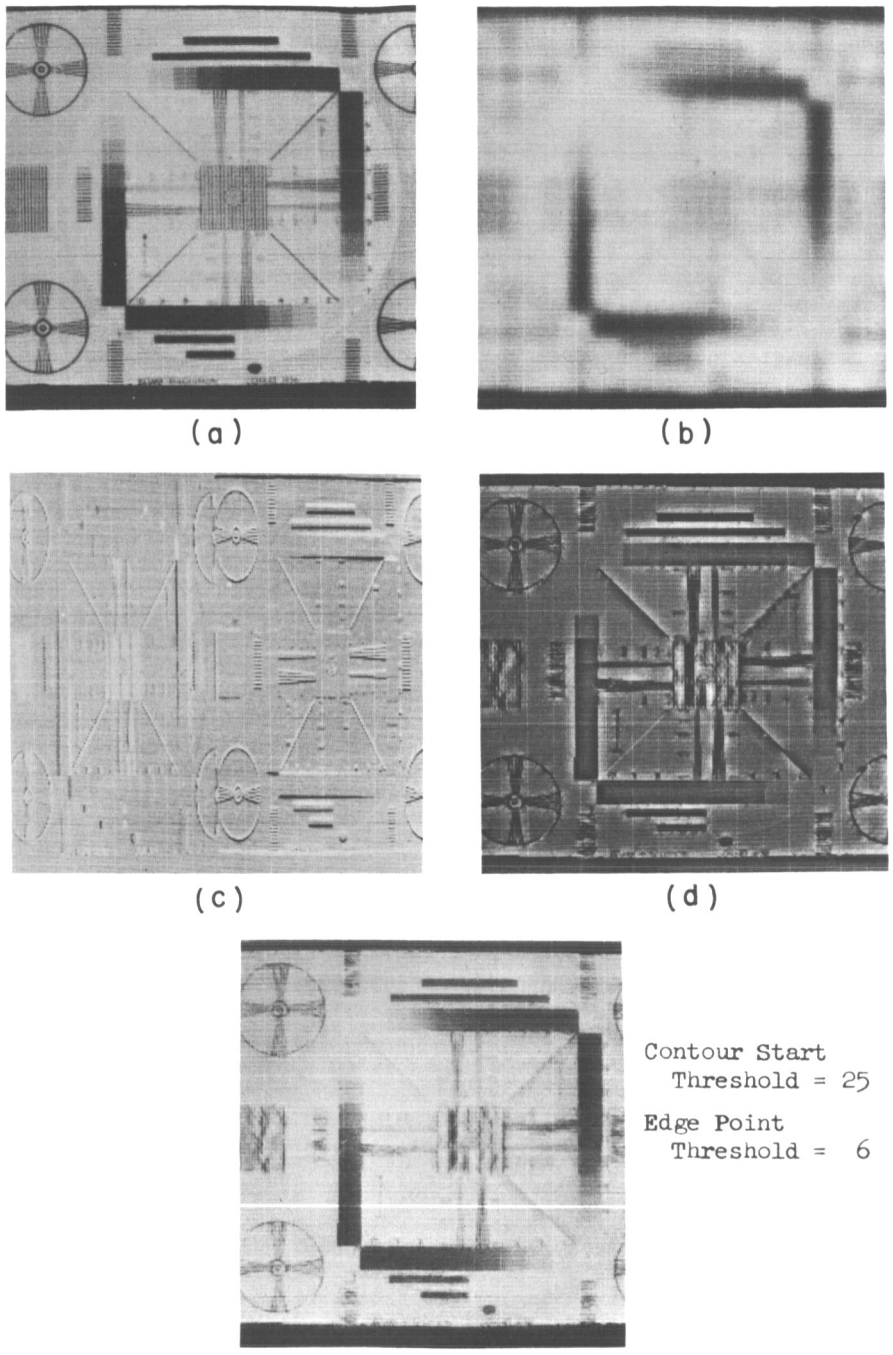

Fig. XXX-6. Simulation result.
(a) Original. (b) Lowpass.
(c) Gradient. (d) Synthetic highs.
(e) Output.

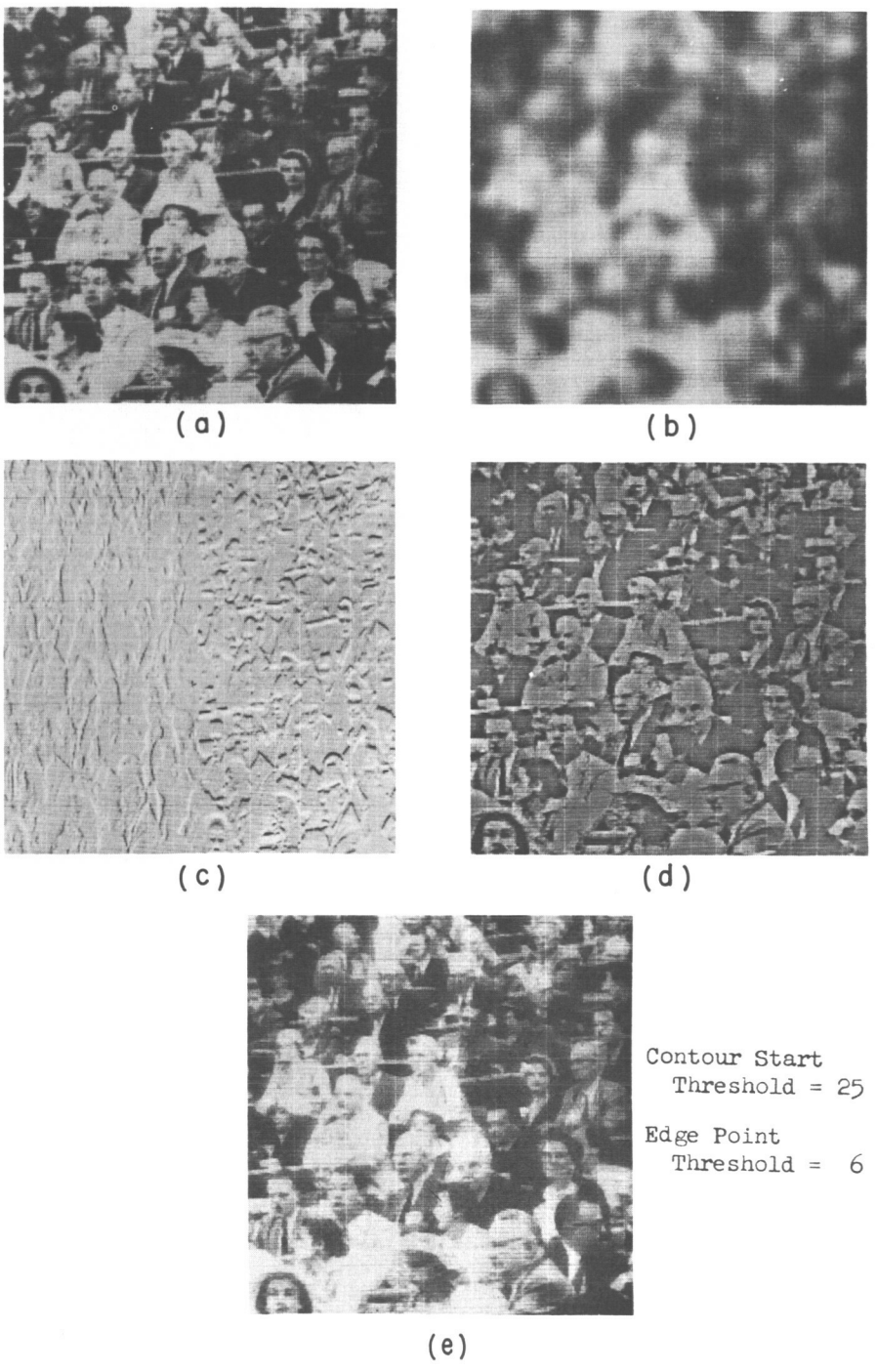

Fig. XXX-7. Simulation result.
(a) Original. (b) Lowpass.
(c) Gradient. (d) Synthetic highs.
(e) Output.

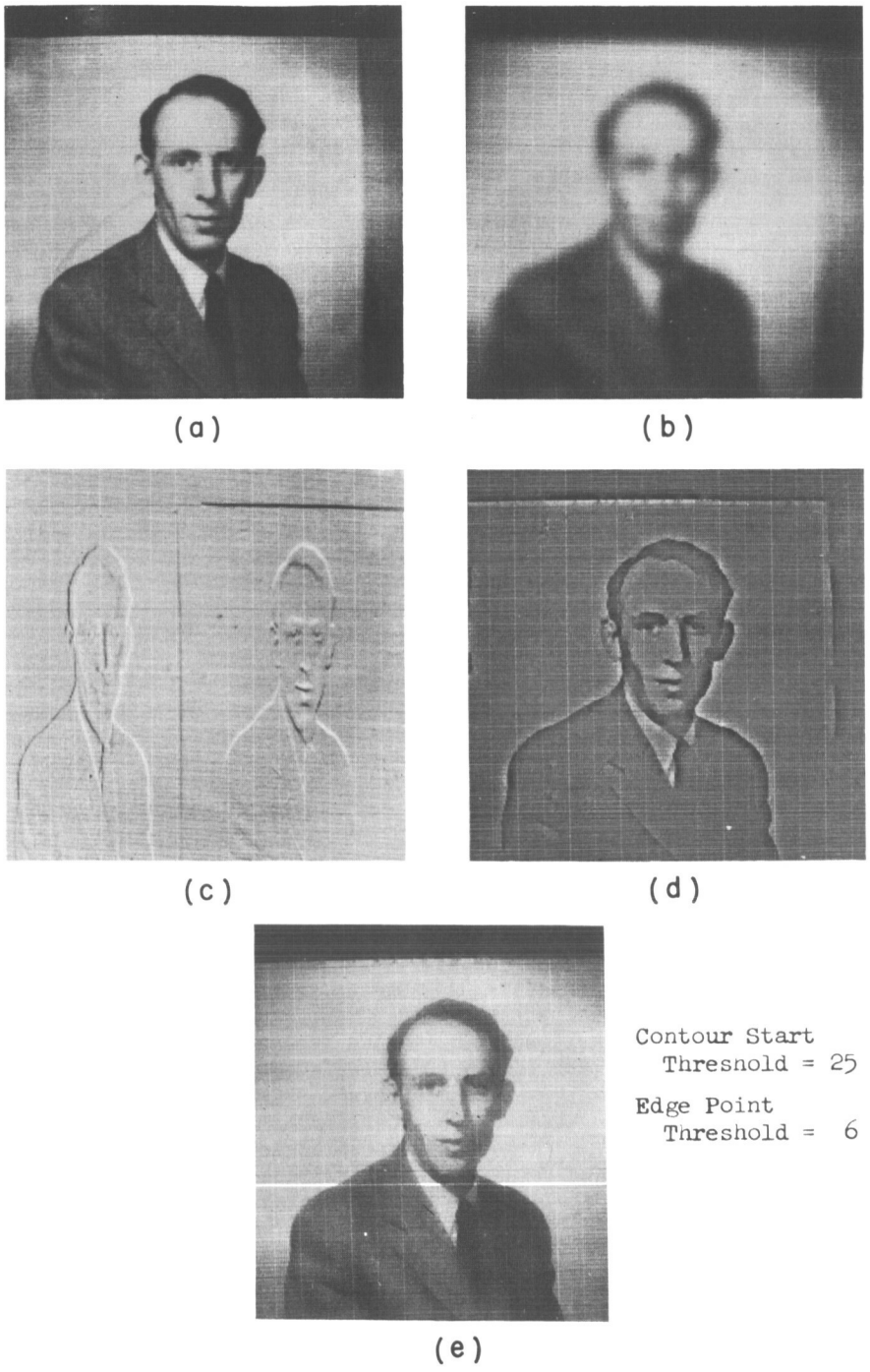

Fig. XXX-8. Simulation result.
(a) Original. (b) Lowpass.
(c) Gradient. (d) Synthetic highs.
(e) Output.

of change from each level.

The output picture with a reduction factor of 13.7 as compared with 6-bit PCM is shown in Fig. XXX-4. A similar bit reduction by two-dimensional bandlimiting is illustrated in Fig. XXX-5.

Figures XXX-6, XXX-7, and XXX-8 show other input pictures and the results of processing. The synthetic highs were accentuated by 1.2 before being added to the lows to give the output pictures. The coding data and bit reduction for each is given in Table XXX-1.

The reduction factor in bit rate over 6-bit PCM as calculated in Table XXX-1 should increase with a higher resolution system. For an $n \times n$ picture the total number of points goes as n^2, while the number of points on the edges is proportional to n. Thus if not many new contours were found in a 512×512 picture the reduction factor would approximately double over that found with a 256×256 picture.

D. N. Graham

References

1. J. W. Pan, "Picture Processing," Quarterly Progress Report No. 61, Research Laboratory of Electronics, M.I.T., July 15, 1962, p. 229.
2. W. F. Schreiber, "The Mathematical Foundation of the Synthetic Highs System," Quarterly Progress Report No. 68, Research Laboratory of Electronics, M.I.T., January 15, 1963, p. 140.
3. D. N. Graham, "Two-dimensional Synthesis of High Spatial Frequencies in Picture Processing," Quarterly Progress Report No. 75, Research Laboratory of Electronics, M.I.T., October 15, 1964, p. 131.
4. D. N. Graham, "Image Transmission by Two-dimensional Contour Coding," Ph.D. Thesis, Department of Electrical Engineering, M.I.T., September 1966.

C. FOURIER-TRANSFORM REPRESENTATION OF PICTURES

With the appearance of the Cooley-Tukey algorithm,[1] which reduces the number of operations in the machine calculation of Fourier series, possibilities for new investigations in picture processing have presented themselves. The use of PCM picture transmission has been well investigated.[2] Now, given an array of numbers, constituting a sampling of image brightness levels, the Fourier series may be determined for a periodic, two-dimensional, discrete function generated from the array. This Fourier series

(a)

(b)

(c)

Fig. XXX-9.

(a) Original picture used in the study.
(b) Result of 5-bit quantization on conventional PAM samples.
(c) Result of 5-bit quantization on Fourier series samples.

will be periodic in two dimensions also. If the image was properly bandlimited before sampling, then the two-dimensional period of the Fourier series, centered around the DC term, is a sampled version of the Fourier transform of the original unsampled image. The coefficients in a period of the Fourier series, which are, in general, complex, are equal in number to the samples taken of the image. The transform of a real function obeys a symmetry condition, $F(u, v) = F^*(-u, -v)$, where $F(u, v)$ is the two-dimensional transform with frequency variables u and v, and * denotes conjugation. This allows representation of the periodic two-dimensional Fourier series by only one-half of the coefficients in any period of the series. Instead of using N real numbers to represent a picture, N/2 complex numbers may be used by Fourier analysis.

Of interest is the result of quantization on picture quality when Fourier series samples are used for picture representation. Partial results in this investigation have been obtained. Figure XXX-9a is the original picture used in this study. This picture was sampled to form a 64×64 array and then quantized to 5 bits per sample. A linear interpolation scheme was then used to obtain the picture in Fig. XXX-9b. Figure XXX-9c was obtained by first calculating a Fourier series using the 64×64 sample array, quantizing the series samples to 5 bits, inverting the series to get a picture array, and then finally interpolating. Figure XXX-9b and 9c are seen to be comparable, thereby indicating that the Fourier series samples are no more susceptible to quantization noise than are conventional PAM samples. The degradation of Fig. XXX-9b and 9c with respect to Fig. XXX-9a is due not only to quantization but also to the heavy aliasing in the sampling process.[3] It is expected that at least a slight improvement is possible for Fig. XXX-9c by using a readjustment of quantization scale, since some of the Fourier series samples were well out of range.

The sampling array was limited to 64×64, because of memory limitations of the IBM 7094 computer.

G. B. Anderson

References

1. J. W. Cooley and J. W. Tukey, "An Algorithm for the Machine Calculation of Complex Fourier Series," Mathematics of Computation, pp. 297-301, April 1965.
2. T. S. Huang, "PCM Picture Transmission," IEEE Spectrum, Vol. 2, No. 12, pp. 57-63, December 1965.
3. O. J. Tretiak, "The Picture Sampling Process," Sc. D. Thesis, Department of Electrical Engineering, M. I. T., 1963.

D. EFFECT OF MULTIPATH ON HOLOGRAM TELEVISION SYSTEMS

1. Introduction

There are three reasons why one might want to transmit a hologram of a scene instead of a conventional picture of the scene.

(i) Although the hologram itself is two-dimensional, the reconstruction of the original scene can be made three-dimensional.

(ii) The effect of channel disturbances on the quality of the reconstructed picture of a hologram television system will be different from its effect on the received picture of a conventional television system. In certain cases, the degradation in picture quality in a hologram TV system may be more acceptable than that in a conventional TV system.

(iii) A hologram may be more amenable to certain bandwidth compression schemes than a conventional picture.

In order to exploit the second point mentioned above, it is necessary to find out how various channel disturbances will affect the reconstructed picture in a hologram TV system. In this report, we present some preliminary results on the effect of multipath or echo on the reconstructed picture of an analog hologram TV system.

2. Theoretical Analysis for Fourier-Transform Holograms

Let $f(x,y)$ be the light (amplitude) distribution, as a function of the spatial coordinates x and y, which we wish to reconstruct at the receiver. Then, except for some scale factors, the Fourier-transform hologram of $f(x,y)$ is

$$H(u,v) = \left|F(u,v)+A\, e^{-jau}\right|^2, \tag{1}$$

where $F(u,v)$ is the Fourier transform of $f(x,y)$, u and v are the spatial frequencies, and A and a are real constants. The term in the right-hand side of Eq. 1, which is responsible for the reconstruction, is[1]

$$H_1(u,v) = A\, F(u,v)\, e^{jau}. \tag{2}$$

If the hologram is scanned (in the v-direction, say), and transmitted in analog fashion, and if there are two different transmission paths, then the received hologram will be

$$H_r(u,v) = H(u,v) + bH(u,v-d), \tag{3}$$

where b and d are real constants. The term on the right-hand side of Eq. 3, which is responsible for the reconstruction, is

$$H_{r1}(u,v) = \left[A\, F(u,v) + Ab\, F(u,v-d)\right] e^{jau} \tag{4}$$

and the reconstructed light (amplitude) distribution will be proportional to

clearly exhibit the fringelike structures predicted by Eq. 6.

4. Fresnel Holograms

A similar analysis of a Fresnel hologram indicated that the effect of multipath in that case is twofold: The reconstructed picture will contain ghost images just as in a conventional TV system, and the overlapping areas of the images will contain fringe-like structures.

T. S. Huang, P. L. Stamm

References

1. T. S. Huang and B. Prasada, "Considerations on the Generation and Processing of Holograms by Digital Computers," Quarterly Progress Report No. 81, Research Laboratory of Electronics, M.I.T., April 15, 1966, p. 199.

E. OPTICAL SPATIAL FILTERING FOR SIMULTANEOUS DELAY AND DOPPLER ESTIMATES OF RADARLIKE SIGNALS

Optical processors have been recognized in recent years as efficient tools for performing spectral analysis and linear filtering, particularly when the data to be processed are two-dimensional.[1] Both coherent and incoherent systems are possible, although the coherent systems are generally more useful. These systems have found application in various kinds of pattern recognition,[2] analysis of nuclear particle tracks in bubble chamber photographs,[3] analysis of seismic data,[4] processing of video signals in synthetic aperture radar,[5] and pulse compression (matched filtering).[6]

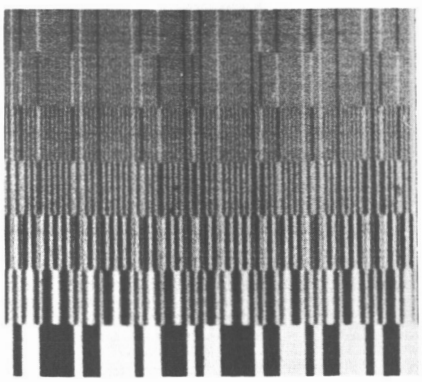

Fig. XXX-13. Space-domain filter function from which the frequency-domain filter was constructed; actual size, 3/8 inch square.

The investigation reported here concerns the use of a coherent spatial matched filter to extract range and Doppler information from a radar or radarlike signal recorded on photographic film, and to present the estimates in a two-dimensional display. An experimental system has been constructed and successfully demonstrated. In the system

the Fourier-transfrom properties of a lens were used to generate the spatial frequency spectrum of an input signal, and the filtering was done in the frequency plane. Computer-generated space-domain filter function transparencies (see Fig. XXX-13) were made with our laboratory's picture-processing equipment, and the frequency plane filter was made photographically with the same optical equipment used for the filtering. Both the signals and frequency plane filter were recorded by modulation on carriers. The signal used was a 49-bit pseudo-random binary shift register code, chosen for its sharply peaked autocorrelation function. The filter was constructed with 7 discrete Doppler channels separated by 1/2 cycle/bit (nothing precludes a continuous filter in the Doppler direction; it was made discrete for simplicity of display). One-half of the spatial frequency plane was blocked to make the system independent of carrier phase.[1]

The system functioned approximately as predicted by theory, although the spurious responses ("self-noise") of the filter were larger than expected (Fig. XXX-14). This

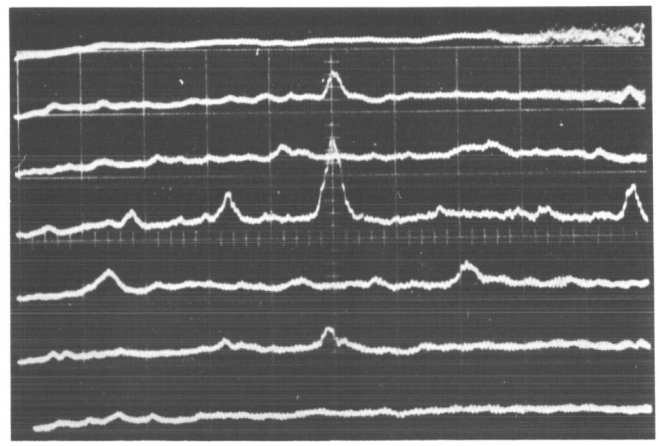

Fig. XXX-14. Response of system to noisefree input; 5 bits/cm horizontal, arbitrary intensity (each trace) vertical; the traces correspond to equidistant channels in the output plane.

we attribute to severe nonlinearity in the photographic process used to construct the frequency-plane filter. The system successfully extracted signals from Gaussian noise with a 0-db S/N energy ratio; a distortionless system should be able to improve this by approximately 10 db (see Fig. XXX-15).

Substantial improvements in performance can probably be obtained by using filters constructed directly in the frequency domain on a computer[7]; this was not attempted because of the low quality of the optical equipment available to us (many of the distortions introduced by an aberrated lens are cancelled if the lens that is to be used for the

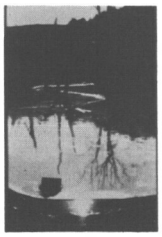

(a)

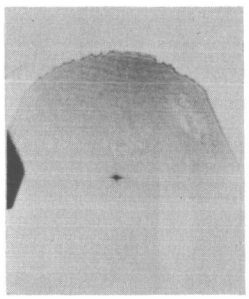

(b)

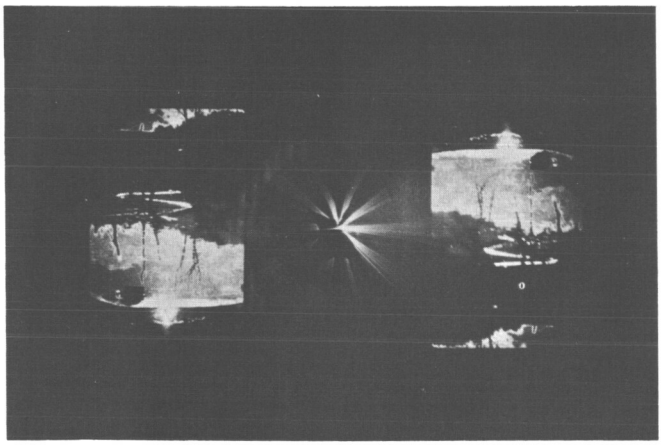

(c)

Fig. XXX-10. (a) Original scene. (b) Its Fourier-transform hologram. (c) Reconstruction from the hologram.

$$g(x,y) = f(x,y)(1 + b\cos dy) + jbf(x,y)\sin dy. \tag{5}$$

The observed intensity distribution then is

$$|g(x,y)|^2 = (1 + b^2 + 2b\cos dy)|f(x,y)|^2. \tag{6}$$

Therefore, the reconstructed scene is the original scene multiplied by a biased sine wave. It will contain fringelike structures, the spacing of the fringes being dependent on d, the delay of one of the transmission paths. The case of more than two transmission paths can be analyzed in a similar way.

3. Experimental Results

The case just discussed was simulated on an optical bench. An apparatus was arranged to make Fourier-transform holograms of a transparency. The multipath was simulated by shifting and double-exposing the film in the hologram plane.

Figure XXX-10 shows the original scene on the transparency, its Fourier-transform

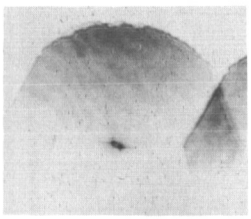

(a)

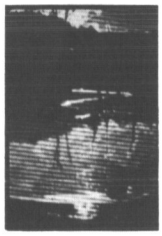

(b)

Fig. XXX-11. (a) A two-path hologram.
(b) Its reconstruction.

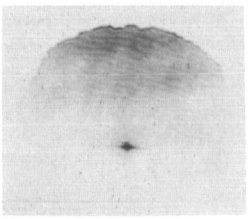

(a)

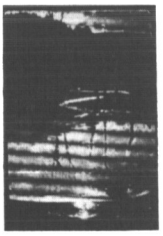

(b)

Fig. XXX-12. (a) Another two-path hologram (with smaller delay).
(b) Its reconstruction.

hologram, and the reconstruction from the hologram. Figures XXX-11 and XXX-12 show two simulated two-path holograms and their reconstructions. The delay, d, in Fig. XXX-12 is approximately 1/4 that in Fig. XXX-11. These reconstructed pictures

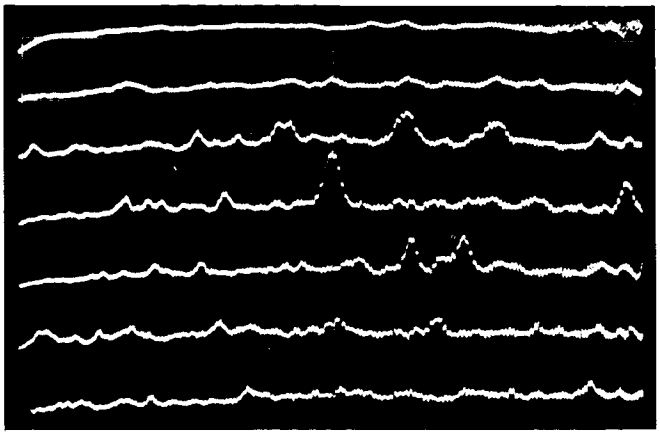

Fig. XXX-15. Response to signal plus Gaussian noise, 0-db S/N energy ratio; same scale as in Fig. XXX-14.

processing is also used for transforming the filter function). High-quality optical equipment and care in the construction of filters should result in improving attainable compression ratios by one or two orders of magnitude.

A. H. M. Ross

References

1. L. J. Cutrona, E. N. Leith, C. J. Palermo, and L. J. Porcello, "Optical Data Processing and Filtering Systems," IRE Trans., Vol. IT-6, p. 386, June 1960.
2. J. D. Armitage and A. W. Lohmann, "Character Recognition by Incoherent Spatial Filtering," Appl. Opt. 4, 461 (April 1965).
3. D. G. Falconer, "Optical Processing of Bubble Chamber Photographs," Appl. Opt. 5, 1365 (September 1966).
4. P. L. Jackson, "Diffractive Processing of Geophysical Data," Appl. Opt. 4, 419 (April 1965).
5. L. J. Cutrona, E. N. Leith, L. J. Porcello, and W. E. Vivian, "On the Application of Coherent Optical Processing Techniques to Synthetic-Aperture Radar," Proc. IEEE 54, 1026 (1966).
6. A. Kozma and D. L. Kelly, "Spatial Filtering for Detection of Signals Submerged in Noise," Appl. Opt. 4, 387 (April 1965).
7. B. R. Brown and A. W. Lohmann, "Complex Spatial Filtering with Binary Masks," Appl. Opt. 5, 967 (June 1966).

XXXI. COMMUNICATIONS BIOPHYSICS*

Academic and Research Staff

Prof. P. R. Gray†
Prof. P. G. Katona
Prof. W. T. Peake‡
Prof. W. M. Siebert
Prof. W. A. Rosenblith ET AL
Prof. T. F. Weiss‡
Dr. J. S. Barlow**
Dr. G. O. Barnett¶
Dr. A. Borbely††
Dr. A. W. B. Cunningham¶¶
N. I. Durlach
Dr. H. Fischler‡‡
Dr. O. Franzen***
Dr. R. D. Hall
Dr. G. Hellekant†††
Dr. N. Y. S. Kiang‡
Dr. R. G. Mark‡‡‡
Dr. M. Nomoto****
Dr. R. Rojas-Corona
Dr. G. F. Songster
R. M. Brown‡
A. H. Crist‡
D. P. Langbein‡

Graduate Students

J. A. Anderson
J. Berliner
G. von Bismarck
L. D. Braida
S. K. Burns
A. N. Chandra
H. S. Colburn
J. E. Evans
J. A. Freeman
J. J. Guinan, Jr.
R. Hershkowitz
H. Hsiao
E. G. Merrill
P. J. Metz
D. C. Milne
E. C. Moxon
M. Nahvi
S. Portny
D. J-M. Poussart
I. H. Thomae
M. L. Wiederhold

RESEARCH OBJECTIVES AND SUMMARY OF RESEARCH

The principal activities of the Communications Biophysics Group tend to combine electrophysiological and behavioral experiments with machine data processing and analytical methods. Our major objective is to obtain a better understanding of sensory

---

*This work was supported principally by the National Institutes of Health (Grant 2 PO1 MH-04737-06), the Joint Services Electronics Programs (U. S. Army, U. S. Navy, and U. S. Air Force) under Contract DA 36-039-AMC-03200(E), the National Science Foundation (Grant GK-835), the National Aeronautics and Space Administration (Grant NsG-496), and in part by the National Institutes of Health (Grant 5 RO1 NB-05462-03).

†Leave of absence, at General Atronics Corporation, Philadelphia, Pennsylvania.

‡Also at Eaton-Peabody Laboratory, Massachusetts Eye and Ear Infirmary, Boston, Massachusetts.

**Research Affiliate in Communication Sciences from the Neurophysiological Laboratory of the Neurology Service of the Massachusetts General Hospital, Boston, Massachusetts.

††Postdoctoral Fellow from the Brain Research Institute, University of Zurich, Zurich, Switzerland.

‡‡From the Department of Electronics, Weizmann Institute of Science, Rehovoth, Israel.

***Postdoctoral Fellow from the Speech Transmission Laboratory, The Royal Institute of Technology, Stockholm, Sweden.

†††Postdoctoral Fellow from the Department of Physiology, Kungl. Veterinarskolan, Stockholm, Sweden.

‡‡‡Assistant Resident, Harvard Medical Service, Boston City Hospital, Boston, Massachusetts.

****Public Health Service International Postdoctoral Research Fellow, from the Department of Physiology, Tokyo Medical and Dental University, Tokyo, Japan.

¶Associate in Medicine, Department of Medicine, Harvard Medical School, and Director, Laboratory of Computor Science, Massachusetts General Hospital.

¶¶Associate in Pathology, Peter Bent Brigham Hospital.

communication – in particular, of hearing. But in addition to our major research interests, we have found it profitable to apply our tools and methods selectively to other organisms and other systems as suggested below.

The group continues close cooperation with the Eaton-Peabody Laboratory of Auditory Physiology at the Massachusetts Eye and Ear Infirmary. This laboratory is operated cooperatively by M. I. T. and the Eye and Ear Infirmary. The cooperative arrangements include joint appointments of scientific staff. Some of the projects described below (Sec. A) will actually be carried out at the Eaton-Peabody Laboratory by staff members and students of the Communications Biophysics Group.

The research program of the Communications Biophysics Group can be divided into five or six major areas. The programs for each area are discussed individually in the following subsections.

A. Research on the Peripheral Auditory System

Our studies of the auditory system in the recent past have ranged from the acoustic properties of the external ear to the electrical activity recorded at the cortex. The principal projects of current interest are the following.

1. Our experimental studies of the signal transmission properties of the middle ear in cat during the past few years have provided a fairly accurate transfer function. Further work on the middle ear will be aimed at achieving (a) a detailed verification of the lumped-element model that we have developed, and (b) making measurements of transfer characteristics in a wider range of conditions.

2. Studies of the dependence of intracochlear potentials on position in the cochlea, as well as on stimulus parameters, could be exceedingly important for the understanding of the mechanical-to-neural transduction process. Techniques have been developed for introducing micropipettes into the basal turn of the cochlea, recording DC, as well as AC, potentials, and for determining histologically the position of the electrode. A series of experiments has been planned to extend systematically our preliminary observations.

3. Recent microelectrode studies of the discharge patterns of single fibers in the auditory nerve have provided a remarkably orderly outline of the relationship between this activity and the acoustic stimulus. Future studies will concentrate on certain aspects of responses to stimuli that are slightly more complex than the clicks and tone bursts that have dominated our earlier work. Our objectives continue to be both to achieve a better understanding of the processes of excitation in the cochlea and to furnish a description of the discharge patterns in terms of a random-process model.

4. Single-unit response patterns in the cochlear nucleus of cats have been studied in some detail in our laboratories. Also, anatomical investigations of the outputs of the cochlear nucleus have begun to describe the connections of the cochlear nucleus to other brain-stem nuclei. In parallel with these anatomical studies, we are starting electrophysiological mapping of the superior olivary region.

5. Electrical stimulation of the olivocochlear bundle has been shown by several workers to have a significant gross effect on the auditory nerve responses to acoustic stimuli. Techniques for studying such efferent influences on single auditory nerve fibers have been developed; the effects on thresholds, tuning curves, and so forth, will be systematically explored.

6. The probabilistic behavior of certain isolated, peripheral nerve fibers in response to electrical stimulation has been observed by various workers for 30 years. We have recently developed the necessary techniques and have repeated some of these observations in isolated, sciatic nerve fibers of the frog. The problem will be further pursued in the frog and in the large unmyelinated fibers of other species. The problem is of interest for two reasons: (i) an understanding of the probabilistic mechanisms in single

fibers has bearing on understanding the coding of messages in fibers of sensory systems, and (ii) understanding the probabilistic generator might lead to some insights into the mechanisms governing the behavior of nerve membrane in general.

7. During the last several years, an attempt has been made to explore the implications for auditory behavior – particularly discrimination – of the observed stochastic nature of the coding of acoustic stimuli in the auditory nerve. The results of these theoretical efforts have suggested, among other things, a plausible mechanism that might underlie the Weber-Fechner law and have yielded new insights into the "place" versus "volley" pitch controversy. Future studies are planned which may be helpful in understanding a variety of other auditory phenomena including various kinds of masking, critical bands, and certain binaural interactions.

N. Y. S. Kiang, W. T. Peake, W. M. Siebert, T. F. Weiss

B. Neuroelectrical Correlates of Conditioning

During the past five years, we have been studying sensory evoked activity during conditioning as a particular example of the study of the brain's electrical activity during the acquisition of learned behavior. In the coming years we plan to extend these studies and also venture into several relatively unexplored problem areas as described below.

1. In the search for neuroelectric correlates of conditioning several lines of evidence suggest that it would be advantageous to examine the activity of central structures that have direct influence on motoneuron pools. Specifically, activity in such structures as the subthalamic nucleus, red nucleus, portions of the mesencephalic and bulbar reticular formations, as well as the motor cortex, would seem to be of interest. In some preliminary studies of activity in motor pathways, we have developed a conditioning situation for the rat that appears to be quite adequate for such work. The principal remaining problems concern the proper choice of recording electrodes and the appropriate types of data analysis.

2. A principal conclusion of our past investigations is that alterations in evoked responses observed in primary sensory pathways during aversive conditioning are not intimately related to the neural substrate of conditioning, but instead are indicative of an emotional response to noxious stimulation. Changes in evoked activity cannot be found in primary sensory systems as the discriminative behavior is acquired if the appetitive instrumental conditioning paradigm is employed. It seems advisable, however, to extend this research to nonspecific, polysensory systems (e.g., medial thalamic nuclei). An experimental situation has been developed (it is essentially an analog for the rate of a human reaction time experiment) that appears to meet the logical requirements, but it will have to be refined in order to reduce the training time and to insure adequate control of stimulus and movement-related variables.

3. The finding that evoked potentials are significantly altered during a fear response raises questions with their own intrinsic interest. The fear response is a very generalized reaction that can readily be brought under stimulus control. The alterations in evoked responses should therefore be quite amenable to experimental analysis. Combined lesion and electrophysiological techniques should carry this analysis quite far.

4. Over the long range, we hope to initiate some electrophysiological conditioning studies on invertebrate species. It is not at all clear that it is possible to develop an invertebrate preparation in which conditioned control of behavior can be readily achieved under conditions suitable for the recording of single-unit potentials, but the promises of such a preparation are sufficiently great to warrant a serious attempt.

R. D. Hall, W. A. Rosenblith

C. Psychophysics

Our research in psychophysics during the last few years has been concerned primarily with binaural hearing. During the coming year we intend to continue research in this area and to initiate research in a number of other areas. Our current interests are outlined as follows.

1. Binaural Hearing

Our previous work on binaural hearing has consisted of constructing a black-box model, the equalization and cancellation (EC) model, and performing a variety of experiments to test it. The projects of current interest in binaural hearing concern (a) the effects of interaural phase shifts and bandwidth on binaural unmasking; (b) the effect on binaural unmasking of introducing interaural relations in the noise that are unlike those encountered in a natural environment; (c) the ability of the EC model to predict just-noticeable differences (jnd's) in interaural time delay, amplitude ratio, and decorrelation; (d) the extent to which an interaural amplitude difference can be discriminated from an interaural time difference; and (e) the development of a new quantitative model of binaural hearing based on physiological data.

2. Effect of Duration on Pitch Discrimination for "Place Pitch" versus "Periodicity Pitch"

It is well known that the sensation of pitch can arise from characteristics of the energy spectrum of the signal (place pitch) or from periodicity characteristics (periodicity pitch). Recent computations based on auditory-nerve data and ideal-observer theory indicate that the effect of duration on pitch discrimination may be different in the two cases. Plans are now being made to explore this question empirically.

3. Short-Term Memory for Sounds

Although much work has been done on short-term memory, relatively little is known about this topic for the situations usually considered in psychoacoustic experiments. Moreover, the knowledge that exists is seldom incorporated into the models constructed for interpreting psychoacoustic data. An effort is now under way to construct a quantitative model of short-term memory for sounds that can be used for interpreting these data, and to perform experiments that will guide the development of this model.

4. Sequential Effects

Past research has shown that a subject's response to a given stimulus is determined not only by that stimulus, but also by previous stimuli, previous responses, and previous feedback in the experimental series. Since the sequence of previous events varies from trial to trial, a portion of the subject's response variability can be ascribed to these variations. Research is now being initiated to study sequential effects in detail, and to separate these effects from other sources of response variability (such as internal noise). In addition to performing specific experiments on this topic, we intend to store the complete history of practically all of our future experiments and to analyze sequential effects as a routine matter, independently of the primary purpose of the experiment.

5. Subjective Estimates of Uncertainty

In most psychophysical experiments, the experiment is structured in such a way that the only means by which the experimenter can obtain information on the subject's

uncertainty about his choice of response is by repeating the same stimulus a number of times and examining the response variability. This method has the advantage of objectivity, but tends to confuse the "instantaneous uncertainty" experienced by the subject on a single trial with variations in the state of the subject from trial to trial. In certain cases, substantial benefits can be obtained by requiring that the subject describe his uncertainty directly on each trial. Experiments are now being planned to study the relation of these subjective estimates of uncertainty to the estimate obtained by examining the variability obtained in repeated trials.

6. Relation of Magnitude Estimation to Absolute Identification

One model for interpreting a subject's behavior in an absolute identification task (in which the stimuli to be identified are selected from a unidimensional, prothetic, continuum) is to assume that the subject estimates the magnitudes of the stimuli, recodes the names of the stimuli chosen by the experimenter into these estimates, and bases his identification choice on a given trial according to his magnitude estimate on that trial. Preliminary research has indicated that this model is capable of precise formulation and that it may be an accurate one. Experiments are now being initiated to test this model. A related effort concerns the search for a precise and useful definition of "unidimensional." Also, experiments are planned to determine the dependence of absolute identification performance on the means available to the subject for storing and recalling his previous sensations.

7. Relation of Magnitude Estimation to Discrimination and Detection (Microscaling)

At present, there is a large schism in psychophysics between discrimination and detection on the one hand, and magnitude estimation and cross-modality matching on the other hand. By studying magnitude estimation and cross-modality matching over very small stimulus ranges (microscaling) and considering intrasubject variability in the estimates, as well as the central tendency, we hope to bridge the gap between these two areas of activity.

N. I. Durlach, W. M. Siebert, W. A. Rosenblith

D. Other Neurophysiological Research

In addition to the programmatic research in specific problem areas described above, our group has always supported a few studies in central nervous system function – particularly those that seem likely to profit from our general interest in analytical and computer techniques. It is impossible to foresee in detail what specific research of this kind will be undertaken during the coming year, since the prospects stem from the particular interests of predoctoral and postdoctoral students and mutual interests (although perhaps not primary interests) of various staff members. Current projects in this more general category (many of which will be continued) include the following.

1. The response pattern of cells in the cerebellum is being studied with specific emphasis upon excitatory and inhibitory states of cells following a sensory stimulus such as a click. The results are used in the formulation of a possible structural model with stochastic properties.

2. A study is also in progress on the behavior of respiratory neurons in the medulla, particularly in the nucleus of the solitary tract.

3. Two studies are under way of single-unit activity evoked in the optic nerve of cat by a variety of photic stimuli. Emphasis in both cases is placed on the quantitative analysis of the unit potentials.

4. Intracellular potentials from units in the cerebral ganglion of Aplysia californicus that respond to tactile stimulation are under investigation. This work also aims at giving a detailed description of the pathways serving touch in this species.

5. Another study of the cerebellum involves exploration of a possible source-sink analysis of cerebellar potentials suggested by the relatively simple laminar morphology of this structure.

W. A. Rosenblith

E. EEG Studies

Several useful techniques have been developed for analyzing the characteristically nonstationary electroencephalographic data obtained from recording from the scalp of a human subject. One method involves observing the cumulative behavior of amplitudes from a sequence of evoked responses. Another useful display is a sequence of frequency spectra in which each individual spectrum is based on a few seconds of data, but the sequence itself covers samples lasting many minutes or even hours. These displays have a third dimension – that of time, and they emphasize changes in the data concomitant with changes in the subject's "state." Apparatus is being designed and constructed which will conveniently implement these displays.

We continue to study the relationships between the EEG alpha rhythm, psychophysical variables, and biochemical phenomena by using facilities and subjects at the M.I.T. Clinical Research Center. So that confidence levels can be established for averaged evoked responses, we plan to develop a method of estimating variance of the evoked response from an examination of the displayed average evoked response. We also plan to examine the possibility of using a matched filter based on the averaged evoked response to enhance individual responses in slow-wave data. We have been involved with and hope to continue a program of evaluation and development of medical instrumentation that is potentially useful clinically.

S. K. Burns, W. A. Rosenblith

F. Cardiovascular System Studies

The aim of our research is the quantitative understanding of the cardiovascular control mechanism. In particular, we are investigating, at present, that part of the carotid-sinus reflex which causes sudden heart-rate changes as a result of the introduction of sudden disturbances in the arterial blood pressure.

Three major projects are being carried out.

1. The quantitative description of the relationship between blood pressure and the firing pattern of pressure receptor nerves.

2. The statistical characterization of the firing pattern of the cardiac vagal efferent nerve fibers.

3. The determination of the relationsip between vagal efferent firing frequency and heart rate.

P. G. Katona

SELECTED PUBLICATIONS

J. S. Barlow, "A Simple Time Division Multiplexing System for Low-Frequency Bioelectric Signals," IEEE Trans., Vol. BME-13, pp. 195-199, 1966.

J. S. Barlow, "Electronic Simulation as an Aid in Evaluating Computer-Analyzed EEG Data," Electroencephal. clin. Neurophysiol. (in press).

S. K. Burns and R. Melzack, "A Method for Analyzing Variations in Evoked Responses," Electroencephal. clin. Neurophysiol. 20, 407-409 (1966).

A. W. B. Cunningham, P. O'Lague, R. Rojas-Corona and J. A. Freeman, "Microelectrode Studies of Spontaneous Potentials from Chick Embryo Telencephalon in vitro," Experientia 22, 439-446 (1966).

N. I. Durlach, "On the Application of the EC Model to Interaural Jnd's," J. Acoust. Soc. Am. (in press).

H. Fischler, N. Peled, and S. Yerushalmi, "FM/FM Multiplex Radio-Telemetry System for Handling Biological Data," IEEE Trans. on Bio-Medical Engineering (in press).

D. B. Geselowitz, "Comment on Core Conductor Model," Biophys. J. 6, 691-692 (1966).

P. R. Gray, "A Statistical Analysis of Electrophysiological Data from Auditory Nerve Fibers in Cat," Technical Report 451, Research Laboratory of Electronics, Massachusetts Institute of Technology, Cambridge, Mass., June 21, 1966.

R. D. Hall, R. J. Clayton, and R. Mark, "A Device for the Partial Restraint of Rats in Operant Conditioning Studies," J. Exptl. Anal. Behav. 9, 143-145 (1966).

R. D. Hall and R. G. Mark, "Acoustically Evoked Potentials in the Rat during Conditioning," Technical Report 455, Research Laboratory of Electronics, Massachusetts Institute of Technology, Cambridge, Mass., November 30, 1966.

N. Y. S. Kiang, with T. Watanabe, E. C. Thomas, and Louise F. Clark, Discharge Patterns of Single Fibers in the Cat's Auditory Nerve (The M.I.T. Press, Cambridge, Mass., 1966).

N. Y. S. Kiang, J. W. Shipley, and M. B. Sachs, "Sensitivity of Single Auditory-Nerve Fibers to Acoustic Stimuli," J. Acoust. Soc. Am. 39, 1253 (A) (1966).

K. Koerber, R. R. Pfeiffer, W. B. Warr and N. Y. S. Kiang, "Spontaneous Spike Discharges from Single Units in the Chochlear Nucleus after Destruction of the Cochlea," Exptl. Neurol. 16, 119-130 (1966).

B. J. Murawski and S. K. Burns, "Day-to-Day Correlation of Urinary Adrenal Steroids and Alpha Frequencies in the EEG," J. Appl. Physiol. 21, 549-553 (1966).

W. T. Peake and J. J. Guinan, Jr., "Circuit Model for Transfer Characteristics of the Cat's Middle Ear," J. Acoust. Soc. Am. 39, 1253 (A) (1966).

R. R. Pfeiffer, "Classification of Response Patterns of Spike Discharges for Units in the Cochlear Nucleus: Tone-Burst Stimulation," Exptl. Brain Res. 1, 220-235 (1966).

R. R. Pfeiffer, "Anteroventral Cochlear Nucleus: Waveforms of Extracellularly Recorded Spike Potentials," Science 154, 667-668 (1966).

L. R. Rabiner, C. L. Lawrence and N. I. Durlach, "Further Results on Binaural Unmasking and the EC Model, J. Acoust. Soc. Am 40, 62-70 (1966).

W. A. Rosenblith, "Physics and Biology—Where do They Meet?," Physics Today, Vol. 19, No. 1, pp. 23-34, January 1966.

W. A. Rosenblith, "On Cybernetics and the Human Brain," The American Scholar 35, 243-248 (1966).

W. A. Rosenblith, "From a Biophysicist Who Came to Supper," R. L. E.: 1946 + 20, Research Laboratory of Electronics, Massachusetts Institute of Technology, Cambridge, Mass., May 1966, pp. 42-44.

M. B. Sachs and N. Y. S. Kiang, "Iso-Rate Contours for Single Auditory-Nerve Fibers," J. Acoust. Soc. Am. 39, 1252 (A) (1966).

R. Suzuki, "Simulation Study of a Hand Controlled by Myoelectric Signals," Conference on Data Acquisition and Processing in Biology and Medicine, Rochester, New York, July 27, 1966 (A).

T. F. Weiss, "A Model of the Peripheral Auditory System," Kybernetik (in press).

M. L. Wiederhold and W. T. Peake, "Effectiveness of Crossed Olivocochlear Bundle Stimulation. Dependence on Acoustic Stimulus Parameters," J. Acoust. Soc. Am. (in press).

F. M. Wiener, R. R. Pfeiffer, and A. S. N. Backus, "On the Sound Pressure Transformation by the Head and Auditory Meatus of the Cat," Acta Oto-Laryngol. 61, 256-269 (1966).

THESES

1. David Assael, "The Effect of Intensity on Pitch in Human Hearing," S. B. Thesis, Department of Electrical Engineering, M.I.T.
2. James E. Brown III, "Research on the 'Vector Model' of Binaural Unmasking," S.B. Thesis, Department of Electrical Engineering, M.I.T.
3. Charles Cain, "Spontaneous Potentials from Chick Embryo Cerebellum in Tissue Culture," S.M. Thesis, Department of Electrical Engineering, M.I.T.
4. Richard E. Doherty, "A Behaviorally Sorted Recording and Averaging System for Electroencephalography," S. B. Thesis, Department of Electrical Engineering, M.I.T.
5. Thomas W. Eggers, "A Magnetic Tape Operating System for a PDP-4 Computer," S.B. Thesis, Department of Electrical Engineering, M.I.T.
6. Robert E. Greenwood, "Computer-Aided Electronic Simulation of the Cochlea," S.M. Thesis, Department of Electrical Engineering, M.I.T.
7. Juergen M. Hahn, "High-Speed Projection System for Visual Neurophysiology," S.B. Thesis, Department of Electrical Engineering, M.I.T.
8. Steven J. Hayashi, "Computer Simulation of Sequence of Activation in Fibrillating Heart," S. B. Thesis, Department of Electrical Engineering, M.I.T.
9. Adrian Houtsma, "Auditory Discrimination of Frequency Ratios," S. M. Thesis, Department of Electrical Engineering, M.I.T.
10. David M. Kettner, "A Statistical Analysis of Four Nonlinear Correlators," S. M. Thesis, Department of Electrical Engineering, M.I.T.
11. John L. Lehr, "Iron Lung Control by Muscle Potentials," S.B. Thesis, Department of Electrical Engineering, M.I.T.
12. Jane Win-Shih Liu, "Probabilistic Models of Neural Networks," S.M. Thesis, Department of Electrical Engineering, M.I.T.
13. Robert Macdonald, "Cochlear Potentials in the Presence of Surgically Produced Endolymphatic Hydrops," S. B. Thesis, Department of Electrical Engineering, M.I.T.
14. Roger Greenwood Mark, "Auditory Evoked Potentials during Conditioning in the Rat," Ph.D. Thesis, Department of Electrical Engineering, M.I.T.
15. David Milne, "Temporal Aspects of Single-Unit Activity in the Optic Tract," S.M. Thesis, Department of Electrical Engineering, M.I.T.
16. Charles E. Molnar, "Model for the Convergence of Inputs upon Neurons in the Cochlear Nucleus," Ph.D. Thesis, Department of Electrical Engineering, M.I.T.
17. Paul H. O'Lague, "Spontaneous Activity in 14-day Chick Embryo Telencephalic Tissue Cultures," S. M. Thesis, Department of Electrical Engineering, M.I.T.
18. William A. Plice, "Temperature Effects on Electrical Activity of Brain Tissue in vitro," S.B. Thesis, Department of Electrical Engineering, M.I.T.

19. Murray B. Sachs, "Auditory Nerve Fiber Responses to Two-Tone Stimuli," Ph.D. Thesis, Department of Electrical Engineering, M.I.T.

20. Martin M. Scholl, "A Study of the Phase of the Alpha Rhythm with Respect to Visual Evoked Response and Visual Reaction time," S.M. Thesis, Department of Electrical Engineering, M.I.T.

21. Alan E. Schutz, "An Electronic Model for the Eye of Limulus," S.M. Thesis, Department of Electrical Engineering, M.I.T.

22. Joshua J. Singer, "Response to Photic Stimulation of the Sixth Abdominal Ganglion of Crayfish," S. M. Thesis, Department of Electrical Engineering, M.I.T.

23. David G. Tweed, "High-Speed Analog-Digital Converter Input and Comparator Circuit Design," S.B. Thesis, Department of Electrical Engineering, M.I.T.

24. Michael Weidner, "Electrical Properties of 3M-kcl Filled Microelectrodes," S.B. Thesis, Department of Electrical Engineering, M.I.T.

25. Francis K. Williams, "A Comparison of the Neuroelectric Characteristics of the Squid and Lobster Axons," S.B. Thesis, Department of Electrical Engineering, M.I.T.

26. J. F. Young, "A Model for Single Baroreceptors," S.M. Thesis, Department of Electrical Engineering, M.I.T.

27. A. N. Kramer, "Irregularities in the Normal Heart Beat: A Statistical Analysis," S.B. Thesis, Department of Electrical Engineering, M.I.T.

28. M. C. Raezer, "Nerve Firing Patterns of Cardio-Inhibitory Vagus Nerve Fibers," S. B. Thesis, Department of Electrical Engineering, M.I.T.

(XXXI. COMMUNICATIONS BIOPHYSICS)

A. CIRCUIT MODEL FOR THE CAT'S MIDDLE EAR

We have derived an analog for the mechanical system of the middle ear based on our recent measurements on anesthetized cats.[1] The general form of our circuit analog (Fig. XXXI-1a) is similar to the form proposed by Zwislocki[2]; whereas the element configurations (Fig. XXXI-1b) that we have found sufficient for "fitting" all of our data are generally simpler than those of other authors.[2-4] In this report we shall (a) describe how we choose the element values to match our data, and (b) show that a model with these element values predicts other results.

Our measurements of the displacement of the incus and stapes relative to the malleus (Fig. XXXI-2) indicate that the two boxes on the right in Fig. XXXI-1a can be approximated by a second-order system with an undamped natural frequency of $\omega_2 = 2\pi\ 9000\ \text{sec}^{-1}$, and a damping factor of $\zeta_2 = 0.46$. R_2, C_2, L_2, and C_J must therefore satisfy two constraints:

$$\omega_2 = \frac{1}{\sqrt{C'L_2}} = 2\pi\ 9000\ \text{sec}^{-1}$$

$$\zeta_2 = \frac{R_2}{2}\sqrt{C'/L_2} = 0.46,$$

where

$$C' = \frac{C_J C_2}{C_J + C_2}.$$

Measurements of the stapes displacement (Fig. XXXI-3) with the cavities open (i.e., with the "cavities" box of Fig. XXXI-1a shorted) suggest that the circuit model should have a heavily damped resonance near 1000 Hz. If we assume that the capacitance C_J is approximately an open circuit in this frequency range, this resonance involves only a simple series circuit. To fit the shape of the amplitude and phase curves, we place two more constraints on the element values:

$$\omega_1 = \sqrt{\frac{1}{L_T C_T}} = 2\pi\ 1500\ \text{sec}^{-1}$$

$$\zeta_1 = \frac{R_T}{2}\sqrt{\frac{C_T}{L_T}} = 0.7,$$

where $R_T = R_1 + R_2$, $L_T = L_1 + L_2$, $C_T = \frac{C_1 C_2}{C_1 + C_2}$. One more constraint is obtained by making the low-frequency transfer ratio of the circuit equal to the measured value

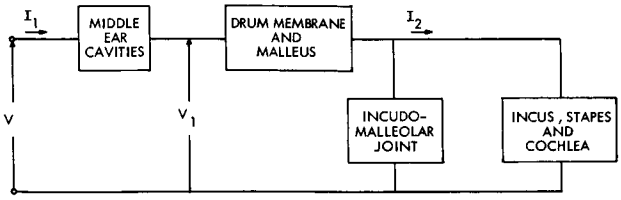

(a)

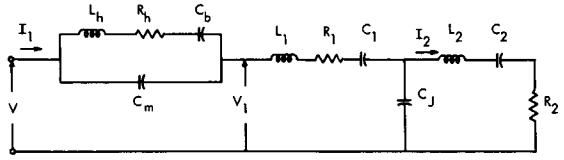

(b)

Fig. XXXI-1. (a) General form of the circuit analog of the middle ear. The input voltage, V_1, is analogous to the sound pressure outside the drum membrane; the current, I_2, is analogous to the velocity of the stapes. The voltage, V_1, is analogous to the pressure across the drum membrane. When the cavities are open, $V = V_1$.

(b) Circuit configuration for the model. The elements might be thought of as analogs of mechanical parameters as follows:

R_2 ~ the net resistance of the incus, stapes, and cochlea.

C_2 ~ the net compliance of the ligaments of the incus and stapes and the cochlea.

L_2 ~ the net inertia associated with the incus, stapes, and cochlea.

C_J ~ the compliance of the incudo-malleolar joint.

C_1, R_1, L_1 ~ the compliance, resistance and inertia, respectively, of the drum membrane and malleus.

C_m ~ the compliance of the air in the middle-ear cavity.

C_b ~ the compliance of the air in the bulla cavity.

L_h, R_h ~ the acoustic mass and resistance, respectively, of the hole connecting the middle-ear cavity to the bulla cavity.

$$\frac{I_2}{j\omega V_1}(\omega \to 0) = \frac{C_1 C_2}{C_1 + C_2} = 3.8 \times 10^{-7} \text{ farads.}$$

Hence we have a total of 5 constraints on the 7 element values indicated in the circuit of Fig. XXXI-3. Since the capacitance C_J is virtually an open circuit for ω near ω_1, the

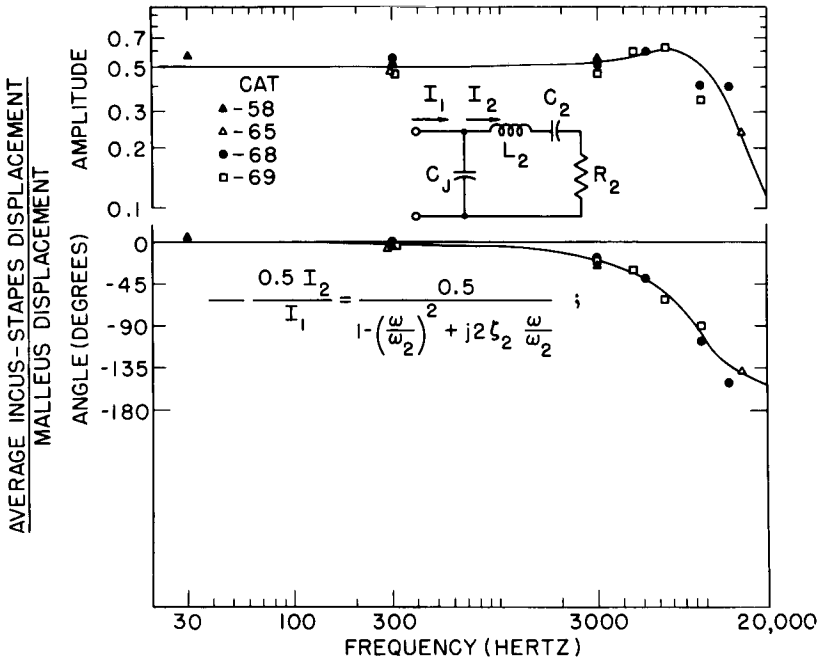

Fig. XXXI-2. Displacement of the incus and stapes relative to the malleus displacement. The combined data from 4 cats have been fitted with curves from the equation shown, with the parameter values $\omega_2 = 2\pi\ 9000\ \text{sec}^{-1}$, and $\zeta_2 = 0.46$.

transfer characteristic of the model is not sensitive to the particular way in which the total resistance is divided between the resistances R_1 and R_2, or the way in which the net capacitance is separated into C_1 and C_2, as long as ω_1, ω_2, ζ_1, ζ_2 are fixed. We have arbitrarily made $C_1 = C_2$ and $R_1 = 0$. Some of Møller's measurements[5] of input impedance before and after interruption of the incudo-stapedial joint indicate that a major portion of the resistance should be on the cochlear side of the joint, and that the compliances are roughly of the same magnitude.

The two coupled cavities of the cat's middle ear are represented by the circuit labeled Z_c in Fig. XXXI-4. The values of these 4 parameters were chosen so that the model would fit measurements of the change in middle-ear transmission when the cavities are opened. The four constraints that were used

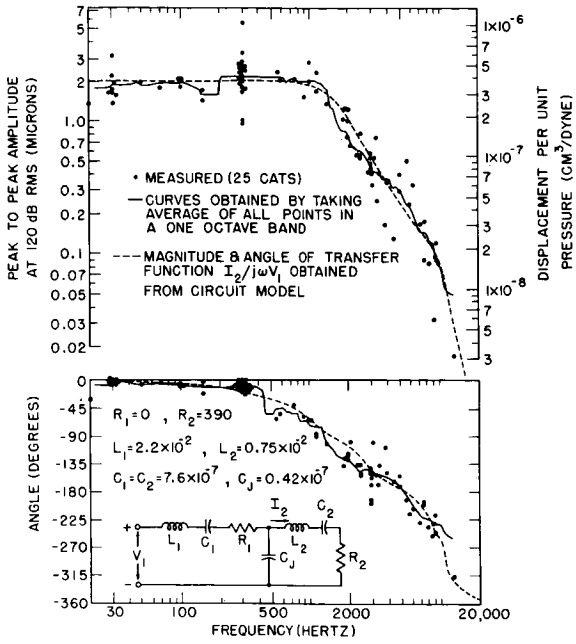

Fig. XXXI-3. Transfer characteristic based on data from 25 cats. The vertical coordinates in the upper figure are stapes displacement (left) and stapes displacement divided by sound pressure at the drum membrane (right). Solid curves represent the "average" transfer function derived from the experimental measurements. Dashed curves were obtained from the circuit model shown.

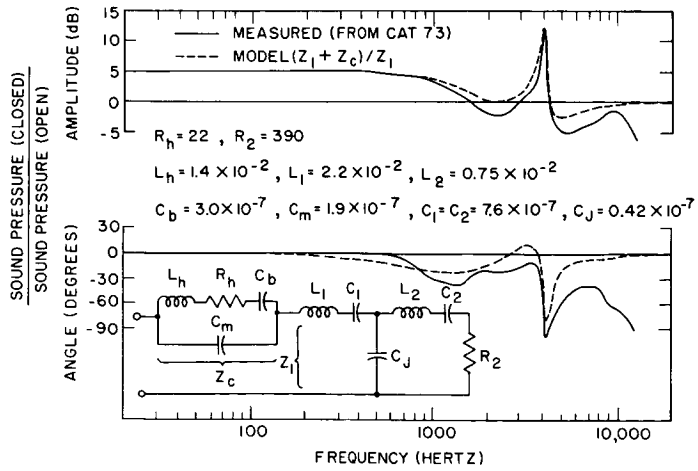

Fig. XXXI-4. Change in transmission through the middle ear resulting from opening both of the middle-ear activities. Solid curve represents a "typical" experimental result; dashed curves were obtained from the circuit model given in the figure.

are (i) the frequency of the maximum effect (cavity resonance)

$$\omega_c = \sqrt{\frac{C_m + C_b}{L_h C_m C_b}} = 2\pi \cdot 4000 \text{ sec}^{-1},$$

(ii) the quality factor of the cavity resonance

$$Q = \frac{\omega_c L_h}{R_h} = 16,$$

(iii) the magnitude of the effect at low frequencies,

$$\frac{Z_1 + Z_c}{Z_1} (\omega \ll \omega_1) = 1.8,$$

and (iv) the magnitude of the effect at the resonant frequency

$$\left| \frac{Z_1 + Z_c}{Z_1} (\omega = \omega_c) \right| = 4.0.$$

The resulting elements values and the measured and computed effects of opening both cavities are shown in Fig. XXXI-4.

The transfer characteristic of the total model and the measured transfer characteristic are shown in Fig. XXXI-5. Since both curves in Fig. XXXI-5 are obtained from curves of Figs. XXXI-3 and XXXI-4, this figure does not contain any new information. We can, however, use the model to predict the change in the transfer function resulting

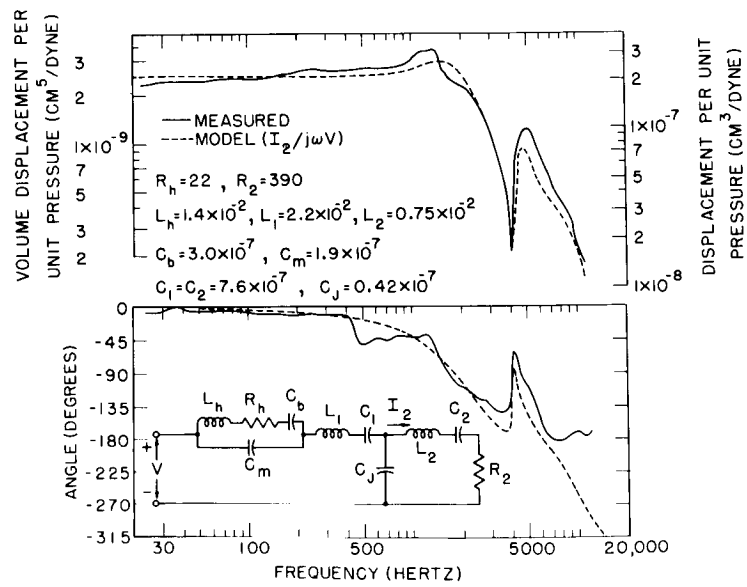

Fig. XXXI-5. Transfer characteristic of cat's middle ear with the bulla and septum intact.

from opening the septum when the bulla is already open. This operation is analogous to setting $1/C_m = 0$, when $1/C_b = 0$. With no new choice of element values we can test the prediction against the measured data. The results (Fig. XXXI-6) indicate that in general the model comes as close to the measured data as do measurements made on other cats.

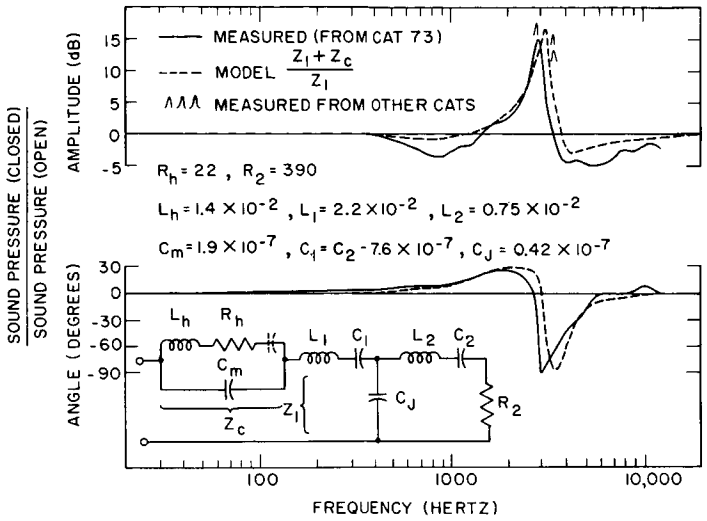

Fig. XXXI-6. Change in transmission through the middle ear resulting from opening the septum in an ear with the bulla previously opened. The small "peaks" measured from "other cats" represent only the parts of the measured curves near the maximum. Then are included to indicate the range of frequencies and amplitudes found.

The circuit-element values have been chosen to give numerical values for the current I_2 in amperes which are equal to the stapes velocity in cm/sec; the value of the voltage in volts is equal to the sound pressure in dynes/cm^2. In order to equate the electric-circuit-element values to the mechanical parameters of the middle ear, we have to take into account: (a) the fact that the motion of the malleus and incus is mainly rotational, (b) the lever ratio from malleus displacement to stapes displacement, (c) the nature of the drum membrane motion, and (d) the coupling of the drum membrane to the manubrium of the malleus. Also, some of the element values that we have used are not unique (i. e. , other values could fit the data equally well), so that we cannot really expect these values to equal the mechanical parameters. Although the validity of this model at the level of the individual elements cannot now be demonstrated, the circuit of Fig. XXXI-5 does provide a fairly accurate and concise description of a relatively large amount of experimental data.

We have received considerable assistance from Thomas Goblick, of Lincoln Laboratory, in computing the characteristics of the model.

W. T. Peake, J. J. Guinan, Jr.

References

1. J. J. Guinan, Jr., and W. T. Peake,"Middle-Ear Characteristics of Anesthetized Cats" (to appear in J. Acoust. Soc. Am.).

2. J. Zwislocki, "Analysis of the Middle-Ear, Part I: Input Impedance," J. Acoust. Soc. Am. 34, 1514-1523 (1962).

3. Y. Onchi, "Mechanism of the Middle Ear," J. Acoust. Soc. Am. 33, 794-805 (1961).

4. A. R. Møller, "Network Model of the Middle Ear," J. Acoust. Soc. Am. 33, 168-176 (1961).

5. A. R. Møller, "An Experimental Study of the Acoustic Impedance of the Middle Ear and Its Transmission Properties," Acta Oto-Laryngol. 60, 129-149 (1965).

B. MULTICHANNEL TIME-DOMAIN FILTERING EMPLOYING TIME-DIVISION MULTIPLEXING AND A MAGNETIC DELAY DRUM

If a signal consists of a message together with a disturbance that is of a single frequency appreciably higher than that of the message, then one way of eliminating the disturbance is to summate the signal with itself delayed by one-half the period of the frequency of the disturbance. A magnetic delay drum[1,2] provides a very convenient method of obtaining the necessary delay; the delay can be adjusted over a very wide range, to match the half-period of the interference. On the other hand, if the magnetic delay drum is limited to providing only a single channel of a signal and its delayed duplicate, then only a single channel of signal could be filtered in this way.

In the present report, a system of time-division multiplexing is employed together with a magnetic drum, in order to provide filtering of two signals in which the disturbance is of the same frequency in both. Although the results from the system described here were carried out with a 10-Hz sine wave and a 10-Hz random noise as the two messages, and a 60-Hz sine wave for the interference, the system is readily adjustable for filtering of other lower or higher frequencies, within the limits of the frequency response in the over-all system.

A block diagram of the system is shown in Fig. XXXI-7. The 10-Hz sine wave is derived from an oscillator; the 10-Hz filtered noise was derived from an Elgenco Model 312A noise generator (DC-120 Hz) and a Spencer-Kennedy Laboratories Variable Electronic Filter (Model 308A), the two channels of which were set at 10-Hz highpass and lowpass, respectively. Samples of these waveforms are shown in the two upper traces of Fig. XXXI-8. The 60-Hz interference was obtained from another sine-wave oscillator

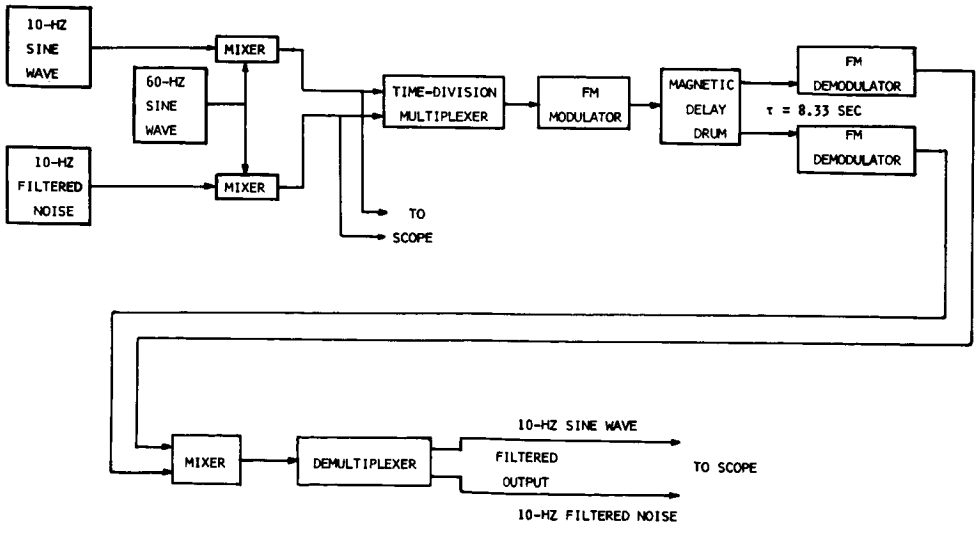

Fig. XXXI-7. System for multichannel time-domain filtering.

and mixed, respectively, with the two above-mentioned waveforms; illustrative examples for 3 different amplitudes of the interference are shown in the two upper traces in Fig. XXXI-9.

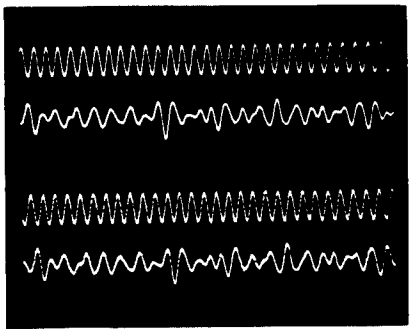

Fig. XXXI-8.

Original (upper 2 traces) and demultiplexed versions (lower 2 traces) of a 10-Hz sine wave and a 10-Hz random signal, without added 60-Hz interference. (The time displacement between the upper 2 traces and the lower 2 traces results from the 31.5-msec delay introduced by the magnetic drum.)

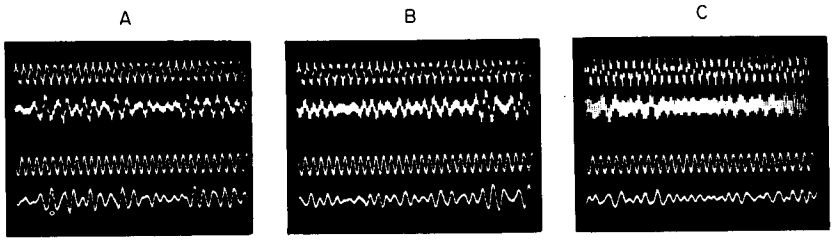

Fig. XXXI-9. Original (upper 2 traces) and demultiplexed versions (lower 2 traces) of a 10-Hz sine wave and a 10-Hz random signal, with 60-Hz interference of 3 different amplitudes (A, B, C) added. Note the elimination of the interference in the demultiplexed versions.

The system for time-division multiplexing which was employed has been described elsewhere.[3] Briefly, 2 traces of a Tektronics Type 3A74 plug-in unit were employed for the multiplexing, the third trace providing the keying pulse that is necessary for demultiplexing; sequentially triggered sample-and-hold circuits[3,4] were employed for the demultiplexing. The output of the multiplexer was fed, in turn, to an FM modulator (Wavetek Voltage-Controlled Generator Model 105), the center frequency of which was set at 13.5 kHz. The magnetic delay drum system employed was that of the Analog Correlator System for Brain Potentials.[2] The delay on the magnetic drum was set at 8.33 msec, half of the period of the 60-Hz interference frequency.

Following FM demodulation (circuits designed by R. M. Brown, Jr.), the two signals delayed relatively to one another were mixed, to eliminate the 60-Hz interference frequency. For this purpose, a vernier adjustment of the multiplexing rate was made so that the relative delay for the pair of multiplexed signals recovered from the magnetic drum, after FM demodulation, was an integral number of periods of the sampling

frequency, that is, so that the phases (with respect to the keying pulses) of the pair of multiplexed waveforms were coincident, as is shown in the two upper traces of Fig. XXXI-10. The summed signals are thus freed of the disturbance frequency, as is

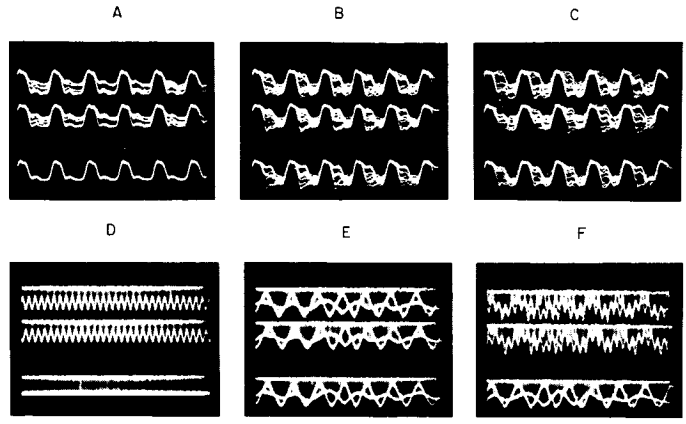

Fig. XXXI-10. Summation of multiplexed signal with itself delayed by 8.33 msec, (upper 2 traces), showing the elimination of the 60-Hz interference before demultiplexing (lowest traces). (The constant-amplitude component is the keying pulse for demultiplexing.) A: 60-Hz interference only; B: information signals only; C: 60-Hz interference base.

evident from the lowest traces of Fig. XXXI-10(A-C) and Fig. XXXI-10(D-F). Correspondingly, the disturbance frequency is also eliminated from the resulting demultiplexed waveforms, as is shown in the lower two traces in Fig. XXXI-9. Comparison of the upper and lower traces in Fig. XXXI-9 with the corresponding traces in Fig. XXXI-8 indicates the efficacy of this method for eliminating the unwanted 60-Hz disturbance.

In the present case, the dwell-time[3] for each channel of the multiplexer was 0.45 msec, so that each channel was sampled at 0.45 msec × 3 or 1.35 msec intervals; the corresponding sampling frequency was thus 740 Hz.

Although only two independent channels of filtering were employed in the results described here, a third channel could easily have been added, were the latter desired [the multiplexing system, in fact, permits the use, under certain circumstances, of 3 channels of continuous information (e.g., EEG's) plus an additional channel of pulse information (e.g., a stimulus pulse), the latter appearing as occasional keying pulses of increased amplitude.]

As mentioned, the system permits a very wide choice of selection of parameters; in particular, it could be arranged for filtering of relatively low-frequency interference of a fixed frequency. (Note that the interference must be of the same frequency for all

channels, although not necessarily of the same amplitude or phase.) In particular, the system would permit the elimination of fixed-frequency interference (i.e., a 60-Hz artefact) in physiological records played back at a lower or a higher speed than the original recordings, from magnetic tape recordings, or from electrically transcribed inked recordings played back at a lower speed than for the original recording, that is, in a multichannel system for reconversion of EEG inked-traces to their electrical form,[5] by employing the principle of phase-modulated analog sampling.[6]

This work was supported at the Massachusetts General Hospital by a U.S. Public Health Service Career Program Award (Number 5-K3-NB-9201), and by a Public Health Service Research Grant (Number NB-03752), from the National Institute of Neurological Diseases and Blindness.

J. S. Barlow

References

1. K. W. Goff, "The Development of a Variable Time Delay," Proc. IRE 41, 1578-15 (1953).
2. J. S. Barlow and R. M. Brown, "An Analog Correlator System for Brain Potentials," Technical Report 300, Research Laboratory of Electronics, M.I.T., July 14, 1955.
3. J. S. Barlow, "A Simple Time-Division Multiplexing System for Low-Frequency Bioelectric Signals," IEEE Trans. Vol. BME-13, No. 4, pp. 195-199, October 1966.
4. J. S. Barlow, "A Small Electronic Analog Averager and Variance Computer for Evoked Potentials of the Brain," Quarterly Progress Report No. 55, Research Laboratory of Electronics, M.I.T., October 15, 1959, pp. 158-165.
5. J. S. Barlow and R. A. DiPerna, "Analog Inked-Trace Reader for Automatic, Continuous, High-Speed Multichannel Operation," Electroenceph. clin. Neurophysiol. (in press).
6. J. S. Barlow, "Automatic Curve Reading by Phase-Modulated Analog Sampling" (submitted for publication to Science).

C. DETERMINISTIC NATURE OF ARTERIAL PRESSURE RECEPTORS

There are some excellent accounts dealing with the qualitative input-output characteristics of arterial pressure receptors.[1] More recently, there have been reports attempting to describe these characteristics quantitatively, in terms of mathematical models.[2] It appears that regardless of whether single fibers or multiple fibers are examined, the output of the pressure receptors is customarily characterized by a continuous function that gives an indication of the "instantaneous frequency" of nerve firing.

Although this type of characterization may be suitable for describing multiple-fiber preparations, it is not adequate for giving an accurate description of the input-output characteristics of single pressure receptor fibers. Our results show that the firing pattern of single pressure receptor nerves is reproducible when the pressure waveform is periodic, and nerve firings tend to occur at well-determined instances of time.

Figure XXXI-11 shows the pressure waveform and associated firing pattern on a single common-carotid pressure receptor nerve of an anaesthetized cat in a particular

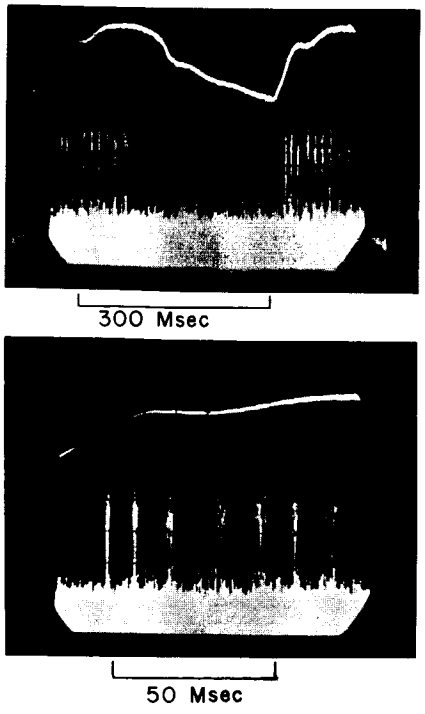

Fig. XXXI-11.

Arterial blood pressure and pressure-receptor nerve firing. In both records: top trace is blood pressure; bottom trace is nerve firing. Pressure minimum: 140 mm Hg; maximum 200 mm Hg. Nerve spikes are approximately 20μvolt. Top record: approximately 25 cycles superimposed, 50 msec/cm. Bottom record: approximately 50 cycles superimposed, 10 msec/cm. (B 31, T116 905-901).

experiment. Approximately 50 cardiac cycles were superimposed, by using the positive derivative of the pressure to trigger the horizontal sweep of the oscilloscope.

The recording shows that the nerve firing pattern was extremely reproducible from cycle to cycle. The first neural firing in each cycle occurred with a maximum jitter of ±1 msec, while the jitter associated with the ninth firing, although approximately eight

times larger than for the first, was still sufficiently small for a definite concentration of impulses to be evident. Computer processing indicated that the first nine firings occurred in all of the cycles, while the tenth developed only in a fraction of the cycles.

Reproducibility of the firing pattern, with the possible exception of the last firing in each cardiac cycle, was observed in several fibers of different animals, and at different levels of blood pressure in the same fiber. Slight cycle-to-cycle variations in blood pressure (2-3 mm Hg) could abolish the repetition of firing patterns. Using the spike in the electrocardiogram as the synchronizing signal, which is the standard procedure, made the regularity of the cycle-to-cycle firing pattern much less apparent than when the positive derivative of the pressure waveform was used.

In some of the experiments the pressure receptor area was perfused with externally generated pressure waveforms. When the perfusion pressure was held constant, the firing frequency was nearly uniform. It was found that the standard deviation of the interspike time interval increased with the mean value of that interval, a finding that had been reported for pacemaker neurons.[3]

P. G. Katona

References

1. S. Landgren, "On the Excitation Mechanism of the Carotid Baroreceptors," Acta Physiol. Scand. 26, 1 (1952).
2. H. R. Warner, "Simulation as a Tool for Biological Research," Simulation 1, 57 (1964).
3. D. Junge and G. P. Moore, "Interspike-Interval Fluctuations in Aplasia Pacemaker Neurons," Biophysical J. 6, 411, (1966).

XXXII. 3 NEUROPHYSIOLOGY* 6

Academic and Research Staff

Dr. 6 W. S. McCulloch	Dr. S-H. Chung	Dr. A. Natapoff
Prof. J. Y. Lettvin	Dr. J. L. S. DaFonseca	Dr. S. A. Papert
Prof. P. D. Wall	Dr. H. Hartman	Dr. A. Taub
Prof. M. Blum	Dr. Dora Jassik-Gerschenfeld	B. Howland
Prof. J. E. Brown ET AL 8	Dr. K. Kornacker	Diane Major
Prof. P. R. Gross	Dr. T. McLardy	W. H. Pitts
Prof. B. Pomeranz	Dr. R. Moreno-Diaz	Sylvia G. Rabin

Graduate Students

E. E. Fetz	J. I. Simpson
G. P. Nelson	W. A. Wright

RESEARCH OBJECTIVES AND SUMMARY OF RESEARCH

1. Basic Theory

Research on the functional organization of the reticular core of the central nervous system continues, in collaboration with Dr. William L. Kilmer of Michigan State University.

Our problem is to construct a theory for the reticular system which is compatible with known neuroanatomy and neurophysiology, and which will lead to testable hypotheses concerning its operation.[1,2]

Our first and second approaches to this problem[3] were outlined in Quarterly Progress Report No. 76 (page 313).

We can report that we are embarked on a kind of iterative net statistical decision theory[4] that is comprehensive, versatile, and penetrating enough to stand a reasonable chance of success.

The computer modeling is being done at the Instrumentation Laboratory, M. I. T., by members of Louis L. Sutro's group.

W. S. McCulloch

References

1. W. S. McCulloch and W. L. Kilmer, "Introduction to the Problem of the Reticular Formation," in Automata Theory (Academic Press, Inc., New York, 1966).
2. W. S. McCulloch, "What's in the Brain That Ink May Character?," Proceedings of the 1964 International Congress for Logic, Methodology and Philosophy of Science, Held in Jerusalem, August 26-September 2, 1964 (North-Holland Publishing Company, Amsterdam, 1965).

*This work is supported by the National Institutes of Health (Grants 5 RO1 NB-04985-04, 5 RO1 NB-04897-04, 5 RO1 NB-06251-02, 1 505 FR-07047-01), the U.S. Air Force (Aerospace Medical Division) under Contract AF33(615)-3885, the U.S. Air Force (Office of Scientific Research) under Contract F 44620-67-C-0030, and by a grant from Bell Telephone Laboratories, Inc.

3. W. L. Kilmer, "On Dynamic Switching in One-Dimensional Iterative Logic Networks," Inform. Contr. 6, 399-415 (1963).

4. W. L. Kilmer, "Topics in the Theory of One-Dimensional Iterative Networks," Inform. Contr. 7, 180-199 (1964).

2. Project Plans

a. Sensory Processes and Multiplexing

The past year's work has suggested to us that the firing pattern of a single neuron which, in the histogram, shows a bimodal or trimodal distribution, conveys information of different sorts with each of the modes. We have spent some time searching for the kind of stimulation needed to separate effects on the different modes, but are not yet able to give a completely satisfactory account of what is happening. There is enough evidence, however, that we have had to consider the characteristics of a system capable of handling information that is distributed or partitioned in the pulse-interval domain. This has led to the making of a new theory of nervous action, an account of which will soon appear.

Color Vision in Amphibia and Reptiles. We have undertaken to study the coding of color in the retinas of frog and turtle, extending the work of Dr. Muntz in this laboratory (4 years ago).

Taste. We shall attempt a study of taste similar to the one that we did on smell.

b. Learning Process

In consequence of the theory of nervous action which we have recently developed, we are studying the notion of the change of probability of invasion into a branch of a single fiber. The work will be done initially on dorsal root-dorsal column system in the cat. We shall try to see if the probability of invasion into the branches at a bifurcation of an axon can be altered permanently in one direction or another by the application of a current across the bifurcation favoring the invasion of one branch more than the other. This is a far-shot experiment, but we feel obliged to do it.

c. Instrumentation

1. We are applying our real-time analyzer of pulse intervals to the study of speech, and for this purpose are devising some new analogue equipment such as a peak picker-outer to take envelopes and a wave-shape detector that works in real time.

2. For the medical profession we are devising an oscillator whose frequency is an exponential function of an applied voltage. This device transforms secular voltage swings such as EKG into a sliding tone that has the same melodic line independent of pitch, i. e., the tune one hears is independent of the DC bias low-applied signal. We have already tried something like this, and it turns out to be very quickly learned for making fine diagnostic distinctions on EKG. We envision a stethoscopelike instrument to replace the ordinary pen recordings of EKG so that screening of patients can be done without accumulation of paper.

3. We are attempting to build an inexpensive low-voltage oscilloscope using crossed galvanometers with 5-kc bandwidth, and a fluorescing paper on which the light spot is cast. One galvanometer gives vertical deflection, the other horizontal deflection.

d. Computer Approach to Diagnosis

Gordon Nelson, a graduate student, during the past two years, has devised a method for handling the diagnostic groupings of a population of rats by similarities of trajectories

in time of the course of a combination of 17 independent measures made on the animals. The program was elegantly simple, and in the end the results were discriminations far higher and more reliable than could be made by any of the people – pediatricians, biologists, students – who handled the animals daily. He is now going to use the same scheme to build an automatic neurological diagnosis machine working in the realm of those diseases that are accompanied by disorders in motion of the body.

J. Y. Lettvin

References

1. M. Takata, W. F. Pickard, J. Y. Lettvin, and J. W. Moore, "Ionic Conduction Changes in Lobster Axon Membrane where Lanthanum Is Substituted for Calcium" (J. Gen. Physiol., in press).
2. R. C. Gesteland, J. Y. Lettvin, and S-H. Chung, "A Code in the Nose," Bionics Symposium, Dayton, Ohio, 1966 (in press).

3. Proposed Research

The work for the coming year will continue an analysis of the organization of the somesthetic system. In the past, we have concentrated on the methods by which cells in the spinal cord handle information that has come in over the dorsal roots. We have unravelled the way in which six stages of abstraction and analysis are organized with respect to each other and to some descending control systems. As a by-product of this research, information has been obtained about synaptic transmission and about sensory processes, particularly those leading to pain reactions. This analysis will continue.

In addition to the system in the spinal cord which receives impulses from the periphery, there is a second more recently evolved system that also receives similar information. The method of handling information in the recent system, the dorsal column-medial lemniscus system, contrasts in many important respects from the method. The relative roles of these two systems in sensory analysis and behavior will be studied.

P. D. Wall

A. ON A CALCULUS FOR TRIADAS

1. Introduction

De Morgan, obstructed by his terminology, thought the construction of a logic of relations impossible. A quarter of a century later, C. S. Peirce initiated it. Repeated attempts to understand him failed because in every paper he changed his terminology. It was not until we attempted to formulate family relations in Gilstrap's matricial calculus that he and we were able to understand Peirce, who had actually invented such a calculus and extended it to three-dimensional arrays which we call "mints." It is now clear what he had done and what stopped him. He also used a symbolism in molecular diagrams which is transparent. Finally, he interpreted these in terms of sentences containing n blanks to be filled by the names of things in the universe of discourse. Whether these be real or imaginary is immaterial to this calculus, which therefore can cope with

intension, not merely extension, and hence is of value in psychophysiological contexts. Many theorems not involving negation can now be proved, but negation is not simple and we are struggling to discover its multifarious consequences. At the moment, we want to present the following useful results.

2. Triadas

A triada is a structure of any kind involving three elements or members of a given set at a time. For example, "a gives b to c" is a triada, G, involving the objects a, b, and c. Peirce suggested different ways to develop a calculus for triadas, i.e., "an art of drawing inferences." For cases in which triadas are of the nature of the previously mentioned example, i.e., of the nature of a sentence or phrase with three blanks that are to be filled by particular members of a given set, a calculus may be developed that is similar to the calculus of functional propositions of three arguments – or you have Boolian tensors of rank 3 – but that is richer in possibilities and consequences. One of the ways to develop such a calculus is to consider two kinds of variables or symbols, one for the elements of the set where the triadas apply (here lower-case letters are used), and the other for the triadas themselves (represented here by upper-case letters). A calculus involving only upper-case letters will be called a "proper calculus for triadas."

In the process of constructing the calculus, operations on or among triadas are defined which have a definite meaning. The object of the calculus is then to combine the operations and to obtain conclusions or theorems about the combined operations of triadas. We concern ourselves here only with closed operations, i.e., operations on or among triadas, which again generate triadas.

3. Definitions and Operations

A triada is a sentence or phrase with three blanks that are to be filled with specific names of objects, or members of a given set, in order for the sentence to have meaning. For example, if in the sentence "a gives b to c," we delete the names a, b, and c, we end with the triada "____ gives ____ to____." We denote by i, j, and k the first, second, and third blanks, respectively. Furthermore, we represent the triada by G_{ijk}, i.e., G_{ijk} means "____ gives ____ to____." If we want to express the fact that the particular member a gives the particular member b to the particular one c, we shall write G_{abc}. Therefore, the subscripts are regarded as variables, as are the blanks, Somewhere in the calculus we shall be able to delete subscripts without confusion, to obtain the calculus proper.

Two triadas are said to be equal if they have the same meaning, i.e., they originate equivalent sentences, when applied to any three objects in the same order. We represent the equality of two triadas by separating them with the sign =. In any expression in which triadas appear, any of them can be replaced by an equivalent one. For example, the

triadas "____gives____to____" and "____is given to____ by____" are not equal because when applied to objects a, b, and c in this order the resulting sentences do not have the same meaning; however, the triadas "____gives ____to ____" and "____is identical to the one who gives____to____" are equal.

We now distinguish three kinds of closed operations. These are unary operations, involving one triada; binary, or nonrelative, involving two triadas; and triadic, or relative, involving three triadas.

a. Unary Operations

Rotation is the clockwise rotation of the order of the blanks in the triada one step. For example, let G_{ijk} be "____gives____to____." Its rotation, represented by $\overset{\frown}{G}_{ijk}$, is the triada "____is given by____the gift____." According to the definition of equality, we may write

$$\overset{\frown}{G}_{ijk} = G_{kij}$$

which indicates that if G applies to objects a, b, and c in this order, then $\overset{\frown}{G}$ applies to them in the order c, a, b.

Reflection, where the first and third blanks interchange positions, for example, the reflection of G_{ijk} is the triada "____is given____ by____," that we represent by $\overset{\smile}{G}_{ijk}$, that is, we may write

$$\overset{\smile}{G}_{ijk} = G_{kji}.$$

By iteratively applying each unary operation to a triada, it is easy to see that

$$G_{ijk} = \overset{\smile\smile}{G}_{ijk} \text{ and } G_{ijk} = \overset{\frown\frown\frown}{G}_{ijk}.$$

Since, in these expressions, subscripts are the same on both sides of the equality sign and they appear in the same order, we may delete them without confusion, to obtain

$$\overset{\smile\smile}{G} = G \text{ and } \overset{\frown\frown\frown}{G} = G.$$

b. Binary Operations (or Nonrelative Operations)

Nonrelative Product: The nonrelative product of two triadas is a triada obtained after joining the two original triadas with the logical connective "and," and making the subscripts in both triadas the same. For example, let G_{ijk} mean "____gives____to____" and let L_{ijk} mean "____lies in between____ and____." The nonrelative product, represented by $G_{ijk} \cdot L_{ijk}$, is the triada "____gives ____to____ and the first lies between the second and the third." It follows that $G_{ijk} \cdot L_{ijk} = L_{ijk} \cdot G_{ijk}$.

Nonrelative Sum: The nonrelative sum of two triadas is the triada obtained after joining the two original triadas with the logical connective "or" (inclusive

or), and making the subscripts in both triadas the same. For example, the nonrelative sum of G_{ijk} and L_{ijk} is the triada "____ gives ____ to ____ or the first lies in between the second and the third." We represent it by $G_{ijk} + L_{ijk}$. It is clear that $G_{ijk} + L_{ijk} = L_{ijk} + G_{ijk}$.

c. Triadic Operations (or Relative Operations)

Now we introduce the existential quantifier Σ (read "there is some ...") and the universal quantifier Π (read "all," or "everybody" or "everything"). Application of a quantifier to a triada gives a lower structure (a structure with a lower number of blanks). For example, $\sum_i G_{ijk}$ reads "there is some who gives__to__," that is, a diadic structure. In order to obtain a closed operation, we could define an "open" or "external" product or sum to obtain a higher structure, and then reduce it to a triada, by applying one or the two quantifiers one or more times. For example, let "and" be the open operation between L_{ijk} and G_{emn} such that $L_{ijk} \cdot G_{emn}$ means "____ lies in between ____ and____ , and____ gives____ to____," that is, a hexada. If we now "contract" by application of the Σ quantifier, we obtain the triada

$$\sum_{iem} L_{ijk} \cdot G_{emn}.$$

This reads "there is some individual who lies in between ____ and____, and someone gives something to____."

More interesting are the combinations of triadas with some elements, or blanks, in common, that is, having colligative terms. Such is the case of the so-called relative products and sum for binary, or diadic, relations. For triadas, let us write the product with one colligative term

$$L_{ijk} \cdot G_{kem}$$

that reads "____ lies in between____ and ____who gives ____ to____," that is, a pentadic structure. If we now contract upon the repeated index, by means of the Σ quantifier, we obtain

$$\sum_{k} L_{ijk} \cdot G_{kem},$$

that is, the tetrada "____ lies in between____ and someone who gives____ to____." If the operation between L_{ijk} and G_{kem} were a sum, we would obtain first the pentada

$$L_{ijk} + G_{kem}$$

that reads "____ lies in between____ and____ or this gives ____ to____." By contracting now on the repeated index by means of the Π quantifier, we obtain

$$\prod_k L_{ijk} + G_{kem},$$

that is, "take any individual; then, either____ lies in between____ and this individual or this gives ____ to____." This is similar to the relative sum of diadas.

The combination of triadas with colligative terms is amenable (Peirce) to clear graphical representation. For example, Diagram XXXII-1 represents the two triadas G_{ijk} and L_{kem}.

Diagram XXXII-1.

The two operations described above could be graphically represented by Diagram XXXII-2, in which the colligative term appears as a "common bound," and the number of blanks left is the number of "free bounds."

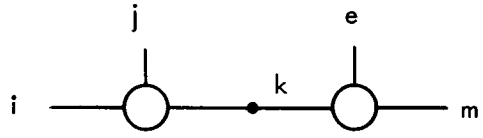

Diagram XXXII-2.

For convenience, we shall define closed relative products and sums among triadas in which the contraction or generalization by the quantifiers is realized upon repeated indexes, and in which each repeated index repeats only once. This permits the use of the above-mentioned type of graph as a means for visualizing the relative operations, and, at the same time, provides us with another tool to prove theorems. It turns out that many of the combinations of open operations which finally result in triadas are particular cases of closed products and sums defined with those rules. Briefly, the rules for forming relative operations of triadas, which permit the use of the above-mentioned graphs, may be stated as follows.

(i) Each repeated index repeats only once.

(ii) Quantifiers act on repeated indexes.

It follows from the graphs that at least three triadas are necessary to verify a closed operation. There are three different ways in which the triadas could be connected (see Diagram XXXII-3):

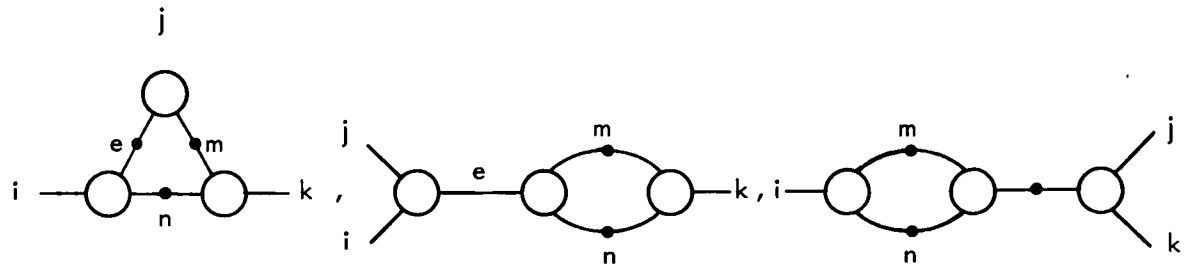

Diagram XXXII-3.

These lead to the relative products and sums that are defined below.

Relative Products

Δ Product of three triadas A, B, and C is the triada

$$\sum_{nem} A_{nie} \cdot B_{ejm} \cdot C_{mkn}$$

which we represent by $\underset{\cdot}{\Delta}(ABC)$.

$\succ$ Product of the triadas A, B, and C is the triada

$$\sum_{emn} A_{ije} \cdot B_{emn} \cdot C_{nmk}$$

which we represent by $\underset{\cdot}{\succ}(ABC)$.

$\prec$ Product of the triadas A, B, and C is the triada

$$\sum_{emn} A_{iem} \cdot B_{men} \cdot C_{njk}$$

which we represent by $\underset{\cdot}{\prec}(ABC)$.

For example, let G be the triada "____gives____to____"; let L be "____lies in between____and____"; and let T be "____thinks____is____." Then, $\underset{\cdot}{\Delta}(GLT)$ reads "someone gives____to somebody who lies in between____and some other who thinks ____is the first," or "there are three individuals such that the first gives____to the

second, this lies in between____ and the third, and this thinks____ is the first."

Relative Sums

Δ Sum of three triadas A, B, and C is the triada

$$\prod_{nem} A_{nie} + B_{ejm} + B_{mkn}$$

which we represent by $\underset{+}{\Delta}(ABC)$

$\succ$ Sum of three triadas A, B, and C is the triada

$$\prod_{nem} A_{ije} + B_{emn} + C_{nmk}$$

which we represent by $\underset{+}{\succ}(ABC)$.

$\prec$ Sum of three triadas A, B, and C is the triada

$$\prod_{emn} A_{iem} + B_{men} + C_{njk}$$

which we represent by $\underset{+}{\prec}(ABC)$.

For example, $\underset{+}{\Delta}(GLT)$ reads "take any three individuals; then, either the first gives ____ to the second, or the second lies in between ____ and the third, or the third thinks ____ is the first."

Resume of Closed Operations for Triadas

- Unary
  - Rotation, $\hat{A}$
  - Reflection, $\check{A}$
- Binary
  - Nonrelative Product $A \cdot B$
  - Nonrelative Sum $A + B$
- Triadic
  - Relative Products
    - $\dot{\Delta}(ABC)$
    - $\dot{\succ}(ABC)$
    - $\dot{\prec}(ABC)$
  - Relative Sums
    - $\underset{+}{\Delta}(ABC)$
    - $\underset{+}{\succ}(ABC)$
    - $\underset{+}{\prec}(ABC)$

4. Immediate Theorems

By combining the closed operations among triadas, we can prove the set of equalities, or theorems, that follow.

First, let P_{ijk} be the triada that results from the nonrelative product of A_{ijk} and B_{ijk}. That is,

$$P_{ijk} = A_{ijk} \cdot B_{ijk}.$$

Rotation of P_{ijk} gives

$$\hat{P}_{ijk} = P_{kij} = A_{kij} \cdot B_{kij} = \hat{A}_{ijk} \cdot \hat{B}_{ijk},$$

that is,

$$\hat{P}_{ijk} = \hat{A}_{ijk} \cdot \hat{B}_{ijk}.$$

Since subscripts now appear in the same order, we may delete them to obtain

$$\widehat{A \cdot B} = \hat{A} \cdot \hat{B}. \tag{1}$$

Similarly, we can prove that

$$\widehat{A + B} = \hat{A} + \hat{B}. \tag{2}$$

By the same method, we can prove that

$$\breve{A \cdot B} = \breve{A} \cdot \breve{B} \tag{3}$$

$$\breve{A + B} = \breve{A} + \breve{B}. \tag{4}$$

Let Q_{ijk} be the triada that results from the operation $\underset{\cdot}{\Delta}(ABC)$, that is,

$$Q_{ijk} = \sum_{emn} A_{nim} \cdot B_{mje} \cdot C_{ekn}.$$

Rotation of Q_{ijk} gives

$$\hat{Q}_{ijk} = Q_{kij}.$$

From the definition of Δ product, we have

$$Q_{kij} = \sum_{emn} A_{nkm} \cdot B_{mie} \cdot C_{ejn}.$$

Since the "and" operation is commutative, we have

$$Q_{kij} = \sum_{emn} B_{mie} \cdot C_{ejn} \cdot A_{nkm}.$$

That is,

$$\hat{Q}_{ijk} = \sum_{emn} B_{mie} \cdot C_{ejn} \cdot A_{nkm}.$$

The subscripts that are not affected by the quantifier appear in the same order in both sides of the last equation. Therefore, we may write

$$\hat{Q} = \underset{\cdot}{\Delta}(BCA).$$

That is,

$$\overset{\frown}{\underset{\cdot}{\Delta}}(ABC) = \underset{\cdot}{\Delta}(BCA). \tag{5}$$

The reflection of Q_{ijk} gives

$$\breve{Q}_{ijk} = Q_{kji}.$$

From the definition of Δ product, we have

$$Q_{kji} = \sum_{emn} A_{nkm} \cdot B_{mje} \cdot C_{ein}.$$

That is,

$$Q_{kji} = \sum_{emn} C_{ein} \cdot B_{mje} \cdot A_{nkm}.$$

From the definition of reflection,

$$\breve{Q}_{ijk} = Q_{kji} = \sum_{emn} \breve{C}_{nie} \cdot \breve{B}_{ejm} \cdot \breve{A}_{mkn}.$$

By deleting subscripts, we obtain

$$\breve{Q} = \underset{\cdot}{\Delta}(\breve{C}\,\breve{B}\,\breve{A}).$$

That is,

$$\overset{\smile}{\underset{\cdot}{\Delta}}(ABC) = \underset{\cdot}{\Delta}(\breve{C}\,\breve{B}\,\breve{A}). \tag{6}$$

By similar procedures, it is possible to show that

$$\overset{\smile}{\underset{\cdot}{\succ}}(ABC) = \underset{\cdot}{\prec}(\breve{C}\,\breve{B}\,\breve{A}) \tag{7}$$

$$\dot{\prec}\overbrace{(ABC)} = \dot{\succ}(\breve{C}\breve{B}\breve{A}). \tag{8}$$

Similarly, we can prove that

$$\dot{\Delta}\overbrace{(ABC)} = \dot{\Delta}(BCA) \tag{9}$$

$$\dot{\Delta}\overbrace{(ABC)} = \dot{\Delta}(\breve{C}\breve{B}\breve{A}) \tag{10}$$

$$\dot{+}(ABC) = \dot{+}(\breve{C}\breve{B}\breve{A}) \tag{11}$$

$$\dot{+}\overbrace{(ABC)} = \dot{+}(\breve{C}\breve{B}\breve{A}). \tag{12}$$

5. Constant Triadas

We define five particular triadas that we shall use in the calculus.

a. Universal triada, I_{ijk}, or simply I, is the triada "____, ____ and ____ are individuals." It has the following properties: Let A be any triada; then A + I = I and A · I = A. It is clear that $\breve{I} = I$ and $\hat{I} = I$.

b. Null triada, θ, or θ_{ijk}, is the triada "neither____ nor____ nor____ are individuals." Let A be any triada; then A + θ = A and A · θ = θ. Also, $\breve{\theta} = \theta$ and $\hat{\theta} = \theta$.

c. Left and Right Identities, denoted by I_λ and I_ρ, respectively, are the following: I_λ is the triada "____ is an individual and ____ is identical to____"; I_ρ is the triada "____ is identical to____, and____ is an individual." It follows that

$$\breve{I}_\lambda = I_\rho \quad ; \quad \breve{I}_\rho = \hat{I}_\lambda \text{ and } I_\lambda = I_\rho. \tag{13}$$

Let A be any triada; then

$$\dot{\Delta}(I_\lambda A I_\rho) = A. \tag{14}$$

For example, let A be "____ gives____ to____". $\dot{\Delta}(I_\lambda A I_\rho)$ reads "there are three individuals such that, the first is an individual and____ is identical to the second, this gives____ to the third, the third is identical to____, and the first is an individual." That is the same as "____ gives____ to____".

d. Central Identity, I_c, is, by definition, $I_c = \hat{I}_\rho$. It follows that

$$\hat{I}_c = I_\lambda \text{ and } \breve{I}_c = I_c. \tag{15}$$

THEOREM. Let R by any triada. Then

$$\hat{R} = \dot{\Delta}(R I_\rho I_\lambda). \tag{16}$$

Proof. According to Eq. 14, $R = \dot{\Delta}(I_\lambda R I_\rho)$. By rotating both members, we obtain

$$\hat{R} = \overbrace{\Delta(I_\lambda R I_\rho)}.$$

And, by applying Eq. 5, $\dot{\Delta}(\widehat{I_\lambda RI_\rho}) = \dot{\Delta}(RI_\rho I_\lambda)$.

THEOREM. Let A, B, and C be any three triadas. Then

$$\dot{\Delta}[\dot{\Delta}(\widehat{B}\,\widehat{\widehat{A}}\,I_c)I_\lambda\,\widehat{C}] = \dot{\prec}(ABC). \tag{17}$$

This theorem could be proved by operating on subscripts, in a form similar to the proofs of Eqs. 5 and 6. It can also be proved by means of a graph. The proof by means of a graph is illustrated in the following diagrams.

The graph for $\dot{\Delta}[\dot{\Delta}(\widehat{B}\,\widehat{\widehat{A}}\,I_c)I_\lambda\,\widehat{C}]$ is shown in Diagram XXXII-4.

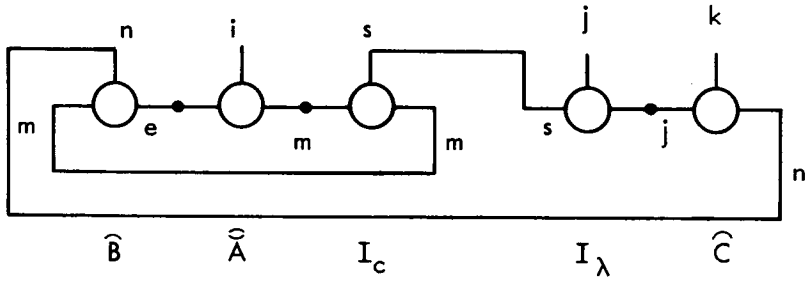

Diagram XXXII-4.

The graph for $\dot{\succ}(ABC)$ is shown in Diagram XXXII-5.

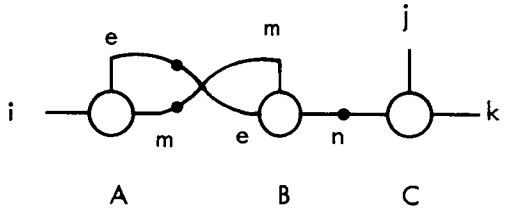

Diagram XXXII-5.

Because of the nature of the identities I_c and I, both graphs are the same. The introduction of the subscript s in the first does not affect this, since it is equivalent to saying that "someone is an individual."

THEOREM. Let A, B, and C be any three triadas. Then

$$\dot{\Delta}[\widehat{\widehat{A}}\,I_\rho\,\dot{\Delta}(I_c\,\widehat{\overset{\times}{C}}\,\widehat{\widehat{B}})] = \dot{\succ}(ABC). \tag{18}$$

Proof. Let R, S, and T be any three triadas.

According to Eq. (17), we have

$$\dot{\prec}(RST) = \dot{\Delta}[\dot{\Delta}(\widehat{S}\,\widetilde{R}\,I_c)I_\lambda\,\widehat{T}].$$

By reflecting both sides, and iteratively applying Eqs. 8 and 6, we obtain

$$\overbrace{\dot{\prec}(RST)} = \dot{\succ}(\breve{T}\,\breve{S}\,\breve{R}) = \Delta[\overset{\times}{T}\breve{I}_\lambda\,\Delta(\breve{I}_c\,\overset{\times}{\breve{R}}\,\overset{\times}{\breve{S}})].$$

But $\breve{I}_\lambda = I_\rho$ and $\breve{I}_c = I_c$. Therefore

$$\dot{\succ}(\breve{T}\,\breve{S}\,\breve{R}) = \dot{\Delta}[\overset{\times}{\breve{T}}\,I_\rho\,\dot{\Delta}(I_c\,\overset{\times}{\breve{R}}\,\overset{\times}{\breve{S}})].$$

Let $A = \breve{T}$, $B = \breve{S}$, and $C = \breve{R}$. Then

$$\widehat{\widehat{T}} = \widehat{\widehat{A}},\ \breve{S} = \widehat{\widehat{B}},\ \text{and}\ \breve{\breve{R}} = \breve{C}.$$

By substitution, we finally prove the theorem.

From theorems (16), (17), and (18), it follows that rotation ($\frown$) and the triadic products $\dot{\succ}$ and $\dot{\prec}$ are reducible to Δ products.

W. S. McCulloch, R. Moreno-Diaz

XXXIII. COMPUTER RESEARCH*

Academic and Research Staff

Prof. J. B. Dennis
W. W. Plummer

RESEARCH OBJECTIVES

The purpose of this group, which is operated jointly by the Research Laboratory of Electronics, the Electronic Systems Laboratory, and the Department of Electrical Engineering, M.I.T., is fourfold:

1. To provide a flexible and readily accessible computation facility oriented toward the Laboratory's research goals.

2. To provide an educational facility where students may learn the principles of automatic computation, and undergraduate and graduate thesis projects may be carried out.

3. To develop computation techniques, especially methods that make program design and construction more convenient, and allow easier communication with the machine.

4. To investigate new principles for organizing multiprogrammed computer systems.

The Computer Research Group operates two general-purpose machines. The TX-0 computer was built by Lincoln Laboratory, M.I.T., as an experimental machine, and was turned over to the Department of Electrical Engineering in 1958. The Digital Equipment Corporation donated one of their PDP-1 machines in 1961. The PDP-1 has become the central processor of a time-shared multiuser system[1] implemented by the group. Our activities have included modifications to the two computer systems to improve their performance, as well as the programming of translators, editors, debugging programs, and executive routines suited to the on-line nature of the use of the two systems.

J. B. Dennis

*This work is supported principally by the Joint Services Electronics Programs (U.S. Army, U.S. Navy, and U.S. Air Force) under Contract DA 36-039-AMC-03200(E); and in part by the National Science Foundation (Grant GP-835) and the National Aeronautics and Space Administration (Grant NsG-496).

XXXIV. COMPUTATION RESEARCH*

Research Staff

Martha M. Pennell
Heather S. Davis
Gail M. Fratar
Joan Harwitt
Elaine C. Isaacs
Eleanor C. River

RESEARCH OBJECTIVES

This group provides a general programming service for Laboratory members who use computers in their research and also acts as liaison with the M. I. T. Computation Center and Project MAC.

The majority of our programming has dealt with the solutions of transcendental and polynomial equations,[1, 2, 4, 5] least-squares fits[3] and Fourier analysis. Undoubtedly, this work will continue.

An increasing amount of our programming, however, has not had direct scientific application. One of our programs has helped to index a book.[6] Another is helping to prepare budgets for the Business Office of our Laboratory.

In addition to actual programming, we also provide other computer-oriented services. We consult with Laboratory members who wish to do their own programming.[7] We have given several demonstrations of the time-sharing system. At present, we are working in conjunction with Professor Sanborn C. Brown of the Plasma Physics Group and Mr. John H. Hewitt of our Document Room to set up our own files for use with the M. I. T. Library's information retrieval program, TIP. Sixty Laboratory members have signed up for our "Fortran IV" course.

Our work in both old and new areas will reflect the increasing needs of Laboratory members for computers as research aids.

Martha M. Pennell

References

1. Martha M. Pennell, "Newton's Method for Finding Complex Roots of a Transcendental Equation," Quarterly Progress Report No. 80, Research Laboratory of Electronics, M. I. T., January 15, 1966, pp. 263-266.
2. Martha M. Pennell, "Numerical Example to Illustrate Kizner's Method for Solving Nonlinear Equations," Quarterly Progress Report No. 80, Research Laboratory of Electronics, M. I. T., January 15, 1966, pp. 266-267.
3. Martha M. Pennell and Heather Davis, "Linearizing the Roots of a Polynomial," Quarterly Progress Report No. 83, Research Laboratory of Electronics, M. I. T., October 15, 1966, pp. 179-181.
4. Martha M. Pennell, "Further Computations Using Newton's Method for Finding Complex Roots of a Transcendental Equation," Quarterly Progress Report No. 81, Research Laboratory of Electronics, M. I. T., April 15, 1966, pp. 253-254.
5. Veronica E. McLoud and Martha M. Pennell, "Example of Symbolic Manipulation of Polynomials in MAD," Quarterly Progress Report No. 82, Research Laboratory of Electronics, M. I. T., April 15, 1966, pp. 294-295.

*This work was supported in part by the Joint Services Electronics Programs (U. S. Army, U. S. Navy, and U. S. Air Force) under Contract DA 36-039-AMC-03200(E).

6. Martha M. Pennell and R. M. Nacamuli, "A Computer Indexing Program," Quarterly Progress Report No. 82, Research Laboratory of Electronics, M.I.T., April 15, 1966, pp. 293-294.

7. M. G. Smith, "Computer Location of Plasma Dispersion Function Multiple Roots," S.M. Thesis, Department of Electrical Engineering, M.I.T., September 1966.

A. UPDATING OF THE COMPUTER INDEXING PROGRAM

In recent months, our basic computer indexing program has undergone marked revision. We feel that the program is now more versatile and hence more readily adaptable to the needs of a small research group.

The basic program permutes and alphabetizes the key words of up to 200 titles for a maximum of 78 characters per title. A second version of the program will do the same for a maximum of 70 titles, each consisting of no more than 132 characters.

In our basic version of the indexing program, the first 6 input characters may contain some sort of identification code, while characters 7-78 contain the title to be permuted. The output consists of the identification code in the first 6 columns, with the output title beginning in column 8. At present, the key word begins in the first permuted word of the output.

The program was originally designed to index upon key words of at least four letters. The disadvantages[1] of this scheme are obvious. Hence, a change was made in the program so that by use of the special character "$", key words of fewer than 4 letters will be indexed upon, and non-key words of more than 4 letters will be ignored. For example, suppose we are given the following input title:

23 ELASTIC COLLISION PROBABILITY FOR ELECTRONS IN ARGON (A)

Under normal circumstances, the key words would be: Elastic, Collision, Probability, Electrons, and Argon. The word "(A)" would be considered as a non-key word. By inserting the special character "$", however, we can generate the minimum desired number of permuted output titles. In our example, by judicious use of the "$", we can cause the phrase "Elastic Collision Probability" to be considered as a key word and also have "(A)" indexed as a key word:

23 ELASTIC$COLLISION$PROBABILITY FOR ELECTRONS IN ARGON (A)$

The "$" is blanked after the permutation for key words has been performed and before the output titles are alphabetized.

The program described here has been used to create an author and subject index in the updating of Basic Data of Plasma Physics[2] by Sanborn C. Brown. The punched output will be used to create listings suitable for photo-offset reproduction.

This work was done in part at the M.I.T. Computation Center.

Elaine C. Isaacs

References

1. Martha M. Pennell and R. M. Nacamuli, "A Computer Indexing Program," Quarterly Progress Report No. 82, Research Laboratory of Electronics, M.I.T., July 15, 1966, p. 23.

2. S. C. Brown, "Computer Programmed 'Basic Data of Plasma Physics'," Quarterly Progress Report No. 80, Research Laboratory of Electronics, M.I.T., January 15, 1966, pp. 83-85.

B. A SIMPLE METHOD FOR FINDING THE ROOTS OF AN ANALYTIC FUNCTION

Preliminary efforts have been made toward implementation of a simple procedure for finding the roots of an arbitrary complex function. The completed program will be especially useful in plasma physics research, in which exact solutions to dispersion equations are usually impossible, and numerical approximations are often valid only for a special type of equation. The method described in this report permits the user to input any analytic function, regardless of whether it happens to be algebraic.

Because the procedure relies on proper selection of curves for evaluation of a line integral, the facilities provided by the ESL Display Console at Project MAC can be profitably used. The techniques of man-machine interaction already developed there give the user a quick and intuitive way to deal with a complicated and formidable dispersion relation. The techniques that we plan to utilize are sketched in the program description below.

We want to find the roots of $f(z) = 0$, where $f(z)$ is given complex function. A simple consequence of Cauchy's residue theorem permits us to state that a root, Z_o, of $f(z)$ can be expressed[1] as

$$Z_o = \frac{1}{2\pi i} \oint_C \frac{zf'(z)}{f(z)}\, dz = \frac{1}{2\pi i} \oint_{f(C)} \frac{z}{f}\, df. \qquad (1)$$

We are interested in the second form of this equation.

Determination of Z_o, using (1), requires the following computational procedures:

1. Display $f(z)$ in the z-plane and determine the existence of a root by inspection.
2. Enclose the root by a curve, C, using the typewriter or the light pen.
3. Compute and display $f(C)$ in the $w = f(z)$ plane. If $f(C)$ does not encircle the origin or encircles it more than once (indicating the presence of additional roots), return to (1) and enter C again.

4. Using Simpson's rule, evaluate the line integral

$$Z_o = \frac{1}{2\pi i} \oint_{f(C)} \frac{z}{f}\, df.$$

This approximation to Z_o is used to obtain a refined value of Z_o, using for C a circle centered at Z_o, and repeating 2) to 4) until a sufficiently precise value is determined. Previous work indicates that convergence is typically quite rapid.[1]

Eleanor C. River

References

1. B. D. Fried, "On Line Root Finding in the Complex Plane," Draft, 21 May 1966.

C. ROOTS, A ROOT-FINDING SUBROUTINE USING MULLER'S METHOD

A reliable polynomial-with-complex-coefficients-root-finding subroutine is the basis for such work as Quixot Dulcin[1] and Mills' display program.[2] In each case the same subroutine, called Roots, was used to perform this vital function. Roots is based on Share Distribution #692 which we modified to handle either a MAD or a Fortran calling program, using Muller's Method[3] to calculate the roots. Because Roots is extremely easy to use (the user need only provide the degree of the polynomial and its coefficients) and seldom fails to converge, it has been extremely useful.

Unfortunately, the program is coded in FAP (the assembly language for the IBM 7090-7094 computers), and consequently incompatible with the IBM 360 series to which the M. I. T. Computation Center will eventually be converting. Moreover, we have been plagued with numerous requests for a compiler language version of Roots. Consequently, we are rewriting Roots in both MAD and Fortran IV languages.

Because of its reliability, we have tried to follow the logic of the original Share Distribution, making modifications only when necessary to prevent cases in which Roots has been known to fail. This usually occurs when the constant term is eight or more orders of magnitude smaller than the other coefficients, i. e., there is a root extremely close to zero.

For example, Roots failed on the following polynomial:

$$x^4 + .076977968x^3 + .0014028739x^2 - .30980169 \times 10^{-5} x - .61770526 \times 10^{-19} = 0,$$

but succeeded on

$$x^4 + .076977968x^3 + .0014258634x^2 - .22131765 \times 10^{-5} x - .77008791 \times 10^{-9} = 0,$$

to give

$-.29337885 \times 10^{-3}$, $.0017075531$, $-.039196071 \pm .00094472884i$.

The method depends on three initial guesses which the program sets internally. These guesses, which remain the same for each polynomial, were not those originally suggested by Muller.

An important problem that we have encountered is round-off. The computer sometimes introduces a seemingly small imaginary or real part. The user is then left to ascertain whether this is a true contribution or whether the root is really pure real or imaginary. For example, on the polynomial whose roots are $\frac{1}{3}$, $\pm i$ (double root):

$$3x^5 - x^4 + 6x^3 - 2x^2 + 3x - 1 = 0 \tag{1}$$

our MAD program gave the following as roots:

$.33333334$

$-.33913844 \times 10^{-13} - .99995337i$

$.80916850 \times 10^{-4} + .9999464i$

$-.43413214 \times 10^{-9} + 1.0000466i$

$-.80916414 \times 10^{-4} - 1.0000053i$

Muller's method is a very easy technique both to understand and program. If we have three points, x_i, x_{i-1}, x_{i-2}, we can approximate the general polynomial:

$$f(x) = a_o x^n + a_1 x^{n-1} + \ldots + a_n = 0 \tag{2}$$

by the quadratic

$$b_o x^2 + b_1 x + b_2 = 0 \tag{3}$$

whose curve passes through the points $(x_i, f(x_i))$, $(x_{i-1}, f(x_{i-1}))$, $(x_{i-2}, f(x_{i-2}))$, and b_1, b_2, b_o satisfy the following system of equations:

$$b_o x_i^2 + b_1 x_i + b_2 = f(x_i)$$

$$b_o x_{i-1}^2 + b_1 x_{i-1} + b_2 = f(x_{i-1})$$

$$b_o x_{i-2}^2 + b_1 x_{i-2} + b_2 = f(x_{i-2}).$$

The quadratic formula easily gives us the roots of Eq. 3. Choosing as x_{i+1} that root of (3) closest in magnitude to x_i, we can again approximate Eq. 2 by Eq. 3, this time using the three points x_{i+1}, x_i, x_{i-1}. This process is repeated until

$$|x_{i+1} - x_i| / |x_{i+1}|$$

has become less than some preassigned number ($3.\times 10^{-8}$). The current value of x_i is then taken to be the root and divided into f(x) to obtain a new polynomial of degree n-1. This entire process is then repeated until a quadratic is formed, at which point the standard formula is used. The question naturally arises, What values does one use for the three initial points x_o, x_1, x_2?

In his article, Muller uses the starting values $x_o = -1$, $x_1 = 1$, $x_2 = 0$ and

$a_n - a_{n-1} + a_{n+1}$ for $f(x_o)$

$a_n + a_{n+1} + a_{n-2}$ for $f(x_1)$

a_n for $f(x_2)$.

The rationale behind this choice is that Eq. 3 then becomes equal to the last three terms of the original equation

$$a_n + a_{n-1}x + a_{n-2}x^2$$

which is a good approximation if a root exists near zero. A second advantage is that this choice saves two evaluations of the original polynomial.

We found, however, that in the Share Distribution the true values for $f(x_o)$, $f(x_1)$, $f(x_2)$ were used. In fact, our first MAD program used Muller's starting guesses and failed on the following polynomial:

$$x^5 - 2x^4 - 6x^3 + 4x^2 + 13x + 6 = 0$$

whose roots are 2, 3, -1 (triple). The Share Distribution did not fail, however, nor did our MAD program when the true values for $f(x_o)$, $f(x_1)$, $f(x_2)$ were used. The same thing occurred on Eq. 1.

An investigation is now under way to determine the reason. Work also continues on debugging and testing our routines.

Martha M. Pennell, Joan Harwitt

References

1. Martha M. Pennell, "Generalized Polynomial Root-Finding Program for a Time-Shared Computer," Quarterly Progress Report No. 79, Research Laboratory of Electronics, M.I.T., October 15, 1965, pp. 263-266.

2. J. M. Mills, "A Computer Display System for Analyzing Polynomial-Type Dispersion Relations," S.M. Thesis, Department of Electrical Engineering, M.I.T., January 1965.

3. D. E. Muller, "A Method for Solving Algebraic Equations Using an Automatic Computer," Mathematical Tables and Other Aids to Computation (National Research Council, Washington, D.C., October 1956), pp. 208-215.

D. LINEARIZING THE ROOTS OF A POLYNOMIAL. II

Using the least-squares method as previously described,[1] we approximated the following sixth-degree polynomial in λ:

$$\begin{vmatrix} \Gamma_{11} - \lambda^2 & \Gamma_{12} & \Gamma_{13} \\ \Gamma_{12} & \Gamma_{22} - \lambda^2 & \Gamma_{23} \\ \Gamma_{13} & \Gamma_{23} & \Gamma_{33} - \lambda^2 \end{vmatrix} = 0$$

where

$$\Gamma_{11} = k_x^2 C_{11} + k_y^2 \tfrac{1}{2}(C_{11}-C_{12}) + k_z^2 C_{44} + 2k_y k_z C_{14}$$

$$\Gamma_{22} = k_x^2 \tfrac{1}{2}(C_{11}-C_{12}) + k_y^2 C_{11} + k_z^2 C_{44} - 2k_y k_z C_{14}$$

$$\Gamma_{33} = \left(k_x^2+k_y^2\right) C_{44} + k_z^2 C_{33}$$

$$\Gamma_{12} = 2k_x k_z C_{14} + \tfrac{1}{2} k_x k_y (C_{11}+C_{12})$$

$$\Gamma_{13} = k_x k_z (C_{44}+C_{13}) + 2k_x k_y C_{14}$$

$$\Gamma_{23} = \left(k_x^2-k_y^2\right) C_{14} + k_y k_z (C_{13}+C_{44})$$

$$k_x = \sin\theta \cos\gamma$$

$$k_y = \sin\theta \sin\gamma$$

$$k_z = \cos\theta$$

$0 \leq \theta \leq 180°$ and $0 \leq \gamma \leq 30°$

$C_{11} = .8694$ $\quad C_{33} = 1.0680$ $\quad C_{44} = .5762$

$C_{12} = .0696$ $\quad C_{13} = .1560$ $\quad C_{14} = .1743$

The problem is to find the set of constants $\phi_1, \ldots, \phi_{14}$ such that one of the following expressions best approximates the three positive real roots of the polynomial:

1) $\phi_1\omega_o + \phi_2\omega_2^1$

2) $\phi_1\omega_o + \phi_2\omega_2 + \phi_3\omega_4$

3) $\phi_1\omega_o + \phi_2\omega_2 + \phi_3\omega_4 + \phi_4\omega_4^3$

4) $\phi_1\omega_o + \phi_2\omega_2 + \phi_3\omega_4 + \phi_4\omega_4^3 + \phi_5\omega_6$

5) $\phi_1\omega_o + \phi_2\omega_2 + \phi_3\omega_4 + \phi_4\omega_4^3 + \phi_5\omega_6 + \phi_6\omega_6^3$

6) $\phi_1\omega_o + \phi_2\omega_2 + \phi_3\omega_4 + \phi_4\omega_4^3 + \phi_5\omega_6 + \phi_6\omega_6^3 + \phi_7\omega_6^6$

7) $\phi_1\omega_o + \phi_2\omega_2 + \phi_3\omega_4 + \phi_4\omega_4^3 + \phi_5\omega_6 + \phi_6\omega_6^3 + \phi_7\omega_6^6 + \phi_8\omega_8$

8) $\phi_1\omega_o + \phi_2\omega_2 + \phi_3\omega_4 + \phi_4\omega_4^3 + \phi_5\omega_6 + \phi_6\omega_6^3 + \phi_7\omega_6^6 + \phi_8\omega_8 + \phi_9\omega_8^3$

9) $\phi_1\omega_o + \phi_2\omega_2 + \phi_3\omega_4 + \phi_4\omega_4^3 + \phi_5\omega_6 + \phi_6\omega_6^3 + \phi_7\omega_6^6 + \phi_8\omega_8 + \phi_9\omega_8^3 + \phi_{10}\omega_8^6$

10) $\phi_1\omega_o + \phi_2\omega_2 + \phi_3\omega_4 + \phi_4\omega_4^3 + \phi_5\omega_6 + \phi_6\omega_6^3 + \phi_7\omega_6^6 + \phi_8\omega_8 + \phi_9\omega_8^3 + \phi_{10}\omega_8^6 + \phi_{11}\omega_{10}$

11) $\phi_1\omega_o + \phi_2\omega_2 + \phi_3\omega_4 + \phi_4\omega_4^3 + \phi_5\omega_6 + \phi_6\omega_6^3 + \phi_7\omega_6^6 + \phi_8\omega_8 + \phi_9\omega_8^3 + \phi_{10}\omega_8^6 + \phi_{11}\omega_{10} + \phi_{12}\omega_{10}^3$

12) $\phi_1\omega_o + \phi_2\omega_2 + \phi_3\omega_4 + \phi_4\omega_4^3 + \phi_5\omega_6 + \phi_6\omega_6^3 + \phi_7\omega_6^6 + \phi_8\omega_8 + \phi_9\omega_8^3 + \phi_{10}\omega_8^6 + \phi_{11}\omega_{10} + \phi_{12}\omega_{10}^3 + \phi_{13}\omega_{10}^6$

13) $\phi_1\omega_o + \phi_2\omega_2 + \phi_3\omega_4 + \phi_4\omega_4^3 + \phi_5\omega_6 + \phi_6\omega_6^3 + \phi_7\omega_6^6 + \phi_8\omega_8 + \phi_9\omega_8^3 + \phi_{10}\omega_8^6 + \phi_{11}\omega_{10} + \phi_{12}\omega_{10}^3 + \phi_{13}\omega_{10}^6 + \phi_{14}\omega_{10}^9$

$\omega_o = 1$

$\omega_2 = \frac{1}{2}(3\cos^2\theta - 1)$

$\omega_4 = \frac{1}{8}(35\cos^4\theta - 30\cos^2\theta + 3)$

$\omega_4^3 = (-1)\,105\sin^3\theta\cos\theta\sin 3\gamma$

$\omega_6 = (-1)\frac{1}{16}(5 - 105\cos^2\theta + 315\cos^4\theta - 231\cos^6\theta)$

$\omega_6^3 = \left(\frac{945}{2}\cos\theta - \frac{3465}{2}\cos^3\theta\right)\sin^3\theta\sin 3\gamma$

$\omega_6^6 = \frac{1}{16}(231\sin^6\theta\sin 6\gamma)$

$\omega_8 = \frac{1}{128}(35 - 1260\cos^2\theta + 6930\cos^4\theta - 12012\cos^6\theta + 6435\cos^8\theta)$

$\omega_8^3 = (-1)\frac{1}{128}\left(6930\cdot 4!\cos\theta - 2002\cdot 6!\cos^3\theta - \frac{429}{8}\cdot 8!\cos^5\theta\right)\sin^3\theta\sin 3\gamma$

$\omega_8^6 = (-1)\frac{1}{128}\left(12012\cdot 6! - \frac{6435}{2}\cdot 8!\cos^2\theta\right)\sin^6\theta\sin 6\gamma$

$\omega_{10} = (-1)\frac{63}{256}\left(1 - 55\cos^2\theta + \frac{1430}{3}\cos^4\theta - 1430\cos^6\theta + \frac{12155}{7}\cos^8\theta - \frac{46189}{63}\cos^{10}\theta\right)$

Table XXXIV-1. Results.

	ϕ_1	ϕ_2	ϕ_3	ϕ_4	ϕ_5	ϕ_6	ϕ_7	ϕ_8	ϕ_9	ϕ_{10}	ϕ_{11}	ϕ_{12}	ϕ_{13}	ϕ_{14}	Standard Deviation	R^2	F-Ratio	Degrees of Freedom
Middle Curve																		
Coefficient	.72523	.03456	.07714	.00267	-.07197										.02030	.9120	165.86	64
Standard Error	(.00285)	(.00672)	(.00822)	(.00012)	(.00982)													
t-value	254.37	5.14	9.38	2.27	-7.33													
Coefficient	.72643	.03725	.06914	-1.07592	-.06686	-.54987	-.879E-6	.00649	-.15134	-.195E-6	-.00932	-.01784	-.165E-7	-.588E-10	.01744	.9410	67.52	55
Standard Error	(.00388)	(.00838)	(.01082)	(.56803)	(.01142)	(.28961)	(.102E-5)	(.01360)	(.07973)	(.105E-7)	(.00959)	(.00939)	(.304E-7)	(.315E-10)				
t-value	187.37	4.44	6.39	-1.89	-5.85	-1.90	.86	.48	-1.90	-1.85	-.97	-1.90	-.54	-1.87				
Lower Curve																		
Coefficient	.60904	.03261	.03980	.00208	.06688	-.00027									.01824	.9067	122.52	63
Standard Error	(.00261)	(.00604)	(.00739)	(.00011)	(.00888)	(.00005)												
t-value	233.40	5.40	5.38	19.20	7.53	-5.18												
Coefficient	.61241	.02393	.04509	.92991	.06949	.47278	-.196E-5	-.00456	.13021	.694E-7	.00825	.01534	.185E-7	.305E-10	.01756	.9214	49.60	55
Standard Error	(.00390)	(.00844)	(.01089)	(.57196)	(.01150)	(.29161)	(.103E-5)	(.01369)	(.08028)	(.106E-6)	(.00966)	(.00945)	(.306E-7)	(.317E-10)				
t-value	156.88	2.84	4.14	1.62	6.04	1.62	1.90	-.33	1.62	.65	.85	1.62	.60	.96				
Outer Curve																		
Coefficient	1.0338	.07636	-.07818	-.00310											.01827	.9375	325.23	65
Standard Error	(.00228)	(.00605)	(.00739)	(.00010)														
t-value	452.79	12.63	-10.58	-29.40														
Coefficient	1.02612	.08434	-.07491	.29992	.00280	.15462	.105E-5	-.00650	.04248	.123E-6	.000430	.00501	-.257E-8	.588E-10	.01714	.9532	86.15	55
Standard Error	(.00381)	(.00824)	(.01063)	(.55837)	(.01123)	(.28468)	(.100E-5)	(.01337)	(.07838)	(.104E-6)	(.00943)	(.00923)	(.297E-7)	(.310E-10)				
t-value	269.25	10.24	-7.04	.54	.25	.54	1.05	-.49	.54	1.18	.04	.54	-.09	1.89				

$$\omega_{10}^{3} = \frac{63}{256}\left(\frac{1430}{3}\cdot 4!\cos\theta - \frac{715}{3}\cdot 6!\cos^3\theta + 12155\cdot 42\cos^5\theta - \frac{46189}{63}\cos^7\theta\right)\sin^3\theta\sin 3\gamma$$

$$\omega_{10}^{6} = \frac{63}{256}\left(1430\cdot 6! - \frac{12155}{14}\cdot 8!\cos^2\theta + \frac{46189}{63}\cdot\frac{10!}{4!}\cos^4\theta\right)\sin^6\theta\sin 6\gamma$$

$$\omega_{10}^{9} = (-1)\frac{1}{256}\cdot 46186\cdot 10!\cos\theta\sin^9\theta\sin 9\gamma$$

n arbitrary roots on the same roots loci were used as data for the least-squares analysis. Because of the nature of the curves and the number of fitting functions, we repeated our calculations with 30, 52, 70, and 90 data points. We found that 30 points were too few and gave spurious results for fitting functions 10 through 13.

We used the following criteria to measure the "goodness" of fit:

R^2 (also called the coefficient of correlation): May be looked upon as the proportion of total "squared error" that is explained by fitting the line as "due to" the linear relationship between the dependent variable and independent variables.[3] A perfect relationship is 1 and no relationship is 0.

Standard Deviation: The measure of dispersion around the fitted line. Two-thirds of the observed points are within one standard deviation of each side of the line.[4]

F-ratio: The explained variation over the unexplained variation of the dependent variables about the least-squares line.[5] For a sample with 37 degrees of freedom and 14 coefficients, 1.89 indicates a good fit; for 55 degrees of freedom and 14 coefficients, 1.88; and for 77 degrees of freedom and 14 coefficients, 1.82. For all equations in our samples, the F-ratio was significant except for the first fitting function.[6]

Standard Error of the coefficient: Similar to the standard deviation of the equation.

t-value: Similar to the F-ratio but is used to test the level of significance of the coefficient rather than the whole equation. At a confidence level of .90, a t-value of 1.645 was significant; at the .95 level the t-value must be 1.960; at the .98 level, 2.326; and at the .99 level, 2.576.[3]

The formulas for calculating these statistical measures are taken from Econometric Models.[7]

The results are summarized in Table XXXIV-1 for the three curves with 70 points used. The fitting functions given here have the best fit as indicated either by the largest F-ratio or the largest R^2 and the smallest standard deviation. The results of the other samples are comparable.

Heather S. Davis

References

1. Martha M. Pennell and Heather Davis, "Linearizing the Roots of a Polynomial," Quarterly Progress Report No. 83, Research Laboratory of Electronics, M.I.T., October 15, 1966, pp. 179-181.

2. G. W. Farnell, "Elastic Waves in Trigonal Chrystals," Can. J. Phys. 39, 65-80 (January 1961).

3. B. L. Nelson, Elements of Modern Statistics (Appleton-Century-Crofts, Inc., New York, 1958), pp. 242-243; see t-value table, p. 341.

4. John F. Kenney, Mathematics of Statistics, Part I (D. Van Nostrand Company, New York, 2d edition, 1961), pp. 68-69.

5. J. Johnston, Econometric Methods (McGraw-Hill Book Company, New York, 1963), pp. 32-33.

6. C. R. C. Standard Mathematical Tables (Student Edition, 1964), pp. 261-264.

7. J. Johnston, op. cit., pp. 134-135.

E. DEVELOPMENT OF PRIVATE LIBRARY TO BE SEARCHED BY TIP

On the initiative of Professor Sanborn C. Brown, a project is under way to create a series of private user files[2] on Project MAC to be searched by the M.I.T. Library TIP Program. The four libraries now being catalogued are those of Professors Allis, Brown, Bers, and Bekefi – all of whom work in the field of Plasma Physics. This project draws extensively upon the facility to create users' files as programmed in the M.I.T. Technical Information Project[1] and upon the user interaction and time-sharing capabilities of Project MAC.

The files are created and maintained by each user or his secretary, except for Professor Allis' whose file is maintained by the Document Room staff of the Research Laboratory of Electronics. Each file contains one entry corresponding to each report, book, etc. in the individual's library. In turn each entry contains the information needed to locate the article, such as the title (unabbreviated), author(s) and source, as well as a code incorporating the Professor's initials to indicate where the publication can be found. Following are examples of entries from each of these four files.

20A 125 - **BROWN**
THE PLASMA PHYSICS OF THERMIONIC CONVERTERS
R. H. BULLIS, L. K. HANSEN, J. M. HOUSTON,
M. F. KOSKINEN, N. S. RASOR, C. WARNER
THERM CONV SPEC CONF SAN DIEGO 1965 SCE 50

ANALYSIS OF BIBLIOGRAPHIC SOURCES IN A GROUP OF PHYSICS-RELATED JOURNALS
M. M. KESSLER
M.I.T. SCE 83

PHYSIC SURVEY AND OUTLOOK
NAT. ACAD. OF SCIENCES
WASHINGTON SCE 89

TRANSACTIONS OF THE ALL-UNION CONF. ON SPACE PHYSICS
G. A. SKURIIN
NASA TT F-389 SCE 102

PLASMA PHYSICS BULLETIN
DEPT. OF PHYSICS
U. OF MIAMI V3 1963 SCE 287

PROCEEDINGS FAR INFRARED PHYSICS SYMPOSIUM
NAVAL ORDANCE LAB. CORONA
CORONA, CAL. SCE 316

PHYSICS OF FLUIDS
A.I.P.
V9 P1437 1966 SCE 359

20E 120 - **BERS**
PLASMA PHYSICS LABORATORY REVIEW
J. E. DRUMMOND ET AL
BOEING JAN-JUN 1965 AE 14

MECHANICAL DESIGN FOR PLASMA PHYSICS RESEARCH
W. S. NEFF, JR.
UCRL 12325 JAN 1965 AE 79

AN ANNOTATED BIBLIOGRAPHY OF ARTICLES ON PLASMA PHYSICS AND CONTROLLED THERMONUCLEAR RESEARCH BY U.K.A.E.A. STAFF, 1958 TO 1962
L. J. ANTHONY
CLM R 24 JAN 1963 AE 119

20A 112 - **BEKEFI**
REPORT OF 1965 NAGOYA MEETING ON SPACE PLASMA PHYSICS
NAGOYA UNIVERSITY IPPJ-44(J) DEC. 1965 GE 5
H. IKEZI AND K. TAKAYAMA
NAGOYA UNIVERSITY IPPJ-48 MARCH 1966 GE 6

PLASMA PHYSICS LABORATORY REVIEW, JAN.-JUNE 1966
SCIENTIFIC RESEARCH LABORATORIES
BOEING, GE 22

26 237 - **ALLIS**
PLASMA PHYSICS LABORATORY REVIEW
J. E. DRUMMOND, ET AL
BOEING SCIENTIFIC RES LAB JULY-DEC 1965 WPA 10

PHYSIQUE DES FAISCEAUX DE PLASMA DE SYNTHESE
J. F. BONNAL, J. GIACOMINI, G. MAINFRAY, C. MANUS,
J. MORELLEC, G. SPIESS
SACLAY SEPT 6-10, 1965 WPA 19

CUMULATIVE LISTING OF PLASMA PHYSICS LABORATORY REPORTS AND PUBLICATIONS (5TH EDITION)
PRINCETON UNIV
PRINCETON UNIV MATT-400 JULY 1966 WPA 48

As we show in the examples above, the file code name indicates the room where the publication can be found.

By using the information retrieval services of the Library TIP Program[2] and Project MAC, these four files may be searched individually or all at once; the latter procedure is facilitated by linking to PRIVAT REPORT in Professor S. C. Brown's files.

We hope that this project will cut down the time and effort spent in organizing and using these private libraries and reduce the number of duplicates. It should make it easier to share information. At the present time, Professor Brown has 466 articles listed; Professor Allis, 52; Professor Bers, 124; and Professor Bekefi, 18.

Heather S. Davis

References

1. M. M. Kessler, Physics Today, Vol. 18, No. 3, pp. 28-36, March 1965.
2. M. M. Kessler, TIP User's Manual, December 1, 1965.

XXXV. STROBOSCOPIC LIGHT RESEARCH*

Academic and Research Staff

Prof. H. E. Edgerton

RESEARCH OBJECTIVES

The Research Laboratory of Electronics has had close association with the research and application of electronic flash-lighting equipment work that is being carried out in the Stroboscopic Light Laboratory of the Department of Electrical Engineering. There are mutual advantages because of common goals in many areas of interest.

First, the aim of both is the education of students. Every opportunity for experimental work should be given to students at the Massachusetts Institute of Technology so that they can become acquainted with the real experimental world and learn the satisfaction of accomplishment. The laboratories and facilities of the Research Laboratory of Electronics are excellent, especially the shops and general service laboratories. As an example, each term, several classes of my students are shown the glass-blowing facilities. Actual devices such as discharge lamps are made during these visits, and the students are given the lamps to exhaust and operate in actual circuits.

Second, the research goal of the Stroboscopic Light Laboratory is the development of instruments and methods by using electronic flash light sources involving the electrical excitation of gas. This field – gaseous conduction of electricity – has engaged the attention of many of the research workers at the Research Laboratory of Electronics. There is much more to be accomplished in the transient pulsing of electricity through gases, so we hope for many years of cooperation.

In our laboratory we wish to know more and more about the fundamental processes that exist in flash lamps so that brighter, shorter-flash or special lamps can be perfected. As knowledge of the physical mechanism evolves, perhaps new goals, at present unperceived, can be reached.

We are called upon from many departments of M.I.T. to help in making measurements for a great variety of problems, mainly involving things that happen fast. Much of our effort is expended along this line of application. Once in a while, a difficult technical problem is easily and quickly solved; more than likely, it is not. A host of problems is waiting for new solutions. This, too, makes it interesting.

For more than ten years we have worked on many applications of electronic flash-lighting equipment to underwater research, with partial financial help from the National Geographic Society and interested individuals. This work has been greatly stimulated by the addition of a pressure-testing facility in Room 20D-009. We have assisted with the photographic devices for both existing bathyscaphes, and helped with the design of new photographic equipment for the French bathyscaphe (ARCHIMEDE) that was built for ultimate depths of 37,000 feet.

At present, two photographic problems in the sea engage our attention. One involves the photography of small jellylike creatures that are almost invisible because their refractive index resembles that of water. A camera equipped with a back light with a special strobe will be made to test the use of the back-lighting principle. This equipment will be used at depths down to 1 mile in seas where abundant plankton life is found.

A second problem, also involving electronic flash photography, is an attempt to apply the elapsed-time principle of motion-picture photography to the study of shallow areas of the sea bottom. For this purpose, stationary cameras will be placed on the bottom of the sea for extended periods of time to study tidal action and biological changes with the seasons.

H. E. Edgerton

*This work is supported in part by the Joint Services Electronics Programs (U.S. Army, U.S. Navy, and U.S. Air Force) under Contract DA 36-039-AMC-03200(E).

Author Index

Allis, W. P., 164
Anderson, G. B., 302
Austin, M.E., 227
Baggeroer, A. B., 243
Barlow, J. S., 327
Barrett, A. H., 33, 36
Bartsch, R. R., 142
Benhaim, N., 253
Bernard, G. D., 121
Bers, A., 141, 144, 173
Billman, K. W., 1, 9
Bitter, F., 63
Black, W. L., 291
Blum, G., 70
Bowers, K. W., 31
Briggs, R. J., 141
Brown, G. A., 171
Brown, S. C., 123, 137
Brown, T. S., 158
Brueck, S. R. J., 155
Burke, B. F., 34, 36
Burnham, D. C., 28
Burns, S. K., 316
Chomsky, N. A., 261
Chu, L; J., 113
Chung, K., 158, 159
Colombant, D. G., 157
Crane, D. E., 175
Davis, Heather S., 355, 359
Davis, J. A., 145
Dennis, J. B., 347
Dupree, T. H., 158
Durlach, N. I., 314
Eberle, F. W., 89
Eden, M., 290, 291
Edgerton, H. E., 363
Elias, P., 205, 206
Ezekiel, S., 70
Fehrs, D. L., 82
Fertel, Jeanne H., 53
Fiocco, G., 63, 64, 66
Gadzuk, J. W., 94, 95
Gallager, R. G., 203, 204, 205, 206
Garland, C. W., 61
Gaut, N. E., 36
Graham, D. N., 294
Grams, G. W., 66
Guinan, J. J. , Jr., 320
Gustafson, T. K., 113
Guttrich, G. L., 9
Hall, R. D., 313
Halle, M., 253, 261
Harwitt, Joan, 352
Haus, H. A., 75, 113, 164
Hofmann, T. J., 263
Hoversten, E. V., 204, 212
Huang, T. S., 289, 304
Ingard, K. U., 97
Isaacs, Elaine C., 350
Katona, P. G., 316, 331
Kennedy, R. S., 204, 206, 212
Kerrebrock, J. L., 171
Kiang, N. Y. S., 311
King, J. G., 1
Kinsey, J. L., 13
Klatt, D. H., 257
Kleppner, D., 27, 28
Kolers, P. A., 290
Kronquist, R. L., 129
Kukolich, S. G., 2
Kusse, B., 151
Kyhl, R. L., 15, 26
Law, Sara, 36
Lee, F. F., 287
Lee, Y. W., 181
Lenoir, W. B., 38, 42
Lettvin, J. Y., 334
Levy, E. K., 171
Lidsky, L. M., 157, 158, 175, 176
Liss, P. H., 290
Lubin, M. D., 175
Manheimer, W. M., 158
Mason, S. J., 287
Massey, J. L., 203
McCulloch, W. S., 333, 335
McNary, C. A., 164
McNelly, T. F., 53
Menyuk, Paula, 254
Milner, J. C., 275
Moir, R. W., 176
Moran, J. M., 34, 36
Moreno-Diaz, R., 335
Murakami, M., 176
Myint, T., 27
Odette, G. R., 157
Offenberger, A. A., 175
Ozier, I., 28
Parker, R. R., 141, 142
Peake, W. T., 311, 320
Pennell, Martha M., 349, 352
Perry, C. H., 51, 53
Pritchard, D. E., 28
Rafuse, R. P., 49, 75
Reznek, S. R., 17
Richters, J. S., 207
River, Eleanor C., 253, 351
Rogers, A. E. E., 34, 36
Rogoff, G. L., 123
Rose, D. J., 157, 158, 175, 176
Rosenblith, W. A., 313, 314, 315, 316
Ross, A. H. M., 307
Ross, J. A., 98, 103
Schafer, R. W., 194
Schindall, J. E., 184
Schneider, H. M., 149
Schreiber, W. F., 289, 291

Schulz, H. M., III, 98
Siebert, W. M., 311, 314
Smullin, L. D., 141
Staelin, D. H., 36
Stamm, P. L., 304
Stevens, K. N., 253
Stickney, R. E., 81, 82, 89
Strandberg, M. W. P., 15, 16
Sullivan, W. T., III, 36
Tretiak, O. J., 291
Troxel, D. E., 287
Van Trees, H. L., 225
Wagner, C. E., 158
Wall, P. D., 335
Warren, B. E., 79
Waugh, J. S., 77
Weiss, R., 69, 70
Weiss, T. F., 311
Williams, J. A., 153
Winkler, P. F., 27
Wright, B. L., 137
Zacharias, J. R., 1